Assembling Multi-Functional Ligands to Smart Materials

Dipankar Ghosh

Faculty of Physical Sciences
University of Iceland
2020

Assembling Multi-Functional Ligands to Smart Materials

Dipankar Ghosh

Dissertation submitted in partial fulfillment of a
Philosophiae Doctor degree in Chemistry

Advisor
Prof. Krishna Kumar Damodaran

PhD Committee
Prof. Ingvar Helgi Árnason
Prof. Már Másson

Opponents
Prof. Thorfinnur Gunnlaugsson
Dr. Stefán Jónsson

Faculty of Physical Sciences
School of Engineering and Natural Sciences
University of Iceland
Reykjavik, June 2020

Assembling Multi-Functional Ligands to Smart Materials

Small molecules arranged to functional materials

Dissertation submitted in partial fulfillment of a *Philosophiae Doctor* degree in Chemistry

Faculty of Physical Sciences
School of Engineering and Natural Sciences
University of Iceland
Dunhagi 3
107 Reykjavik
Iceland

Telephone: 525 4000

Bibliographic information:

Dipankar Ghosh, 2020, *Assembling Multi-Functional Ligands to Smart Materials*, PhD dissertation, Faculty of Physical Sciences, University of Iceland, 342pp.

Author ORCID: 0000-0002-1165-2819

ISBN 978-9935-9452-5-9

Printing: Haskolaprent Ehf.
Reykjavik, Iceland, June 2020

Abstract

Nature has been successful in self-assembling simple building blocks to complex functional architectures and the concept of supramolecular chemistry has enabled chemists to mimic nature's self-assembly principles. The understanding of the assembly/reassembly process is challenging but this will enable us to design and synthesize complex functional materials with predictable properties. In this doctoral work, the assembly of hydrogen bond functionalized organic molecules via non-bonding interactions and metal coordination have been studied. The metal coordination induced assembly was studied by converting the multi-functional ligand into metalloligands, which were converted to metal organic material (MOMs) and the catalytic properties of the MOMs were evaluated. The self-assembly based on hydrogen bonding was analyzed in low molecular weight supramolecular gels (LMWGs), which are stimuli-responsive supramolecular systems where the self-assembly/reassembly process can be either switched on/off by an external stimulus. The role and importance of various non-bonding interactions in the formation of gel network were studied in amide based LMWGs and metallogels. The self-assembly process in multi-component amide/urea supramolecular gels was analyzed by various analytical techniques and have reported the crystallographic evidence of specific co-assembly in mixed enantiomeric gel. The application of LMWGs as efficient crystallizing media was explored and have shown the crystallization of inorganic compounds using gel medium. These studies enabled us to understand the key interactions of the self-assembly process in these systems, which will be beneficial in designing new supramolecular systems with predictable properties

Útdráttur

Náttúran notar einfaldar, sjálfskipulangar (e. self-assembling) byggingareiningar til þess að mynda flóknari efni með ákveðna virkni tengda byggingu þeirra, hugmyndir þversameinda efnafræði hafa gert efnafræðingum kleift að herma sjálfskipulagningu náttúrulegra efna. Að auka skilning á samsetniningarferlinu er krefjandi en mun gera okkur kleift að hanna og smíða flókin efni með fyrirsjáanlega virkni og eiginleika. Í þessu doktors verkefni, verður skoðuð samsöfnun vetninstengjandi virktra lífrænna efna með ósamgildumtengjum og girðitengjum við málma. Málm hvötuð samsetning var skoðuð með því að umbreyta fjöl virkum bindli (e. ligand) í málm-bindli, sem var innlimaður í málmlífrænt efni (MOMs) (e. metal organic material) og kvötunar eiginleikar þess greindir. Sjálfskipulangningin byggð á vetnins tengjum var rannsökuð í þversameindagelum byggðum á lág-massa sameindagelum (LMWGs) (e. low molecular weight gelators), sem eru þversameinda kerfi með ákveðna örvunar svörun þar sem sjálfskipulagning/endurmyndun ferli getur verið stillt af/á eftir utanaðkomandi örvun eins og hita, ljósi, hljóðbylgjum, pH eða jónum. Tilgangur og mikilvægi ýmissa ósamgildra tengja í myndun gelkerfa voru rannsökuð í LMWGs byggðum á amíðum og málmgelum (e. metallogels). Sjálfskipulagningar ferlið í fjölþátta-amíð/urea þversameindagelum var rannsakað með fjölbreyttum greiningar aðferðum og hefur sértæk samsöfnun byggingareingina (e. specific co-assembly) í blönduðum handhverfu gelum verið sýnd með kristalbyggingar greiningu. Notkun á LMWGs sem skilvirkum kristalræktunar miðil var könnuð og hefur sýnt kristöllun ólífrænna efna í gel miðil. Þessar ransóknir gera okkur kleift að skilja lykil víxlverkanir í sjálskipulagningar ferli þessara kerfa, sem mun gagnast í hönnun nýrra þversameinda kerfa með for ákveðna eiginleika.

Preface

The word 'supramolecular' is defined as the process of self-assembly of molecules via non-covalent bonding or interactions. Although the concept of supramolecular chemistry was developed over a century ago, yet the design, understanding of mechanism and the control over supramolecular self-assembly process is largely unexplored. This is typically due to the dynamic nature of the non-covalent interactions such as hydrogen-bonding, π-π stacking, electrostatic attraction, van der Waals force, solvophilic/solvophobic interaction and coordination bonding. The structural properties of self-assembled network rely on the combination of several non-bonding interactions, thus, constructing a supramolecular architecture with desired functionality from simple building blocks is a daunting task. The doctoral dissertation focuses on understanding the role of different non-bonding interactions in the formation of self-assembled hierarchical network. We have classified the self-assembly in three categories- (a) self-assembly of coordinating ligands with metal centers via coordination bond, (b) self-assembly of low molecular weight gelators via non-bonding interactions to form supramolecular gels and (c) self-assembly of multi-component gelators based on enantiomers to analyze different self-assembly modes. This thesis includes the published articles and the manuscripts which are at the final stage or ready to be submitted in a peer reviewed journal. The references for the articles are cited separately within the manuscripts, and citation style was used according to the journal.

In the first part, various multi-functional ligands with different binding sites were synthesized and reacted with various metal ions. This resulted in a number of metalloligands and metal-organic materials (MOMs) with specific architecture and functionality. This was achieved by synthesizing metalloligands with specific geometry and spatial arrangement of the functional groups. The complexes and MOMs were characterized by X-ray diffraction and catalytic properties of the materials were evaluated for various organic reactions including CO_2 conversion.

In the second part, the role of different non-bonding interactions in formation of supramolecular gels were explored. We have selected several low molecular weight gelators, which act as stimuli-responsive gelators and offers better control of the self-

assembly/reassembly process due to their tunable properties to external stimuli such as heat, light, sound, pH, coordination, salts/ions, etc. Understanding of the role of specific non-bonding interactions was accomplished by structural modification of existing gelators. The comparison of non-bonding interactions observed in crystal structure of parent gelator and modified gelator and the corroboration to their relative gel strength clearly indicate the importance of the particular non-bonding interaction in self-assembly process. This was further evidenced by inducing gelation to non-gelators via metal coordination to form supramolecular metallogels. It was observed that the specific non-bonding interaction, which was responsible for the formation of metallogel was absent in the non-gelator ligand indicating the importance of a particular interaction in the self-assembly process.

Unraveling of self-assembly process in multi-component supramolecular gels is even more challenging due to the self-recognition of gelators across various length scales. The individual gelators in multi-component gels rearrange either constructively or destructively to form well-ordered fibers containing individual gelators (self-sorting) or both gelators (specific co-assembly) or a mixed system (random co-assembly). In the third section of the thesis, self-assembly was investigated in multi-component gels derived from mixing enantiomeric gelators. We report the first crystallographic evidence of specific co-assembly in an enantiomeric multi-component gel, which resulted in the enhanced thermal and mechanical strength of the mixed gel system. In the last section, we show the application of supramolecular gel as a media for crystal growth and crystal habit modification of inorganic complexes. We believe that these findings will contribute to the ongoing efforts to understand self-assembly process and help chemists to design supramolecular architectures with desirable properties.

Table of Contents

List of Figures

List of Schemes

List of Tables

Abbreviations

1D	One-dimensional
2D	Two-dimensional
3D	Three-dimensional
AFM	Atomic force microscopy
BDA	Benzene-1,4-diamide
BDC	Benzene-1,4-dicarboxylate
CD	Circular dichroism
CLSM	Confocal laser scanning microscope
Cryo	Cryogenic
DMF	N,N-Dimethylformamide
DMSO	Dimethyl sulfoxide
FT-IR	Fourier-transform infrared
IRMOF	Isoreticular metal organic framework
LMWG	Low molecular weight gelator
mCPBA	*meta*-Chloroperoxybenzoic acid
MGC	Minimum gel concentration
ML	Metalloligand
MOF	Metal-organic framework
MOM	Metal-organic material
NMR	Nuclear magnetic resonance
PG	Polymeric gel
PSM	Post-synthetic modification
PXRD	Powder X-ray diffraction
SBU	Secondary building unit
SCSC	Single crystal to single crystal
SCXRD	Single crystal X-ray diffraction
SEM	Scanning electron microscopy
TEM	Transmission electron microscopy
TGA	Thermogravimetric analysis
T_{gel}	Sol-gel transition temperature
UV–vis	Ultraviolet–visible
XRPD	X-ray powder diffraction

Acknowledgements

I would like to thank Prof. Krishna Kumar Damodaran for giving me the opportunity to conduct this research. I truly appreciate his constant help and encouragement which has been enriching my professional and personal experience. My sincere thanks goes to all the present and past members of our group, and all the researchers working in Raunvísindastofnun Háskólans for their support, especially Daníel Arnar Tómasson (for Icelandic translation), Kristinn Ragnar Óskarsson (for helping in CD), Sreejith Sudhakaran Jayabhavan, and Dr. Subham Saha who helped me immensely in every aspect. I am grateful to Dr. Sigríður Jónsdóttir for helping with NMR and mass spectroscopy, Prof. Snorri Th. Sigurdsson for his valuable suggestions, Svana Hafdís Stefánsdóttir, Sverrir Guðmundsson and Óskar Rudolf Kettler for helping with chemicals and laboratory equipment. I would also like to thank all the academic and technical staff from other institutes; Sigurður Sveinn Jónsson from ISOR (for powder X-ray), Birgir Jóhannesson from Nýsköpunarmiðstöð Íslands (SEM), Iwona T. Myszor and Prof. Gudmundur H. Gudmundsson (Life and environmental sciences, Læknagarður, University of Iceland) for the research collaboration. I would also like to thank the University of Iceland Doctoral Grant and University of Iceland Teaching Assistantship Grant for funding. I thank COST action CM1402 for funding STSM and Erasmus+ for exchange study.

I take this opportunity to thank my doctoral committee members Prof. Ingvar Helgi Árnason and Prof. Már Másson to scrutiny my work and provide their valuable feedback during my study. I also thank my distinguished opponents Prof. Thorfinnur Gunnlaugsson and Dr. Stefán Jónsson for finding time from their busy schedule and willing to review this dissertation and my work.

This work would not have been possible without the help of our international collaborators, Prof. Jonathan Steed and Dr. Matthew T. Mulvee (Durham University, U.K), Prof. Pall Thordarson, Dr. Adam Martin and Dr. Abbas Darestanifarahani (UNSW, Australia), Prof. António A. Vicente and Dr. Luiz Henrique Fasolin (University of Minho, Portugal), Dr. Marcin Górecki and Prof. Gennaro Pescitelli (University of Pisa, Italy), and Dr. Ragnar Björnsson (MPI CEC, Germany), I am grateful to all of them for the fruitful collaboration.

1 Introduction

Self-assembly is the process by which individual components are spontaneously organized into well-ordered hierarchical network by some specific, local interactions. Nature has been successful in self-assembling small subunits into complex biomolecules such as proteins, enzymes, nucleic acids etc.[1] Chemists are striving to mimic nature's principles to construct complex molecular architecture[2-5] by self-assembling small molecules. The idea of 'supramolecular chemistry'[6-8] empower us to assemble individual molecules via coordination bond or non-bonding interactions to form a three-dimensional superstructure.[9-10] Macroscopic properties of a material arise from the supramolecular aggregation, hence complex architectures and functionality can be accomplished from comparatively simple and small molecular building blocks. Organic linkers aggregated by metal ion coordination[11] is a prevalent example of assembling building block via coordination. The energy of the coordination bonds typically range between 15-50 kcal/mol, which is lower than usual covalent bonds (60-120 kcal/mol) but higher than other non-bonding interactions (0.5-20 kcal/mol).[12] The metal ions are Lewis acidic in nature and bind readily with suitable Lewis basic sites present in the organic ligands. These hybrid metal-organic materials (MOMs) possess well-ordered three-dimensional architecture and are used in gas adsorption, storage, sensing, separation, and catalysis.[13-15] In contrast, non-covalent interactions are weaker interactions but the impact of these interactions on molecular assembly as well as their material properties is promising. For example, the self-assembly of small organic molecules via non-bonding interactions lead to an unique class of soft materials, known as low molecular weight gels (LMWGs).[16-17] LMWGs are formed by self-assembly of gelator molecules via various non-bonding interaction (H-bonding, π—π interaction, van der Waals interaction, halogen bonding), resulting in immobilization of solvent molecules.[17-19] During the last decade, there is an upsurge interest in LMWGs due to their potential application in dynamic gels, cell culture, drug delivery, and media of crystal growth.[20-22] Usually gels are formed by a single gelator, however, recently supramolecular gels based on multi-component gels have drawn considerable attraction because of the tunability of gel state properties.[23-26] This doctoral dissertation will illustrate the use of various interactions (metal coordination and non-bonding) in constructing supramolecular architectures from simple organic molecules to functional smart materials by probing the key interactions responsible for the formation of the self-assembled network.

1.1 Assembling multi-functional ligands by metal coordination

Metal-organic materials (MOMs) are hybrid inorganic-organic compounds consisting of metal ions or clusters connected via organic linkers.[27-28] The metal center is usually transition metal ions or inorganic clusters, also known as the secondary building units (SBUs)[29] and a ligand with two or more binding sites (*Scheme 1.1*). The extended structure of MOMs is constructed by stitching the SBUs and organic linkers via coordination bonds.[30] MOMs can be discrete complexes or polymers growing infinitely in one, two or three dimensions, which include coordination polymers, porous materials and metal-organic frameworks (MOFs). MOMs often display unique property such as diverse structure, large pore size, high surface area, and selective gas adsorption affinity and specific catalytic property.[31-32] The framework constructed by metal-ligand coordination depends on the geometry of the metal nodes and structure of the complementary organic linkers.[33-35] Ligands with highly directional binding properties and rigid architectures are chosen as linkers. Linkers with pyridyl or carboxylic acid groups are commonly used due to the capability of forming stable coordination bonds with most of the metal ions.

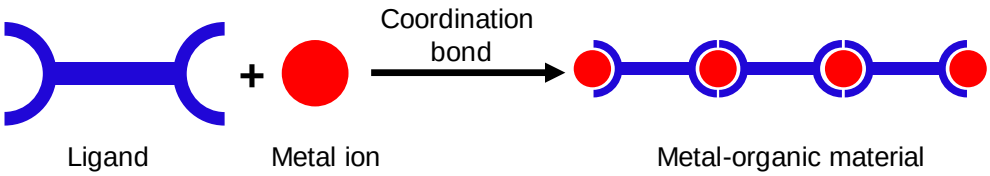

Scheme 1.1 Formation of MOMs.

The research on functional metal-organic materials (MOMs) has received enormous attention in last two decades. The crystalline nature, microporous structure and tunable properties make these materials highly attractive in inorganic and materials chemistry. Furthermore, the potential application in gas storage, separation, sensing, purification, catalysis and drug delivery is the reason why the study is increasing in both industry and academia.[11, 31-32, 36-41]

1.1.1 Advantage of MOMs

Inorganic porous solids such as zeolites or silicates have been extensively used as functional porous materials, but the diversity of zeolites is rather restricted due to the

exclusive use of tetrahedral building units like SiO_4 or AlO_4.[42] In contrast, MOMs have emerged as superior class of porous materials since the 'secondary building unit' (SBU), as well as the length, shape and functionality of the organic linker can be freely varied.[11, 43-45] This enables to construct MOMs with different pore sizes and functionalization of the organic part. The existence of free coordinating site at metal node or SBU plays crucial role in determining properties of MOMs, such as interaction with guest molecules and catalysis.[46-48] Catalytic MOMs can be obtained by incorporating catalytically active metal centers or ligands in the framework. However, the catalytically active sites are not retained due to the limitations in the synthetic procedures of MOFs, which requires high temperature and pressure and the MOFs prepared at room temperature lack a systematic synthetic approach. Efforts have been made to incorporate catalytic moiety (organic or inorganic) after building the MOF skeleton via post-synthetic modification but the catalytic properties may be reduced due to blockage and diffusion rate. Thus, it will be interesting and challenging to develop a systematic approach to retain these catalytically active metal centers in the resulting MOMs. An elegant approach is to assemble metal centers with multi-functional organic ligands, which are linkers with predetermined functional groups such as catalytically active metalloligands or organic groups to form catalytically active MOMs.[40, 49-51] The multi-functional organic ligands can be classified into two categories (*Scheme 1.2*): (a) ligands with two different binding sites and (b) ligands with a binding site and a hydrogen bonding unit. The reaction of metal centers with ligands with two different binding sites will result in the formation of metalloligands (MLs).[52]

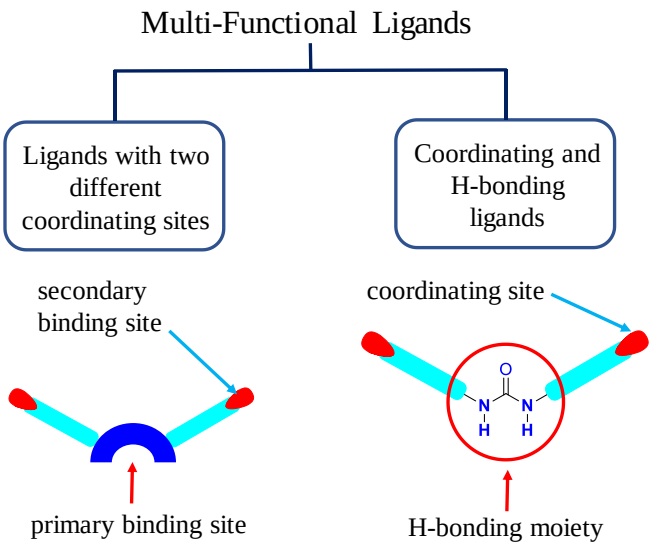

Scheme 1.2 Design of multi-functional ligands.

1.1.2 Category 1: multi-functional ligands based on metalloligands (MLs)

Metalloligands are hybrid inorganic-organic complexes having at least two or more free coordinating sites,[45, 53] making them unique building blocks for the construction of a designed architecture. These compounds offer several advantages: (i) highly ordered architectures with high density of single catalytic sites, (ii) induce structural rigidity resulting in stable frameworks, (iii) tunable topology and surface functionality by changing the nature of metal ions and organic linkers, and (iv) assembly of catalytically active homogeneous metal complexes into heterogeneous networks.[30] The ligands used in MLs are multi-functional organic ligands,[45, 54-57] which ideally contain two types of coordinating sites, primary and secondary. The primary group of a multi-functional ligand bind with the first metal ion to form MLs whereas the secondary binding site remains free. In contrast, simple coordination complexes are made of a metal ion surrounded by simple ligands that lack a secondary binding group. The metalloligands interact or coordinate with a second metal ion through the secondary binding site or another metalloligand containing complementary appended functional groups. Thus, MLs serve as unique building blocks for the construction of a designed architecture (*Scheme 1.3*), offering better control in geometry and enhanced structural rigidity.

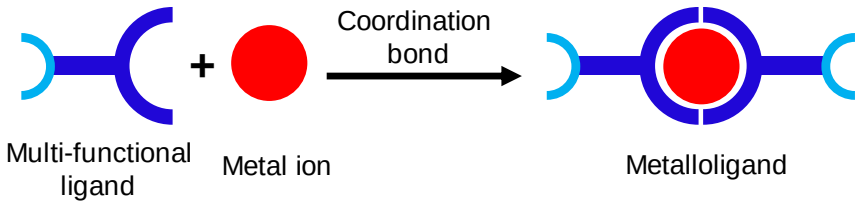

Scheme 1.3 Synthesis of metalloligand.

The propagation of metalloligands depend upon the number of binding sites, symmetry and the nature of second ion or complementary functional linker.[58-61] The tentative coordination modes of MLs are shown in *Scheme 1.2*. The *Scheme 1.4a* represents different MLs based on number of appended groups and symmetry. *Scheme 1.4b* shows the coordination behavior of a planar C_3 symmetric metalloligand with a secondary metal ion. The metalloligand is likely to offer three secondary binding sites and the geometrical orientation will lead to coordinate to three secondary metal ions. As a result, a two-dimensional (2D) layer or sheet network is likely to generate via coordinate bonds between the ML and second metal ion.

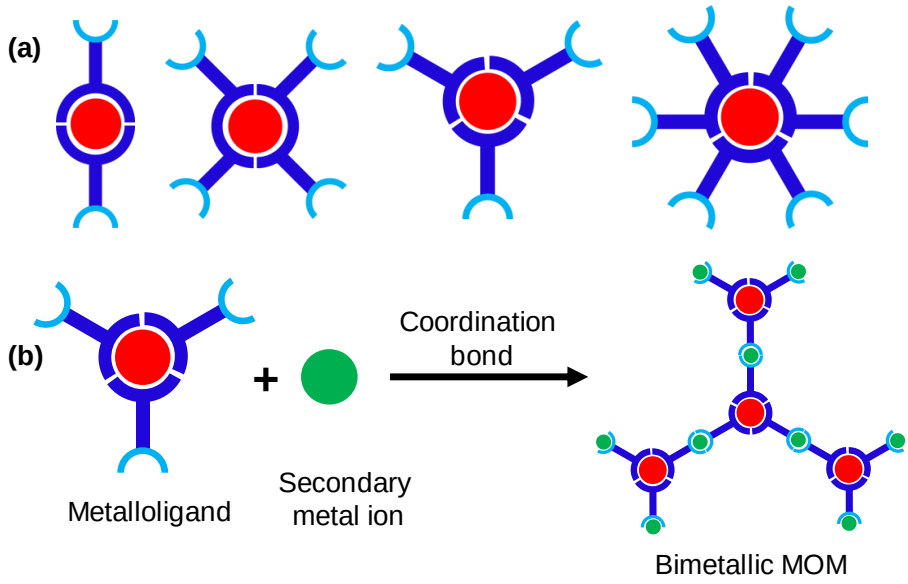

Scheme 1.4 (a) Metalloligands with assorted appended groups and (b) its propagation.

There are several multi-functional organic ligands that have been used as MLs,[45, 54-57] which ideally contain two types of coordinating sites, primary and secondary (*Scheme 1.5*, the blue color indicates primary functional group and red color indicates secondary functional group).

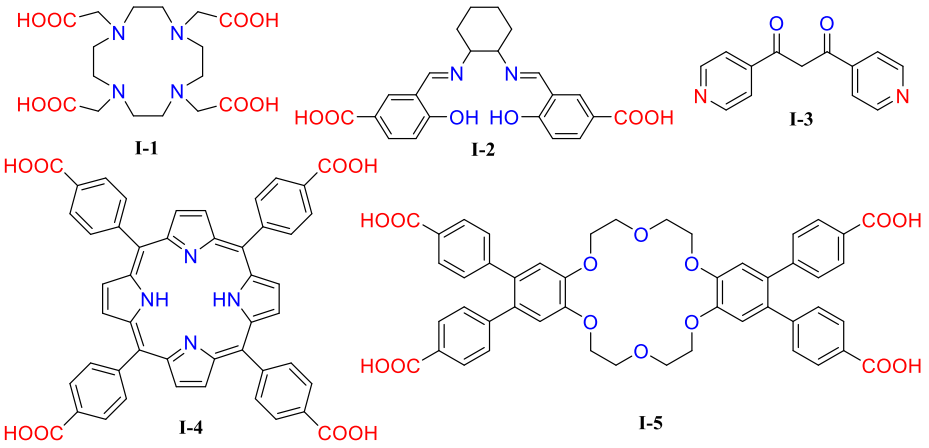

Scheme 1.5 Various multi-functional ligands used as a linker.[30]

Among the numerous multi-functional ligands reported so far, salen, porphyrin, cyclam, crown ether and cryptand-based ligands are most common and widely used due to the structural rigidity, tunable backbone, highly directional binding and ability to form stable complexes and coordination polymer.[62] The linking of multi-functional ligands with metal ions will lead to multi-functional MOMs, which often display diverse properties that are not achieved in MOMs with simple linkers. The nomenclature and the classification of metalloligands depends on the primary functional group. The pivotal structure and utilization of the MLs also depend on the primary group. For example, acetylacetonate and *β*-diketonate MLs are commonly used to construct mixed-metal coordination polymers. Burrows and coworkers used a series of dipyridyl *β*-diketonate complexes as versatile polydentate MLs for the synthesis of MOFs and hydrogen-bonded networks.[63-65] The acetylacetone and β-diketone (ligand **I-3**) moieties are easily deprotonated to form stable anions due to delocalized electron clouds, which forms stable metal complex with large number of *d*-block and *f*-block elements. Introducing appended pyridyl groups in the backbone makes the complexes efficient MLs, which coordinate with a second metal ion to form various coordination polymer or MOFs.[63] The study also reveals the importance of the choice of primary metal ions in resulting complexes. The use of highly reactive metal

ions like copper(II) and zinc(II) leads to polymeric structures, where the *β*-diketone moieties are coordinated in equatorial positions and two pyridyl groups occupy the axial position. The high affinity of these metal ions towards pyridyl groups prevents the formation of discrete MLs. While using iron(III) ion with three molecules of the ligand **I-3**, a metalloligand obtained was further coordinated to silver(I) ion to form MOMs was achieved (*Figure 1.1a*). The metalloligand with *f*-block elements were self-assembled into 3D network via hydrogen bonding (*Figure 1.1b*).

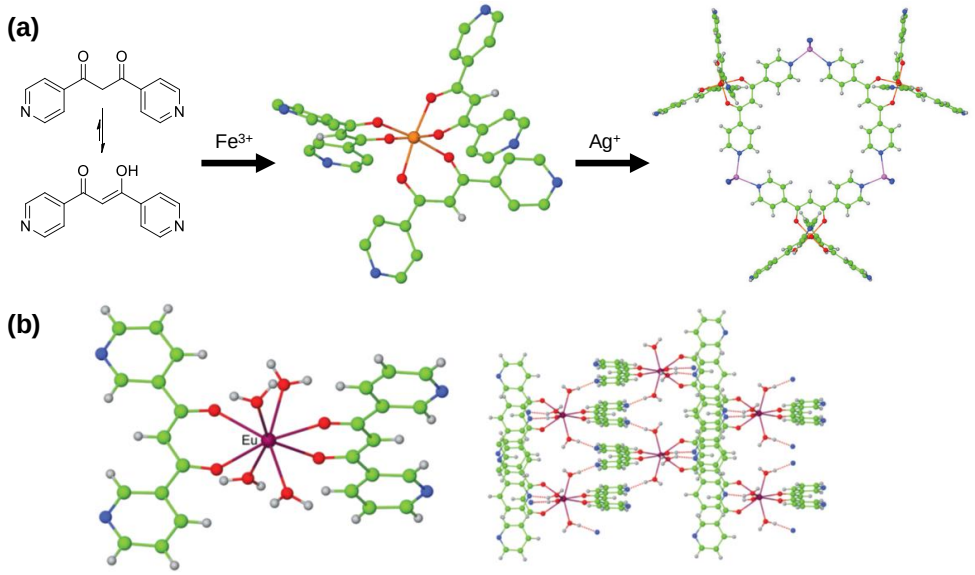

Figure 1.1 (a) Synthesis of metalloligands and MOMs from dipyridyl β-diketonate ligand and (b) hydrogen-bonded aggregated network of the Eu metalloligand.[63]

Metal-salen complexes are one of the most widely recognized metalloligands with numerous applications in coordination chemistry.[66-67] Salen (*N*,*N*'-bis(salicylidene)ethylene-diamine dianion) is a Schiff-base ligand derived from salicylaldehyde and 1,2-diamine moieties. There are several advantages of this ligand including ease of synthesis, rigid structure, opportunity to modify the functionality in backbone and formation of highly stable metal complexes. The substituents in the salen backbone can affect the property of the ligand, and also its metal complexes. A coordinating group can be introduced to the backbone to construct salen based metalloligands[68] (*Scheme 1.6*).

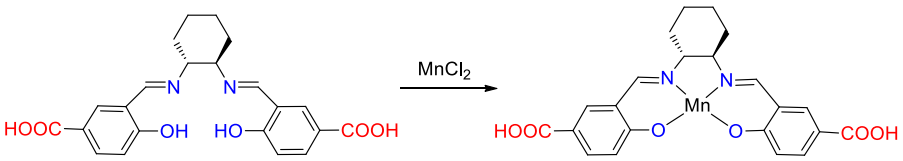

Scheme 1.6 Synthesis of Mn-salen metalloligand.[68]

Cao *et al* reported a pyridyl-functionalized nickel(II) salen metalloligand, where one of the two appended pyridyl moiety was coordinated to the metal center to form one-dimensional (1D) homochiral nickel coordination polymer.[69] The nickel(II) center was chelated to the salen unit in the equatorial position, and possessed one vacant axial position (*Figure 1.2*). The MOM displayed comparable catalytic activity to the homogeneous counterpart in the oxidation of styrene to styrene oxide.

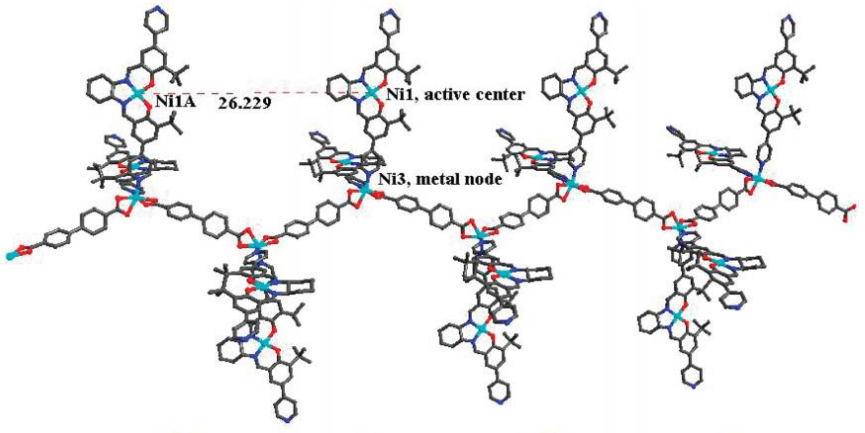

Figure 1.2 Synthesis of MOM based on Ni-salen metalloligand, reported by Cao et al.[69]

Metalloporphyrins are another important class of metalloligands.[70-72] Porphyrins are well known organic chromophores that absorb visible light and extensively used as chemical sensors. Porphyrins possess a rigid planner structure with well-defined pores, yet easily modifiable periphery to append a variety of auxiliary moieties. The metal ion is coordinated at the center of the porphyrin ring, along with the customized functionality at the backbone provide diverse opportunity to construct novel networks and porous materials. Choe and coworkers synthesized a MOF (PPF-1) by combining $Zn(COO)_4$ paddle-wheel unit and zinc(II) porphyrin metalloligand with four appended carboxylate groups (*Figure 1.3*).[73] The central metal ion zinc(II) was replaced by cobalt(II) to obtain PPF-1Co. The porous architecture of PPF-1 is evident from its large surface area and high H_2 uptake value.

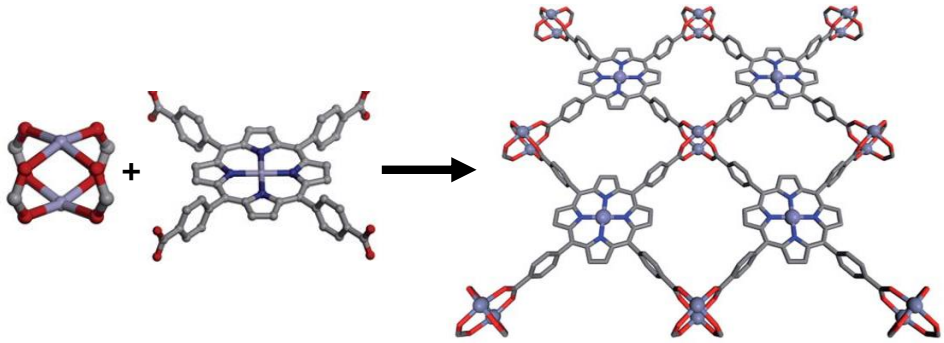

Figure 1.3 Synthesis of MOF combining paddlewheel and porphyrin metalloligand units, reported by Choe et al.[73]

Constructing functional MOMs using the metalloligand approach offers several advantages over the conventional method of mixing the ligand and metal. The main advantage is that the metalloligand approach offers precise control over the placement of auxiliary functional group in a framework.[60] A predesigned network can be constructed by appropriate combination of metalloligand and second metal ions (*Scheme 1.4b*). The metalloligands tend to generate more rigid and highly ordered architectures compared to a traditional organic scaffold.[74] Secondly, the pore sizes and pore environments can be easily tuned by modifying the metal ion or counter anion of the auxiliary functional group. The methodology allows us to place two different metals in close proximity, constructing such heterometallic networks is challenging in the conventional route. Hence, the metalloligand approach is very appealing for synthesizing multifunctional materials with diverse chemical functionality.

1.1.3 Category 2: multi-functional ligands based on hydrogen bonding moieties

An alternate way to construct multi-functional ligands is to incorporate a hydrogen bonding motif along with a coordinating site. Here the coordinating site fabricates the network by binding with a metal ion, where the hydrogen-bonding moiety is placed in well-arranged location in the framework. The coordinating site can be a carboxylic acid or pyridyl group, which is an excellent choice in constructing MOMs. The hydrogen bonding moiety is typically urea, amide or amine, which can interact with specific guest molecules (*Scheme 1.7*).[75-78]

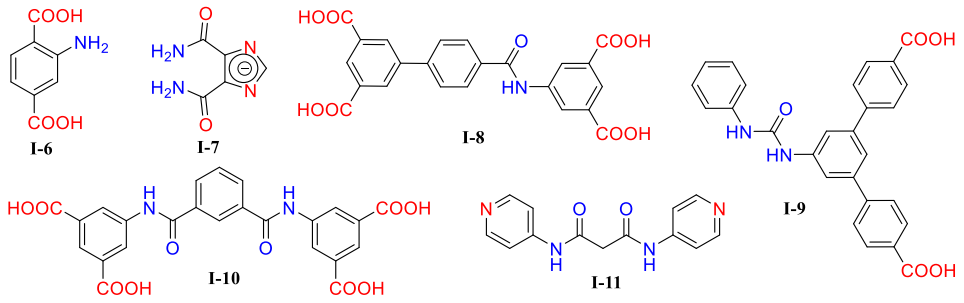

Scheme 1.7 Examples of hydrogen-bonding multi-functional ligands as MOM linker.

Scheme 1.7 shows some of the reported hydrogen-bonding multi-functional ligands that are used as linkers.[79-82] Introducing hydrogen bonding moiety in a simple carboxylate linker often results in 'smart materials' based on MOMs. Also, the well-arranged hydrogen bonding moieties display 'host-guest interactions', resulting enhanced activity of the MOM. For example, Zhang *et al* replaced the simple carboxylate inker H_4TPTC ([1,1':4',1''-terphenyl]-3,3'',5,5''-tetracarboxylic acid) of NOTT-101 with an amide-based linker **I-8** in modified MOF NJU-Bai45 (*Figure 1.4*).[83] The modified MOF NJU-Bai45 displayed sharp enhancement in volumetric and gravimetric methane storage working capacity presumably due to the cooperative efforts of balanced pore volume and material density.

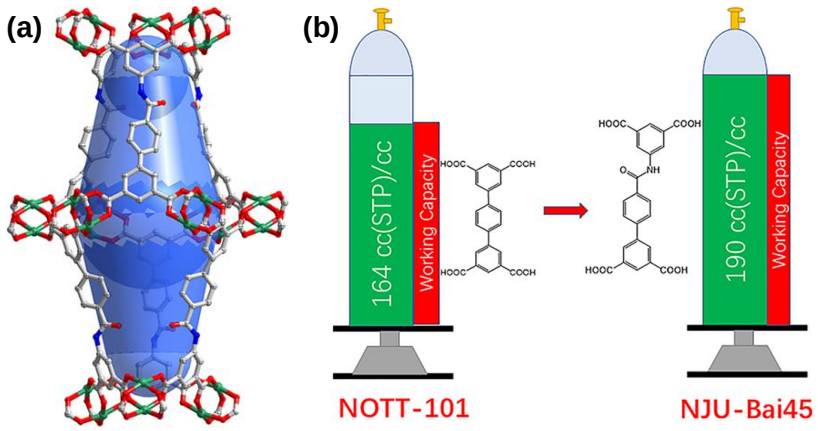

Figure 1.4 (a) Crystal structure of NJU-Bai45 showing Shuttle-shaped cage and (b) schematic representation of ligand functionalization leading to enhanced methane storage working capacity, reported by Zhang and coworkers.[83]

Urea group is known for its two-point hydrogen bond-donating ability. Zhu *et al.* incorporated a urea moiety in a dicarboxylate linker **I-9**, and synthesized a 2D MOF by reacting the ligand with copper(II) ion.[84] The N—H group in the linker interacts with substrates with hydrogen-bond acceptor groups, resulting in activation of the functional group. Thus, the MOF served as a hydrogen-bond donor catalyst and demonstrated excellent activity in cyanosilylation, Henry reaction and methanolysis of epoxides (*Figure 1.5*).

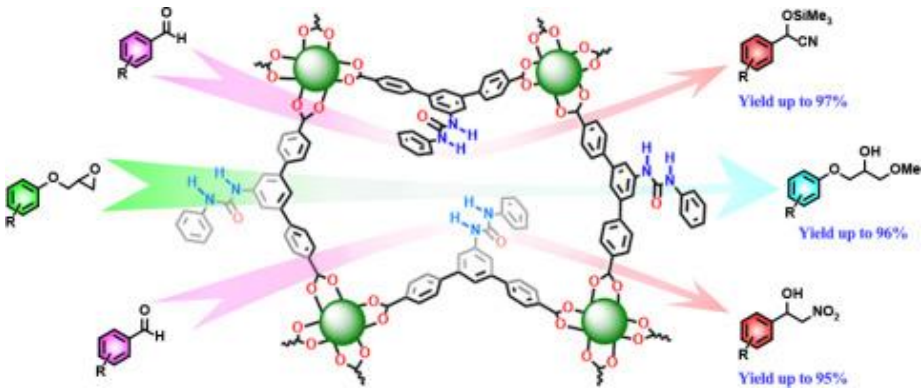

Figure 1.5 Multi-functional heterogeneous catalyst by urea containing MOF reported by Zhu et al.[84]

1.1.4 Synthesis of MOMs

Metal-organic materials (MOMs) are coordination polymers or metal-organic frameworks, which are hybrid solid constructed from inorganic metal nodes and organic bridging ligands propagating infinitely in one, two or three dimensions.[27, 85-87] The chemistry of MOMs has developed rapidly in last two decades due to unique properties and wide range of potential applications including gas storage,[88-90] separation,[91] sensing,[92-93] lithium/sodium ion rechargeable batteries,[94] catalysis [51, 95-98] etc. In this work, we will limit our focus on using MOMs as heterogeneous catalysts. The possibility of incorporating functional groups into MOMs makes them ideal candidates for heterogeneous catalysis. The rigid structure, uniform micropores and well-arranged active sites in MOMs can result in size- and shape-selective catalysis.

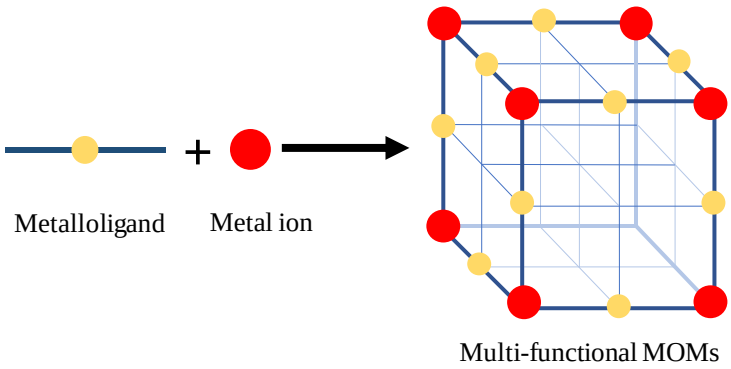

Scheme 1.8 Synthesis of functional metal-organic materials.

The concept of utilizing metalloligand approach to synthesize MOMs is well established.[45, 54-57] On treating the metalloligands having a specific geometry and binding site with the appropriate metal ion will result in multi-functional MOMs with well-arranged auxiliary functional groups (*Scheme 1.8*). The metalloligand having a preinstalled catalytically active site results in incorporating catalytic sites into the framework. For example, chiral ruthenium(II) salen complexes were known to be proficient homogeneous catalyst in asymmetric cyclopropanation reaction. Lin and coworkers modified the salen ligand to introduce two carboxylate moieties in the backbone, and reacted with zinc(II) nitrate to synthesize chiral MOFs CMOF1 and CMOF2.[99] The MOFs (CMOF1 and CMOF2) possessed ruthenium(III) center, which was subsequently reduced to ruthenium(II) to obtain CMOF1R and CMOF2R. Thus, the catalytically inactive MOFs CMOF1 and CMOF2 were converted to catalytically active CMOF1R and CMOF2R, showing high activity in asymmetric cyclopropanation of alkenes with high diastereo- and enantioselectivity (*Figure 1.6*). This clearly shows that the homogeneous catalytic site was incorporated in the heterogeneous analogue and the site retained its catalytic activity.

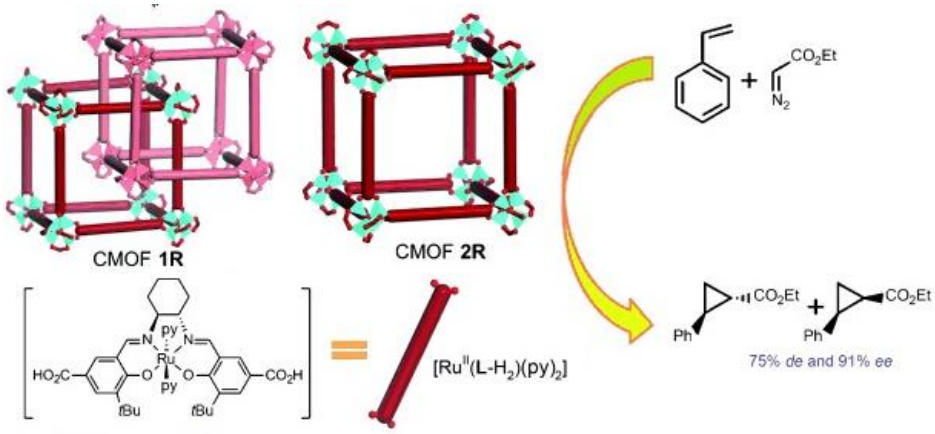

Figure 1.6 Structure and catalytic activity of CMOF1R and CMOF2R reported by Lin et al.[99]

The same group incorporated a cobalt(III)-porphyrin complex in a bimetallic indium-cobalt MOF (In-Co[TBP]-MOF) where cobalt(III) is the active catalytic center in hydration reaction of alkynes to form carbonyl derivatives.[100] The MOF possessed a two-fold interpenetrated structure and as a result, the catalytically active metalloporphyrin centers were placed adjacent to each other. This allowed cooperative activation of the catalytic centers, and the MOF turned out to be more efficient catalyst compared to its homogeneous analogues (*Figure 1.7*).

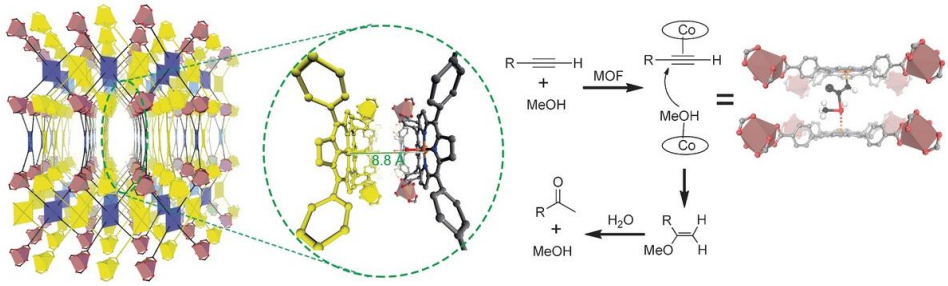

Figure 1.7 Structure and cooperative catalysis in In-Co(TBP)-MOF reported by Lin et al.[100]

One of the main challenges to incorporate catalytic centers into MOFs is the typical high temperature, high pressure synthetic procedure which results in decomposition of the active center. A good strategy is to employ soft-synthetic techniques such as layering, vapor phase diffusion etc. in the synthesis process rather than the conventional solvothermal method to ensure the retention of the active sites in MOMs. Terfort *et al*

demonstrated a rapid room temperature synthesis to grow well-ordered HKUST-1 crystallite.[101] Similarly, room temperature synthesis of Fe–BTC (BTC = 1,3,5-benzenetricarboxylate) was reported by Pérez-Ramírez.[102] Such soft-synthetic preparation of the MOMs further extends the applicability of the materials. The stable rigid architectures with highly ordered catalytic sites will make the MOMs ideal candidate for heterogeneous catalysis.

1.2 Assembling multi-functional ligands by non-bonding interaction

Molecular self-assembly through non-bonding interaction was one of the most exciting concepts that arrived with the development of supramolecular chemistry in the first half of the twentieth century. These interactions are hydrogen bonding (4-60 kJ/mol), dipole-dipole forces (5-50 kJ/mol), π-π interactions (5-20 kJ/mol), van der Waals forces (<5 kJ/mol) and various solvophilic and solvophobic effects.[103] Self-assembly occurs when molecules spontaneously sort in a specific order to form complex architecture stabilized by non-covalent forces. The supramolecular architecture is formed by weak intermolecular forces, which makes the self-assembly process often reversible and the process can be triggered by "switching on/off" external stimuli (*Scheme 1.9*). Supramolecular low molecular weight gelators (LMWGs)[20, 104-111] offers better control of the self-assembly/reassembly process, which can be either switched on/off by an external stimulus such as anion, heat, light, sound etc., which will enable us to study the self-assembly process of the molecules from nano-scale to mesoscopic scale.

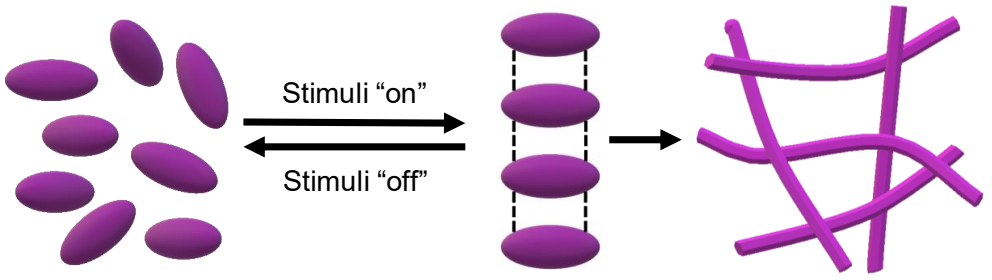

Scheme 1.9 Self-assembly based on non-bonding interaction triggered by external stimuli.

1.2.1 Supramolecular gel

Gels are usually recognized by their jelly-like appearance– a soft semi-solid material that exhibits no macroscopic flow. These materials are colloidal dispersion in which a gelator is dispersed (the solid, continuous phase) within a solvent (the liquid, dispersed phase), and are found in everyday applications such as cosmetics, medicine and food industries. Gels are liquid at high temperature and solidifies upon cooling. Gelation is often recognized by simple 'inversion test' – i.e., the material doesn't flow when turned upside down (*Scheme 1.10*). Commonly gels are consisted of 1.0–2.0 wt% of gelator and 98.0–99.0 wt% of solvent, where the fluid component that is immobilized in a 3D network. Gels typically displays fibrous network that spans the entire sample in 3D cross-linked network stopping the free flow of the liquid.

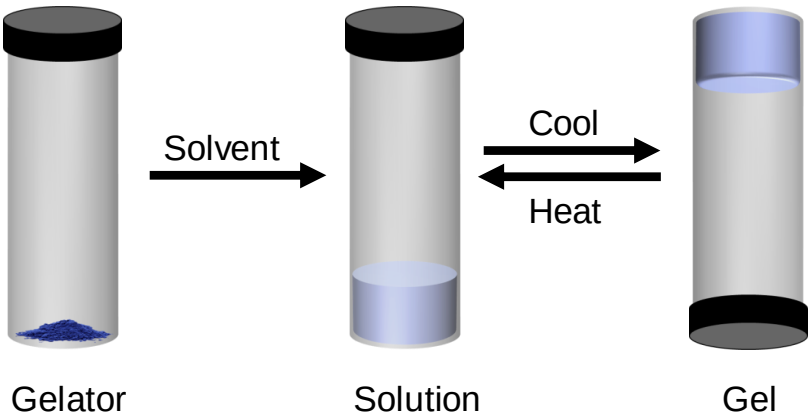

Scheme 1.10 Formation of supramolecular gel.

1.2.2 Classification of supramolecular gels

Supramolecular gels are classified in many different categories depending on the structure of the gelator, the types of cross-linking that creates the 3D networks and the medium where the gelator is surrounded.[111] Based on the molecular weight of the gelator, gels are usually classified into two categories, polymeric gels and low molecular weight gelators (LMWGs). Traditionally, supramolecular gels were synthesized from polymeric gels. Polymer gels consist of three-dimensional (3D) polymeric networks cross-linked via covalent bonds that can immobilize solvent molecules. In contrast, LMWGs are small

organic molecules that are aggregated via non-covalent interactions to form fibers and the individual fibrils further entangle, cross-link to form 3D networks. For example, agarose, gelatin etc. are the example of common polymeric hydrogel. Polymer gels are one of the most attractive soft materials found in our daily lives such as cosmetics, health care, food, textile and oil industries.[112-113] The disadvantage of conventional polymer gels is that the networks are interconnected by covalent bonds resulting limited application as a chemical or thermal 'switch' (*Scheme 1.11*).[114] Depending upon the type of aggregation, gels are classified as cross-linked polymeric gels (PGs)[115] and stimuli-responsive supramolecular gels (*Scheme 1.11*). Polymer gelators make supramolecular gels through physical cross-linking,[115] among them cross-linked hydrogels are most important because of their inherent property of biocompatibility. Back in 1960, Wichterle and Lim developed cross-linked poly(hydroxyethyl methacrylate) (pHEMA), first synthetic hydrogels of hydroxyethyl methacrylate (HEMA) using ethylene glycol dimethyl acrylate (EGDMA) as cross-linker.[116] Cross-linking between polymer chains results in significant change in physical properties such as elasticity, viscosity, solubility, sol-gel transition temperature, melting pint etc. Because of the versatile and unique properties, cross-linked PGs have vast potential applications including in farming and civil engineering,[117] cosmetics,[118] healthcare, fiber cable and drug delivery. The main drawback of cross-linked PGs is the formation of covalent bonds resulting in formation of irreversible systems. On the other hand, stimuli-responsive supramolecular gels are formed by weak non-covalent interaction and offers flexibility and tunable gel state properties. [119-122] Most of the stimuli-responsive gels are based on LMWGs.

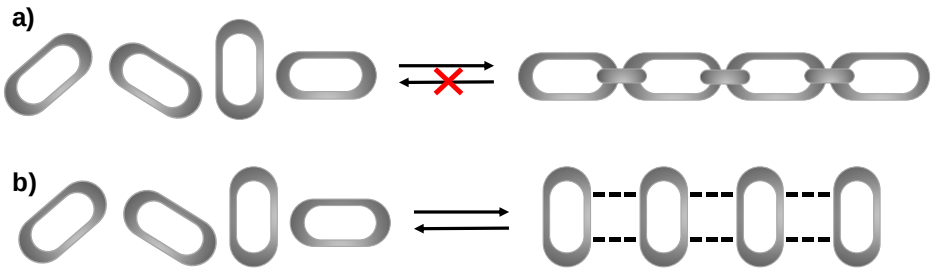

Scheme 1.11 Type of supramolecular gelators based on aggregation: a) cross-linked polymer, b) stimuli-responsive gelator.

Supramolecular gels are formed by self-assembly via weak non-covalent interactions,[123] and the individual molecules of supramolecular gelators aggregate by non-bonding interactions such as hydrogen bonding, π–π stacking, van der Waals force, solvophilic and solvophobic interactions etc. The initial self-assembly most commonly lead to 1D fibers, which further entangle or cross-link to 3D network that immobilizes the solvent system through surface tension and capillary forces. Since the gels do not possess permanent covalent cross-linking, supramolecular gelation can be reversed by various external stimuli, for example heat, light, sound, anion or metal salts and termed as 'stimuli-responsive gel'.

Supramolecular gels obtained from small organic molecules, typically having molecular weight less than 3000 amu/molecule is classified as low molecular weight gelators (LMWGs).[16] Back in 1974 Flory distinguished gels in four main categories[124] - a) highly ordered lamellar structures, b) disordered polymeric networks formed by covalent bond, c) polymer networks formed by physical aggregation or cross-link and d) microscopic particles of solid suspended in liquid to form disordered structures. The fourth category includes the gel formed by self-assembly of low molecular weight gelators, and since then the focus on such systems was grown among supramolecular chemists.[17] In 1997, Terech and Weiss reviewed organogels based on LMWGs, where organic liquids are essentially used as solvent component.[125] Later in 2004, Hamilton and Estroff described the field of LMWGs in water or mixed aqueous solvent systems, namely hydrogels.[107] During last two decades, supramolecular gels based on LMWGs (*Scheme 1.12b*) became an emerging class of soft materials due to the tunable gel state properties and wide range of applications in dynamic gels, cell culture, drug delivery and media to control crystal growth.[20, 22, 125-130] Unlike the covalent network in polymeric gels, LMWGs are self-assembled via weak non-covalent interactions such as hydrogen bonding, π–π stacking, van der Waals interactions etc., thus respond to external stimuli to switch on/off gelation.

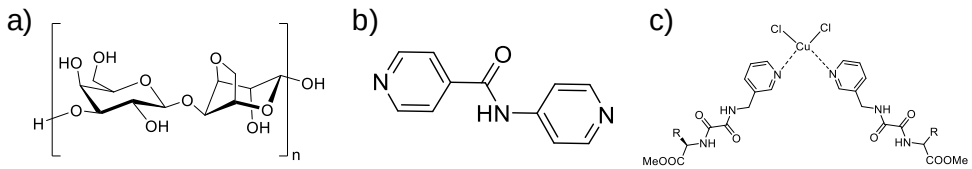

Scheme 1.12 Type of supramolecular gelators based on structure: a) polymeric gelator, b) low-molecular weight gelator, c) metallogelator.

Supramolecular gels are classified into hydrogel and organogels depending upon the nature of solvents. In hydrogel, water is used as solvent whereas organogels are composed of organic solvents.[131] Removal of solvents is often necessary to analyze the gel network by scanning electron microscopy (SEM), atomic force microscopy (AFM), powder X-ray diffraction (XRPD) etc. When the solvent is removed by filtration or dried by slow evaporation at room temperature, the resulting dried gel is called xerogel. Drying gel at supercritical condition leads to highly porous solid material, known as aerogel (*Scheme 1.13*).

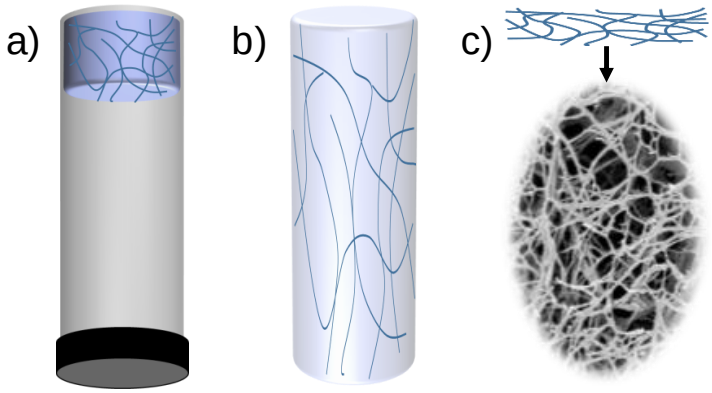

Scheme 1.13 Type of supramolecular gelators based on gelling medium: a) organogel/ hydrogel, b) aerogel, c) xerogel showing fibrous network.

Recently, metal-based gelators or metallogelators[132-133] also drawn significant interest in supramolecular gels. Metallogel is formed by coordination interaction between an organic moiety and a metal center, which is a weaker interaction compared to covalent bonds but stronger than other non-bonding interactions observed in LMWGs. The gel fibers of metallogels can be formed by the self-assembly of discrete complexes via non-bonding interactions,[134-136] coordination polymers,[137-139] or cross-linked coordination polymers.[140] The presence of metal ions in gel fiber offers a variety of applications in catalysis, sensing, optics and magnetic materials.[133]

1.2.3 Low molecular weight gelators (LMWGs)

The LMWGs are usually associated to form a fiber level assembly, which further entangles or cross-link to form three-dimensional networks. The process of forming hierarchical aggregation should be divided across all length scales to correlate the molecular structure and gel network.[107] The molecular level aggregation starts with various non-covalent interactions between the gelator molecules such as hydrogen bonding, π—π interaction, van der Waals interaction, halogen bonding, etc. The molecular interactions control the nanostructure and it observed that most of the time the molecular aggregation leads to one-dimensional chain. The 1D chains further interact with each other and generate fibrils. The generation of 1D chain in bis(urea) systems is shown in *Scheme 1.14*. The individual molecules are assembled into 1D chain to form the primary α-tape structure, which further entangles and cross link to form the secondary and tertiary structures.

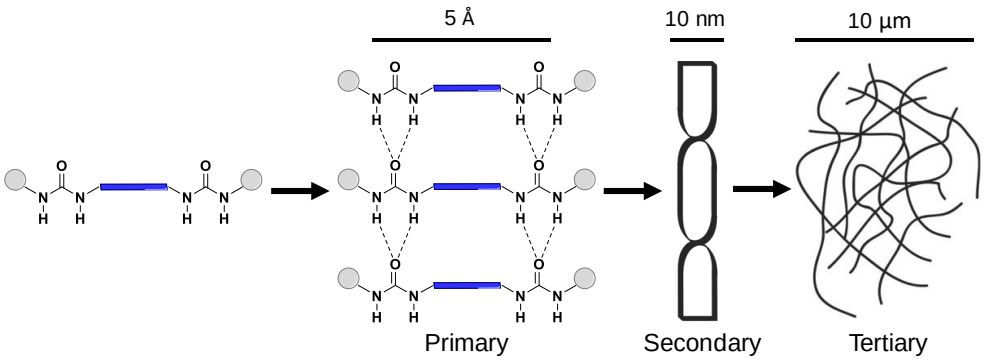

Scheme 1.14 Self-assembly of bis(urea) gelators to form primary, secondary and tertiary structure.[107]

Damodaran *et al* synthesized a series of pyridyl amides and it was found that only N-(4-pyridyl)isonicotinamide (**4PINA**) is able to form hydrogel whereas the other amides did not show any gelation properties.[141] The single crystal structure revealed that **4PINA** displays 1D zig-zag chain structure, which explains the strong gelation ability of the compound (*Scheme 1.15*). This indicates the importance of the relative position of the pyridyl nitrogen in gel formation.

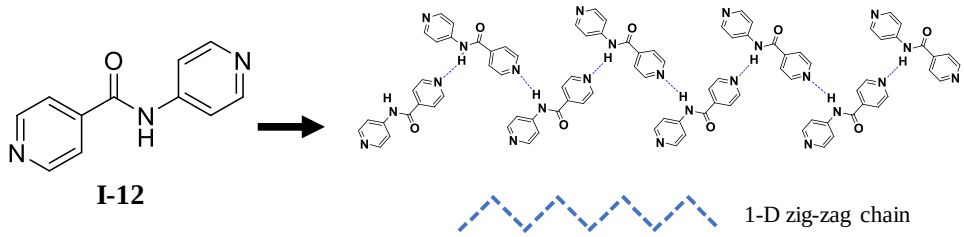

*Scheme 1.15 Self-assembly of the gelator **4PINA (I-12)** to 1D chain.*[141]

The aggregated fibrils from nano- to micrometer scale can be observed by microscopic techniques like scanning electron microscopy (SEM), atomic force microscopy (AFM) etc. Steed and coworkers synthesized a series of LMWGs by combing several chiral functionalities with urea motif.[142] The gelators formed gel in wide range of solvents and displayed different morphologies in SEM (*Figure 1.8*). The gels displayed varied gel strength and rheological characteristics, and various parameters such as chirality, thixotropic nature were correlated to the gel fibers observed in SEM images. Two bis(urea) compounds with two —CH_2 groups and four —CH_2 groups in the linker is shown in *Figure 1.8a* and *Figure 1.8b* respectively. SEM images of the xerogel *1.8a* revealed rod-shaped architecture (bottom) compared to thread-like morphology of *1.8b* xerogel. This indicated that *1.8a* was more crystalline, which was in good agreement with the rheological measurements.

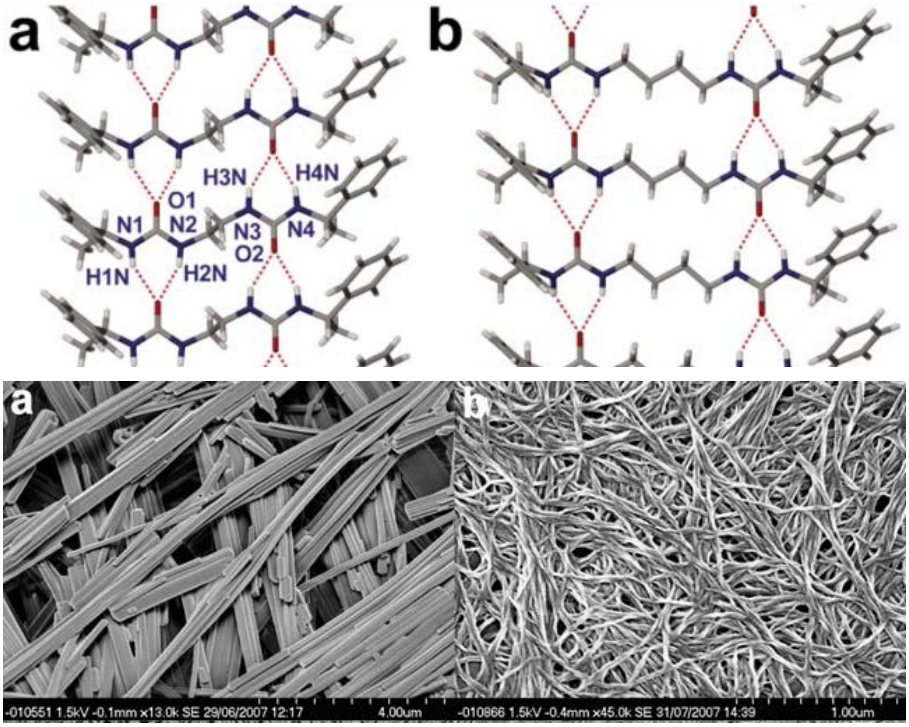

Figure 1.8 Crystal structure and SEM image of the xerogels of bis(urea) compounds.[142]

The choice of solvent is crucial since solvophilic/solvophobic interactions play an important role in gelation. If the solvophilic interaction is too strong, the solid remains in solution and strong solvophobic interaction cause precipitation. Hence the delicate balance between solvophilic and solvophobic interaction allows the formation of gel fibers that is stabilized within the solvent. The solvent molecules are trapped in the 3D fibrous network to form a semi-solid soft material resulting in gel formation. For example, Li and coworkers synthesized a bis(amide) gelator BOXDH-T12 with long alkyl chains at the periphery (*Figure 1.9*).[143] Based on the UV–vis, FTIR, ^{1}H-NMR, fluorescence and TGA analysis, the packing mode of the gelator is portrayed in *Figure 1.9*. In ethanolic medium, hydrogen bonding between the gelator molecules is predominant, thus the 'H-aggregate' is formed. Strong interaction between the gelator molecules indicates high solvophobic interaction between the gelator and ethanol. This results in precipitation of the material and no gel is obtained in ethanol. On the other hand, strong interaction of the gelator with DMSO solvent leads (high solvophilic interaction) to 'slipped aggregation', which also fails to form the gel. But interestingly, in a mixture of DMSO/EtOH, within the range from 50% DMSO to 80% DMSO amount, the solvophilic/solvophobic interaction is balanced and gel is formed.

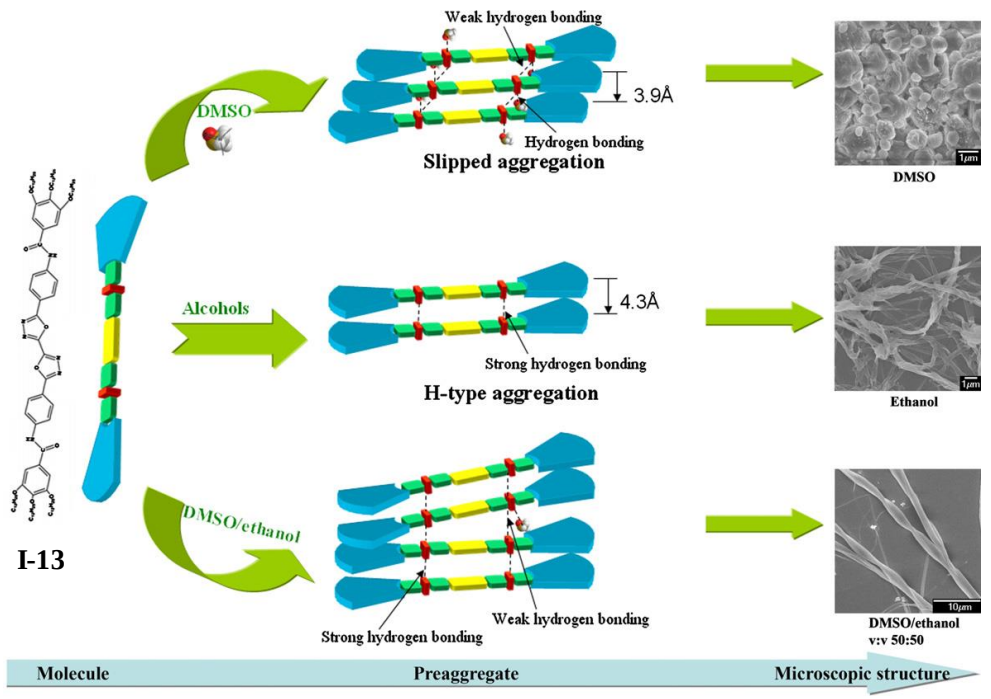

*Figure 1.9 Schematic representation of the aggregated structure of **I-13** (BOXDH-T12) in ethanol, DMSO and DMSO/ethanol as reported by Li and coworkers.*[143]

1.2.4 Characterization of supramolecular gel

Self-assembly of the molecules leading to the formation of 1D chain is considered as the primary structure of supramolecular gel (*Scheme 1.14*). Thus, primary structure of a gel arises from the molecular level assembly of the gelator, with a typical length of a few angstrom. The 1D chains are aggregated in a nanometer scale to generate the secondary microstructure of the gel. Finally, the fibers are further entangled or cross-linked to construct the 3D network or tertiary structure. In order to characterize a gel, it is necessary to identify the key interactions at various length scale. However, characterizing supramolecular gels across different length scale is difficult due to the dynamic nature of noncovalent interactions that assemble the gelator molecules. Numerous techniques are applied to extract the information about self-assembly and the combination of various techniques provide better insight into the self-assembly process.[111] However, each characterization method has its own advantages and disadvantages. A few of the standard characterization methods and their application in investigating self-assembly is discussed here.

Molecular-level assembly arises from intermolecular non-covalent interactions and in general, non-covalent interactions involve exchanges of energy and momentum between the molecules.[111] Thus, spectroscopic techniques are reliable to explore molecular level assembly in supramolecular gelators. Ultraviolet-visible (UV-vis) spectroscopy, infrared (IR) spectroscopy, nuclear magnetic resonance (NMR) spectroscopy, fluorescence spectroscopy, circular dichroism (CD) spectroscopy etc. are used to probe the interactions between the gelator molecules. The difference of intensity or position of the peaks in solution state and gel state or dispersed gel state elucidate the information of molecular self-assembly.

Escuder, Miravet and coworkers studied the structural properties of amino acid derivative hydrogels by spectroscopic techniques.[144] The shifts in IR and ^{1}H-NMR spectra (*Figure 1.10b* and *1.10c*) in solution and gel state revealed that the hydrophobic effect is dominant in the self-assembly process in water. This study shows that although the intermolecular hydrogen bonding is a key force in the aggregation of gelators, other weak non-bonding interactions also play an important role in determining overall gelation properties.

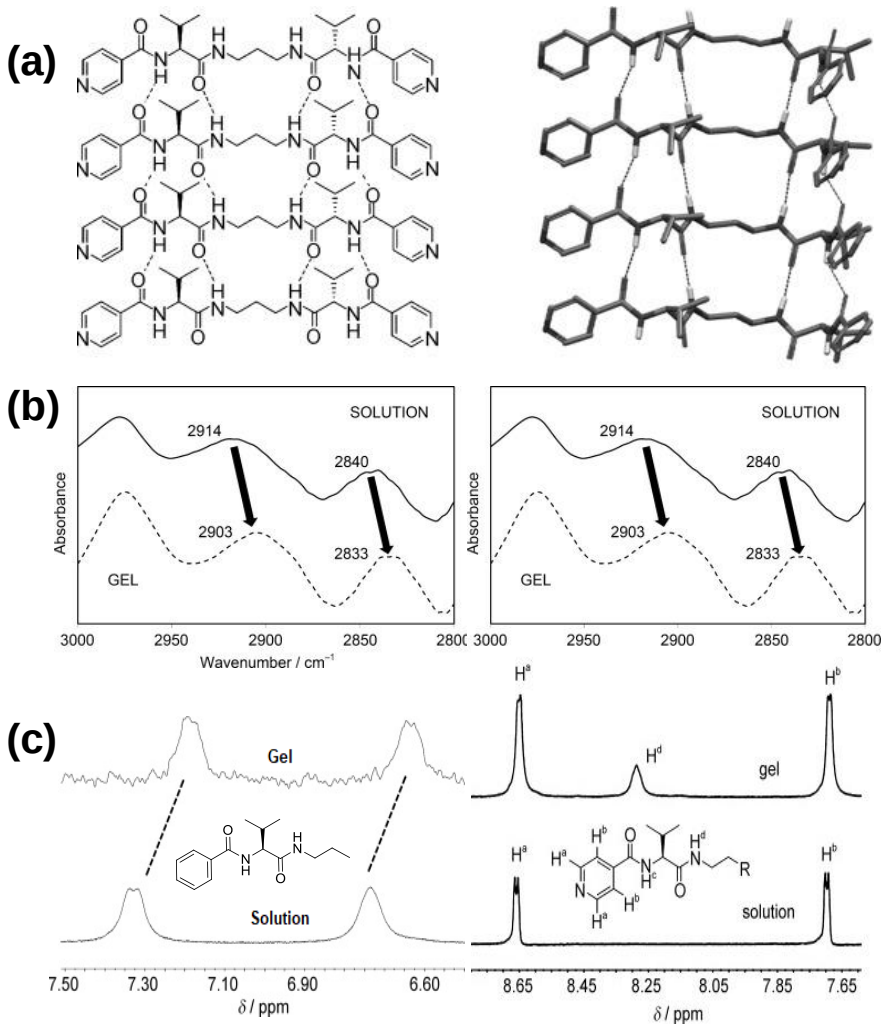

Figure 1.10 Investigating self-assembly by spectroscopic techniques: a) schematic aggregation model of bis(urea) gelator in energy minimized model, b) FTIR spectra of the bis(urea) gelator in D_2O solution and gel state, and c) fragment of the ^1H NMR spectra showing the shift in CD_3CN (left) and D_2O (right) reported by Escuder and Miravet.[144]

The hierarchical assembly of supramolecular gelators involves the formation of fibrous network. The contemporary microscopic techniques allow chemists to observe the morphology of the native gel or dried gel (xerogel) network. A few standard microscopy techniques include scanning electron microscopy (SEM), atomic force microscopy (AFM), transmission electron microscopy (TEM), confocal laser scanning microscopy (CLSM), cryogenic SEM and TEM (cryo-SEM and cryo-TEM) etc.[111] Each of these instruments

have its own scope and limitations, and different imaging can be beneficent to visualize aggregation across different magnification. For example, SEM has relatively large depth of field due to the narrow electron beam used for focusing. Thus, a large area of the sample can be focused at a time and very high-resolution images can be generated. SEM is the most applied microscopic technique, where the overall network is observed at a low magnification and detailed structures can be examined at higher magnification. Whereas in AFM, a 3D surface profile ranging from nanometer to sub-millimeter length scales is provided. On the other hand, TEM accrues images from the interaction of electron beams with the specimen as it passes through. TEM can produce high magnified and focused images even at sub-nanometer scale resolution. The key feature of CLSM is optical sectioning, where point-by-point images are acquired and reconstructed by software. CLSM is very effective to obtain high-resolution optical images with depth selectivity. It can be noted that most of the microscopy requires drying of the gel and the xerogel may not provide the actual morphology at solvated state. Cryo-SEM and cryo-TEM are conducted by freezing the solvent at cryogenic temperature to lower the morphological changes during sample preparation.[145]

The network level assembly of the gelators arise from entanglement or cross-linking of the fibers. The most used technique to elucidate information on network level assembly is rheology. Rheology measures the stiffness (solid-like characteristics) and/or resistance of flow (viscosity) in a semi-solid soft material on applying external stress or strain. Rheology is considered as the ultimate characterization of gel behavior of a system and provides insight on mechanical strength of the network.

In case where the single crystal structure of the gelator is available, it is possible to analyze the non-covalent interactions in self-assembly of the gelator by correlating simulated powder X-ray diffraction (PXRD) pattern from crystal data and PXRD obtained from either native gel or xerogels. However, the crystal structure of a gelator does not always represent the packing of molecules in gelator fibers[146] and in some cases removal of solvent from gel network may result in artefacts due to dissolution, recrystallization or changes in morphology or polymorphic phase transition.[147-148] Still, this is one of the most practical method to analyze the role of non-bonding interactions in the self-assembly of a gelator.

1.3 Multi-component gel

In most cases, gel is formed by a single gelator and a solvent. However, there are examples where gel is formed by more than one gelator, or a mixture of a gelator and non-gelator, or even a mixture of two non-gelators, these are called multi-component gel.[23, 149] Recently, supramolecular gels obtained from multi-component systems have drawn significant attention due to the tunable property that is beyond the scope of single component systems. Combining two individual gelators can lead to form a mixed gel either constructively or destructively, i.e., the resulting gel can be a stronger or weaker gel compared to the parent gelators.[107] Alternatively, mixed gelator with new properties can be constructed by mixing known gelators with non-gelling components. Multi-component gels can even be formed by mixing two non-gelators or weak gelators, where mixing induces or strengthen the gelation process.[150] These studies indicate that multi-component gels are special class of soft materials having diverse range of properties.

One of the earliest research field in multi-component supramolecular gels was the study to combine two non-gelators to obtain a gel. A good strategy to obtain such systems is to induce hydrogen bonding by mixing a hydrogen bond donor and an acceptor. Hirst and Smith wrote one of the earliest review on this field in 2005,[151] and they reported a multicomponent gel based on hydrogen-bonded carboxylic acid dendrons mixed with diamines (*Scheme 1.16*).[152] The hydrogen bonded (acid−base) interaction between carboxylic acid dendrons and diamine influence the gel formation whereas the spacer unit in the diamine determines the gel strength. This approach was later utilized in several carboxylic acid/amine systems and many gels based on organic salts were synthesized.[153-154]

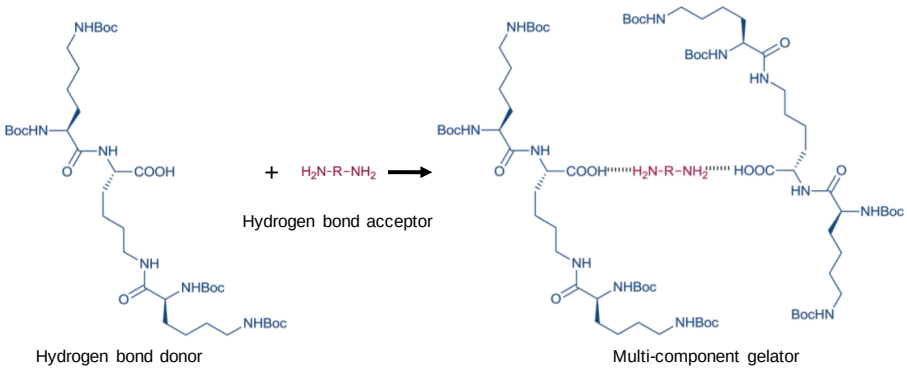

Scheme 1.16 Formation of multi-component gel by acid-base interaction.[152]

Another strategy to obtain multi-component gel is to mix a non-gelling additive to a gelator. Such systems can be designed to tune the functional properties of the gel by impacting the gelator self-assembly. The non-gelling additive can also increase the lifetime of the gel. For example, hydrogelator *N*-octyl-*D*-gluconamide was stable for a few hours until the gel network is collapsed to form crystals. However, Fuhrhop *et al*. have shown that the gel can be stabilized for short term in the presence of phosphotungstic acid[155] and at least for five months in the presence of the charged surfactant, sodium dodecyl sulfate surfactant.[156] It was hypothesized that any nucleation point of *N*-octyl-*D*-gluconamide crystal was dissolved in the micelles formed by the sodium dodecyl sulfate surfactant.

The most exciting class of multi-component gel is obtained by mixing two individual gelators. The fine tuning of gelation in these systems enable chemists to design new systems with precise properties. Maitra, and coworkers have used one achiral (**I-14**) and two chiral (**I-15R** and **I-16R**) alkyl-1-pyrenyl urethanes (*Figure 1.11a*) to examine the effect of chirality and gel strength in the mixed gels.[157] The achiral/chiral gels displayed amplification of chirality in isooctane, although no such phenomenon was observed in dodecane gels. Doping achiral **I-14** with chiral **I-15R** or **I-16R** coerce the system to adopt a preferred helical arrangement at the supramolecular level, and the mechanism is named "sergeants and soldiers" principle. Interestingly, the mixed achiral/chiral gels in dodecane did not show any signal in CD, indicating that the transformation of molecular chirality to the mixed assembly leading to helical bias depends on the solvent.

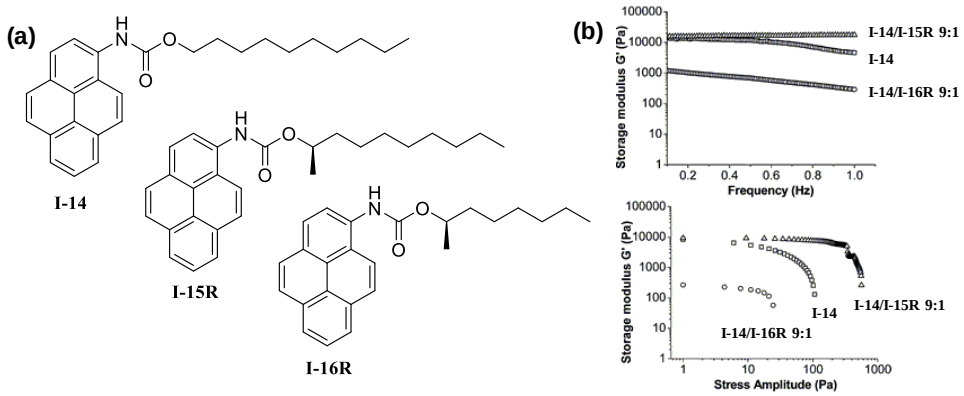

Figure 1.11 (a) Structure of the urethanes gelators, (b) Rheological measurements showing destructive and constructive assembly in ***I-14/I-16R*** *(9:1 mixture) and* ***I-14/I-15R*** *(9:1 mixture) mixed gels respectively.*[157]

They have also shown that how mixing two gelators can affect the thermal and mechanical stability. The gels of **I-14**/**I-16R** were thermally and mechanically weaker and more fragile compared to the gels obtained from the individual component, indicating that the gelators interacted destructively in the mixed gel. In contrast, the **I-14**/**I-15R** gels showed comparable thermal stability (to the native gel of **I-14**), significantly improved yield stress (*Figure 1.11b*), and the mixed gel displayed fibers of larger width in SEM images. The reduced gel strength in **I-14**/**I-16R** mixed gel is attributed to the structural dissimilarity in length of the alkyl side chains of the two gelators.

1.3.1 Self-assembly of multi-component gel

Mixing two compounds leads to self-recognition at the molecular level, and two alike molecules can combine themselves to form 'self-sorted' fibers or they can interact to produce well-ordered fibers containing both gelators (specific co-assembly).[25, 149] Random co-assembly is also possible where the compounds are mixed randomly to form the fibers (*Scheme 1.17*).

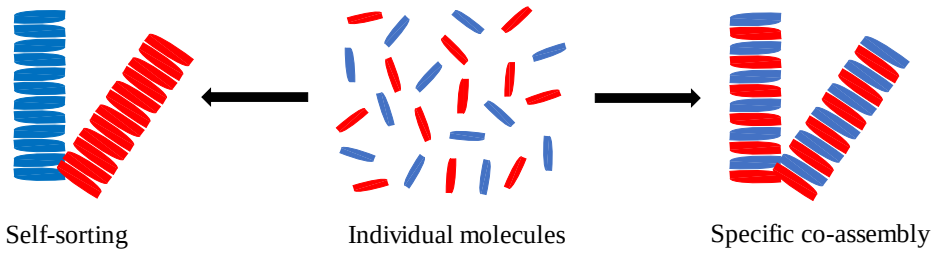

Scheme 1.17 Self-sorting and co-assembly of multi-component gels.

The utilization of different self-assembly opens the scope to synthesize new fascinating materials with finely tuned properties. For example, self-sorted systems of gelators having appropriate electronic property can be utilized to generate bulk heterojunctions (BHJ) for optoelectronic devices. Sugiyasu *et al* synthesized two semiconducting molecule-based organogelators 'Thio' and 'Pery', which act as opposite '*p*-type' and '*n*-type' charge carriers respectively (*Figure 1.12*).[158] The mixture of 'Thio' and 'Pery' forms self-sorted individual fibers, and the multi-component system consists of precise π-stacking structures entangled at *p-n* heterojunction points.

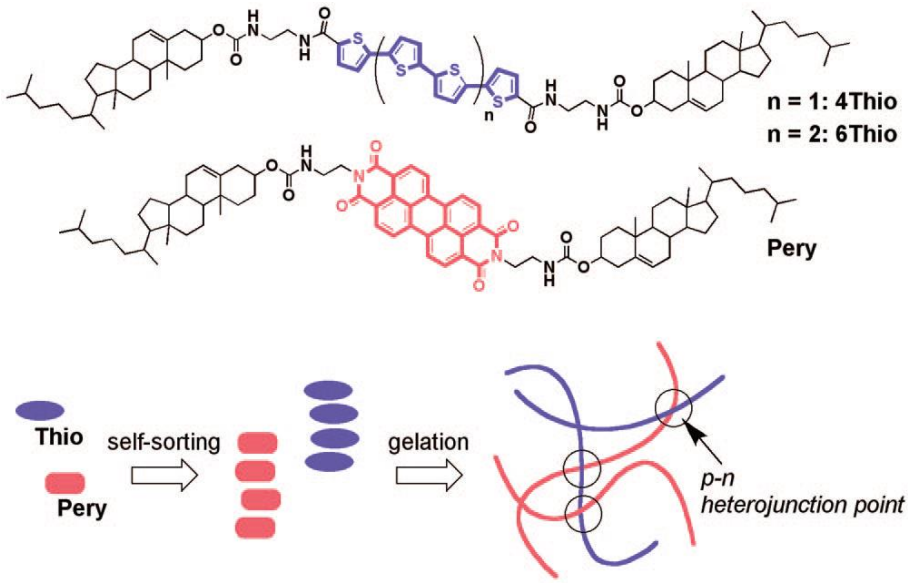

Figure 1.12 Structures of 'Thio' and 'Pery', schematic representation of the self-sorted network and formation of p-n heterojunction points reported by Sugiyasu et al.[158]

The specific co-assembly of two gelators can arise synergic gelation effect, especially in case of two structurally similar gelators. For example, Zinic and coworkers have reported that equimolar mixture of (*S*,*S*)-bis(LeuOH) oxalamide [**I-17*S***] and (*S*,*S*)-bis(leucinol) oxalamide [**I-18*S***] co-assemble and due to the synergic effect, the gelation ability of the multi-component gel is increased at least seven-fold compared to any single-component gels (*Figure 1.13*).[159] Interestingly, the synergistic effect is observed only in homochiral mixed gel [**I-17*S*** + **I-18*S***], and the gelation ability of the heterochiral mixed gel [**I-17*S*** + **I-18*R***] is only slightly improved in the mixed gel. The difference in the gelling ability of the two mixed gels is attributed to the different orientations of the isobutyl side chain, which impacts negatively the packing of the heterochiral complex. This indicates the chirality of the gelator plays an important role in the self-assembly process.

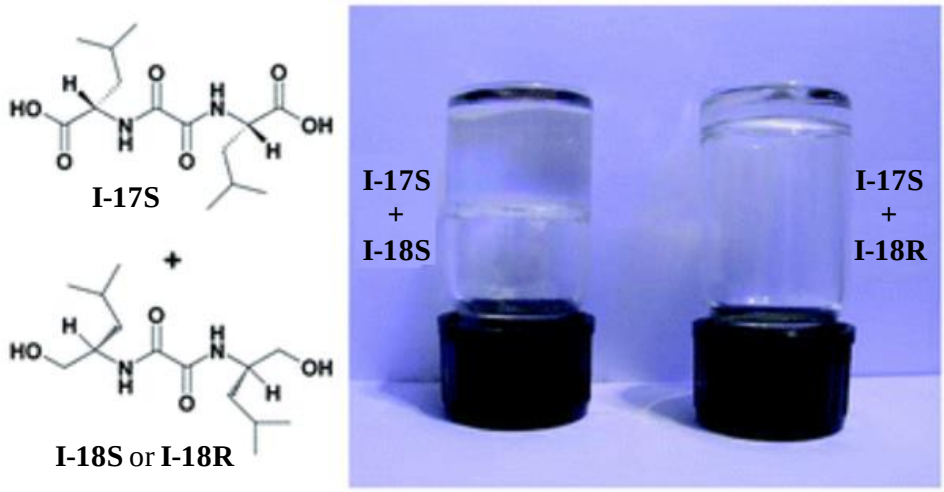

Figure 1.13 Structures of the gelators and enhanced gelation ability of the multi-component gel. [159]

Probing random co-assembly in multi-component gel is challenging since the dynamic nature is expected to be very high in such systems. Such assembly is assumed to be somewhere in between self-sorting and specific co-assembly. Wang and coworkers obtained a co-assembled system by mixing a phenothiazine-based and a naphthalene-based LMWG.[160] The co-assembly of system is predicted from changes in the fluorescence spectra, increase in gel-to-sol transition temperature, different diameter observed in transmission electron microscopy (TEM) and enhanced rheological properties structure. The exact aggregation is presumably random co-assembly since there are no specific interactions present.[149]

1.3.2 Multi-component gels based on enantiomers

Mixing two enantiomers is an easy and simple way to obtain multi-component systems with structurally similar compounds.[149, 161-163] Supramolecular gels constructed from chiral compounds often display interesting properties since the molecular chirality is translated to the hierarchical assembly. Chiral gelators self-assemble to form chiral nanostructures and can work as a matrix for enantioselective recognition on chiral analytes.[164] This unique property has made chiral LMWGs potentially applicable in the field of chiral nanomaterials, chiral recognition and asymmetric catalysis.[24, 161, 164-165]

Co-assembly of chiral gelator and chiral guest molecules leads to chiral recognition in supramolecular gels. The gelator and guest form a diastereomeric aggregate, and different diastereomers obtained from specific enantiomeric mixtures often display different structure and strength. For example, van Esch and Feringa demonstrated cooperative chiral recognition of a bis(ureido)cyclohexane gelator (**I-19*R*** and **I-19*S***) and bis(ureido)-cyclohexane tagged with azobenzene chromophores (**I-20*R*** and **I-20*S***) guest (*Figure 1.14).*[166] The incorporation of the guest **I-20*R*** with same configuration of the gelator **I-19*R*** is packed distinctly compared to the gelator with opposite configuration (**I-19*S***). The association constant of the **I-20*R*** guest was found to be almost double with the **I-19*S*** gelator compared to the **I-19*R*** gelator. This indicates that incorporation of the guest is preferred in the gelator having reverse configuration, which can be attributed to the reduced steric bulk in the aggregates with opposite chirality (*Figure 1. 14b*).

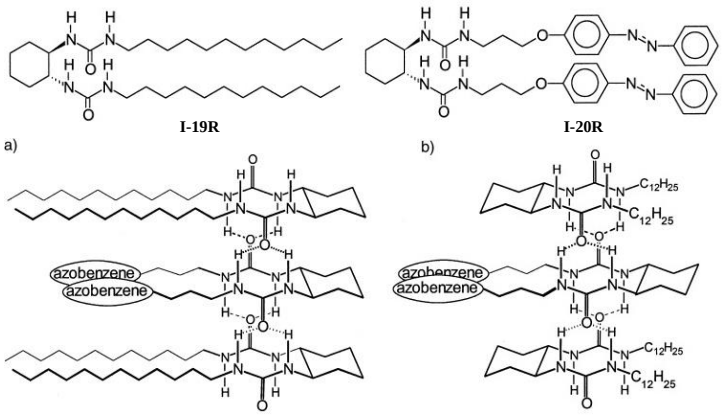

*Figure 1.14 Structure of chiral bis(ureido)cyclohexane gelator **I-19R** (R,R isomer) and the guest molecule **I-20R** (R,R isomer). Model for the incorporation of guest molecule in gelator aggregation: (a) with same configuration **I-19R** in **I-20R** and (b) with different configuration **I-20R** in **I-19S**.*[166]

1.3.3 Characterizations of multi-component gel

In a recent review, Draper and Adams described how the self-sorting or co-assembly might occur at various length scales (from nano to micro).[25] Predicting self-sorting or co-assembly of multi-component systems is challenging because of the dynamic nature of supramolecular gels across different length scales. The self-assembly process is often directed by structural similarity of the individual components.[167] Gelators with different molecular structure tend to self-sort and structurally similar gelators prefer mixing to form co-assembled fibers. Several techniques have been applied till date to study the hierarchical aggregation of multi-component gels from molecular to network level, and some of them is described below.

Similar to single-component gels, multi-component gels are also formed by the intermolecular association of the gelators leading to one-dimensional fibrils, which are entangled and cross-linked in three-dimensional network. The property of the gels depends on the self-assembly of LMWGs into the primary fibrous network and the entanglement of the primary structures. Hence, in order to characterize gels, it is important to unveil the molecular aggregation across different length scales, starting from molecular level to network scale. However, the characterization of supramolecular gels from molecular to mesoscopic level is difficult due to the dynamic nature of gel media. Characterizations of multi-component gel is even more challenging because of the various possibilities in the aggregation process.[25, 149, 168] In mixed gel, the individual components can retain the original fibers (self-sorting) or rearrange to generate new type of fibers (co-assembly). Some of the most common techniques to identify self-sorted or co-assembled network is discussed here.

The primary structure of a gel network is formed due to the self-recognition of the individual gelators at molecular level. Various spectroscopic techniques such as UV-vis absorption spectroscopy, infra-red spectroscopy, nuclear magnetic resonance (NMR), fluorescence spectroscopy and circular dichroism (CD) are effective tools to probe molecular level assembly.[158, 169-173] In a self-sorted system, absorption of the mixed gel system is expected to be an overlay of the spectra of individual components. On the other hand, any change in the multi-component spectra from the parent gelator system is expected due to co-assembly of the individual molecules. For example, Ghosh and Das have shown H-bonding and charge-transfer mediated self-sorting and specific co-assembly

between aromatic donor and acceptor chromophores by UV-visible absorption spectra.[167] *Scheme 1.18* shows schematic representation how a self-sorting and co-assembly can be predicted when a change in UV-visible spectrum is observed in multi-component systems.

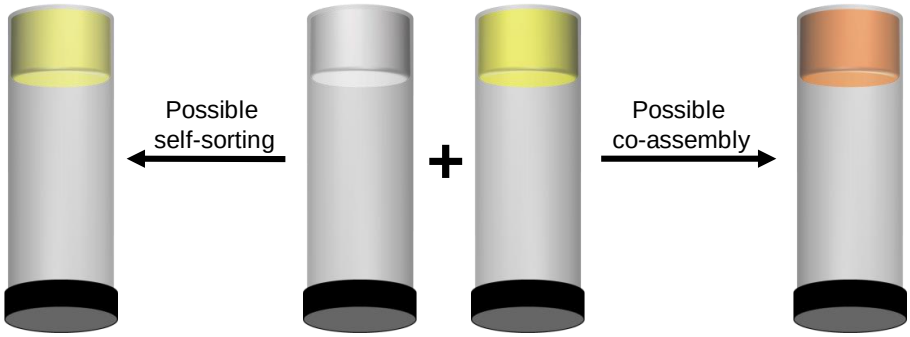

Scheme 1.18 Investigating self-assembly by UV-vis spectroscopy.

Since the self-assembly in multi-component gel still involves the formation of fibrous network, comparison of the fibers of the mixed gel with individual parent gel in either native gel or dried gel state provides information about the self-assembly process. Recent advancement in microscopic techniques like scanning electron microscopy (SEM), transmission electron microscopy (TEM), cryogenic transmission electron microscopy (cryo-TEM), atomic force microscopy (AFM), confocal laser scanning microscopy (CLSM) have allowed chemists to examine the self-assembled fibers and elucidate the information of network level self-assembly.[174-178] SEM is one of the best techniques to visualize the fibrous network in dried gel, which is often used to differentiate self-sorted or co-assembled fibers in multi-component systems. Although it is not always clear whether the morphology imaged in SEM represent in the same in native gel state, as artefacts can occur during drying process leading to aggregation or structural change.[147] However, in most of the cases, SEM provides clear evidence of self-assembly in multi-component gels. Self-sorted systems lead to fibers with similar morphologies (helical/ twisted/ tape/ rod etc.) and dimension (length/ thickness/ diameter etc.) as observed in the individual component but in co-assembled gels, it is possible to visualize fibers with different morphology. For example, Steed and co-workers have shown co-assembly of two gelators to form helical fibers, while flat ribbons were observed in SEM of the individual gelator.[179] Moffat and Smith showed a system[174] where two different types of fibers with very different diameters were visible together in SEM. The fibers seen in mixed gel were

similar to the fibers observed in individual gelators, indicating that the gelators were self-sorted.

The overall property of a mixed gel is outcome of not only the primary assembly, but also the entanglement to a larger length-scale in 3D network. Assembly of these fibers into gel network can be studied by its physical properties, gel-sol transition temperature (T_{gel}), rheology and powder X-ray diffraction (PXRD).[159-160, 180-184] Although it is difficult to elucidate exact information on the type or extent of self-assembly from macroscopic properties of multi-component gels, sometimes the comparison of physical properties of individual and mixed gel provide an indication to the assembly type.[25] Li *et al* showed that a multi-component gel obtained by mixing two short peptide-based gelators PTZ-GFFY and Nap-GFFY displayed storage modulus (G′) value of 5000 Pa, whereas the individual gels of PTZ-GFFY and Nap-GFFY was relatively weak with G′ of about 500 and 150 Pa respectively.[160] Thus, mixing gelators to form multi-component gel became popular strategy to improve the mechanical property of supramolecular gels.

1.4 Application of supramolecular gels

Among the numerous applications of supramolecular gels in the field of chemistry and biochemistry, a few are mentioned here.

Cell culture

Hydrogels have great potential in tissue engineering, primarily due to the biocompatibility, specific cell-scaffold interactions and rheological similarities to the extracellular matrix.[185-186] The bioactive behavior of LMWGs can be easily tuned by altering the chemical structure, thus, the LMWGs became an attractive material that promotes cell adhesion and growth.[187]

Drug delivery

Supramolecular hydrogels consist of amphiphilic oligopeptide or sugar-based composite are excellent drug delivery systems due to the biocompatible and biodegradable nature.[188] The weak non-bonding interactions holding the gel structure can respond to various stimuli, such as pH, ionic strength, or enzyme activity. The enzyme-mediated hydrolysis of gelator-drug conjugate system can be employed for drug release at specific targets.[189-190]

Sensing

The self-assembly of LMWGs is fabricated by weak non-bonding interactions, which can be either switched on/off by an external stimulus such as heat, light, pH, salts/ions, etc. Most of the supramolecular gels are thermoreversible, thus, gels possess inherent thermoresponsive property. The weak non-bonding interactions can be easily disrupted by adding salt/ions, which can be utilized as a sensing property. Furthermore, incorporation of a receptor site in the gelator molecule imparts sensitivity towards external stimuli. For example, azobenzene and anthracene based gelators have been used as photoresponsive gels, and pH-responsive gels were obtained by introducing an acidic or basic site in the gelator.[191]

Catalysis

Supramolecular LMWGs constitute an important class of multitopic catalyst, where the self-assembly leads nanofibers with well-ordered catalytic sites.[192] In addition to the single site catalysis, the organization of catalytic sites in gel state could generate interesting features such as neighboring effects, cooperativity and amplification of chirality.[193] Spatial separation of two incompatible catalytic functionalities was achieved in self-sorted gel, resulting one-pot tandem catalysis.[176]

Media of crystal growth

During the last decade, supramolecular gels have emerged as a promising crystallization media,[20] and our group is mainly focused on applying gels as media to control crystal growth. The aspect of using LMWGs in crystallization is discussed in details, *vide infra*.

1.4.1 Crystallization vs gelation

Crystallization and gelation can be viewed as alternative outcomes of different self-assembly process in a supersaturated solution, and the balance between high-order crystallinity and less-ordered fibrous aggregation leading to gel is not completely understood. Both gels and crystals are usually obtained in similar process, the most common method is to dissolve a substance in a solvent at supersaturation point by heating followed by cooling to room temperature. Thus, gelation resembles crystallization where both have similar nucleation point in the solution (*Scheme 1.19*) [194-196] Entanglement of gel fibers to form a solid-like 3D network in the solution is a parallel process of crystallization.

Crystals are grown by high ordered packing of the molecules in 3D whereas gels are formed by the self-assembly of the gelator in 1D to form fibrils, which subsequently entangle in 3D network.[105, 197] The crystallization vs gelation process depends largely on molecular structure, choice of solvent and external stimuli, and the formation of gels and crystals are often unpredictable.[146, 195] The crystal engineering approach in the design of gelators has revealed that there is often a link between the non-bonding interactions observed in a crystal structure and the ability in gel formation.[105] There are many gel-to-crystal transitions reported to explore the link between crystallization and gelation[197-200] and the non-bonding interactions observed in crystal structures of the gelators were used to rationalize the gelation ability.[105, 141-142, 201] Correlation of powder X-ray pattern (PXRD) of the crystalline state and native gel or xerogels is used to elucidate the structural information. However, the XRPD pattern does not always reveal the actual structure due to artefacts caused during sample preparation.[20] As a result, the mechanistic understanding of the two self-assembly processes and their correlation is still limited.

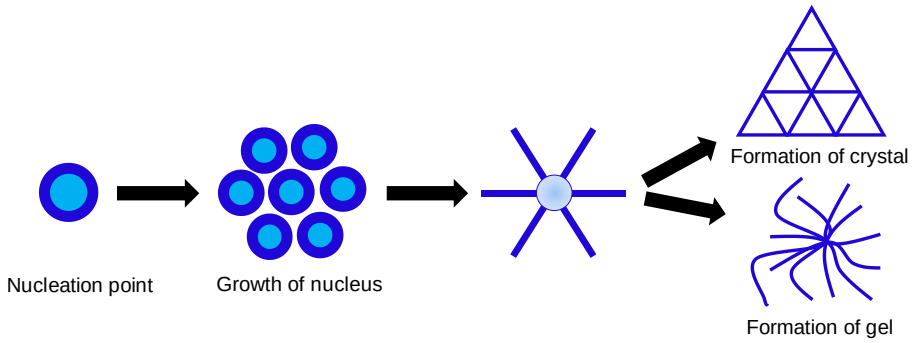

Scheme 1.19 Formation of crystalline network and gel fiber from similar nucleation point.

1.4.2 Gel as crystallizing media

Supramolecular gel phase crystallization using low molecular weight gelators (LMWG) has witnessed tremendous growth over the last decade where the gel fibers can potentially act as a template for the discovery of novel solid forms.[20] Crystallization in the gel matrix is a time-resolved process where both gelator and crystallizing substrate is dissolved initially in the same solvent. The gel is formed at first, followed by the growth of crystals within the gel. Holmes described the early examples of formation of crystals in gels in his review a century ago in 1917,[202] and the technique became popular in 1970-80s. In a

review in 1982, Patel and Rao covered the information on the crystal growth in gels, nucleation mechanism and problems associated with gel phase crystallization.[203] However, the crystals were grown in polymer gels. Hamilton group first used LMWG (*Figure 1.15a*) to grow calcite crystals in aqueous medium (*Figure 1.15b*).[204]

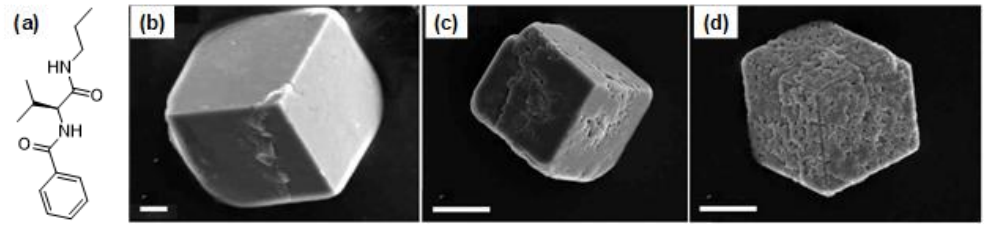

Figure 1.15 (a) structure of the LMWG used to crystallize calcite and the changes in calcite surface texture as a function of time. Image shows the crystals removed from a gel of (a) after (b) 3.5 h, scale bar: 5 µm, (c) 10.5 h, scale bar: 20 µm, and (d) 24 h, scale bar: 20 µm.[204]

Gunnlaugsson, Boland and co-workers have demonstrated the fascinating growth of the single crystal halide (NaCl, KCl and KI) salt wires facilitated by the supramolecular gel (**I-21** and $EuCl_3$- **I-21**) upon dehydration to give "chemical nano-gardens" (*Figure 1.16*).[205]

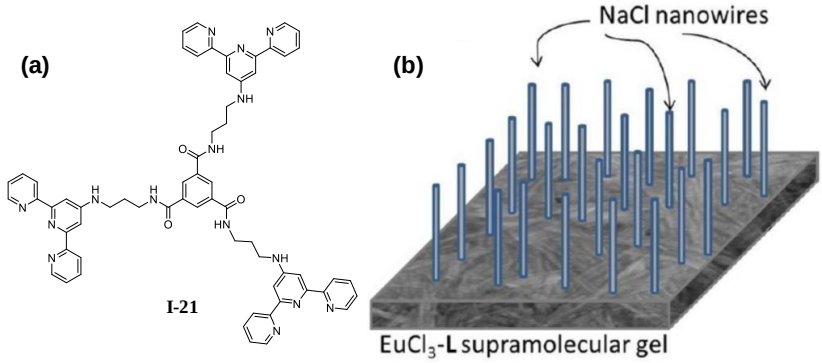

*Figure 1.16 (a) structure of the LMWG **I-21**, (b) formation of the NaCl nanowires.*[205]

The gel phase crystallization of pharmaceuticals offers several advantages but surprisingly, this technique is vastly underexplored. In 2006, Pauchet *et al* isolated a new polymorph of (±)-modafinil (form-III, orthorhombic form) in gel medium which was not obtained by crystallization in solution.[206] Steed and coworkers have crystallized a series of drug precursors including carbamazepine, sparfloxacin, piroxicam, theophylline, caffeine,

ibuprofen, paracetamol, sulindac and indomethacin in bis(urea) based supramolecular organogels (*Scheme 1.20a*).[207] Sanchez and coworkers also utilized bis(amide) type organogelators (*Scheme 1.20b*) to crystallize carbamazepine, aspirin, caffeine and indomethacin.[208]

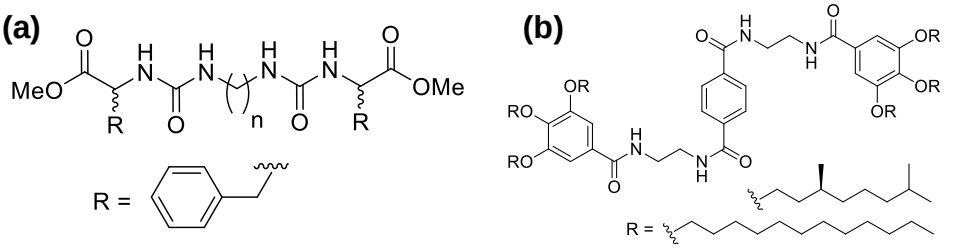

Scheme 1.20 LMWGs used in crystallizing drug molecules.[207-208]

The crystals grown in gel often display improved physical characteristics due to restricted Brownian motions and sedimentation in the gel medium.[209] For example, McPherson *et al.* used a silica gel matrix to obtain larger and better-quality crystals of a macromolecule thaumatin with enhanced stability.[210] The results suggested that the gel matrix suppressed nucleation and reduced the rate of crystal growth by decreasing the mobility of thaumatin and its flux at the crystal surface (*Figure 1.17*).

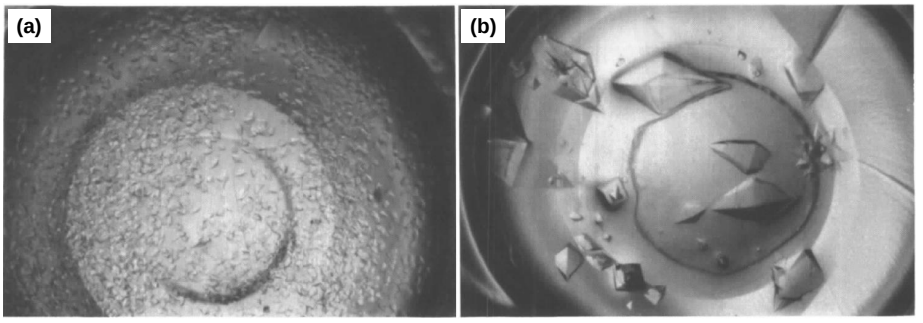

Figure 1.17 Crystals of thaumatin grown in (a) absence of gel (b) presence of gel.[210]

Another interesting feature of gel phase crystallization is using chiral gels to influence the handedness of a crystallite. For example, the achiral inorganic salt sodium chlorate ($NaClO_3$) crystallizes in a chiral space group $P2_13$ and form conglomerate of two enantiomorphic crystals (*Figure 1.18a*). Crystallization of $NaClO_3$ in pure water yields 1:1 mixture of *L*- and *D*-crystals, but crystallization in chiral biopolymer agarose gel can be selectively biased towards excesses of either *L*- or *D*-crystals depending upon the gelation condition (*Figure 1.18b*).[211]

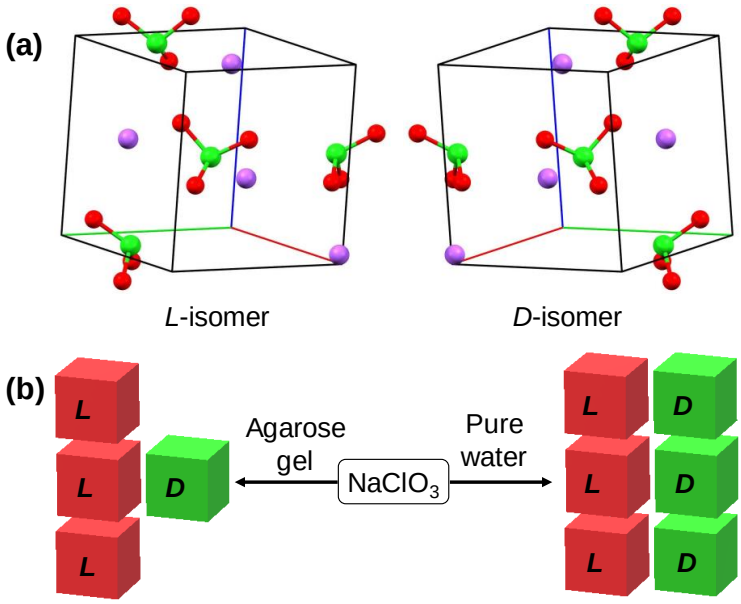

Figure 1.18 (a) L- and D-isomers of $NaClO_3$ (b) Crystallization in agarose gel showing the biasness towards a specific isomer.

The stimuli-responsive properties of the LMWGs can be employed to recover the crystallized drug molecules from the gel matrix. The gel network is disrupted by an external stimulus without affecting the crystals. Steed and coworkers used acetate anion to break the bis(urea) gel, from where the carbamazepine (CBZ) crystals were isolated by filtration (*Figure 1.19*).[207]

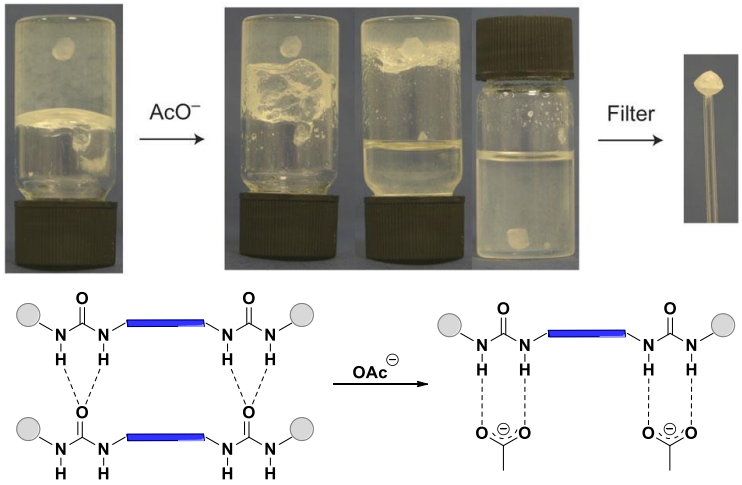

Figure 1.19 Recovery of crystals grown in gel by anion switching.[207]

Usually, the gel acts as an inert matrix in the growth of crystals, but there are reports where the gel medium is also utilized to modify crystal habit or polymorphic form.[22, 207, 212-213] Steed and co-workers synthesized a series of platinum bearing LMWGs mimicking the anticancer drug cisplatin.[212] Crystallization of cisplatin in the mimicked gel resulted in crystal habit modification and a novel solvate form was isolated. This was the first evidence of using a drug-mimicked LMWG to influence the outcome of the crystallization process. Later, the same group showed that the metastable polymorph of highly polymorphic drug precursor ROY can be selectively crystallized by using supramolecular gelator that is structurally similar (**I-22**) to the crystallizing substrate (*Figure 1.20*).[22] The gelator mimicking the crystallizing substrate leads to a gel matrix that can potentially lower the nucleation barrier of a particular polymorph,[214] and the designed nucleation of a substrate could be a promising strategy to control polymorphism. Thus, LMWGs can act as an excellent medium for crystallization of organic and inorganic materials.

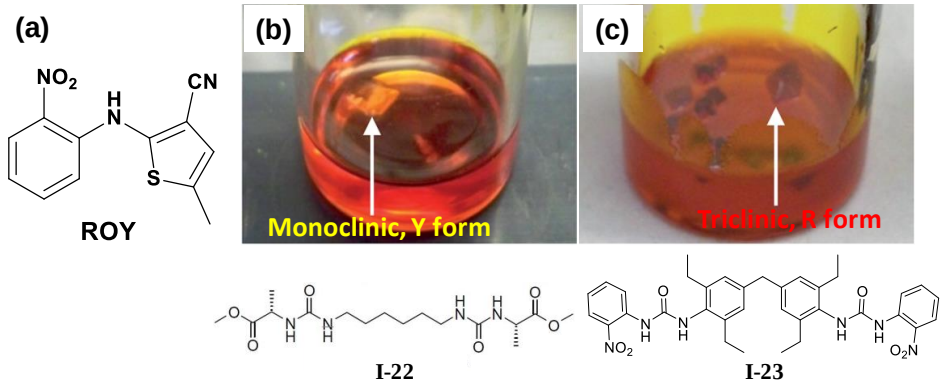

*Figure 1.20 (a) Chemical structure of ROY (b) Crystallization of ROY in solution state or LMWG having no structural similarity (**I-22**) (c) Crystallization of ROY in structurally similar LMWG (**I-23**).*[22]

1.5 Objective of the thesis

Assembling small molecules into hierarchical superstructure to obtain functional material is an active area of research. Using small molecules as the network building block offers tunability and a system with specific properties is obtained. The assembly of the subunits are classified in two categories- (a) coordination to metal ions resulting in metal organic material (MOMs) and (b) self-assembly via non-bonding interaction leading to supramolecular gelation. The specific aims and objectives of the work is discussed below.

The overall doctoral dissertation is divided in four main projects. The first part, which will be elaborated in chapter two, is directed to develop multi-functional MOMs and its application in heterogeneous catalysis including CO_2 conversion. Our aim was to synthesize metalloligands based on multi-functional ligands and incorporate to robust bimetallic frameworks. The incorporation of functional metalloligands in highly ordered three-dimensional array make it promising candidate for heterogeneous catalysis. Various soft-synthetic methods used in the synthetic process ensure the retention of catalytic cites in the framework. We have synthesized a series of multi-functional ligands and metalloligands. A MOF with functional urea moiety was synthesized by room temperature layering, and it was applied as heterogeneous catalyst in various organic reaction such as CO_2 fixation of epoxides, alcohol oxidation and methanolysis.

Chapter three describes the assembly of small molecules via non-bonding interactions to construct supramolecular gels (LMWGs). Probing the role of different non-bonding interactions in gel formation is difficult due to the dynamic nature of the material. We accomplished structural modification of existing LMWGs and investigated the non-covalent interactions by single crystal X-ray structure. The structures in crystalline state and gel state was rationalized by comparing powder X-ray pattern of simulated data obtained from single crystal structure and the pattern of bulk xerogel samples. It was observed that gelation can be induced or hindered by structural modification. Comparing relative gel strength of the parent and structurally modified gelator with the interactions observed in both crystal structures elucidate significant information about the specific non-bonding interaction. A second strategy is to induce gelation to a non-gelator by coordinating with a metal center (metallogel). Although the strong coordination bond between the metal center and organic ligand is the key driving force in metallogel

formation, but the nature of other non-bonding interactions also plays an important role in the assembly. We have compared the interactions observed in the non-gelator ligands with the metal complexes to investigate the contribution in gel formation.

Although most of the gels are obtained by a single gelator, supramolecular gels constructed from multi-component systems have gained significant attention in recent time due to potential tuning in gel state properties. We are interested in multi-component gels obtained from enantiomeric gelators and the findings are explained in chapter four. Mixing two or more gelators leads to self-recognition at molecular level, and individual gelators can self-sort or co-assemble for more favorable interactions. We investigated the self-assembly modes by SEM, CD, rheology and SCXRD and correlated to the enhanced gel strength in multi-component enantiomeric gels. Finally, the last part of the thesis illustrates the application of supramolecular gels in crystallization of inorganic complexes. We have shown that the LMWGs can act as a media for selective crystallization of thermodynamically stable form of a copper(II) complex. Also, selective crystallization of specific enantiomer of a chiral MOM using chiral LMWGs is in progress. We believe that these studies will have significant contribution to ongoing research in supramolecular chemistry. The detail investigation of the molecular self-assembly will help the chemists to design new functional ‘smart materials’ with fine-tuned properties.

2 Assembling Multi–Functional Ligands via Coordination to form Catalytically Active MOMs

The chemistry of catalysis has been evolved 200 years ago, yet the design and synthesis of new and efficient catalysts remains as the important field in chemistry and biochemistry[215-216] due to their application in industry and biological process. Catalysts accelerate chemical reaction by offering an alternative and energetically more favorable pathway compared to the non-catalyzed reaction, thus, the discovery of improved catalytic systems is always in demand for laboratories and industries.[217-218] Earlier, most of the catalytic reactions were based on homogeneous catalysts due of the excellent efficiency. Generally, homogenous catalytic reactions often suffer from disadvantages such as problem of the recovery of the metal from the reaction products and environmental pollution resulting from potentially hazardous heavy–metal catalysts. Extensive efforts have been directed toward the development of efficient and recyclable heterogeneous catalysts[219-220] to overcome these problems, resulting in heterogeneous catalyst, which are efficient as its homogeneous analogue.[99-100]

Metal-organic materials (MOMs)[221-223] are very interesting hybrid materials, which consists of metal ion and bridging organic ligands. During the last two decades MOMs have attracted intense research interest due to their highly ordered crystalline structure, specific surface area, large pore volume and tunable pore surface.[224-227] The uses of MOMs in adsorption and gas storage are well known,[79, 228] and the current interest is to develop MOM as catalyst.[40] In heterogeneous catalysts, the substrates have to be adsorbed on the catalyst surface and MOMs are very good absorbents[229-230] as well as stable under high temperature,[231-232] which make them ideal candidates for catalysis. Furthermore, the well-arranged active sites[233] in MOM cluster makes the catalytic activity even more promising. MOMs with bimetallic assembly have been reported,[224, 234] which contain a catalytically active metal center for catalysis, and a second metal ion for network formation and structural rigidity. There are two ways to introduce catalytically active metal centers in MOMs (a) direct incorporation[235-236] and (b) post synthetic modification.[237-239] One of the

main challenges in direct incorporation is to retain these catalytically active sites in MOM cluster during synthesis. MOMs are generally synthesized under high temperature and pressure,[49, 240] leading to decomposition of active sites. Post synthetic modification (PSM) affect the properties of MOMs, which are harnessed by incomplete conversion, loss of crystallinity and reduced pore size resulting in reduced catalytic activity due to blockage and diffusion rate.

Another approach is to incorporate catalytically active metal sites by utilizing metalloligand,[30, 222, 241-242] which has been very successful. Metalloligands are coordination complexes of organic ligands and metal ion, with two or more vacant coordinating sites. The organic ligands have two types of coordination sites- primary and secondary. The primary group forms catalytically active centers by coordinating to suitable metal ions whereas the secondary group binds with a second metal to construct MOMs.

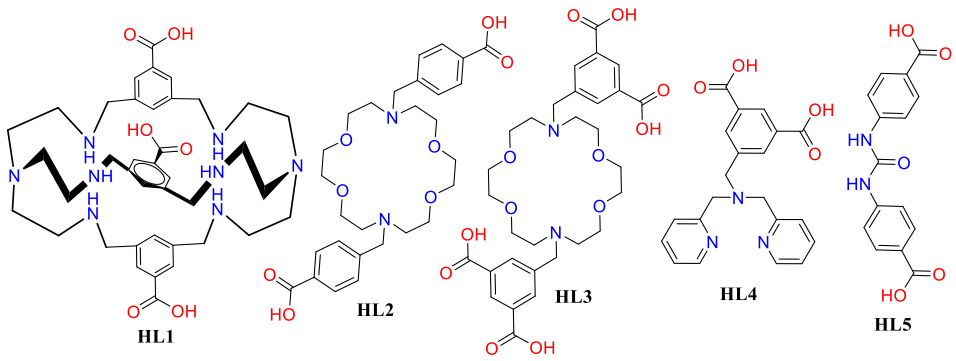

Scheme 2.1 Designed multi-functional ligands.

The metalloligands (MLs) will be assembled into a 3D array with transition metals to form MOMs with well-arranged catalytically active site with suitable pore size, which will great potential as efficient heterogeneous catalysts. One of the major aims of the doctoral research is to construct catalytically active MOMs for chemical fixation of carbon dioxide to useful organic compounds. The ever-increasing emission of CO_2 from combustion processes is one of the main reasons behind global warming and climate change. The capture, storage and conversion of atmospheric CO_2 still remained a profound challenge for chemists. Furthermore, CO_2 serves as attractive C1 building block in organic synthesis in laboratory and industrial processes. Metal–organic frameworks (MOFs) are promising candidates for CO_2 uptake[231] and catalytic conversion of CO_2 into methanol, formic acid,

methane or cyclic carbonates by catalytic MOFs has been reported.[243] Thus, the possibility to construct new and improved MOMs for carbon capture and sequestration (CSS) was further explored in this doctoral study. We have used metalloligand approach to achieve this task and in this doctoral study, various multi-functional ligands were designed and synthesized (*Scheme 2.1*), the blue color indicates primary functional group and red color shows secondary functional group (**HL1** – **HL4**). Various chelating ligands were chosen as primary functional group due to the ability to trap catalytically active metal ions resulting in the formation of highly stable coordination complexes. The secondary functional group was chosen as pyridyl or carboxylate moiety owing to the ability to bind with various metal ions to form a rigid network. A second strategy is to incorporate a hydrogen bonding moiety in the framework (**HL5**), which can interact with the guest molecules and activate the substrate for catalytic conversion. We have designed ligands with urea or amide groups with pyridyl or carboxylate functionality as secondary group were synthesized for this purpose. Thus, multi-functional ligands based on aza-cryptand, aza-crown, dipicolylamine, paddlewheel complexes and hydrogen bonding moieties were synthesized.

2.1 Multi-functional ligand based on aza-cryptand

Dinuclear metalloenzymes are known to bind with CO_2 and catalyze the hydrolysis and redox reactions at ambient conditions.[244-246] Specifically, nickel containing enzymes have shown high efficiency in binding CO_2 and complexes consisting Ni–OH center is widely known to promote CO_2 fixation.[247] Holm and co-workers have used various nickel complexes that can selectively bind with CO_2 and act as the catalyst for CO_2 conversion.[248-249] However, one of the major drawbacks of such systems was the lack of reversibility due to the conversion to oligomer with bridging carbonates. The nickel complexes of aza-cryptands are structurally similar to these metalloenzymes but they have rigid binding units with well-defined cavities. The size of the cavity can also be freely varied by designing linker molecules connecting two tris(2-aminoethyl)amine or *tren*-moieties.[250] Furthermore, the binding mode of the aza-cryptand molecules can be tuned by choosing specific ions. The larger ions are usually placed into the center of the macrocycle, whereas small transition metal ions bind in a binuclear fashion (*Figure 2.1*).

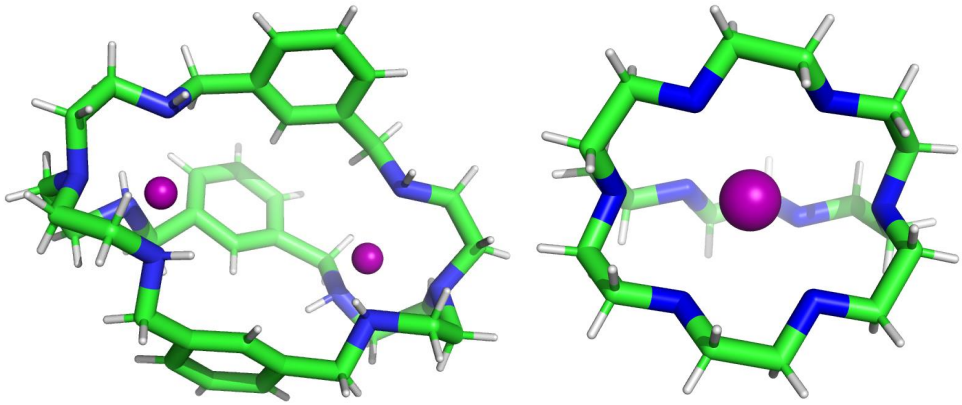

Figure 2.1 Chelating modes of aza-cryptand ligands with small and large size metals.

The cryptand and aza-cryptand macrocycle have been extensively used in supramolecular chemistry for anion recognition and metal chelation,[251-253] and the possibility of using dinuclear nickel-cryptand complexes in CO_2 fixation was also explored. Möller and Apfel have reported dinickel aza-cryptand complex for highly selective CO_2 capture under ambient conditions.[244] The predefined cavity of the system for hosting CO_2 (*Figure 2.2*) resulted in high stability and selectivity. Chemical fixation and transformation of CO_2 was

also shown by Chen and Lu using a dinuclear copper aza-cryptate. Our aim was to incorporate the aza-cryptand moiety in a MOM framework, which would enable the CO_2 uptake and conversion by a single system. Also, the rigid framework would prevent the formation of oligomer during catalytic reaction, which will lead to reusable heterogeneous catalyst. Thus, a carboxylic acid moiety was introduced in the aza-cryptand backbone which can bind with a secondary metal ion to facilitate the formation of bimetallic MOM.

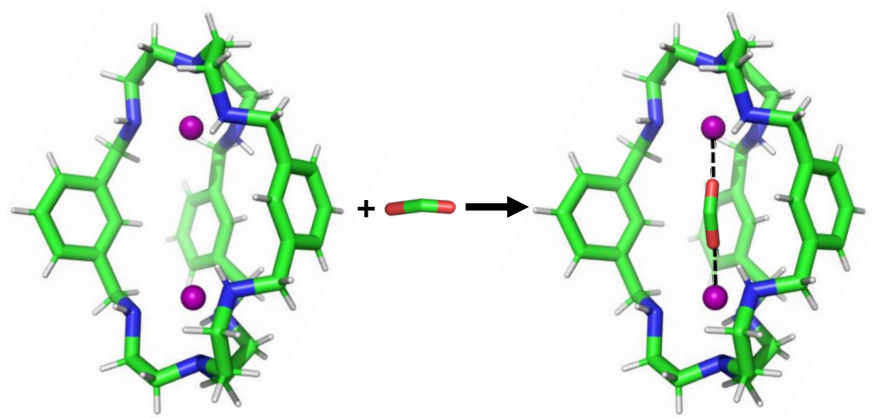

Figure 2.2 CO_2 binding with dimetallic aza-cryptand.

We have introduced three carboxylic acid groups to the aromatic ring of isocryptand (**HL1**). The ligand was synthesized by multi-step organic synthesis (*Scheme 2.2*). Initially, the trimethyl-1,3,5-benzenetricarboxylate was reduced with sodium borohydride to form a mixture of a mono- and a di-alcohol. The minor product methyl 3,5-bis(hydroxymethyl)benzoate was isolated by column chromatography and was oxidized with pyridinium chlorochromate (PCC) to obtain methyl-3,5-diformylbenzoate. The dialdehyde was reacted with tris(2-aminoethyl)amine to obtain a Schiff base, which was reduced *in-situ* by sodium borohydride to form the ester protected ligand (**MeL1**). Finally, the ester group was hydrolyzed by sodium hydroxide to isolate the ligand **HL1** (*Scheme 2.2*).

The ligand was characterized by ^{1}H- and ^{13}C-NMR and mass spectroscopy. The crystals of the ester **MeL1** obtained was analyzed by single crystal X-ray diffraction. However, single crystals of **HL1** with acid group was not obtained. Crystal structure of **MeL1** revealed that the compound crystallized in Pī space group with two molecules in the asymmetric unit (*Figure 2.3*). The molecule did not participate in any hydrogen bonding interaction.

Interestingly, an ester group of the molecule resided in the core of the neighboring molecule and this was stabilized via various non-bonding interactions.

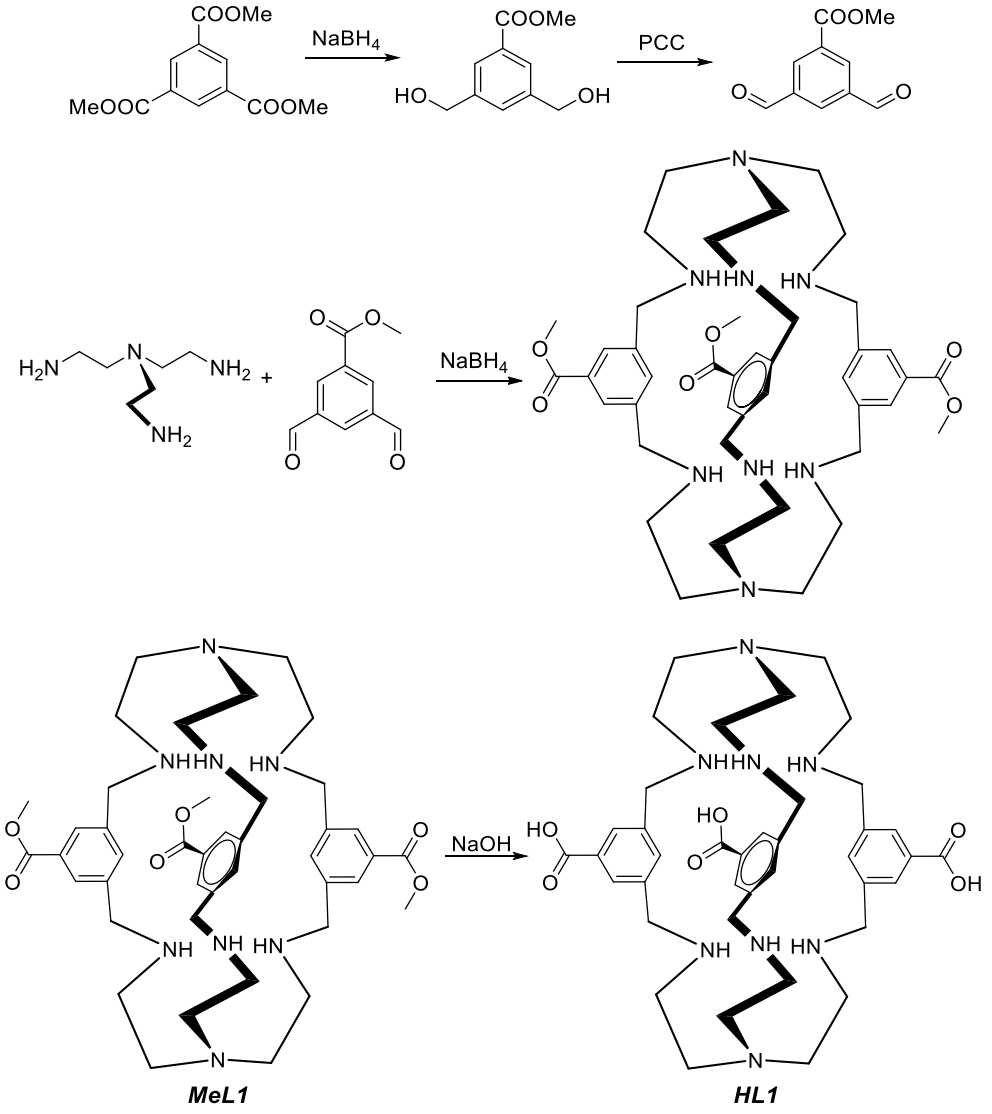

Scheme 2.2 Synthesis of ***HL1***

The ligand **HL1** was proved to be highly soluble in water but sparingly soluble in any organic solvents. **HL1** was treated with various metal salts such as copper(II), zinc(II), iron(II) and (III), and cadmium (II) in 3:2 metal:ligand ratio (1:1 for Fe^{3+}) in pure water or aqueous solution of various hydrophilic solvents. Layering a solution of the metal salts (in water or organic solvents) over an aqueous solution of the ligand produced white precipitate after 3-4 days. ^{1}H-NMR of the precipitate suggested that the material was the starting material. Hydrothermal reactions in pure water or DMF at 100-150 °C for 48 h produced a clear solution (color corresponding to the color of the metal salt), which subsequently produced a white precipitate of the unreacted **HL1** ligand. Similar observation was recorded for solvothermal in mixed aqueous solvents such as water/MeOH, water/EtOH and water/DMF mixtures. Thus, **HL1** displayed poor reactivity towards metal salts, presumably due to the interpenetration of the carboxylate moiety into the cryptand cavity, making the binding site unavailable for metal coordination.

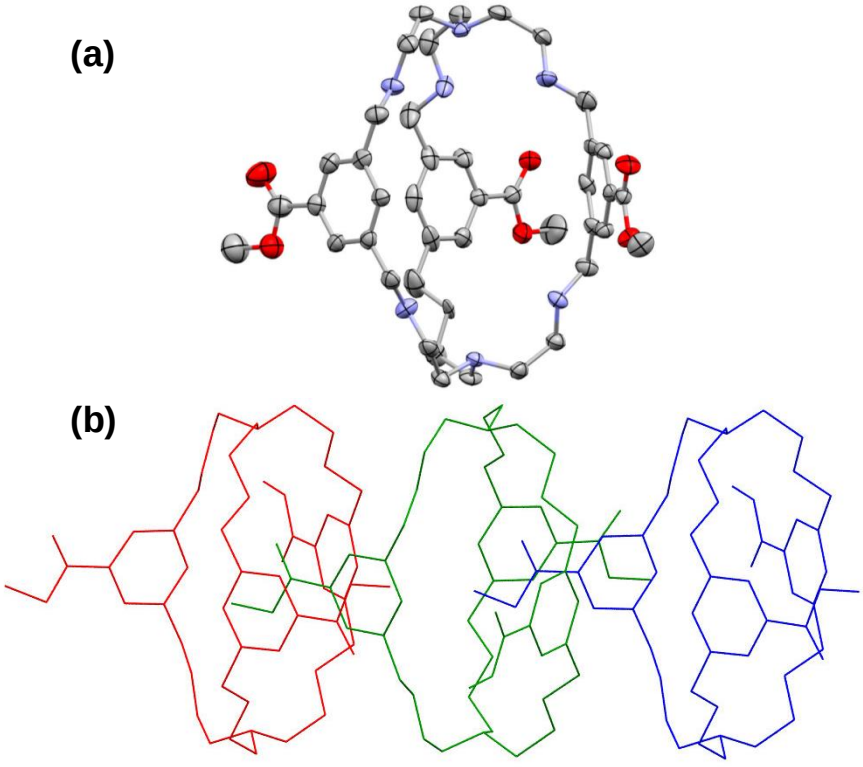

*Figure 2.3 Crystal structure of cryptand ligand (**MeL1**): (a) individual molecule and (b) interpenetrated network.*

2.2 Multi-functional ligand based on diaza-18-crown-6 derivatives

In order to avoid interpenetration of the ligand and to make the chelating unit free for metal coordination, the C_3-symmetric cryptand moiety was modified to C_2-symmetric aza-crown ether (*Figure 2.4*). The crown ether moieties have been widely used to form complexes with s-block and transition metal ions[254-256] and metals of different sizes can be trapped in the ring by varying the number of ring members.

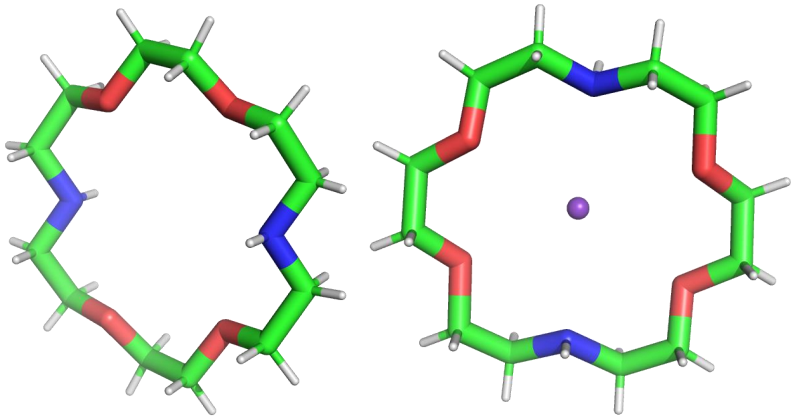

Figure 2.4 1,10-diaza-18-crown-6 ligand (left) and metal ion captured by the ligand (right).

There are various ways to attach the secondary functional group to the periphery of crown-ethers. One simple strategy is to use catechol derivatives as a precursor to obtain substituted crown ethers (*Scheme 2.3*). For example, Cohen *et al* used ester protected 2,3-dihydroxy-terephthalic acid to synthesize crown ether- and thiacrown ether-appended benzene dicarboxylic acids, and incorporated the ligands into isoreticular MOFs (IRMOF) and UiO-66 materials.[257] This approach allows to incorporate one of the fundamental units of supramolecular chemistry into highly stable MOFs, and the combination of the macrocycle with modular architectures of MOFs can be utilized in guest molecule capture and separation. However, drawback of such ligands are the limited availability, expensive catechol derivatives and also the difficulty in synthesizing the macrocycles due to multiple steps and low yield.

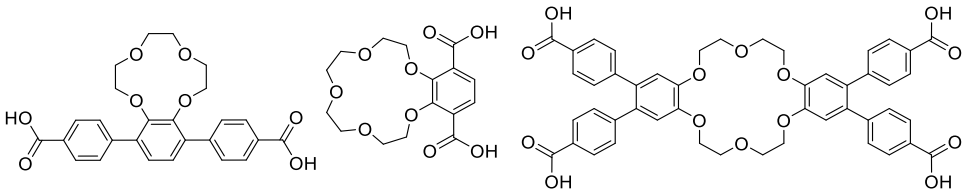

Scheme 2.3 Reported examples of crown ether-appended ligands in MOF synthesis.

An alternative strategy is to use diaza-crown ethers instead of simple crown ether, which will enable us to link the secondary functional groups through the nitrogen atoms. We have synthesized 1,10-diaza-18-crown-6[258-259] to attach carboxylic acid groups at the backbone. 1,10-diaza-18-crown-6 was synthesized according to a procedure described in literature,[260] and two ligands (**HL2** and **HL3**) were synthesized by incorporating two and four carboxylic acid groups to the ligands, respectively (*Scheme 2.4*). **HL2** was synthesized by reacting 1,10-diaza-18-crown-6 with methyl-4-(bromomethyl)benzoate and the ester group was deprotected by sodium hydroxide. **HL3** was synthesized by reacting 1,10-diaza-18-crown-6 and dimethyl 5-(bromomethyl)-isophthalate, followed by the ester hydrolysis reaction.

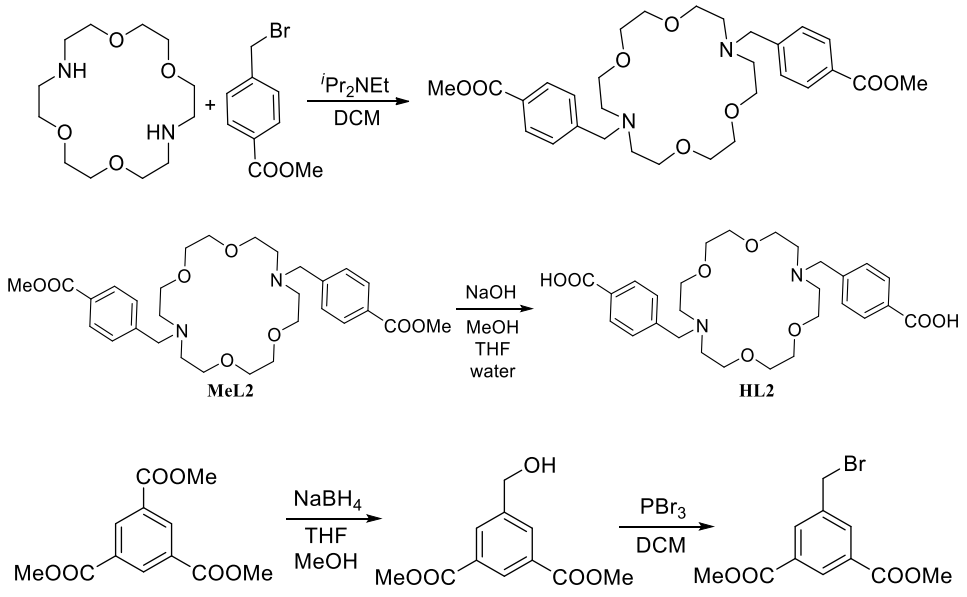

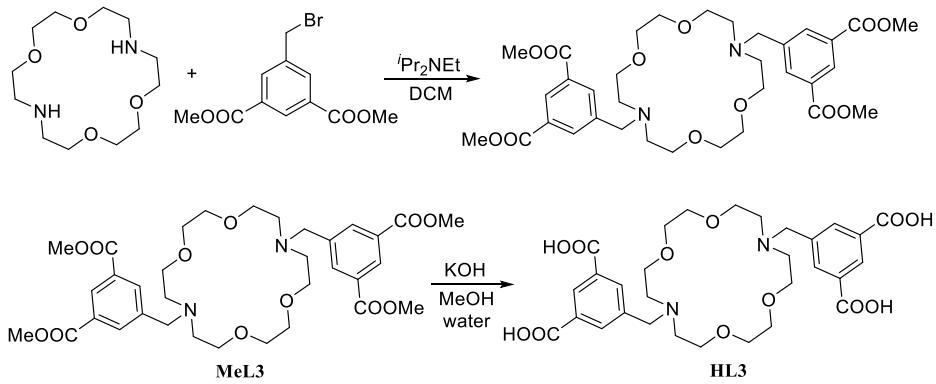

*Scheme 2.4 Synthesis of **HL2** and **HL3**.*

X-ray quality single crystals of **HL2** was obtained by slow evaporation of a MeOH/water solution. SCXRD analysis revealed that **HL2** was obtained as a metal complex in the ester hydrolysis step, and the metal hydroxide used in the reaction was the source of the metal ion. Hydrolyzing the ester with LiOH, NaOH and KOH resulted in Li, Na and K-complex of **HL2**, respectively. The carboxylate groups of the two adjacent molecules were connected through a proton (H^+), which was shared between the two carboxylates to balance the charge. However, free **HL2** crystals were also obtained accidentally from a solvothermal reaction of **HL2** and $Zn(BF_4)_2.6H_2O$. In contrast, **HL3** was obtained as free ligand irrespective of choice of the base in the hydrolysis step, and both the **HL3** ligand and the tetramethyl ester ***MeL3*** were recrystallized from methanol.

Analysis of the crystal structures of **HL2** ligand, the dimethyl ester ***MeL2*** and sodium-adduct ***Na-HL2*** revealed that the aromatic rings were directed away of the crown ether moiety (*Figure 2.5*), leading the aza-crown ether macrocycle open for metal coordination. The structures of **HL2**, **HL3** and their derivatives were also compared. Interestingly, in both **HL3** and **MeL3** structures, the aromatic moiety was oriented towards the aza-crown ether moiety (*Figure 2.6*), blocking both of the sides of the macrocycle. The structures corroborate well with the fact that a metal complex was formed in the hydrolysis of **HL2** whereas **HL3** was obtained as a free ligand.

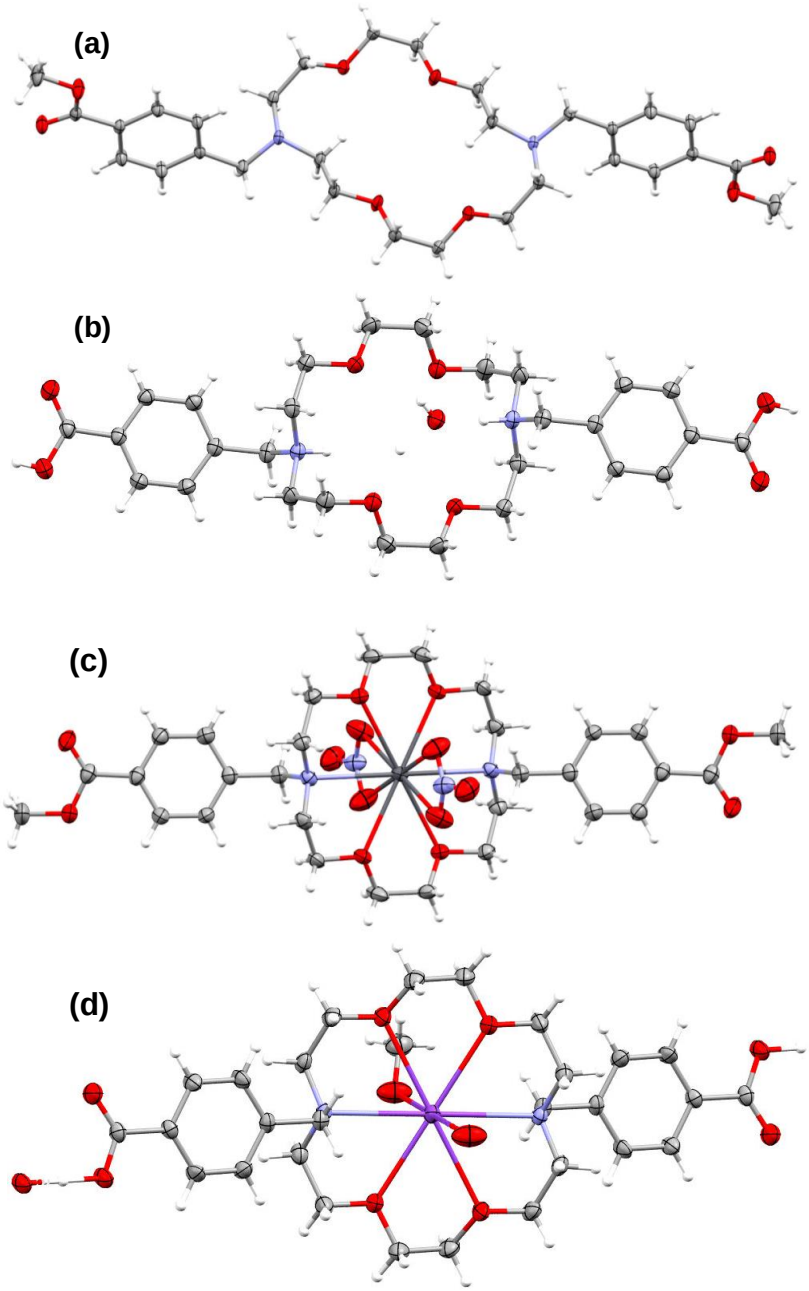

Figure 2.5 Crystal structure of the ligand: (a) ***MeL2****, (b)* ***HL2*** *and metalloligand: (c)* ***Pb-MeL2*** *and (d)* ***Na-HL2*** *complex.*

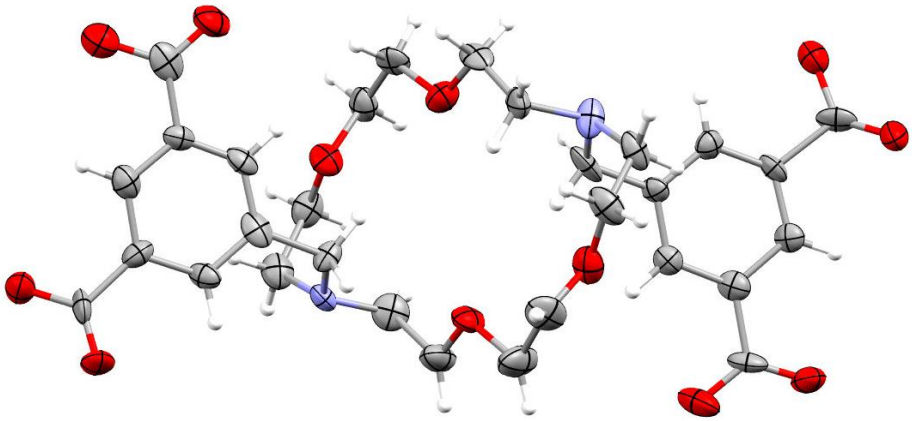

*Figure 2.6 Crystal structure of **HL3**.*

Metalation of aza-crown ether carboxylic acids **HL2** and **HL3** was performed with a series of metal salt. Since **HL2** was obtained as a monocarboxylate salt with trapped Li/ Na/K ion, the ligand was highly soluble in water and high polar organic solvents such as DMF, DMA and DMSO. However, the solubility was much lower in hydrophilic solvents such as methanol, ethanol, acetonitrile and THF even at hot condition. Layering dilute solutions of **HL2** in water, methanol, DMF or DMA over aqueous metal salt solutions at 1:1 metal:ligand ratio resulted in unreacted **HL2** crystals. Similarly, solvothermal reactions in either water/MeOH, water/DMF, water/DMA, methanol or DMF resulted in isolation of **HL2** crystals. In a few cases, the counter anions from the metal salts (e.g., tetrafluoborate) was present at the crystal structures, but no metal coordination was achieved under these reaction conditions. The failure of the metal complexation of **HL2** can be attributed to the presence of strongly coordinated alkali metals in the aza-crown ether cavity, from where displacement of the metal ion was proved to be a daunting task.

The ligand **HL3** was moderately soluble in water and other organic solvents (methanol, ethanol, DMF, DMA and DMSO). The solution of **HL3** in organic solvents was layered over aqueous metal salt solutions at 1:1 and 2:1 metal:ligand ratio, which resulted in **HL3** crystals in 3-4 days. The solvothermal or hydrothermal reactions with zinc(II), cobalt (II), nickel (II) and cadmium(II) salts also produced unreacted **HL3** crystals. The copper(II) and iron(II)/(III) produced blue and red precipitate respectively in DMF under solvothermal condition, indicating that metal complexation might take place. The mixture was filtered and the solution was layered or diffused with THF/Et_2O/MeCN/1,4-dioxane etc., but single

crystal of MOMs was not obtained. The unsuccessful attempt in isolating single crystals limited the characterization of the materials.

The solvothermal reaction of **HL3** with lead(II) nitrate in DMF or a mixture of water/DMF (1:1 v/v) at 120.0 °C for 48 h produced white plate shaped single crystals. Single crystal X-ray diffraction revealed that a coordination polymer of molecular formula $[Pb_2(\mathbf{L3})(NO_3)_2]_n$ was obtained (*Figure 2.7*), where one carboxylate form each of the aromatic ring was coordinated to the lead(II) center, and the other carboxylic acid remained free. Analysis of the crystal packing revealed that the MOM does not possess a porous structure, which prevented us to study the adsorption and catalytic property of the MOM.

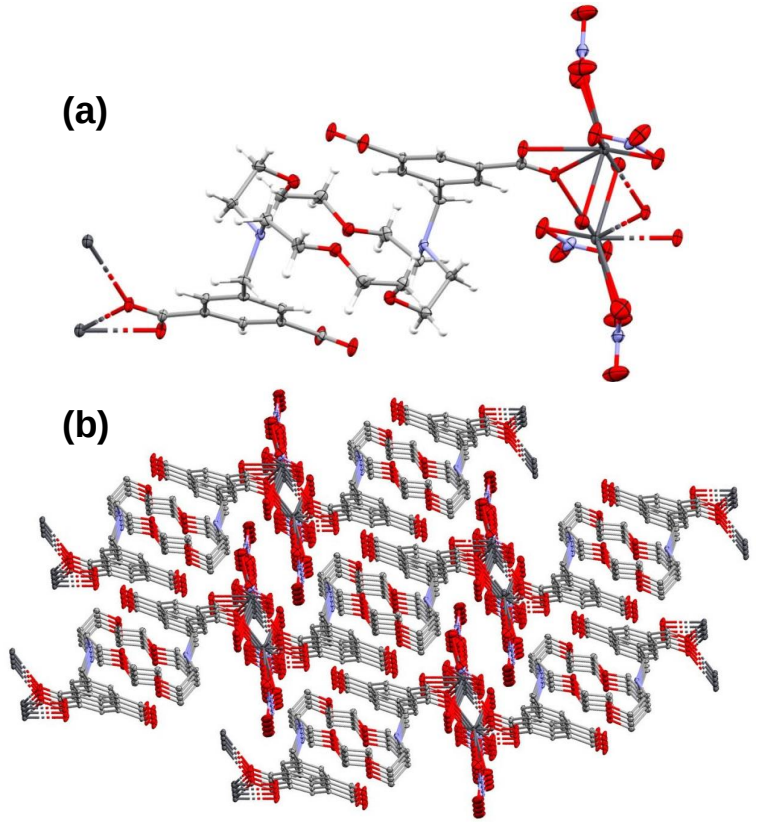

*Figure 2.7 Coordination polymer of **L3** with $Pb(NO_3)_2$: (a) asymmetric unit and (b) 3D packing.*

2.3 Multi-functional ligand based on dipicolylamine derivative

Since metalloligands were not obtained from the C_3- and C_2-macrocycles, the primary functional group was modified to simple chelating unit. Thus, di(2-picolyl)amine (DPA) moiety was chosen as the primary group, which can be considered as a subunit of the aza-cryptand or aza-crown macrocycle (*Figure 2.8*). Using the tridentate ligand will facilitate the formation of metalloligand, and the secondary functional group can be attached through the N–H moiety.

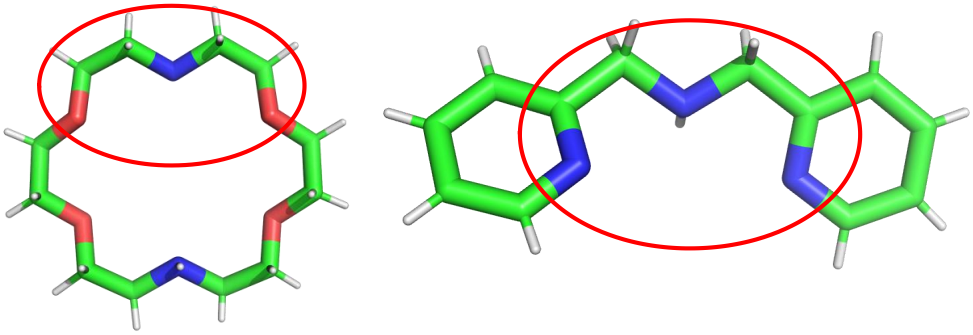

Figure 2.8 Comparison of primary functional groups in aza-crown ether and DPA.

The metal complexes of di-pyridyl ligand DPA and its transition and post-transition metal complexes have been widely investigated due to their biological, catalytic and sensing applications.[261-264] The coordination complexes of DPA are exceptionally stable, and often consist of coordinatively unsaturated metal centers, making them useful platforms for anion recognition and catalysis.[265-266] Gomez and co-workers linked two DPA units with different spacers, and coordinated to copper(II) and zinc(II) perchlorate to obtain binuclear complexes.[267] The coordinatively unsaturated copper(II) complexes showed strong binding property with different phosphorylated anions, and were used in DNA cleavage (*Figure 2.9a*). Joshi *et al* utilized similar chelating moiety to synthesize palladium complexes of NNN/CNN pincer ligands, and the complex was proved to be efficient catalysts in hetero cross-dehydrogenative coupling reaction of thiophene, furan, and benzothiazole derivatives (*Figure 2.9b*).[268] These examples indicate the large scope to utilize DPA units as an active site in MOMs.

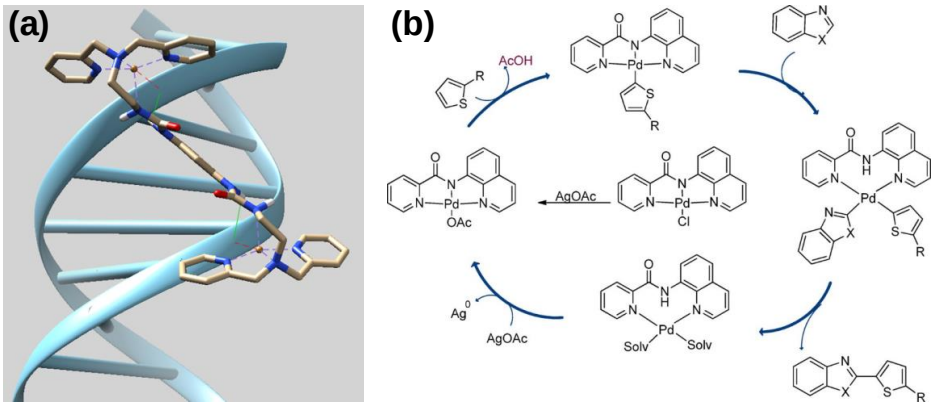

Figure 2.9 Application of DPA complexes in (a) DNA cleavage reported by Gomez and co-workers[267] *and (b) dehydrogenative coupling reported by Joshi and co-workers.*[268]

Herein, we attached an isophthalate moiety as a secondary functional group with DPA to obtain multi-functional ligand **HL4** (*Scheme 2.5*). The ligand was synthesized by reacting dipicolylamine with dimethyl 5-(bromomethyl)isophthalate to produces diester protected **HL4** (**MeL4**), which was hydrolyzed with sodium hydroxide to yield **HL4**. The ligand **HL4** was obtained as hydrochloride salt (on neutralizing the carboxylate salt with hydrochloric acid), and characterized by NMR and mass spectroscopy.

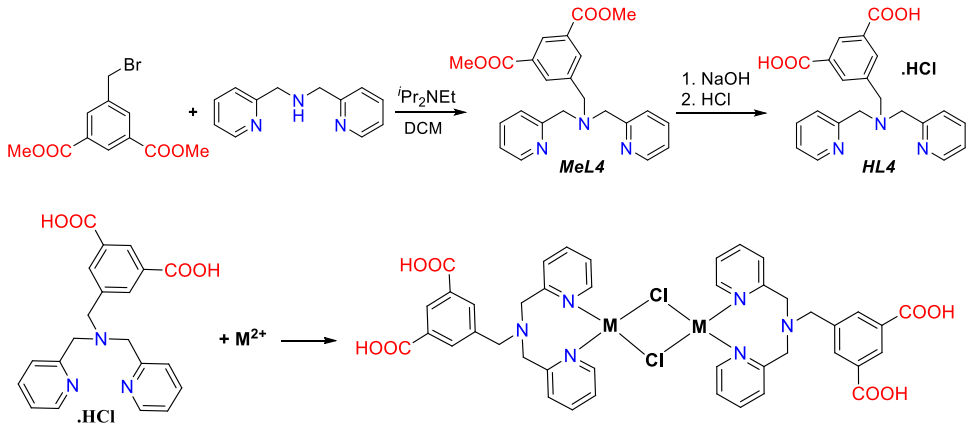

*Scheme 2.5 Synthesis of **HL4** ligand and **HL4**-metalloligands.*

Metalloligands were obtained with **HL4** on treating with various transition metals such as Cu^{2+}, Zn^{2+}, Cd^{2+} and Co^{2+} (*Figure 2.10*). X-ray quality single crystals were obtained in different solvent or solvent mixtures, for example in water, ethanol, water/ethanol and

water/DMF mixture, indicating high affinity of the chelating moiety to transition metals. In a typical experiment, a solution of the metal salt was layered over a solution of **HL4.HCl**, and X-ray quality single crystals were obtained in 1-2 days. Interestingly, the counter anion chloride was involved in the formation of the metalloligand, which was evident by the presence of chloride anion in the crystal structure and the crystals were obtained by reacting **HL4** with various nitrate salts. The metalloligands of cadmium(II) and zinc(II) were obtained as dimer of two individual complexes bridged by the chloride ions.

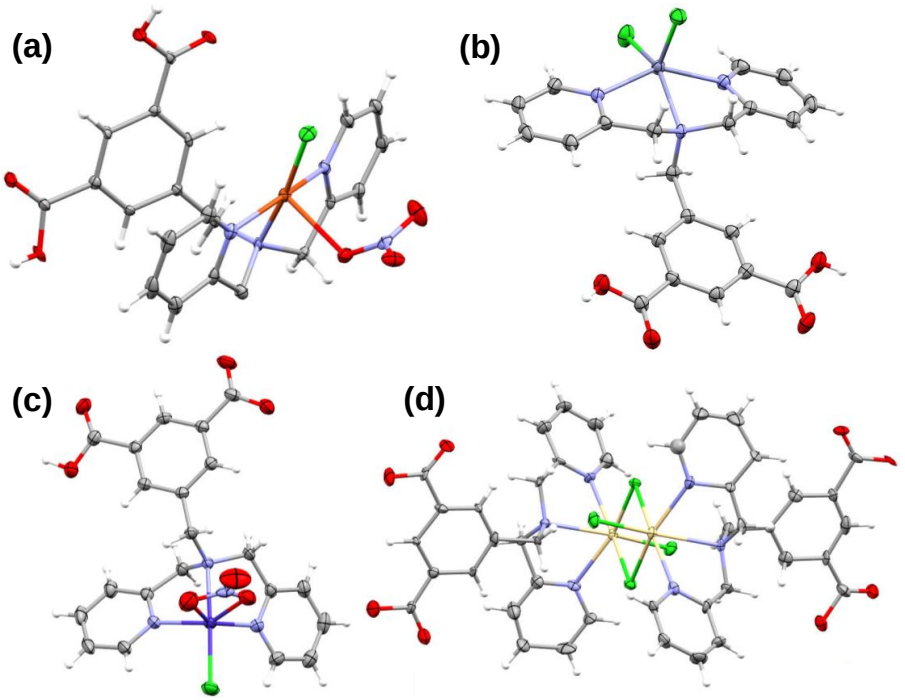

Figure 2.10 ***HL4****-metalloligands with (a)* Cu^{2+}*, (b)* Zn^{2+}*, (c)* Co^{2+} *and (d)* Cd^{2+} *salts.*

Unfortunately, the attempts to obtain bimetallic MOMs using the DPA-metalloligands were not successful. A reaction of the metalloligand and a second metal salts at room temperature or high temperature produced either the unreacted metalloligand, or a different metalloligand produced by the metal exchange. For example, reaction of Cu-DPA metalloligand with other metal salts always resulted in unreacted Cu-DPA crystals. On the other hand, mixing Zn-DPA, Cd-DPA or Co-DPA metalloligands with copper(II) salts produced the Cu-DPA crystals, indicating that the Zn^{2+}, Cd^{2+} or Co^{2+} ions were replaced by the Cu^{2+} ion. This can be attributed to the strong coordinating ability of the copper(II) ion, which always forms the complex with DPA moiety.

2.4 Metalloligands based on copper(II) paddle-wheel complexes

The unsuccessful attempt with multi-functional ligands prompted us to explore paddle-wheel complexes of simple ligands as metalloligands. Among several types of SBUs known till date, paddle-wheel type clusters have been most ubiquitous and mostly utilized as catalytic center. Paddle-wheel clusters possesses general formula of $[M_2(\mu–O_2C–R)_4]$ where the metal ion acquires an octahedral geometry with four bridging carboxylate oxygen at equatorial position and the solvent molecules occupy the axial position (*Figure 2.11a*). Paddle-wheel metal complex units have been extensively used as homogenous and heterogeneous catalyst across a remarkable range of organic reactions such as cyclopropanation, C–H insertion, C–N coupling, formation of cyclic carbonates, oxidation of alcohols to aldehydes, three-component coupling etc.[269-274] Dirhodium(II,II) paddle-wheel complex is recognized as one the most efficient paddle-wheel clusters due to high stability and excellent catalytic activity, but the major drawback of rhodium complexes is the limited availability and utmost cost. Thus, paddle-wheels based on copper(II) center became popular, and in recent time, copper(II) paddle-wheels have emerged as a very important class of heterogeneous catalyst. Back in 1999, Williams *et al* synthesized the MOF HKUST-1 consisting a copper(II) paddle-wheel SBU and benzene-1,3,5-tricarboxylate[275] and since then the incorporation of copper(II) paddle-wheel SBU in MOFs has grown rapidly. MOFs with paddle-wheel SBU offer enhanced thermal stability of the cluster, and the functionalization promotes interesting properties including catalysis. *Figure 2.11b* displays a typical example of asymmetric aminolysis catalyzed by copper(II) paddle-wheel SBU.[276]

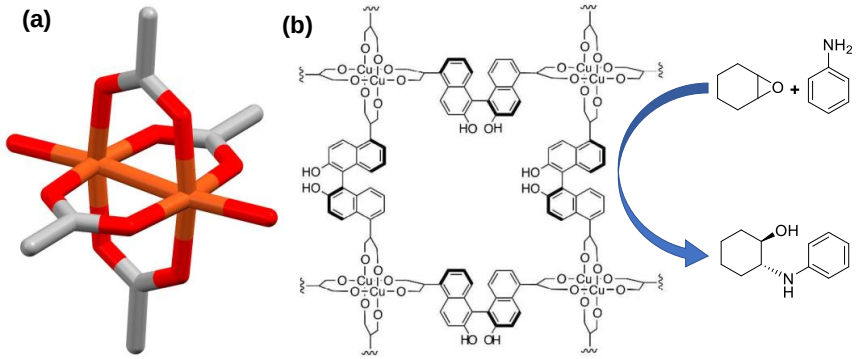

Figure 2.11 (a) Paddle-wheel SBU and (b) catalytic activity of paddle-wheel center reported by Hirao et al.[276]

Our aim is to incorporate the paddle-wheel units in bimetallic MOMs, where copper(II) paddle-wheel complexes can be utilized as metalloligands. We have developed an experimental procedure to obtain paddle-wheel cluster having a general formula $[Cu_2(OOC\text{-}C_6H_4\text{-}X)_4]$ by reacting bifunctional ligands ($X\text{-}C_6H_4\text{-}COOH$) with copper(II) salt (X = COOR/ OH/ SH etc.). All these complexes have free secondary binding site such as carboxylate esters, hydroxy, thiol etc., thus the complexes can be considered as metalloligands. The paddle-wheel complexes can further coordinate with a different metal ion to form bimetallic coordination polymers or MOMs. Single crystal X-ray structure revealed that the axial position of paddle-wheel cluster is occupied by solvent molecules. Removal of weakly coordinating solvents leads to coordinatively unsaturated metal centers, which are excellent catalytically active sites. Easy and quick synthesis of the complexes and inexpensive starting materials make this ideal candidate for the synthesis of bulk catalyst. These paddle-wheel complexes can be treated as secondary building units (SBU) and combine a second metal ion to form porous crystalline motifs.

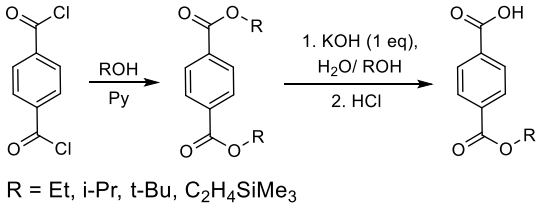

Scheme 2.6 Synthesis of mono-ester protected terephthalic acids.

The monoester derivatives of terephthalic acid were synthesized following the general two step synthetic procedure. In the first step, the diesters were synthesized by the reaction of terephthaloyl dichloride and appropriate alcohol, followed by the removal of one ester group by treating with one equivalent of potassium hydroxide (*Scheme 2.6*), or lithium hydroxide (for benzyl ester) or tetra-n-butylammonium fluoride (for 2-trimethylsilyl ethyl ester).

Copper(II) paddle-wheel complexes of monoester protected terephthalic acid were synthesized by reacting $Cu(NO_3)_2.3H_2O$ and corresponding ligand in ethanol, DMF or water. The axial positions were occupied by two solvent molecules in every case (*Scheme 2.7 and Figure 2.12*).

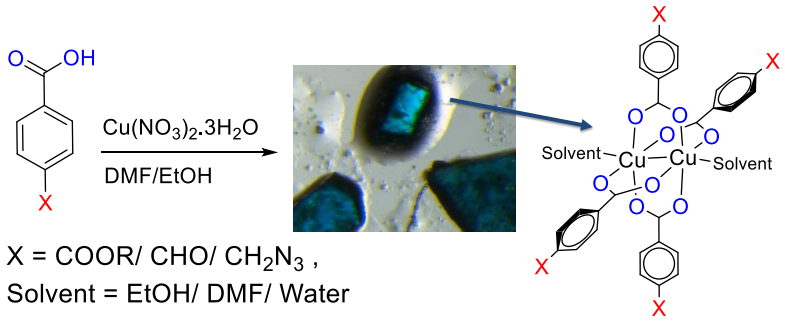

Scheme 2.7 Synthesis of Cu(II)-paddlewheel complexes.

Our aim was to hydrolyze the ester group in theses complexes to make copper(II) paddle-wheel complexes with free carboxylic acids, which will be used for second metalation. But unfortunately, both acid- and base-catalyzed hydrolysis reactions resulted in decomposition of the paddle-wheel complex. The *in situ* hydrolysis of the complex and a second metalation was also tried at high temperature, but a simple copper(II)-terephthalic acid coordination polymer was obtained after the reaction. In order to overcome the problem, we tried to synthesize a copper(II)-terephthalic acid monobenzyl ester paddle-wheel complex, since the benzyl esters can be hydrolyzed in much mild condition (10%Pdin activated charcoal and H_2 gas).[277] Thus, the dibenzyl terephthalate was synthesized by the reaction of terephthaloyl dichloride and benzyl alcohol, and one of the ester groups was hydrolyzed with one equivalent of LiOH. Copper(II) paddle-wheel complex of the monoester was synthesized following the similar procedure. The complex was synthesized in ethanol, DMF and also in 1:1 (v/v) DMF/EtOH mixture. The axial position was found to

be coordinated with EtOH molecule in the first case whereas DMF coordinated in other two experiment. It was observed that the DMF-coordinated complex was more stable, as it retained the crystallinity and original color for much longer time. Thus, the ester hydrolysis was carried out mainly on the DMF-coordinated complex.

The hydrolysis of the benzyl ester in the paddle-wheel complex was attempted in different conditions. First, the EtOH coordinated complex was dissolved in absolute ethanol and was placed in Parr reactor with 10% Pd/C. After the reaction, the blueish green color of the solution turned colorless, and the evaporation of the ethanol produced a white solid. On characterization, it was observed that paddle-wheel framework was decomposed and ester group was not hydrolyzed. Thus, the hydrolysis was attempted for the DMF-coordinated complex by dissolving in minimum volume of DMF and adding absolute ethanol. The mixture was placed in Parr reactor along with 10% Pd/C, and subjected to hydrogenation at 60 psi pressure for 48 h. After the reaction, ethanol was evaporated and a light green solution of the product in DMF was obtained. The solution was left for crystallization and unreacted starting material crystals were obtained after few days. A green solid was obtained after the complete evaporation of DMF.

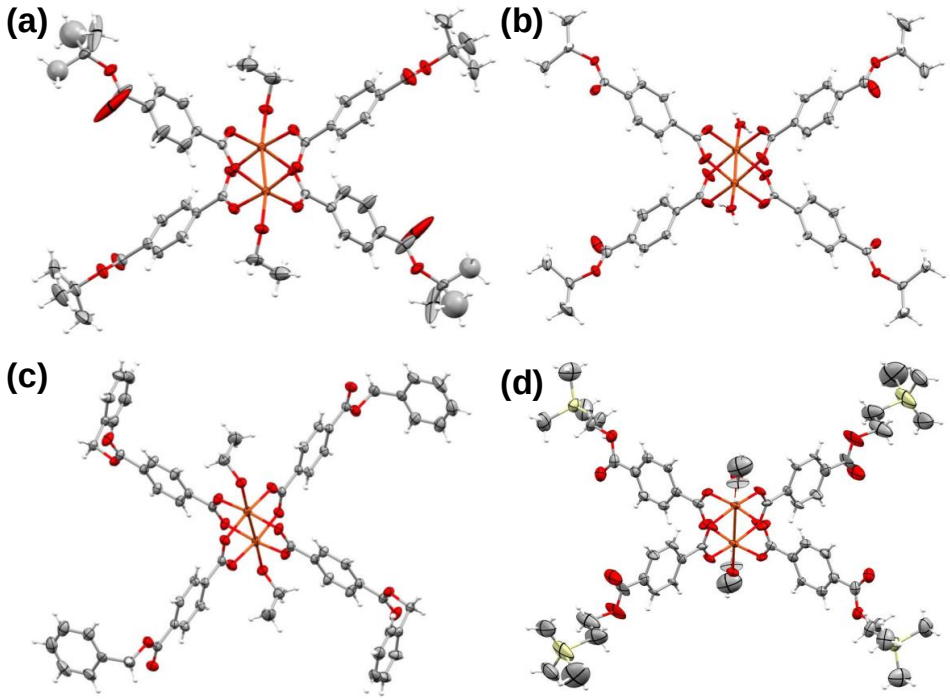

Figure 2.12 Copper(II) paddle-wheel complexes of terephthalic acid monoester derivatives: (a) tBu ester, (b) iPr ester, (c) benzyl ester and (d) 2-(trimethylsilyl)ethyl ester.

After the unsuccessful attempts to hydrolyze the ester groups, we aimed to incorporate different functional groups in paddle-wheel framework and attach the SBUs via organic reactions. A paddle-wheel complex from commercially available 4-formyl benzoic acid was successfully synthesized (*Figure 2.13a*). Attempts were made to connect the aldehyde functionalized SBUs by reacting with *p*-phenylenediamine to get a Schiff base polymer.

However, the attempts turned out to unsuccessful and a black precipitate was obtained in all cases. Similar results were observed when *p*-toluenesulfonic acid (*p*-TSA) salt (2:1) of *p*-phenylenediamine was used instead of free p-phenylenediamine. A paddle-wheel complex with 4-(azidomethyl) benzoic acid was also synthesized (*Figure 2.13b*), which was subjected to 'click reaction' with 1,4-diethynylbenzene. Unfortunately, this attempt also turned out to be unsuccessful and no product was obtained.

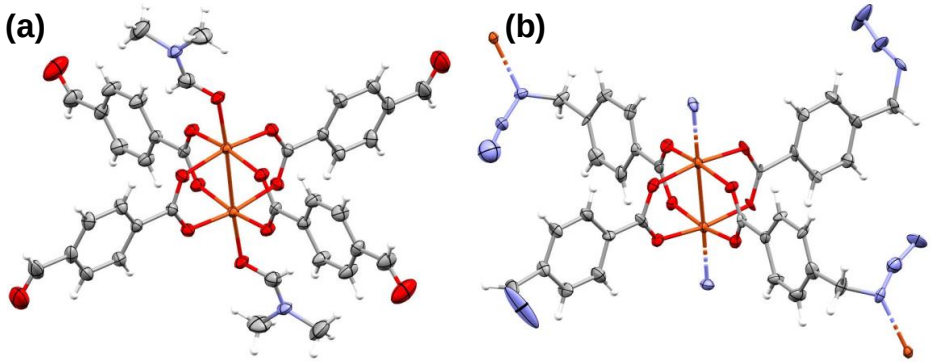

Figure 2.13 Copper(II) paddle-wheel complexes of (a) 4-formyl benzoic acid and (b) 4-azidomethyl benzoic acid.

The reaction of $Cu(NO_3)_2.3H_2O$ with 4-mercaptobenzoic acid at 1:2 metal:ligand ratio in ethanol resulted in a coordination polymer instead of a complex. Crystal structure of the MOM revealed that two copper(II) centers were bridged by four carboxylates of four ligand molecules, forming a typical paddle-wheel unit, and the solvent ethanol is coordinated to the axial positions (*Figure 2.14a*). Interestingly, the sulfur atoms of the –SH moiety were connected by S–S bond, resulting in the formation of a 2D coordination polymer. The 3D packing of the MOM indicated very small pores, which were occupied by water molecules (*Figure 2.14b*). The possibility to utilize the MOM and all the paddle-wheel complexes as homo/ heterogeneous catalyst in C–H and N–H insertion reactions is ongoing.

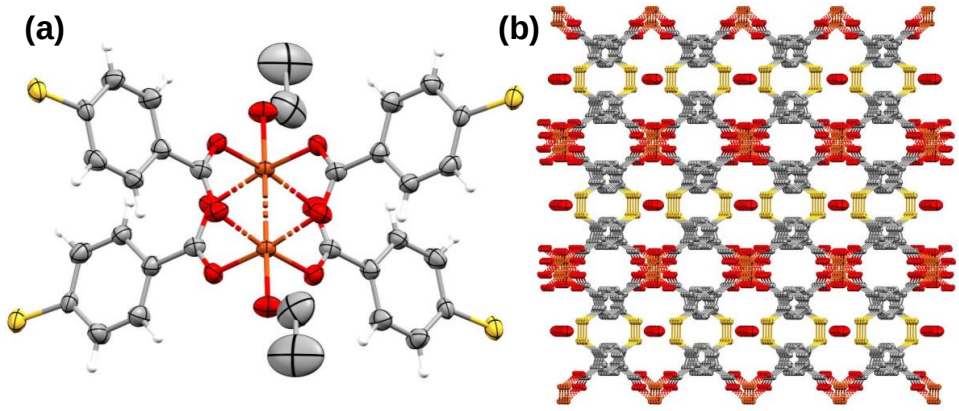

Figure 2.14 Copper(II) paddle-wheel polymer of 4-mercapto benzoic acid (a) asymmetric unit and (b) 3D packing.

2.5 Multi-functional ligand based on hydrogen bonding motifs

As mentioned above, an alternative approach to construct multi-functional MOMs is to utilize ligands with a binding site and a preinstalled functional organic moiety. Usually, hydrogen-bonding groups such as urea, amide, amine etc. are chosen as the functional moieties, which can interact to the substrate via hydrogen-bonding. We have selected urea group as the functional organic moiety and carboxylic acid as binding site. The Urea groups are known to form two-point hydrogen bonding through N–H moiety and interacts with electron rich substrate like CO_2. Thus, urea-based catalyst have been widely used for various reactions including CO_2 conversion in homogenous medium.[278] A dicarboxylic acid with urea group (**HL5**) was synthesized to incorporate the urea-motif in MOM. The ligand was previously reported,[75-76, 78, 279] and was synthesized by modifying the reported procedure. In the first step, isopropyl-4-aminobenzoate was reacted with triphosgene in presence of triethylamine to obtain the ester protected ligand (**^{i}PrL5**), which was hydrolyzed with sodium hydroxide to yield the compound **HL5** (*Scheme 2.8*).

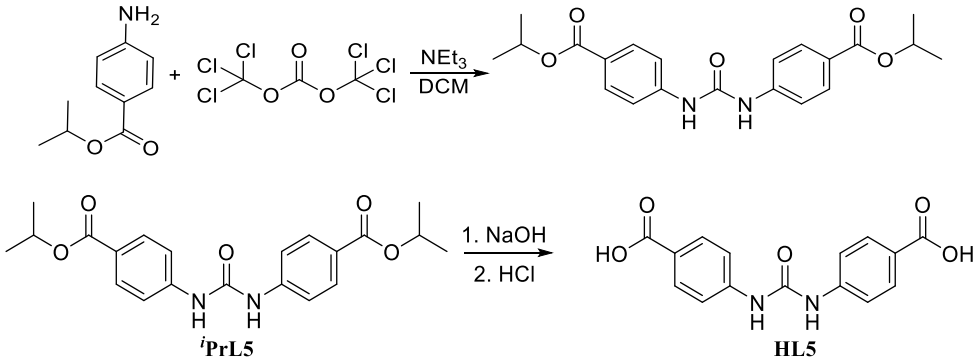

*Scheme 2.8 Synthesis of **HL5**.*

2.6 Synthesis, characterization and application of MOMs in heterogeneous catalysis

The urea-containing multi-functional ligand *N*,*N*′-bis(4-carboxyphenyl)urea (**HL5**) were reacted with various metals at different reaction conditions (layering, high temperature, solvothermal etc.). Layering of **HL5** with copper(II) salts yielded a green needle-shaped crystalline material. The ligand was treated with copper(II) nitrate, perchlorate, sulfate, chloride and acetate salts but X-ray quality crystals were obtained only with copper(II) sulfate (*Scheme 2.9*). Different experiments by varying solvent suggested that water/DMF mixture was best solvent system to obtain crystals. SCXRD data revealed that a porous coordination polymer (**HI-101**) was obtained.

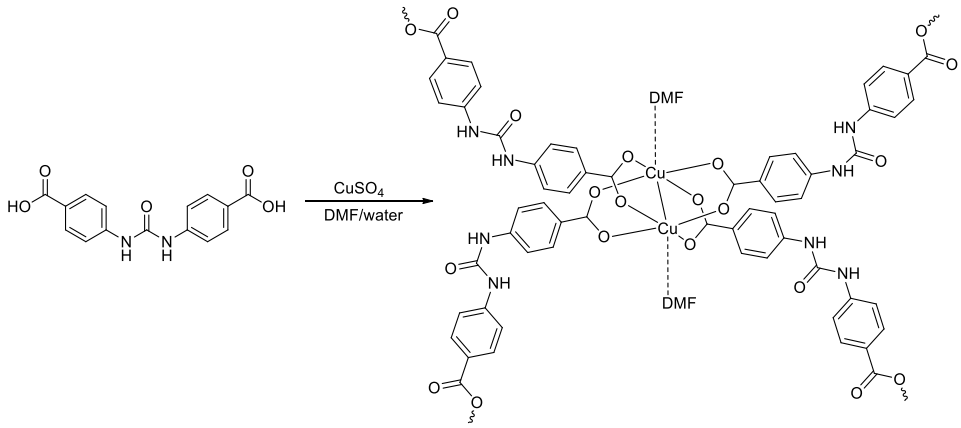

*Scheme 2.9 Synthesis of **HI-101**.*

Single crystal X-ray diffraction revealed that **HI-101** crystallized in the tetragonal space group P4/mcc with a formula of $[Cu_2(\mathbf{L5})_2(DMF)_2]_n$. The copper(II) center formed a paddle-wheel cluster with four ligands at the equatorial positions, and the axial positions are occupied by two DMF molecules. The paddle-wheel moieties are connected by the ligand to form a 4,4' network, and a planner 2D sheet is generated. The orthogonal 2D sheets interpenetrated each other to form a two-fold interpenetrated network (*Figure 2.15*), resulting in the overall 3D framework.

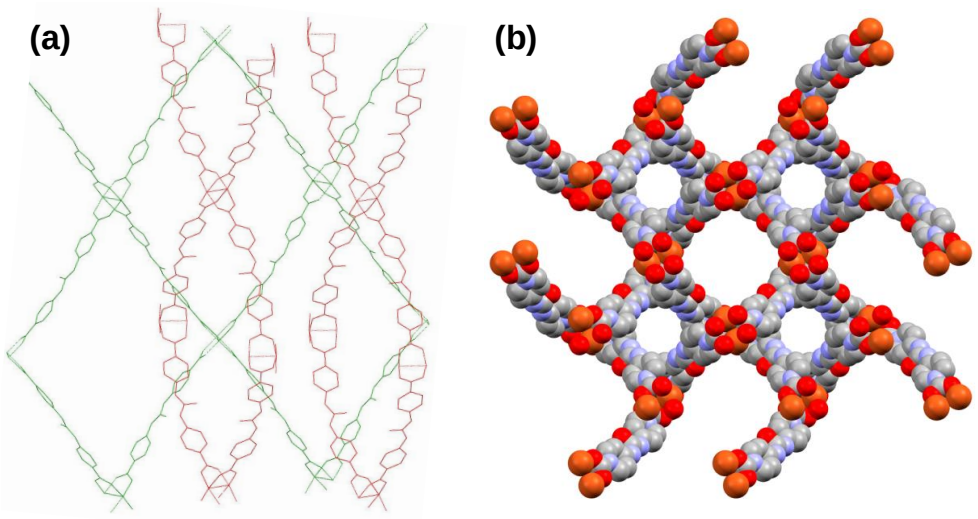

*Figure 2.15 Single crystal structure of **HI-101**: (a) 2-fold interpenetrating network and (b) spacefill model displaying porous architecture.*

2.6.1 Evaluation of catalytic property

The combination of copper paddle-wheel cluster and a urea functionalized linker, along with the porous architecture of **HI-101** prompted us to analyze the catalytic activity of **HI-101**.[273, 280] The crystalline material was isolated and dried under high vacuum at 60.0 °C for 36 h to activate the catalyst. The catalytic activity of **HI-101** was tested in three different reactions such as CO_2 fixation, methanolysis and alcohol oxidation (*Scheme 2.10*).

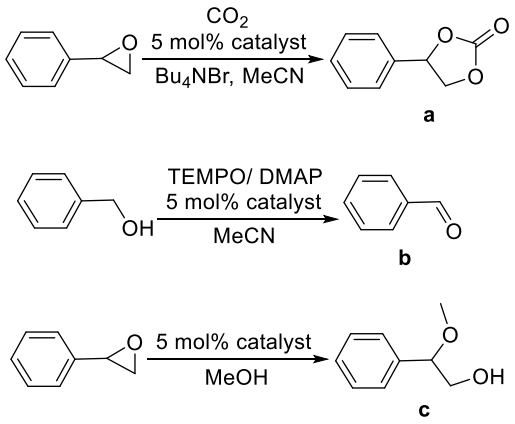

*Scheme 2.10 Catalytic reactions by **HI-101**: (a) CO_2 fixation (b) alcohol oxidation and (c) methanolysis.*

CO_2 fixation

The conversion of CO_2 to useful organic compounds have emerged as a prolific area of current research because of the fact that CO_2 can be used as renewable, non-toxic, environmentally friendly and inexpensive C1 resource. Due to the non-reactive nature and stable configuration, the activation of inert CO_2 is usually achieved by catalysts.[281-282] The chemical fixation of CO_2 with epoxides to form cyclic carbonates is particularly noteworthy due to extensive use of the product as synthetic intermediate of complex molecules, polar aprotic solvents, lithium ion batteries, precursor for polycarbonates and raw material for engineering plastics.[281-282] Recently, MOMs based catalytic conversion of CO_2 to cyclic carbonate [283-285] have gained immense attention because of their remarkable affinity for CO_2. For example, the presence of coordinatively unsaturated metal sites are well known to bind with CO_2 and converting it into useful organic products.[243, 286] This prompted us to test the catalytic activity of **HI-101** in CO_2 conversion reaction in the cycloaddition reaction of epoxide and CO_2 to form cyclic carbonate. The experiments performed at room temperature and normal pressure with styrene oxide as starting epoxide did not yield the desired product. The catalytic reaction performed at elevated temperature or by increasing the pressure (up to 3 bar) and in presence of various additives such as tetrabutylammonium bromide (TBAB) and tetrabutylammonium fluoride (TBAF) also resulted in similar results.

Interestingly, CO_2 conversion was achieved when the pressure was increased to 10 bar. This was achieved by stirring styrene oxide (240.0 mg, 2.0 mmol), **HI-101** (75.0 mg, 0.1 mmol) and TBAB (64.0 mg, 0.2 mmol) as co-catalyst in 2.0 mL of acetonitrile at room temperature under 10 bar CO_2 pressure for 36 h. The reaction performed without TBAB additive resulted in very low yield indicating the importance of the additive in these reactions. We have also tested the reaction with only $Cu(OAc)_2.H_2O$ to see the effect of metal salts in the reaction and no product formation was observed. A blank reaction under same reaction conditions, a reaction with only free ligand **HL5** and reaction with only $Cu(OAc)_2.H_2O$ were also performed. The product was not formed in all these cases indicating the presence of both Cu-paddle-wheel moiety and urea functionality in **HI-101** for the catalytic activity. The reaction was repeated under similar condition (2 mmol substrate, 0.1 mmol **HI-101** and 0.2 mmol TBAB) with epichlorohydrin as starting material, and epichlorohydrin carbonate was obtained at 80.0% yield.

*Table 2.1 CO_2 fixation of styrene oxide catalyzed by **HI-101**.*

Entry	Additive	CO_2 pressure (bar)	Time (h)	Temperature (°C)	% Yield[¶]
1	-	3	48	RT	-
2	-	3	48	100	-
3	TBAB	3	48	RT	-
4	TBAB	3	48	100	-
5	TBAB	10	30	RT	75
6[†]	TBAB	10	30	RT	-
7	-	10	30	RT	trace

Reaction conditions: epoxides (1.0 mmol), **HI-101** (5.0 mol %), additives (5.0 mol %), solvent- MeCN (2.0 mL), [¶]Isolated yield, [†]**HI-101** was not added.

The heterogeneous mixture obtained after reaction was centrifuged, and the supernatant liquid was decanted. The solid residue (**HI-101**) was washed three times with acetonitrile and was reactivated by heating at 60.0 °C under vacuum for 24 h. The recovered catalyst

was reused without further purification for the second run with fresh epoxide and TBAB. When the recovered MOM catalyst was used in cycloaddition of epichlorohydrin and CO_2, 50.0% cyclic carbonate product was obtained under same reaction condition. The decrease in product formation may be attributed to leaching of **HI-101** during the reaction, hence a partial regeneration of the catalyst taking place. When the catalyst was recovered second time and was subjected to third catalytic cycle, 45.0% product was obtained. In agreement with previously reported works,[287-289] a possible mechanism of the cycloaddition reaction has been proposed. First epoxide binds with coordinatively unsaturated copper(II) center, hence activating the epoxide toward nucleophilic substitution. In next step, nucleophilic bromide ion generated from cocatalyst TBAB attacks terminal carbon of the epoxide. The urea group of the linker simultaneously activates CO_2 by hydrogen bonding and facilitates the interaction between epoxide oxygen and CO_2 C atom. Formation of cyclic carbonate is accomplished by bond formation between CO_2 oxygen and terminal carbon of epoxide, with release of bromide.

Methanolysis

The ring-opening reaction of epoxides by alcohols (alcoholysis) is catalyzed by a variety of Lewis or Bronsted acid resulting in 1,2-bifunctional compounds having pharmaceutical and agrochemical interest.[280, 290] The catalytic activity of **HI-101** in methanolysis of styrene oxide was evaluated. A mixture of styrene oxide (120.0 mg, 1.0 mmol) and **HI-101** (35.0 mg, 0.05 mmol) in 2.0 mL methanol was stirred at room temperature, and the formation of 2-methoxy-2-phenylethanol was monitored by ^{1}H-NMR. Conversion of the starting material to the product was calculated from the ratio of peak integration. About 60.0% conversion was observed after 2 days, the reaction mixture was stirred for another 3 days and the starting materials completely disappeared (isolated product yield: 95.0%). Methanolysis of epichlorohydrin was also performed with **HI-101**, where complete conversion of the starting material was observed in 4 days. The catalyst was recovered after reaction by centrifugation, the recovered catalyst was activated by heating at 60.0 °C under vacuum for 24 h and was recycled. On using recovered **HI-101** as catalyst under identical reaction condition, 65.0% and 70.0% methanolysis product were obtained from styrene oxide and epichlorohydrin respectively. The decrease in yield after multiple cycles indicate leaching of the active catalytic center. The reaction performed with only free ligand **HL5,** reaction with only $Cu(OAc)_2.H_2O$ and a blank reaction under same reaction conditions resulted in trace amount of the product (~ 10%).

Table 2.2 ***HI-101*** *catalyzed methanolysis of styrene oxide.*

Entry	Catalyst	Time (d)	% Yield[¶]
1	-	5	9
2	$Cu(OAc)_2.H_2O$	5	10
3	**HL5** ligand	5	9
4	**HI-101**	5	95
5	**HI-101**	2	60
6	**HI-101**[†]	5	64
7	**HI-101**[‡]	5	41

Reaction conditions: epoxides (1.0 mmol), **HI-101** (5.0 mol %), MeOH (2.0 mL), temperature- RT, [¶]Isolated yield, [†]catalyst after 1st recycle, [‡]catalyst after 2nd recycle.

Alcohol oxidation

Catalytic activity of **HI-101** was further investigated for aerobic oxidation of primary alcohol with 2,2,6,6-tetramethylpiperidine 1-oxyl (TEMPO) free radical.[291] Benzyl alcohol was selected as representative primary alcohol. A series of experiments were carried out at room temperature and at 70.0 °C under atmospheric pressure using air (O_2) as the oxidant, and the results are summarized in Table 2.3. Table 2.3 shows the role of different catalyst and additive. The product benzaldehyde was obtained only in presence of 4-(dimethylamino)-pyridine (DMAP) as base and was isolated in good yield (90.0%) within 8 h. The reaction preformed with $Cu(OAc)_2.H_2O$ in presence of 4-dimethylaminopyridine (DMAP) also resulted in moderate yield (60.0%). However, the reactions performed with only free ligand and blank reaction resulted in trace amount of the product (<10%), which indicates that the oxidation reaction is catalyzed by copper(II) center.

Table 2.3 ***HI-101*** *catalyzed oxidation of benzyl alcohol.*

Entry	Catalyst	Additive	Time (h)	% Yield[¶]
1	-	DMAP	24	Trace
2	$Cu(OAc)_2.H_2O$	DMAP	24	60
3	**HL5** ligand	DMAP	24	Trace
4	**HI-101**	-	24	-
5	**HI-101**	DMAP	8	90

Reaction conditions: epoxides (1.0 mmol), **HI-101** (5.0 mol %), additives (5.0 mol %), solvent- MeCN (6.0 mL), temperature- 70.0 °C [¶]Isolated yield.

2.7 Experimental section

The synthetic procedure for multi-functional ligands, metalloligands and MOMs are described below.

2.7.1 Cryptand derivative

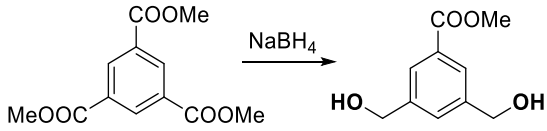

Synthesis of methyl 3,5-bis(hydroxymethyl)benzoate: Trimethyl-1,3,5-tricarboxybenzoate (5.0 g, 19.8 mmol) was placed, along with a stirring bar, in a two-neck 100 mL flask equipped with a reflux condenser and a 20 mL addition funnel. While maintaining a dry nitrogen atmosphere, anhydrous THF (15.0 mL) was added to the reaction flask resulting in a clear solution. $NaBH_4$ (1.8 g, 47.6 mmol) was then added to this solution thus forming a suspension which was stirred continuously at room temperature. While stirring, a mixture of THF/MeOH (12.5 mL / 3.7 mL) was added dropwise via the addition funnel. The reaction mixture was then refluxed for 30 min; during this time the reaction mixture changed from a transparent solution to a light yellow and back to transparent again. After cooling, the reaction was quenched with 20.0 mL of 1.0 N HCl. The product was then extracted with EtOAc (3 x 25.0 mL). The organic phase was dried over Na_2SO_4 and the solvent was removed in vacuum affording a white solid. The crude mixture was purified by silica gel column chromatography with EtOAc to give 1.47 g of the product (7.5 mmol, yield 38.0%) as a white solid. ^{1}H NMR (400 MHz, $CDCl_3$): δ = 7.89 (s, 2H), 7.54 (s, 1H), 4.69 (s, 4H), 3.86 (s, 3H), 1.63 (bs, 2H) ppm; 13C NMR (100 MHz, $CDCl_3$) δ 165.37, 140.90, 130.21, 128.86, 127.12, 63.43, 51.50 ppm.

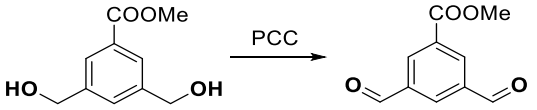

Synthesis of methyl 3,5-diformylbenzoate: Methyl 3,5-bis(hydroxymethyl)benzoate (0.9 g; 4 mmol) was added to the suspension of pyridinium chlorochromate (3.0 g, 12.0 mmol) in CH_2Cl_2 (15.0 mL). The mixture which turned quickly from orange to black was stirred overnight. Diethyl ether (20.0 mL) was added, and the residue was further extracted with

diethyl ether (3 × 10.0 mL) until the gummy residue became granular solid. The combined extracts were passed through silica, and the solvent was removed in rotavapor. ^{1}H NMR (400 MHz, $CDCl_3$): δ= 10.19 (s, 2H, CHO), 8.79 (d, J = 7.8 Hz, 2H, aromatic), 8.56 (t, J = 7.8 Hz, 1H, aromatic), 3.90 (s, 3H, COOMe).

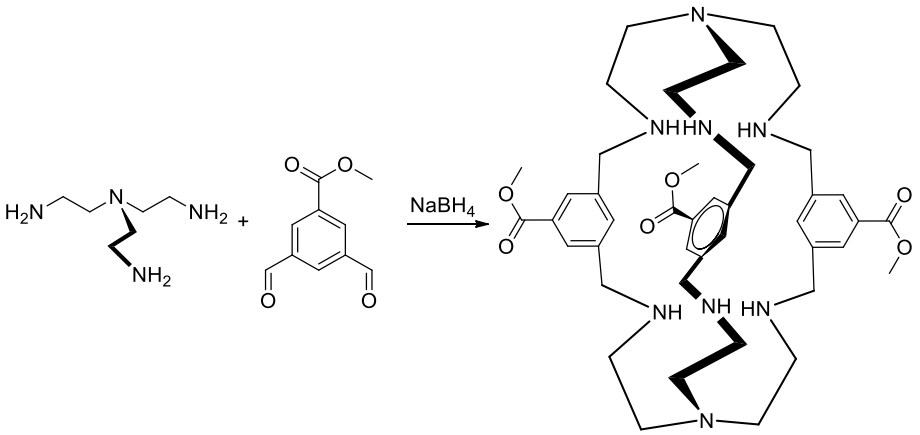

*Synthesis of substituted isocryptand ester (**MeL1**):* Methyl 3,5-diformylbenzoate (1.1 g, 5.5 mmol) was dissolved in 80.0 mL of dry MeOH and 10.0 mL (minimum volume) dry THF in a 2-neck round-bottom flask equipped with a dropping funnel and magnetic stirrer. The solution was cooled to 5.0-10.0 °C using an ice bath. A solution of tren (530.0 mg, 3.6 mmol) in 20.0 mL of dry MeOH was added dropwise (2-3 drops/min) allowing the complete dispersion of each drop between the additions with constant stirring under N_2 atmosphere. The addition of tren solution was completed in approximately 1 h and the temperature was maintained at 5.0-10.0 °C with constant stirring. After adding tren solution, the yellow solution was allowed to stir at room temperature for another 8 h. The reduction of the Schiff base thus formed was achieved by hydrogenating the mixture with $NaBH_4$ (portion-wise) for 1 hour at room temperature. The reaction mixture was stirred at room temperature for 3 h. MeOH was evaporated to dryness under reduced pressure, and the residue was treated with cold distilled water (50.0 mL). The desired cryptand was extracted with $CHCl_3$ (3 x 50 mL). The organic layer was further washed with (3 x 100 mL) distilled water and was dried over anhydrous Na_2SO_4, filtered and evaporated to obtain a colorless semisolid. The semisolid product was redissolved in hot MeCN and was allowed to crystallize at room temperature. Colorless crystals suitable for single crystal X-ray diffraction was obtained overnight. Yield 1.0 g, 71.0%. ^{1}H NMR (400 MHz, $CDCl_3$):

δ= 7.48 (s, 6H, aromatic), 7.14 (s, 3H, aromatic), 3.79 (s, 12H, $COOCH_3$), 3.56 (s, 12H, benzyl), 2.56-2.51 (m, 24H, CH_2), 1.79 (s, 6H, N-H).

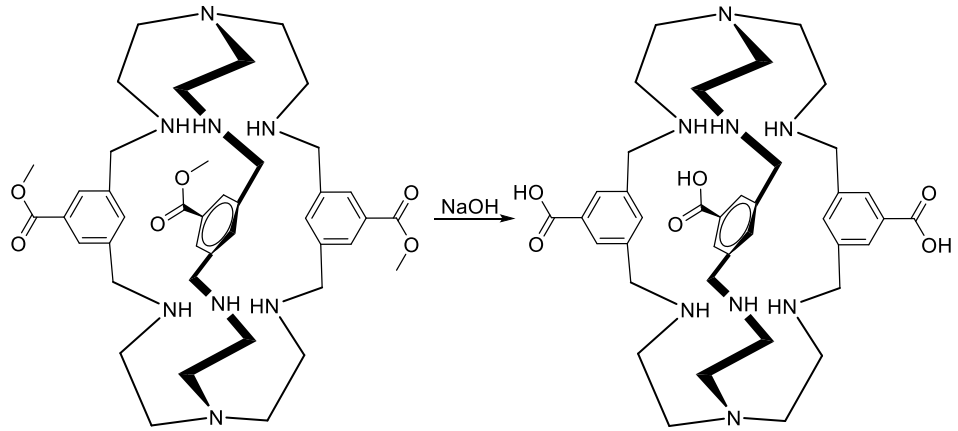

*Synthesis of substituted isocryptand acid (**HL1**):* The ester (1.0 g, 1.3 mmol) was dissolved in 50.0 mL 1:2 THF/ methanol solution, and a solution of 650.0 mg (11.7 mmol, 9.0 equivalent) KOH in 15.0 mL water was added to it. The solution was refluxed for 14 h and was cooled to room temperature. The THF/methanol was evaporated and the residue was neutralized by 1.0 N HCl. The white precipitate was centrifuged and washed with water, again centrifuged and washed with acetone. The residue was dried to yield 85.0% of the corresponding isocryptand carboxylic acid.

2.7.2 Diaza-18-crown-6 derivatives

4,13-diaza-18-crown-6 was synthesized following literature procedure[260] and the derivatives were synthesized by N-alkylation.

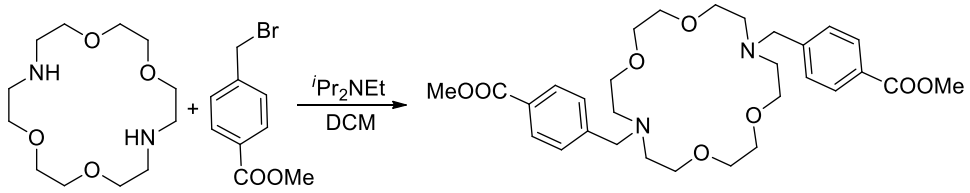

*Synthesis of N,N'-di(4-methyl benzoate)-4,13-diaza-18-crown-6 (**MeL2**):* $^{i}Pr_2NEt$ (4.0 mL, 22.8 mmol) and methyl 4-(bromomethyl)benzoate (1.83 g, 8.0 mmol) were added sequentially to a stirred solution of 4,13-diaza-18-crown-6 (1.0 g, 3.9 mmol) in dry CH_2Cl_2

(100.0 mL) at room temperature. The resultant solution was heated to 45.0°C for 24 h and allowed to cool to room temperature. DCM was evaporated and crude product was recrystallized from hot ethanol. The solution was cooled to room temperature to yield pure crystalline product (yield: 1.5 g, 69.0%).

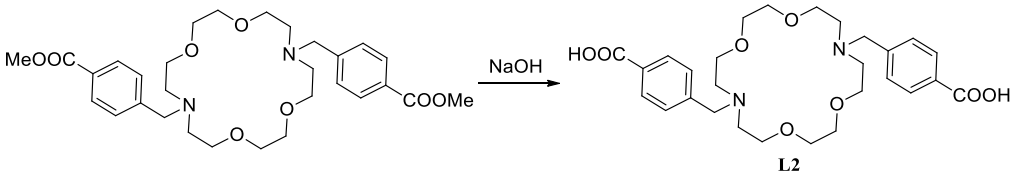

*Synthesis of N,N'-di(4-benzoic acid)-4,13-diaza-18-crown-6 (**HL2**):* The ester was dissolved in 15.0 mL ethanol, and a solution of 450.0 mg KOH in 15.0 mL water was added to it. The resulting mixture was refluxed for 14 h and was cooled to room temperature. The ethanol was evaporated and was neutralized by 50.0% HCl. The brownish precipitate was centrifuged and washed with water, centrifuged again and washed with acetone. The residue was dried to yield 85.0% of the corresponding aza-crown ether acid (yield 80.0%).

*Synthesis of N,N'-Di(4-methyl benzoate)-4,13-diaza-18-crown-6-Pb complex (**Pb-MeL2**):* A methanolic solution of *N,N*'-di(4-methyl benzoate)-4,13-diaza-18-crown-6 was layered over an aqueous solution of $Pb(NO_3)_2$. X-ray quality single crystals were obtained in 4-5 days.

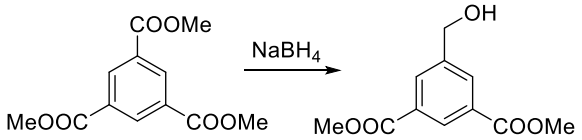

Synthesis of dimethyl 5-(hydroxymethyl)isophthalate: Trimethyl-1,3,5-tricarboxybenzoate (5.0 g, 19.8 mmol) was placed, along with a stirring bar, in a two-neck 100 ml flask equipped with a reflux condenser and a 20.0 mL addition funnel. While maintaining a dry nitrogen atmosphere, anhydrous THF (15.0 mL) was added to the reaction flask causing dissolution of the white solid. $NaBH_4$ (0.9 g, 23.8 mmol) was then added to this solution

thus forming a suspension which was stirred continuously at room temperature. While stirring, a mixture of THF/MeOH (12.5 mL/3.7 mL) was added dropwise via the addition funnel. The reaction mixture was then refluxed for 30 min; during this time the reaction mixture changed from a transparent solution to a light yellow and back to transparent again. After cooling, the reaction was quenched with 20.0 mL of 1.0 N HCl. The product was then extracted with EtOAc (3 x 25.0 ml). The organic phase was dried over Na_2SO_4 and the solvent was removed in vacuum affording a white solid. The crude mixture was purified by silica gel column chromatography with EtOAc to give 2.53 g of the product (11.3 mmol, yield 57.0%) as a white solid. ^{1}H NMR (400 MHz, $CDCl_3$): δ = 8.59 (t, 1H, J = 1.6Hz), 8.23 (t, 2H, J = 0.8Hz), 4.81 (d, 2H, J = 5.9Hz), 3.95 (s, 6H), 1.86 (s, 1H) ppm; 13C NMR (100 MHz, $CDCl_3$) δ 166.49, 142.28, 132.37, 130.93, 129.84, 64.32, 52.59 ppm.

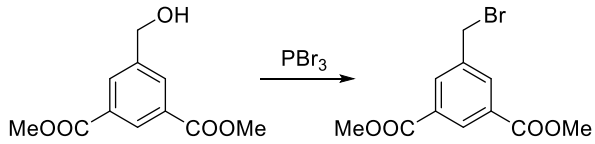

Synthesis of dimethyl 5-(bromomethyl)isophthalate: To a solution of dimethyl 5-(hydroxymethyl)isophthalate (2.24 g, 10.0 mmol) in DCM (100.0 mL), PBr_3 (5.4 g, 1.9 mL, 20 mmol) was added dropwise at room temperature. The mixture was stirred at room temperature for 15 h. The mixture was then washed with ice water, dried over Na_2SO_4 and concentrated under reduced pressure to give dimethyl 5-(bromomethyl)isophthalate in 90.0% yield. ^{1}H-NMR (400 MHz, $CDCl_3$): δ = 8.54 (t, J = 2 Hz, 1H, aromatic), 8.22 (d, J = 2 Hz, 2H, aromatic), 4.55 (s, 2H, CH_2Br), 3.90 (s, 6H, $COOCH_3$).

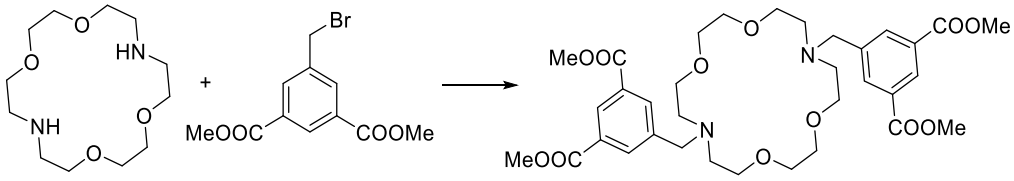

*Synthesis of tetramethyl 5,5'-((1,4,10,13-tetraoxa-7,16-diazacyclooctadecane-7,16-diyl)bis (methylene))diisophthalate (**MeL3**):* ^{i}Pr$_2$NEt (1.5 mL, 8.5 mmol) and dimethyl 5-(bromomethyl)isophthalate (1.58 g, 5.5 mmol) were added sequentially to a stirred solution of 4,13-diaza-18-crown-6 (700 mg, 2.67 mmol) in dry CH_2Cl_2 (100 mL) at room

temperature. The resultant solution was heated to 45.0°C for 24 h and allowed to cool to room temperature. DCM was evaporated and the crude product was recrystallized from hot ethanol. Cooling the solution to room temperature yield pure crystalline product (yield: 1.6 g, 89%) ^{1}H-NMR (400 MHz, $CDCl_3$): δ = 8.47 (s, 2H, aromatic), 8.13 (s, 4H, aromatic), 3.87 (s, 12H, $COOCH_3$), 3.72 (s, 4H, benzyl), 3.54-3.58 (m, 16H, O-CH_2), 2.77 (t, 8H, J = 6.0 Hz, N-CH_2).

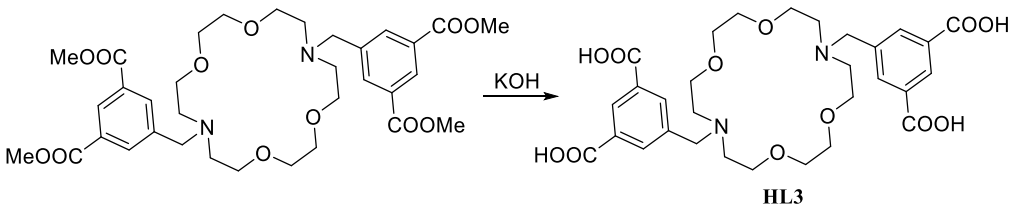

*Synthesis of 5,5'-((1,4,10,13-tetraoxa-7,16-diazacyclooctadecane-7,16-diyl)bis(methylene)) diisophthalic acid (**HL3**):* The ester **MeL3** (1.6 g, 2.47 mmol) was dissolved in 30.0 mL 1:1 THF/ methanol solution, and a solution of 450.0 mg KOH in 15.0 mL water was added to it. The reaction mixture was refluxed for 15 h, cooled to room temperature, THF/methanol was evaporated and was neutralized by 1.0 N HCl. The white precipitate was centrifuged and washed with water, centrifuged again and washed with acetone. The residue was dried to yield 1.3 g (85.0%) of the corresponding aza-crown ether tetra acid. ^{1}H-NMR (protonated compound) (400 MHz, DMSO-d_6): δ = 8.55 (s, 2H, aromatic), 8.52 (s, 4H, aromatic), 4.64 (s, 4H, benzyl), 3.94 (s, 8H, N-CH_2), 3.43-3.35 (m, 16H, O-CH_2).

2.7.3 Dipicolylamine derivative

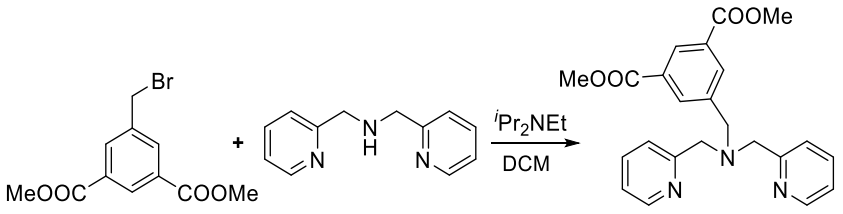

*Synthesis of dimethyl 5-((bis(pyridin-2-ylmethyl)amino)methyl)isophthalate (**MeL4**):* ^{i}Pr_2NEt (1.4 mL, 7.8 mmol) and dimethyl 5-(bromomethyl)isophthalate (2.2 g, 7.5 mmol) were added sequentially to a stirred solution of dipicolylamine (1.5 g, 7.5 mmol) in dry CH_2Cl_2 (100.0 mL) at room temperature. The resultant solution was heated to 45.0°C for

24 h and allowed to cool to room temperature. The mixture was washed with 2.0% $NaHCO_3$ solution. The organic phase was dried over sodium sulfate and evaporated. The crude product was obtained as pale yellow solid (yield: 2.7 g, 88.8%) ^{1}H-NMR (400 MHz, $CDCl_3$): δ = 8.53 (m, 3H), 8.26 (s, 2H), 7.67 (dt, 2H, J = 8.0 Hz, 4.0 Hz), 7.56 (d, 2H, J = 8.0 Hz), 7.15 (t, 2H, J = 8.0 Hz), 3.95 (s, 6H), 3.83 (s, 4H), 3.80 (s, 2H).

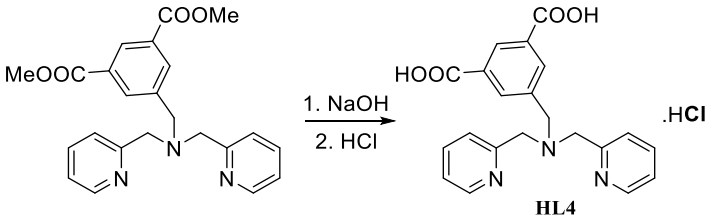

Synthesis of 5-((bis(pyridin-2-ylmethyl)amino)methyl)isophthalic acid ***(HL4):*** The ester **MeL4** (2.0 g, 5.0 mmol) was dissolved in 30.0 mL methanol, and a solution of 0.9 g KOH (16.0 mmol) in 15 mL water was added. The reaction mixture was refluxed for 12 h, cooled to room temperature, methanol was evaporated and was neutralized by 0.5 N HCl. The white precipitate was centrifuged and washed with small amount of ethanol and dried to yield 1.6 g (77.5%) of the corresponding acid as hydrochloride salt (**HL4.HCl**). ^{1}H-NMR (400 MHz, DMSO-d_6): δ = 8.43 (d, 2H, 8.0 Hz), 8.14 (t, 2H, 7.6 Hz), 7.66 (d, 3H, J = 7.2 Hz), 7.60 (t, 2H, J = 8.0 Hz), 7.48 (s, 2H), 4.09 (s, 4H), 3.54 (s, 2H).

Multi-functional ligand containing urea motif

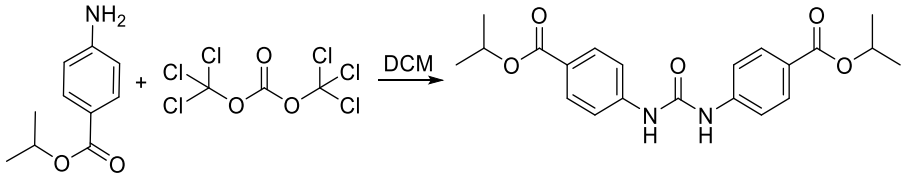

Synthesis of di-isopropyl 4,4'-(carbonylbis(azanediyl))dibenzoate ***(iPrL5):*** *iso*propyl 4-aminobenzoate (1.0 equivalent) and NEt_3 (2.0 equivalent) were dissolved in anhydrous DCM and cooled in an ice bath at 0-5.0 °C. 741.0 mg (2.5 mmol) of triphosgene was added, and the reaction was gradually brought to room temperature. It was stirred overnight at room temperature. The solvent was then removed in vacuum, and the oily compound was stirred with 2.0% sodium bicarbonate solution. It was filtered and washed with water to obtain the product. Yield 92.0%.

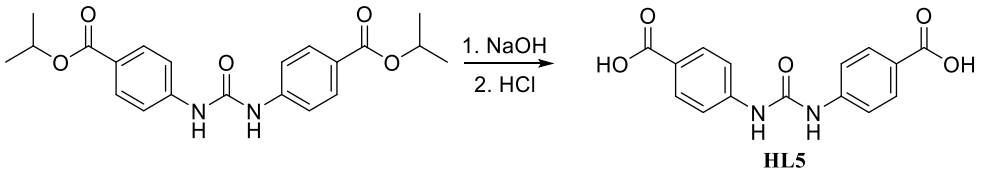

HL5

*Synthesis of 4,4'-(carbonylbis(azanediyl))dibenzoic acid (**HL5**): N,N*'-urea dicarboxylic acid isopropyl ester was dissolved in a mixture of THF/methanol and 30.0 mL sodium hydroxide solution (2.0 M) was added. The solution was stirred overnight at room temperature. After hydrolysis was complete, methanol and THF were evaporated and resulting aqueous solution was extracted with ethyl acetate to remove the unreacted ester. The aqueous layer was filtered, washed with distilled water and dried to obtain the title acid.

*Synthesis of Cu-urea acid MOF (**HI-101**):* A DMF solution of ***HL5*** (30.0 mg, 0.1 mmol) was layered over an aqueous solution of $CuSO_4.5H_2O$ (25.0 mg, 0.1 mmol). X-ray quality single crystals were obtained within one week.

2.7.4 Synthesis of monoester protected terephthalic acid

The compound was synthesized following general procedure reported in literature.[270, 292-294] First, a diester was synthesized by reacting terephthaloyl dichloride and corresponding alcohol in presence of pyridine. Then one of the ester groups was selectively deprotected by reacting with one equivalent of suitable reagent.

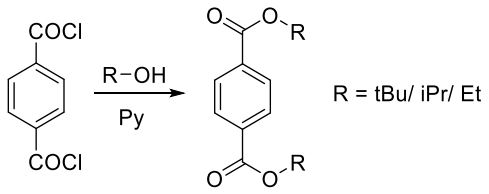

Synthesis of ethyl, isopropyl, tertbutyl diesters: Pyridine (1.0 mL) was added to a mixture of terephthaloyl dichloride (464.0 mg, 2.28 mmol) in corresponding alcohol (7.0 mL). After stirring overnight, saturated aqueous NH_4Cl was added, and the mixture was extracted with CH_2Cl_2, dried (Na_2SO_4), and evaporated in vacuum. The diesters were obtained as white solid at 95.0-98.0% yield.

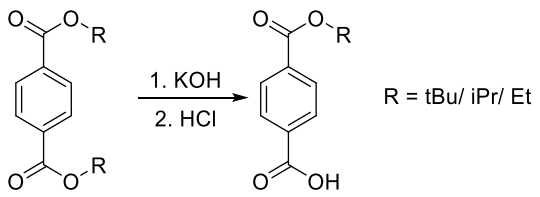

Synthesis of ethyl, isopropyl, tertbutyl monoesters: To the starting diester (10.0 mmol), 30.0 mL of corresponding alcohol was added, and the mixture was heated for 15 min. Potassium hydroxide (1.0 equivalent) was poured into the solution, and then the mixture was heated for 3.5 h under reflux. The mixture was cooled, and the alcohol was evaporated. The resulting crude product was dissolved in water and extracted with DCM. The aqueous layer was acidified with concentrated hydrochloric acid. The precipitate was then filtered or extracted with ethyl ether, dried over magnesium sulfate, and concentrated under reduced pressure.

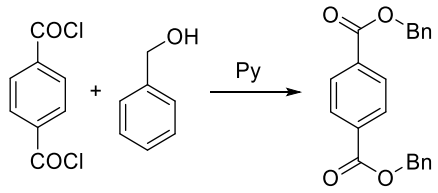

Synthesis of dibenzyl terephthalate: A solution of 5.0 mL pyridine, 10.0 mL benzyl alcohol and 30.0 mL dry DCM was added dropwise to a mixture of terephthaloyl dichloride (4.64 g, 22.8 mmol) in dry DCM (50.0 mL). After stirring overnight, the DCM was evaporated and saturated aqueous NH_4Cl was added. The mixture was extracted with CH_2Cl_2, dried (Na_2SO_4), and evaporated in fume hood. The product was obtained as a mixture with excess benzyl alcohol. It was purified by column chromatography (pet ether) to obtain pure dibenzyl terephthalate as a white solid. Yield: 7.34 g, 93.0%. ^{1}H NMR (400 MHz, $CDCl_3$): δ = 7.52 (s, 4 H, terephthaloyl-H), 7.35-7.48 (m, 10 H, phenyl-H), 5.39 (s, 4 H, benzyl-H).

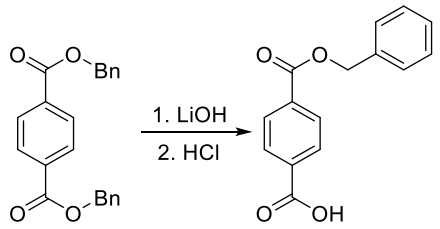

Synthesis of 4-((benzyloxy)carbonyl)benzoic acid: To the starting solution of dibenzyl terephthalate (3.88 g, 20.0 mmol) in 50.0 mL of methanol, finely powdered lithium hydroxide (1.122 g, 20.0 mmol, 1.0 equivalent) was added, and then the mixture was heated for 3.5 h under reflux. The mixture was cooled, and methanol was evaporated. The resulting crude product was dissolved in water and extracted with dichloromethane. The aqueous layer was acidified with 50.0% hydrochloric acid. The precipitate was then filtered or extracted with DCM, dried over sodium sulfate, and concentrated under reduced pressure. 4-((benzyloxy)carbonyl)-benzoic acid, yield 2.77 g 77.0%. ^{1}H NMR (400 MHz, $CDCl_3$): δ = 8.10 (s, 4H, terephthaloyl-H), 7.29 – 7.40 (m, 5H, phenyl-H), 5.33 (s, 2H, benzyl-H).

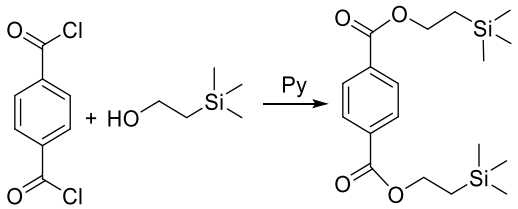

Synthesis of 2-(trimethylsilyl)ethyl diester: Pyridine (0.55 mL, 6.84 mmol) was added dropwise to a mixture of terephthaloyl chloride (464.0 mg, 2.28 mmol) and 2-(trimethylsilyl)ethanol (0.66 mL, 4.57 mmol) in chloroform. After stirring overnight, a saturated aqueous NH_4Cl was added and the mixture was extracted with CH_2Cl_2.The organic layer was dried over Na_2SO_4 and evaporated in vacuum. Column chromatography (hexanes:EtOAc 95:5) was performed to yield the product (728.0 mg, 87.0%) as a colorless oil. ^{1}H NMR (400 MHz, $CDCl_3$) ä 8.70 (dd, 1H, J = 1.7, 1.7 Hz), 8.23 (dd, 2H J = 1.8, 7.8 Hz), 7.54 (dd, 1H, J = 7.8, 7.8 Hz), 4.43-4.49 (m, 4H), 1.13-1.19 (m, 4H), 0.11 (s, 18H).

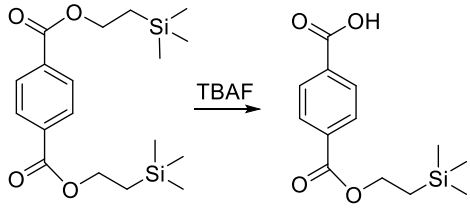

Synthesis of 2-(trimethylsilyl)ethyl monoester: 2.0 mL of tetrabutylammonium fluoride (1.0 M in THF, 2.0 mmol) was added to bis[2-(trimethylsilyl)ethyl]-1,4-Benzenedicarboxylate (733.0 mg, 2.0 mmol) in THF (15.0 mL). After stirring overnight, diethyl ether (50.0 mL) and HCl (5 mL, 1.0 N) were added in sequence, and the organic layer was separated, dried over sodium sulfate and evaporated in vacuum. Column chromatography was performed (CH_2Cl_2: MeOH 100: 0 to 97:3) to yield the monoester (315.0 mg, 63.0%) as a white solid: ^{1}H NMR (400 MHz, $CDCl_3$) 8.79 (dd, 1H, J = 1.5, 1.5 Hz), 8.30-8.33 (m, 2H), 7.60 (dd, 1H, J = 7.8, 7.8 Hz), 4.45-4.51 (m, 2H), 1.16-1.27 (m, 2H), 0.12 (s, 9H).

Synthesis of Cu-paddle-wheel complexes: 0.2 mmol of the monoester protected terephthalic acid and 0.1 mmol of $Cu(NO_3)_2.3H_2O$ (24.1 mg) were taken in a 7.0 mL screw cap vial and 2.0 mL of ethanol was added to it. The mixture was heated at 85.0°C overnight and X-ray quality single crystals were obtained from the reaction mixture.

3 Assembling Multi–Functional Ligands to Low Molecular Weight Gels

Supramolecular gels based on low molecular weight gelators (LMWGs) have attracted immense attention due to the feasibility of tuning the gel state properties and potential applications in dynamic gels, cell culture, drug delivery and media of crystal growth. LMWGS are self-assembled to one-dimensional (1D) fibrils via non-covalent interactions such as hydrogen bonding, van der Waals interactions, π–π stacking and the gel is formed by immobilizing the solvent molecules in the 3D fibrous network. Predicting supramolecular interactions to control or tune the gel property is challenging because of the dynamic nature of noncovalent interactions leading to the self-assembly of gelator. The engineering and tuning of the gel structure can be explored with respect to an external stimulus such as heat, sonication, additives or seeding, which can lead to controllable performance of the gel. Although, various characterization methods have been applied to investigate gelation mechanism and unveil the influencing factors behind the formation of supramolecular gels, characterizing supramolecular gels from molecular to mesoscopic scale have been remained a daunting task. A good strategy to analyze the self-assembly is to modify an existing supramolecular gel and compare the structural difference between the parent gelator and its derivative with their gelation property. In this chapter we have studied the self-assembly of LMWGs by structural modification of the gelators and also effect of addition of metal centers in supramolecular gel formation. This chapter is divided into four articles.

3.1 Article I

The presence of 1D network is considered to be one of the basic criteria for gel formation and the growth of 1D hydrogen bonded chains from urea and amide moieties are well established. Thus, we have chosen amide and urea based LMWG for structural modification. The first system we have chosen is a pyridyl amide based hydrogelator,

namely N-(4-pyridyl)isonicotinamide (**4PINA**)[141] due to the remarkably low molecular weight and minimum gel concentration. The structural modification was achieved by oxidizing the pyridyl group to pyridyl-*N*-oxide moiety, and two mono-*N*-oxides (**PNO** and **INO**) and a di-*N*-oxide (**diNO**) were synthesized. The effect of the structural modification on gelation property and the outcome in understanding the role of specific non-bonding interactions is discussed in *Article-I*.

3.2 Article II

Structural modification was also performed on two pyridyl urea based hydrogelators *N,N'*-bis(3-pyridyl)urea (**3-BPU**) and *N,N'*-bis(4-pyridyl)urea (**4-BPU**).[295] Among the two isomeric parent gelators, **4-BPU** is a supergelator but **3-BPU** is a non-gelator. This prompted us to check the possibility of inducing gelation to the non-gelator by structural modification. Thus, the N—H···N interaction of the pyridyl urea was replaced with N—H···O interaction by oxidizing the pyridyl group to pyridyl-*N*-oxide moiety. The relative gelation ability of the parent compounds and the derivatives was correlated to the hydrogen bond strengths of the corresponding N—H···N and N—H···O synthons by DFT calculations of the dimer interactions in gas phase using a state-of-the-art protocol. The stimuli-responsive properties of the parent and the derivative gelators were compared. Also, the supramolecular gels derived from pyridyl-aryl urea are known for antibacterial properties.[296] We have studied the antibacterial properties of the gels in collaboration with Prof. Gudmundur H Gudmundsson, and the results are described in *Article-II*.

3.3 Article III

Gelation can also be induced by metal coordination (metallogel),[297] where the combination of strong coordination bond between the organic ligand and metal center and various other non-bonding interactions contribute together in gel formation. Inclusion of metal ions in supramolecular gels offers potential applications in catalysis, sensing, optics and magnetic materials. We have investigated the ability of metal salts to induce gelation in pyridyl amides-based ligand N-(4-pyridyl)nicotinamide (**4PNA**) and the detail analysis is reported in *Article-III*.

3.4 Article IV

In this project we analyzed the metallogel formation from the structurally modified non-gelators **PNO** and **INO**. The parent gelator **4PINA** is self-assembled via hydrogen bonding between N—H···N synthon involving the amide moiety and pyridyl nitrogen atom, which is similar to complementary amide N—H···O hydrogen bonding. The modification of pyridyl nitrogen to pyridyl *N*-oxide disrupted the hydrogen bonding, thus no gelation was observed in **PNO** and **INO**. This prompted us to investigate the possibility to restore the N—H···O hydrogen bonding (between amide and *N*-oxide moieties) in metal complexes of **PNO** and **INO**. The stimuli-responsive property of the metallogels were also analyzed and the results are detailed in *Article-IV*.

Article-I

This project is published in a peer reviewed journal and included as it was published. Slight differences might appear from the original article due to the formatting issue.

Publication details:

"**Tuning gel state properties of supramolecular gels by functional group modification**"

Dipankar Ghosh, Matthew T. Mulvee and Krishna K. Damodaran*

Molecules, **2019**, *24*, 3472.

Author contributions:

D.G. and K.K.D planned and designed the research; **D.G.** synthesized the gelators, performed characterizations, solved single crystal structures and evaluated gelation properties. T.M. carried out the rheology measurements. **D.G.** and K.K.D. wrote the initial manuscript draft and all authors reviewed the main manuscript.

molecules

MDPI

Article

Tuning Gel State Properties of Supramolecular Gels by Functional Group Modification

Dipankar Ghosh [1], Matthew T. Mulvee [2] and Krishna K. Damodaran [1,*]

[1] Department of Chemistry, Science Institute, University of Iceland, Dunhagi 3, 107 Reykjavík, Iceland
[2] Department of Chemistry, Durham University, South Road, Durham DH1 3LE, UK
* Correspondence: krishna@hi.is; Tel.: +354-525-4846; Fax: +354-552-8911

Received: 31 August 2019; Accepted: 24 September 2019; Published: 25 September 2019

Abstract: The factors affecting the self-assembly process in low molecular weight gelators (LMWGs) were investigated by tuning the gelation properties of a well-known gelator *N*-(4-pyridyl)isonicotinamide (**4PINA**). The N—H···N interactions responsible for gel formation in **4PINA** were disrupted by altering the functional groups of **4PINA**, which was achieved by modifying pyridyl moieties of the gelator to pyridyl *N*-oxides. We synthesized two mono-*N*-oxides (**INO** and **PNO**) and a di-*N*-oxide (**diNO**) and the gelation studies revealed selective gelation of **diNO** in water, but the two mono-*N*-oxides formed crystals. The mechanical strength and thermal stabilities of the gelators were evaluated by rheology and transition temperature (T_{gel}) experiments, respectively, and the analysis of the gel strength indicated that **diNO** formed weak gels compared to **4PINA**. The SEM image of **diNO** xerogels showed fibrous microcrystalline networks compared to the efficient fibrous morphology in **4PINA**. Single-crystal X-ray analysis of **diNO** gelator revealed that a hydrogen-bonded dimer interacts with adjacent dimers via C—H···O interactions. The non-gelator with similar dimers interacted via C—H···N interaction, which indicates the importance of specific non-bonding interactions in the formation of the gel network. The solvated forms of mono-*N*-oxides support the fact that these compounds prefer crystalline state rather than gelation due to the increased hydrophilic interactions. The reduced gelation ability (minimum gel concentration (MGC)) and thermal strength of **diNO** may be attributed to the weak intermolecular C—H···O interaction compared to the strong and unidirectional N—H···N interactions in **4PINA**.

Keywords: LMWGs; hydrogel; structural modification; pyridyl amides; *N*-oxides

1. Introduction

Supramolecular gels based on low molecular weight gelators (LMWGs) [1–10] are an excellent class of soft materials with tunable gel state properties and potential applications [9–16], such as dynamic gels, cell culture, drug delivery, and media of crystal growth. LMWGs are formed by the immobilization of the solvent molecules in the three-dimensional (3-D) network of the gelator, which are stabilized by various noncovalent interactions [1–9], such as hydrogen bonding, van der Waals interactions, π−π stacking, etc. The gelation properties of LMWGs depend on various factors such as concentration [17,18], sonication [19–21], additives [22], and seeding [21,23]. The understanding and prediction of the gel structure and self-assembly process of LMWGs to control or tune the gelation properties are difficult because of the dynamic nature of noncovalent interactions [1–10]. This is due to the low molecular order of the gel state as a whole because of the variation in the length scales (ranging from nano to micro) of the gel structure. Efforts have been made to investigate the gelation mechanism and unveil the factors influencing the gel using various methods [8,19,24–32], such as ultraviolet–visible (UV–Vis) spectroscopy, nuclear magnetic resonance spectroscopy (NMR), Fourier transform infrared spectroscopy (FT-IR), scanning electron microscopy (SEM), atomic force microscopy

(AFM), transmission electron microscopy (TEM), rheology and X-ray diffraction techniques including X-ray diffraction (XRD), small-angle X-ray scattering (SAXS), small-angle neutron scattering (SANS), etc. Although the characterization of supramolecular gels from molecular to mesoscopic scale has been challenging, X-ray diffraction techniques can be used to correlate the crystal structure of the gelator with the powder diffraction pattern of either native gel or the xerogel [4,8,33–35]. However, the removal of solvent to prepare a xerogel can result in artifacts due to dissolution, recrystallisation, and changes in morphology or polymorphic phase transition, but this approach still remains as one of the practical methods to gain insight into the gelator structure and aggregation behavior. Furthermore, this technique enables us to correlate the intermolecular interactions observed in the single-crystal structure with the molecular aggregation in the gel state, which may be different from its crystalline network [34]. We were interested in studying the effect of hydrogen-bonding motifs in the self-assembly process of LMWGs, to enable us to tune the gel state properties. However, the design, mechanism, and understanding of gel structure and the self-assembly process of new LMWGs are challenging because the structure and properties rely mostly on the geometry and spatial arrangement of the building blocks and also the nature of intermolecular noncovalent interactions [36,37]. Thus, modifying an existing supramolecular gel can be considered as a good strategy to analyze the self-assembly, enabling us to compare the structural and gelation properties of new LMWGs with the parent gelator [38].

Amide and urea moieties have been used extensively as supramolecular synthons [39] to generate LMWGs with tunable properties [40–42]. Amide-based LMWGs contain an amide N−H donor and C=O acceptor resulting in a strong N−H···O=C interaction, which self-assemble to a 3-D network via cooperative and unidirectional hydrogen bonding involving amide units [43]. These 3-D networks are capable of immobilizing solvent molecules to form organo/hydrogels [34,44–49]. Recently, we reported the structural modification of trimesic amide-based gelator N^1,N^3,N^5-tri(pyridin-3-yl)benzene-1,3,5-tricarboxamide [50] to corresponding tris-*N*-oxide compound (**L-3Nox**) [38]. The gelation properties suggested that **L-3Nox** is a weaker gelator compared to the parent amide and the structure–property correlation was not performed due to the lack of a single-crystal X-ray structure. This prompted us to select low molecular weight pyridyl amide gelators, which are classified as stimuli-responsive supramolecular gels due to their tunable properties to external stimuli such as pH, coordination, salts/ions, etc. [6,51–65]. The advantage of using pyridyl amide is twofold: (a) the opportunity to modify each ring selectively by simple organic reactions (Scheme 1) and (b) the easiness of obtaining the crystal structure. Thus, a pyridyl amide-based hydrogelator, namely *N*-(4-pyridyl)isonicotinamide (**4PINA**) [34], with remarkably low molecular weight and minimum gel concentration was selected. The derivatives of **4PINA** are ideal candidates to study the molecular aggregation enabling us to compare the role of non-bonding interactions in gel formation with **4PINA**. The aggregation mode of molecules in the xerogel fibrils was found to be N—H···N hydrogen bonding, which had a prominent effect in the self-assembly of **4PINA**. The structural modification of **4PINA** was achieved by oxidizing the pyridine ring to the corresponding *N*-oxide, which may restrict the N—H···N hydrogen bonding-based molecular aggregation.

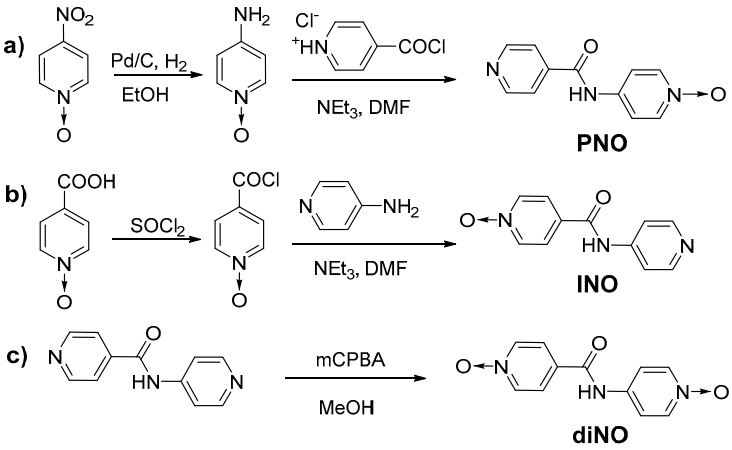

Scheme 1. Synthesis of the *N*-oxide amides: (**a**) 4-(isonicotinamido)pyridine-1-oxide (**PNO**), (**b**) 4-(pyridin-4-ylcarbamoyl)pyridine-1-oxide (**INO**), and (**c**) 4-((1-oxidopyridin-4-yl)carbamoyl)pyridine-1-oxide (**diNO**).

2. Results

2.1. Design and Synthesis

We synthesized three *N*-oxides compounds by modifying the pyridyl group of *N*-(4-pyridyl)isonicotinamide (**4PINA**) [34]. This included a di-*N*-oxide (4-((1-oxidopyridin-4-yl)carbamoyl) pyridine-1-oxide, **diNO**) and two mono-*N*-oxides, namely 4-(isonicotinamido) pyridine-1-oxide (**PNO)** and 4-(pyridin-4-ylcarbamoyl)pyridine-1-oxide (**INO**) with the *N*-oxide group at the aminopyridine and isonicotinoyl end, respectively. Mono-*N*-oxide amides were synthesized by reacting acid chlorides with corresponding amines in anhydrous DMF in the presence of triethylamine (Scheme 1a,b). The precipitates obtained for **INO** and **PNO** were washed with aqueous sodium bicarbonate solution followed by water to ensure the removal of salts. The di-*N*-oxide (**diNO**) was synthesized by oxidizing **4PINA** with *m*-chloroperoxybenzoic acid (Scheme 1c) and the product was washed with water and dried. All compounds were characterized by NMR, HRMS, IR, and X-ray diffraction (single-crystal and powder).

2.2. Gelation Experiments

The gelation experiments for **diNO**, **INO**, and **PNO** were tested in various solvents (Table S1, Supplementary Materials). In a typical experiment, a 10.0 mg portion of the compound was heated in 1.0 mL of solvent (1.0 wt %) to get a clear solution and was cooled to room temperature. The hydrogel formation of these amides tested at 1.0 wt % indicated no gelation, which prompted us to increase the concentration to 4.0 wt %. The mixture was heated (80.0–90.0 °C) and on cooling to room temperature, gelation was observed only for the di-*N*-oxide (**diNO**) after 1 h, which was confirmed via inversion test. Crystalline materials were obtained for both the mono-*N*-oxides (**PNO** and **INO**). The gelation experiment performed with an equimolar mixture of **PNO** and **INO** resulted in concomitant crystallization of the individual compounds, which was confirmed by single-crystal X-ray diffraction (SCXRD). The gel strength of **diNO** was analyzed by sol–gel transition temperature (T_{gel}) and minimum gel concentration (MGC) experiments. The lowest concentration at which the gel was obtained was recorded as the minimum gel concentration (MGC). The MGC experiment of the hydrogel was performed in 1.0 mL of water by weighing different amounts of **diNO** gelator (30.0 to 50.0 mg) in a 7.0 mL vial. The mixture was heated and then cooled to room temperature, and the vial

was left undisturbed for gel formation. After 24 h, the gel formation was confirmed by the inversion test and the MGC of the gelator was found to be 4.0 wt %.

2.3. Thermal Stability

The thermal stability of the gel network of **diNO** was evaluated using gel-to-solution transition temperature (T_{gel}) experiments, which is the critical temperature at which the gel converts to a solution. The experiment was performed by placing a small spherical glass ball (92.0 mg) on top of the **diNO** preformed hydrogel in a standard vial. The vial was heated and the temperature at which the ball touched the bottom of the vial was recorded as T_{gel}. The experiments were performed at 4.0 and 6.0 wt % and the T_{gel} did not vary much with the concentration of **diNO**, which was found to be 78.0 °C and 80.0 °C at 4.0 and 6.0 wt %, respectively.

2.4. Rheology

Rheological analysis was undertaken to determine the mechanical properties of the supramolecular hydrogels (4.0 wt %) [66,67]. The oscillatory amplitude sweeps, at a constant frequency (1.0 Hz), demonstrated a linear viscoelastic region (LVR) in which the storage (elastic) G′ modulus was approximately an order of magnitude higher than the loss (viscous) G″ modulus for both samples (Figure 1a) [66,68]. Thus, both samples had a linear elastic response to low stress amplitudes. This behavior is indicative of a solid-like network throughout the sample gelling the aqueous solvent. At increased shear stresses, a stress softening behavior was observed, the viscous moduli (G″) increased, and at a crossover point, there was a concomitant sharp decrease in the storage moduli (G′) indicating a transition from an elastic gel to a viscous fluid [69,70]. At low shear stresses, **4PINA** had an elastic modulus of approximately 140,000 Pa and a yield stress of approximately 500 Pa. **diNO** was a significantly softer gel with an elastic modulus of approximately 5000 Pa and was also weaker, with a yield stress of approximately 60 Pa.

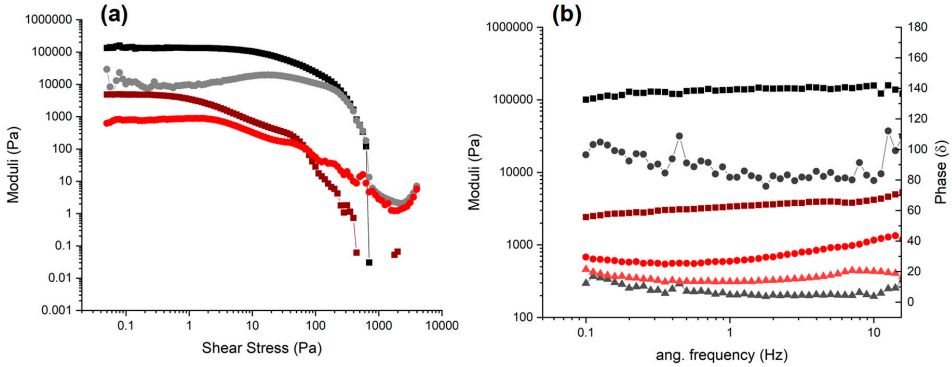

Figure 1. (**a**) Oscillatory amplitude sweeps and (**b**) oscillatory frequency sweeps, for *N*-(4-pyridyl) isonicotinamide (**4PINA**) (black) and **diNO** (red). For both, **.** refers to G′ and • refers to G″, the storage modulus and viscous modulus, at 4.0 wt %, respectively. ▲ refers to the phase lag (δ).

Oscillatory frequency sweeps (Figure 1b) at a fixed amplitude (0.05 Pa) demonstrated that G′, arising from the elastic network, was higher than G″ across all frequencies for **4PINA**, which is characteristic of the presence of a solid-like network of filaments that are temporally persistent in the viscoelastic gel. These moduli were effectively indifferent to the frequency and this was true for **diNO** as well at low frequencies (<10 Hz). However, with increasing frequencies G′ increased, the typical behavior of viscoelastic liquids rather than supramolecular gels [66], which further indicates that **diNO** formed weaker gels than **4PINA**. Furthermore, the ratio of G′:G″ is not at least an order of magnitude,

the generally accepted ratio for supramolecular gels. Instead the ratio is roughly 7:1, further indicating that the modifications made to **diNO** severally affect its gelling ability. However, the phase angle, the lag between the applied shear stress and the measured strain, for **diNO** of approximately 15.0 δ is comparable to that of the original gelator, **4PINA**, with a measured phase lag of approximately 7.0 δ. Moreover, the phase angle is not dependent on the frequency, a key Watson–Chambon criterion for gels. Thus, as the **diNO** samples do not meet the moduli requirements but demonstrated other viscoelastic behavior typical of a physical gel, it can, with caveats, be considered a very weak gel.

2.5. Scanning Electron Microscopy (SEM)

The morphology of gel fibers was studied by analyzing the SEM images of dried **diNO** gel. The gel was prepared at 4.0 wt % in water, filtered after 24 h, and dried under a fume hood. A small portion of the dried gel was placed on a carbon tab and was coated with gold for 2 min. The SEM images revealed that the xerogel displayed a rod-type architecture with needle-shaped microcrystalline materials in the network. The diameter of the small needle-shaped fibers ranged from 1.2 to 2.5 μm and the width of the larger microcrystalline rods ranged from 8.0 to 30.0 μm (Figure 2).

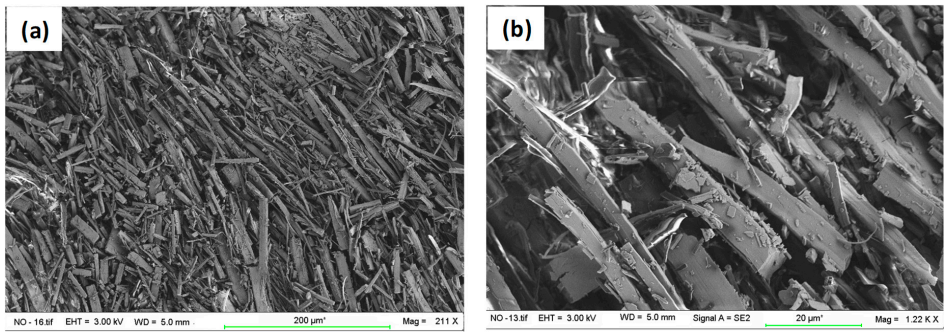

Figure 2. SEM images of **diNO** show the microcrystalline fibrous network: (**a**) overview; (**b**) magnified images.

2.6. Crystal Structure

The crystallization experiments of *N*-oxides and an equimolar mixture of two mono-*N*-oxides were performed in water and various organic solvents. The compounds were proved to be sparingly soluble in most of the organic solvents, hence the experiments were carried out in a water or aqueous solution of methanol, ethanol, acetonitrile, and tetrahydrofuran. About 20.0 mg of the material were dissolved by heating in 1.0 mL of water, and the solution was cooled to room temperature. Crystallization from mixed solvents (1:1, v/v) such as methanol/water, ethanol/water, acetonitrile/water, and tetrahydrofuran/water resulted in precipitates. In some cases, needle-shaped crystals were obtained with low yield and the crystal quality was not good for single-crystal X-ray diffraction. The crystallization experiments performed in water produced X-ray quality single crystals for all *N*-oxides. The crystals of **diNO** were found to be needle-shaped, whereas block-shaped crystals were observed for both mono-*N*-oxides. Interestingly, crystallization of a 1:1 mixture of **PNO** and **INO** also resulted in block-shaped crystals.

The gelator **diNO** crystallized in a triclinic space group (Pī) with the carbonyl moiety of the amide group slightly deviated from the amide plane (15.74(8)°) and the pyridyl *N*-oxide rings were twisted at an angle of 58.71(3)° (Figure 3a). The N-H moiety was involved in hydrogen-bonding interaction (N—H···O) with the oxygen atom of the adjacent molecule to form a dimer. This dimer was further stabilized by a strong π–π interaction (3.6563(9) Å) between the isonicotinoyl *N*-oxide ring of **diNO** (Figure 3b) and also N—H···O interactions (2.8178(16) Å) between the amide N-H moiety and isonicotinoyl *N*-oxide moieties (Figure S9, Supplementary Materials). The aminopyridine *N*-oxide moieties of the **diNO** dimer interact with the isonicotinoyl *N*-oxide moieties of adjacent dimers via

offset π–π interactions (3.8745(9) and 3.8219(9) Å) and also display bifurcated C—H···O interactions (3.1789(18) and 3.1621(19) Å) with adjacent dimers (Figure 3c).

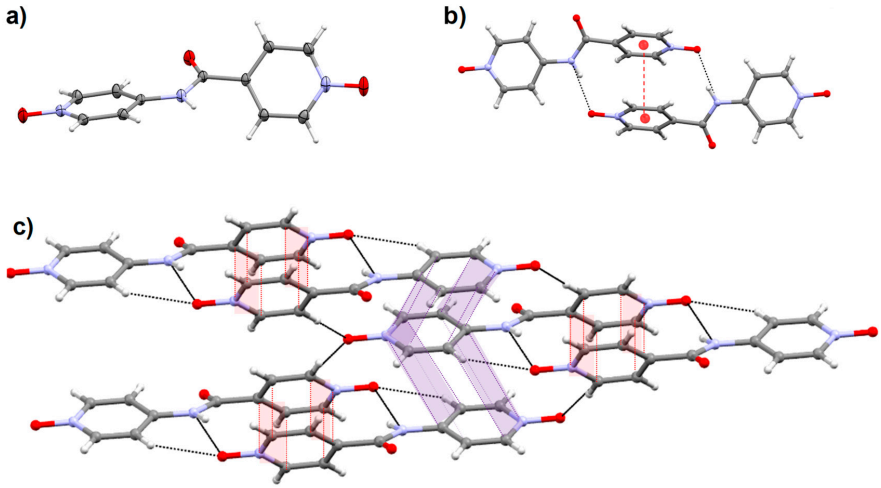

Figure 3. (**a**) Crystal structure of **diNO**, (**b**) showing hydrogen-bonded dimer stabilized with π–π interaction and (**c**) interaction of the individual dimer with adjacent dimer via various non-bonding interactions (dotted lines); black lines indicate hydrogen bonding, red line for π–π interactions of the individual dimer, and blue line for π–π interactions with adjacent dimers.

Compound **INO** crystalized in a triclinic space group (Pī) and the twisting of the pyridyl *N*-oxide ring (58.86°) was similar to **diNO** (Figure 4a). The hydrogen-bonding pattern was exactly the same as in **diNO** resulting in a dimer, which was stabilized by N—H···O and π–π interactions. The only difference between these two structures was the connection between adjacent dimers and the dimer in **INO** propagates via C—H···N interaction (3.4391(16) and 3.5489(16) Å), whereas C—H···O and π–π interactions are observed in **diNO**. The solvated form of **INO** was also isolated (**INO.2H$_2$O**) and the crystals belong to a monoclinic $C2_{/c}$ space group (Figure S10). The asymmetric unit contains one **INO** and two molecules of water, and the isonicotinoyl *N*-oxide and pyridyl moieties are coplanar to the amide groups compared to the de-solvated form. The hydrogen-bonding pattern of **INO.2H$_2$O** was different from **INO** due to the presence of dimeric water clusters. The isonicotinoyl *N*-oxide was hydrogen-bonded to two water molecules via O—H···O interactions (2.793(3) and 2.796(2) Å), and the pyridyl nitrogen atom interacted with a water molecule through O—H···N interaction (2.771(2) Å). This resulted in the formation of a hydrogen-bonded macrocycle involving two **INO** molecules and four water molecules. The amide moieties of the macrocycle were hydrogen bonded to adjacent macrocycles via N—H···O (2.921(2) Å) interactions to form a hydrogen-bonded 3-D network.

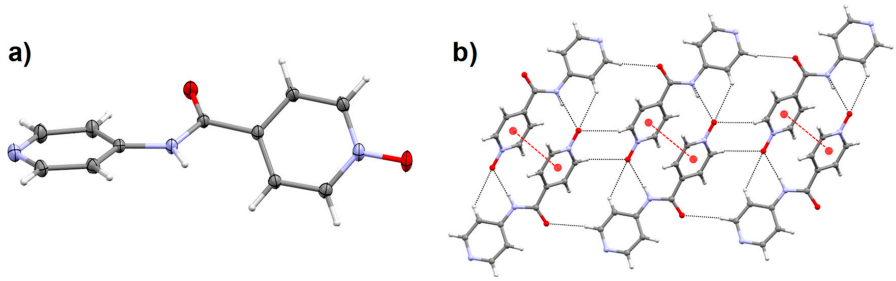

Figure 4. (**a**) Crystal structure of **INO** and (**b**) interaction of individual dimers via various non-bonding interactions; black dotted lines indicate hydrogen bonding and red dotted lines represent the π–π interactions.

The structural analysis of the pyridyl *N*-oxide compound (**PNO**) revealed that the compound crystallized in a similar space group as **diNO** but with two solvent water molecules (**PNO.2H$_2$O**, Figure 5a). The pyridyl *N*-oxide and isonicotinoyl moieties are almost planar to each other but slightly twisted from the amide plane (16.70 and 18.72°). The N-H moiety of the amide group, the pyridyl nitrogen atom, and the N-oxide moieties are hydrogen bonded to the water molecules. The amide acts as donor (N—H···O = 2.8617(15) Å), whereas the *N*-oxide (O—H···O = 2.7412(15) and 2.7701(16) Å) and isonicotinoyl groups (O—H···N = 2.8598(17) Å) act as acceptor, resulting in four water molecules interacting with one **PNO** molecule. The hydrogen bonding between water molecules and **PNO** resulted in a hexagonal architecture of oxygen atoms formed by *N*-oxide oxygen atoms of two **PNO** and four water molecules, which was stabilized by various interactions with amide and pyridyl nitrogen atoms of adjacent **PNO** molecules (Figure 5b).

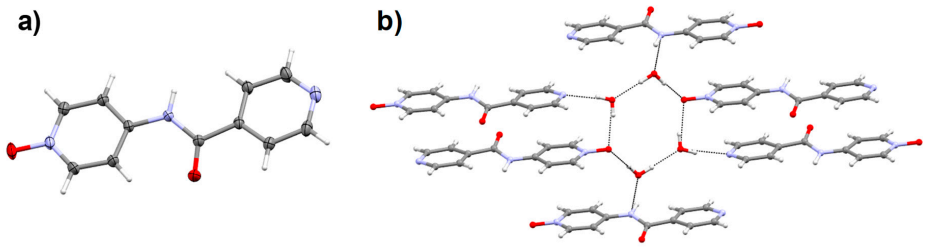

Figure 5. Single-crystal structure of **PNO**: (**a**) Asymmetric unit (water molecules not shown); (**b**) two-dimensional (2-D) sheet constructed by H-bonding between the ligand and solvent (water) molecules.

We also performed the crystallization of a 1:1 mixture of **INO** and **PNO** in water (2.0 wt %) and block-shaped crystals appeared on cooling after 1 h. The SCXRD data matched the **PNO.2H$_2$O** crystals. The crystals of **INO.2H$_2$O** were also obtained from the same mixture after 24 h. The experiments repeated by varying the ratios of **INO** and **PNO** (1:3 and 3:1) also resulted in the co-crystallization of the individual components.

2.7. X-ray Powder Diffraction (XRPD)

The phase purity of the compounds was further analyzed by comparing the XRPD pattern of the bulk crystals with the simulated pattern obtained from the single-crystal data. XRPD was performed on the bulk solid of recrystallized **diNO** from water and the xerogel obtained from water at 4.0 wt %. The powder X-ray pattern of the re-crystallized **diNO** matches perfectly well the simulated graph obtained from the single-crystal data (Figure 6). However, the powder X-ray pattern of the xerogel did not match the calculated pattern from the crystal structure of **diNO**. The XRPD patterns

of mono-*N*-oxides were performed with the recrystallized samples from water, which were filtered and dried in air. The XRPD pattern of **PNO** revealed that the pattern of bulk solid was virtually super-imposable on the simulated pattern of **PNO** (Figure S11). The XRPD pattern of the bulk crystalline material of **INO** was also similar to the simulated pattern of **INO** (Figure S12). We also performed the XRPD of the hydrated form of **INO**, but the pattern was different from the calculated pattern of the **INO.2H$_2$O** crystal structure (Figure S13). Interestingly, the **INO.2H$_2$O** bulk crystal pattern matched the simulated pattern of **INO** (Figure S12).

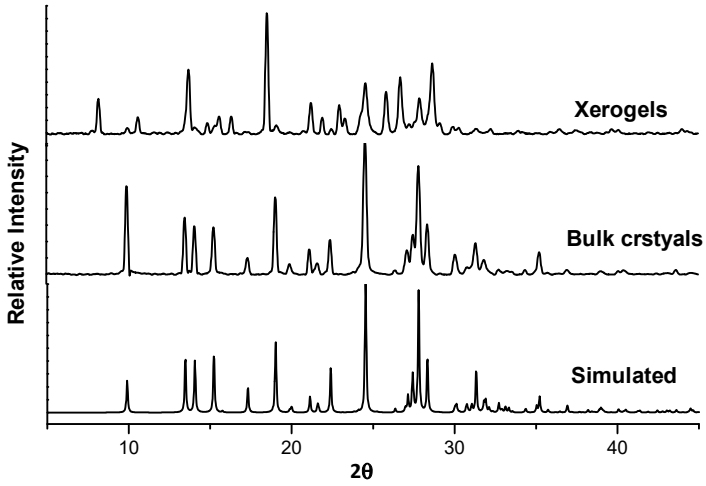

Figure 6. X-ray powder diffraction (XRPD) comparison of **diNO**: simulated pattern from single-crystal X-ray diffraction (SCXRD) data, bulk crystals, and xerogel obtained from water.

3. Discussion

The ability of pyridyl amides to form a one-dimensional (1-D) hydrogen-bonded network is well established, which makes them ideal candidates in designing LMWGs with tunable properties. The availability of single-crystal X-ray structures of many organo/hydrogelators based on pyridyl amides enabled us to identify the key factors responsible for the formation of gel networks, for example, the formation of 1-D networks. The structural analysis of pyridyl amides indicates that these compounds self-assemble through mainly two types of hydrogen bonding, namely N—H···O synthon of the amide moiety and N—H···N synthon involving the amide and pyridyl nitrogen. These two types of interactions are predominant in the molecular aggregation of *N*-(4-pyridyl)isonicotinamide (**4PINA**) [34] along with various other non-bonding interactions. However, the impact of these types of interactions was not studied in detail. For example, what is the role of N—H···N synthon in gel network stabilization? What happens if these interactions are replaced by another synthon? We addressed this question by restricting the N—H···N synthon by modifying the pyridyl nitrogen to pyridyl-*N*-oxide moiety. Thus, we modified the pyridyl groups of **4PINA** [34] to *N*-oxides; two mono-*N*-oxides were synthesized by oxidizing the nitrogen atoms at the pyridyl amine end (**PNO**) and the isonicotinic acid end (**INO**), and oxidation of both pyridyl nitrogen atoms resulted in **diNO**. This restricts N—H···N interactions between the gelators and hinders the one-dimensional growth of the gel fibril, which may facilitate the formation of either a two-dimensional (2-D) or 3-D network of gelator. Another advantage of pyridyl-*N*-oxides is the ease of crystallization in an aqueous medium, enabling us to compare the crystal structures of mono-*N*-oxides and di-*N*-oxide for structure–property correlation.

The gelation properties of all the *N*-oxides in various solvents resulted in selective gelation of **diNO** in the water at higher concentration (4.0 wt %). The formation of needle-shaped crystals at

lower concentration revealed that crystallization and gelation properties [71] were concentration dependent. The mono-*N*-oxides (**PNO** and **INO**) did not form gel in any solvents but formed crystals indicating the importance of similar groups at both ends in gel formation, which corroborates well with the gelation properties of **4PINA** [34]. We also prepared a mixture of **PNO** and **INO** in different ratios to test the ability of these compounds to form multi-component gels. Such gels are obtained by mixing two or more compounds (gelator/non-gelator) where individual molecules interact either constructively or destructively to form well-ordered fibers containing individual components (self-sorting), both components (specific co-assembly), or a mixture of both (random co-assembly) [72,73]. We showed that mixing enantiomeric supramolecular gels based on bis(urea) compounds tagged with a phenylalanine methyl ester leads multi-component gels with enhanced thermal and mechanical strength [74]. However, the experiments performed with the mixtures of **PNO** and **INO** resulted in concomitant crystallization of individual compounds. **INO** was proved to be more soluble between the two mono-*N*-oxides leading to slow crystallization. The crystallization of the individual compounds suggests self-sorting of the components in the mixture.

The minimum gel concentration (MGC) of **diNO** (4.0 wt %) indicates that the gel network formed was weaker compared to **4PINA** (MGC 0.37 wt %) [34]. This may be attributed to the fact that converting the pyridyl group of **4PINA** to pyridyl-*N*-oxide increased the hydrophilic interactions preferring crystalline form, which hindered the gel formation at low concentration [75]. The gel-to-solution transition temperature (T_{gel}) experiments performed at MGC of **diNO** to evaluate the thermal stability of the gel revealed that the gel network collapsed at 78.0 °C. This indicates that the gel network of **diNO** is slightly weaker compared to **4PINA** and the T_{gel} of **diNO** network did not change drastically with concentration. This is in agreement with the rheological measurements that revealed that **diNO** gels were weaker compared to the **4PINA** gelator. The rheology experiments enabled us to elucidate the information regarding factors controlling the gelation, gel strength, and the solid-like properties of pure gels, and the mechanical strength of the **4PINA** and **diNO** gels was evaluated using rheology. The rheological measurements performed for both **4PINA** and **diNO** gels revealed that **diNO** gels were significantly softer than **4PINA** gels. At a low strain of 1.0%, both **diNO** and **4PINA** samples had an effectively infinite shear stress relaxation time, typical of a temporally persistent supramolecular elastic network. On the other hand, at a higher strain of 10.0% the relaxation time for the **4PINA** sample, which had sheared, now displayed a finite relaxation time and behaved like a viscous liquid (Figures S14 and S15). The morphologies of the gel fibers were analyzed using SEM images of the dried gel, and the results indicated that a microcrystalline network was observed in **diNO** gels. The xerogels of **4PINA** at a similar concentration displayed fibrous morphology with tape-type architecture with widths ranging from 0.57 to 5.7 μm [34], which was different from **diNO** gels. This is quite interesting because changing the pyridyl groups to *N*-oxide resulted in a drastic change in the morphology of the gel fibers. The stronger gelation properties of **4PINA** may be attributed to the ability of **4PINA** to immobilize the solvent molecules more efficiently in the fibrous network compared to the *N*-oxide network.

The crystallization experiments of the *N*-oxides performed in aqueous solutions of polar solvents resulted in either needle-shaped crystals or precipitate, which prompted us to explore the crystallization in pure water. The crystallization of **INO** and **PNO** in water resulted in blocked-shaped crystals in 3–5 h, but needle-shaped **diNO** crystals were formed in 1 to 2 days. The solid-state structures of the *N*-oxides were analyzed by single-crystal *X*-ray diffraction. The structure of *N*-oxides with both ends modified (**diNO**) was compared to the parent **4PINA** structure and these two structures differ mainly in the type of non-bonding interactions. The crystal structure of **4PINA** showed that the pyridyl nitrogen atoms and the amide moieties were hydrogen bonded via N—H···N interaction to form a 1-D hydrogen-bonded network. However, discrete dimers were formed in **diNO** by N—H···O hydrogen bonding, which was stabilized by π–π interactions. These dimers interact with each other via bifurcated C—H···O interactions and π–π interactions to form a 2-D supramolecular structure. The comparison of the intermolecular interactions in both the structures indicated that the N—H···N

interaction in **4PINA** is replaced by bifurcated C—H···O interactions in **diNO**. This explains why **4PINA** is a good gelator, which indicates the importance of N—H···N interaction in the formation of supergelators. The phase purity of the *N*-oxide compounds was analyzed by comparing the diffraction pattern of the crystal structures with the powder X-ray pattern of the bulk materials. The analysis of the pattern revealed that the recrystallized form of **diNO** matched the single-crystal structure of **diNO**, indicating an identical structure. However, the XRPD pattern of the xerogels of **diNO** did not match the pattern obtained from the crystal structure of **diNO**. This is presumably due to the presence of hydrogen-bonded solvent molecules in the xerogels. The XRPD data of the bulk materials of **INO** and **PNO.2H$_2$O** matched their corresponding crystal structures. However, the XRPD pattern of **INO.2H$_2$O** matched the crystal structure of the **INO** pattern, confirming the transformation of **INO.2H$_2$O** crystals due to the loss of water molecules during the drying process.

The crystal structure analysis of **INO** obtained from water revealed the presence of two forms, namely **INO** and **INO.2H$_2$O**. These two forms were crystallized from water and the rapid crystallization process produced large block-shaped crystals of **INO.2H$_2$O**. The gelation experiments performed at higher concentration (>40.0 mg in 1.0 mL water) also favored the crystallization of **INO.2H$_2$O**. The selective crystallization of **INO** was obtained by the slow crystallization in dilute aqueous solution over a period of five days. This indicates that **INO.2H$_2$O** was the kinetically favored form and these crystals were slowly converted to the thermodynamically stable **INO** form, which was confirmed by powder X-ray analysis. The solid-state structure of these two forms was different and the molecule was planar in **INO.2H$_2$O** compared to **INO**. This was due to the hydrogen-bonding interaction of the water molecules resulting in a hydrogen-bonded macrocycle involving two **INO** molecules and four water molecules. The structures of **INO** and **diNO** were compared to analyze the importance of identical groups on both ends in the gelation process. The solid-state structures of **INO** and **diNO** were similar resulting in the dimer formation, but the non-bonding interaction responsible for the propagation of the dimers was different. The dimer in **diNO** propagated via C—H···O interactions (3.1789(18) and 3.1621(19) Å) and this was replaced by a C—H···N interaction (3.4391(16) and 3.5489(16) Å) in **INO**. The selective gelation of **diNO** may be attributed to the strong C—H···O interaction compared to the non-bonding interaction in **INO**. The structure analysis of **PNO** revealed the presence of two water molecules in the crystal structure, which helped the molecule to retain the molecular planarity. The water molecules play a crucial role in overall packing of the crystal, and a hexagonal architecture of oxygen atoms was formed by the hydrogen bonding between **PNO** and the water molecules. The structural analysis of **4PINA** and the *N*-oxides confirm the importance of the non-bonding interactions and the presence of identical groups at both ends of the compounds in gel formation.

4. Materials and Methods

4.1. Chemicals and Reagents

All starting materials and solvents were purchased from Sigma-Aldrich (MEDOR ehf, Reykjavik, Iceland) and were used as supplied. Deionized water was used for all the experiments and anhydrous methanol was obtained by distilling the solvent over Mg turnings and iodine. 4-aminopyridine-1-oxide [76] and *N*-(4-pyridyl)isonicotinamide (**4PINA**) [34] were synthesized following the reported procedures. ^{1}H NMR and IR spectra were recorded on a Bruker Advance 400 spectrometer (Rheinstetten, Germany) and a Nicolet iN10 (Thermo Fisher Scientific, Hvidovre, Denmark), respectively. Single-crystal X-ray diffraction (SCXRD) was performed on a Bruker D8 VENTURE (Karlsruhe, Germany), and X-ray powder diffraction (XRPD) was carried out using a Bruker D8 Focus instrument (Karlsruhe, Germany). The morphology of the xerogel was analyzed by scanning electron microscopy (SEM) using a Leo Supra 25 Microscope (Carl Zeiss, Oberkochen, Germany).

4.2. Synthesis

General procedure for **INO** and **PNO:** The acid chloride was prepared by stirring the carboxylic acid (10.0 mmol) with 5.0 mL of thionyl chloride overnight in a round-bottom flask at 65.0 °C. The pale-yellow solution obtained was cooled and the excess thionyl chloride was removed by distillation. The resulting white solid/crystal was transferred to a 100 mL two-neck RB flask containing 4-aminopyridine/4-aminopyridine-1-oxide (10.0 mmol). A pale yellowish solution was obtained by adding 20.0 mL anhydrous DMF to the flask, the solution was cooled to 0 °C, and triethylamine (1.5 mL, 10.8 mmol) was added dropwise to this solution. The resulting mixture was stirred overnight at room temperature and the solution was added to a beaker containing 200 mL diethyl ether resulting in a white suspension. The mixture was filtered, and the residue was stirred with 4.0% $NaHCO_3$ for 5 h, filtered, and washed with cold water. The resulting white solid was recrystallized from water to obtain the desired product.

4-(pyridin-4-ylcarbamoyl)pyridine-1-oxide (**INO**): Isonicotinic acid-*N*-oxide (1.39 g, 10.0 mmol) and 4-aminopyridine (0.94 g, 10.0 mmol). Yield: 72.0% (1.55 g, 7.2 mmol). ^{1}H NMR (400 MHz, DMSO-d_6) δ: 10.68 (1H, s), 8.47 (2H d, J = 8.0), 8.36 (2H d, J = 8.0), 7.95 (2H d, J = 8.0), 7.73 (2H d, J = 8.0). MS (ESI) m/z for $C_{11}H_9N_3O_2Na^+$: expected 238.20, found 238.20.

4-(isonicotinamido)pyridine-1-oxide (**PNO**): Isonicotinic acid (1.23 g, 10.0 mmol) and 4-aminopyridine-1-oxide (1.10 g, 10.0 mmol). Yield: 79.0% (1.70 g, 7.9 mmol). ^{1}H NMR (400 MHz, DMSO-d_6) δ: 10.98 (1H, s), 8.80 (2H d, J = 6.0), 8.19 (2H d, J = 7.6), 7.85 (2H d, J = 4.4, 1.4), 7.82 (2H dd, J = 5.4, 2.2). MS (ESI) m/z for $C_{11}H_9N_3O_2Na^+$: expected 238.20, found 238.19.

4-((1-oxidopyridin-4-yl)carbamoyl)pyridine-1-oxide (**diNO**): To a solution of *N*-(4-pyridyl)isonicotinamide (1.35 g, 6.8 mmol) in MeOH (25 mL), *m*-chloroperoxybenzoic acid (3.80 g, 17.0 mmol) was added in portions for 15 min. The reaction mixture was refluxed overnight at 70.0 °C and cooled to room temperature. The solid was collected by filtration, washed with hot methanol, and then dried. Yield 0.88 g, 56.0%. ^{1}H NMR (400 MHz, DMSO-d_6) δ: 10.81 (1H, s), 8.39 (2H d, J = 7.2), 8.18 (2H d, J = 7.2), 7.95 (2H d, J = 7.2), 7.79 (2H d, J = 7.2). MS (ESI) m/z for $C_{11}H_9N_3O_3Na^+$: expected 254.05, found 254.05.

4.3. Gelation Studies

Gelation experiments were initially carried out by weighing 10.0 mg of the *N*-oxide ligands (**INO**, **PNO**, **diNO**, and an equimolar mixture of **INO** and **PNO**) in a 7.0 mL vial and 1.0 mL of distilled water was added to the compounds. The mixtures were heated until a clear solution was obtained; cooling to room temperature resulted in no gelation in any case after 24 h. Since the compounds were soluble only in water, gelation experiments were carried out in aqueous solution of organic solvents. An aqueous solution (1:1, v/v) was prepared by mixing 500 μL of organic solvents (methanol, ethanol, tetrahydrofuran, acetonitrile, or nitrobenzene) with 500 μL of water. These solutions were added to 10.0 mg of the *N*-oxide compounds and the mixtures were heated; cooling to room temperature resulted in a white precipitate after 24 h in all cases. The higher solubility of the compounds in water compared to other solvents prompted us to check the gelation experiments at higher concentration. Crystals were obtained when the gelation experiments were performed in 1.0 mL water with 20.0 mg compounds (2.0 wt %). The gelation ability tested in mixed solvents at 2.0 wt % mostly produced precipitate, whereas some crystalline materials were observed in a few experiments (in methanol/water).

The gelation experiments at higher concentration (4.0 wt %) also resulted in crystals for **INO**, **PNO**, and their equimolar mixture but an opaque gel was formed under identical conditions (confirmed by inversion test) for **diNO**. The gelation experiments at higher concentration in a mixed solvent were avoided due to insolubility of these materials. The solubility of **diNO** was found to be approximately 60.0 mg/mL in water, and the solution formed gel at concentrations between 4.0 and 6.0 wt %. The two

mono-*N*-oxides and their equimolar mixture at high concentration (>4.0 wt %) were dissolved in boiling water, which readily formed crystals on cooling.

4.4. Minimum Gel Concentration (MGC)

The MGC was performed by taking various amounts (30.0 to 50.0 mg) of **diNO** in a standard 7.0 mL vial and the vial was sealed after adding 1.0 mL of distilled water. The mixtures were heated to dissolve the compound and left undisturbed to form gel. The minimum concentration at which gel was obtained was noted as MGC. The MGC of **diNO** was found to be 4.0 wt % in pure water.

4.5. T_{gel} Experiments

The gel-to-solution transition temperature (T_{gel}) experiment was performed at two different concentrations (4.0 and 6.0 wt %) of **diNO**. The required amount (40.0 or 60.0 mg) of **diNO** was placed in a 7.0 mL vial and 1.0 mL of water was added. The vial was sealed, and the mixture was heated to obtain a clear solution and cooled to room temperature to form the gel. After 24 h, a small spherical glass ball (92.0 mg) was carefully placed over the gel. The vial was gradually heated in an oil bath equipped with a magnetic stirrer and a thermometer. The temperature at which the glass ball touched the bottom of the vial was recorded as T_{gel}. The T_{gel} of **diNO** was found to be 78.0 °C and 80.0 °C at 4.0 and 6.0 wt %, respectively.

4.6. Rheology

The rheology experiments were performed at Durham University using a TA Instruments AR 2000 (New Castle, DE, USA) fitted with a rough Peltier plate and a 25 mm rough plate geometry (gap width of 2500 μm) at 25 °C. Supramolecular gels were prepared as discussed previously at a concentration of 4.0 wt %. The top plate was lowered and the normal force was allowed to reach equilibrium. Oscillatory amplitude sweeps were performed at a constant frequency (1.0 Hz) and the oscillatory frequency sweeps were performed at a constant shear stress (0.5 Pa). These experiments were performed in triplicate and the mean moduli and standard deviation were calculated.

4.7. Scanning Electron Microscopy (SEM)

The gelator **diNO** (40.0 mg) was dissolved in 1.0 mL of water by heating and cooled to room temperature to form the gel. After 24 h, the yellowish opaque gel was filtered through a filter paper and the residue was air dried in a fume hood. The xerogels were gold-coated for 2 min and SEM was performed using a Leo Supra 25 Microscope.

4.8. Crystallography

X-ray quality single-crystals were isolated from water, immediately immersed in cryogenic oil, and mounted. The diffractions were collected using MoK_α radiation (λ = 0.71073 Å) on a Bruker D8 VENTURE (Photon100 CMOS detector) diffractometer equipped with a Cryostream (Oxford Cryosystems, Oxford, UK) open-flow nitrogen cryostat at room temperature. The unit cell determination, data collection, data reduction, structure solution/refinement, and empirical absorption correction (SADABS) were carried out using Apex III (Bruker AXS, Madison, WI, USA). The structure was solved by a direct method and refined by the full-matrix least-squares on F^2 for all data using SHELXTL [77] (Version 2017/1, University of Göttingen, Göttingen, Germany) and Olex2 [78] (Version 1.2, OlexSys Ltd., Durham, U.K.) software. All non-disordered non-hydrogen atoms were refined anisotropically, and the hydrogen atoms were placed in the calculated positions and refined using a riding model.

4.9. X-ray Powder Diffraction (XRPD)

The *N*-oxide compounds (20.0 mg) were dissolved in 1.0 mL of hot water and left undisturbed for crystallization. After crystallization, the mixture was filtered and the residue was dried in air. The crystals were ground to fine powder and XRPD was carried out using a Bruker D8 Focus instrument. The xerogel of **diNO** was prepared by heating 40.0 mg of the compound in 1.0 mL of water (4.0 wt %), and the gel formed was filtered after 24 h followed by drying the residue overnight in a fume hood.

5. Conclusions

We synthesized two mono-*N*-oxides (**INO** and **PNO**) and a di-*N*-oxide (**diNO**) by altering the pyridyl moieties of a known hydrogelator (**4PINA**) to *N*-oxide moieties. The gelation ability of these compounds tested in various solvent/solvent mixtures indicated that selective gelation of **diNO** was observed in water. The mechanical strength and the thermal stability of **diNO** were evaluated using rheology and gel-to-solution transition temperature (T_{gel}) experiments, respectively. The gelation properties of **diNO** were compared with the parent **4PINA** gelator, which indicated that **diNO** is a weaker gelator. SEM images were used to visualize the changes in the morphology of the gel fibers due to the alteration in the functional groups. The effect of various non-bonding interactions in the crystalline state and dried gel was studied using X-ray diffraction. Single-crystal X-ray analysis of the di-*N*-oxide structure revealed the formation of a hydrogen-bonded dimer, which interacted with adjacent dimers via C—H···O interactions to form the extended network, and similar dimers observed in non-gelator **INO** were interconnected through C—H···N interaction. The strong interaction of the mono-*N*-oxide with water molecules indicates the increased hydrophilic nature of these compounds to form solvated crystals. The reduced gelation ability (MGC) and thermal strength of **diNO** may be attributed to the weak intermolecular C—H···O interaction. The absence of strong N—H···N interactions in the *N*-oxide compounds compared to **4PINA** clearly indicate the role of these interactions in gel formation. The tuning of gelation ability (MGC) and thermal/mechanical strength of **4PINA** by alerting the functional group proves the importance of non-bonding interactions and functional groups in designing LMWGs with tunable properties, which contributes to the ongoing efforts to identify the key structural features of gel network formation.

Supplementary Materials: The following are available online at http://www.mdpi.com/1420-3049/24/19/3472/s1, Figure S1: ^{1}H NMR of **diNO** in DMSO-d_6, Figure S2: ^{1}H NMR of **INO** in DMSO-d_6, Figure S3: ^{1}H NMR of **PNO** in DMSO-d_6, Figure S4: IR spectrum of **diNO**, Figure S5: IR spectrum of **INO** (anhydrous form), Figure S6: IR spectrum of **INO** (hydrated form), Figure S7: IR spectrum of **PNO**, Figure S8: IR spectrum of 1:1 mixture of **INO + PNO**, Figure S9: Crystal structure of **diNO**, Figure S10: Crystal structure of **INO.2H$_2$O**, Figure S11: XRPD comparison of **PNO**, Figure S12: XRPD comparison of **INO**, Figure S13: XRPD comparison of **INO.2H$_2$O**, Figure S14: Stress relaxation experiments performed at 1.0% strain, Figure S15: Stress relaxation experiments performed at 10.0% strain, Figure S16: Amplitude and frequency sweeps, Scheme S1: Chemical structure of **4PINA**, Table S1: Gelation table of *N*-oxide compounds, Table S2: Determination of MGC of **diNO**, Table S3: Determination of T_{gel} of **diNO**, Table S4: Crystal data for the *N*-oxide compounds.

Author Contributions: Conceptualization, K.K.D.; Data curation, D.G.; Formal analysis, D.G.; Funding acquisition, K.K.D.; Investigation, D.G.; Methodology, D.G. and M.T.M.; Project administration, K.K.D.; Resources, K.K.D.; Validation, K.K.D.; Writing—original draft, D.G.; Writing—review & editing, K.K.D.

Funding: This research received no external funding.

Acknowledgments: We thank the University of Iceland Research Fund and the Science Institute for funding. D.G. thanks the University of Iceland for the Doctoral Research and Teaching Assistantship grant. We thankfully acknowledge Jonathan Steed, Durham University, Durham, UK for rheology experiments, Sigurjur Sveinn Jonsson, ISOR-Iceland for X-ray powder diffraction analysis, and Sigridur Jonsdottir, University of Iceland for NMR and mass spectroscopy. We thank Rannís Iceland for granting an infrastructure grant for a single-crystal X-ray diffractometer.

Conflicts of Interest: The authors declare no conflict of interest.

References

1. Estroff, L.A.; Hamilton, A.D. Water Gelation by Small Organic Molecules. *Chem. Rev.* **2004**, *104*, 1201–1218. [CrossRef] [PubMed]
2. De Loos, M.; Feringa, B.L.; van Esch, J.H. Design and Application of Self-Assembled Low Molecular Weight Hydrogels. *Eur. J. Org. Chem.* **2005**, *2005*, 3615–3631. [CrossRef]
3. George, M.; Weiss, R.G. Molecular Organogels. Soft Matter Comprised of Low-Molecular-Mass Organic Gelators and Organic Liquids. *Acc. Chem. Res.* **2006**, *39*, 489–497. [CrossRef] [PubMed]
4. Dastidar, P. Supramolecular gelling agents: Can they be designed? *Chem. Soc. Rev.* **2008**, *37*, 2699–2715. [CrossRef] [PubMed]
5. Hirst, A.R.; Escuder, B.; Miravet, J.F.; Smith, D.K. High-Tech Applications of Self-Assembling Supramolecular Nanostructured Gel-Phase Materials: From Regenerative Medicine to Electronic Devices. *Angew. Chem. Int. Ed.* **2008**, *47*, 8002–8018. [CrossRef] [PubMed]
6. Piepenbrock, M.-O.M.; Lloyd, G.O.; Clarke, N.; Steed, J.W. Metal- and Anion-Binding Supramolecular Gels. *Chem. Rev.* **2010**, *110*, 1960–2004. [CrossRef]
7. Steed, J.W. Anion-tuned supramolecular gels: A natural evolution from urea supramolecular chemistry. *Chem. Soc. Rev.* **2010**, *39*, 3686–3699. [CrossRef]
8. Yu, G.; Yan, X.; Han, C.; Huang, F. Characterization of supramolecular gels. *Chem. Soc. Rev.* **2013**, *42*, 6697–6722. [CrossRef]
9. Kumar, D.K.; Steed, J.W. Supramolecular gel phase crystallization: Orthogonal self-assembly under non-equilibrium conditions. *Chem. Soc. Rev.* **2014**, *43*, 2080–2088. [CrossRef]
10. Banerjee, S.; Das, R.K.; Maitra, U. Supramolecular gels 'in action'. *J. Mater. Chem.* **2009**, *19*, 6649–6687. [CrossRef]
11. Foster, J.A.; Damodaran, K.K.; Maurin, A.; Day, G.M.; Thompson, H.P.G.; Cameron, G.J.; Bernal, J.C.; Steed, J.W. Pharmaceutical polymorph control in a drug-mimetic supramolecular gel. *Chem. Sci.* **2017**, *8*, 78–84. [CrossRef] [PubMed]
12. Terech, P.; Weiss, R.G. Low Molecular Mass Gelators of Organic Liquids and the Properties of Their Gels. *Chem. Rev.* **1997**, *97*, 3133–3160. [CrossRef] [PubMed]
13. Du, X.; Zhou, J.; Shi, J.; Xu, B. Supramolecular Hydrogelators and Hydrogels: From Soft Matter to Molecular Biomaterials. *Chem. Rev.* **2015**, *115*, 13165–13307. [CrossRef] [PubMed]
14. Babu, S.S.; Praveen, V.K.; Ajayaghosh, A. Functional π-Gelators and Their Applications. *Chem. Rev.* **2014**, *114*, 1973–2129. [CrossRef] [PubMed]
15. Worthington, P.; Pochan, D.J.; Langhans, S.A. Peptide Hydrogels—Versatile Matrices for 3D Cell Culture in Cancer Medicine. *Front. Oncol.* **2015**, *5*, 92. [CrossRef] [PubMed]
16. Truong, W.T.; Su, Y.; Meijer, J.T.; Thordarson, P.; Braet, F. Self-Assembled Gels for Biomedical Applications. *Chem. Asian J.* **2011**, *6*, 30–42. [CrossRef] [PubMed]
17. Li, J.-L.; Wang, R.-Y.; Liu, X.-Y.; Pan, H.-H. Nanoengineering of a Biocompatible Organogel by Thermal Processing. *J. Phys. Chem. B* **2009**, *113*, 5011–5015. [CrossRef] [PubMed]
18. Li, J.-L.; Liu, X.-Y.; Wang, R.-Y.; Xiong, J.-Y. Architecture of a Biocompatible Supramolecular Material by Supersaturation-Driven Fabrication of its Fiber Network. *J. Phys. Chem. B* **2005**, *109*, 24231–24235. [CrossRef] [PubMed]
19. Afrasiabi, R.; Kraatz, H.-B. Sonication-Induced Coiled Fibrous Architectures of Boc-L-Phe-L-Lys(Z)-OMe. *Chem. Eur. J.* **2013**, *19*, 1769–1777. [CrossRef] [PubMed]
20. Dhibar, S.; Dey, A.; Majumdar, S.; Ghosh, D.; Mandal, A.; Ray, P.P.; Dey, B. A supramolecular Cd(ii)-metallogel: An efficient semiconductive electronic device. *Dalton Trans.* **2018**, *47*, 17412–17420. [CrossRef] [PubMed]
21. Wang, R.-Y.; Liu, X.-Y.; Li, J.-L. Engineering Molecular Self-Assembled Fibrillar Networks by Ultrasound. *Cryst. Growth Des.* **2009**, *9*, 3286–3291. [CrossRef]
22. Alexander, S.L.M.; Korley, L.T.J. Nucleation effects of high molecular weight polymer additives on low molecular weight gels. *Polym. J.* **2018**, *50*, 775–786. [CrossRef]
23. Wang, R.-Y.; Liu, X.-Y.; Narayanan, J.; Xiong, J.-Y.; Li, J.-L. Architecture of Fiber Network: From Understanding to Engineering of Molecular Gels. *J. Phys. Chem. B* **2006**, *110*, 25797–25802. [CrossRef] [PubMed]
24. Draper, E.R.; Adams, D.J. How should multicomponent supramolecular gels be characterised? *Chem. Soc. Rev.* **2018**, *47*, 3395–3405. [CrossRef] [PubMed]

25. Cao, X.; Meng, L.; Li, Z.; Mao, Y.; Lan, H.; Chen, L.; Fan, Y.; Yi, T. Large Red-Shifted Fluorescent Emission via Intermolecular π–π Stacking in 4-Ethynyl-1,8-naphthalimide-Based Supramolecular Assemblies. *Langmuir* **2014**, *30*, 11753–11760. [CrossRef] [PubMed]
26. Wang, C.; Zhang, D.; Zhu, D. A Chiral Low-Molecular-Weight Gelator Based on Binaphthalene with Two Urea Moieties: Modulation of the CD Spectrum after Gel Formation. *Langmuir* **2007**, *23*, 1478–1482. [CrossRef]
27. Wang, C.; Zhang, D.; Xiang, J.; Zhu, D. New Organogels Based on an Anthracene Derivative with One Urea Group and Its Photodimer: Fluorescence Enhancement after Gelation. *Langmuir* **2007**, *23*, 9195–9200. [CrossRef]
28. Wang, G.; Cheuk, S.; Yang, H.; Goyal, N.; Reddy, P.V.N.; Hopkinson, B. Synthesis and Characterization of Monosaccharide-Derived Carbamates as Low-Molecular-Weight Gelators. *Langmuir* **2009**, *25*, 8696–8705. [CrossRef]
29. Gao, W.; Liang, Y.; Peng, X.; Hu, Y.; Zhang, L.; Wu, H.; He, B. In situ injection of phenylboronic acid based low molecular weight gels for efficient chemotherapy. *Biomaterials* **2016**, *105*, 1–11. [CrossRef]
30. Das, U.K.; Banerjee, S.; Dastidar, P. Remarkable Shape-Sustaining, Load-Bearing, and Self-Healing Properties Displayed by a Supramolecular Gel Derived from a Bis-pyridyl-bis-amide of L-Phenyl Alanine. *Chem. Asian J.* **2014**, *9*, 2475–2482. [CrossRef]
31. Tang, Y.-T.; Dou, X.-Q.; Ji, Z.-A.; Li, P.; Zhu, S.-M.; Gu, J.-J.; Feng, C.-L.; Zhang, D. C2-symmetric cyclohexane-based hydrogels: A rational designed LMWG and its application in dye scavenging. *J. Mol. Liq.* **2013**, *177*, 167–171. [CrossRef]
32. Li, P.; Dou, X.-Q.; Tang, Y.-T.; Zhu, S.; Gu, J.; Feng, C.-L.; Zhang, D. Gelator-polysaccharide hybrid hydrogel for selective and controllable dye release. *J. Colloid Interface Sci.* **2012**, *387*, 115–122. [CrossRef] [PubMed]
33. Ghosh, D.; Lebedytė, I.; Yufit, D.S.; Damodaran, K.K.; Steed, J.W. Selective gelation of *N*-(4-pyridyl)nicotinamide by copper(ii) salts. *CrystEngComm* **2015**, *17*, 8130–8138. [CrossRef]
34. Kumar, D.K.; Jose, D.A.; Dastidar, P.; Das, A. Nonpolymeric Hydrogelator Derived from *N*-(4-Pyridyl)isonicotinamide. *Langmuir* **2004**, *20*, 10413–10418. [CrossRef] [PubMed]
35. Sahoo, P.; Kumar, D.K.; Raghavan, S.R.; Dastidar, P. Supramolecular Synthons in Designing Low Molecular Mass Gelling Agents: L-Amino Acid Methyl Ester Cinnamate Salts and their Anti-Solvent-Induced Instant Gelation. *Chem. Asian J.* **2011**, *6*, 1038–1047. [CrossRef] [PubMed]
36. Bhattacharjee, S.; Bhattacharya, S. Role of synergistic [small pi]-[small pi] stacking and X-H[three dots, centered]Cl (X = C, N, O) H-bonding interactions in gelation and gel phase crystallization. *Chem. Commun.* **2015**, *51*, 7019–7022. [CrossRef] [PubMed]
37. Jones, C.D.; Steed, J.W. Gels with sense: Supramolecular materials that respond to heat, light and sound. *Chem. Soc. Rev.* **2016**, *45*, 6546–6596. [CrossRef]
38. Ghosh, D.; Ferfolja, K.; Drabavičius, Ž.; Steed, J.W.; Damodaran, K.K. Crystal habit modification of Cu(ii) isonicotinate–*N*-oxide complexes using gel phase crystallisation. *New J. Chem.* **2018**, *42*, 19963–19970. [CrossRef]
39. Desiraju, G.R. Supramolecular Synthons in Crystal Engineering—A New Organic Synthesis. *Angew. Chem. Int. Ed.* **1995**, *34*, 2311–2327. [CrossRef]
40. Weiss, R.G.; Terech, P. *Molecular Gels: Materials with Self-Assembled Fibrillar Networks*; Springer: Heidelberg, Germany, 2006; p. 978.
41. Fages, F.; Voegtle, F.; Zinic, M. Systematic design of amide- and urea-type gelators with tailored properties. *Top. Curr. Chem.* **2005**, *256*, 77–131.
42. Isare, B.; Pensec, S.; Raynal, M.; Bouteiller, L. Bisurea-based supramolecular polymers: From structure to properties1. *C. R. Chim.* **2016**, *19*, 148–156. [CrossRef]
43. Gale, P.A.; Busschaert, N.; Haynes, C.J.E.; Karagiannidis, L.E.; Kirby, I.L. Anion receptor chemistry: Highlights from 2011 and 2012. *Chem. Soc. Rev.* **2014**, *43*, 205–241. [CrossRef] [PubMed]
44. Dzolic, Z.; Cametti, M.; Dalla Cort, A.; Mandolini, L.; Zinic, M. Fluoride-responsive organogelator based on oxalamide-derived anthraquinone. *Chem. Commun.* **2007**, *34*, 3535–3537. [CrossRef] [PubMed]
45. Kotova, O.; Daly, R.; dos Santos, C.M.G.; Boese, M.; Kruger, P.E.; Boland, J.J.; Gunnlaugsson, T. Europium-Directed Self-Assembly of a Luminescent Supramolecular Gel from a Tripodal Terpyridine-Based Ligand. *Angew. Chem. Int. Ed.* **2012**, *51*, 7208–7212. [CrossRef] [PubMed]
46. Feng, L.; Cavicchi, K.A. Investigation of the relationships between the thermodynamic phase behavior and gelation behavior of a series of tripodal trisamide compounds. *Soft Matter* **2012**, *8*, 6483–6492. [CrossRef]

47. Mukhopadhyay, S.; Ira; Krishnamoorthy, G.; Maitra, U. Dynamics of Bound Dyes in a Nonpolymeric Aqueous Gel Derived from a Tripodal Bile Salt. *J. Phys. Chem. B* **2003**, *107*, 2189–2192. [CrossRef]
48. Li, Z.; Cao, J.; Li, H.; Liu, H.; Han, F.; Liu, Z.; Tong, C.; Li, S. Self-assembled drug delivery system based on low-molecular-weight bis-amide organogelator: Synthesis, properties and in vivo evaluation. *Drug Deliv.* **2016**, *23*, 3168–3178. [CrossRef] [PubMed]
49. Bradberry, S.J.; Dee, G.; Kotova, O.; McCoy, C.P.; Gunnlaugsson, T. Luminescent lanthanide (Eu(iii)) cross-linked supramolecular metallo co-polymeric hydrogels: The effect of ligand symmetry. *Chem. Commun.* **2019**, *55*, 1754–1757. [CrossRef] [PubMed]
50. Kumar, D.K.; Jose, D.A.; Dastidar, P.; Das, A. Nonpolymeric Hydrogelators Derived from Trimesic Amides. *Chem. Mater.* **2004**, *16*, 2332–2335. [CrossRef]
51. Meazza, L.; Foster, J.A.; Fucke, K.; Metrangolo, P.; Resnati, G.; Steed, J.W. Halogen-bonding-triggered supramolecular gel formation. *Nat. Chem.* **2013**, *5*, 42–47. [CrossRef]
52. Pal, A.; Ghosh, Y.K.; Bhattacharya, S. Molecular mechanism of physical gelation of hydrocarbons by fatty acid amides of natural amino acids. *Tetrahedron* **2007**, *63*, 7334–7348. [CrossRef]
53. Kawamoto, K.; Grindy, S.C.; Liu, J.; Holten-Andersen, N.; Johnson, J.A. Dual Role for 1,2,4,5-Tetrazines in Polymer Networks: Combining Diels–Alder Reactions and Metal Coordination to Generate Functional Supramolecular Gels. *ACS Macro Lett.* **2015**, *4*, 458–461. [CrossRef]
54. Das, U.K.; Banerjee, S.; Dastidar, P. Primary Ammonium Monocarboxylate Synthon in Designing Supramolecular Gels: A New Series of Chiral Low-Molecular-Weight Gelators Derived from Simple Organic Salts that are Capable of Generating and Stabilizing Gold Nanoparticles. *Chem. Asian J.* **2013**, *8*, 3022–3031. [CrossRef] [PubMed]
55. Jin, Q.; Zhang, L.; Liu, M. Solvent-Polarity-Tuned Morphology and Inversion of Supramolecular Chirality in a Self-Assembled Pyridylpyrazole-Linked Glutamide Derivative: Nanofibers, Nanotwists, Nanotubes, and Microtubes. *Chem. Eur. J.* **2013**, *19*, 9234–9241. [CrossRef] [PubMed]
56. Karak, S.; Kumar, S.; Bera, S.; Diaz, D.D.; Banerjee, S.; Vanka, K.; Banerjee, R. Interplaying anions in a supramolecular metallohydrogel to form metal organic frameworks. *Chem. Commun.* **2017**, *53*, 3705–3708. [CrossRef] [PubMed]
57. Kartha, K.K.; Praveen, V.K.; Babu, S.S.; Cherumukkil, S.; Ajayaghosh, A. Pyridyl-Amides as a Multimode Self-Assembly Driver for the Design of a Stimuli-Responsive π-Gelator. *Chem. Asian J.* **2015**, *10*, 2250–2256. [CrossRef] [PubMed]
58. Liu, Q.; Wang, Y.; Li, W.; Wu, L. Structural Characterization and Chemical Response of a Ag-Coordinated Supramolecular Gel. *Langmuir* **2007**, *23*, 8217–8223. [CrossRef] [PubMed]
59. Lee, H.H.; Jung, S.H.; Park, S.; Park, K.-M.; Jung, J.H. A metal-organic framework gel with Cd2+ derived from only coordination bonds without intermolecular interactions and its catalytic ability. *New J. Chem.* **2013**, *37*, 2330–2335. [CrossRef]
60. Aoyama, R.; Sako, H.; Amakatsu, M.; Yamanaka, M. Palladium ion-induced supramolecular gel formation of tris-urea molecules. *Polym. J.* **2015**, *47*, 136–140. [CrossRef]
61. Ghosh, K.; Panja, S.; Bhattacharya, S. Naphthalene linked pyridyl urea as a supramolecular gelator: A new insight into naked eye detection of I- in the gel state with semiconducting behaviour. *RSC Adv.* **2015**, *5*, 72772–72779. [CrossRef]
62. Kumar, D.P. Synthesis of gold nanoparticles and nanoclusters in a supramolecular gel and their applications in catalytic reduction of p-nitrophenol to p-aminophenol and Hg(ii) sensing. *RSC Adv.* **2014**, *4*, 45449–45457. [CrossRef]
63. Byrne, P.; Lloyd, G.O.; Applegarth, L.; Anderson, K.M.; Clarke, N.; Steed, J.W. Metal-induced gelation in dipyridyl ureas. *New J. Chem.* **2010**, *34*, 2261–2274. [CrossRef]
64. Pandurangan, K.; Kitchen, J.A.; Blasco, S.; Paradisi, F.; Gunnlaugsson, T. Supramolecular pyridyl urea gels as soft matter with antibacterial properties against MRSA and/or *E. coli*. *Chem. Commun.* **2014**, *50*, 10819–10822. [CrossRef] [PubMed]
65. Stanley, C.E.; Clarke, N.; Anderson, K.M.; Elder, J.A.; Lenthall, J.T.; Steed, J.W. Anion binding inhibition of the formation of a helical organogel. *Chem. Commun.* **2006**, *30*, 3199–3201. [CrossRef] [PubMed]
66. Goodwin, J.W.; Hughes, R.W. *Rheology for Chemists: An Introduction*, 2nd ed.; Royal Society of Chemistry: Cambridge, UK, 2008; p. 264.

67. Guenet, J.-M. Rheological Aspects. In *Organogels: Thermodynamics, Structure, Solvent Role, and Properties*; Guenet, J.-M., Ed.; Springer International Publishing: Cham, Switzerland, 2016; pp. 83–94.
68. Sathaye, S.; Mbi, A.; Sonmez, C.; Chen, Y.; Blair, D.L.; Schneider, J.P.; Pochan, D.J. Rheology of peptide- and protein-based physical hydrogels: Are everyday measurements just scratching the surface? *Wiley Interdiscip. Rev. Nanomed. Nanobiotechnol.* **2015**, *7*, 34–68. [CrossRef] [PubMed]
69. Zuidema, J.M.; Rivet, C.J.; Gilbert, R.J.; Morrison, F.A. A protocol for rheological characterization of hydrogels for tissue engineering strategies. *J. Biomed. Mater. Res. B* **2014**, *102*, 1063–1073. [CrossRef]
70. Gaharwar, A.K.; Avery, R.K.; Assmann, A.; Paul, A.; McKinley, G.H.; Khademhosseini, A.; Olsen, B.D. Shear-Thinning Nanocomposite Hydrogels for the Treatment of Hemorrhage. *ACS Nano* **2014**, *8*, 9833–9842. [CrossRef]
71. Dasgupta, D.; Thierry, A.; Rochas, C.; Ajayaghosh, A.; Guenet, J.M. Key role of solvent type in organogelation. *Soft Matter* **2012**, *8*, 8714–8721. [CrossRef]
72. Colquhoun, C.; Draper, E.R.; Eden, E.G.B.; Cattoz, B.N.; Morris, K.L.; Chen, L.; McDonald, T.O.; Terry, A.E.; Griffiths, P.C.; Serpell, L.C.; et al. The effect of self-sorting and co-assembly on the mechanical properties of low molecular weight hydrogels. *Nanoscale* **2014**, *6*, 13719–13725. [CrossRef]
73. Raeburn, J.; Adams, D.J. Multicomponent low molecular weight gelators. *Chem. Commun.* **2015**, *51*, 5170–5180. [CrossRef]
74. Tómasson, D.A.; Ghosh, D.; Kržišnik, Z.; Fasolin, L.H.; Vicente, A.A.; Martin, A.D.; Thordarson, P.; Damodaran, K.K. Enhanced Mechanical and Thermal Strength in Mixed-Enantiomers-Based Supramolecular Gel. *Langmuir* **2018**, *34*, 12957–12967. [CrossRef] [PubMed]
75. Sauvée, C.; Ström, A.; Haukka, M.; Sundén, H. A Multi-Component Reaction towards the Development of Highly Modular Hydrogelators. *Chem. Eur. J.* **2018**, *24*, 8071–8075. [CrossRef]
76. Gardner, J.N.; Katritzky, A.R. 875. *N*-oxides and related compounds. Part V. The tautomerism of 2- and 4-amino- and -hydroxy-pyridine 1-oxide. *J. Chem. Soc.* **1957**, 4375–4385. [CrossRef]
77. Sheldrick, G.M. Crystal structure refinement with SHELXL. *Acta Crystallogr. Sect. C Struct. Chem.* **2015**, *71 Pt 1*, 3–8. [CrossRef] [PubMed]
78. Dolomanov, O.V.; Bourhis, L.J.; Gildea, R.J.; Howard, J.A.K.; Puschmann, H. OLEX2: A complete structure solution, refinement and analysis program. *J. Appl. Crystallogr.* **2009**, *42*, 339–341. [CrossRef]

Sample Availability: Samples of the compounds **diNO**, **INO**, and **PNO** are available from the authors.

Supplementary Information

Tuning gel state properties of supramolecular gels by functional group modification

Dipankar Ghosh, Matthew T. Mulvee and Krishna K. Damodaran*

Table of content

Chemical Structure of 4PINA

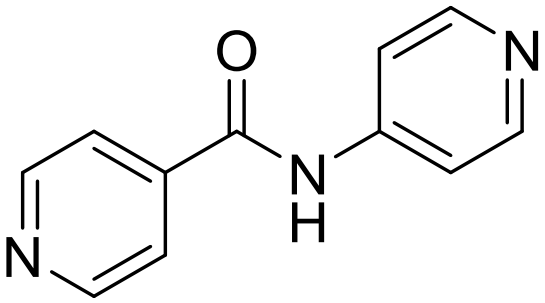

Scheme S1: Chemical structure of 4PINA

NMR spectra of the *N*-oxide compounds

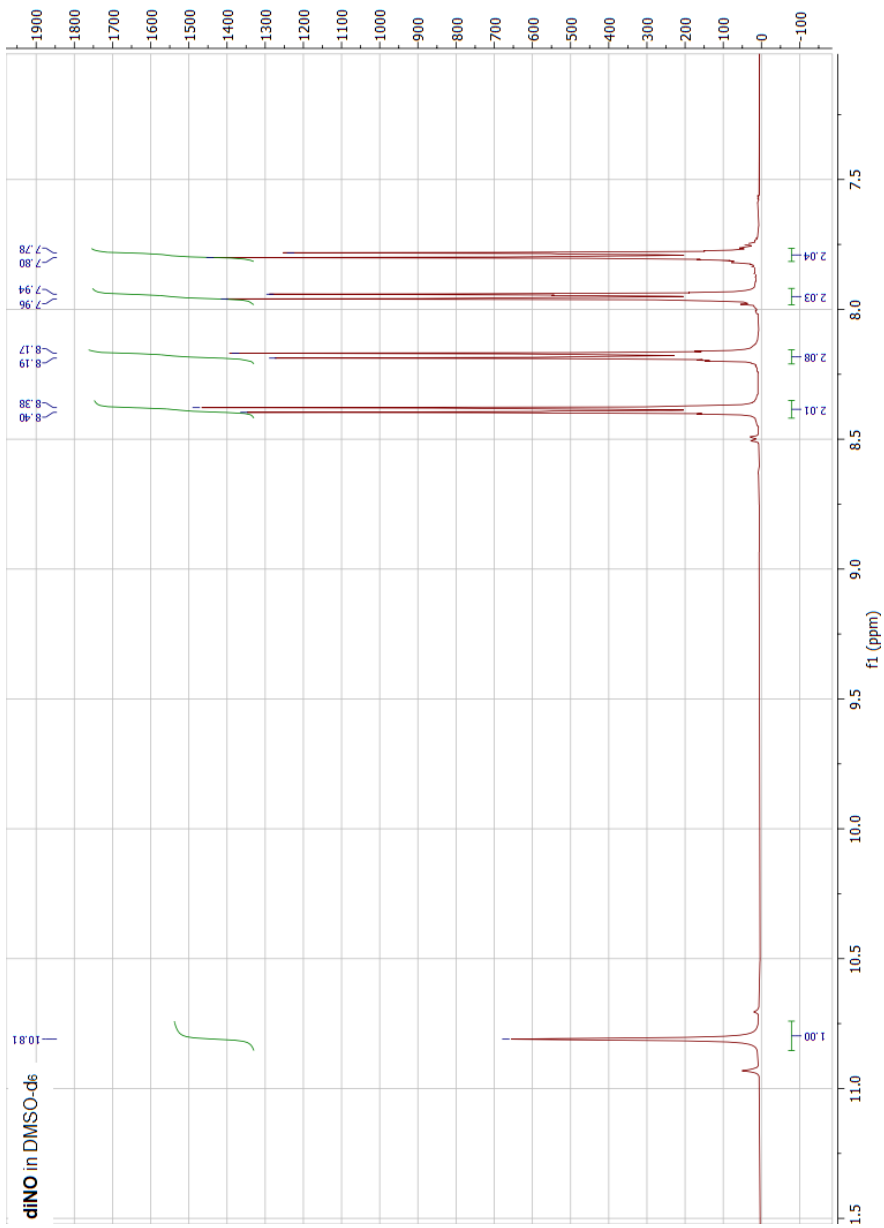

Figure S1: ^{1}H-NMR of **diNO** in DMSO-d_6

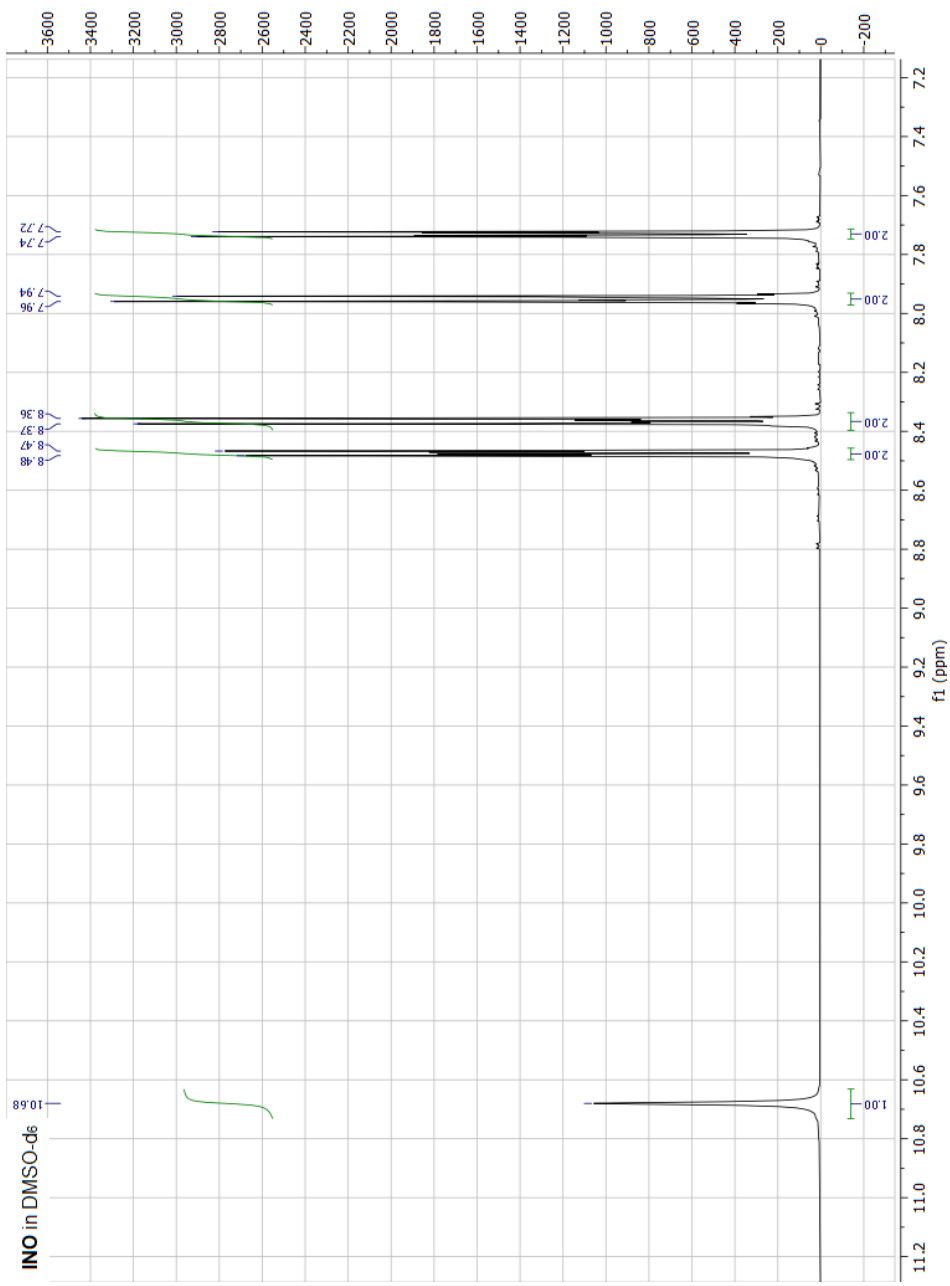

Figure S2: ^{1}H-NMR of **INO** in DMSO-d_6

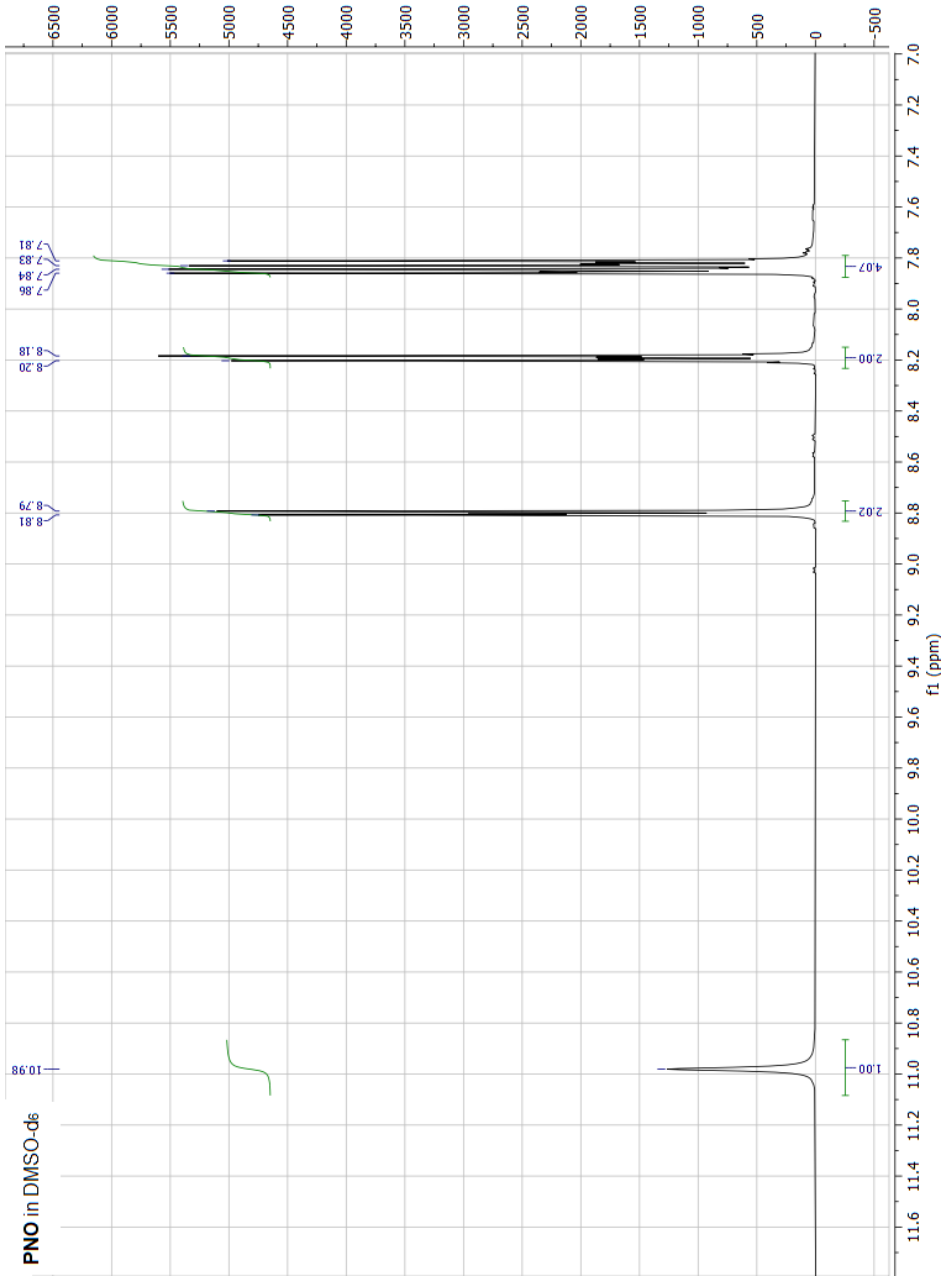

Figure S3: ^{1}H-NMR of **PNO** in DMSO-d_6

IR spectra of the *N*-oxide compounds

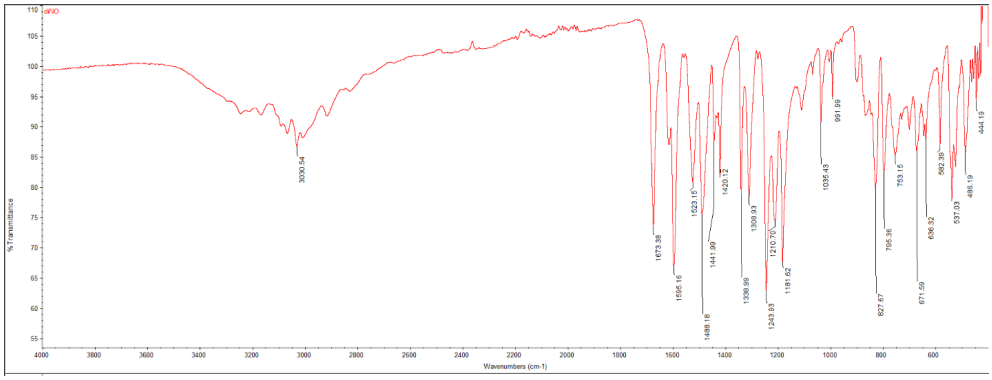

Figure S4: IR spectrum of **diNO**

Figure S5: IR spectrum of **iNO** (anhydrous form)

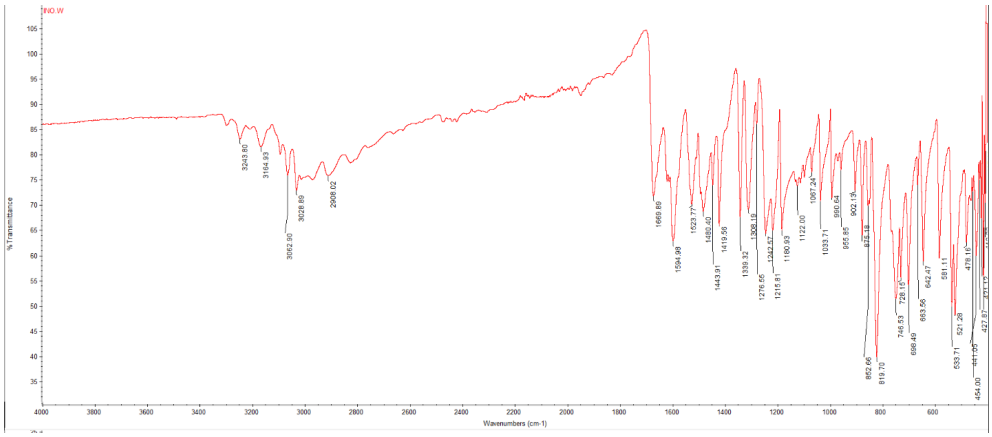

Figure S6: IR spectrum of **INO** (hydrated form)

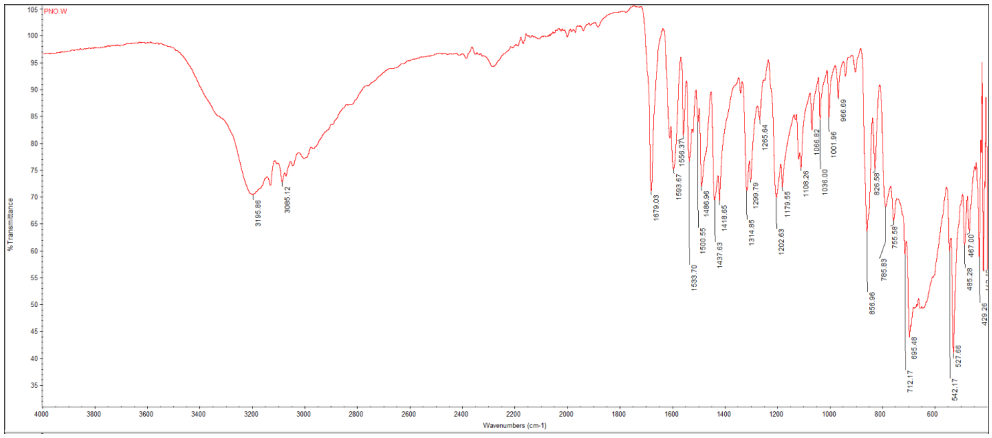

Figure S7: IR spectrum of **PNO**

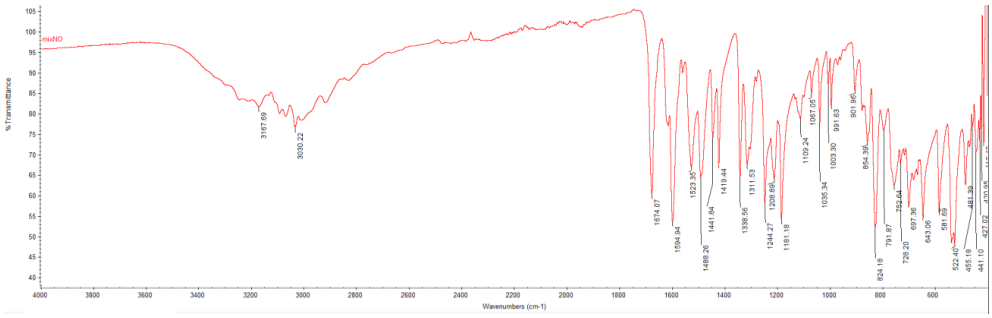

Figure S8: IR spectrum of 1:1 mixture of **INO + PNO**

Gelation experiments

Table S1: Gelation Table of *N*-oxide compounds

Compound	Amount	Solvent (1.0 mL)	Initial Observation	Observation in 24 h
diNO	10 mg	Methanol	Insoluble	Precipitate
diNO	10 mg	Ethanol	Insoluble	Precipitate
diNO	10 mg	Tetrahydrofuran	Insoluble	Precipitate
diNO	10 mg	Acetonitrile	Insoluble	Precipitate
diNO	10 mg	Nitrobenzene	Insoluble	Precipitate
diNO	10 mg	Water	Solution	Solution
diNO	20 mg	Water	Solution	Crystal
diNO	30 mg	Water	Solution	Crystal
diNO	40 mg	Water	Solution	Gel
diNO	60 mg	Water	Solution	Gel
diNO	10 mg	Water/MeOH	Colloidal	Crystalline precipitate
diNO	10 mg	Water/EtOH	Colloidal	Precipitate
diNO	10 mg	Water/THF	Colloidal	Precipitate
diNO	10 mg	Water/MeCN	Colloidal	Precipitate
diNO	10 mg	Water/$PhNO_2$	Insoluble	Precipitate
diNO	20 mg	Water/MeOH	Insoluble	Precipitate
diNO	20 mg	Water/EtOH	Insoluble	Precipitate
INO	10 mg	Methanol	Insoluble	Precipitate
INO	10 mg	Ethanol	Insoluble	Precipitate
INO	10 mg	Tetrahydrofuran	Insoluble	Precipitate
INO	10 mg	Acetonitrile	Insoluble	Precipitate
INO	10 mg	Nitrobenzene	Insoluble	Precipitate
INO	10 mg	Water	Solution	Solution
INO	20 mg	Water	Solution	Crystal
INO	30 mg	Water	Solution	Crystal
INO	40 mg	Water	Solution	Crystal
INO	60 mg	Water	Solution	Crystal
INO	10 mg	Water/MeOH	Solution	Precipitate
INO	10 mg	Water/EtOH	Solution	Precipitate
INO	10 mg	Water/THF	Colloidal	Precipitate
INO	10 mg	Water/MeCN	Colloidal	Precipitate
INO	10 mg	Water/$PhNO_2$	Insoluble	Precipitate
INO	20 mg	Water/MeOH	Insoluble	Precipitate
INO	20 mg	Water/EtOH	Insoluble	Precipitate
PNO	10 mg	Methanol	Insoluble	Precipitate
PNO	10 mg	Ethanol	Insoluble	Precipitate
PNO	10 mg	Tetrahydrofuran	Insoluble	Precipitate
PNO	10 mg	Acetonitrile	Insoluble	Precipitate
PNO	10 mg	Nitrobenzene	Insoluble	Precipitate

*Table **S1** continued*				
PNO	10 mg	Water	Solution	Solution
PNO	20 mg	Water	Solution	Crystal
PNO	30 mg	Water	Solution	Crystal
PNO	40 mg	Water	Solution	Crystal
PNO	60 mg	Water	Solution	Crystal
PNO	10 mg	Water/MeOH	Colloidal	Precipitate
PNO	10 mg	Water/EtOH	Colloidal	Precipitate
PNO	10 mg	Water/THF	Colloidal	Precipitate
PNO	10 mg	Water/MeCN	Colloidal	Precipitate
PNO	10 mg	Water/$PhNO_2$	Insoluble	Precipitate
INO + PNO	10 mg	Methanol	Insoluble	Precipitate
INO + PNO	10 mg	Ethanol	Insoluble	Precipitate
INO + PNO	10 mg	Tetrahydrofuran	Insoluble	Precipitate
INO + PNO	10 mg	Acetonitrile	Insoluble	Precipitate
INO + PNO	10 mg	Nitrobenzene	Insoluble	Precipitate
INO + PNO	10 mg	Water	Solution	Solution
INO + PNO	20 mg	Water	Solution	Crystal
INO + PNO	30 mg	Water	Solution	Crystal
INO + PNO	40 mg	Water	Solution	Crystal
INO + PNO	60 mg	Water	Solution	Crystal
INO + PNO	10 mg	Water/MeOH	Colloidal	Precipitate
INO + PNO	10 mg	Water/EtOH	Colloidal	Precipitate
INO + PNO	10 mg	Water/THF	Colloidal	Precipitate
INO + PNO	10 mg	Water/MeCN	Colloidal	Precipitate
INO + PNO	10 mg	Water/$PhNO_2$	Insoluble	Precipitate

Table S2: Determination of MGC of **diNO**

Amount	Solvent (1.0 mL)	Initial Observation	Observation in 24 h
30 mg	Water	Solution	Crystal
33 mg	Water	Solution	Crystal
36 mg	Water	Solution	Partial Gel
38 mg	Water	Solution	Partial Gel
40 mg	Water	Solution	Gel
45 mg	Water	Solution	Gel
50 mg	Water	Solution	Gel

Table S3: Determination of T_{gel} of **diNO**

Amount	Solvent (1.0 mL)	Time	T_{gel}
40 mg	Water	24 h	78.0 °C
60 mg	Water	24 h	80.0 °C

Crystal Data of the *N*-oxide compounds

Table S4: Crystal Data for the *N*-oxide compounds

Crystal data	**diNO**	**INO**	**INO.2H$_2$O**	**PNO.2H$_2$O**
Empirical formula	$C_{11}H_9N_3O_3$	$C_{11}H_9N_3O_2$	$C_{11}H_{13}N_3O_4$	$C_{11}H_{13}N_3O_4$
Colour	Colourless	Colourless	Colourless	Colourless
Formula weight	231.21	215.21	251.24	251.24
Crystal size (mm)	0.3x0.18x0.08	0.45x0.2x0.08	0.48x0.24x0.18	0.24x0.21x0.14
Crystal system	triclinic	triclinic	monoclinic	triclinic
Space group	Pī	Pī	C2/c	Pī
a (Å)	6.6694(9)	6.8242(10)	18.2418(15)	7.4444(6)
b (Å)	8.5614(12)	8.5382(13)	13.0771(11)	8.1856(7)
c (Å)	9.2107(13)	9.1542(13)	13.6389(11)	10.0952(9)
α (°)	95.653(4)	98.243(4)	90	95.322(3)
β (°)	101.326(4)	105.184(4)	130.390(2)	103.371(3)
γ (°)	104.266(4)	103.773(4)	90	90.353(3)
Volume (Å^3)	493.77(12)	487.77(12)	2478.1(4)	595.67(9)
Z	2	2	8	2
$D_{calc.}$ (g/cm^3)	1.555	1.465	1.347	1.401
F(000)	240	224	1056	264
μ MoKα (mm^{-1})	0.117	0.105	0.104	0.109
Temperature (K)	296(2)	296(2)	300(2)	296(2)
Reflections collected/ unique/observed [I>2σ(I)]	23437/2796/2258	22681/2860/2515	37643/3488/2490	23800/3371/2722
Data/restraints/parameters	2796/0/154	2860/0/145	3488/0/179	3371/0/179
Goodness of fit on F^2	1.033	1.050	1.043	1.090
Final R indices [I>2σ(I)]	R_1 = 0.0453 wR_2 = 0.1271	R_1 = 0.0423 wR_2 = 0.1221	R_1 = 0.0457 wR_2 = 0.1309	R_1 = 0.0423 wR_2 = 0.1272
R indices (all data)	R_1 = 0.0601 wR_2 = 0.1355	R_1 = 0.0482 wR_2 = 0.1280	R_1 = 0.0687 wR_2 = 0.1441	R_1 = 0.0546 wR_2 = 0.1351

Crystal Structures

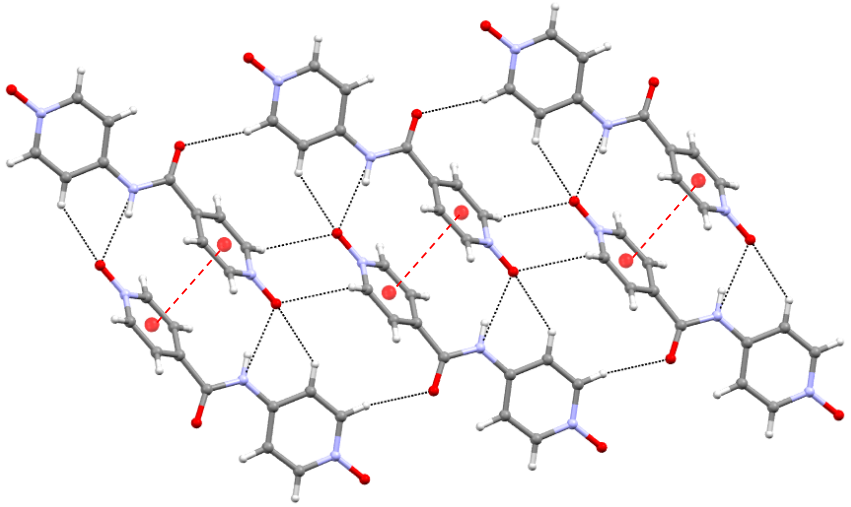

Figure S9: Crystal structure of **diNO** showing π—π and C—H···O interactions

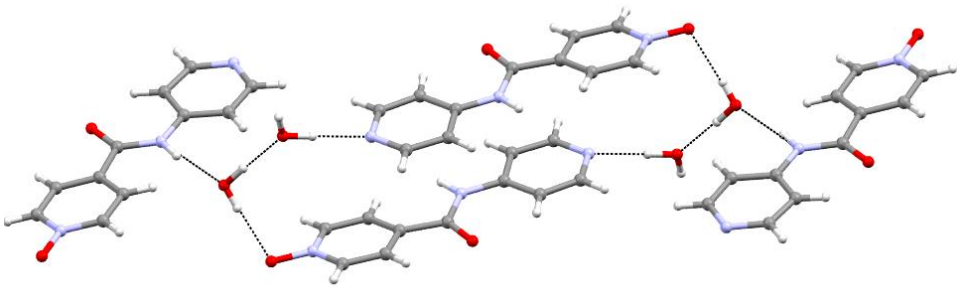

Figure S10: Crystal structure of **INO.2H$_2$O** showing hydrogen-bonding with water molecules

X-ray powder diffraction (XRPD)

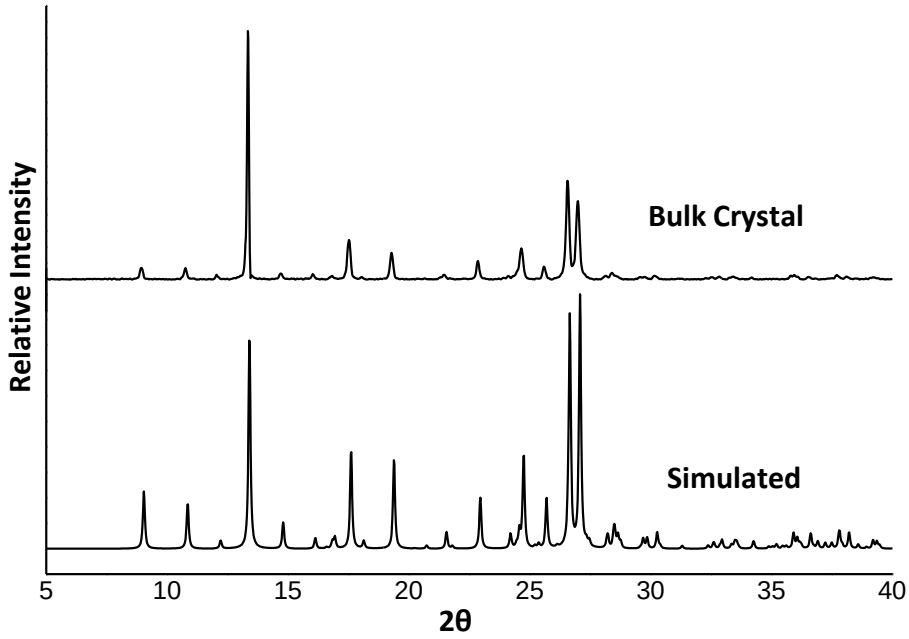

Figure S11: XRPD comparison of **PNO**: simulated pattern from SCXRD data and bulk crystals obtained from water

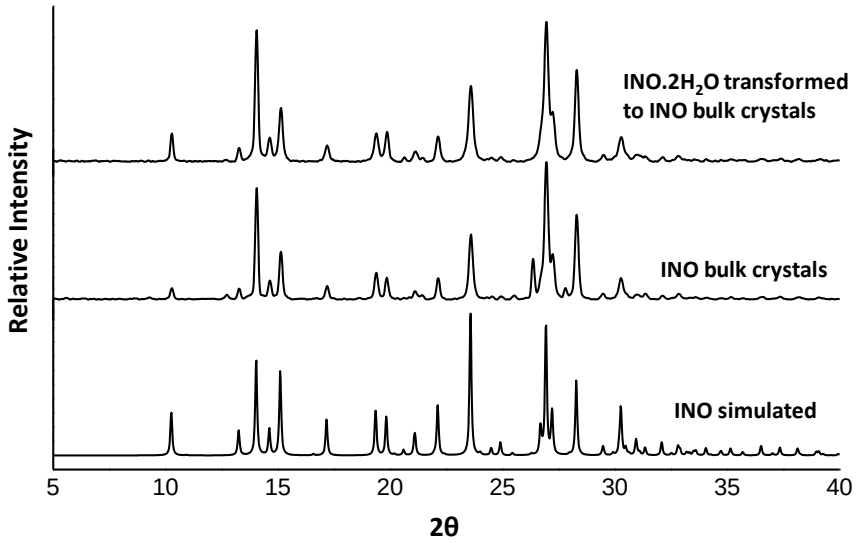

Figure S12: XRPD comparison of **INO**: simulated pattern of **INO**, bulk crystals of **INO** and **INO.2H$_2$O**. The pattern indicates that the kinetically favored form **INO.2H$_2$O** was slowly converted to the thermodynamically stable **INO** form.

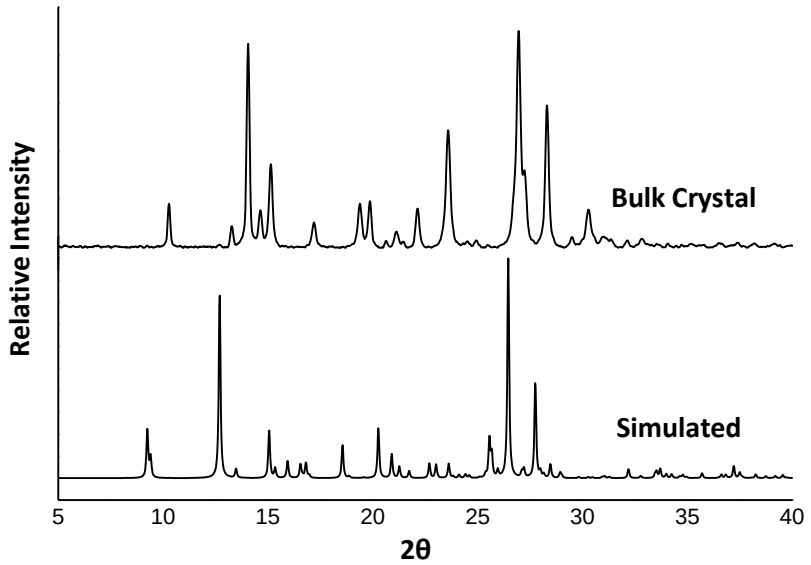

Figure S13: XRPD comparison of **INO.2H$_2$O** (hydrated form): Simulated pattern and bulk crystals obtained from water.

Rheology experiments

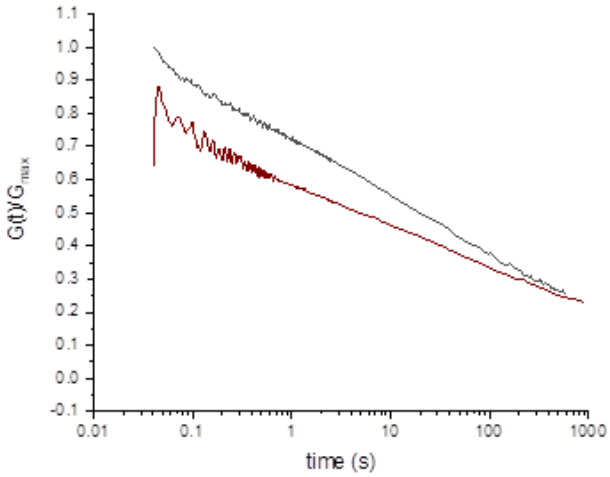

Figure S14: Stress relaxation experiments performed at 1.0% strain indicating that both samples show an extensive relaxation time, indicative of a gel-like response which have a temporally persistent entangled network.

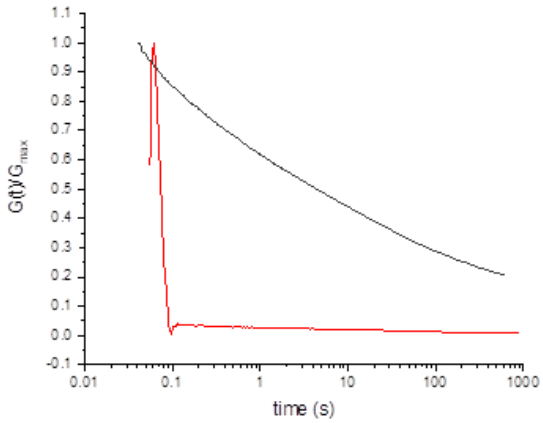

Figure S15: Stress relaxation experiments performed at 10.0% strain showing the difference between the relaxation time of **4PINA** and **diNO**.

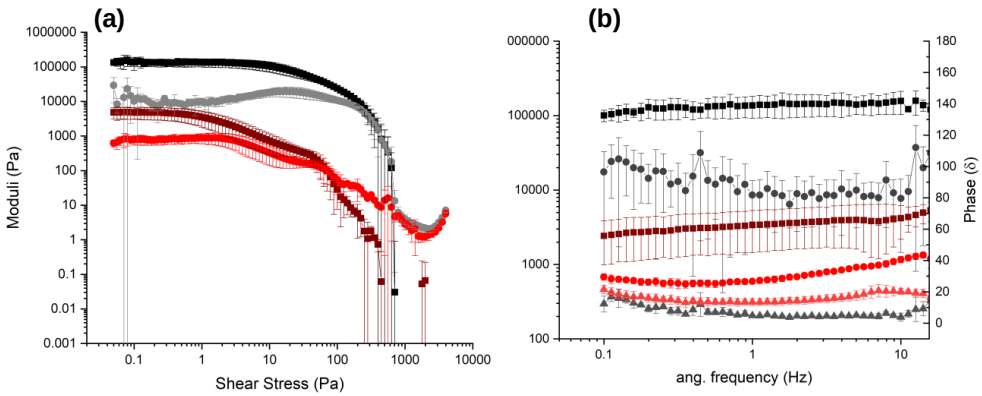

Figure S16: Oscillatory amplitude sweeps (a) and oscillatory frequency sweeps (b), for **4PINA** (black) and **diNO** (red). For both ▪ refer to G' and ● refer to G", the storage modulus and viscous modulus, at 4.0 wt% respectively. Δ refer to the phase lag (δ). Error bars indicate the standard deviation calculated from the repeated measurements

Article-II

This manuscript is in final form and ready for submission in a peer reviewed journal, and included as it is at the current version.

Project details:

″Tuning the gelation properties of supramolecular gel based on (bis)pyridyl urea by altering the non-bonding interactions″

Dipankar Ghosh, Ragnar Björnsson, Iwona T. Myszor, Gudmundur H. Gudmundsson and Krishna K. Damodaran*

Author contributions:

D.G. and K.K.D. planned and designed the research. **D.G.** synthesized the gelators, performed characterizations, solved single crystal structures and evaluated gelation properties, stimuli-responsive properties and rheology measurements. R.B. and I.T.M. carried out the theoretical calculation and antibacterial properties, respectively. K.K.D. and **D.G.** wrote the initial manuscript draft and all authors are reviewing the manuscript.

FULL PAPER

Tuning the gelation properties of supramolecular gel based on (bis)pyridyl urea by altering the non-bonding interactions

Dipankar Ghosh,[a] Ragnar Bjornsson,[b] Iwona T. Myszor,[c] Gudmundur H. Gudmundsson[c] and Krishna K. Damodaran*[a]

[a] Mr. Dipankar Ghosh and Dr. Krishna K Damodaran
Department of Chemistry, Science Institute,
University of Iceland
Dunhagi 3, 107 Reykjavík, Iceland; Fax: +354 552 8911
E-mail: krishna@hi.is
[b] Dr. Ragnar Bjornsson
Department of Inorganic Spectroscopy, Max-Planck-Institut für Chemische Energiekonversion
Campus de Stiftstrasse 34-36, 45470 Mülheim an der Ruhr, Germany
[c] Ms. Iwona T Myszor and Dr. Gudmundur H Gudmundsson
Department of Life and environmental sciences, School of Engineering and Natural Sciences,
University of Iceland
Læknagarður, Room-550, Vatnsmýrarvegi 16, 101 Reykjavik

Supporting information for this article is given via a link at the end of the document.

Abstract: The structural modification of the gelator/non-gelator by altering the non-bonding interactions responsible for gel formation enabled us to tune the gelation properties and study the self-assembly process of LMWGs. This was achieved by modifying pyridyl moieties of bis(pyridyl) urea based hydrogelator (**4-BPU**) and the isomer (**3-BPU**) to pyridyl N-oxides compounds (**L_1** and **L_2** respectively). The modification of the functional groups induced/enhanced gelation properties and the modified compounds displayed enhanced mechanical and thermal stabilities. The introduction of the N-oxide moieties had prominent effect on the morphologies of the gel network. The role of specific non-bonding interactions in gel formation were analyzed by comparing the solid-state interactions of the compounds using single crystal X-ray diffraction, which was correlated with the enhanced gelation properties. This study shows the importance of specific non-bonding and the spatial arrangement of the functional groups in supramolecular gel network formation.

Introduction

Supramolecular gels based on low molecular weight gelators (LMWGs)[1] emerged as an important class of stimuli-responsive soft materials due to their potential applications[1g-j, 2] as hosts in slow-release drug delivery, tissue engineering, sensing, crystallizing media, catalysis etc. The stimuli-responsive properties of LMGWs will enable us to tune the gelation properties by adding an external stimulus[1g, 3] such as heat, light, sound, pH, redox, and salts/ions. LMWGs are formed by the self-assembly of the gelator molecules in presence of solvent molecules into a 3-dimensional network and the solvent molecules are entrapped in these networks. These networks are stabilized by various non-covalent interactions[1] such as hydrogen bonding, van der Waals interactions, π−π stacking etc. The mechanism and understanding of the self-assembly process of LMWGs and the gel structure is difficult due to the dynamic and reversible nature of these non-covalent interactions.[1] Although, the characterization of supramolecular gels from molecular to mesoscopic scale have been challenging, efforts have been made to identify the key structural features of gel-network formation in LMWGs using various spectroscopic and microscopic techniques.[1i] The correlation of the crystal structure of the gelator with the powder diffraction pattern of either native gel or the xerogel using X-ray diffraction enable us to compare the intermolecular interactions observed in the single crystal structure with the molecular aggregation in gel state. This will enable us to study the effect of hydrogen bonding motifs in the solid-state of the gelators and correlate with the gel properties and the self-assembly process of LMWGs. However, the structure and properties of LMWGs depends on the geometry and spatial arrangement of the building blocks and also the nature of intermolecular non-covalent interactions, which makes it challenging to design new LMWGs with specific properties.

An excellent strategy is to modify a well-known gelator that contain supramolecular synthons[4] or hydrogen bonding moieties, which enable us to compare the gelation and structural properties of the modified gelator with the parent gelator. The modification of the groups attached to the hydrogen bonding motif also have prominent effect in gel formation for example, changing the length of alkyl-chains will alter the hydrophobic - hydrophilic balance and the van der Waals forces.[5] McNeil *et.al* have modified azosulfonate gelator scaffold to develop nitrite-based sensor based on LMWGs.[6] We have shown that the gelation properties can be altered by modifying the pyridyl groups of trimesic amide based gelator *N^1,N^3,N^5*-tri(pyridin-3-yl)benzene-1,3,5-tricarboxamide[7] to *N*-oxide groups resulting in *tris*-*N*-oxide compound.[8] Recently, we showed the importance of non-bonding interactions and functional groups in designing LMWGs by modifying a pyridyl amide based gelator namely *N*-(4-pyridyl)isonicotinamide (**4PINA**)[9] to di-*N*-oxide compound (**diNO**).[10] The modification of the pyridyl group resulted in the disruption strong and unidirectional N—H···N interactions of the parent gelator and a weak intermolecular C—H···O interaction was observed in **diNO**. The absence of strong N—H···N interactions in *N*-oxide compound resulted in the reduced gelation ability and thermal strength of **diNO**.[10] The tuning of gelation properties by functional group modification prompted us to check the possibility of inducing gelation in non-gelators, which is challenging and this approach has not been reported. This was achieved by modifying the functional groups to alter the non-

bonding interactions in bis(pyridyl) urea compounds, which are an excellent class of stimuli-responsive soft materials with tunable properties.[1h, 11]

Single crystal X-ray diffraction (SCXRD) has been used to identify the key interactions in the solid-state structure of LMWGs,[3m, 9, 11e, 12] which may provide insight into the packing modes of these molecules in gel fibers. Generally, in urea based LMWGs, the urea motifs self-assemble via self-complementary hydrogen bonding (N—H···C=O) into one-dimensional arrays of hydrogen bonds to form α-tapes (fibrils) and these fibrils aggregate to form an interconnected, entangled 3-D framework. Steed *et. al* reported that N—H···N interactions also play an important role in the crystal structure of pyridyl-urea compounds.[13] This prompted us to alter the N—H···N interactions to N—H···O interactions and analyze the role of the resulting interaction in supramolecular gelation of and the effect of these structural modification on gelation of bis(pyridyl)urea compounds. We have selected *N,N'*-bis(3-pyridyl) urea (**3-BPU**) and *N,N'*-bis(4-pyridyl) urea (**4-BPU**) as the parent compounds[11e] and the pyridine rings of **3BPU**/**4-BPU** were oxidized to corresponding *N*-oxides. The structural modification induced gelation or enhanced gelation properties were studied by analyzing the key non-bonding interactions of the parent and modified compounds.

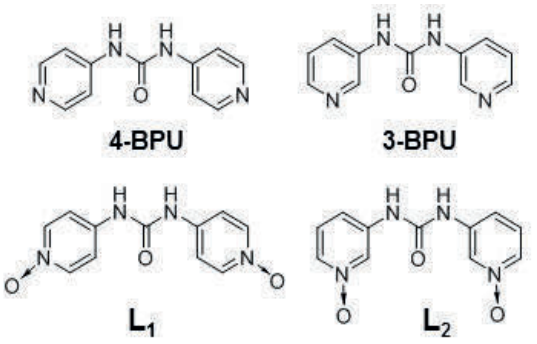

Scheme 1. Parent bis-pyridyl urea and the corresponding *N*-oxide compounds obtained by modifying the pyridyl groups.

Results and Discussion

The reaction of 4-aminopyridine and triphosgene in presence of triethylamine in anhydrous dichloromethane resulted in *N,N'*-bis(4-pyridyl) urea (**4-BPU**). The structural isomer *N,N'*-bis(3-pyridyl) urea (**3-BPU**) was synthesized by reacting 3-aminopyridine and triphosgene in DCM in presence of Et_3N.[11e] **3-BPU** did not form hydrogels in pure water and in majority of aqueous solutions whereas **4-BPU** formed gels in water/aqueous solutions and the structural details of **4-BPU** interacting with the gelling solvents has been reported.[11e] The structural modifications of the bis(pyridyl) urea compounds were achieved by oxidizing the pyridyl groups of **4-BPU** and **3-BPU** to pyridyl *N*-oxide moieties using 3-chloroperoxybenzic acid, resulting in di-*N*-oxide urea 4,4'-(carbonylbis(azanediyl))bis(pyridine 1-oxide) (**L_1**) and 3,3'-(carbonylbis(azanediyl))bis(pyridine 1-oxide) (**L_2**) respectively.

Gelation experiments: The compound **L_1** was found to be insoluble in most of the organic solvents but and **L_2** was partially soluble at room temperature. The experiments to test gel formation in water resulted in hydrogels of **L_1** and **L_2** at 0.7 wt% and 0.8 wt% respectively. The insolubility of **L_1** at higher concentration (>1.5 wt%) in water prompted us to check the gelation ability of **L_1** in aqueous solutions of highly polar solvents. The gelation was tested in water and 9 different solvent/water mixtures (1:1, v/v) at 1.0 wt% of **L_1** (Table 1). The (bis)urea **L_1** was dissolved in highly polar solvent such as DMF, DMA, DMSO, ethylene glycol (EG), 1,2-dimethoxyethane (DME), MeOH, EtOH, MeCN or THF, and the addition of water to this solution resulted in immediate precipitate, which was reheated to obtain a clear solution. The gelation experiments performed in 1:1 (v/v) mixture of DMSO/water, EG/water and DME/water resulted in gel formation after 1-2 hours but gelation was not observed for **L_1** in other solvent mixtures. The gelation experiments were performed by varying the concentration of ethylene glycol in EG/water mixtures and the results indicated that decreasing the concentration of the water prevents gel formation.

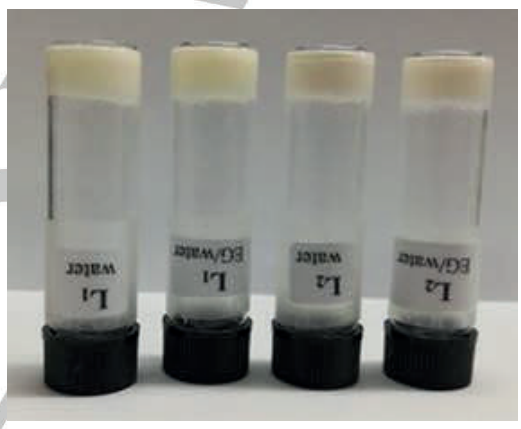

Figure 1. **L_1** and **L_2** gels obtained from water and EG/water (3:7 v/v) mixture.

The minimum gel concentration (MGC) of **L_1** was determined by varying the concentration of gelator and the MGC was found to be 0.7 wt% in both water and EG/water mixture (3:7, v/v). The MGC of the parent **4-BPU** gelator was found to be 0.8 wt% in water and 0.7 wt% in EG/water mixture (3:7, v/v). These results clearly indicated that **4-BPU** and the modified compound **L_1** can form the entangled network, which showed the important role of urea moieties in gel formation. The analysis of the gelation properties of **3-BPU** isomer indicated that gelation was observed in EG/water and DME/water mixture (1:1, v/v) but **3-BPU** failed to form hydrogels in pure water and various aqueous mixture (1:1, v/v) of polar solvents (Table S1) due to the higher solubility of **3-BPU**. We have tested the gelation properties of **L_2**, which was synthesized by modifying **3-BPU**. The solubility of **L_2** was higher compared to **L_1** in water or aqueous solution of organic solvents. The ability of **L_2** to form hydrogel was tested by dissolving 10.0 mg of **L_2** in 1.0 mL solvent by heating and the solution was left undisturbed. Interestingly, hydrogel was obtained within an hour (Table 1), which was confirmed by inversion test and the MGC of

L_2 in water was found to be 0.8 wt% (Table S2). Thus, replacing the pyridyl groups with *N*-oxide groups induced hydrogel formation in **L_2**, which was not observed in parent **3-BPU**. The gelation experiments performed in (1:1, v/v) aqueous solutions of highly polar solvents (EG, DMF, DMA, DMSO, MeOH, EtOH, MeCN & THF) at 1.0 wt% resulted in gelation of **L_2** in all cases. The MGC of **L_2** in EG/water mixture (3:7, v/v) was found to be 1.1 wt%. We have also performed gelation experiments by varying the concentration of ethylene glycol and the results showed that increasing the concentration of ethylene glycol in EG/water mixture increased the MGC of **L_2** gels, indicating weaker gel.

Table 1. Gelation test for **L_1** and **L_2** at 1.0 wt% in various solvent/water mixtures (1:1, v/v).

Solvent	**L_1**	**L_2**
Water	Gel	Gel
THF/water	Colloidal	Gel
EtOH/water	Colloidal	Gel
MeOH/water	Colloidal	Gel
Acetonitrile/water	Colloidal	Gel
DMF/water	Colloidal	Gel
DMA/water	Colloidal	Gel
DMSO/water	Gel	Gel
EG/water[†]	Gel	Gel [*]
1,2-dimethoxyethane/water[†]	Gel	Gel [*]

[*] 1.5 wt% and [†] 3:7 v/v.

Gel Strength: The thermal stabilities of the gel networks were evaluated by gel-to-solution transition temperature (T_{gel}) experiments. The thermal stabilities of **4-BPU**, **3-BPU**, **L_1** and **L_2** were measured in water and various EG/water ratio, and the results are summarized in Table 2. The T_{gel} comparison of **4-BPU** and **L_1** revealed that both the networks displayed similar thermal stabilities in pure water. However, increasing the ethylene glycol concentration resulted in enhanced thermal stability (10.0 to 15.0 °C) in the modified *N*-oxide gels. The increased thermal stability may be attributed to the high solubility of **4-BPU**/**3-BPU** in EG, which weakened the solid-like network of the **4-BPU**/**3-BPU** gel.

Table 2. T_{gel} (°C) comparison of **4-BPU** and **L_1** at 1.0 wt%, and **3-BPU** and **L_2** at 2.5 wt% in water and various EG/water ratio.

Water:EG	**4-BPU**[*]	**L_1**[*]	**3-BPU**[**]	**L_2**[**]
10:0	98.1	95.2	Crystal	88.2
9:1	85.6	94.5	Crystal	83.6
8:2	81.2	91.7	57.1	79.1
7:3	74.0	91.0	56.4	74.5
6:4	71.6	89.4	Crystal	72.3
5:5	69.5	84.1	Crystal	71.0

[*]1.0 wt% and [**] 2.5 wt%.

The T_{gel} comparison of **3-BPU** and **L_2** clearly indicate that the thermal stability of **L_2** network is much higher compared to **3-BPU**. Furthermore, **L_2** is capable of forming gel in a wide range of solvent composition. Thus, modifying the pyridyl groups of bis(pyridyl) urea compounds have prominent effect on the thermal stability of the gel network.

Rheology: The structural characteristics of the bis(pyridyl) and bis(pyridyl-*N*-oxide) urea gels were analyzed by rheology, which will enable us to compare the solid-like properties and relative strength of the gel networks. The **4-BPU**, **L_1** and **L_2** gels were prepared at 1.0 wt% in water, and oscillatory strain sweep experiments were carried out to determine the linear viscoelastic region (LVR), where the elastic modulus (G') was constant irrespective of the shear stress. The experiments were performed within the LVR to ensure that the gel networks undergo reversible deformation, which will enable us to estimate the actual characteristic of the materials. The **4-BPU** gel displayed quite narrow LVR, and the G' decreased on increasing the shear strain above 0.05% (Figure S3). In contrast, the **L_1** and **L_2** gels were more rigid, and the LVR of these gels were stretched to 0.1% (Figure S4-S5). The cross-over point, where the solid-like property of the gel transformed to liquid-like property was also higher for the **L_1** and **L_2** gels. These indicates that the *N*-oxide gels are capable of resisting higher applied forces without irreversible deformation compared to the **4-BPU** gel. The frequency sweep experiments performed on the gels at 1.0 wt% in water revealed that both of the storage and loss moduli (G' and G'') were independent of frequency, supporting the gel behavior (Figure 2). The **4-BPU** and **L_1** gels displayed quite similar G', but the G' of **L_2** gel was significantly higher, indicating that the **L_2** gel possessed a stronger network with higher mechanical stability.

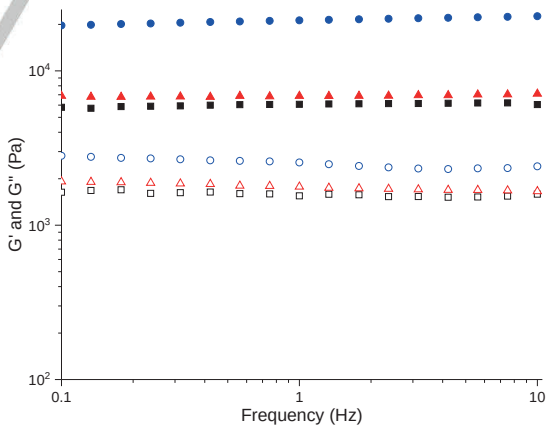

Figure 2. Frequency sweep experiments performed on **4-BPU**, **L_1** and **L_2** gels at 1.0 wt% in water at 20.0 °C at a constant strain of 0.05%. Color codes: G', **4-BPU** (■), G'', **4-BPU** (□), G', **L_1** (▲), G'', **L_1** (△), G', **L_2** (●), G'', **L_2** (○).

The relative gel strength of **3-BPU** and **L_2** were also compared by performing rheology on the gels prepared at 2.5 wt% in EG/water (3:7 v/v). The strain sweep (Figure S6-S7) and frequency sweep (Figure S8) experiments performed on both gels revealed that **L_2** displayed about 1000 times higher G' compared to the parent **3-**

BPU. Also, the G' and G'' of **3-BPU** did not show a constant value at low frequency range, indicating that the **3-BPU** gel network is soft resulting in a weak solid-like network. This is in excellent agreement with the overall gelation properties of the compounds, which suggested that **4-BPU**, **L_1** and **L_2** were efficient hydrogelators but **3-BPU** is a weak gelator.

Gel morphology: The morphologies of **4-BPU**, **3-BPU**, **L_1** and **L_2** were analyzed by scanning electron microscopy (SEM). The **4-BPU** (1.0 wt%) and **3-BPU** (2.5 wt%) gels were prepared from EG/water (3:7, v/v) and the gels of **L_1** (1.0 wt%) and **L_2** (2.5 wt%) were prepared in water, EG/water (3:7, v/v) and DMSO/water (1.0 wt% for both **L_1** and **L_2**). After 24 hours, the gels were filtered, dried under a fume hood for 2 days. A small portion of the dried gel was placed on a pin mount with carbon tab on top and coated with gold for three minutes. The SEM images of the dried gels revealed that various morphologies such as needles, fibrous, tape like and plates were observed.

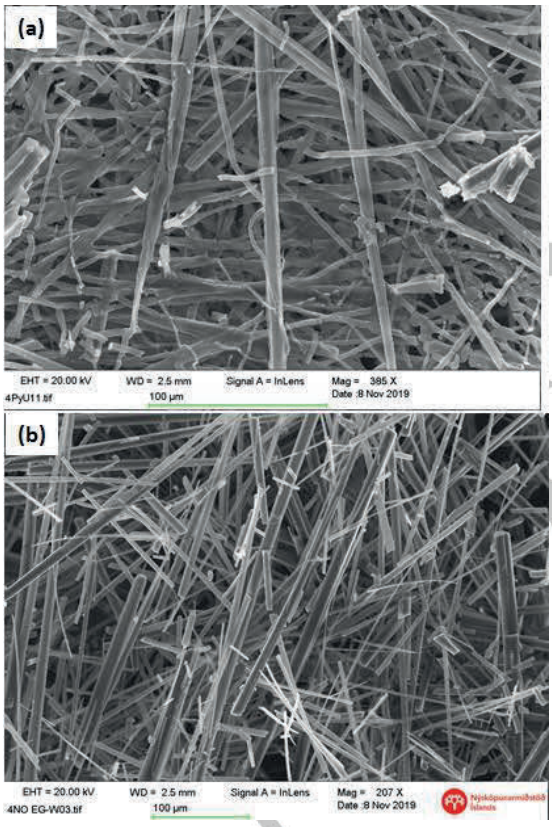

Figure 3. SEM images of (a) **4-BPU** and (b) **L_1** xerogels obtained from EG/water (3:7, v/v) at 1.0 wt%.

The **4-BPU** xerogels obtained from EG/water (3:7, v/v) displayed typical fibrous network with thickness varying from 2.0 to 8.0 µm (Figure 3a). The morphology of **L_1** gels from both EG/water mixture (Figure 3b) and pure water (Figure S9) were slightly different from the parent **4-BPU** gelator. The xerogels of **L_1** displayed crystalline fibers with thickness ranging from 4.0 to 12.0 µm whereas tape like fibrous network was observed in **4-BPU**. The xerogel of **L_1** (1.0 wt%) obtained from DMSO/water mixture (1:1, v/v) showed fibrous tape like morphology with thickness varying from 0.1 to 1.6 µm (Figure S10). The xerogels of **3-BPU** from EG/water (3:7, v/v) displayed crystalline network with brick like morphology (Figure 4a) varying from 5.0 to 20.0 µm but a different morphology was observed for **L_2** xerogels in both EG/water (3:7 v/v) (Figure 4b) and pure water (Figure S11).

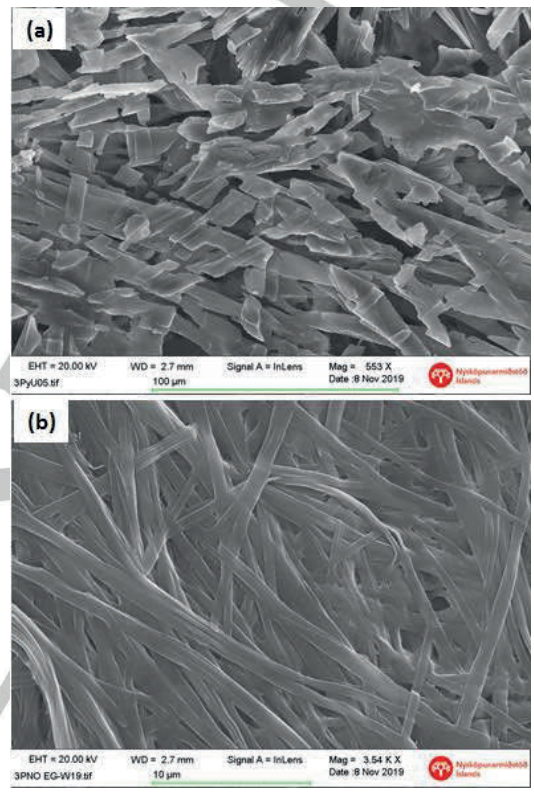

Figure 4. SEM images of (a) **3-BPU** and (b) **L_2** xerogels obtained from EG/water (3:7, v/v) at 2.5 wt%.

The thickness of the fibers observed for **L_2** xerogels from EG/water, 3:7 v/v and pure water varied from 0.8 to 1.2 µm and 0.2 to 0.8 µm respectively. The SEM images **L_2** (1.0 wt%) gel obtained from 1:1 DMSO/water mixture (v/v) showed morphologies similar to EG/water gels with varying thickness (0.05 to 1.0 µm, Figure S12). These results clearly indicate that modifying the pyridyl group to *N*-oxide groups induced prominent change in the morphology of the gel fibers. Thus, the mode of intermolecular non-bonding interactions plays an important role in altering the morphology of gel fibers, which prompted us to corelate the solid-state structure of the modified compounds with the parent gelator structure using X-ray diffraction.

Single Crystal X-ray diffraction: The structural details of the parent gelator **4-BPU** [11e], the isomer **3-BPU** [11e] and the *N*-oxide **$L_2.H_2O$** [14] were compared to the modified **4-BPU** gelator (**L_1**). We were successful in isolating the crystals of the gelators in various

solvated forms such as **L_1.H_2O**, **3-BPU.2EG** and **L_2.EG**. X-ray quality crystals of **L_1** was obtained by the slow evaporation of **L_1** from water below MGC over a period 1-2 days. The crystal data and parameters of refinement are listed in Table S3 and the hydrogen-bonding parameters are provided in Table S4. Single crystal X-ray diffraction revealed that **L_1** crystallized in monoclinic space group *$P2_1/c$* with one solvent water molecule (**L_1.H_2O**). The molecular plane consists of one of the pyridyl *N*-oxide moieties and the urea moiety were planar to each other but the second pyridyl moiety was slightly twisted from the molecular plane (15.6°). The hydrogen bonding modes of the two pyridyl *N*-oxide moieties were different and the twisted pyridyl *N*-oxide moiety displayed N—H···O interaction (2.7990(16) & 2.7851(16) Å) with the urea moiety, which was similar to complementary urea interaction. This interaction resulted in a one-dimensional chain with **L_1** orienting orthogonal to each other displaying urea α–tape like architecture (Figure 5a). The 1-D chains displayed bifurcated hydrogen bonding with adjacent chains via O—H···O interactions (2.7466(19) & 2.7612(19) Å) involving the planar pyridyl N-oxide moiety and the solvent water molecule (Figure 5b).

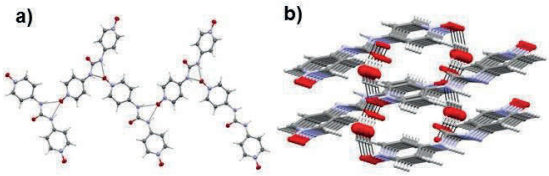

Figure 5. (a) Hydrogen bonded 1-D chain observed in **L_1** and (b) 1-D chains displaying bifurcated hydrogen bonding with adjacent chains and solvent water molecules via O—H···O interactions.

The comparison of the solid-state structure of **L_1** with the parent gelator (**4BPU**) revealed the absence of complementary hydrogen bonding motifs in **4BPU** [11e] but the pyridyl groups and the urea moieties were involved in hydrogen bonding with the solvent molecules. The structural analysis of the crystals of **L_2** revealed the formation of solvated form of **L_2** (**L_2.H_2O**) was obtained and the unit cell parameters matched with the reported structure [14]. The hydrogen bonding modes of the pyridyl *N*-oxide and urea moieties of **L_2** were similar to **L_1** and the 1-D hydrogen bonded chain formed was stabilized by the complementary hydrogen bonding [14]. The structure was compared with the parent compound **3-BPU** [11e], which existed in two forms (**3-BPU** & **3-BPU.H_2O**). The pyridyl groups of **3-BPU** were involved in N—H···N interactions and these groups were hydrogen bonded to the solvent water molecules in **3-BPU.H_2O** [11e]. Thus, replacing the non-bonding interactions resulted in a 1-D hydrogen bonded chain in **L_1** and **L_2** stabilized by complementary urea-like hydrogen bonding (N—H···O). Moreover, the alteration of the pyridyl group to the pyridyl *N*-oxide moiety induced gelation resulting in **L_2** hydrogels but the parent **3-BPU** was a non-gelator in water. The gelation ability of **3-BPU**, **L_1** and **L_2** in EG/water prompted us to analyze the crystal structure of these compounds obtained from ethylene glycol. The structural analysis of crystals of **3-BPU** obtained from ethylene glycol revealed that **3-BPU** crystallized in monoclinic space group *$P2_1/c$* with two ethylene glycol molecules (**3-BPU.2EG)**. The pyridyl nitrogen atoms were oriented *trans* to each other resulting in an *anti*-confirmation compared to the reported *syn*-confirmation of **3-BPU** & **3-BPU.H_2O** structures [11e]. The urea moiety and the pyridyl nitrogen atom of **BPU.2EG** were hydrogen bonded to one of the ethylene glycol molecules via N—H···O (2.9122(14) & 2.7496(13) Å) and O—H···N (2.7932(15) Å) interactions resulting in a hydrogen bonded macrocycle (Figure 6a).

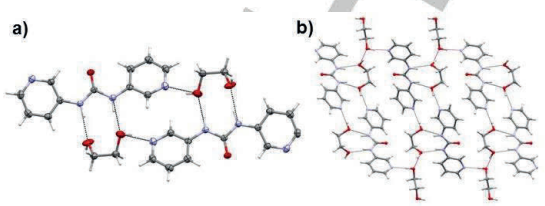

Figure 6. (a) Hydrogen bonded macrocycle obtained by the interaction of solvent ethylene glycol and **BPU** molecules in **BPU.2EG** (b) macrocycle interacting with adjacent macrocycles via O—H···O interactions.

This macrocycle interacts with adjacent macrocycles via O—H···O interactions (2.7026(15) Å) between the other pyridyl moieties and the second ethylene glycol molecule to form a 2-D hydrogen bonded corrugated sheet like architecture (Figure 6b). The modified compound **L_2** crystallized in an orthorhombic *$C222_1$* space group with a formula of **L_2.EG** and a *syn*-confirmation of pyridyl *N*-oxides was observed. One of the N—H groups of the urea moiety interacted with the pyridyl *N*-oxide group via complementary urea-like hydrogen bonding (N—H···O = 2.690(2) Å) interaction similar to **L_2.H_2O** resulting in a 1-D chain (Figure 7a), which interact with adjacent chains via N—H···O interaction (2.690(2) Å) between the pyridyl *N*-oxide groups and the other NH groups of the urea moiety. The pyridyl *N*-oxide groups also interact with ethylene glycol molecule via O—H···O (2.741(2) Å) hydrogen bonding interaction (Figure 7b) resulting in a three-dimensional hydrogen bonded network.

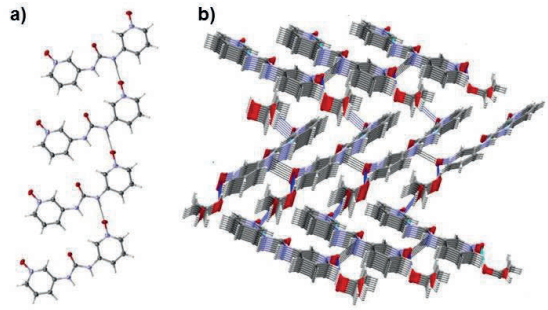

Figure 7. Hydrogen bonded chains in **L_2.EG** stabilized by N—H···O interactions between urea and pyridyl *N*-oxide moieties, (b) 1-D chains interacting with adjacent chains via N—H···O interaction involving pyridyl *N*-oxide groups and the other N—H groups of the urea moiety.

X-ray Powder diffraction (XRPD): The combination of single crystal X-ray structure of the gelator and powder diffraction pattern of either the native gel or the xerogel will enable us to correlate the intermolecular interactions observed in the single

crystal structure with the molecular aggregation in the gel state. Although, the removal of solvent to prepare a xerogel can result in artefacts due to dissolution, recrystallization and changes in morphology or polymorphic phase transition, but this approach still remains as one of the practical methods to get insight to self-assembly process in LMWGs.[1d, i, 9, 15] The self-assembly of **L_1** and **L_2** in gel state was correlated with respective crystal structures by comparing powder X-ray pattern of the bulk crystals and dried gels with the crystal structure. XRPD was performed on the bulk solid of **L_1** (recrystallized from water) and the xerogel obtained from water at MGC. The powder pattern for the bulk crystal and xerogel pattern also matched with the simulated graph obtained from the single-crystal structure of **L_1**. The powder X-ray pattern of the recrystallized **L_1** was virtually superimposable on the xerogel pattern (Figure S13).

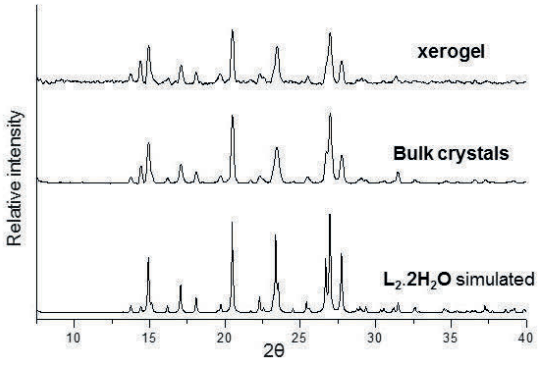

Figure 8. Comparison of the XRPD pattern of simulated, as synthesized and the xerogel from water at 1.0 wt% of **L_2**.

This indicates that the single-crystal structure of **L_1** truly represents the packing in bulk crystal and the hierarchical gel network. We have performed the XRPD of xerogels obtained from water and EG/water mixture (3:7, v/v) and the pattern matched each other but the xerogel pattern obtained from water was less crystalline indicating that ethylene glycol induced crystalline nature in gel fibers. The PXRD of the **L_2** xerogels were compared with the simulated pattern and bulk crystal of **L_2.H_2O** and **L_2.EG** and the powder pattern of both bulk crystals matched with the simulated pattern of **L_2.H_2O** (Figure 8). Interestingly, the bulk crystals (**L_2.EG**) from ethylene glycol and the xerogel obtained from EG/water mixture (3:7, v/v) did not match the **L_2.EG** simulated pattern but both matched perfectly with **L_2.H_2O** simulated pattern, presumably due to the loss of hydrogen loosely bonded ethylene glycol molecules during the drying process. We observed similar trends for **3-BPU**, where XRPD pattern of **3-BPU.EG** bulk crystals and xerogels obtained from EG/water mixture (3:7, v/v) showed perfect match with the simulated **3-BPU** pattern (Figure S14-S17) but these patterns were different from the simulated **3-BPU.EG** pattern. This confirms the loss of EG molecules in the crystal during the drying process. The xerogel patterns obtained for **L_1** and **L_2** from water and EG/water mixture (3:7, v/v) indicates that the 1-D urea α–tape like architecture was preserved in the xerogel network.

Stimuli-responsive property: The urea functionalized LMWGs are excellent class of stimuli-responsive soft materials,[1h] and the self-assembly of the gelator can be tuned by anion binding, resulting in the construction or deconstruction of the gel networks. The hydrogels of **4-BPU**, **L_1** and **L_2** at 1.0 wt% were treated with different anions such as halides, acetate and cyanide (sodium or potassium salt), and the relative gel strength of the anionic mixtures were compared with the corresponding gels. The **4-BPU** gel was stable after the addition of three equivalents of fluoride, chloride, bromide, iodide, acetate and cyanide salts (Figure S18). However, the gel network was collapsed by the addition of four equivalents of iodide, acetate and cyanide ions (Figure 9) but higher amounts were required for other halides such as bromide (5 equiv), fluoride (6 equiv) and chloride (7 equiv). This indicated that the ions with larger size were more effective in breaking the gel network, presumably due to the interference to a greater number of N—H···N hydrogen bonding synthons. The higher efficiency of fluoride in collapsing the gel compared to the chloride ion was attributed to the higher electronegativity resulting in strong hydrogen bonding capability of the fluoride ion. However, **L_1** gel proved to be more sensitive to the anions (Figure S19), and the gel was broken by the addition of two equivalents of iodide and cyanide ions. The gel network was collapsed in presence of three equivalents of bromide, and four equivalents of acetate ions (Figure 9). These results clearly indicate that **L_1** gel was more responsive compared to the parent **4-BPU** gel.

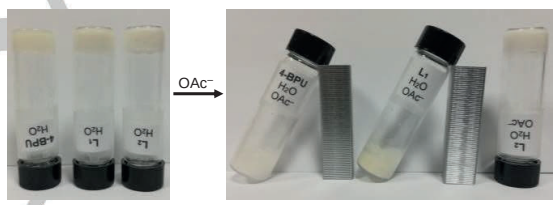

Figure 9. The effect of four equivalents of acetate anion on **4-BPU**, **L_1** and **L_2** gels.

Interestingly, the **L_2** hydrogel displayed much higher stability towards anions compared to **4-BPU** and **L_1** gels, and the gel network was stable after adding six equivalents of anions in all cases. This was due to the rigid network of **L_2** compared to **4-BPU** and **L_1** gels, thus **L_2** exhibited more resistance towards anions. The effect of the anions on the gel network was also studied by rheology. The addition of three equivalents of anions to **L_2** gel resulted in reduction of the storage modulus, however, no significant difference in the G' values was observed for various anions (Figure S20). On increasing the amount of the anions to six equivalents, G' of the gels dropped for bromide, iodide, acetate and cyanide ions (Figure 10). The larger ions such as acetate and cyanide showed lowest G' values, which corroborates well to the experiments with **4-BPU** and **L_1** gels. The analysis of the anion sensing experiments suggest that the modification of the functional groups can potentially generate gels with higher sensitivity as well as higher resistance.

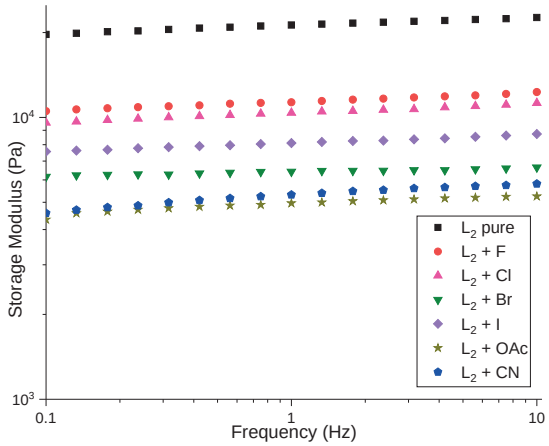

Figure 10. Frequency sweep experiments performed at 20.0 °C at a constant strain of 0.02% on **L_2** hydrogel at 1.0 wt%, in presence of six equivalents of anions.

Computational Studies: To rationalize these observations we calculated the strengths of different hydrogen-bonding interactions using quantum chemical calculations via a state-of-the-art density functional theory (DFT)-based protocol (ωB97M-D3BJ/def2-TZVP). Interactions of gelators/non-gelators with themselves as well as with single solvent molecules ethylene glycol (EG) and water molecule were calculated. These calculations were performed in the gas phase and they allow us to compare the hydrogen-bonding interaction strength of different functional groups; they are not intended, however, to mimic the complex solution/gel environment. Figure S21-S24 (see Supporting Information) shows the optimized geometries as well as interaction energies.

Calculations of the non-gelator 3BPU reveals that the strongest 3BPU-dimer interaction is -17.5 kcal/mol (ΔE) and involves N—H···O hydrogen-bonding. This is about equal to the 3BPU-EG interaction of -17.8 kcal/mol. The **4-BPU** dimer can hydrogen-bond via either N—H···O or N—H···N. The stronger N—H···O interaction within the **4-BPU** dimer (-15.4 kcal/mol) is, however, calculated to be weaker than the N—H···O interaction between 4BPU-EG interaction (-16.6 kcal/mol). The hydrogen-bonding interactions with water and **3-BPU**/**4-BPU** are generally calculated to be weaker than **3-BPU**/**4-BPU** dimer interactions but interactions with EG are predicted to be strongest overall.

Calculations of **L_1** and **L_2** dimers reveal a rather different picture. The **L_1**-**L_1** dimer interaction via a N—H···O hydrogen bond is a rather strong interaction (-19.9 kcal/mol) that can be compared to the relatively weak H_2O-**L_2** O—H···O—N interaction (-10.4 kcal/mol) and the EG-**L_1** N—H···O interaction (-16.6 kcal/mol).

For the **L_2**-**L_2** dimer we found two different conformations. One with an approximately parallel alignment of the **L_2** units and another with more perpendicular alignment. The parallel conformation had an interaction energy of -19.6 kcal/mol while the perpendicular conformation had an interaction energy of -24.3 kcal/mol. Both of these conformations were found to be stronger than **L_2**-EG interactions (-15.1 kcal/mol) and an **L_2**.H_2O interaction (-8.8 kcal/mol).

These simple hydrogen-bonding calculations in the gas phase do not offer an explanation for why **4-BPU** is a gelator while **3-BPU** is not. More complex calculations that take the solution/gel environment into account are likely required to understand the nature of the gelation process. The increased dimer hydrogen-bonding interaction strength in going from **3-BPU** to **L_2** via pyridyl nitrogen to *N*-oxide substitution is, however, a plausible model for why **L_2** becomes a gelator.

Antibacterial Property: An inhibition zone assay was used in thin plates (1.0 mm) made of 1.0% (w/v) agar in 2.5% (w/v) LB broth seeded with Bacillus megaterium (Bm11). Single colonies of bacteria were grown overnight on 1.5% agar plates containing LB broth (2.5%) and streptomycin (100 µg/mL), and then inoculated in 2.5% LB medium overnight at 30.0 °C in an incubator. Bacteria were added to the agar plate just before plating to a concentration of 8.5 × 10^4 cells/mL. Small wells (3.0 mm diameter, 3.0 µL volume) were pierced in the plates, and a 3.0 µL suspension of 2.0 wt% **3-BPU**, **4-BPU**, **L_1** and **L_2** in water was added. After incubating for overnight at 30.0 °C, the diameters of bacteria-free zone was measured. **3-BPU**, **4-BPU** and **L_2** showed no antibacterial activity, and no area of clearance was observed in the agar plate. Interestingly, **L_2** was found to have some activity, resulting an area of clearance with 6.0 mm diameter (Figure 11). This result demonstrated that the simple modification of pyridyl group to pyridyl-*N*-oxide could potentially lead to antibacterial functionality.

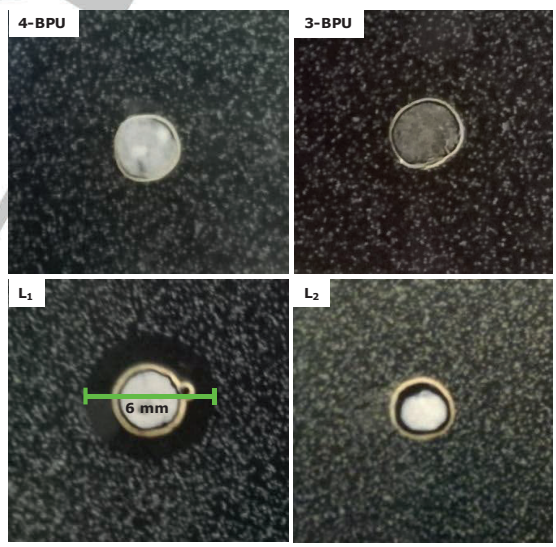

Figure 11. Antibacterial study performed on **3-BPU**, **4-BPU**, **L_1** and **L_2**, where **L_2** is showing an area of clearance having a diameter of 6.0 mm.

Conclusion

The structural modification of the gelator/non-gelator was used as a strategy to alter the non-bonding interactions responsible for gel formation to induce/enhance the gelation properties of LMWGs. This was achieved by modifying pyridyl moieties of a bis(pyridyl)

urea based hydrogelator (**4-BPU**) and a non-gelator (**3-BPU**) to pyridyl *N*-oxides compounds (**L_1** and **L_2** respectively). The gelation properties of the modified compounds and the parent compounds were analyzed by standard gelation techniques and improved gelation property was observed for **L_1** compared to the parent **4-BPU**. The hydrogel formation of **L_2** clearly indicate that the structural modification of **3-BPU** induced gelation. The modified gelator **L_2** turned out to be an excellent gelator in water and mixed aqueous solvents. The modification of the functional groups had prominent effect on the mechanical and thermal stability of the gel network and the modified gelators showed higher sol-gel transition temperatures (T_{gel}). The morphologies of the xerogels were analyzed by comparing the SEM images, which showed that the crystalline brick like morphology of **3-BPU** was replaced by an efficient fibrous network in **L_2** in water, which corroborates well with the gelation results. The comparison of the solid-state structures revealed that a one-dimensional chain was formed via N—H···O interaction similar to complementary urea interaction, which was crucial for formation of gel network. The enhanced gelation properties resulting from the alteration of N—H···N interaction to N—H···O interaction were also supported by the rheological measurements, which established the stiffer network of the modified gelators. The stimuli-responsive property was studied by adding various anions to the hydrogels, which revealed that **L_1** gel was a good anion sensor whereas **L_2** gel displayed significant resistance towards anions. Density functional theory calculations confirm the increased hydrogen-bonding strength of N—H···O vs N—H···N interactions. This implicates that the spatial arrangement of the functional groups in the gelator and the nature of intermolecular non-covalent interactions of the gelators are crucial for the 3-D arrangement of the gel network. Furthermore, antibacterial activity studied on Bm11 bacteria indicated that the functional group modification could potentially lead to antibacterial properties.

Experimental Section

All starting materials and solvents were purchased from commercial sources and used as supplied. Deionized water was used for all the experiments and anhydrous dichloromethane was obtained by distilling the solvent over CaH_2. **3-BPU** and **4-BPU** were synthesized following reported procedure [11e] and the analytical data matched with the reported compounds. ^{1}H and ^{13}C NMR spectra were recorded on a Bruker Advance 400 spectrometer (^{1}H-NMR: 400 MHz, ^{13}C-NMR: 100 MHz) and SEM was performed on a Leo Supra 25 microscope.

1. Synthesis of the ligand

*1.1: 4,4'-(carbonylbis(azanediyl))bis(pyridine 1-oxide) (**L_1**)*: To a solution of **4-BPU** (1.1 g, 5.1 mmol) in DMF (30 mL), 3-chloroperoxybenzic acid (3.4 g, 14.8 mmol) was added in portions over a period of 15 minutes at room temperature and the mixture was stirred overnight. The white precipitate obtained was filtered and stirred overnight in 0.05 *N* HCl. The mixture was filtered, washed with water and dried to obtain **L_1** as a white powder. Yield = 0.62 g (2.5 mmol, 49.4%). ^{1}H-NMR (400 MHz, DMSO-d_6): δ = 9.45 (2H, s), 8.10 (4H, d, J = 8.0), 7.49 (4H, d, J = 8.0). ^{13}C-NMR (100 MHz, DMSO-d_6): δ = 151.47, 138.76, 136.66, 115.25. MS (ESI) m/z for $C_{11}H_{10}N_4O_3Na^+$: expected 269.0651, found 269.0663.

*1.2: 3,3'-(carbonylbis(azanediyl))bis(pyridine 1-oxide) (**L_2**)*: **L_2** was synthesized following similar procedure as above by reacting **3-BPU** (1.1 g, 5.1 mmol) and 3-chloro-peroxybenzic acid (3.4 g, 14.8 mmol) in 30 mL DMF. The product was recrystallized from methanol. Yield = 0.72 g (2.9 mmol, 56.5%). ^{1}H-NMR (400 MHz, DMSO-d_6): δ = 9.31 (2H, s), 8.53 (2H, d, J = 4.0), 7.92 (2H, m), 7.33-7.34 (4H, m). ^{1}H-NMR (400 MHz, DMSO-d_6): δ = 9.31 (2H, s), 8.53 (2H, d, J = 4.0), 7.92 (2H, m), 7.33-7.34 (4H, m). ^{13}C-NMR (100 MHz, DMSO-d_6): δ = 151.83, 138.49, 132.88, 129.52, 126.06, 115.45. MS (ESI) m/z for $C_{11}H_{10}N_4O_3Na^+$: expected 269.0651, found 269.0659.

2. Gelation Studies

2.1 Gelation test: The gelation properties of **L_1** and **L_2** were tested in various solvents by adding 1.0 mL of the solvent to 10.0 mg of *N*-oxide compounds (1.0 wt%) in a standard 7.0 mL vial and the mixture was heated to obtain a clear solution. The solution was cooled to room temperature and gelation was confirmed by inversion test. The gelation experiments in mixed solvent system (1:1, v/v) were performed by dissolving the gelator in 500 µL of the appropriate solvent and distilled water (500 µL) was added as co-solvent. The mixture was heated to obtain a clear solution, cooled to room temperature and left undisturbed. We also performed gelation experiments in the solvent mixtures by varying the concentration of the polar solvents. Gelation was observed in water and also in three solvents mixtures such as dimethyl sulfoxide (DMSO)/water, ethylene glycol (EG)/water and 1,2-dimethoxyethane (DME)/water for **L_1** and **L_2**. However, gelation was not achieved in other solvent/mixtures for **L_1** but **L_2** was soluble in water and mixed aqueous solvents on heating resulting in gels in all solvent mixtures studied.

*2.2 Minimum gel concentration (MGC)***:** The MGC experiment was performed by weighing various amounts of gelator in a standard 7.0 mL vial, followed by adding 1.0 mL of solvent (or solvent mixture). The ligand was dissolved by heating the mixture and the solution was left at room temperature for gelation. The minimum concentration at which the gel was obtained after 24 hours was recorded as MGC.

2.3 T_{gel} experiments: The gel to solution transition temperature (T_{gel}) was evaluated in different solvent systems. The required amount of the gelator was dissolved in the solvent or solvent mixtures by heating the mixture in a sealed vial to obtain a clear solution. The solution was cooled to room temperature and after 24 hours, a spherical glass ball (52.0 mg) was placed on the top of the gel. The vial was placed into an oil bath equipped with a magnetic stirrer and a thermometer. The oil bath was gradually heated and the temperature at which the glass ball touched the bottom of the vial was recorded as T_{gel}.

3. Rheology: Rheological measurements were performed in an Anton Paar MCR 302 rheometer using a 25.0 mm stainless steel parallel plate geometry configuration. The **4-BPU**, **L_1** and **L_2** gels were prepared by dissolving 10.0 mg of the compound in 1.0 mL of water and experiments were performed by scoping a ~1.0 mL portion of gel on the plate. **3-BPU** and **L_2** gels were also prepared at 2.5 wt% in EG/water (3:7 v/v). Viscoelastic properties were evaluated by oscillatory measurements at a constant temperature of 25.0 °C. Amplitude sweeps were performed with constant frequency (f) of 1.0 Hz and log ramp strain (γ) = 0.01 – 100% and frequency sweeps were carried out between 0.1 and 10.0 Hz within the linear viscoelasticity domain (0.05% strain).

4. Scanning electron microscopy (SEM): The **4-BPU** and **3-BPU** gels were prepared from EG/water (3:7, v/v) at 1.0 wt% and 2.5 wt% respectively. The gels of **L_1** (1.0 wt%) and **L_2** (2.5 wt%) were prepared in water and EG/water (3:7, v/v) and 1.0 wt% gels were prepared for both **L_1** and **L_2** in DMSO/water (1:1, v/v). The resulting gels were filtered after 24 hours and dried under fume hood. A small portion of the dried gels were placed on pin mount with carbon tab on top and coated with gold for 2 minutes. SEM images of the dried gels were analyzed using Leo Supra 25 microscope.

5. Single Crystal X-ray diffraction (SCXRD): X-ray quality single-crystals of **3-BPU**, **L_1** and **L_2** were obtained by the slow evaporation of the

compounds from corresponding solvents. Needle shaped crystals of **L_1.H_2O** were obtained by the slow evaporation of an aqueous solution (2.0 mL) of **L_1** (10.0 mg) in an open vial. The crystallization experiment of **L_2** in ethylene glycol was performed by dissolving 20.0 mg of **L_2** in 1.0 mL of ethylene glycol and left for slow evaporation under the fume hood. Concomitant crystals of block shaped **L_2.H_2O** and plate shaped **L_2.EG** were obtained in 2-3 days. The crystallization experiment performed with **3-BPU** in ethylene glycol resulted in long needle shaped crystals in 1-2 days, which was obtained by the slow evaporation of 40.0 mg of **3-BPU** in 1.0 mL of ethylene glycol. The crystals were isolated from the solvent and immersed in cryogenic oil before mounting. The crystals were mounted on a Bruker D8 VENTURE (Photon100 CMOS detector) diffractometer equipped with a Cryostream open-flow nitrogen cryostat and the data collection were performed using CuK_α radiation (λ = 1.54178 Å) at 150.0(2) K. The unit cell determination, data collection, data reduction, structure solution/refinement, and empirical absorption correction (SADABS) were carried out using Apex III. The structure was solved by a direct method and refined by the full-matrix least-squares on F^2 for all data using SHELXTL[16], version 2017/1 and Olex2, version 1.2 software [17]. All non-disordered non-hydrogen atoms were refined anisotropically, and the hydrogen atoms were placed in the calculated positions and refined using a riding model except for **L_1.H_2O** where the hydrogen atoms of the water molecules were located on the Fourier map and refined. The free variables of disordered carbon atoms in ethylene glycol molecule in **3-BPU.2EG** were refined by the FVAR instruction. The crystallographic data for this paper were deposited at Cambridge Crystallographic Data Centre and the CCDC numbers are 1965865-1965867. These data can be obtained free of charge via www.ccdc.cam.ac.uk/data_request/cif, or by emailing data_request@ccdc.cam.ac.uk

6. X-ray Powder diffraction (XRPD): The bulk crystals of **L_1** were obtained by the slow evaporation of the solution of **L_1** (10.0 mg in 2.0 mL water). The gelator **L_2** (20.0 mg) was dissolved in 1.0 mL of ethylene glycol and left under a fume hood for crystallization resulting in bulk crystals of **L_2**. The crystals of 3-BPU was obtained from ethylene glycol solution (40.0 mg in 1.0 mL). The crystals were filtered, dried in air and grinded to fine powder. The xerogel of **3-BPU**, **4-BPU**, **L_1** and **L_2** were prepared by filtering the corresponding gels in water or in 3:7 EG/water (v/v) mixture at concentration closer to MGC, followed by drying the residue in a fume hood. XRPD was carried out on the bulk crystals and xerogels using a Bruker D8 Focus instrument.

7. Quantum chemical calculations: Calculations were performed with the ORCA program, version 4.2.1.[18] The density functional theory-based protocol consisted of the ωB97M-D3BJ[19] functional (including the D3 dispersion correction by Grimme and coworkers)[20] and the triple-zeta basis set def2-TZVPP.[21] The RIJCOSX[22] approximation was used to calculate Coulomb and Exchange integrals, using the def2/J auxiliary basis set by Weigend et al.[23] and the GridX5 (ORCA keyword) grid was used. Tigher grids for the exchange-correlation terms were also used (Grid5, FinalGrid6 keywords in ORCA). Interaction energies were calculated as electronic energies from relaxed structural optimizations in the gas phase.

Acknowledgements

We thank the Science Institute and University of Iceland Research Fund for financial support. DG thanks University of Iceland Research Fund for Doctoral Research and Teaching grant. We thank Rannis Iceland for Infrastructure grant (150998-0031) for a single-crystal X-ray diffractometer, Sigurður Sveinn Jonsson, ISOR-Iceland for X-ray powder diffraction analysis and Sigridur Jonsdottir, University of Iceland for NMR and mass spectroscopy.

Keywords: LMWGs • hydrogen bonding • pyridyl urea • structural modification • antibacterial study

[1] a) L. A. Estroff and A. D. Hamilton, *Chem. Rev.* **2004**, *104*, 1201-1218; b) M. de Loos, B. L. Feringa and J. H. van Esch, *Eur. J. Org. Chem.* **2005**, *2005*, 3615-3631; c) M. George and R. G. Weiss, *Acc. Chem. Res.* **2006**, *39*, 489-497; d) P. Dastidar, *Chem. Soc. Rev.* **2008**, *37*, 2699-2715; e) A. R. Hirst, B. Escuder, J. F. Miravet and D. K. Smith, *Angew. Chem. Int. Ed.* **2008**, *47*, 8002-8018; f) S. Banerjee, R. K. Das and U. Maitra, *J. Mater. Chem.* **2009**, *19*, 6649-6687; g) M.-O. M. Piepenbrock, G. O. Lloyd, N. Clarke and J. W. Steed, *Chem. Rev.* **2010**, *110*, 1960-2004; h) J. W. Steed, *Chem. Soc. Rev.* **2010**, *39*, 3686-3699; i) G. Yu, X. Yan, C. Han and F. Huang, *Chem. Soc. Rev.* **2013**, *42*, 6697-6722; j) D. K. Kumar and J. W. Steed, *Chem. Soc. Rev.* **2014**, *43*, 2080-2088.

[2] a) W. Fang, Y. Zhang, J. Wu, C. Liu, H. Zhu and T. Tu, *Chem. Asian J.* **2018**, *13*, 712-729; b) X. Du, J. Zhou, J. Shi and B. Xu, *Chem. Rev.* **2015**, *115*, 13165-13307; c) D. K. Smith in *Applications of Supramolecular Gels*, *Vol.* (Ed. R. Weiss), Royal Society of Chemistry, Cambridge, **2018**, pp. 300-371; d) J. A. Foster, K. K. Damodaran, A. Maurin, G. M. Day, H. P. G. Thompson, G. J. Cameron, J. C. Bernal and J. W. Steed, *Chem. Sci.* **2017**, *8*, 78-84.

[3] a) L. Meazza, J. A. Foster, K. Fucke, P. Metrangolo, G. Resnati and J. W. Steed, *Nat Chem* **2013**, *5*, 42-47; b) A. Pal, Y. K. Ghosh and S. Bhattacharya, *Tetrahedron* **2007**, *63*, 7334-7348; c) K. Kawamoto, S. C. Grindy, J. Liu, N. Holten-Andersen and J. A. Johnson, *ACS Macro Lett.* **2015**, *4*, 458-461; d) U. K. Das, S. Banerjee and P. Dastidar, *Chem. Asian J.* **2013**, *8*, 3022-3031; e) Q. Jin, L. Zhang and M. Liu, *Chem. Eur. J.* **2013**, *19*, 9234-9241; f) S. Karak, S. Kumar, S. Bera, D. D. Diaz, S. Banerjee, K. Vanka and R. Banerjee, *Chem. Commun.* **2017**, *53*, 3705-3708; g) K. K. Kartha, V. K. Praveen, S. S. Babu, S. Cherumukkil and A. Ajayaghosh, *Chem. Asian J.* **2015**, *10*, 2250-2256; h) Q. Liu, Y. Wang, W. Li and L. Wu, *Langmuir* **2007**, *23*, 8217-8223; i) H. H. Lee, S. H. Jung, S. Park, K.-M. Park and J. H. Jung, *New J. Chem.* **2013**, *37*, 2330-2335; j) R. Aoyama, H. Sako, M. Amakatsu and M. Yamanaka, *Polym. J.* **2015**, *47*, 136-140; k) K. Ghosh, S. Panja and S. Bhattacharya, *RSC Advances* **2015**, *5*, 72772-72779; l) D. P. Kumar, *RSC Advances* **2014**, *4*, 45449-45457; m) P. Byrne, G. O. Lloyd, L. Applegarth, K. M. Anderson, N. Clarke and J. W. Steed, *New J. Chem.* **2010**, *34*, 2261-2274; n) K. Pandurangan, J. A. Kitchen, S. Blasco, F. Paradisi and T. Gunnlaugsson, *Chem. Commun.* **2014**, *50*, 10819-10822; o) C. E. Stanley, N. Clarke, K. M. Anderson, J. A. Elder, J. T. Lenthall and J. W. Steed, *Chem. Commun.* **2006**, 3199-3201.

[4] G. R. Desiraju, *Angew. Chem. Int. Ed.* **1995**, *34*, 2311-2327.

[5] a) M. Suzuki and K. Hanabusa, *Chem. Soc. Rev.* **2009**, *38*, 967-975; b) N. Zweep, A. Hopkinson, A. Meetsma, W. R. Browne, B. L. Feringa and J. H. van Esch, *Langmuir* **2009**, *25*, 8802-8809.

[6] D. M. Zurcher, Y. J. Adhia, J. D. Romero and A. J. McNeil, *Chem. Commun.* **2014**, *50*, 7813-7816.

[7] D. K. Kumar, D. A. Jose, P. Dastidar and A. Das, *Chem. Mater.* **2004**, *16*, 2332-2335.

[8] D. Ghosh, K. Ferfolja, Ž. Drabavičius, J. W. Steed and K. K. Damodaran, *New J. Chem.* **2018**, *42*, 19963-19970.

[9] D. K. Kumar, D. A. Jose, P. Dastidar and A. Das, *Langmuir* **2004**, *20*, 10413-10418.

[10] D. Ghosh, M. T. Mulvee and K. K. Damodaran, *Molecules* **2019**, *24*, 3472.

[11] a) M. George and R. G. Weiss in *Low Molecular-Mass Organic Gelators*, *Vol.* Eds.: R. G. Weiss and P. Terech), Springer Netherlands, Dordrecht, **2006**, pp. 449-551; b) E.-M. Schön, E. Marqués-López, R. P. Herrera, C. Alemán and D. D. Díaz, *Chem. Eur. J.* **2014**, *20*, 10720-10731; c) B. Isare, S. Pensec, M. Raynal and L. Bouteiller, *C.R. Chim.* **2016**, *19*, 148-156; d) M. George, G. Tan, V. T. John and R. G. Weiss, *Chem. Eur. J.* **2005**, *11*, 3243-3254; e) D. K. Kumar, D. A. Jose, A. Das and P. Dastidar, *Chem. Commun.* **2005**, 4059-4061.

[12] a) S. Abraham, Y. Lan, R. S. H. Lam, D. A. S. Grahame, J. J. H. Kim, R. G. Weiss and M. A. Rogers, *Langmuir* **2012**, *28*, 4955-4964; b) Y. Xu, C. Kang, Y. Chen, Z. Bian, X. Qiu, L. Gao and Q. Meng, *Chem. Eur. J.* **2012**, *18*, 16955-16961; c) Y. Wang, L. Tang and J. Yu, *Cryst. Growth Des.* **2008**, *8*, 884-889; d) D. Braga, S. d'Agostino, E. D'Amen and F. Grepioni,

Chem. Commun. **2011**, *47*, 5154-5156; e) P. Dastidar, R. Roy, R. Parveen and K. Sarkar, *Adv. Ther.* **2019**, *2*, 1800061.

[13] a) P. Byrne, D. R. Turner, G. O. Lloyd, N. Clarke and J. W. Steed, *Cryst. Growth Des.* **2008**, *8*, 3335-3344; b) A. M. Todd, K. M. Anderson, P. Byrne, A. E. Goeta and J. W. Steed, *Cryst. Growth Des.* **2006**, *6*, 1750-1752.

[14] L. S. Reddy, S. Basavoju, V. R. Vangala and A. Nangia, *Cryst. Growth Des.* **2006**, *6*, 161-173.

[15] a) D. Ghosh, I. Lebedyté, D. S. Yufit, K. K. Damodaran and J. W. Steed, *CrystEngComm* **2015**, *17*, 8130-8138; b) P. Sahoo, D. K. Kumar, S. R. Raghavan and P. Dastidar, *Chem. Asian J.* **2011**, *6*, 1038-1047.

[16] G. M. Sheldrick, *Acta Crystallogr. Sect. C: Struct. Chem.* **2015**, *71*, 3-8.

[17] O. V. Dolomanov, L. J. Bourhis, R. J. Gildea, J. A. K. Howard and H. Puschmann, *J. Appl. Crystallogr.* **2009**, *42*, 339-341.

[18] a) F. Neese, *WIREs Comput. Mol. Sci.* **2012**, *2*, 73-78; b) F. Neese, *WIREs Comput. Mol. Sci.* **2018**, *8*, e1327.

[19] a) N. Mardirossian and M. Head-Gordon, *J. Chem. Phys.* **2016**, *144*, 214110; b) A. Najibi and L. Goerigk, *J. Chem. Theory Comput.* **2018**, *14*, 5725-5738.

[20] a) S. Grimme, J. Antony, S. Ehrlich and H. Krieg, *J. Chem. Phys.* **2010**, *132*, 154104; b) S. Grimme, S. Ehrlich and L. Goerigk, *J. Comput. Chem.* **2011**, *32*, 1456-1465.

[21] F. Weigend and R. Ahlrichs, *Phys. Chem. Chem. Phys.* **2005**, *7*, 3297-3305.

[22] a) F. Neese, F. Wennmohs, A. Hansen and U. Becker, *Chem. Phys.* **2009**, *356*, 98-109; b) R. Izsák and F. Neese, *J. Chem. Phys.* **2011**, *135*, 144105.

[23] F. Weigend, *Phys. Chem. Chem. Phys.* **2006**, *8*, 1057-1065.

Supporting Information

Tuning the gelation properties of (bis)pyridyl urea supramolecular gel by altering non-bonding interactions

Dipankar Ghosh, Ragnar Bjornsson, Iwona T. Myszor, Gudmundur H. Gudmundsson and Krishna K. Damodaran*

Table of content

1. ^{1}H-NMR of L_1 and L_2

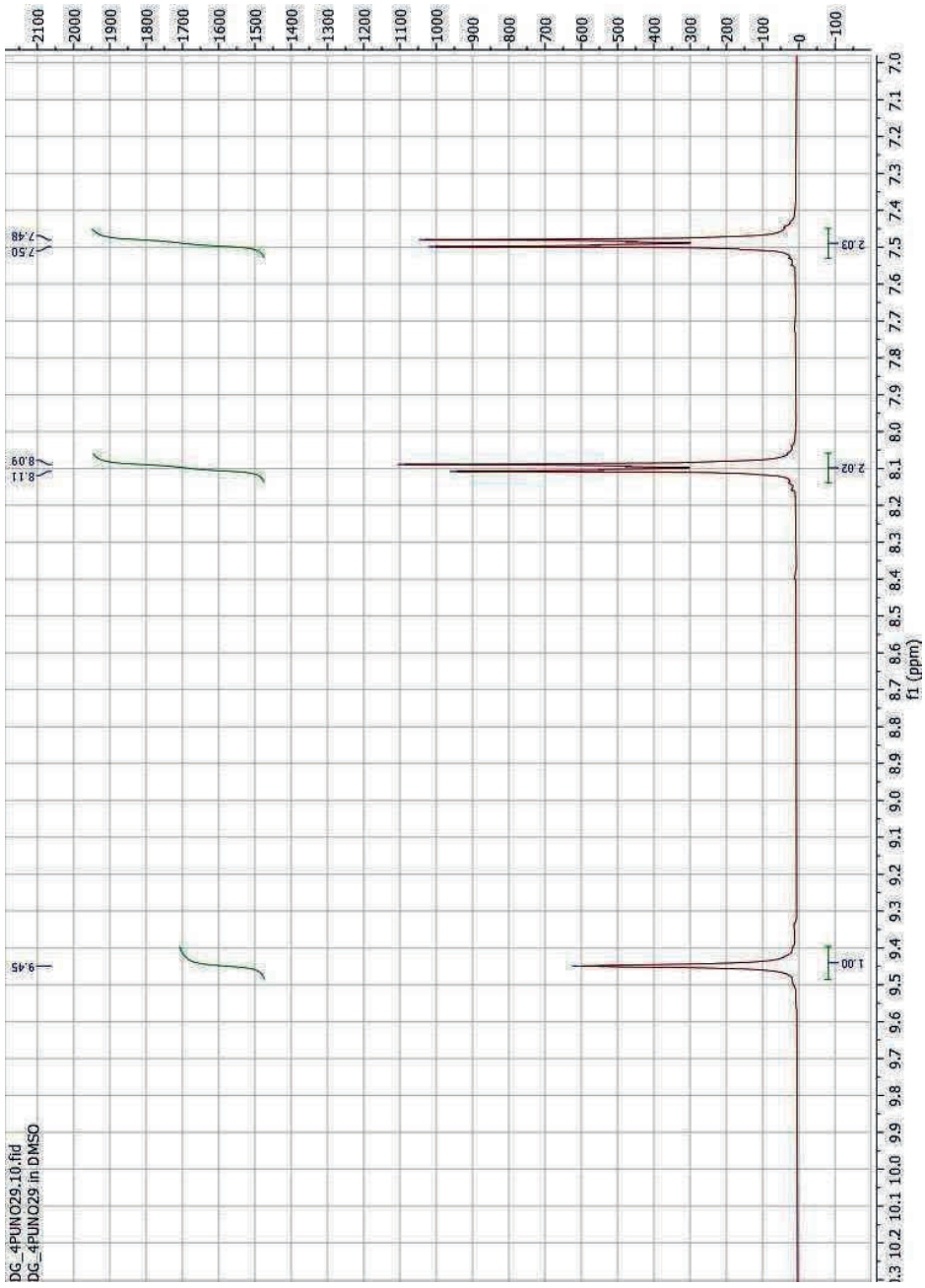

Figure S1: ^{1}H-NMR of $\mathbf{L_1}$

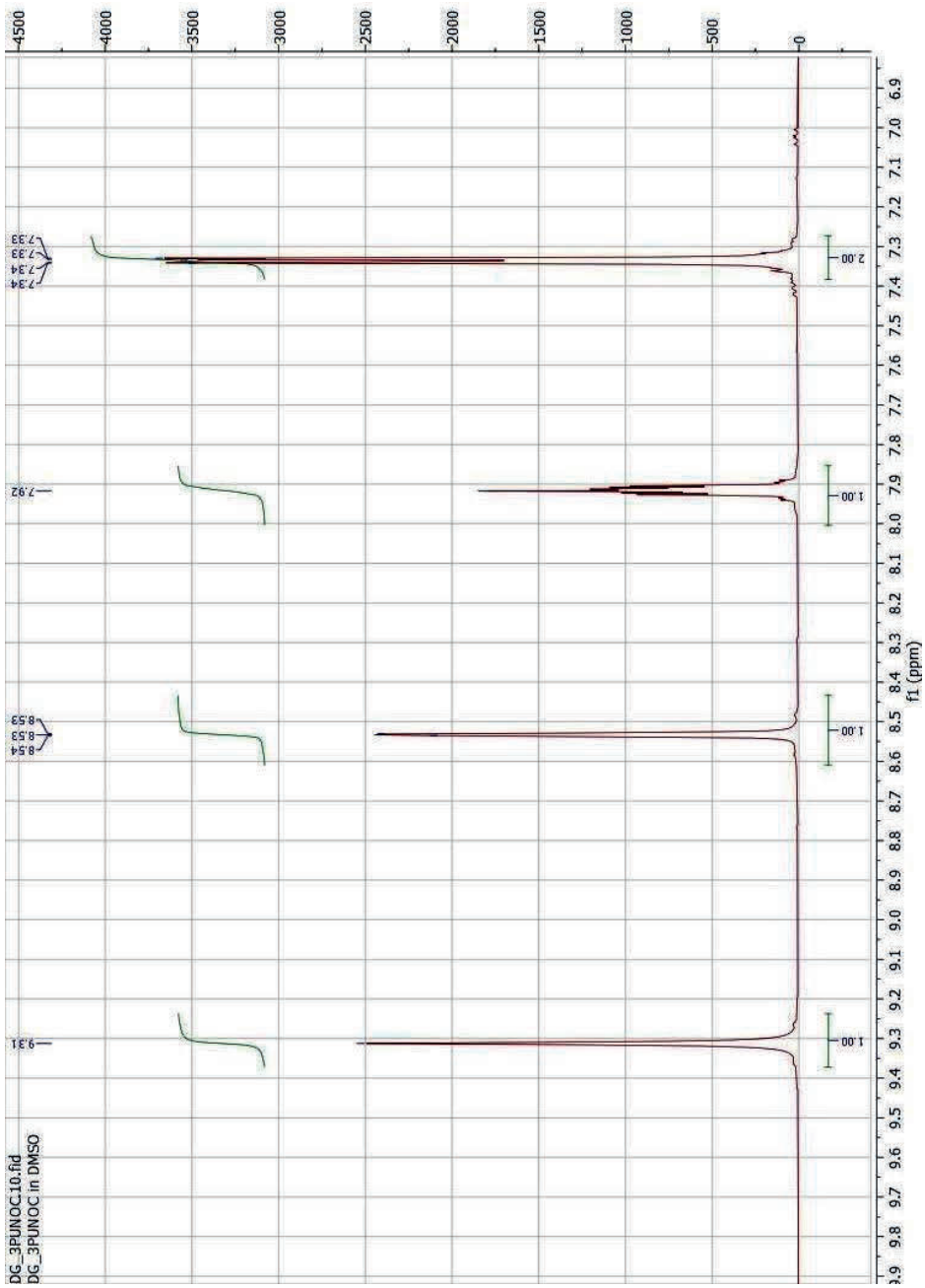

Figure S2: ^{1}H-NMR of **L$_2$**

2. Gelation details

Table S1: Gelation experiment with **4-BPU** and **3-BPU** in water and 1:1 solvent/water mixture

Solvent	**4-BPU***	**3-BPU**[§]
Water	Gel	Insoluble
DMF/water	Gel	Crystal
DMA/water	Gel	Crystal
DMSO/water	Gel	Crystal
MeOH/water	Gel	Crystal
EtOH/water	Gel	Crystal
MeCN/water	Gel	Crystal
THF/water	Gel	Crystal
EG/water	Gel	Gel[†]
1,2-DME/water	Gel	Gel[†]

*= 1.0 wt%, [§]= 6.0 wt%, [†]= 3.0 wt%

Table S2: Determination of MGC

Amount	**Initial observation**	**Observation in 24 h**
L_1 in water		
5.0 mg	Solution	Colloidal
6.0 mg	Solution	Partial gel
7.0 mg	Solution	Gel
8.0 mg	Solution	Gel
L_1 in EG/water (3:7 v/v)		
5.0 mg	Solution	Colloidal
6.0 mg	Solution	Colloidal
7.0 mg	Solution	Gel
8.0 mg	Solution	Gel
L_2 in water		
6.0 mg	Solution	Colloidal
7.0 mg	Solution	Partial gel
8.0 mg	Solution	Gel
9.0 mg	Solution	Gel

L_2 in EG/water (3:7 v/v)		
7.0 mg	Solution	Colloidal
8.0 mg	Solution	Colloidal
9.0 mg	Solution	Colloidal
10.0 mg	Solution	Partial gel
11.0 mg	Solution	Gel
12.0 mg	Solution	Gel
4-BPU in EG/water (3:7 v/v)		
5.0 mg	Solution	Colloidal
6.0 mg	Solution	Partial gel
7.0 mg	Solution	Gel
8.0 mg	Solution	Gel
3-BPU in EG/water (3:7 v/v)		
20.0 mg	Solution	Colloidal
21.0 mg	Solution	Colloidal
22.0 mg	Solution	Gel
24.0 mg	Solution	Gel

3. Rheology

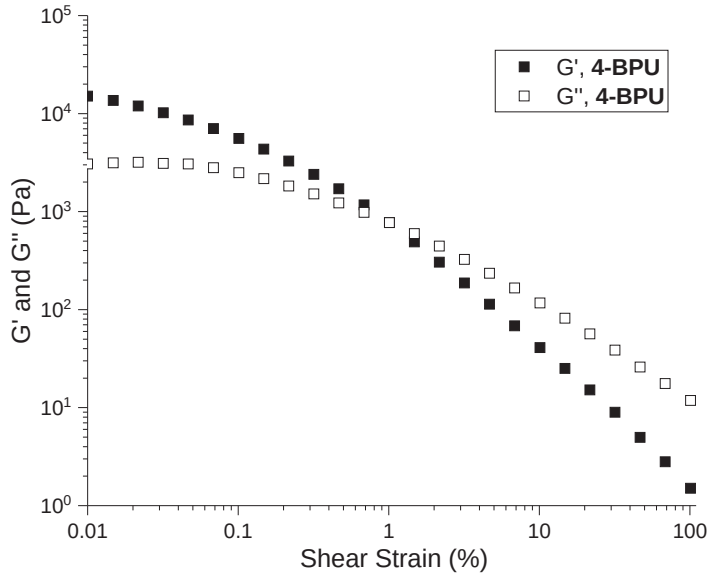

Figure S3: Strain sweep experiment performed on **4-BPU** gel at 1.0 wt% in water, at 25.0 °C and constant frequency of 1.0 Hz.

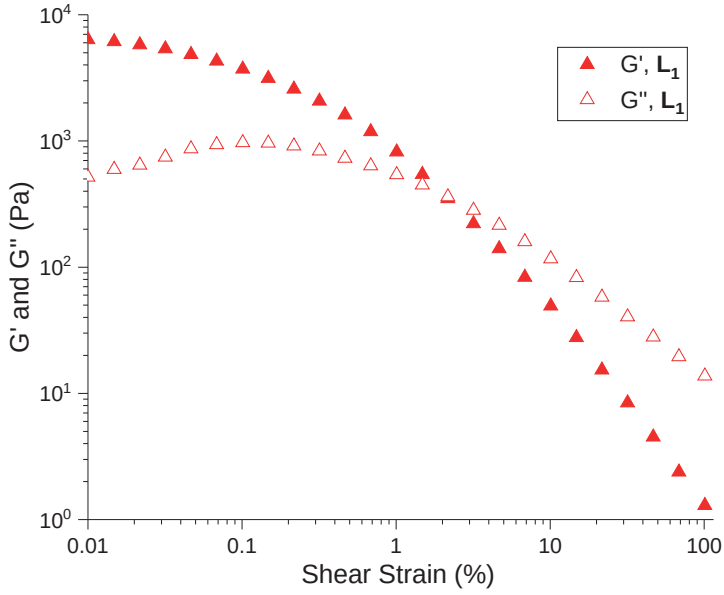

Figure S4: Strain sweep experiment performed on **L_1** gel at 1.0 wt% in water, at 25.0 °C and constant frequency of 1.0 Hz.

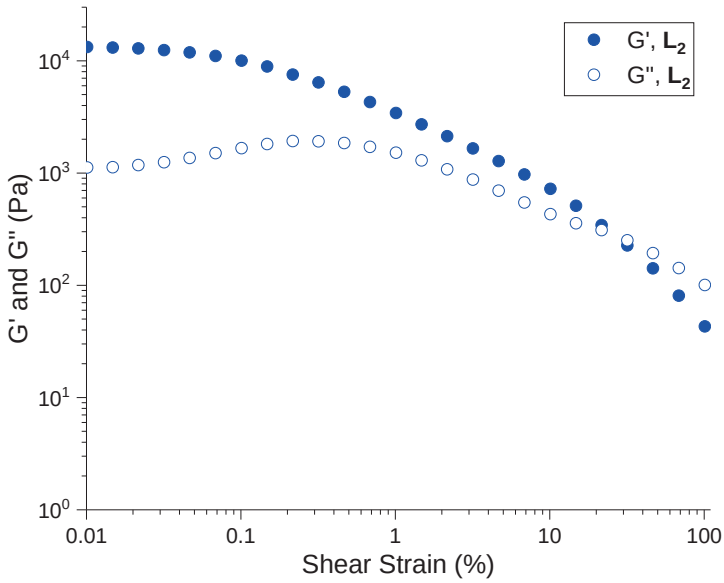

Figure S5: Strain sweep experiment performed on **L**$_2$ gel at 1.0 wt% in water, at 25.0 °C and constant frequency of 1.0 Hz.

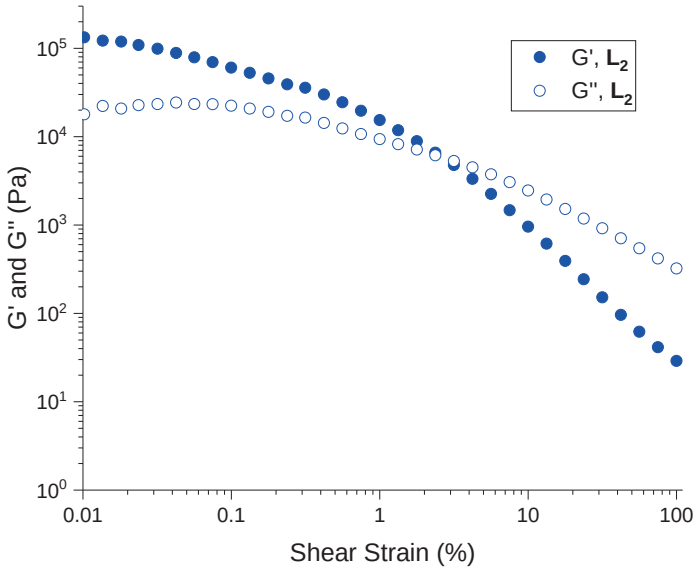

Figure S6: Strain sweep experiment performed on **L**$_2$ gel at 2.5 wt% in EG/water (3:7 v/v), at 25.0 °C and constant frequency of 1.0 Hz.

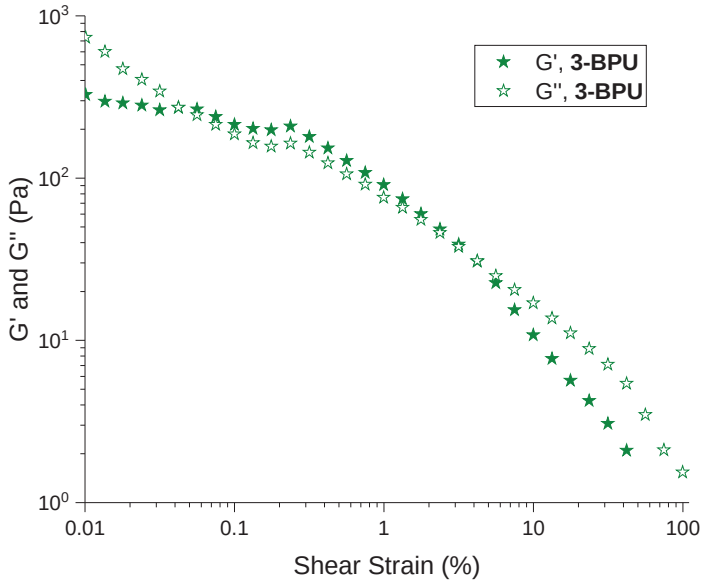

Figure S7: Strain sweep experiment performed on **3-BPU** gel at 2.5 wt% in EG/water (3:7 v/v), at 25.0 °C and constant frequency of 1.0 Hz.

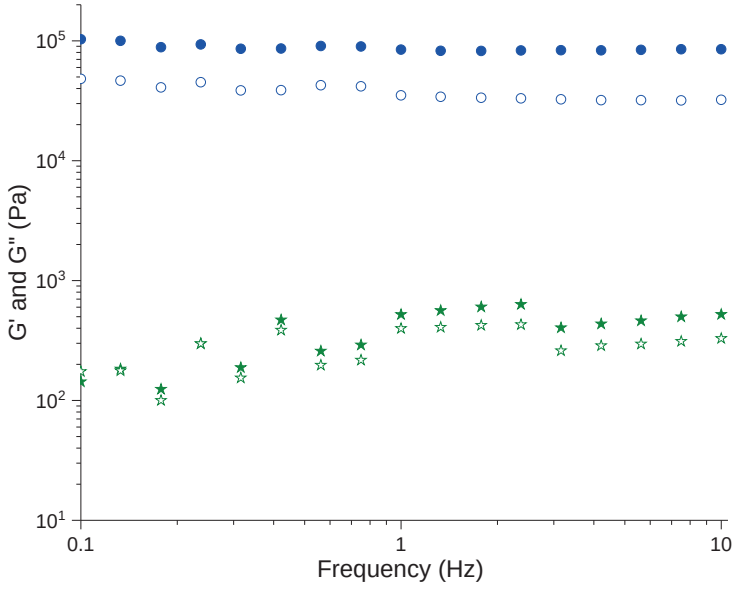

Figure S8: Frequency sweep experiment performed on **3-BPU** and $\mathbf{L_2}$ gels at 2.5 wt% in EG/water (3:7 v/v), at 25.0 °C and a constant strain of 0.05%. Colour codes: G', **3-BPU** (★), G'', **3-BPU** (☆), G', $\mathbf{L_2}$ (●) and G'', $\mathbf{L_2}$ (○).

4. Scanning Electron Microscopy (SEM)

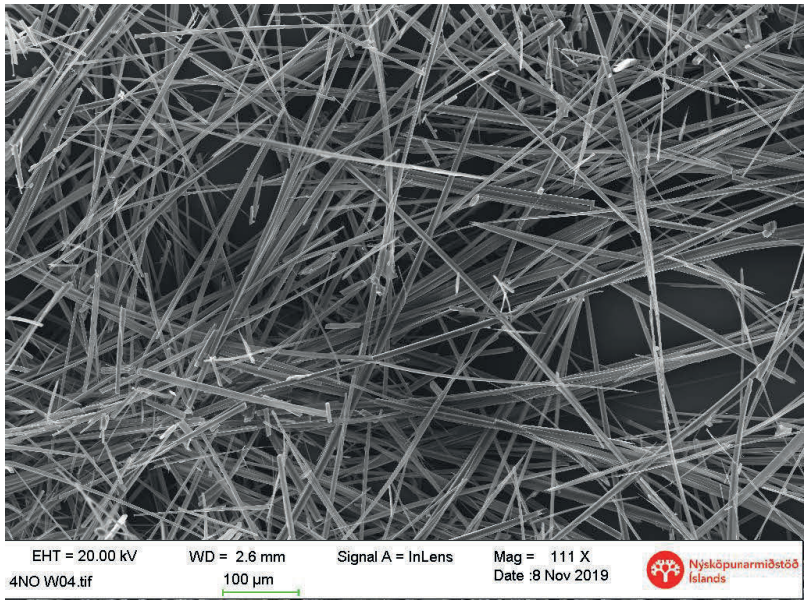

Figure S9: Xerogels of $\mathbf{L_1}$ obtained from water at 1.0 wt%.

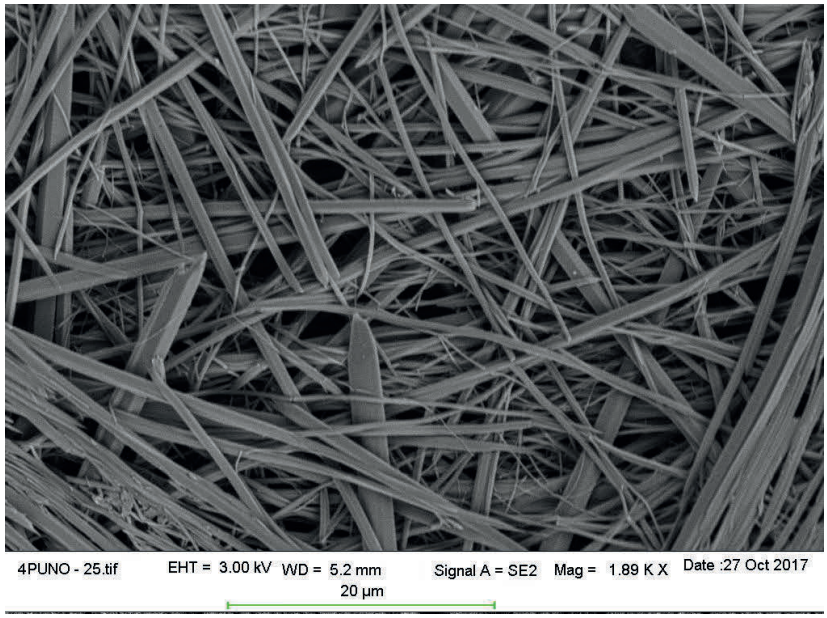

Figure S10: Xerogels of $\mathbf{L_1}$ obtained from DMSO/water (1:1 v/v) at 1.0 wt%.

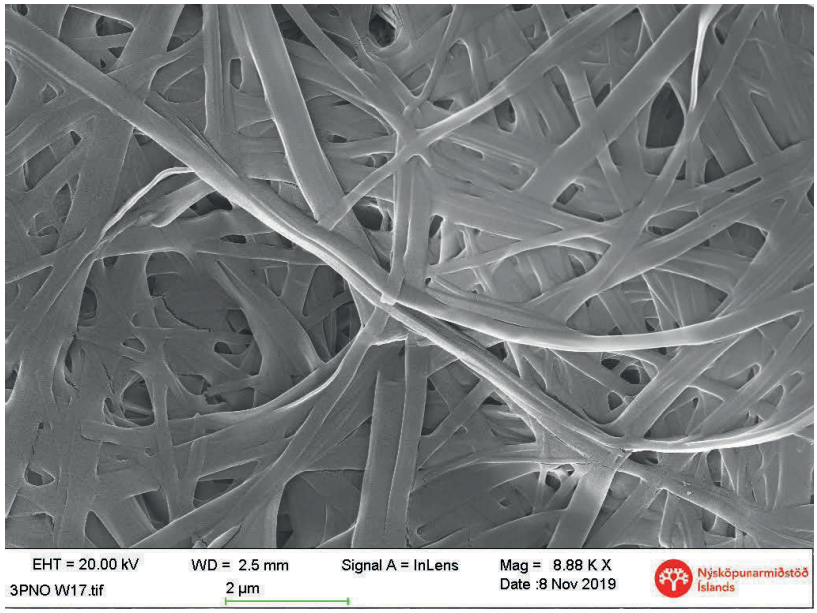

Figure S11: Xerogels of **L**$_2$ obtained from water at 2.5 wt%.

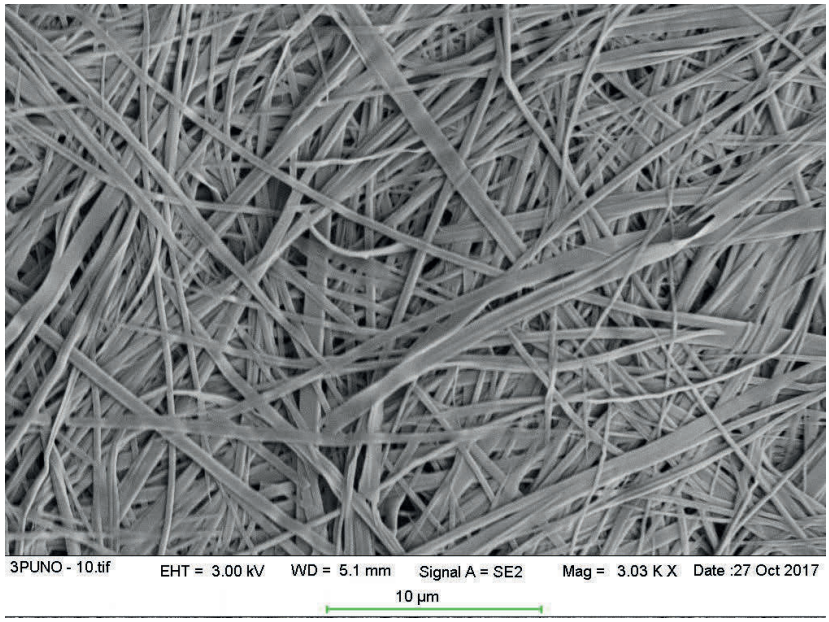

Figure S12: Xerogels of **L**$_2$ obtained from DMSO/water (1:1 v/v) at 1.0 wt%.

5. Crystal data

Table S3: Crystal data

Crystal data	**$L_1.H_2O$**	**L_2.EG**	**3-BPU.EG**
Empirical formula	$C_{11}H_{12}N_4O_4$	$C_{13}H_{16}N_4O_5$	$C_{14}H_{19}N_4O_4$
Colour	Colourless	Colourless	Colourless
Formula weight	264.25	308.30	307.33
Crystal size (mm)	0.23×0.05×0.04	0.28×0.1×0.05	0.42×0.1×0.075
Crystal system	monoclinic	orthorhombic	monoclinic
Space group	$P2_1/c$	$C222_1$	$P2_1/c$
a (Å)	3.79670(10)	7.8647(4)	18.3475(7)
b (Å)	12.2604(3)	11.0925(5)	4.7351(2)
c (Å)	24.6800(5)	15.9892(8)	17.5516(6)
α (°)	90	90	90
β (°)	90.3160(10)	90	98.4340(10)
γ (°)	90	90	90
Volume ($Å^3$)	1148.81(5)	1394.88(12)	1508.34(10)
Z	4	4	4
$D_{calc.}$ (g/cm^3)	1.528	1.468	1.353
F(000)	552	648	652
μ CuKα (mm^{-1})	1.011	0.972	0.843
Temperature (K)	150(2)	150(2)	150(2)
Reflections collected/ unique/observed [I>2σ(I)]	13589/2026/ 1794	4732/1366/1334	23481/2950/2768
Data/restraints/parameters	2026/0/180	1366/0/103	2950/0/223
Goodness of fit on F^2	1.045	1.138	1.017
Final R indices [I>2σ(I)]	R_1 = 0.0350 wR_2 = 0.0817	R_1 = 0.0296 wR_2 = 0.0853	R_1 = 0.0370 wR_2 = 0.0957
R indices (all data)	R_1 = 0.0411 wR_2 = 0.0855	R_1 = 0.0302 wR_2 = 0.0858	R_1 = 0.0389 wR_2 = 0.0972

Table S4: Hydrogen-bonding table

$L_1.H_2O$						
Nr	Donor---H···Acceptor	D–H/**Å**	H···A/**Å**	D···A/**Å**	∠D---H···A/°	Symmetry operation
1	N(8)---H(8)···O(16)	0.88	1.98	2.7990(16)	153	1-x,1/2+y,3/2-z
2	N(11)---H(11)···O(16)	0.88	1.96	2.7851(16)	156	1-x,1/2+y,3/2-z
3	O(19)---H(19A)···O(1)	0.96(3)	1.80(3)	2.7466(19)	172(2)	x,y,z
4	O(19)---H(19A)···N(2)	0.96(3)	2.50(3)	3.2906(19)	141(2)	x,y,z
5	O(19)---H(19B)···O(1)	0.90(2)	1.87(2)	2.7612(19)	168(2)	-1+x,y,z
6	C(3)---H(3)···O(10)	0.95	2.53	3.2099(18)	128	1-x,1-y,1-z
7	C(6)---H(6)···O(19)	0.95	2.46	3.280(2)	144	2-x,2-y,1-z
8	C(17)---H(17)···O(19)	0.95	2.59	3.415(2)	146	-1+x,3/2-y,1/2+z
$L_2.EG$						
Nr	Donor---H···Acceptor	D–H/**Å**	H···A/**Å**	D···A/**Å**	∠D---H···A/°	Symmetry operation
1	N(8)---H(8)···O(1)	0.88	2.07	2.690(2)	127	1/2+x,-1/2+y,z
2	O(11)---H(11)···O(1)	0.77(3)	1.97(3)	2.741(2)	175.1(17)	x,y,z
3	C(3)---H(3)···O(11)	0.95	2.45	3.377(3)	164	-1/2+x,3/2-y,1-z
4	C(4)---H(4)···O(11)	0.95	2.52	3.208(3)	129	-1/2+x,-1/2+y,z
3-BPU.EG						
Nr	Donor---H···Acceptor	D–H/**Å**	H···A/**Å**	D···A/**Å**	∠D---H···A/°	Symmetry operation
1	N(7)---H(7)···O(17)	0.88	1.92	2.7496(13)	158	x,1/2-y,1/2+z
2	N(10)---H(10)···O(20)	0.88	2.13	2.9122(14)	147	x,1/2-y,1/2+z
3	O(17)---H(17)···O(21)	0.84	1.88	2.7026(15)	166	x,y,z
4	O(20)---H(20)···N(13)	0.84	1.97	2.7932(15)	166	1-x,-1/2+y,3/2-z
5	O(21)---H(21)···N(1)	0.908(19)	1.838(19)	2.7344(14)	168.6(17)	x,y,z

6. Powder X-ray diffraction

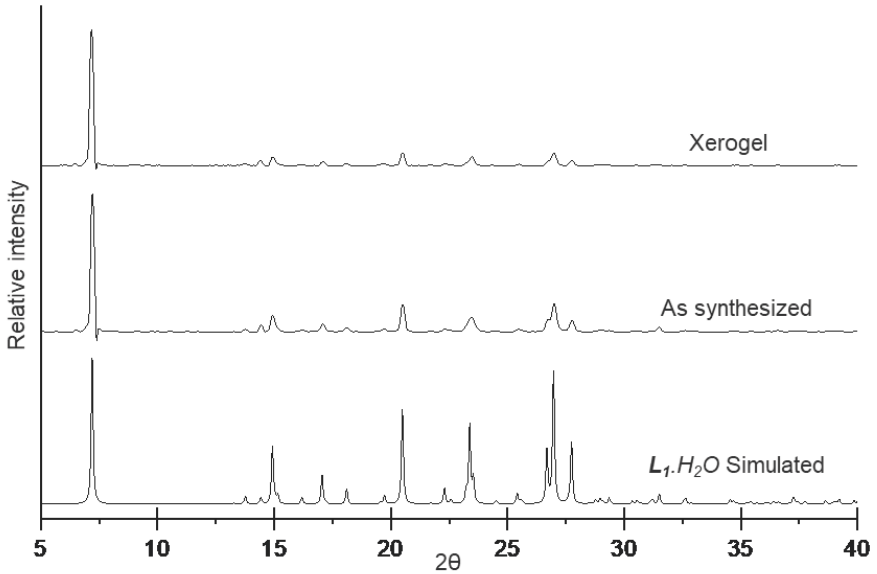

Figure S13. Comparison of the XRPD pattern of simulated $\mathbf{L_1.H_2O}$, as synthesised and the xerogel from water at 1.0 wt%.

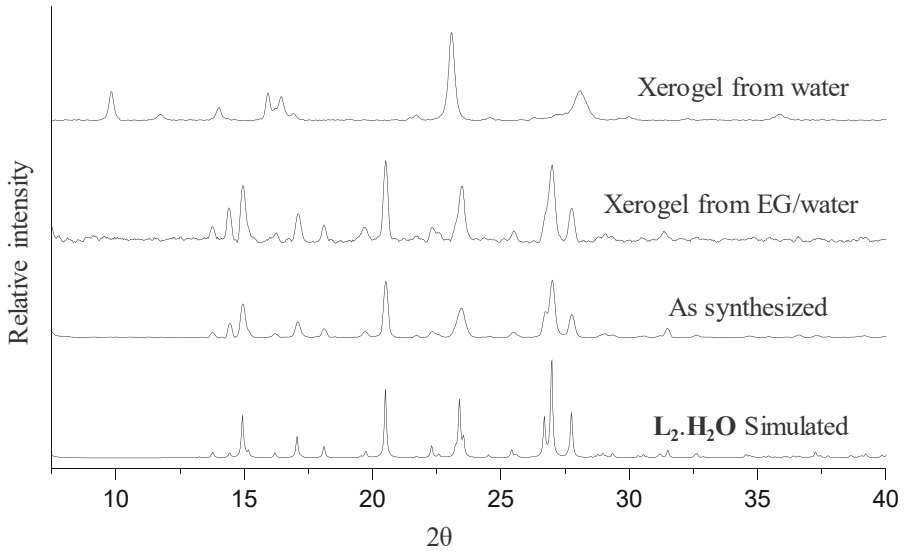

Figure S14: XRPD comparison of simulated $\mathbf{L_2.H_2O}$, bulk crystals of $\mathbf{L_2}$, xerogels obtained from EG/water (3:7 v/v) and pure water: (top) full spectra (bottom) selected region.

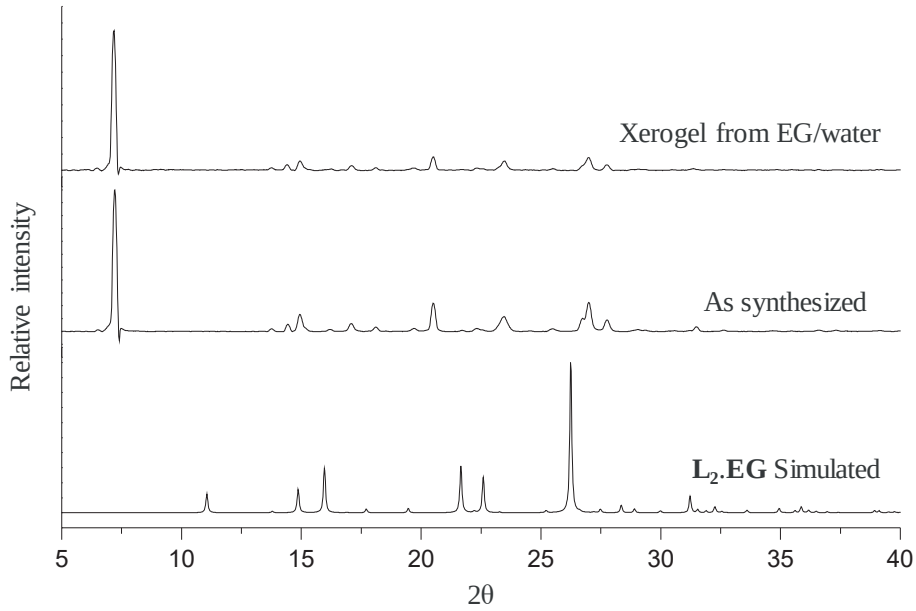

Figure S15: XRPD comparison of simulated **L_2.EG**, bulk crystals of **L_2** and xerogels obtained from EG/water (3:7 v/v).

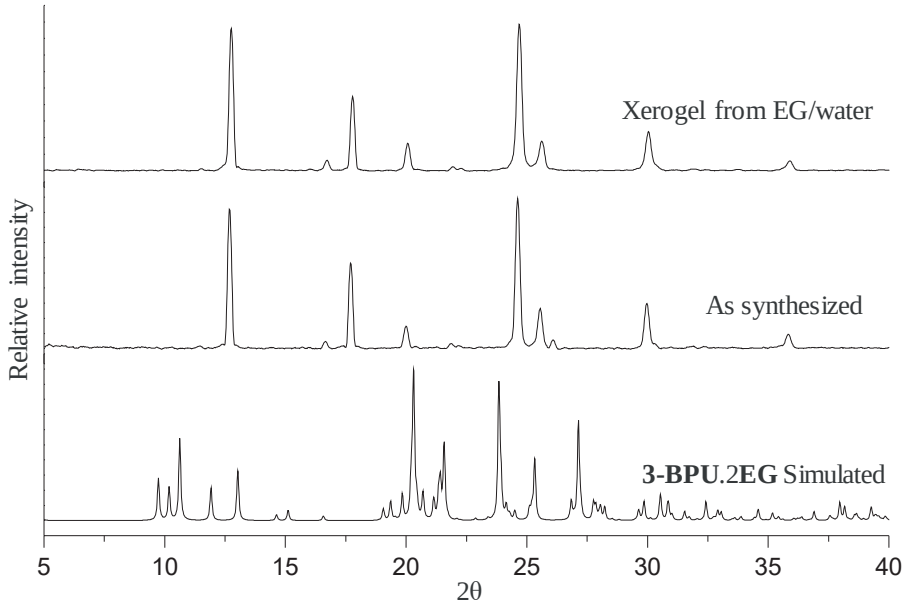

Figure S16: XRPD comparison of simulated **3-BPU.2EG**, bulk crystals of **3-BPU** and xerogels obtained from EG/water (3:7 v/v).

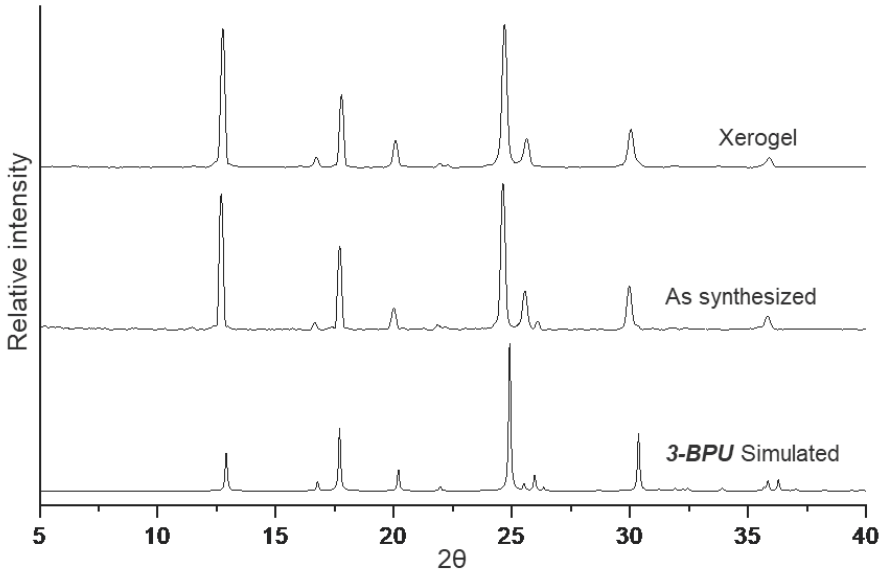

Figure S17: XRPD comparison of simulated **3-BPU**, bulk crystals of **3-BPU** and xerogels obtained from EG/water (3:7 v/v).

7. Anion sensing

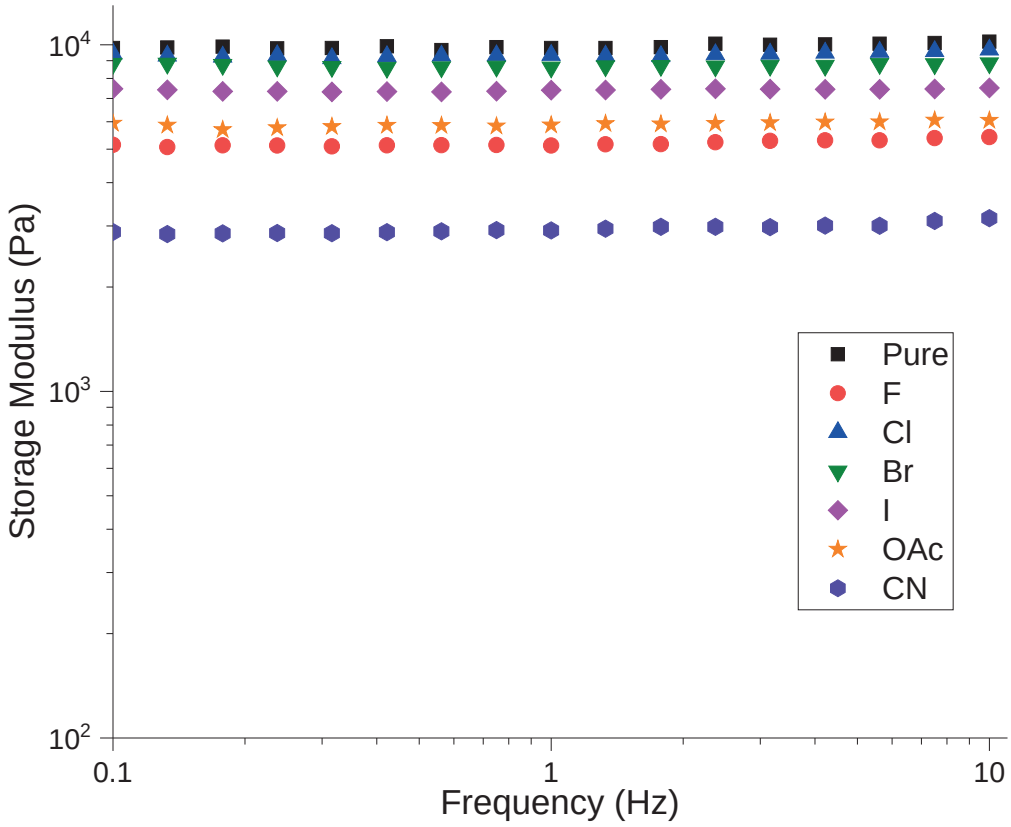

Figure S18: Frequency sweep experiments performed at 20.0 °C at a constant strain of 0.02% on **4-BPU** hydrogel at 1.0 wt%, in presence of three equivalents of anions.

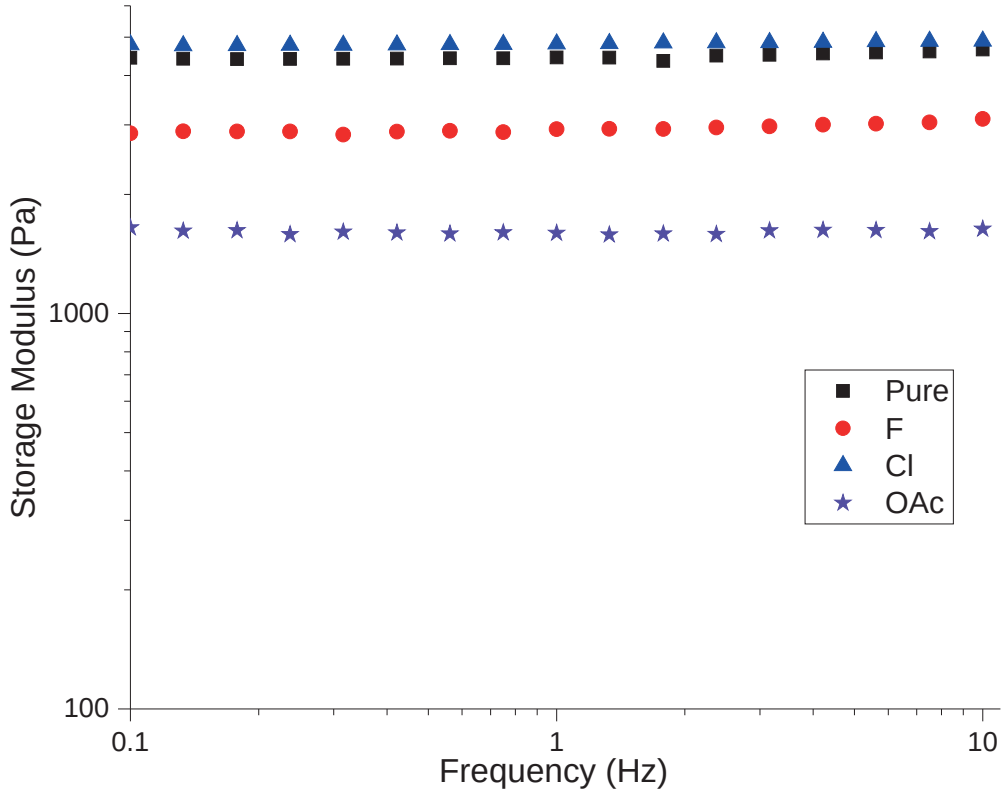

Figure S19: Frequency sweep experiments performed at 20.0 °C at a constant strain of 0.02% on $\mathbf{L_1}$ hydrogel at 1.0 wt%, in presence of three equivalents of anions.

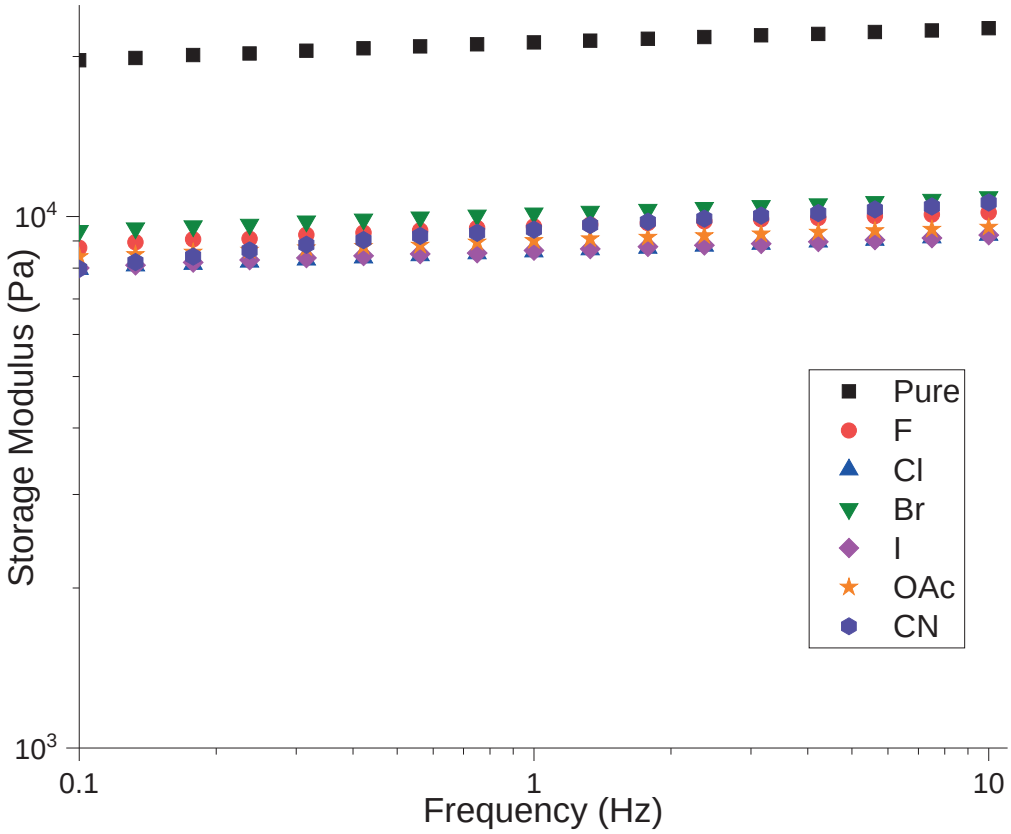

Figure S20: Frequency sweep experiments performed at 20.0 °C at a constant strain of 0.02% on $\mathbf{L_2}$ hydrogel at 1.0 wt%, in presence of three equivalents of anions.

7. Computational Study

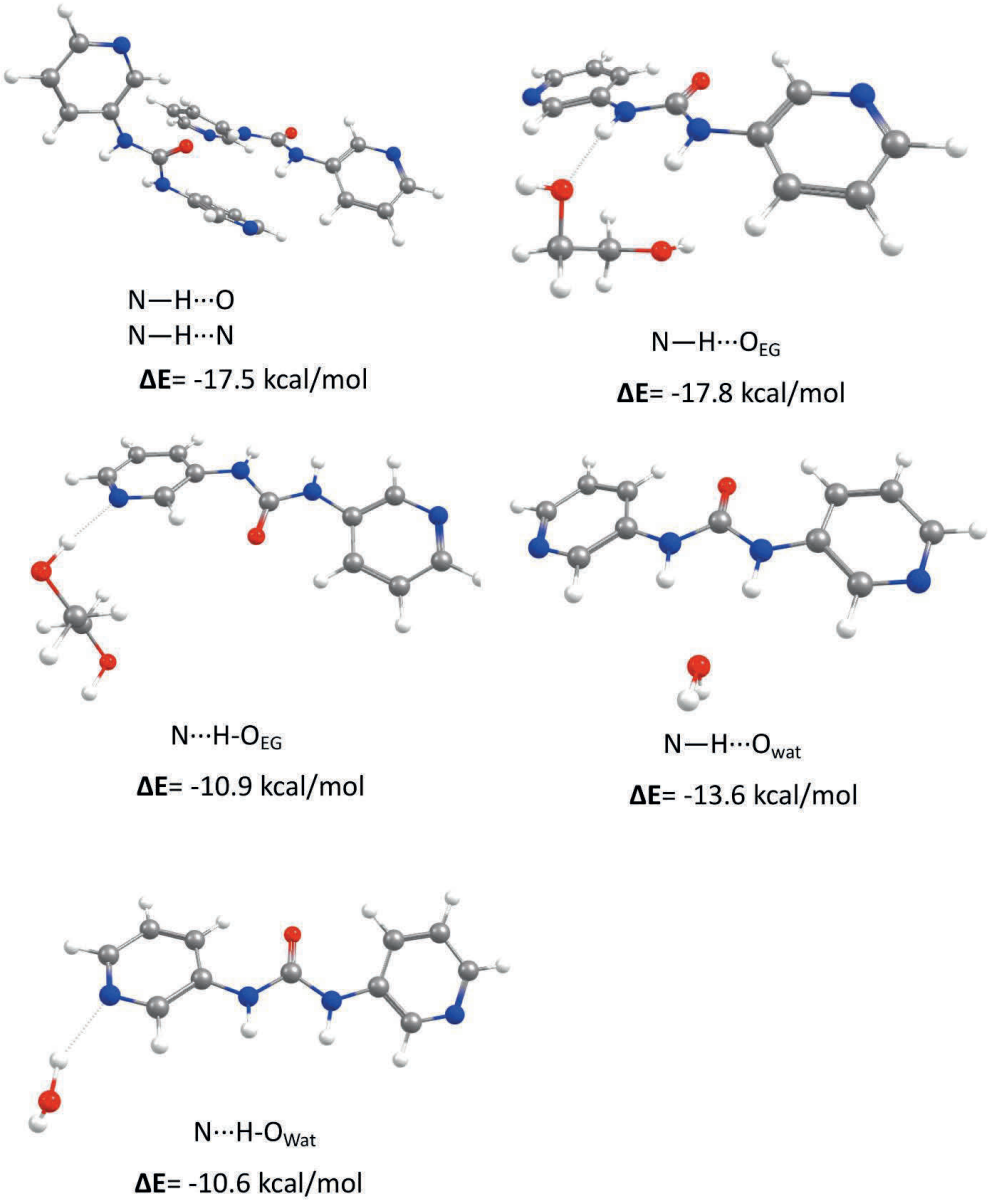

Figure S21: DFT-optimized geometries and calculated interaction energies of various **3-BPU** hydrogen-bonding interactions.

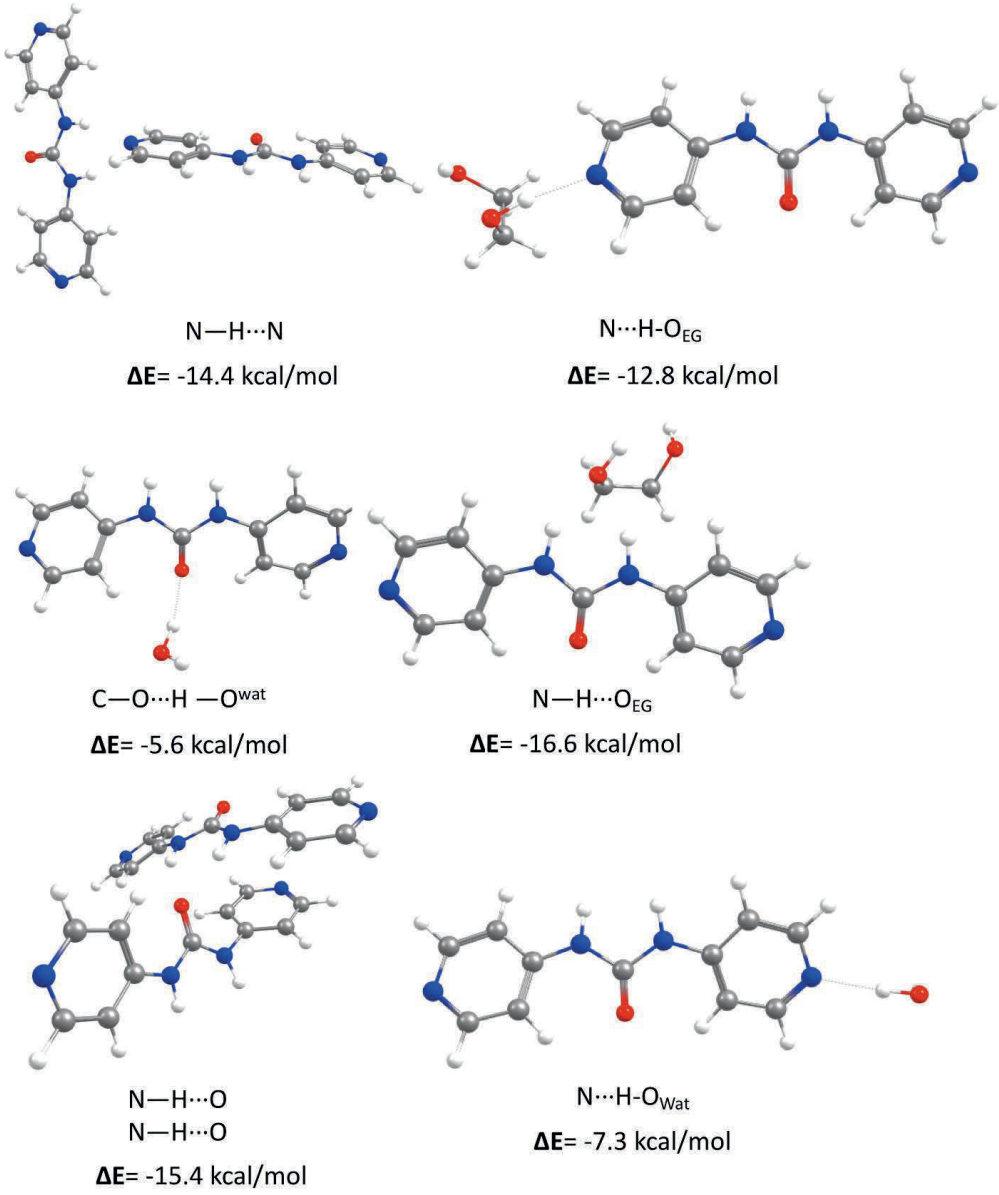

Figure S22: DFT-optimized geometries and calculated interaction energies of various **4-BPU** hydrogen-bonding interactions.

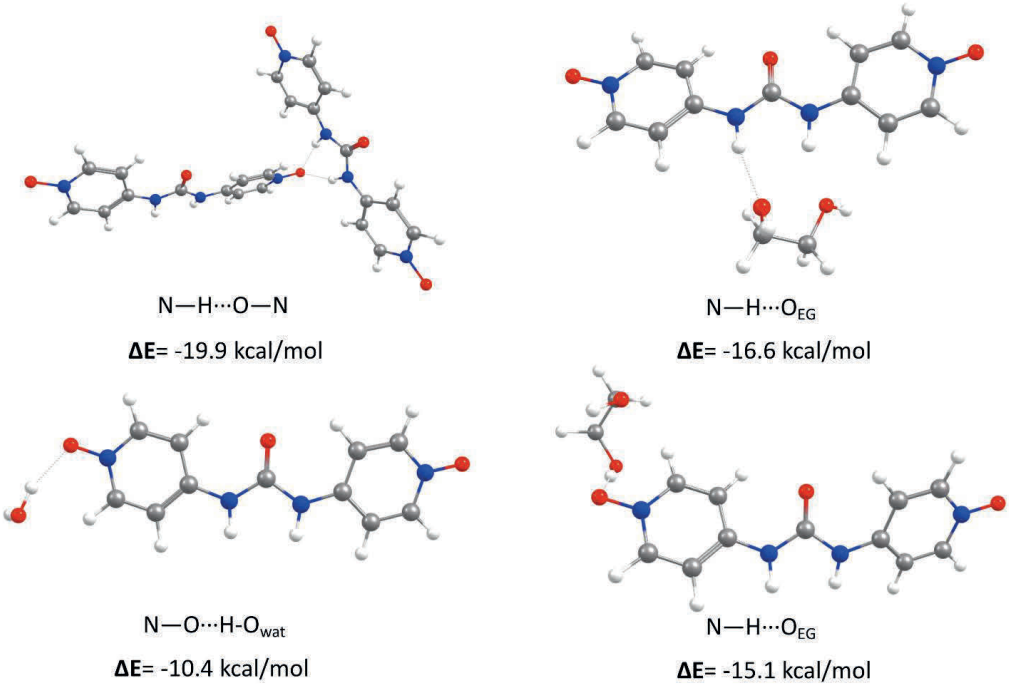

Figure S23: DFT-optimized geometries and calculated interaction energies of various **L$_1$** hydrogen-bonding interactions.

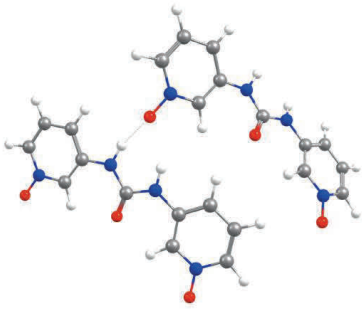

N—H···O—N

ΔE= -19.6 kcal/mol

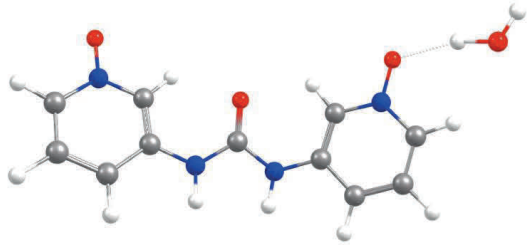

N—O···H-O_{wat}

ΔE= -8.8 kcal/mol

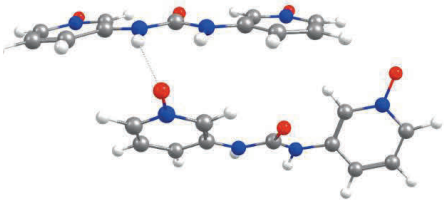

N—H···O-N

ΔE= -24.3 kcal/mol

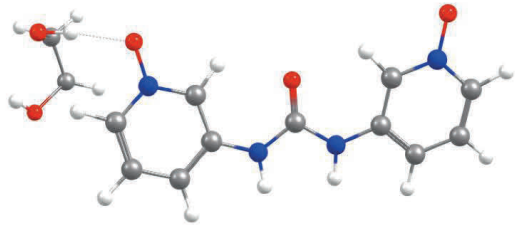

N—O···H-O_{EG}

ΔE= -15.1 kcal/mol

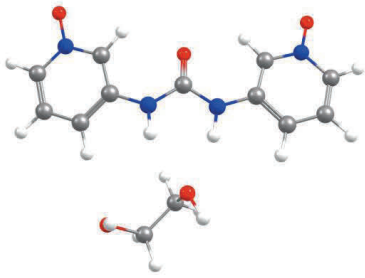

N—H···O_{EG}

ΔE= -15.0 kcal/mol

Figure S24: DFT-optimized geometries and calculated interaction energies of various $\mathbf{L_2}$ hydrogen-bonding interactions.

Article-III

This project is published in a peer reviewed journal and included as it was published. Slight differences might appear from the original article due to the formatting issue.

Publication details:

″Selective gelation of N-(4-pyridyl)nicotinamide by copper(II) salts″

Dipankar Ghosh, Ieva Lebedytė, Dmitry S. Yufit, Krishna K. Damodaran* and Jonathan W. Steed*

CrystEngComm, **2015**, *17*, 8130-8138.

Author contributions:

K.K.D planned and designed the research; I.L. synthesized the ligand and $Cu(OAc)_2$ complex. **D.G.** synthesized the ligand, performed the metal complexation, found the selective gelation property and performed gel characterizations. D.S.Y. solved single crystal structures and K.K.D. wrote the initial manuscript draft. **D.G.**, K.K.D. and J.W.S. reviewed the main manuscript.

CrystEngComm

PAPER

View Article Online
View Journal | View Issue

Cite this: *CrystEngComm*, 2015, **17**, 8130

Selective gelation of *N*-(4-pyridyl)nicotinamide by copper(II) salts†

Dipankar Ghosh,[a] Ieva Lebedytė,[a] Dmitry S. Yufit,[b] Krishna K. Damodaran*[a] and Jonathan W. Steed*[b]

Received 7th May 2015,
Accepted 18th August 2015

DOI: 10.1039/c5ce00901d

www.rsc.org/crystengcomm

We report the selective gelation properties of the copper(II) complexes of *N*-(4-pyridyl)nicotinamide (**4PNA**). The morphology of the xerogels was examined by scanning electron microscopy (SEM). The correlation between the X-ray powder diffraction (XRPD) pattern of the xerogels and the single crystal structure of the copper(II) acetate complex suggests that the single crystal X-ray data represent a good structural model for the gel fibers, and that gelation arises from the presence of a 1D hydrogen-bonded chain between gelator amide groups and coordinated anions, while the presence of strongly bound water in non-gelator systems results in the formation of more extensively hydrogen-bonded crystalline networks. The selective gelation of all the copper(II) salts compared to the other metal salts may be attributed to the Jahn–Teller distorted nature of copper(II), which weakens water binding in all copper(II) salts.

Introduction

Supramolecular gels based on low molecular weight gelators (LMWGs)[1–10] have emerged as a prolific area of current research due to their potential applications as functional soft materials for separation,[11] drug delivery,[12–14] as well as templating of inorganic and polymer materials[15,16] and as media to control crystal growth.[17] Gels are formed by the immobilisation of solvent molecules in the 3D fibrous network of the gelators, which self-assemble *via* non-covalent interactions[18,19] such as hydrogen bonding, van der Waals interactions, π–π stacking and halogen bonding. Recently, there has been an upsurge of interest in metal-based supramolecular gels (metallogels).[8,20] These metal-containing LMWGs have strong coordination interactions between the organic moiety and metal centre, which act as a key driving force in the formation of the gel fibre network in combination with various non-covalent interactions.[8,21,22] The gel fibres themselves can arise from the self-assembly of discrete complexes,[23–28] coordination polymers,[29–34] or cross-linked coordination polymers.[35] Non-coordinated metal ions or metallic nanoparticles may also be incorporated into the gel matrix.[36–39] The inclusion of metal ions in LMWGs leads to the formation of multifunctional metallogels which offer potential applications[20] in catalysis, sensing, optics and magnetic materials.

The understanding of the structure of LMWGs and metallogels in the gel state is still in its infancy because of the low ordering of the gel as a whole and the wide range of length scales of the gel structure from the nano- to the micro-scale. Efforts have been made to determine the gel structure by analysis of the X-ray diffraction pattern of the dried gel (xerogel). Nevertheless, removal of solvent to prepare a xerogel can result in artefacts due to dissolution and recrystallization, changes in morphology or polymorphic phase transition. However, the combination of the crystal structure and the powder diffraction pattern of either a native gel or a xerogel remains one of the most practical methods to gain insight into the gelator structure and aggregation behaviour. Based on this approach, efforts have been made to identify the key structural features of gel network formation in LMWGs by analysis of their potential using supramolecular synthons.[40]

Although there are a few reports on the structure–property correlation of metallogels,[41–45] designing metallogels with specified properties and structures is still a daunting task. We have shown that binding of metal to functional groups such as a pyridyl group can 'switch on' gelation by removing the competing urea–pyridyl hydrogen bonding interaction.[18,46] In previous work, one of us has reported a series of pyridyl amide compounds and

[a] *Department of Chemistry, Science Institute, University of Iceland, Dunhagi 3, 107 Reykjavík, Iceland. E-mail: krishna@hi.is; Fax: +354 552 8911; Tel: +354 525 4846*
[b] *Department of Chemistry, Durham University, South Road, Durham DH1 3LE, UK*

† Electronic supplementary information (ESI) available: Crystallographic information in CIF format for the structure of **1**, **2**, **3** & **4**. Details of gelation experiments, PXRD comparison, SEM of copper(II) nitrate gel and T_{gel} measurement. CCDC 1062590–1062592 and 1062883. For ESI and crystallographic data in CIF or other electronic format see DOI: 10.1039/c5ce00901d

established that *N*-(4-pyridyl)isonicotinamide can selectively form a hydrogel.[47] Other *N*-(pyridyl)isonicotinamide isomers do not form hydrogels, highlighting the importance of the relative position of ring nitrogen atoms for gel formation. In this work, we explore the ability of metal salts to bring about gelation in pyridyl amides. Specifically, we report the gelation properties of the metal salts of *N*-(4-pyridyl)nicotinamide (**4PNA**) as depicted in Scheme 1.

Experimental

Materials and methods

All starting materials were purchased from commercial sources and were used as supplied. Dichloromethane was freshly distilled from calcium hydride prior to use for the synthesis of amide, while the other solvents were used without further purification. Deionized water was used for all the experiments. ^{1}H and ^{13}C NMR spectra were recorded on a Bruker Advance 400 spectrometer (^{1}H-NMR: 400 MHz, ^{13}C-NMR: 100 MHz). IR spectra were measured on a Nicolet iS10, SEM was performed on a Leo Supra 25 microscope and PXRD was carried out using a Bruker D8 Focus instrument.

Synthesis of the ligand

The synthesis and characterisation of **4PNA** have been reported previously[47] and the analytical and spectroscopic data matched those reported in the literature.

Synthesis of complexes

[Cu(4PNA)$_2$(OAc)$_2$] (1). A solution of **4PNA** (25 mg, 0.125 mmol) in 5 mL of ethanol was layered over 5 mL of aqueous Cu(OAc)$_2$·2H$_2$O (12.4 mg, 0.062 mmol) solution. Blue crystals of **1** were obtained in a week (23 mg, 0.04 mmol). Yield: 64%. Anal. data for $C_{26}H_{24}CuN_6O_6$: calc. C, 53.84; H, 4.17; N, 14.49. Found: C, 53.72; H, 4.04; N, 14.42. FT-IR (cm^{-1}): 3255m, 3171m, 3075m, 3002m, 1687vs, 1601vs, 1507vs, 1429vs, 1332s, 1298s, 1240w, 1209w, 1117s, 1065w, 1026s, 895m, 839s, 728s, 679m, 622m, 601m, 542s.

[Cd(4PNA)$_2$(OAc)$_2$(H$_2$O)]·2H$_2$O (2). The cadmium complex was synthesised by layering an ethanolic solution (1.5 mL) of **4PNA** (20 mg, 0.1 mmol) over an aqueous solution (1 mL) of Cd(OAc)$_2$·2H$_2$O (13.3 mg, 0.05 mmol). Colourless crystals suitable for X-ray analysis were obtained after a period of one week (8 mg, 0.012 mmol). Yield: 25%. Anal. data for $C_{26}H_{30}CdN_6O_9$: calc. C, 45.72; H, 4.43; N, 12.31. Found: C, 45.87; H, 4.12; N, 12.30. FT-IR (cm^{-1}): 3247w, 3170w, 3069w, 1686s, 1597vs, 1523vs, 1421vs, 1333s, 1301s, 1212s, 1117s, 1065w, 1045m, 1015s, 936w, 896m, 834s, 730s, 711s, 672m, 622m, 591m, 538s.

[Zn(4PNA)$_2$(NO$_3$)$_2$(H$_2$O)$_2$] (3). Complex **3** was synthesized by layering an ethanolic solution (10 mL) of **4PNA** (39.8 mg, 0.2 mmol) over an aqueous solution (10 mL) of Zn(NO$_3$)$_2$·6H$_2$O (29.7 mg, 0.1 mmol). After a period of two weeks, X-ray quality single crystals were obtained (48.6 mg, 0.078 mmol). Yield: 78%. Anal. data for $C_{22}H_{22}N_8O_{10}Zn$: calc. C, 42.36; H, 3.55; N, 17.96. Found: C, 42.27; H, 3.38; N, 17.79. FT-IR (cm^{-1}): 3430b, 2516w, 2427w, 2356m, 1858w, 1678vs, 1620s, 1568s, 1492vs, 1426m, 1384vs, 1341m, 1315m, 1292s, 1108m, 1063s, 1023s, 920m, 900s, 873w, 842w, 828m, 811m, 756m, 700vs, 651s, 602m, 528m, 420m.

[Cd(4PNA)$_2$(NO$_3$)$_2$(H$_2$O)$_2$] (4). An ethanolic solution (10 mL) of **4PNA** (39.8 mg, 0.200 mmol) was layered over an aqueous solution of Cd(NO$_3$)$_2$·4H$_2$O (30.8 mg, 0.1 mmol). After a period of one week, X-ray quality single crystals were obtained (36.0 mg, 0.053 mmol). Yield: 54%. Anal. data for $C_{22}H_{22}CdN_8O_{10}$: calc. C, 39.39; H, 3.31; N, 16.70. Found: C, 39.22; H, 3.26; N, 16.64. FT-IR (cm^{-1}): 3668w, 3391b, 3306b, 2446w, 2361s, 1929b, 1769w, 1681vs, 1596vs, 1523vs, 1418m, 1384vs, 1333vs, 1297vs, 1208s, 1115s, 1065m, 1047m, 1021vs, 930m, 897s, 822vs, 729m, 699vs, 596m, 530s, 418m.

Gel preparation

Copper(II) acetate gel. Gels were prepared at various wt% by dissolving the required amount of Cu(OAc)$_2$·2H$_2$O in water (0.5 mL) and mixing it with the corresponding amount (1 : 2 metal : ligand ratio) of **4PNA** in DMF (0.5 mL). The mixture was sonicated for 2–4 minutes and allowed to stand overnight. The blue copper(II) acetate–**4PNA** gel was obtained and confirmed by the tube inversion test. Yield: 45%. The spectroscopic data for the xerogels matched those for **1**.

Copper(II) chloride gel. The gelation experiments were performed by mixing an aqueous solution of $CuCl_2$ (0.5 mL of water) with the corresponding amount (1 : 2 metal : ligand ratio) of **4PNA** in DMF (0.5 mL). The resulting solution was sonicated for one minute and allowed to stand overnight to yield a green gel. Yield: 38%. Anal. data for $C_{17}H_{23}Cl_2CuN_5O_3$: calc. C, 42.55; H, 4.83; Cu, 13.24; N, 14.60. Found: C, 42.72; H, 4.49; Cu, 13.49; N, 13.84. FT-IR (cm^{-1}): 3303m, 3228m, 3152m, 3066m, 1693vs, 1600vs, 1512vs, 1428s, 1331s, 1297vs,

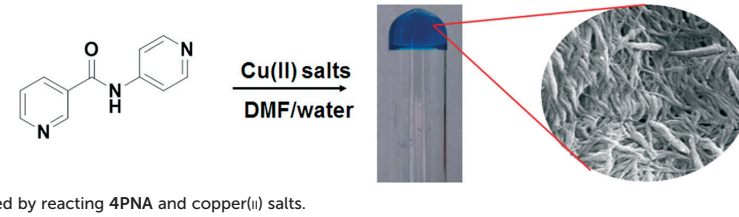

Scheme 1 Gels obtained by reacting **4PNA** and copper(II) salts.

1209s, 1117s, 1049m, 1024m, 896m, 835s, 725w, 696m, 675w, 645w, 599w, 537m, 445w.

Copper(II) nitrate gel. Gelation was observed at 3–7 wt% and the gel was prepared by mixing $Cu(NO_3)_2{\cdot}3H_2O$ (in water, 0.5 mL) with the corresponding amount (1 : 2 metal : ligand ratio) of **4PNA** in DMF (0.5 mL). The solution was mixed together without sonication and allowed to stand overnight to yield a greenish-blue gel. Yield: 19%. Anal. data for $C_{14}H_{18}CuN_6O_9$: calc. C, 35.19; H, 3.80; Cu, 13.30; N, 17.59. Found: C, 35.51; H, 3.49 Cu, 12.59; N, 16.10. FT-IR (cm^{-1}): 3319m, 3084w, 1695s, 1600vs, 1513vs, 1429s, 1380vs, 1335s, 1295s, 1211s, 1117m, 1057w, 1029w, 897w, 832s, 738w, 690m, 653w, 599w, 536m, 450w.

Copper(II) perchlorate gel. The gelation experiments performed at various concentrations of $Cu(ClO_4)_2{\cdot}6H_2O$ and **4PNA** in 1 : 2 DMF/water (v/v) resulted in partial gelation. Gelation was observed above 4 wt% at higher DMF concentration (9 : 1 DMF/water, v/v) and in pure DMF. This was achieved by mixing a solution of $Cu(ClO_4)_2{\cdot}6H_2O$ (0.1 mL of water or DMF) with the corresponding amount (1 : 2 metal : ligand ratio) of **4PNA** in DMF (0.9 mL). The resulting solution was sonicated for one minute and allowed to stand overnight to yield a greenish-blue gel. Yield: 13%. Anal. data for $C_{25}H_{25}Cl_2CuN_7O_{11}$: calc. C, 40.91; H, 3.43; Cu, 8.66; N, 13.36. Found: C, 41.86; H, 3.11; Cu, 9.69; N, 12.96. FT-IR (cm^{-1}): 3448b, 3069m, 1692s, 1600vs, 1514vs, 1476w, 1425s, 1395w, 1335s, 1298s, 1210s, 1116vs, 1029m, 898w, 834s, 734w, 687m, 627m, 599m, 535m.

Copper(II) sulphate gel. The copper(II) sulphate complexes of **4PNA** displayed similar properties as the copper(II) perchlorate salts. In this case, the required amount of $Cu(SO_4){\cdot}5H_2O$ in water (0.2 mL) was mixed with the corresponding amount (1 : 2 metal : ligand ratio) of **4PNA** in DMF (0.8 mL). The mixture was sonicated for one minute and allowed to stand overnight to yield a greenish-blue gel. Yield: 44%. Anal. data for $C_{22}H_{28}CuN_6O_{11}S$: calc. C, 40.77; H, 4.35; Cu, 9.80; N, 12.97; S, 4.95. Found: C, 40.88; H, 3.94; Cu, 10.58; N, 12.96; S, 5.91. FT-IR (cm^{-1}): 3401b, 3084w, 1691s, 1654m, 1605vs, 1516vs, 1421s, 1387w, 1336s, 1302s, 1212s, 1120vs, 1029m, 899w, 839m, 738m, 698m, 652w, 619m, 541m.

Scanning electron microscopy

The copper(II) salt dissolved in water was mixed with a solution of **4PNA** in DMF in a 1 : 2 metal : ligand ratio. In the case of copper(II) acetate, copper(II) chloride and copper(II) nitrate, 1 : 1 DMF/water (v/v) was used. For copper(II) perchlorate and copper(II) sulphate, 9 : 1 DMF/water (v/v) and 8 : 2 DMF/water (v/v) mixtures were used, respectively. It was then allowed to stand overnight. The resulting blue gel was filtered and dried under high vacuum. The copper(II) acetate and copper(II) chloride gels in pure water were also prepared in a similar fashion and dried. A small portion of the dried gel was placed on a pin mount with graphite planchets on top and coated with gold in the SEM (Leo Supra 25 microscope).

Crystallography

X-ray quality single crystals were obtained by slow evaporation of **4PNA** and a metal salt solution such as $Cu(OAc)_2{\cdot}2H_2O$ (**1**), $Cd(OAc)_2{\cdot}2H_2O$ (**2**), $Zn(NO_3)_2{\cdot}6H_2O$ (**3**), $Cd(NO_3)_2{\cdot}4H_2O$ (**4**) and $Cu(NO_3)_2{\cdot}3H_2O$ (**5**); however, the crystals of **5** did not diffract. X-ray single crystal data have been collected using MoKα radiation (λ =0.71073 Å) on Bruker D8 Venture (Photon 100 CMOS detector, IμS microsource, focusing mirrors for complexes **2**, **3** and **4** and for complex **1**, sealed tube and graphite monochromator) diffractometers equipped with Cryostream (Oxford Cryosystems) open-flow nitrogen cryostats at a temperature of 120.0(2) K. All structures were solved by direct methods and refined by full-matrix least-squares on F^2 for all data using Olex2 (ref. 48) and SHELXTL (ref. 49) software. All non-disordered non-hydrogen atoms were refined anisotropically, hydrogen atoms in structure **1** were refined isotropically, and the hydrogen atoms in structures **2**, **3** & **4** (except those of amide groups and H_2O molecules) were placed in their calculated positions and refined in riding mode. Disordered atoms in structures **3** and **4** were refined isotropically with fixed SOF = 0.5. The crystal data and parameters of refinement are listed in Table S14, ESI.† Crystallographic data for the structures have been deposited with the Cambridge Crystallographic Data Centre as supplementary publication (CCDC 1062590–1062592 and 1062883).

Results and discussion

Synthesis

The **4PNA** ligand was prepared by reacting nicotinoyl chloride and 4-aminopyridine in dichloromethane in the presence of triethylamine.[47] The gelation ability of the free ligand was examined in various solvents (Table S2, ESI†) and gelation was observed only in water at a higher concentration (3 wt%). The gelation ability of **4PNA** was further analysed in the presence of various salts of metal ions such as Mn(II), Fe(II), Co(II), Ni(II), Cu(II), Zn(II) and Cd(II) (Table 1). We have selected various anions of these metal salts with different hydrogen bonding properties such as acetate, chloride, nitrate, perchlorate and sulphate. The copper(II) acetate, cadmium(II) acetate, zinc(II) nitrate and cadmium(II) nitrate complexes of **4PNA** were also isolated and structurally characterised by single crystal X-ray diffraction (*vide infra* and ESI†).

Gelation studies

All of the metal salts were screened for gel formation with **4PNA** in a variety of solvents; however, the starting metal complexes only proved to be soluble in highly polar solvents, particularly water, DMF and DMSO. Gelation tests were performed *in situ* by mixing the metal salt and the ligand. In a typical experiment, an aqueous solution of the metal salt was mixed with a DMF solution of **4PNA** (1 : 1 or 1 : 2 metal : ligand ratio), sonicated for a short period of time and left to stand overnight. The manganese(II), iron(II), cobalt(II), nickel(II), cadmium(II) and zinc(II) complexes of **4PNA** did not

Table 1 Gelation studies with different metal salts in 1 : 1 DMF/water (v/v)

Metal salts	Initial observation	Final observation	wt%
$Cu(OAc)_2{\cdot}2H_2O$	Blue solution (C)	Blue gel (T)	2.0–6.0
$Cu(OAc)_2{\cdot}2H_2O$	Blue solution (C)	Blue gel (O)	7.0–10.0
$CuCl_2$	Light green solution (O)	Green gel (O)	2.6–10.0
$Cu(NO_3)_2{\cdot}3H_2O$	Blue solution (O)	Blue gel (O)	3.0–6.0
$Cu(ClO_4)_2{\cdot}6H_2O$[a]	Greenish-blue solution (O)	Greenish-blue gel (O)	4.0–11.7
$CuSO_4{\cdot}5H_2O$[b]	Blue solution	Blue gel (O)	3.5–9.0
$Zn(NO_3)_2{\cdot}6H_2O$	Clear solution	Clear solution	3.0–9.0
$Zn(OAc)_2{\cdot}2H_2O$	Clear solution	Clear solution	3.0–8.0
$ZnCl_2$	Clear solution	Crystalline material	3.0–6.0
$ZnSO_4{\cdot}7H_2O$	Clear solution	White precipitate	3.0–6.8
$Zn(BF_4)_2{\cdot}H_2O$	Clear solution	Clear solution	3.0–6.0
$Cd(NO_3)_2{\cdot}4H_2O$	Clear solution	White precipitate	3.0–9.0
$Cd(OAc)_2{\cdot}2H_2O$	White solution	White precipitate	3.0–8.0
$CdCl_2$	White solution	White precipitate	3.0–6.0
$CdSO_4{\cdot}8/3H_2O$	White solution	White precipitate	3.0–6.0
$FeSO_4{\cdot}7H_2O$	Green solution (C)	Yellow precipitate	3.0–6.0
$FeCl_2{\cdot}4H_2O$	Yellow solution (C)	Crystalline material	3.0–6.0
$Ni(OAc)_2{\cdot}4H_2O$	Green solution (C)	Green solution (C)	3.0–6.0
$NiCl_2{\cdot}6H_2O$	Green solution (C)	Green solution (C)	3.0–6.0
$Ni(NO_3)_2{\cdot}6H_2O$	Green solution (C)	Green solution (C)	3.0–6.0
$Co(OAc)_2{\cdot}4H_2O$	Red solution (C)	Red solution (C)	3.0–6.0
$CoCl_2{\cdot}6H_2O$	Red solution (C)	Pink precipitate	3.0–6.0
$Co(NO_3)_2{\cdot}6H_2O$	Red solution (C)	Red solution (C)	3.0–6.0
$MnCl_2{\cdot}4H_2O$	Clear solution	Clear solution	3.0–6.0
$MnSO_4{\cdot}H_2O$	Clear solution	Crystalline material	3.0–6.0
$Mn(NO_3)_2{\cdot}4H_2O$	Clear solution	Clear solution	3.0–6.0

C = clear, O = opaque & T = transparent. [a] Gelation experiments were performed in 9 : 1 DMF/water (v/v). [b] Gelation experiments were performed in 8 : 2 DMF/water (v/v).

form gels; a clear solution was observed initially and further evaporation yielded precipitates/crystals (Table 1). In contrast, all copper(II) salts formed gels with **4PNA** at a 1 : 2 metal : ligand ratio (assessed by a simple inversion test) in different DMF/water concentrations (Fig. 1).

Addition of varying ratios of copper(II) salts and **4PNA** in a 1 : 1 DMF/water mixture (v/v) established that a ratio of 1 : 2 metal : ligand resulted in optimal gel formation.

In the case of copper(II) acetate, mixing an aqueous solution of the metal salt and a DMF solution of the ligand (1 : 2 metal : ligand ratio) resulted in a clear solution from 2 wt% to 6 wt% which formed transparent blue gels after leaving to stand overnight. These gels subsequently yielded crystals over 24–48 h depending on the concentration (2–6 wt%), whereas a higher concentration (above 7 wt%) resulted in the formation of an opaque gel (Fig. 2). However, in a 1 : 1 metal : ligand ratio, gelation was observed above 4 wt%. We repeated these gelation experiments using copper(II) chloride in a 1 : 1 DMF/water mixture (v/v) and similar results were obtained. An opaque green solution was obtained by mixing an aqueous solution of the metal salt and a DMF solution of the ligand (1 : 2 metal : ligand ratio), which formed opaque green gels after leaving to stand overnight at various concentrations (from 2.6 wt% to 10 wt%). Gels were also observed in a 1 : 1 metal : ligand ratio at 3.3 wt%. The copper(II) nitrate complex of **4PNA** formed a gel in a 1 : 2 metal : ligand ratio at 3 wt%

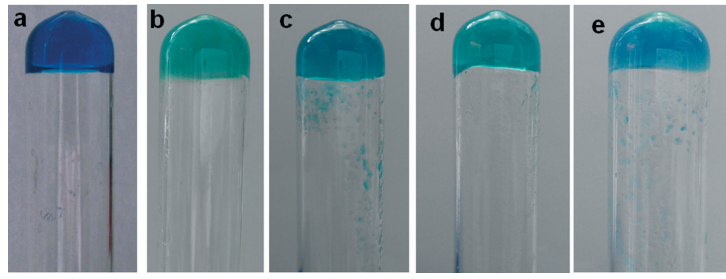

Fig. 1 Reaction of copper(II) salts with **4PNA** in a 1 : 2 metal : ligand ratio forming gels: (a) Cu(II) acetate and **4PNA** at 3 wt% in 1 : 1 DMF/water (v/v); (b) Cu(II) chloride and **4PNA** at 3 wt% in 1 : 1 DMF/water (v/v); (c) Cu(II) nitrate and **4PNA** at 4 wt% in 1 : 1 DMF/water (v/v); (d) Cu(II) perchlorate and **4PNA** at 4 wt% in 9 : 1 DMF/water (v/v); (e) Cu(II) sulphate and **4PNA** at 4.5 wt% in 8 : 2 DMF/water (v/v).

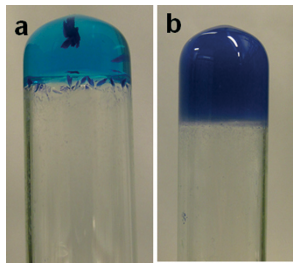

Fig. 2 Reaction of copper(II) acetate with **4PNA** (1 : 2 ratio): (a) crystals and gel formed at 3 wt% of the gelator and (b) opaque gel formed at higher gelator concentration (9 wt%) in 1 : 1 DMF/water (v/v).

concentration. Gelation was also observed by changing the anion to stronger hydrogen bonding anions, namely perchlorate and sulphate. In the case of perchlorate, gels were observed at a higher concentration of DMF (9 : 1 DMF/water mixture, v/v) at 4 wt% gelator concentration, whereas for the sulphate anion, gelation occurred at 3.5 wt% in a 8 : 2 DMF/water mixture (v/v). Increasing the proportion of DMF led to increased solubility and no gelation was observed for copper(II) acetate and copper(II) nitrate. In the case of copper(II) perchlorate, copper(II) chloride and copper(II) sulphate, gelation was observed at higher DMF concentrations.

Similar results were observed in the DMSO/water mixture for all copper(II) complexes. These results indicate that copper(II) coordination selectively enhances the gelation ability of **4PNA**, particularly in the case of copper(II) acetate and copper(II) chloride, to a much lesser degree in the other analogues. The selective effect of copper(II) is also noteworthy. The selectivity of metal salts in the gelation process has been reported. The perchlorate and nitrate salts of Ag(I) selectively formed metallogels indicating the importance of metal salts in gelation.[50] The selectivity of copper(II) chloride salts over other copper(II) salts in metallogel formation has been reported.[51] Recently, the selectivity of copper(II) chloride and bromide over perchlorate, nitrate, sulphate and acetate anions was reported.[52] These studies reveal the importance of metal salts, specifically copper(II) salts, in metallogel formation. In the present study, a series of copper(II) salts enhanced the gelation properties of the ligand (**4PNA**) over other metal salts. This is presumably due to the versatile properties of the copper(II) geometry such as its Jahn–Teller distorted nature, which weakens water binding in all copper(II) salts.

Gelation experiments for the complexes of all copper(II) salts were also performed in pure water. Addition of copper(II) acetate and copper(II) chloride to **4PNA** (1 : 2 metal : ligand ratio) in pure water gave gels above 1.5 wt% and 3 wt%, respectively, whereas reaction of other copper(II) salts with **4PNA** in water immediately gave a precipitate in every case. These results indicate that DMF acts as a solubilising medium while water acts as an antisolvent. This delicate balance between hydrophobic effects and other intermolecular interactions is required to achieve three-dimensional elastic self-assembled networks of the gel. These results clearly indicate that the 1 : 2 metal : ligand ratio is optimal.

Gel thermal stability

The formation of supramolecular gels at room temperature is relatively unusual, implying slow coordination or slow nucleation of the gel fibres. Slow cooling is a more common method to bring about the necessary supersaturated solution from which gel fibre growth can occur. The thermal stability of the room-temperature copper(II) metallogels of **4PNA** was evaluated by analysing the temperature at which the gel was converted into a liquid phase (T_{gel}). Copper(II) acetate gels displayed T_{gel} values of 58 °C and 61 °C for 2 wt% and 4 wt%, respectively. The T_{gel} for copper(II) chloride at 3 wt% was 64 °C and that for copper(II) nitrate gels at 6.4 wt% was 53 °C. In comparison, the T_{gel} values for the analogous copper(II) perchlorate and sulphate gels at 4 wt% and 5 wt% were 55 °C and 65 °C, respectively. These results indicate that the thermal stability depends on the hydrogen bonding ability of the anions. The copper(II) acetate and copper(II) chloride gels are thermoreversible at minimum gel concentrations, whereas copper(II) nitrate and copper(II) sulphate gels are thermoreversible at higher concentrations (5–6 wt%). However, prolonged heating at an elevated temperature (<90 °C) resulted in the decomposition of these complexes.

Scanning electron microscopy

The morphologies of the copper(II) gels of **4PNA** were studied by SEM analysis. The gels prepared from water and DMF/water (1 : 1, v/v) were filtered and dried under high vacuum. A small portion of the dried gel was placed on a pin mount with graphite planchets on top and was coated with gold. The SEM images of the copper(II) acetate complex of **4PNA** (4 wt%) revealed that both xerogels display a fibrous network, although some crystalline material is also evident in the xerogels obtained from DMF/water (Fig. 3a). This may arise from the drying process given the relative volatility of water compared to DMF, which may well result in partial dissolution and reprecipitation. The width of the gel fibrils varies from 13 nm to 40 nm regardless of the anion and solvent in which the gel is prepared (Fig. S3, ESI†).

Crystal structures

The complexes obtained from the reaction of **4PNA** with metal salts such as copper(II) acetate, cadmium(II) acetate, zinc(II) nitrate and cadmium nitrate were characterised by single crystal X-ray crystallography. Crystals were isolated by slow evaporation of an EtOH/water mixture of **4PNA** and metal salts. Crystallographic details (Table S14†) and hydrogen bonding parameters (Table S15†) are given in the ESI.†

Crystalline structure of $[Cu(4PNA)_2(OAc)_2]$. X-ray quality crystals were obtained by slow evaporation of an ethanol–water mixture of copper(II) acetate and **4PNA** to give a mononuclear 1 : 2 complex of formula $[Cu(4PNA)_2(OAc)_2]$ (**1**), with a

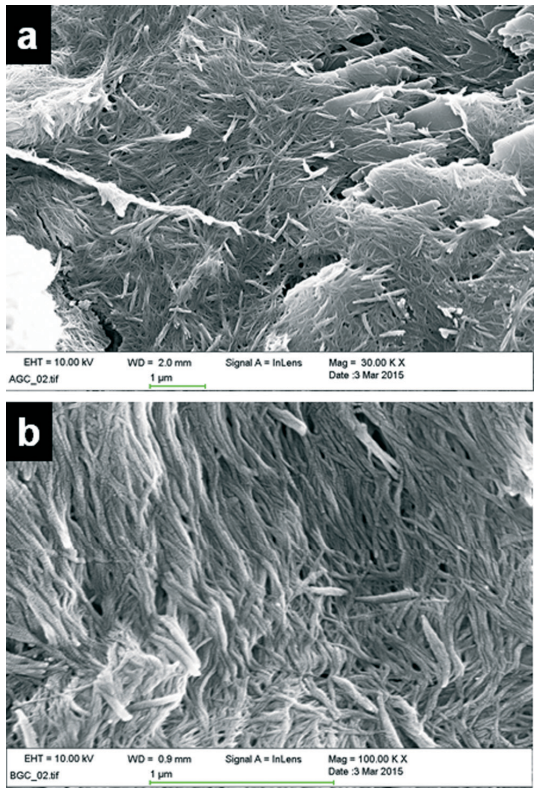

Fig. 3 SEM images of 1 : 2 copper acetate gels of **4PNA** (a) in DMF/water and (b) in only water, displaying a fibrous network.

stoichiometry consistent with the optimal ratio required for gel formation.

The copper(II) metal centre lies on an inversion centre and displays a Jahn–Teller distorted octahedral geometry with the oxygen atoms of the acetate anion adopting an asymmetric chelate coordination mode in the equatorial position. The axial positions are occupied by the pyridyl nitrogen atoms of the **4PNA** ligands which coordinate *via* the 4-aminopyridine-derived end of the molecule. The nicotinoyl-derived pyridyl group is uncoordinated in the structure and does not take part in strong intermolecular interactions. The nitrogen atom of the amide moiety of **4PNA** is hydrogen-bonded to the oxygen atom of the metal-coordinated acetate anion resulting in the formation of a 1D hydrogen-bonded chain (N⋯O = 2.8188(19) Å, ∠N–H⋯O = 164.0(17)°). This type of structure could give rise to hydrogen-bonded 1D fibre formation and hence gelation[53] (Fig. 4b).

Crystalline structure of $[Cd(4PNA)_2(OAc)_2(H_2O)]\cdot 2H_2O$. Slow evaporation of a solution of cadmium(II) acetate and **4PNA** in EtOH/water at a 1 : 2 metal : ligand ratio resulted in the formation of a complex of formula $[Cd(4PNA)_2(OAc)_2(H_2O)]\cdot 2H_2O$ (**2**) over a period of one week. Although the coordination modes of acetate and **4PNA** are similar to those in **1**, water coordination results in a distorted pentagonal bipyramidal Cd(II) metal centre (Fig. 5a). The nitrogen atom of the amide moiety of **4PNA** displays hydrogen bonding to the metal-coordinated acetate anion resulting in N–H⋯O interactions (N⋯O = 2.856(2)–2.950(2) Å, ∠N–H⋯O = 166(3)–172(2)°). The uncoordinated water molecules are hydrogen-bonded to the oxygen atoms of the metal-bound acetate anions. One of these water molecules is further hydrogen-bonded to the nitrogen atom of the nicotinoyl-derived pyridyl

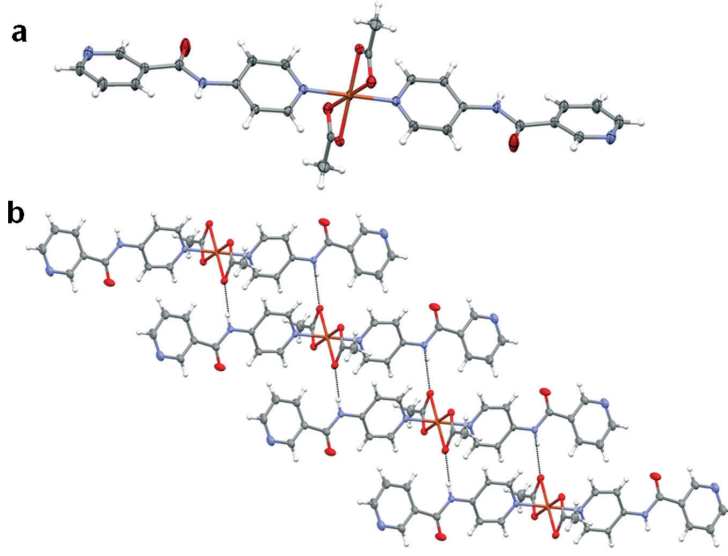

Fig. 4 (a) Molecular structure of **1** and (b) the 1D hydrogen-bonded chain observed in the solid state.

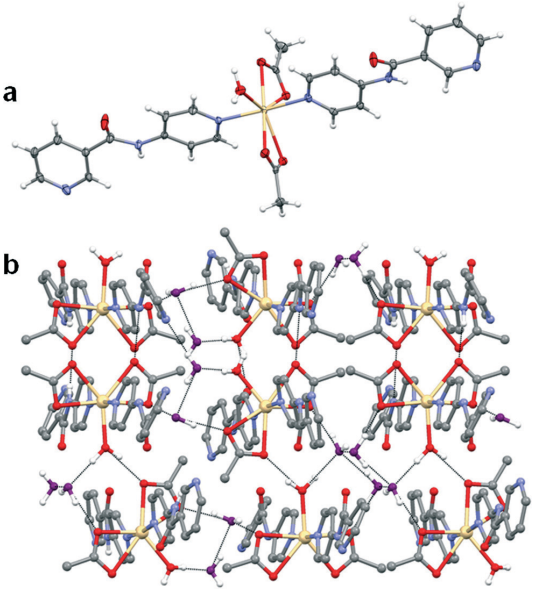

Fig. 5 (a) Molecular structure of **2** (uncoordinated water molecules are not shown) and (b) the 2D hydrogen-bonded chain observed in the solid state (uncoordinated water molecules are shown in purple).

group resulting in the formation of a 2D hydrogen-bonded network (Fig. 5b). The cross-linking provided by the hydrogen bonding to the additional water molecules may explain why this material forms a crystalline solid rather than a gel.

Crystalline structure of $[Zn(4PNA)_2(NO_3)_2(H_2O)_2]$. Single crystals of formula $[Zn(4PNA)_2(NO_3)_2(H_2O)_2]$ (**3**) suitable for X-ray analysis were obtained by slow evaporation of an EtOH/water mixture of zinc(II) nitrate and **4PNA** (1 : 2 metal : ligand ratio) over a period of one week. The Zn(II) atom lies on an inversion centre and the structure of **3** is very similar to that of **1** except that the poorer ligating properties of the nitrate anion and smaller size of zinc(II) result in monodentate coordination and completion of the coordination sphere by two adventitious water molecules. The nitrogen atom of the amide moiety forms hydrogen bonds to the oxygen atom of the nitrate anion (N⋯O = 2.920(2) Å, ∠N–H⋯O = 161(2)°) and the oxygen atoms are hydrogen-bonded to the metal-coordinated water molecules. These hydrogen bonding interactions result in the formation of a 2D hydrogen-bonded network (Fig. 6b).

Crystalline structure of $[Cd(4PNA)_2(NO_3)_2(H_2O)_2]$. Crystallization of **4PNA** from a solution of cadmium(II) nitrate in EtOH/water at a 1 : 2 metal : ligand ratio gives a complex of formula $[Cd(4PNA)_2(NO_3)_2(H_2O)_2]$ (**4**) with cadmium(II) lying on an inversion centre, which is isomorphous with **3**. Although the metal–ligand bond distances are slightly longer than those in the zinc analogue, the hydrogen bonding patterns are similar (for example, the amide moiety and oxygen atom of the nitrate anion, N⋯O = 2.959(4) Å, ∠N–H⋯O = 164.0°), resulting in the formation of a 2D hydrogen-bonded network (Fig. S4, ESI†).

It is quite interesting to note that in all these structures, the N–H⋯O synthon is observed where the nitrogen atom of the amide moiety of **4PNA** is hydrogen-bonded to the oxygen atom of the metal-coordinated anion. Comparison of the

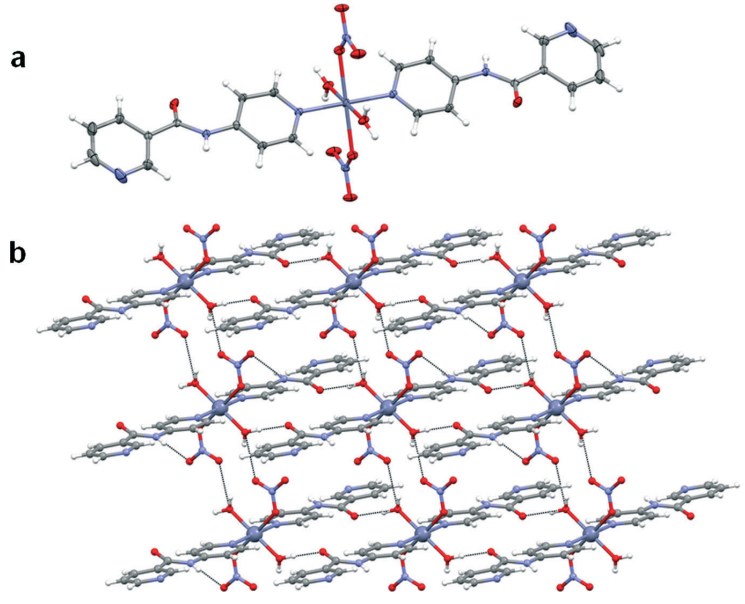

Fig. 6 (a) Molecular structure of **3** and (b) the 2D hydrogen-bonded chain observed in the solid state.

hydrogen bonding distances clearly indicates that compound **1** has strong hydrogen bonds (N···O = 2.8188(19) Å). These strong interactions may be attributed to the lack of water molecules, resulting in a large electron density around the donor atom, thereby forming a rigid 1D network which could account for its gelation ability.

X-ray powder diffraction (XRPD)

It is interesting to note that the hydrogen bonding pattern in compound **1** is 1D, whereas the solid state structures of non-gelators **2**, **3** and **4** are 2D hydrogen-bonded networks. In order to determine whether these single crystal structures are of relevance to the gels formed by the copper(II) complexes with a stoichiometry of 1 : 2, we compared the XPRD pattern calculated from the single crystal data with the experimental patterns of the xerogel obtained from DMF/water and the bulk precipitate from EtOH/water (Fig. 7). These data showed that the structure of the aqueous DMF-derived copper acetate xerogel is similar to that of the single crystal despite the fact that the sample crystallized from a different solvent. The precipitate obtained from aqueous ethanol is also the same solid form. Given the simple nature of the complex in **1**, its 1 : 2 stoichiometry which matches the ratio needed for optimal gelation and the persistence of this solid form in all three samples, we believe that this complex is the gelator and the formation of a 1D hydrogen-bonded tape due to the lack of coordinated water is a key factor in the gelation behaviour.

While the structural information on the copper(II) chloride complex was not available due to the lack of single crystals, we have performed Cambridge Structural Database (CSD)[54] analysis and found that 91% of the copper(II) chloride structures do not have coordinated water molecules (ESI†). This might be the reason that the copper(II) chloride complex of **4PNA** shows excellent gelation properties. Although the structure of the copper(II) nitrate complex of **4PNA** has not been determined, the closely related *N*-phenyl-4-pyridinecarboxamine (**4PPC**) complex $[Cu(\mathbf{4PPC})_2(NO_3)_2(H_2O)_2]$ contains two aqua ligands,[55] suggesting that the relatively inefficient gelation behaviour of the copper(II) nitrate complex of **4PNA** may also arise from additional water hydrogen bonding interactions. The perchlorate and sulphate salts of copper(II) are known to have coordinated water molecules. The fact that these copper(II) complexes do form weak gels at high weight percent, as opposed to the crystalline complexes expected for the other hydrated metal complexes, may arise from the Jahn–Teller distorted nature of copper(II) meaning that water is relatively weakly bound in comparison to the zinc(II) analogue. Further evidence for the hydrated nature of the copper(II) complexes of **4PNA** comes from the IR spectrum of the material. We compared the IR spectra of the complexes (as-synthesised) with those of the xerogels. The IR spectra of the xerogels of copper(II) acetate and the crystals were similar. The other complexes displayed a slight broad *ν*(OH) band compared to the bulk solid (as-synthesised), which supports the effect of metal-bound water in the gelation process (Fig. S8–S12, ESI†).

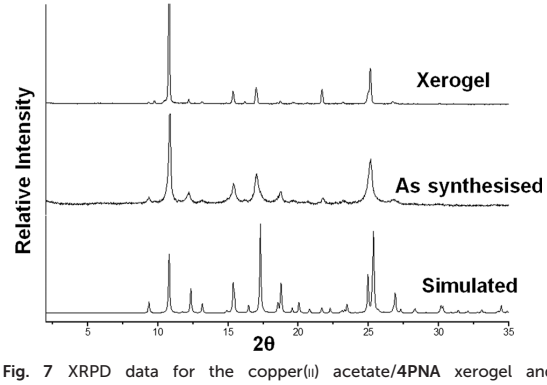

Fig. 7 XRPD data for the copper(II) acetate/**4PNA** xerogel and precipitated product and the simulated pattern from the single crystal X-ray data.

Conclusions

The gelation ability of **4PNA** was analysed in the presence of the salts of various metal ions such as manganese(II), iron(II), cobalt(II), nickel(II), copper(II), zinc(II) and cadmium(II). Interestingly, gelation of **4PNA** metal complexes was observed only in the case of copper(II) salts. The selective gelation of all the copper(II) salts compared to the other metal salts may be attributed to the Jahn–Teller distorted nature of copper(II), which weakens water binding in all copper(II) salts. Specifically, the copper(II) acetate complex of **4PNA** is a good gelator of polar solvents while the analogous zinc and cadmium nitrate and acetate complexes do not form metallogels. We suggest that this selective gelation ability of the copper(II) acetate salt has a structural origin and is correlated with the lack of coordinated water in the complex gelators, preventing 2D hydrogen-bonded network formation and favouring the formation of 1D hydrogen-bonded fibrils. An interesting feature of the gelators is the availability of non-coordinated pyridyl nitrogen atoms for further modification[34] and work directed towards the incorporation of metallic nanoparticles using these anchor points is currently in progress.

Acknowledgements

We are thankful to Prof. P. Dastidar, IACS-Kolkatta, India for the support and help with the initial results. We thank ÍSOR Iceland (Dr. Sigurður Sveinn Jónsson) for powder X-ray diffraction analysis and Nýsköpunarmiðstöð Íslands (Dr. Jón Matthíasson and Dr. Birgir Jóhannesson) for help in collecting the SEM images. KKD thanks the University of Iceland Start-up Grant and Research Fund (6459 and 7274) for funding.

Notes and references

1 S. Banerjee, R. K. Das and U. Maitra, *J. Mater. Chem.*, 2009, **19**, 6649–6687.

2 P. Dastidar, *Chem. Soc. Rev.*, 2008, **37**, 2699–2715.
3 M. de Loos, B. L. Feringa and J. H. van Esch, *Eur. J. Org. Chem.*, 2005, **2005**, 3615–3631.
4 L. A. Estroff and A. D. Hamilton, *Chem. Rev.*, 2004, **104**, 1201–1218.
5 M. George and R. G. Weiss, *Acc. Chem. Res.*, 2006, **39**, 489–497.
6 A. R. Hirst, B. Escuder, J. F. Miravet and D. K. Smith, *Angew. Chem., Int. Ed.*, 2008, **47**, 8002–8018.
7 D. K. Kumar and J. W. Steed, *Chem. Soc. Rev.*, 2014, **43**, 2080–2088.
8 M.-O. M. Piepenbrock, G. O. Lloyd, N. Clarke and J. W. Steed, *Chem. Rev.*, 2010, **110**, 1960–2004.
9 J. W. Steed, *Chem. Soc. Rev.*, 2010, **39**, 3686–3699.
10 G. Yu, X. Yan, C. Han and F. Huang, *Chem. Soc. Rev.*, 2013, **42**, 6697–6722.
11 E. Krieg, H. Weissman, E. Shirman, E. Shimoni and B. Rybtchinski, *Nat. Nanotechnol.*, 2011, **6**, 141–146.
12 S. Sutton, N. L. Campbell, A. I. Cooper, M. Kirkland, W. J. Frith and D. J. Adams, *Langmuir*, 2009, **25**, 10285–10291.
13 P. D. Thornton, R. J. Mart, S. J. Webb and R. V. Ulijn, *Soft Matter*, 2008, **4**, 821–827.
14 K. J. C. van Bommel, M. C. A. Stuart, B. L. Feringa and J. van Esch, *Org. Biomol. Chem.*, 2005, **3**, 2917–2920.
15 B. Li, L. Tang, L. Qiang and K. Chen, *Soft Matter*, 2011, **7**, 963–969.
16 Q. Wei and S. L. James, *Chem. Commun.*, 2005, 1555–1556.
17 J. A. Foster, M.-O. M. Piepenbrock, G. O. Lloyd, N. Clarke, A. K. HowardJudith and J. W. Steed, *Nat. Chem.*, 2010, **2**, 1037–1043.
18 L. Meazza, J. A. Foster, K. Fucke, P. Metrangolo, G. Resnati and J. W. Steed, *Nat. Chem.*, 2013, **5**, 42–47.
19 R. G. Weiss, *P*, *Terech and Editors, Molecular Gels: Materials with Self-Assembled Fibrillar Networks*, Springer, 2006.
20 A. Y.-Y. Tam and V. W.-W. Yam, *Chem. Soc. Rev.*, 2013, **42**, 1540–1567.
21 N. N. Adarsh, P. Sahoo and P. Dastidar, *Cryst. Growth Des.*, 2010, **10**, 4976–4986.
22 B. Xing, M.-F. Choi and B. Xu, *Chem. Commun.*, 2002, 362–363.
23 R. Gavara, J. Llorca, J. C. Lima and L. Rodriguez, *Chem. Commun.*, 2013, **49**, 72–74.
24 T. Ishi-i, R. Iguchi, E. Snip, M. Ikeda and S. Shinkai, *Langmuir*, 2001, **17**, 5825–5833.
25 K. Isozaki, K. Ogata, Y. Haga, D. Sasano, T. Ogawa, H. Kurata, M. Nakamura, T. Naota and H. Takaya, *Chem. Commun.*, 2012, **48**, 3936–3938.
26 D. López and J.-M. Guenet, *Macromolecules*, 2001, **34**, 1076–1081.
27 P. Terech, G. Gebel and R. Ramasseul, *Langmuir*, 1996, **12**, 4321–4323.
28 Y. Zhang, B. Zhang, Y. Kuang, Y. Gao, J. Shi, X. X. Zhang and B. Xu, *J. Am. Chem. Soc.*, 2013, **135**, 5008–5011.
29 N. N. Adarsh and P. Dastidar, *Cryst. Growth Des.*, 2011, **11**, 328–336.
30 X. de Hatten, N. Bell, N. Yufa, G. Christmann and J. R. Nitschke, *J. Am. Chem. Soc.*, 2011, **133**, 3158–3164.
31 T. D. Hamilton, D.-K. Bučar, J. Baltrusaitis, D. R. Flanagan, Y. Li, S. Ghorai, A. V. Tivanski and L. R. MacGillivray, *J. Am. Chem. Soc.*, 2011, **133**, 3365–3371.
32 T. Ishiwata, Y. Furukawa, K. Sugikawa, K. Kokado and K. Sada, *J. Am. Chem. Soc.*, 2013, **135**, 5427–5432.
33 M. Paul, N. N. Adarsh and P. Dastidar, *Cryst. Growth Des.*, 2012, **12**, 4135–4143.
34 M.-O. M. Piepenbrock, N. Clarke and J. W. Steed, *Soft Matter*, 2011, **7**, 2412–2418.
35 K. Hanabusa, Y. Maesaka, M. Suzuki, M. Kimura and H. Shirai, *Chem. Lett.*, 2000, 1168–1169.
36 S. Bhattacharjee and S. Bhattacharya, *Chem. Commun.*, 2014, **50**, 11690–11693.
37 S. Bhattacharjee, S. K. Samanta, P. Moitra, K. Pramoda, R. Kumar, S. Bhattacharya and C. N. R. Rao, *Chem. – Eur. J.*, 2015, **21**, 5467–5476.
38 P. Kumar Vemula, U. Aslam, V. Ajay Mallia and G. John, *Chem. Mater.*, 2007, **19**, 138–140.
39 M. Paul, K. Sarkar and P. Dastidar, *Chem. – Eur. J.*, 2015, **21**, 255–268.
40 G. R. Desiraju, *Angew. Chem., Int. Ed. Engl.*, 1995, **34**, 2311–2327.
41 T. Klawonn, A. Gansauer, I. Winkler, T. Lauterbach, D. Franke, R. J. M. Nolte, M. C. Feiters, H. Borner, J. Hentschel and K. H. Dotz, *Chem. Commun.*, 2007, 1894–1895.
42 P. Sahoo, V. G. Puranik, A. K. Patra, P. U. Sastry and P. Dastidar, *Soft Matter*, 2011, **7**, 3634–3641.
43 A. Y.-Y. Tam, K. M.-C. Wong and V. W.-W. Yam, *J. Am. Chem. Soc.*, 2009, **131**, 6253–6260.
44 B. Xing, M.-F. Choi and B. Xu, *Chem. – Eur. J.*, 2002, **8**, 5028–5032.
45 S. Yoon, W. J. Kwon, L. Piao and S.-H. Kim, *Langmuir*, 2007, **23**, 8295–8298.
46 P. Byrne, G. O. Lloyd, L. Applegarth, K. M. Anderson, N. Clarke and J. W. Steed, *New J. Chem.*, 2010, **34**, 2261–2274.
47 D. K. Kumar, D. A. Jose, P. Dastidar and A. Das, *Langmuir*, 2004, **20**, 10413–10418.
48 O. V. Dolomanov, L. J. Bourhis, R. J. Gildea, J. A. K. Howard and H. Puschmann, *J. Appl. Crystallogr.*, 2009, **42**, 339–341.
49 G. Sheldrick, *Acta Crystallogr., Sect. A: Found. Crystallogr.*, 2008, **64**, 112–122.
50 J. H. Lee, S. Kang, J. Y. Lee and J. H. Jung, *Soft Matter*, 2012, **8**, 6557–6563.
51 Z. Džolić, M. Cametti, D. Milić and M. Žinić, *Chem. – Eur. J.*, 2013, **19**, 5411–5416.
52 S. Sarkar, S. Dutta, S. Chakrabarti, P. Bairi and T. Pal, *ACS Appl. Mater. Interfaces*, 2014, **6**, 6308–6316.
53 T. K. Adalder, U. K. Das, J. Majumder, R. Roy and P. Dastidar, *J. Indian Inst. Sci.*, 2014, **94**, 9–24.
54 F. Allen, *Acta Crystallogr., Sect. B: Struct. Sci.*, 2002, **58**, 380–388.
55 G. Chun-Hua, Z. Xiang-Dong, G. Wei, G. Fang and L. Qi-Tao, *Chin. J. Chem.*, 2005, **23**, 1001–1006.

Supporting Information

Selective gelation of N-(4-pyridyl)nicotinamide by copper(II) salts

Dipankar Ghosh,[a] Ieva Lebedytė,[a] Dmitry S. Yufit,[b] Krishna K. Damodaran[a]* and Jonathan W. Steed[b]*

1. ^{1}H-NMR ($CDCl_3$): 4-pyridyl nicotinamide (**4PNA**)

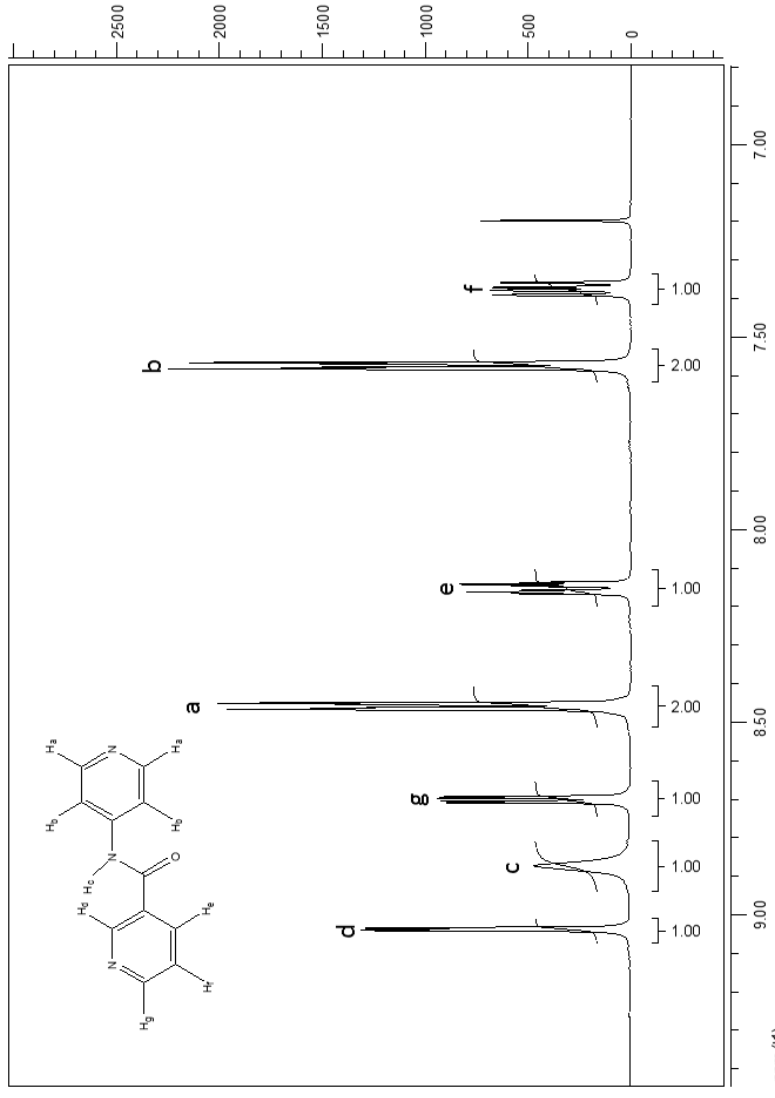

Figure S1: ^{1}H-NMR spectrum of 4-pyridyl nicotinamide (**4PNA**) in $CDCl_3$

2. ^{13}C-NMR (CD_3OD): *4-pyridyl nicotinamide (**4PNA**)*

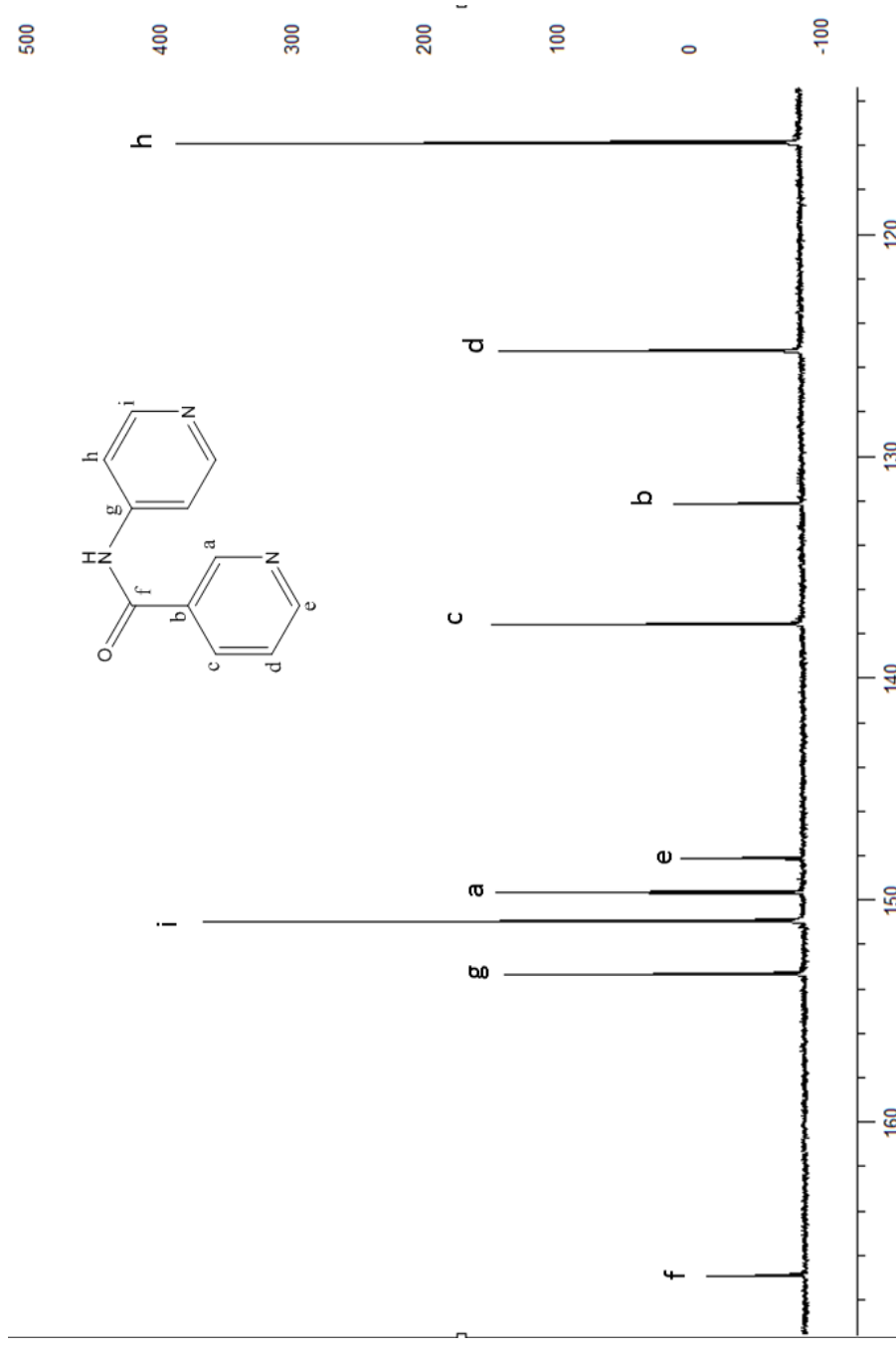

Figure S2: ^{13}C-NMR spectrum of **4PNA** in CD_3OD

3. Synthesis of metal complexes of 4PNA in a 1:2 metal:ligand ratio

Table S1: Preparation of complexes					
Entry	**Metal Salts**	**Metal Salts (mmol)**	**Ligand**	**Crystallising Medium**	**Outcome**
1	$Cu(OAc)_2.2H_2O$	0.1	0.2	Water-EtOH	Crystals
2	$Cd(OAc)_2.2H_2O$	0.1	0.2	Water-EtOH	Crystals
3	$Zn(NO_3)_2.6H_2O$	0.1	0.2	Water-EtOH	Crystals
4	$Cd(NO_3)_2.4H_2O$	0.1	0.2	Water-EtOH	Crystals
5	$Cu(NO_3)_2.3H_2O$	0.062	0.125	DMF	Crystals
6	$Zn(OAc)_2.2H_2O$	0.1	0.2	Water-EtOH	Powder

Synthesis of Copper(II) nitrate complex of **4PNA***:* A solution of **4PNA** (25 mg, 0.125 mmol) in 0.5 mL DMF was mixed with a solution of $Cu(NO_3)_2.3H_2O$ (15.2 mg, 0.062 mmol) in DMF (0.5 mL). Blue crystals of copper(II) nitrate complex of ***4PNA*** were obtained overnight (18 mg).

4. FT-IR (cm^{-1}) of metal complexes.

Entry 1*:* 3255m, 3171m, 3075m, 3002m, 1687vs, 1601vs, 1507vs, 1429vs, 1332s, 1298s, 1240w, 1209w, 1117s, 1065w, 1026s, 895m, 839s, 728s, 679m, 622m, 601m, 542s.

Entry 2*:* 3247w, 3170w, 3069w, 1686s, 1597vs, 1523vs, 1421vs, 1333s, 1301s, 1212s, 1117s, 1065w, 1045m, 1015s, 936w, 896m, 834s, 730s, 711s, 672m, 622m, 591m, 538s.

Entry 3*:* 3430b, 2516w, 2427w, 2356m, 1858w, 1678vs, 1620s, 1568s, 1492vs, 1426m, 1384vs, 1341m, 1315m, 1292s, 1108m, 1063s, 1023s, 920m, 900s, 873w, 842w, 828m, 811m, 756m, 700vs, 651s, 602m, 528m, 420m.

Entry 4*:* 3668w, 3391b, 3306b, 2446w, 2361s, 1929b, 1769w, 1681vs, 1596vs, 1523vs, 1418m, 1384vs, 1333vs, 1297vs, 1208s, 1115s, 1065m, 1047m, 1021vs, 930m, 897s, 822vs, 729m, 699vs, 596m, 530s, 418m.

Entry 5*:* 3432b, 3077w, 1693s, 1655m, 1600vs, 1518vs, 1429s, 1384vs, 1335vs, 1302vs, 1213s, 1118m, 1059w, 1029m, 898w, 837m, 738m, 699m, 601w, 540m.

Entry 6*:* 3262b, 3081m, 3013w, 1683vs, 1594vs, 1516vs, 1478m, 1397vs, 1331s, 1293s, 1243w, 1210s, 1114s, 1064m, 1024s, 928w, 897m, 838s, 738m, 707s, 678s, 619m, 595m, 540s, 429w.

5. Gelation Experiments:

5.1 Gelation test for Ligand (4PNA)

The gelation ability of the ligand **4PNA** was studied at various concentration in different solvents and also in solvent mixtures. The ligand **4PNA** was dissolved in 1 mL of corresponding solvent by heating followed by sonication until a clear solution is obtained. The solution was left undisturbed overnight and checked for gel formation.

Table S2: Gelation studies of 4PNA in different solvents with different concentrations

Ligand conc.	Water	Ethanol	Methanol	DMF	DMSO	DMF-water (1:1)	DMSO-water (1:1)
1 wt%	Solution	Solution	Solution	Solution	Solution	Solution	Solution
2 wt%	Partial gel	Solution	Solution	Solution	Solution	Solution	Solution
4 wt%	Gel	Solution	Solution	Solution	Solution	Solution	Solution
6 wt%	Gel	Solution	Solution	Solution	Solution	Solution	Precipitate
8 wt%	Gel	Solution	Solution	Solution	Solution	Precipitate	Precipitate

5.2 Gelation test for metal salt with 4PNA

Gelation experiment of **4PNA** was studied with Mn(II), Fe(II), Co(II), Ni(II), Cu(II), Zn(II) and Cd(II) salts. The required amount of metal salt was dissolved in 0.5 mL of water, and mixed with corresponding amount (1:2 ratio) of **4PNA** in 0.5 mL of DMF. It was sonicated for 1-4 minutes and kept without disturbing. Only copper(II) salt formed gel and was confirmed by tube inversion test.

5.3 Gelation test for copper(II) acetate with 4PNA at various concentrations

(a) 1:2 metal:ligand ratio: Gelation experiments were performed with $Cu(OAc)_2.2H_2O$ and **4PNA** in 1:2 metal:ligand ratio at different concentrations in 50 % DMF/water mixture (v/v) (Table S3). The minimum gelator concentration (MGC) was found to be 2 wt% in 50 % DMF/water mixture (v/v) and 1.5 wt% in pure water.

Table S3: Gelation test for copper(II) acetate complex (1:2 metal:ligand ratio)

Total conc. (metal salt+ligand) wt%	**Observation**
1.5%	Partial gel
2%	Gel
3%	Gel + Crystal
6%	Gel + Crystal
9%	Gel + Precipitate

(b) 1:1 metal:ligand ratio: Gelation experiments were performed with different concentration of $Cu(OAc)_2.2H_2O$ and **4PNA** in 1:1 metal:ligand ratio in 50 % DMF/water mixture (v/v) (Table S4). The minimum gelator concentration (MGC) was found to be 4 wt% in 50 % DMF/water mixture (v/v).

Table S4: Gelation test for copper(II) acetate complex (1:1 metal:ligand ratio)	
Total conc. (metal salt+ligand) wt%	Observation
2 %	Clear solution
4%	Gel
6%	Gel
8%	Gel + Precipitate

(c) Varying solvent composition: To evaluate the effect of DMF/water ratio in gelation, we fixed the gelator concentration as 4 wt% (1:2 metal-ligand ratio) and experiments were performed with varying solvent composition (Table S5).

Table S5: Gelation test for copper(II) acetate complex in various solvent composition	
DMF/H_2O	**Observations**
20% DMF	Solution + Crystals
30% DMF	Solution + Crystals
40% DMF	Gel
50% DMF	Gel
60% DMF	Gel
70% DMF	Clear solution
80% DMF	Clear solution

5.4 Gelation test for copper(II) chloride with 4PNA at various concentrations

(a) 1:2 metal:ligand ratio: A solution of $CuCl_2$ in 0.5 mL of water was mixed with of **4PNA** in 0.5 mL of DMF and was sonicated for one minute resulting in opaque greenish blue solution, which was allowed to stand overnight to yield green gel 2.6 - 10 wt% concentration (Table S6).

Table S6: Gelation test for copper(II) chloride complex (1:2 metal:ligand ratio)	
Total conc. (metal salt+ligand) wt%	**Observation**
1.5 wt%	Partial gel
2 wt%	Partial gel
2.6 wt%	Opaque greenish blue gel
3 wt%	Opaque greenish blue gel
6 wt%	Opaque greenish blue gel
8 wt%	Opaque greenish blue gel
10 wt%	Opaque greenish blue gel

(b) 1:1 metal:ligand ratio: Gelation experiments were performed with $CuCl_2$ and **4PNA** in 1:1 metal:ligand ratio at 3.3 wt% concentration in 1:1 and 3:1 DMF/water mixture (v/v) yielded greenish blue gels.

(c) Varying solvent composition: The total concentration (metal salt+ligand) was fixed at 3 wt% (1:2 metal-ligand ratio) and gelation was observed at various DMF/water mixture (Table S7).

Table S7: Gelation test for copper(II) chloride complex in various solvent composition

DMF/H_2O	**Observations**
Pure water	Gel
10 % DMF	Partial gel
20 % DMF	Partial gel
30 % DMF	Partial gel
40 % DMF	Gel
50 % DMF	Gel
60 % DMF	Gel
70 % DMF	Gel
80 % DMF	Gel
90 % DMF	Gel
Pure DMF	Partial gel

5.5 Gelation test for copper(II) nitrate with 4PNA at various concentrations

(a) 1:2 metal:ligand ratio: A solution of $Cu(NO_3)_2.3H_2O$ in 0.5 mL of water was mixed with of **4PNA** in 0.5 mL of DMF and it was kept without disturbing. Sonication was avoided due to immediate precipitation and an opaque deep blue gel was observed in 3-6 wt% concentration (Table S8). The gel was deformed upon shaking, indicating lower gel strength compared to copper acetate gel.

Table S8: Gelation test for copper(II) nitrate complex (1:2 metal:ligand ratio)

Total conc. (metal salt+ligand) wt%	Observation
2%	Partial gel
2.5%	Partial gel
3%	Opaque blue gel
4.5%	Opaque blue gel
6.4%	Opaque blue gel

(b) 1:1 metal:ligand ratio: Gelation experiments were performed with $Cu(NO_3)_2.3H_2O$ and **4PNA** in 1:1 metal:ligand ratio at different concentrations in 50 % DMF/water mixture (v/v) (Table S9).

Table S9: Gelation test for copper(II) nitrate complex (1:1 metal:ligand ratio)

Total conc. (metal salt+ligand) wt%	Observation
3%	Clear solution
5%	Clear solution
7%	Precipitate
9%	Precipitate

(c) Varying solvent composition: The total concentration (metal salt+ligand) was fixed at 6 wt% (1:2 metal-ligand ratio) and gelation was observed only at 1:1 DMF/water (Table S10).

Table S10: Gelation test for copper(II) nitrate complex in various solvent composition

DMF/H_2O	Observations
20% DMF	Precipitate
30% DMF	Precipitate
40% DMF	Precipitate
50% DMF	Gel
60% DMF	Clear solution
70% DMF	Clear solution
80% DMF	Clear solution

5.6 Gelation test for copper(II) perchlorate with 4PNA at various concentrations

(a) Varying solvent composition: Gelation was observed above 4 wt% (1:2 metal:ligand ratio) at higher DMF concentration (9:1 DMF/water, v/v) and pure DMF. This was achieved by mixing an aqueous solution of $Cu(ClO_4)_2.6H_2O$ (0.1 mL water or DMF) with corresponding amount (1:2 metal:ligand ratio) of 4PNA in DMF (0.9 mL). The resulting solution was sonicated for one minute and allowed to stand overnight to yield greenish-blue gel (Table S11).

Table S11: Gelation test for copper(II) perchlorate complex in various solvent composition

DMF/H_2O	Observations
Pure water	Complete precipitate
20% DMF	Complete precipitate
40% DMF	Little precipitate with a blue solution
60% DMF	Little precipitate with a blue solution
80% DMF	Blue solution
90% DMF	Gel
Pure DMF	Gel
Pure water	Complete precipitate

(b) 1:2 metal:ligand ratio: Gelation experiments were performed at various gelator concertation in 9:1 DMF/water and pure DMF . (Table S12).

Table S12: Gelation test for copper(II) perchlorate complex in various concentration

wt %	DMF	90% DMF
8 wt%	Gel	Gel
6 wt%	Gel	Gel
4 wt%	Gel	Gel
3 wt%	Partial gel	Partial gel

5.7 Gelation test for copper(II) sulphate with 4PNA at various concentrations

(a) Varying solvent composition: Copper(II) sulphate complexes of 4PNA displayed similar properties as copper(II) perchlorate salts. In this case, the required amount of $Cu(SO_4).5H_2O$ in water (0.2 mL) and mixing with the corresponding amount (1:2 metal:ligand ratio) of 4PNA in DMF (0.8 mL), the mixture was sonicated for one minute and allowed to stand overnight to yield greenish-blue gel (Table S13).

Table S13: Gelation test for copper(II) sulphate complex in various conditions				
wt%	**40% DMF**	**60% DMF**	**70% DMF**	**80% DMF**
4.5	Blue ppt	Blue ppt	Broken gel	Gel with slight ppt
6	Blue ppt	Partial gel	Broken gel	Gel with more ppt
7.5	Blue ppt	Partial gel	Partial gel	Gel with more ppt

5.8. SEM: Xerogel of copper(II) complexes of **4PNA** (1:2 metal:ligand ratio) were prepared for SEM analysis. The morphologies of the xerogels were similar to that of copper(II) acetate xerogels (Figure S3)

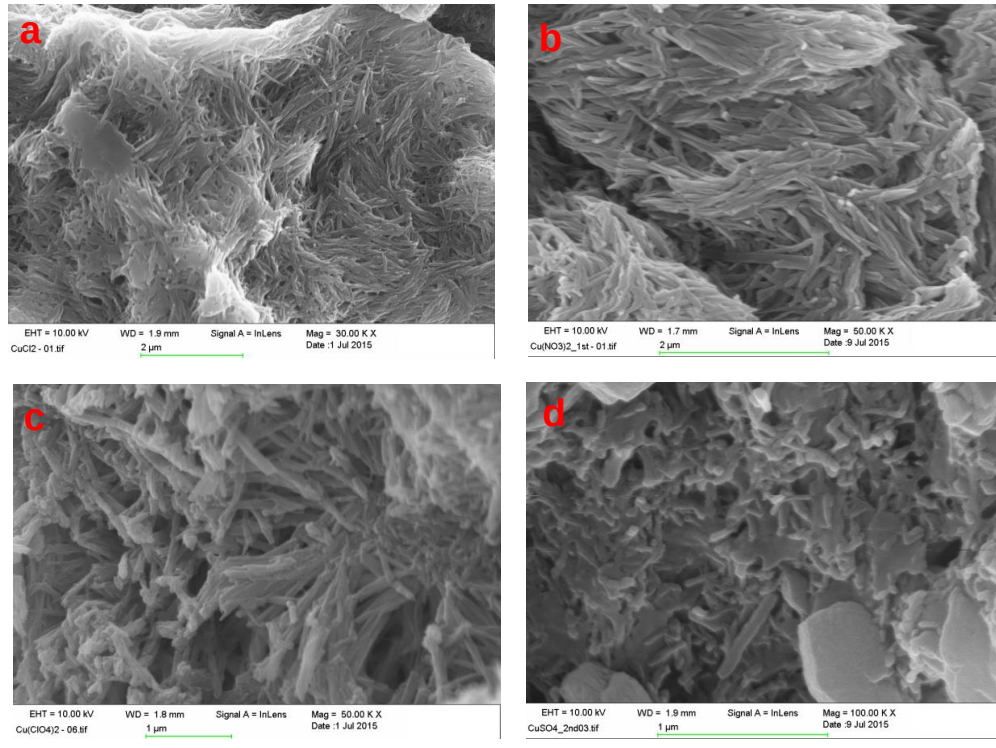

Figure S3: SEM images of (a) copper chloride gels of 4PNA at 3 wt% in 1:1 DMF/water (v/v); (b) copper nitrate gels of 4PNA at 4 wt% in 1:1 DMF/water (v/v); (c) copper perchlorate gels of 4PNA at 4 wt% in 9:1 DMF/water (v/v; (d) copper sulfate gels of 4PNA at 6 wt% in 8:2 DMF/water (v/v).

5.9 T_{gel} Experiment: $Cu(OAc)_2.2H_2O$ (6.7 mg, 0.033 mmol) in 0.5 mL water was mixed with a solution of (13.3 mg 0.066 mmol) **4PNA** in 0.5 mL DMF in a standard 7 mL vial and was sonicated for 4 minutes. A blue gel of copper(II) acetate complex of **4PNA** was obtained overnight. A small spherical glass ball (360 mg) was placed on the top of the gel and was heated in an oil bath. The temperature at which the ball touched the bottom of the vial was recorded (58 ^{0}C for 2 wt% and 61 ^{0}C for 4 wt%) as T_{gel}. The gel was reformed on keeping overnight at room temperature. Although, the gels were thermoreversible, heating at elevated temperature (<90 ^{0}C) resulted in a brown mass.

T_{gel} of copper nitrate gel (6.4 wt%) was prepared in similar fashion. Gel was synthesized by mixing a solution of $Cu(NO_3)_2.3H_2O$ (24.1 mg 0.1 mmol) in 0.5 mL of water with a solution of **4PNA** (40 mg 0.2 mmol) in 0.5 mL of DMF. T_{gel} was found to be 53 ^{0}C. However, the solution didn't form gel after cooling back to room temperature, indicating that the gels are thermoirreversible.

Copper chloride gel (3 wt%) was synthesized by mixing a solution of $CuCl_2$ (7.5 mg 0.05 mmol) in 0.5 mL of water with a solution of **4PNA** (22.5 mg, 0.11 mmol) in 0.5 mL of DMF. T_{gel} was found to be 64^{0}C. The gel was reformed on keeping overnight at room temperature.

Copper perchlorate gel (4 wt%) was synthesized by mixing a solution of $Cu(ClO_4)_2.6H_2O$ (19.2 mg 0.05 mmol) in 0.1 mL of water with a solution of **4PNA** (20.8 mg, 0.10 mmol) in 0.9 mL of DMF. T_{gel} was found to be 55^{0}C. However, the solution didn't form gel after cooling back to room temperature, indicating that the gels are thermoirreversible.

Copper sulphate gel (5 wt%) was synthesized by mixing a solution of $CuSO_4.5H_2O$ (19.3 mg 0.077 mmol) in 0.2 mL of water with a solution of **4PNA** (30.7 mg, 0.154 mmol) in 0.8 mL of DMF. T_{gel} was found to be 65^{0}C. The gel was reformed on keeping overnight at room temperature.

6. Characterisation

6.1 Cambridge Structural database search: A search motif was introduced with two chlorides and two pyridyl moieties (with hydrogen atoms at 2 and 6 position only) resulted in 98 hits. Adding one water molecule to the above search resulted in only 9 hits.

6.1 Crystal data

	Table S14: Crystal data for Complex 1, 2, 3 & 4			
Crystal data	**1**	**2**	**3**	**4**
Empirical formula	$C_{26}H_{24}CuN_6O_6$	$C_{26}H_{26}CdN_6O_7.2H_2O$	$C_{22}H_{22}N_8O_{10}Zn$	$C_{22}H_{22}CdN_8O_{10}$
Colour	Clear dark violet	Colourless	Colourless	Colourless
Formula weight	580.05	682.96	623.85	670.88
Crystal size (mm)	0.40 x 0.22 x 0.09	0.15 x 0.08 x 0.05	0.14 x 0.12 x 0.015	0.25 x 0.16 x 0.04
Crystal system	triclinic	Monoclinic	triclinic	triclinic
Space group	Pī	$P2_1/c$	Pī	Pī
a (Å)	8.0578(6)	16.3055(3)	7.4378(4)	7.3668(5)
b (Å)	8.3568(6)	22.8004(4)	8.9941(4)	9.1365(6)
c (Å)	10.1944(6)	15.2496(3)	9.8914(5)	9.9565(6)
α (^{0})	79.288(5)		75.2719(17)	76.1428(18)
β (^{0})	69.725(6)	97.353(2)	72.7974(17)	73.5323(18)
γ (^{0})	82.953(6)		82.7345(17)	83.610(2)
Volume (Å^3)	631.44(7)	5622.75(18)	610.39(5)	623.27(7)
Z	1	8	1	1
$D_{calc.}$(g/cm^3)	1.525	1.614	1.697	1.787
F(000)	299	2784	320	338
μ MoKα (mm^{-1})	0.920	0.841	1.083	0.951
Temperature (K)	120.0(2)	120.0(2)	120.0(2)	120.0(2)
Reflections collected/ unique/observed [I>2σ(I)]	7769/3689/3339	112852/14250/10961	13125/3403/2891	19999/3310/3264
Data/restraints/parameters	3689/0/226	14250/1/789	3403/0/199	3310/1/157
Goodness of fit on F^2	1.080	1.023	1.040	1.008
Final R indices [I>2σ(I)]	R_1 = 0.0348 wR_2 = 0.0768	R_1 = 0.0329 wR_2 = 0.0608	R_1 = 0.0343 wR_2 = 0.0736	R_1 = 0.0592 wR_2 = 0.1492
R indices (all data)	R_1 = 0.0403 wR_2 = 0.0810	R_1 = 0.0570 wR_2 = 0.0675	R_1 = 0.0463 wR_2 = 0.0777	R_1 = 0.0595 wR_2 = 0.1497

6.3 Illustration of the Crystalline structure of $[Cd(4PNA)_2(NO_3)_2(H_2O)_2]$

The nitrogen atom of the amide moiety is hydrogen bonded to the oxygen atom of the nitrate anion (N–H…O) to form a 1-D hydrogen bonded network similar to **3**. These 1-D chains are further hydrogen bonded to adjacent 1-D chains via hydrogen bonding oxygen atom of amide moiety and nitrate anions with the metal coordinated water molecule. These hydrogen bonding interactions result in a 2-D hydrogen bonded network (Figure S4).

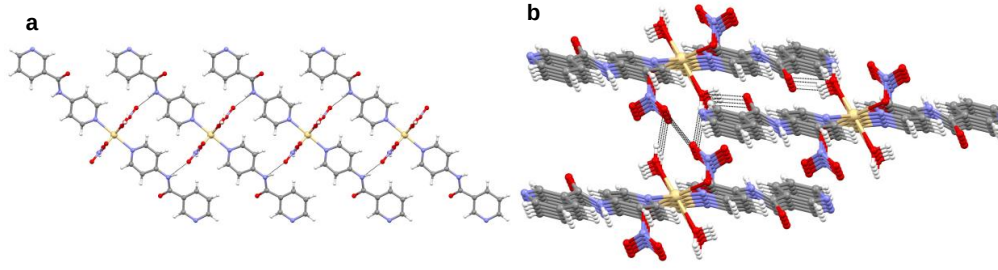

Figure S4: (a) I-D hydrogen bonded network in **4** and (b) the formation of a 2-D hydrogen bonded network from 1-D hydrogen bonded chains.

Hydrogen Bonding Parameters

Table S15: Hydrogen bonding parameters for Complex 1, 2, 3 & 4					
D–H•••A	**D–H (Å)**	**H•••A (Å)**	**D•••A (Å)**	**D–H•••A (^{0})**	**Symmetry operation for A**
Complex 1					
N(2)–H(2)•••O(3)	0.85(2)	1.99(2)	2.8188(19)	164.0(17)	1+x, y, z
C(2)–H(2A)•••O(3)	0.95(2)	2.52(3)	3.174(2)	126.2(15)	1+x, y, z
C(5)–H(5)•••O(1)	0.95(2)	2.37(2)	3.300(2)	166.5(17)	-x, -y, 2-z
C(8)–H(8)•••O(3)	0.95(2)	2.36(2)	3.270(2)	161(2)	1+x, y, z
Complex 2					
O(1W)–H(1WA)•••O(15)	0.85	1.85	2.682(2)	163	x, y, z
N(2)–H(2)•••O(13)	0.89(3)	1.99(3)	2.856(2)	166(3)	x, 1/2-y, -1/2+z
O(1W)–H(1WB)•••O(3W)	0.94	1.80	2.710(2)	163	x, y, z
N(2A)–H(2A)•••O(12)	0.84(3)	2.12(3)	2.950(2)	172(2)	x, 1/2-y, 1/2+z
N(2B)–H(2B)•••N(3B)	0.78(3)	2.41(3)	3.149(3)	158(3)	1-x, 1-y, -z
N(2C)–H(2C)•••O(18)	0.87(3)	2.10(3)	2.947(3)	165(2)	x, 3/2-y, 1/2+z
O(2W)–H(2WA)•••O(1B)	0.79	1.98	2.720(2)	155	x, 3/2-y, 1/2+z
O(2W)–H(2WB)•••O(6W)	0.85	1.86	2.706(2)	175	1-x, 1-y, 1-z
O(3W)–H(3WA)•••O(4W)	0.88	1.98	2.792(3)	154	-x, 1-y, 1-z
O(3W)–H(3WB)•••O(17)	0.88	1.86	2.710(2)	162	x, y, z
O(4W)–H(4WA)•••O(3W)	0.89	1.92	2.794(2)	167	x, y, z
O(4W)–H(4WB)•••O(11)	0.96	1.83	2.748(2)	157	x, y, z
O(5W)–H(5WA)•••O(14)	0.88	2.11	2.946(2)	158	x, y, z
O(5W)–H(5WB)•••O(16)	0.95	1.76	2.691(2)	167	1-x, 1-y, 1-z
O(6W)–H(6WA)•••N(3)	0.82	2.08	2.895(3)	173	x, 1/2-y, 1/2+z
O(6W)–H(6WB)•••O(5W)	0.83	1.98	2.776(3)	161	x, y, z
C(3A–H(3A)•••O(12)	0.95	2.37	3.203(3)	146	x, 1/2-y, 1/2+z
C(3C)–H(3C)•••O(18)	0.95	2.52	3.450(3)	166	x, 3/2-y, 1/2+z
C(4A)–H(4A)•••O(11)	0.95	2.53	3.444(3)	162	x, y, 1+z
C(4C)–H(4C)•••O(17)	0.95	2.59	3.465(3)	153	x, y, 1+z
C(5B)–H(5B)•••O(6W)	0.95	2.48	3.426(3)	173	1-x, 1-y, -z
C(6)–H(6)•••O(1C)	0.95	2.28	3.232(3)	175	x, y, -1+z
C(6A)–H(6A)•••O(1A)	0.95	2.39	3.123(3)	133	-x, 1-y, 2-z
C(10A) –H(10A)•••N(3A)	0.95	2.62	3.211(3)	121	x, 1/2-y, -1/2+z
C(11A)–H(11A)•••O(12)	0.95	2.57	3.349(3)	139	x, 1/2-y, 1/2+z
C(11C)–H(11C)•••O(18)	0.95	2.50	3.271(3)	138	x, 3/2-y, 1/2+z
C(4S)–H(4SA)•••O(2W)	0.98	2.56	3.468(3)	155	1-x, 1-y, 1-z
C(6S)–H(6SC)•••O(14)	0.98	2.41	3.385(3)	176	x, y, z
Complex 3					
N(2)–H(2)•••O(3)	0.83(3)	2.12(2)	2.920(2)	161(2)	x, 1+y, z
O(5)–H(5A)•••O(4)	0.81(3)	2.08(3)	2.852(2)	160(3)	1+x, y, z
O(5)–H(5B)•••O(1)	0.82(3)	1.90(3)	2.7114(19)	176(3)	1-x, -y, 1-z
C(3)–H(3)•••O(3)	0.95	2.51	3.282(2)	138	x, 1+y, z
C(5)–H(5)•••O(4)	0.95	2.43	3.364(3)	166	-x, 1-y, 1-z
Complex 4					
N(2)–H(2)•••O(4)	0.88	2.10	2.959(4)	164	x, 1+y, z
O(5)–H(5A)•••O(1)	0.88	1.92	2.726(4)	152	x, y, -1+z
O(5)–H(5B)•••O(3)	0.80	2.08	2.861(4)	169	-x, 1-y, 1-z
C(9A)–H(9A)•••O(3)	0.95	2.54	3.287(6)	136	x, 1+y, 1+z
C(9A)–H(9A)•••O(3)	0.95	2.45	3.341(6)	156	-x, 2-y, 2-z
C(10B)–H(10B)•••O(3)	0.95	2.37	3.296(7)	165	-x, 2-y, 2-z
C(11A)–H(11A)•••O(4)	0.95	2.55	3.367(7)	145	x, 1+y, z
C(11B)–H(11B)•••O(2)	0.95	2.46	3.410(5)	175	x, 1+y, z
C(11B)–H(11B)•••O(4)	0.95	2.58	3.307(7)	133	x, 1+y, z

6.4. Powder X-Ray: XRPD experiments were carried out in order to establish their crystalline phase purity. The simulated pattern obtained from the crystal structures were matched with the bulk solid (as synthesised).

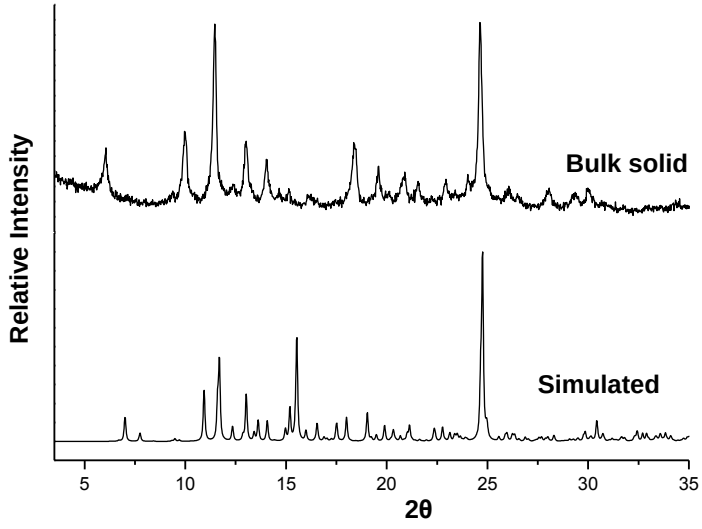

Figure S5: Comparison of PXRD pattern of complex **2** (as synthesised) with the crystal structure. The XRPD pattern do not correlate with the all the peaks of simulated pattern presumably due to the loss of the uncoordinated water molecule in **2.**

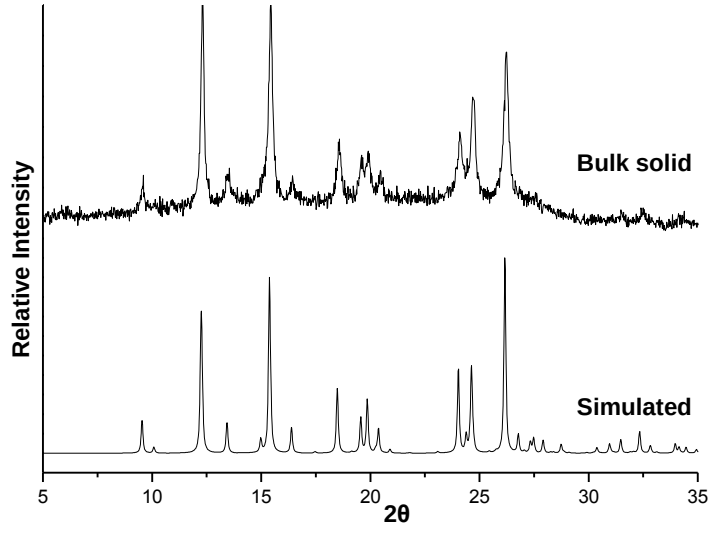

Figure S6: Comparison of PXRD pattern of complex **3** (as synthesised) with the crystal structure.

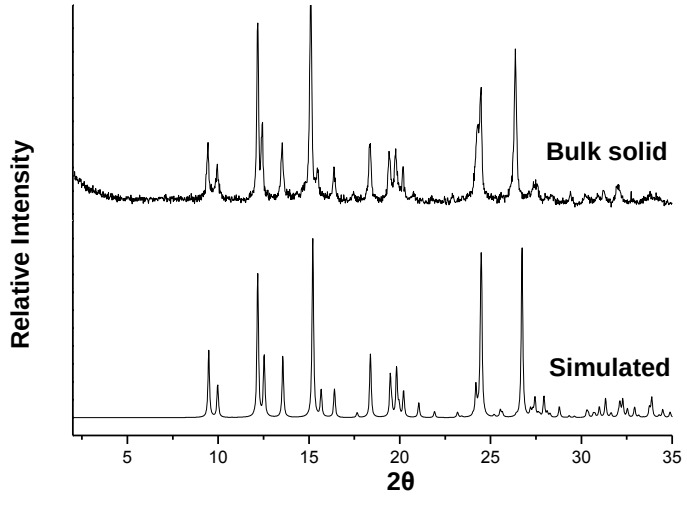

Figure S7: Comparison of PXRD pattern of complex **4** (as synthesised) with the crystal structure.

6.5. of FT-IR (cm^{-1}) of metal complexes: Comparison of complex and xerogels

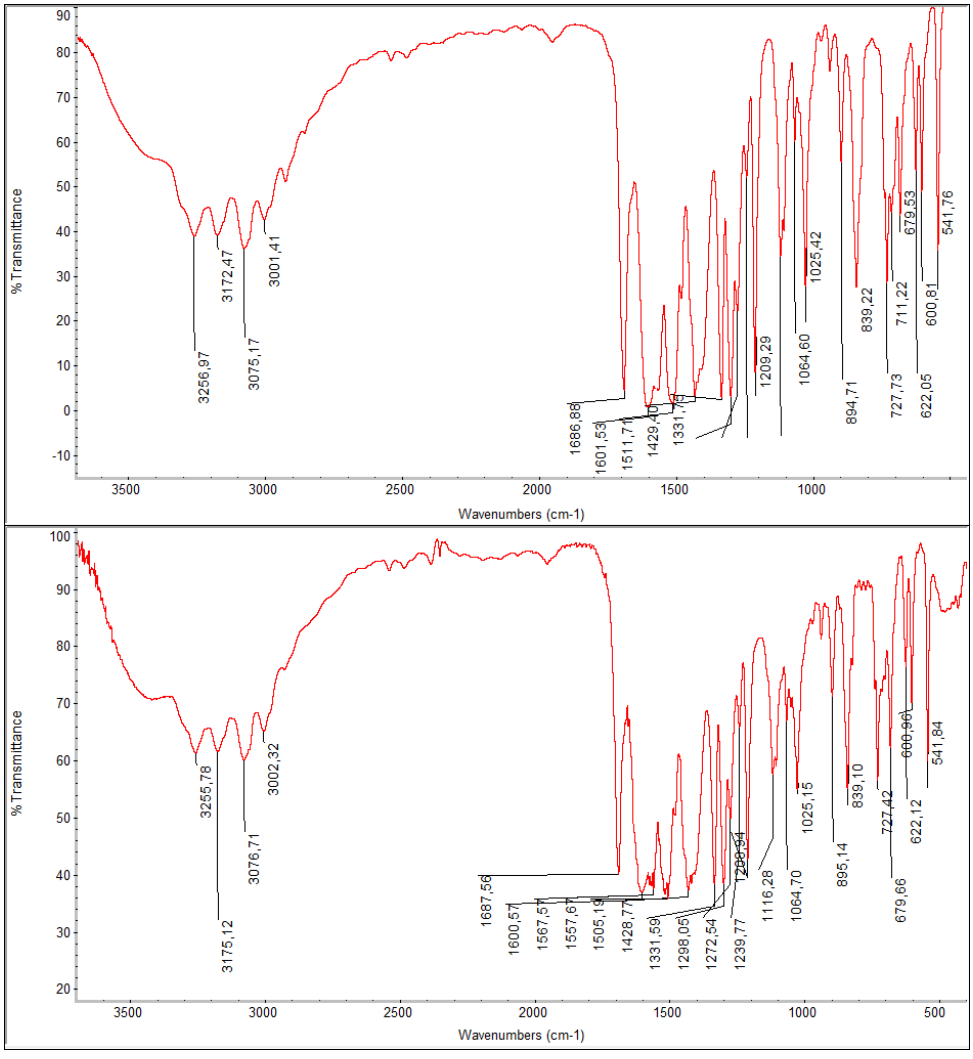

Figure S8: IR spectra comparison of the complexes (top) and xerogels (bottom) of copper(II) acetate and **4PNA.**

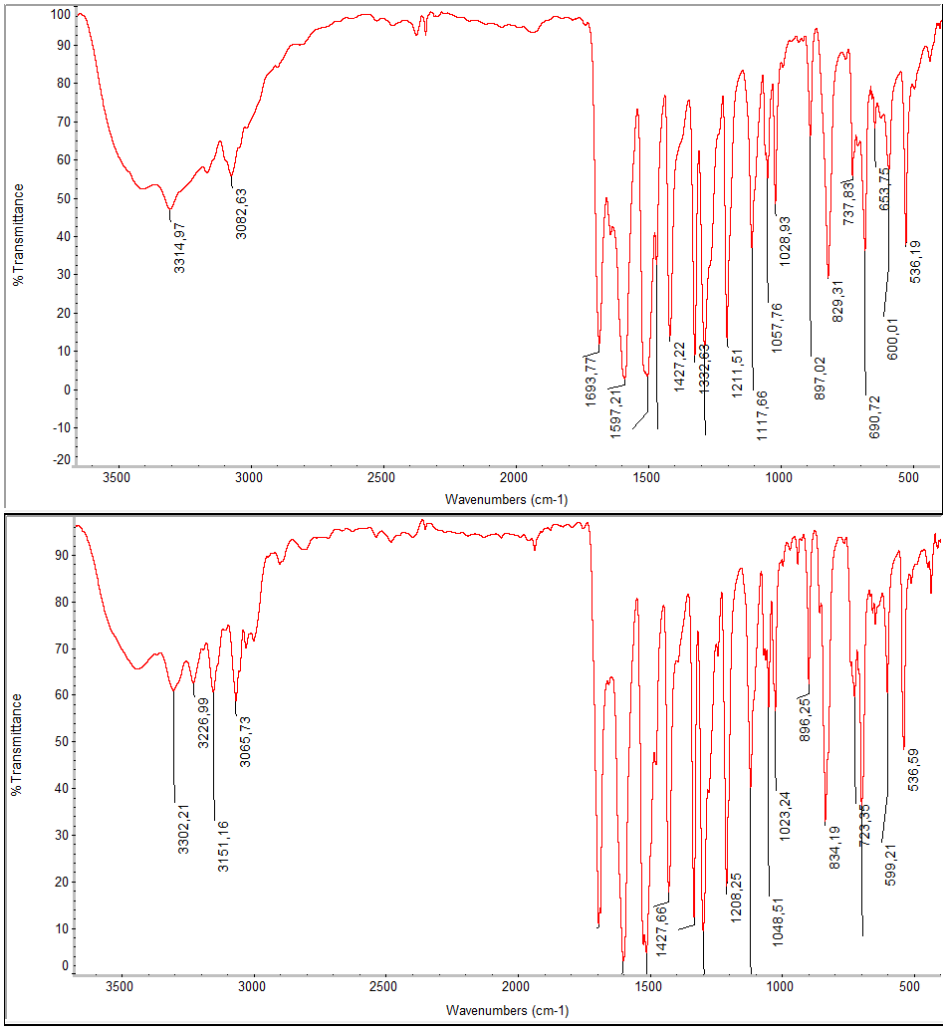

Figure S9: IR spectra comparison of the complexes (top) and xerogels (bottom) of copper(II) chloride and **4PNA.**

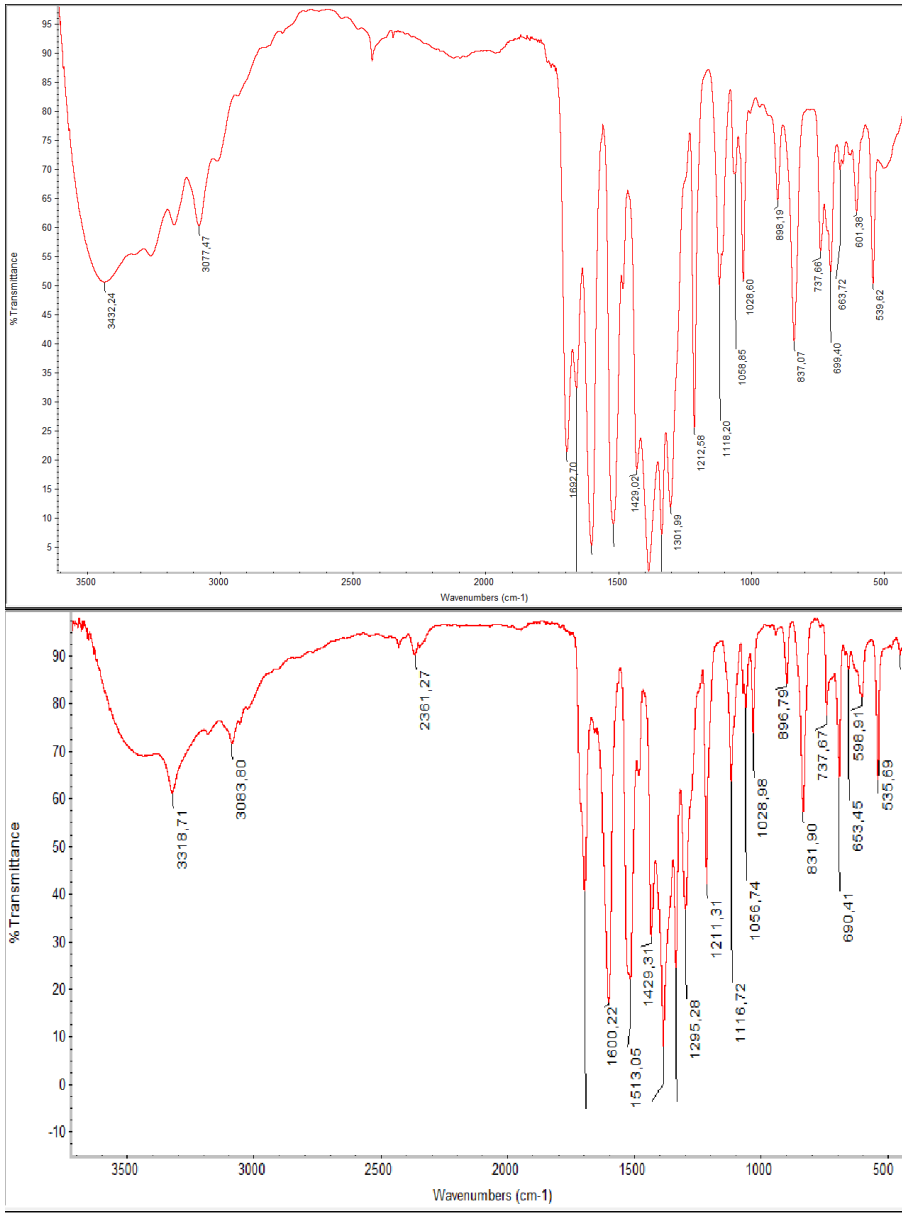

Figure S10: IR spectra comparison of the complexes (top) and xerogels (bottom) of copper(II) nitrate and **4PNA.**

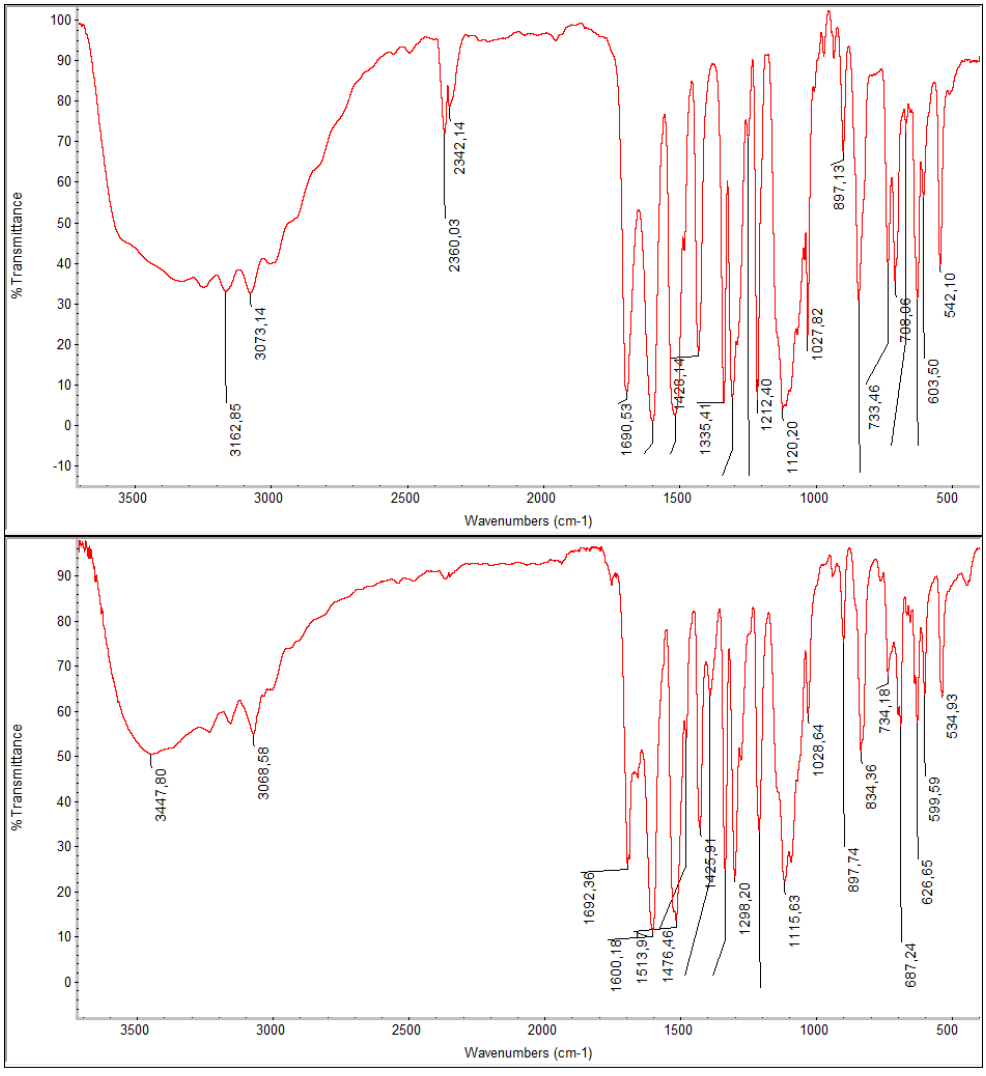

Figure S11: IR spectra comparison of the complexes (top) and xerogels (bottom) of copper(II) perchlorate and **4PNA.**

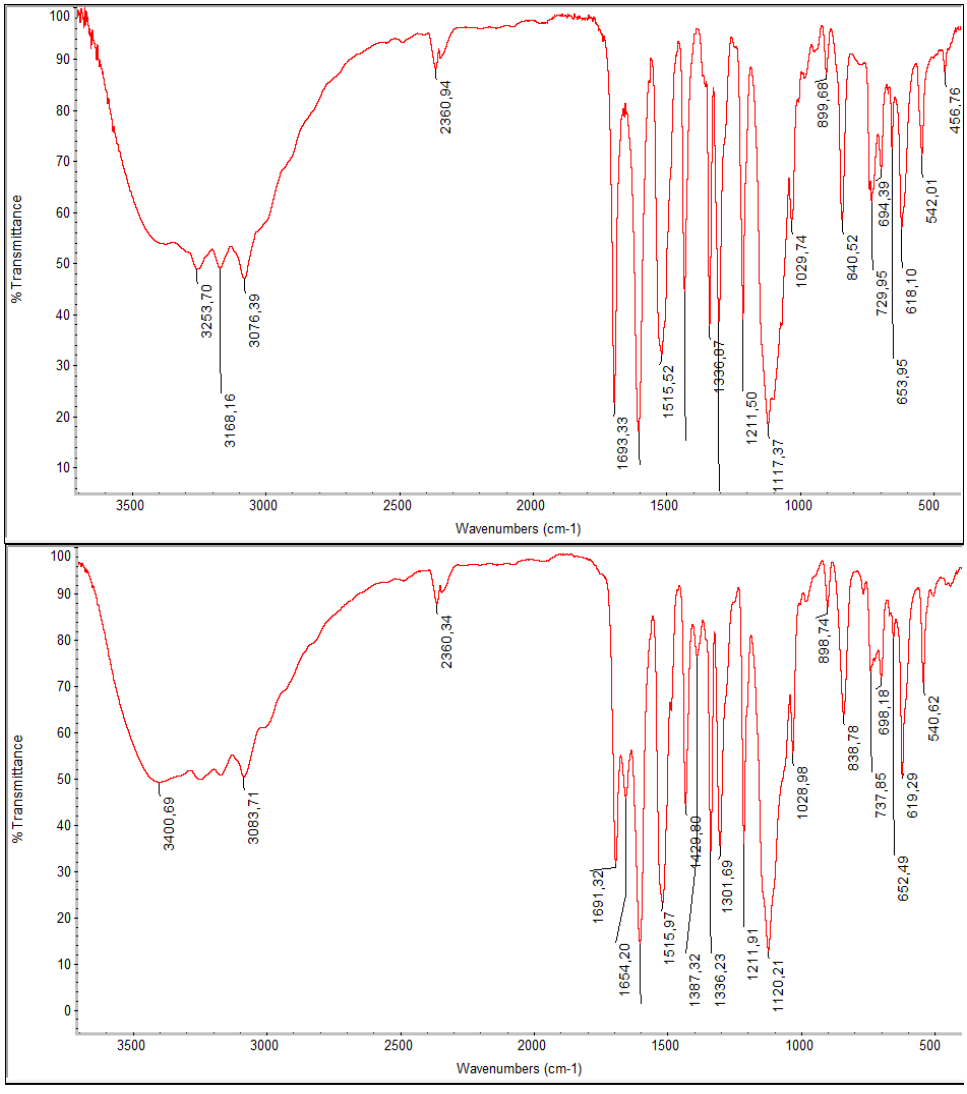

Figure S12: IR spectra comparison of the complexes (top) and xerogels (bottom) of copper(II) sulphate and **4PNA.**

Article-IV

This project is published in a peer reviewed journal and included as it was published. Slight differences might appear from the original article due to the formatting issue.

Publication details:

″Metal complexation induced supramolecular gels for the detection of cyanide in water″

Dipankar Ghosh, Deepa and Krishna K. Damodaran*

Supramol. Chem., **2020**, 1-11

Author contributions:

D.G. and K.K.D planned and designed the research; **D.G.** synthesized the gelators, performed characterizations, solved single crystal structures and evaluated gelation properties and anion sensing. Deepa repeated the gelation experiments. K.K.D. wrote the initial manuscript draft and **D.G.** and K.K.D reviewed the main manuscript.

SUPRAMOLECULAR CHEMISTRY
https://doi.org/10.1080/10610278.2020.1751845

Taylor & Francis
Taylor & Francis Group

ARTICLE

Metal complexation induced supramolecular gels for the detection of cyanide in water

Dipankar Ghosh, Deepa and Krishna K. Damodaran

Department of Chemistry, Science Institute, University of Iceland, Reykjavik, Iceland

ABSTRACT

The role of metal salts in inducing supramolecular gel network formation was analysed by reacting two pyridyl-*N*-oxide amides with various diamagnetic zinc(II) and cadmium(II) salts. Metal induced supramolecular gelation was observed for zinc(II) and cadmium(II) chloride complexes in water and the morphologies of the xerogels were analysed by scanning electron microscopy (SEM). The relative gel strength was corroborated with various non-bonding interactions observed in the solid-state structures of zinc(II) complexes using X-ray diffraction. The non-bonding interactions of the pyridyl-*N*-oxide amides and the metal complexes were compared to find the key interactions responsible for metallogel formation. The anion induced stimuli-responsive property of the metallogels was studied in the presence of halides and cyanide anions. The cadmium(II) gels were stable in presence of two equivalents of halides but the network collapsed in presence of cyanide anion in water and this property can be used to detect cyanide anions in water.

ARTICLE HISTORY
Received 31 December 2019
Accepted 26 March 2020

KEYWORDS
Supramolecular gels; metallogels; hydrogen bonding; pyridyl-*N*-oxide amide; anion sensing

1. Introduction

Supramolecular gels based on low molecular weight gelators (LMWGs) [1–3] have witnessed a tremendous growth over last decade due to the emerging potential applications [3–11] as functional soft materials for separation, drug delivery and as media to control crystal growth. The gelator self-assemble in presence of the solvent into a 3-dimensional network within which the solvent molecules are entrapped and these networks are stabilised by various non-covalent interactions [3–16] such as hydrogen bonding, van der Waals interactions, $\pi - \pi$ stacking, etc. The structure and properties of the LMWGs rely mostly on the geometry and spatial arrangement of the building blocks and also the nature of intermolecular non-covalent interactions [17,18]. We have shown that the gelation properties can be altered by modifying the pyridyl groups of trimesic amide-based gelator N^1,N^3,N^5-tri(pyridin-3-yl) benzene-1,3,5-tricarboxamide [19] to *N*-oxide groups resulting in *the tris*-*N*-oxide compound [20]. Recently, we showed the importance of non-bonding interactions and functional groups in designing LMWGs by modifying a pyridyl amide-based gelator, namely, *N*-(4-pyridyl)isonicotinamide [21] to two mono-*N*-oxides [4-(pyridin-4-ylcarbamoyl)pyridine-1-oxide (**INO**) and 4-(isonicotinamido) pyridine-1-oxide (**PNO**)] and a di-*N*-oxide compound (4-((1-oxidopyridin-4-yl)carbamoyl)pyridine-1-oxide) [22]. The modification of the pyridyl group resulted in the disruption of strong and unidirectional N—H···N interactions of the parent gelator and a weak intermolecular C—H···O interaction was observed in the di-*N*-oxide compound. The gelation studies revealed the importance of *N*-oxide moieties on both ends for gelation of the di-*N*-oxide compound in water, but the two mono-*N*-oxides formed crystals. These studies will help researchers to understand the nature of supramolecular interactions, which will enable them to control/tune the gelation abilities of LWMGs. However, the mechanism and understanding of the self-assembly process in LMWGs is challenging due to the dynamic nature of noncovalent interactions and efforts have been made to analyse the self-assembly process at the molecular level in LMWGs [4,23–31] using various spectroscopic techniques.

Stimuli-responsive supramolecular systems [32–35] offer better control of the self-assembly/reassembly process, which can be either switched on/off by an external stimulus such as light, redox, pH and metal complexes, salts/ions, etc. Stimuli-responsive materials based on pyridyl amides are an excellent class of compounds due to the presence of metal-binding pyridyl groups and hydrogen bonding amide groups [5,36]. The inclusion of metal ions in these materials can induce/disrupt the stimuli-responsive properties, for example, the gelation properties. This will lead to the formation of metal-based supramolecular gels (metallogels) [5,37], which offer potential applications [37] in catalysis, sensing, optics and magnetic materials. The key driving force in the formation of the gel fibre network in

CONTACT Krishna K. Damodaran krishna@hi.is Department of Chemistry, Science Institute, University of Iceland, Dunhagi 3, 107 Reykjavík, Iceland

metallogels is the strong coordination interactions between the organic moiety and metal centre resulting in a 3-dimensional network, which is further stabilised by various non-covalent interactions [5,38,39]. Metallogels are obtained by the self-assembly of discrete complexes [40–45], coordination polymers [46–51], or cross-linked coordination polymers [52] into a 3-D network. Interestingly, the incorporation of non-coordinated metal ions or metallic nanoparticles can also induce gelation [53–56]. We have reported the gelation ability of metallogels based on metal complexes of N-(4-pyridyl)nicotinamide (4PNA) and showed that copper(II) complexes of 4PNA formed gels selectively [36]. Steed *et al.* reported that metal ions could induce the gelation in bis-pyridyl urea ligands [57] whereas Zhang and co-workers showed that the organogel network in tripeptide-based gelators collapsed in presence of metal cations [58]. It is interesting to note that despite metal coordination is the major structure determining factor in these systems, various non-bonding interactions also play a key role in gel network formation. Thus, it is important to study the role of metal ions and the other factors responsible for the self-assembly process in supramolecular gels, which will enable us to design/predict the formation of metallogels. We have used single-crystal diffraction to analyse the factors influencing gel formation by comparing the mode of interactions in the structures of the ligands and metal complexes. Single-crystal X-ray diffraction has been used to get some insight into the packing modes of these molecules in gel fibres by analysing the key interactions in the solid-state structure of LMWGs [21,57,59–66]. We have selected two non-gelators mono-*N*-oxide pyridyl amides **INO** and **PNO** [22] and the effect of metal coordination in these *N*-oxide amides were analysed by reacting these compounds with diamagnetic zinc(II) and cadmium(II) metal salts such as acetate, chloride and nitrate.

2. Experimental section

All starting materials and solvents were purchased from commercial sources and were used as supplied. Deionised water was used for gelation and crystallisation experiments. **PNO** and **INO** were synthesised following the reported procedure [22]. ^{1}H NMR and IR spectra were recorded on a Bruker Avance 400 spectrometer and a Nicolet iZ10, respectively. The morphology of the xerogel was analysed by scanning electron microscopy (SEM) using a Leo Supra 25 Microscope at 30 µm aperture, 3.0 kV ETH and In-Lens focusing. Single-crystal X-ray diffraction was performed on a Bruker D8 VENTURE and X-ray powder diffraction (XRPD) was carried out using a Bruker D8 Focus instrument.

2.1. Gelation studies

The corresponding metal salt (0.05 mmol) was dissolved in 0.5 mL of water and added to an aqueous or DMF solution (0.5 mL) of the *N*-oxide ligands (21.5 mg, 0.1 mmol) in a 7.0 mL vial. The mixture was heated, and a clear solution was obtained (colloidal solution in some cases) and left at room temperature for gel formation. After 24 h, gelation was tested by the vial inversion test. The gelation experiments were also performed at higher concentration with 0.075 mmol of metal salt in 0.5 mL water and 0.15 mmol of ligand (**INO** or **PNO**) in 0.5 mL of water or DMF. Experiments were not performed beyond this concentration due to the limiting solubility of the ligands.

2.2. Minimum Gel Concentration (MGC)

The MGC experiment was performed by taking various amounts of appropriate metal salts and ligands at 1:2 metal–ligand ratio. The metal salt (one equivalent) was dissolved in 0.5 mL of water and added to a 0.5 mL aqueous or DMF solution of the ligand (two equivalents). The mixture was heated to obtain a clear solution and left undisturbed to form the gel. The minimum concentration at which gel was obtained was recorded as MGC.

2.3. T_{gel} experiments

An aqueous solution (0.5 mL) of the metal salt (1 equivalent) was added to 0.5 mL of the ligand solution (2 equivalents) in water or DMF. The gel was obtained by heating the mixture in a 7.0 mL sealed vial until a clear solution was observed and the mixture was left undisturbed at room temperature. After 24 h, a small spherical glass ball (53.0 mg) was placed over the gel. The vial was gradually heated in an oil bath equipped with a magnetic stirrer and a thermometer. The temperature at which the glass ball touched the bottom of the vial was recorded as T_{gel}.

2.4. Synthesis of the complexes

The metal chloride complexes were synthesised and characterised via standard analytical methods.

Zn-PNO: An aqueous solution of $ZnCl_2$ (6.8 mg, 0.05 mmol in 1.0 mL water) was added to a DMF solution of **PNO** (21.5 mg, 0.1 mmol in 1.0 mL DMF). The mixture was left at room temperature. Needle shaped crystals were obtained in overnight. ATR-FTIR (cm^{-1}): 3044, 2873, 1686, 1596, 1556, 1533, 1516, 1489, 1473, 1439, 1418, 1313, 1296, 1266, 1246, 1210, 1175, 1147, 1102, 1065,

1029, 964, 897, 866, 854, 842, 796, 753, 713, 700, 689, 666, 545, 530, 492, 465, 443.

Zn-INO: A solution of $ZnCl_2$ (6.8 mg, 0.05 mmol) and **INO** (21.5 mg, 0.1 mmol) in 1.0 mL water was heated at 80°C in a sealed vial. Plate-shaped crystals were grown in the solution in 2–3 h. ATR-FTIR (cm^{-1}): 3323, 3111, 3083, 3014, 1683, 1595, 1518, 1498, 1477, 1425, 1326, 1298, 1231, 1202, 1175, 1100, 1058, 1024, 943, 890, 849, 836, 759, 657, 587, 537, 485, 429.

Cd-PNO: An aqueous solution of $CdCl_2$ (9.1 mg, 0.05 mmol in 0.5 mL water) was added to a solution of **PNO** (21.5 mg, 0.1 mmol in 0.5 mL water). After overnight, the white precipitate formed was filtered and dried. ATR-FTIR (cm^{-1}): 3042, 2881, 1689, 1596, 1559, 1532, 1517, 1487, 1473, 1437, 1422, 1316, 1296, 1272, 1214, 1173, 1121, 1109, 1074, 1034, 1017, 895, 868, 843, 800, 748, 711, 691, 553, 530, 492, 464, 430.

Cd-INO: Cd-INO was synthesised following a similar procedure of **Cd-PNO**. An aqueous solution (0.5 mL) of $CdCl_2$ (9.1 mg, 0.05 mmol) was added to 0.5 mL aqueous solution of **INO** (21.5 mg, 0.5 mmol). The precipitate obtained after 24 h was filtered and dried. ATR-FTIR (cm^{-1}): 3248, 3176, 3112, 3078, 3039, 1697, 1614, 1595, 1532, 1507, 1474, 1437, 1422, 1335, 1293, 1239, 1213, 1177, 1101, 1070, 1030, 1014, 957, 902, 862, 852, 837, 825, 814, 759, 728, 688, 665, 652, 641, 579, 525, 506, 484, 429.

2.5. Crystallography

X-ray quality single crystals were isolated from the mother liquor, immediately immersed in cryogenic oil, and mounted. The diffractions were collected using CuK_α radiation (λ = 1.54178 Å) on a Bruker D8 VENTURE (Photon100 CMOS detector) diffractometer equipped with a Cryostream open-flow nitrogen cryostat at room temperature. The unit cell determination, data collection, data reduction, structure solution/refinement, and empirical absorption correction (SADABS) were carried out using Apex III. The structure was solved by a direct method and refined by the full-matrix least-squares on F^2 for all data using SHELXTL [67] and Olex2 [68] software. All non-disordered non-hydrogen atoms were refined anisotropically, and the hydrogen atoms were placed in the calculated positions and refined using a riding model. Crystallographic data for the structures have been deposited with the Cambridge Crystallographic Data Centre as supplementary publication (CCDC 1974718 and 1974719).

2.6. Anion sensing

A solution of $ZnCl_2$ (9.5 mg, 0.07 mmol) or $CdCl_2$ (12.8 mg, 0.07 mmol) in 0.25 mL water was added to an aqueous solution (0.75 mL) of **PNO** or **INO** (30.1 mg, 0.14 mmol) in a sealed vial. After the gel was formed, 0.14 mmol of the suitable anion in solid form (sodium or potassium salt) was added on the top of the gel. The addition of anion (0.14 mmol) was repeated if the gel was found to be stable upon inversion test and the process was repeated up to the addition of 0.7 mmol of the salt. The experiments were also performed by adding the anion *in situ* during gel formation. A solution of $ZnCl_2$ (9.5 mg, 0.07 mmol) or $CdCl_2$ (12.8 mg, 0.07 mmol) in 0.25 mL water was added to an aqueous solution (0.75 mL) of **PNO** or **INO** (30.1 mg, 0.14 mmol) and 0.14 mmol of the particular anion. The mixture was heated in a sealed vial and cooled to room temperature. Gel formation was checked by the inversion test and if a gel was obtained, the experiment was repeated by adding another equivalent of the anion.

3. Results and discussion

The mono-*N*-oxide amide **PNO** was synthesised as per the reported procedure [22] by reacting isonicotinic acid chloride with 4-aminopyridine-1-oxide and the reaction of isonicotinic acid-*N*-oxide chloride with 4-aminopyridine yielded **INO**. We have chosen diamagnetic zinc(II) and cadmium(II) salts such as chloride, nitrate and acetate to analyse the effect of metal coordination in these compounds, for example, can metal ions induce gelation in these complexes? The structural details of **INO** and **PNO** [22] are reported, which will enable us to compare the mode of interactions of the ligands and the metal complexes. The gelation abilities were evaluated *in situ* by mixing the metal complex and ligand in water or an aqueous solution of highly polar solvents.

3.1. Gelation experiments

The gelation experiments were performed by mixing the solution of metal salts (0.05 mmol) and ligand (0.1 mmol) in water (1:2 metal:ligand ratio). The mixture was heated to get a clear solution (colloidal solutions were obtained in some cases, see Table S1 and Table S2) and left undisturbed for gel formation, which resulted in precipitate or crystals but no gelation. Gelation was not observed for experiments performed at a lower concentration. This prompted us to check the gelation of these mixtures at higher concentration and gelation experiments performed at a concentration higher than 3.0 wt % (see Table 1) resulted in gel formation (Figure 1) for zinc(II) chloride-**PNO** (**Zn-PNO**, 0.06 mmol $ZnCl_2$ and 0.12 mmol **PNO**), zinc(II) chloride-**INO** (**Zn-INO**, 0.065 mmol $ZnCl_2$ and 0.13 mmol **INO**), cadmium(II) chloride-**PNO** (**Cd-PNO**, 0.06 mmol $CdCl_2$ and

Table 1. Gelation test for **PNO** and **INO** with Zn(II)/Cd(II) salts at 1:2 metal–ligand ratio.

Solvent (1.0 mL)	Metal salt (0.075 mmol)	**PNO** (0.15 mmol)	**INO** (0.15 mmol)
Water	$ZnCl_2$	Gel	Gel
Water	$Zn(OAc)_2$	Ligand crystal	Ligand crystal
Water	$Zn(NO_3)_2$	Ligand crystal	Precipitate
Water	$CdCl_2$	Gel	Gel
Water	$Cd(OAc)_2$	Colloidal	Ligand crystal
Water	$Cd(NO_3)_2$	Ligand crystal	Ligand crystal
DMF/water (1:1 v/v)	$ZnCl_2$	Gel	Precipitate
DMF/water (1:1 v/v)	$Zn(OAc)_2$	Precipitate	Solution
DMF/water (1:1 v/v)	$Zn(NO_3)_2$	Solution	Solution
DMF/water (1:1 v/v)	$CdCl_2$	Precipitate	Colloidal
DMF/water (1:1 v/v)	$Cd(OAc)_2$	Solution	Solution
DMF/water (1:1 v/v)	$Cd(NO_3)_2$	Solution	Solution

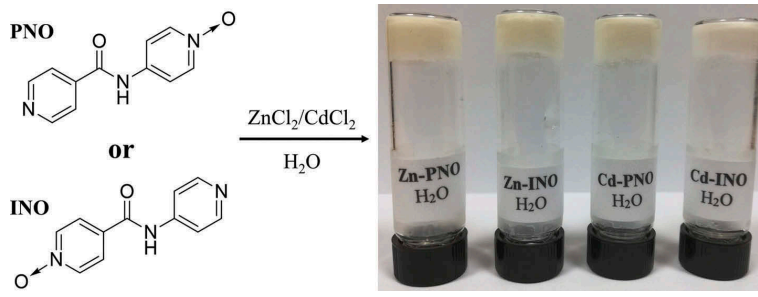

Figure 1. Metallogels of **Zn-PNO** (4.2 wt%), **Zn-INO** (4.2 wt%), **Cd-PNO** (4.6 wt%) and **Cd-INO** (4.6 wt%) obtained from water.

0.12 mmol **PNO**) and cadmium(II) chloride-**INO (Cd-INO**, 0.07 mmol $CdCl_2$ and 0.14 mmol **INO**). The gelation experiments with acetate and nitrate salts of cadmium-(II) and zinc(II) did not yield metallogels for both **PNO** and **INO** (see Table S1 and Table S2). This indicates that zinc(II) and cadmium(II) chloride complexes selectively form metallogels, which can be correlated to the electron affinity and the steric hindrance of the counter anions. This is due to the highest electron affinity and spherical geometry of chloride anions, which enable a stronger interaction between the metal centre and the anions.

The solubility of the metal complexes in water was one of the issues for testing the gelation properties at higher concentration. Thus, we decided to test the gelation properties of these complexes in an aqueous solution of highly polar solvent (1:1, v/v, DMF/water, Table 1). The gelation experiments performed by mixing the metal chloride salts (0.05 mmol) in water and the ligand (0.1 mmol) in DMF revealed that gelation was observed for only **Zn-PNO** complex. The gelation experiments performed for other mixtures at higher concentration did not yield gels.

The gelation ability of the complexes was compared by analysing the MGC. Both **Zn-PNO** and **Cd-PNO** complexes required 0.06 mmol of metal salt and 0.12 mmol of **PNO** to form a gel in water (the MGC was 3.4 and 3.7 wt%, respectively). The MGC of **Zn-INO** and **Cd-INO** gel in water was found to be 3.7 wt% and 4.3 wt%, respectively. The MGC experiments revealed that **PNO** complexes formed better hydrogelators compared to **INO** complex. The **Zn-PNO** gel in 1:1 DMF/water (v/v) displayed a lower MGC of 2.8 wt% (0.05 mmol of $ZnCl_2$ and 0.1 mmol of **PNO**), indicating that **Zn-PNO** complex formed efficient metallogel at lower concentration (see Table S3-S6).

3.2. Gel strength

The thermal stability of the gel network was evaluated using gel-to-solution transition temperature (T_{gel}) experiments. The T_{gel} of the **Zn-PNO** was evaluated in DMF/water (1:1, v/v), which was found to be 98.3°C and 112.6°C at 2.8 wt% and 4.2 wt%, respectively. The T_{gel} of the complexes was also determined in water and the results are summarised in Table S7. The results indicate that **PNO** complexes formed stronger network compared to the **INO** metallogel. The metallogels of cadmium complexes did not transform into solution upon heating presumably due to the presence of polymeric networks or coordination polymers.

3.3. Gel morphology

The morphologies of the xerogels were analysed by SEM. The gels of **Zn-INO** (3.7 wt%) and **Cd-PNO** (3.7 wt%) were prepared in water and **Zn-PNO** (2.8 wt%) gel was prepared in DMF/water (1:1, v/v). After 24 h, the gels were filtered, dried under a fume hood for 30 h. A small portion of the dried gel was placed on a pin mount with carbon tab on top and coated with gold for 2 min. The SEM images of **Zn-PNO** and **Cd-PNO** complexes revealed that all xerogels display fibrous needle-type morphology (Figure 2). The individual fibrils of **Cd-PNO** aggregates displayed needles with varying dimensions (Figure 2(a)) with thickness ranging from 0.1 to 0.65 µm (see Figure S1a). The morphologies of the xerogels of **Zn-PNO** displayed fibrous needles (Figure 2(b)) and the thickness of the fibres ranged from 0.25 to 1.5 µm and the dimensions of the needles varied from 2.0 to 8.0 µm (see Figure S1b). The SEM images of **Zn-INO** displayed crystalline fibrous block morphology with thickness varying from 0.25 to 2.0 µm (see Figure S2).

3.4. Structural analysis of the metal complexes

As mentioned above, the characterisation of supramolecular gels in its native form is challenging and efforts have been made to correlate the solid-state structure with the gel state using X-ray diffraction techniques. In this method, the crystal structure of the gelator is compared to the powder diffraction pattern of either native gel or the xerogel [1,4,21,36,69]. This approach still remains as one of the practical methods to gain insight into the gelator structure and aggregation behaviour, but the removal of solvent while preparing xerogel can result in artefacts due to dissolution, recrystallisation and changes in morphology or polymorphic phase transition [70]. This technique will enable us to compare the intermolecular interactions observed in the single-crystal structure with the molecular aggregation in the gel state, which might be different from its crystalline network [21].

The solid-sate structures of **PNO** and **INO** [22] were compared with the crystal structures of the metal complex using single-crystal diffraction data. The crystallographic data and the hydrogen bonding parameters are provided in Table 2 and Table S8, respectively.

X-ray quality single crystals of **Zn-PNO** were obtained by mixing an aqueous solution of $ZnCl_2$ with a solution of **PNO** in DMF at room temperature. Single-crystal X-ray analysis confirmed the formation of the complex [$ZnCl_2$(**PNO**)$_2$] with zinc(II) metal centre displaying slightly distorted tetrahedral geometry. The metal centre was coordinated to two chloride anions and two **PNO** molecules

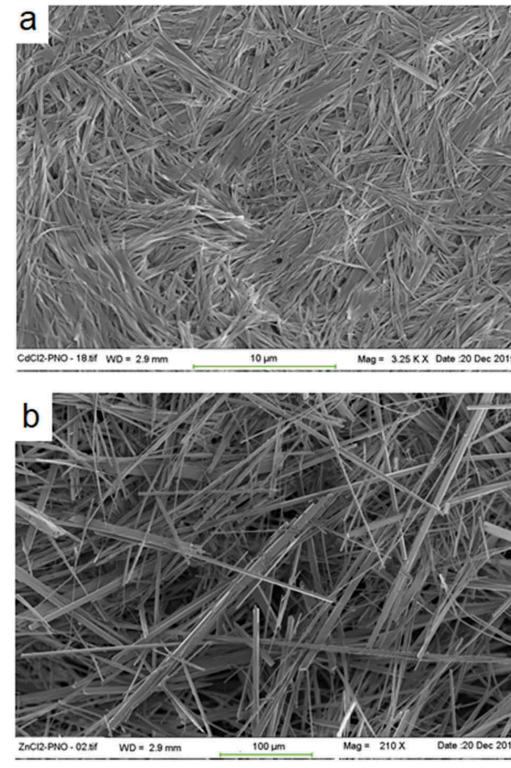

Figure 2. SEM images of xerogels of (a) **Cd-PNO** obtained from water at 3.7 wt% and (b) **Zn-PNO** obtained from DMF/water (1:1, v/v) at 2.8 wt%.

were coordinated to the zinc(II) via the pyridyl nitrogen atom of the isonicotinoyl moiety (Figure 3(a)). The amide moiety of one of the **PNO** molecules displayed hydrogen bonding with the *N*-oxide group via N—H···O interaction (2.783 [3] Å), which was similar to the complementary amide hydrogen bonding resulting in a hydrogen bonded 1-D corrugated sheet (Figure 3(b)). These 1-D sheets interacted with adjacent sheets via N—H···O interaction (2.783 [3] Å) involving the other amide and *N*-oxide moieties to form a 3-D hydrogen bonded network, which was stabilised by various non-covalent interactions.

The complex **Zn-INO** was obtained from a hot aqueous solution of $ZnCl_2$ and **INO** by heating the mixture at 80°C for 2 h resulting in plate-shaped crystals. The mixture was cooled to room temperature and X-ray quality single crystals were isolated. The structural analysis of these crystals revealed that a complex of formula [$ZnCl_2$(**INO**)$_2$] was obtained. The coordination geometry of the metal centre was similar to **Zn-PNO** with two chloride and **INO** moieties coordinated zinc(II) atoms,

Table 2. Crystal data of $ZnCl_2$(**PNO**)$_2$ and $ZnCl_2$(**INO**)$_2$.

Crystal data	$ZnCl_2$(**PNO**)$_2$	$ZnCl_2$(**INO**)$_2$
Empirical formula	$C_{22}H_{18}Cl_2N_6O_4Zn$	$C_{22}H_{18}Cl_2N_6O_4Zn$
Colour	colourless	colourless
Formula weight	566.69	566.69
Crystal size (mm)	0.30 × 0.07 × 0.06	0.22 × 0.10 × 0.02
Crystal system	orthorhombic	monoclinic
Space group	Fdd2	P2/c
a (Å)	21.8375 [16]	7.0586 [6]
b (Å)	45.335 [3]	6.5219 [5]
c (Å)	4.6374 [4]	24.986 [2]
α (°)	90	90
β (°)	90	93.451 [2]
γ (°)	90	90
Volume (Å^3)	4591.1 [6]	1148.14 [16]
Z	8	2
$D_{calc.}$ (g/cm^3)	1.640	1.639
F(000)	2304	576
μ CuKα (mm^{-1})	4.010	4.009
Temperature (K)	302 [2]	302 [2]
Reflections collected/unique/ observed [I > 2σ(I)]	36,527/2202/2175	17,901/2248/2095
Data/restraints/parameters	2202/1/160	2248/0/159
Goodness of fit on F^2	1.047	1.085
Final R indices [I > 2σ(I)]	R_1 = 0.0202 wR_2 = 0.0595	R_1 = 0.0270 wR_2 = 0.0780
R indices (all data)	R_1 = 0.0205 wR_2 = 0.0599	R_1 = 0.0292 wR_2 = 0.0795

respectively (Figure 4(a)) but the pyridyl and pyridyl-*N*-oxide rings were slightly twisted compared to **Zn-PNO** and these rings were oriented at an angle of 50.64° to each other. The amide and *N*-oxide moieties were involved in hydrogen bonding with adjacent molecule via N—H···O interaction (2.8146 [19] Å) resulting in a hydrogen-bonded 1-D chain. This 1-D chain can be considered as complementary amide hydrogen bonding, which was further stabilised by π–π interaction between the pyridyl-*N*-oxide moieties and the 1-D chains interact with adjacent chains via π–π interaction and C—H···Cl interaction (Figure 4(b)).

The crystal structures of **PNO** and **INO** [22] were compared to the crystal structure of the metal complexes to elucidate the key parameters responsible for the conversion of the non-gelator to metallogels. In the ligand structure, the amide and *N*-oxide moieties interacted with the solvent water molecules via N—H···O and O—H···O interactions. However, these interactions were replaced by N—H···O interaction in zinc(II) chloride complexes of **PNO** and **INO** resulting in a 1-D corrugated sheets, which were similar to the complementary amide hydrogen bonding. These results clearly indicate that N—H···O interactions play a crucial role in gel formation in metallogels.

Infrared spectroscopy can be used to analyse the self-assembly modes of LMWGs based on amides [21,71–74] due to their characteristic bands such as amide-A/amide-B (originated from mainly N—H stretching vibration), amide-I (C=O stretching), amide-II (N—H bending) etc. Hydrogen bonding affects the bond length of the interacting species, for example, the increased hydrogen bonding will shift the corresponding peaks to lower wavenumbers/frequencies (red shift) and vice versa (blue shift). The comparison of the IR-bands of the free ligand and the corresponding metal complexes will enable us to study the extent of hydrogen-bonding in these complexes. The selected peaks of the free ligands and metal complexes are summarised in Table S9. The **PNO** ligand displayed a broad peak at 3193 cm^{-1} and sharp peaks at 1679 and 1556 cm^{-1}. In **PNO** complexes (**Zn-PNO** and **Cd-PNO**), the N—H stretching peaks were shifted to 3044 and 3042 cm^{-1} respectively (see Figure S3). The C=O bands of the free ligands were

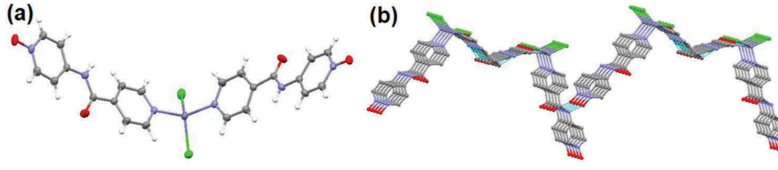

Figure 3. (a) Crystal structure of **Zn-PNO** and (b) hydrogen-bonded 1-D corrugated sheet stabilised by N—H···O interaction.

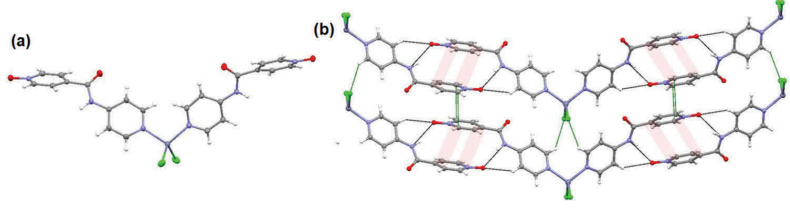

Figure 4. (a) Crystal structure of **Zn-INO** and (b) hydrogen-bonded 1-D chain stabilised by N—H···O (black-dotted line) and π–π interactions (red shade) and the adjacent chains interacted each other via π–π and C—H···Cl interactions (green-dotted lines).

blue-shifted after complex formation indicating that the strength of interaction based on the carbonyl moieties of the amide group were slightly reduced in complexes [75,76]. The N-H bands (amide-A and amide-II) of the complexes appeared at lower frequencies (red shifted) indicating stronger hydrogen bonds compared to the free ligand except in the case **Cd-INO** (see Figure S4). This is presumably due to the weaker hydrogen bond in **Cd-INO**, which supports that fact that complex **Cd-INO** displayed higher MGC compared to other complexes. These results corroborate well with the solid-state interactions observed in the crystal structures of the complexes (**Zn-INO** and **Zn-PNO**) where the amide N-H moieties displayed strong N—H···O interactions, which was not observed in the free ligand structure. These interactions were similar to the complementary amide hydrogen bonding resulting in a 1-D hydrogen-bonded architecture, which plays an important role in metallogel formation.

3.5. X-ray powder diffraction (XRPD)

XRPD was performed on the xerogels of **Zn-PNO** and **Zn-INO** to correlate the structural factors in gel state and solid-state. The comparison of these data with crystal structure will enable us to correlate the solid-state structure of the xerogel and the crystal structure. We have compared the XPRD pattern calculated from the single-crystal data with the experimental patterns of the xerogel of **Zn-PNO** obtained from DMF/water (1:1, v/v) at 2.8 wt% and 3.7 wt% for **Zn-INO** in water. The analysis of both patterns revealed that the crystals and the xerogels have similar crystal phase (Figure 5 and Figure S5). The similarity in two patterns indicate that the structure obtained from the single-crystal data has been translated to hierarchical xerogel network, and the crystal structure of **Zn-PNO** and **Zn-INO** truly represents the structure in xerogel state.

3.6. Stimuli-responsive properties of metallogels

The tuning of gel properties based on anion binding is an area of current interest because anion affect the flow characteristics of supramolecular gels and induce conformational changes in LMWGs [3,5,77]. Cyanide has been widely used in various industrial processes and the detection of cyanide anion is very important due to their extreme toxicity [78–80]. The stimuli-responsive property of supramolecular gels make them an ideal candidate to detect cyanide anions [81–84] and this prompted us to analyse the stimuli-responsive property of the metallogels in presence of anions [3,5,81,85–89] such as fluoride, chloride, bromide, iodide and cyanide (Table S10). The metallogels were treated with two equivalents of the anion (with respect to the metal counter-anion) in solid form and the gels were left undisturbed for an hour. The **Zn-PNO** and **Zn-INO** metallogels collapsed in case of cyanide, fluoride and iodide anions, but the gels were stable for chloride and bromide anions (Figure 6). The gelation was turned *ON* by the addition of

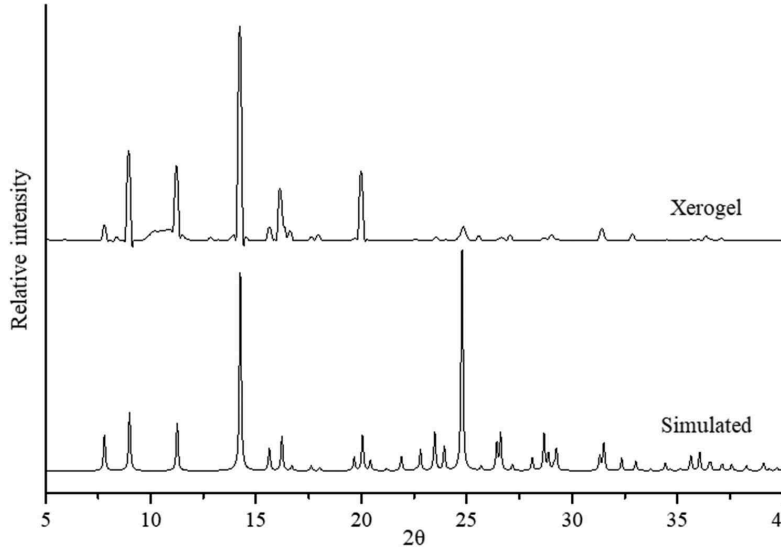

Figure 5. XRPD comparison of **Zn-PNO**: simulated pattern obtained from single-crystal data (bottom) and xerogel (top) obtained from DMF/water (1:1, v/v) at 2.8 wt%.

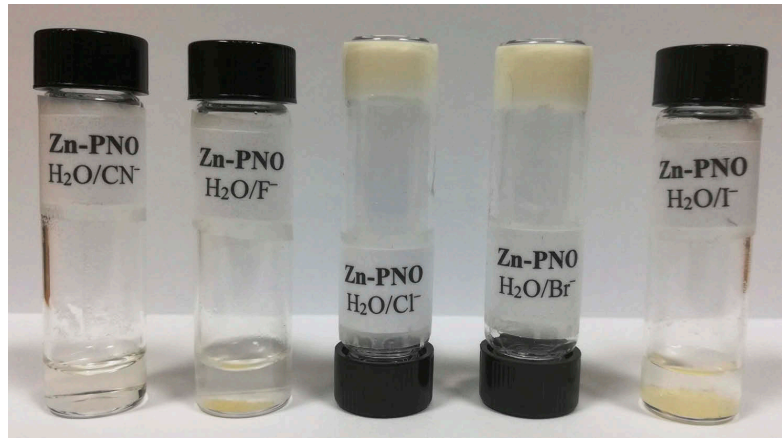

Figure 6. Effect of various anions to **Zn-PNO** gel network.

two equivalents of chloride anion in case of **Zn-PNO** and **Zn-INO** metallogels treated with fluoride anions, but the gelation was not observed for the iodide and cyanide anion treated metallogels even after adding an excess of chloride anions. The gelation property of **Cd-PNO** and **Cd-INO** was not affected by the addition of fluoride, chloride, bromide and iodide but the gelation was turned *OFF* selectively by two equivalents of cyanide anion. This is presumably due to the fact that the gel network in cadmium(II) metallogel are polymeric in nature and cyanide anion is a stronger ligands compared to the halides, which resulted in the disruption of the network at this particular concentration.

The experiments repeated by heating the anions and gels together also produced the same results. We have also performed experiments at higher anion concentration (five equivalents) and similar results were obtained except for iodide anions where the **Cd-PNO** and **Cd-INO** gel network collapsed by the addition of five equivalents of iodide anion. This can be correlated to the soft–soft interaction between the cadmium(II) metal centre and iodide anion at higher concentration. These results indicate that all the four metallogels can detect cyanide anions in water by monitoring gel–sol transition whereas **Cd-PNO** and **Cd-INO** can selectively detect cyanide over fluoride, chloride, bromide and iodide anions in water.

4. Conclusions

In summary, the role of metal coordination in supramolecular gel formation was analysed by coordinating zinc(II) and cadmium(II) salts with pyridyl amide-based non-gelator ligands (**PNO** or **INO**). The gelation studies revealed that metal-induced gelation was observed in water for zinc(II) chloride and cadmium(II) chloride complexes and gels were not formed for acetate and nitrate salts of these metals for both **PNO** and **INO**. The complex **Zn-INO** formed weaker metallogel compared to **Zn-PNO** gel. The gelation experiments performed in DMF/water (1:1, v/v) revealed selective gelation of **Zn-PNO** complex. The morphologies of the xerogels were analysed by SEM, which displayed fibrous needle/block type network. The metal complex-induced gelation was further supported by FT-IR, single-crystal X-ray and X-ray powder diffraction. The self-assembly process was analysed by comparing the single-crystal X-ray structure of the ligands and the zinc complexes, which indicated that the amide and pyridyl-*N*-oxide moieties interacted each other via N—H···O interactions. These interactions resulted in a 1-D hydrogen-bonded chain similar to complementary amide hydrogen bonding, which was one of the key factors for gel network formation. The stimuli-responsive properties of the metallogels in presence of anions were studied and the results indicated that the gel networks of **Zn-PNO** and **Zn-INO** collapsed in presence of cyanide, fluoride and iodide anions, whereas addition of chloride and bromide anion did not affect the gelation. The metallogels of **Cd-PNO** and **Cd-INO** collapsed in presence of cyanide anions but the addition of two equivalents of halide anions did not affect the gel network, which indicates that **Cd-PNO** and **Cd-INO** can be used to detect cyanide anions in water by gel to sol transition. These results indicate that the role of metal coordination, hydrogen bonding and the nature of anions are crucial in supramolecular gel formation.

Acknowledgments

We thank the Science Institute and University of Iceland Research Fund for financial support. DKK and Deepa thank EU for the Erasmus Exchange Program, D.G. thanks the University of Iceland for the Doctoral Research fund. We thank Rannis Iceland for Infrastructure grant (150998-0031), Sigurður Sveinn Jónsson, ISOR-Iceland for X-ray powder diffraction analysis and Dr Sigríður Jónsdóttir, University of Iceland for NMR spectroscopy.

Disclosure statement

No potential conflict of interest was reported by the authors.

Funding

This work was supported by the Icelandic Centre for Research (Rannis) [Infrastructure Grant-150998-0031].

ORCID

Krishna K. Damodaran http://orcid.org/0000-0002-9741-2997

References

[1] Dastidar P. Supramolecular gelling agents: can they be designed? Chem. Soc. Rev. **2008**;37:2699–2715.
[2] Draper ER, Adams DJ. Low-molecular-weight gels: the state of the art. Chem. **2017**;3(3):390–410.
[3] Steed JW. Anion-tuned supramolecular gels: a natural evolution from urea supramolecular chemistry. Chem. Soc. Rev. **2010**;39:3686–3699.
[4] Yu G, Yan X, Han C, et al. Characterization of supramolecular gels. Chem. Soc. Rev. **2013**;42:6697–6722.
[5] Piepenbrock M-OM, Lloyd GO, Clarke N, et al. Metal- and anion-binding supramolecular gels. Chem. Rev. **2010**;110:1960–2004.
[6] Kumar DK, Steed JW. Supramolecular gel phase crystallization: orthogonal self-assembly under non-equilibrium conditions. Chem. Soc. Rev. **2014**;43:2080–2088.
[7] Fang W, Zhang Y, Wu J, et al. Recent advances in supramolecular gels and catalysis. Chem. Asian J. **2018**;13:712–729.
[8] Du X, Zhou J, Shi J, et al. Supramolecular hydrogelators and hydrogels: from soft matter to molecular biomaterials. Chem. Rev. **2015**;115:13165–13307.
[9] Smith DK. Applications of supramolecular gels. Weiss R, editor. In: Molecular gels: structure and dynamics. Cambridge: Royal Society of Chemistry; 2018. p. 300–371.
[10] Foster JA, Damodaran KK, Maurin A, et al. Pharmaceutical polymorph control in a drug-mimetic supramolecular gel. Chem. Sci. **2017**;8:78–84.
[11] Gagni P, Romanato A, Bergamaschi G, et al. A self-assembling peptide hydrogel for ultrarapid 3D bioassays. Nanoscale Adv. **2019**;1:490–497.
[12] Estroff LA, Hamilton AD. Water gelation by small organic molecules. Chem. Rev. **2004**;104:1201–1218.
[13] de Loos M, Feringa BL, van Esch JH. Design and application of self-assembled low molecular weight hydrogels. Eur. J. Org. Chem. **2005**;2005:3615–3631.
[14] George M, Weiss RG. Molecular organogels. soft matter comprised of low-molecular-mass organic gelators and organic liquids. Acc. Chem. Res. **2006**;39:489–497.
[15] Hirst AR, Escuder B, Miravet JF, et al. High-tech applications of self-assembling supramolecular nanostructured gel-phase materials: from regenerative medicine to electronic devices. Angew. Chem. Int. Ed. **2008**;47:8002–8018.
[16] Banerjee S, Das RK, Maitra U. Supramolecular gels 'in action'. J. Mater. Chem. **2009**;19:6649–6687.
[17] Bhattacharjee S, Bhattacharya S. Role of synergistic π–π stacking and X–H···Cl (X = C, N, O) H-bonding interactions in gelation and gel phase crystallization. Chem. Commun. **2015**;51:7019–7022.
[18] Jones CD, Steed JW. Gels with sense: supramolecular materials that respond to heat, light and sound. Chem. Soc. Rev. **2016**;45:6546–6596.
[19] Kumar DK, Jose DA, Dastidar P, et al. Nonpolymeric hydrogelators derived from trimesic amides. Chem. Mater. **2004**;16:2332–2335.
[20] Ghosh D, Ferfolja K, Drabavičius Ž, et al. Crystal habit modification of Cu(II) isonicotinate–*N*-oxide complexes using gel phase crystallisation. New J. Chem. **2018**;42:19963–19970.
[21] Kumar DK, Jose DA, Dastidar P, et al. Nonpolymeric hydrogelator derived from *N*-(4-pyridyl)isonicotinamide. Langmuir. **2004**;20:10413–10418.
[22] Ghosh D, Mulvee MT, Damodaran KK. Tuning gel state properties of supramolecular gels by functional group modification. Molecules. **2019**;24:3472.
[23] Draper ER, Adams DJ. How should multicomponent supramolecular gels be characterised? Chem. Soc. Rev. **2018**;47:3395–3405.
[24] Cao X, Meng L, Li Z, et al. Large red-shifted fluorescent emission via intermolecular π–π stacking in 4-ethynyl-1,8-naphthalimide-based supramolecular assemblies. Langmuir. **2014**;30:11753–11760.
[25] Wang C, Zhang D, Zhu D. A chiral low-molecular-weight gelator based on binaphthalene with two urea moieties: modulation of the CD spectrum after gel formation. Langmuir. **2007**;23:1478–1482.
[26] Wang C, Zhang D, Xiang J, et al. New organogels based on an anthracene derivative with one urea group and its photodimer: fluorescence enhancement after gelation. Langmuir. **2007**;23:9195–9200.
[27] Wang G, Cheuk S, Yang H, et al. Synthesis and characterization of monosaccharide-derived carbamates as low-molecular-weight gelators. Langmuir. **2009**;25:8696–8705.
[28] Gao W, Liang Y, Peng X, et al. In situ injection of phenylboronic acid based low molecular weight gels for efficient chemotherapy. Biomaterials. **2016**;105:1–11.
[29] Das UK, Banerjee S, Dastidar P. Remarkable shape-sustaining, load-bearing, and self-healing properties displayed by a supramolecular gel derived from a bis-pyridyl-bis-amide of L-phenyl alanine. Chem. Asian J. **2014**;9:2475–2482.
[30] Tang Y-T, Dou X-Q, Ji Z-A, et al. C_2-symmetric cyclohexane-based hydrogels: a rational designed

LMWG and its application in dye scavenging. J. Mol. Liq. **2013**;177:167–171.
[31] Li P, Dou X-Q, Tang Y-T, et al. Gelator-polysaccharide hybrid hydrogel for selective and controllable dye release. J. Colloid Interface Sci. **2012**;387:115–122.
[32] McConnell AJ, Wood CS, Neelakandan PP, et al. Stimuli-responsive metal–ligand assemblies. Chem. Rev. **2015**;115:7729–7793.
[33] Theato P, Sumerlin BS, O'Reilly RK, et al. Stimuli responsive materials. Chem. Soc. Rev. **2013**;42:7055–7056.
[34] Hajime S, Itaru H. Supramolecular assemblies responsive to biomolecules toward biological applications. Chem. Asian J. **2015**;10:2026–2038.
[35] Segarra-Maset MD, Nebot VJ, Miravet JF, et al. Control of molecular gelation by chemical stimuli. Chem. Soc. Rev. **2013**;42:7086–7098.
[36] Ghosh D, Lebedytė I, Yufit DS, et al. Selective gelation of N-(4-pyridyl)nicotinamide by copper(II) salts. CrystEngComm. **2015**;17:8130–8138.
[37] Tam A-Y-Y, Yam V-W-W. Recent advances in metallogels. Chem. Soc. Rev. **2013**;42:1540–1567.
[38] Adarsh NN, Sahoo P, Dastidar P. Is a crystal engineering approach useful in designing metallogels? A case study. Cryst. Growth Des. **2010**;10:4976–4986.
[39] Xing B, Choi M-F, Xu B. A stable metal coordination polymer gel based on a calix[4]arene and its "uptake" of non-ionic organic molecules from the aqueous phase. Chem. Commun. **2002**;362–363.
[40] Gavara R, Llorca J, Lima JC, et al. A luminescent hydrogel based on a new Au(I) complex. Chem. Commun. **2013**;49:72–74.
[41] Ishi-i T, Iguchi R, Snip E, et al. Fullerene can reinforce the organogel structure of porphyrin-appended cholesterol derivatives: novel odd–even Effect of the $(CH_2)_n$ spacer on the organogel stability. Langmuir. **2001**;17:5825–5833.
[42] Isozaki K, Ogata K, Haga Y, et al. Metal array fabrication through self-assembly of Pt-complex-bound amino acids. Chem. Commun. **2012**;48:3936–3938.
[43] López D, Guenet J-M. Behavior of a self-assembling bicopper complex in organic solutions. Macromolecules. **2001**;34:1076–1081.
[44] Terech P, Gebel G, Ramasseul R. Molecular rods in a zinc-(II) porphyrin/cyclohexane physical gel: neutron and X-ray scattering characterizations. Langmuir. **1996**;12:4321–4323.
[45] Zhang Y, Zhang B, Kuang Y, et al. A redox responsive, fluorescent supramolecular metallohydrogel consists of nanofibers with single-molecule width. J. Am. Chem. Soc. **2013**;135:5008–5011.
[46] Adarsh NN, Dastidar P. A new series of Zn^{II} coordination polymer based metallogels derived from bis-pyridyl-bis-amide ligands: a crystal engineering approach. Cryst. Growth Des. **2011**;11:328–336.
[47] de Hatten X, Bell N, Yufa N, et al. A dynamic covalent, luminescent metallopolymer that undergoes sol-to-gel transition on temperature rise. J. Am. Chem. Soc. **2011**;133:3158–3164.
[48] Hamilton TD, Bučar D-K, Baltrusaitis J, et al. Thixotropic hydrogel derived from a product of an organic solid-state synthesis: properties and densities of metal –organic nanoparticles. J. Am. Chem. Soc. **2011**;133:3365–3371.
[49] Ishiwata T, Furukawa Y, Sugikawa K, et al. Transformation of metal–organic framework to polymer gel by cross-linking the organic ligands preorganized in metal–organic framework. J. Am. Chem. Soc. **2013**;135:5427–5432.
[50] Paul M, Adarsh NN, Dastidar P. Cu^{II} coordination polymers capable of gelation and selective SO_4^{-2} separation. Cryst. Growth Des. **2012**;12:4135–4143.
[51] Piepenbrock M-OM, Clarke N, Steed JW. Rheology and silver nanoparticle templating in a bis(urea) silver metallogel. Soft Matter. **2011**;7:2412–2418.
[52] Hanabusa K, Maesaka Y, Suzuki M, et al. Low molecular weight gelator containing β-diketonato ligands: stabilization of gels by metal coordination. Chem. Lett. **2000**;29:1168–1169.
[53] Bhattacharjee S, Bhattacharya S. Pyridylenevinylene based Cu^{2+}-specific, injectable metallo(hydro)gel: thixotropy and nanoscale metal-organic particles. Chem. Commun. **2014**;50:11690–11693.
[54] Bhattacharjee S, Samanta SK, Moitra P, et al. Nanocomposite made of an oligo(*p*-phenylenevinylene)-based trihybrid thixotropic metallo(organo)gel comprising nanoscale metal-organic particles, carbon nanohorns, and silver nanoparticles. Chem. Eur. J. **2015**;21:5467–5476.
[55] Kumar Vemula P, Aslam U, Ajay Mallia V, et al. In situ synthesis of gold nanoparticles using molecular gels and liquid crystals from vitamin-C amphiphiles. Chem. Mater. **2007**;19:138–140.
[56] Paul M, Sarkar K, Dastidar P. Metallogels derived from silver coordination polymers of C_3-symmetric tris(pyridylamide) tripodal ligands: synthesis of Ag nanoparticles and catalysis. Chem. Eur. J. **2015**;21:255–268.
[57] Byrne P, Lloyd GO, Applegarth L, et al. Metal-induced gelation in dipyridyl ureas. New J. Chem. **2010**;34:2261–2274.
[58] Xue P, Wu H, Wang X, et al. Cation tuning toward the inference of the gelation behavior of supramolecular gels. Sci. Rep. **2016**;6:25390.
[59] Kumar DK, Jose DA, Das A, et al. First snapshot of a nonpolymeric hydrogelator interacting with its gelling solvents. Chem. Commun. **2005**;4059–4061.
[60] Abraham S, Lan Y, Lam RSH, et al. Influence of positional isomers on the macroscale and nanoscale architectures of aggregates of racemic hydroxyoctadecanoic acids in their molecular gel, dispersion, and solid states. Langmuir. **2012**;28:4955–4964.
[61] Xu Y, Kang C, Chen Y, et al. In situ gel-to-crystal transition and synthesis of metal nanoparticles obtained by fluorination of a cyclic β-aminoalcohol gelator. Chem. Eur. J. **2012**;18:16955–16961.
[62] Wang Y, Tang L, Yu J. Investigation of spontaneous transition from low-molecular-weight hydrogel into macroscopic crystals. Cryst. Growth Des. **2008**;8:884–889.
[63] Braga D, D'Agostino S, D'Amen E, et al. Polymorphs from supramolecular gels: four crystal forms of the same silver(I) supergelator crystallized directly from its gels. Chem. Commun. **2011**;47:5154–5156.
[64] Dastidar P, Roy R, Parveen R, et al. Supramolecular synthon approach in designing molecular gels for advanced therapeutics. Adv. Ther. **2019**;2:1800061.
[65] Pizzi A, Lascialfari L, Demitri N, et al. Halogen bonding modulates hydrogel formation from Fmoc amino acids. CrystEngComm. **2017**;19:1870–1874.

[66] Meazza L, Foster JA, Fucke K, et al. Halogen-bonding-triggered supramolecular gel formation. Nat. Chem. **2013**;5:42–47.
[67] Sheldrick G. Crystal structure refinement with *SHELXL*. Acta Crystallogr. Sect. C. **2015**;71:3–8.
[68] Dolomanov OV, Bourhis LJ, Gildea RJ, et al. *OLEX2*: a complete structure solution, refinement and analysis program. J. Appl. Crystallogr. **2009**;42:339–341.
[69] Sahoo P, Kumar DK, Raghavan SR, et al. Supramolecular synthons in designing low molecular mass gelling agents: L-amino acid methyl ester cinnamate salts and their anti-solvent-induced instant gelation. Chem. Asian J. **2011**;6:1038–1047.
[70] Adams DJ. Does drying affect gel networks? Gels. **2018**;4:32.
[71] Fornaro T, Burini D, Biczysko M, et al. Hydrogen-bonding effects on infrared spectra from anharmonic computations: uracil–water complexes and uracil dimers. J. Phys. Chem. A. **2015**;119:4224–4236.
[72] Saha A, Roy B, Garai A, et al. Two-component thermoreversible hydrogels of melamine and gallic acid. Langmuir. **2009**;25:8457–8461.
[73] Xing P, Chu X, Li S, et al. Switchable and orthogonal self-assemblies of anisotropic fibers. New J. Chem. **2013**;37:3949–3955.
[74] Nebot VJ, Armengol J, Smets J, et al. Molecular hydrogels from bolaform amino acid derivatives: a structure-properties study based on the thermodynamics of gel solubilization. Chem. Eur. J. **2012**;18:4063–4072.
[75] Zhong J-L, Jia X-J, Liu H-J, et al. Self-assembled metallogels formed from *N*,*N*′,*N*″-tris(4-pyridyl)trimesic amide in aqueous solution induced by Fe(III)/Fe(II) ions. Soft Matter. **2016**;12:191–199.
[76] Banerjee S, Adarsh NN, Dastidar P. A crystal engineering rationale in designing a Cd^{II} coordination polymer based metallogel derived from a C_3 symmetric tris-amide-tris-carboxylate ligand. Soft Matter. **2012**;8:7623–7629.
[77] Lloyd GO, Steed JW. Anion-tuning of supramolecular gel properties. Nat. Chem. **2009**;1:437–442.
[78] Ma J, Dasgupta PK. Recent developments in cyanide detection: a review. Anal. Chim. Acta. **2010**;673:117–125.
[79] Bencini A, Lippolis V. Metal-based optical chemosensors for CN^- detection. Environ. Sci. Pollut. Res. Int. **2016**;23:24451–24475.
[80] Udhayakumari D. Detection of toxic fluoride ion via chromogenic and fluorogenic sensing. A comprehensive review of the year 2015–2019. Spectrochim. Acta A. **2020**;228:117817.
[81] Fang H, Qu W-J, Yang -H-H, et al. A self-assembled supramolecular gel constructed by phenazine derivative and its application in ultrasensitive detection of cyanide. Dyes Pigm. **2020**;174:108066.
[82] Samanta SK, Dey N, Kumari N, et al. Advanced porous materials for sensing, capture and detoxification of organic pollutants toward water remediation. ACS Sustain. Chem. Eng. **2019**;7:12304–12314.
[83] Hu J-H, Yin Z-Y, Gui K, et al. A novel supramolecular polymer gel-based long-alkyl-chain-functionalized coumarin acylhydrazone for the sequential detection and separation of toxic ions. Soft Matter. **2020**;16:1029–1033.
[84] Wei T-B, Ma X-Q, Fan Y-Q, et al. Aggregation-induced emission supramolecular organic framework (AIE SOF) gels constructed from tri-pillar[5]arene-based foldamer for ultrasensitive detection and separation of multi-analytes. Soft Matter. **2019**;15:6753–6758.
[85] Karak S, Kumar S, Bera S, et al. Interplaying anions in a supramolecular metallohydrogel to form metal organic frameworks. Chem. Commun. **2017**;53:3705–3708.
[86] James SJ, Perrin A, Jones CD, et al. Highly interlocked anion-bridged supramolecular networks from interrupted imidazole–urea gels. Chem. Commun. **2014**;50:12851–12854.
[87] Lin Q, Lu -T-T, Zhu X, et al. A novel supramolecular metallogel-based high-resolution anion sensor array. Chem. Commun. **2015**;51:1635–1638.
[88] Tom L, Kurup MRP. A stimuli responsive multifunctional ZMOF based on an unorthodox polytopic ligand: reversible thermochromism and anion triggered metallogelation. Dalton Trans. **2019**;48:16604–16614.
[89] Ganta S, Chand DK. Multi-stimuli-responsive metallogel molded from a Pd_2L_4-type coordination cage: selective removal of anionic dyes. Inorg. Chem. **2018**;57:3634–3645.

Supplementary Information

Metal complexation induced supramolecular gels for the detection of cyanide in water

Dipankar Ghosh, Deepa and Krishna K. Damodaran*

Table of content

1. Gelation studies

Table S1: Gelation experiment of **PNO** in presence of zinc(II) and cadmium(II) salts at 1:2 metal-ligand ratio

Metal salt	Amount (mg)	mmol	**PNO** amount (mg)	Solvent (1.0 mL)	Initial Observation	Observation after 24 h
$ZnCl_2$	6.8	0.05	21.5	Water	Solution	Partial gel
$ZnCl_2$	8.2	0.06	25.8	Water	Solution	Gel
$ZnCl_2$	10.2	0.075	32.3	Water	Solution	Gel
$ZnCl_2$	6.8	0.05	21.5	DMF/ Water (1:1 v/v)	Solution	Gel
$ZnCl_2$	8.2	0.06	25.8	DMF/ Water (1:1 v/v)	Solution	Gel
$Zn(NO_3)_2{\cdot}6H_2O$	14.9	0.05	21.5	Water	Solution	**PNO** Crystal
$Zn(NO_3)_2{\cdot}6H_2O$	22.3	0.075	32.3	Water	Solution	**PNO** Crystal
$Zn(NO_3)_2{\cdot}6H_2O$	14.9	0.05	21.5	DMF/ Water (1:1 v/v)	Solution	Solution
$Zn(NO_3)_2{\cdot}6H_2O$	22.3	0.075	32.3	DMF/ Water (1:1 v/v)	Solution	**PNO** Crystal
$Zn(OAc)_2{\cdot}2H_2O$	9.2	0.05	21.5	Water	Solution	**PNO** Crystal
$Zn(OAc)_2{\cdot}2H_2O$	13.8	0.075	32.3	Water	Solution	**PNO** Crystal
$Zn(OAc)_2{\cdot}2H_2O$	9.2	0.05	21.5	DMF/ Water (1:1 v/v)	Colloidal	Precipitate
$Zn(OAc)_2{\cdot}2H_2O$	13.8	0.075	32.3	DMF/ Water (1:1 v/v)	Colloidal	Precipitate
$CdCl_2$	9.1	0.05	21.5	Water	Colloidal	Partial gel
$CdCl_2$	13.7	0.075	32.3	Water	Colloidal	Gel
$CdCl_2$	9.1	0.05	21.5	DMF/ Water (1:1 v/v)	Colloidal	Precipitate
$CdCl_2$	13.7	0.075	32.3	DMF/ Water (1:1 v/v)	Colloidal	Precipitate
$Cd(NO_3)_2{\cdot}4H_2O$	15.4	0.05	21.5	Water	Solution	**PNO** Crystal
$Cd(NO_3)_2{\cdot}4H_2O$	23.1	0.075	32.3	Water	Solution	**PNO** Crystal
$Cd(NO_3)_2{\cdot}4H_2O$	15.4	0.05	21.5	DMF/ Water (1:1 v/v)	Solution	Solution
$Cd(NO_3)_2{\cdot}4H_2O$	23.1	0.075	32.3	DMF/ Water (1:1 v/v)	Solution	Solution
$Cd(OAc)_2{\cdot}2H_2O$	13.3	0.05	21.5	Water	Colloidal	Colloidal
$Cd(OAc)_2{\cdot}2H_2O$	20.0	0.075	32.3	Water	Colloidal	Precipitate
$Cd(OAc)_2{\cdot}2H_2O$	13.3	0.05	21.5	DMF/ Water (1:1 v/v)	Solution	Solution
$Cd(OAc)_2{\cdot}2H_2O$	20.0	0.075	32.3	DMF/ Water (1:1 v/v)	Solution	Precipitate

Table S2: Gelation experiment of **INO** in presence of Zinc(II) and cadmium(II) salts at 1:2 metal-ligand ratio

Metal salt	Amount (mg)	mmol	**INO** amount (mg)	Solvent (1.0 mL)	Initial Observation	Observation after 24 h
$ZnCl_2$	6.8	0.05	21.5	Water	Solution	Partial gel
$ZnCl_2$	9.0	0.065	28.0	Water	Solution	Gel
$ZnCl_2$	10.2	0.075	32.3	Water	Solution	Gel
$ZnCl_2$	6.8	0.05	21.5	DMF/ Water (1:1 v/v)	Solution	Solution
$ZnCl_2$	10.2	0.075	32.3	DMF/ Water (1:1 v/v)	Solution	Colloidal
$Zn(NO_3)_2{\cdot}6H_2O$	14.8	0.05	21.5	Water	Solution	**INO** Crystal
$Zn(NO_3)_2{\cdot}6H_2O$	22.3	0.075	32.3	Water	Colloidal	Precipitate*
$Zn(NO_3)_2{\cdot}6H_2O$	14.8	0.05	21.5	DMF/ Water (1:1 v/v)	Solution	Solution
$Zn(NO_3)_2{\cdot}6H_2O$	22.3	0.075	32.3	DMF/ Water (1:1 v/v)	Solution	Solution
$Zn(OAc)_2{\cdot}2H_2O$	10.9	0.05	21.5	Water	Solution	Solution
$Zn(OAc)_2{\cdot}2H_2O$	13.8	0.075	32.3	Water	Solution	**INO** Crystal
$Zn(OAc)_2{\cdot}2H_2O$	10.9	0.05	21.5	DMF/ Water (1:1 v/v)	Solution	Solution
$Zn(OAc)_2{\cdot}2H_2O$	13.8	0.075	32.3	DMF/ Water (1:1 v/v)	Solution	Solution
$CdCl_2$	9.1	0.05	21.5	Water	Colloidal	Partial gel
$CdCl_2$	13.7	0.075	32.3	Water	Colloidal	Gel
$CdCl_2$	9.1	0.05	21.5	DMF/ Water (1:1 v/v)	Colloidal	Precipitate
$CdCl_2$	13.7	0.075	32.3	DMF/ Water (1:1 v/v)	Colloidal	Precipitate
$Cd(NO_3)_2{\cdot}4H_2O$	15.4	0.05	21.5	Water	Solution	**INO** Crystal
$Cd(NO_3)_2{\cdot}4H_2O$	23.1	0.075	32.3	Water	Solution	**INO** Crystal
$Cd(NO_3)_2{\cdot}4H_2O$	15.4	0.05	21.5	DMF/ Water (1:1 v/v)	Solution	Solution
$Cd(NO_3)_2{\cdot}4H_2O$	23.1	0.075	32.3	DMF/ Water (1:1 v/v)	Solution	Solution
$Cd(OAc)_2{\cdot}2H_2O$	13.3	0.05	21.5	Water	Solution	**INO** Crystal
$Cd(OAc)_2{\cdot}2H_2O$	20.0	0.075	32.3	Water	Solution	**INO** Crystal
$Cd(OAc)_2{\cdot}2H_2O$	13.3	0.05	21.5	DMF/ Water (1:1 v/v)	Solution	Solution
$Cd(OAc)_2{\cdot}2H_2O$	20.0	0.075	32.3	DMF/ Water (1:1 v/v)	Solution	Solution

*A gel was obtained in 5 minutes, but the gel was broken after an hour and precipitate was observed.

Table S3: Determination of MGC of **Zn-PNO** gel

$ZnCl_2$ amount (mg)	mmol	**PNO** amount (mg)	Solvent (1.0 mL)	Initial Observation	Observation after 24 h
6.8	0.05	21.5	Water	Solution	Partial gel
7.5	0.055	23.7	Water	Solution	Partial gel
8.2	0.06	25.8	Water	Solution	Gel
8.8	0.065	28.0	Water	Solution	Gel
5.4	0.04	17.2	DMF/ Water (1:1 v/v)	Solution	Precipitate
6.1	0.045	19.3	DMF/ Water (1:1 v/v)	Solution	Partial gel
6.8	0.05	21.5	DMF/ Water (1:1 v/v)	Solution	Gel
7.5	0.055	23.7	DMF/ Water (1:1 v/v)	Solution	Gel

Table S4: Determination of MGC of **Zn-INO** gel

$ZnCl_2$ amount (mg)	mmol	**INO** amount (mg)	Solvent (1.0 mL)	Initial Observation	Observation after 24 h
7.5	0.055	23.7	Water	Solution	Partial gel
8.2	0.06	25.8	Water	Solution	Partial gel
8.8	0.065	28.0	Water	Solution	Gel
9.5	0.07	30.1	Water	Solution	Gel

Table S5: Determination of MGC of **Cd-PNO** gel

$CdCl_2$ amount (mg)	mmol	**PNO** amount (mg)	Solvent (1.0 mL)	Initial Observation	Observation after 24 h
9.2	0.05	21.5	Water	Colloidal	Partial gel
10.1	0.055	23.7	Water	Colloidal	Partial gel
11.0	0.06	25.8	Water	Colloidal	Gel
11.9	0.065	28.0	Water	Colloidal	Gel

Table S6: Determination of MGC of **Cd-INO** gel

$CdCl_2$ amount (mg)	mmol	**INO** amount (mg)	Solvent (1.0 mL)	Initial Observation	Observation after 24 h
11.0	0.06	25.8	Water	Colloidal	Partial gel
11.9	0.065	28.0	Water	Colloidal	Partial gel
12.8	0.07	30.1	Water	Colloidal	Gel
13.7	0.075	32.2	Water	Colloidal	Gel

Table S7: T_{gel} experiment for the metallogels

Complex	**Solvent**	*wt%*	T_{gel} (°C)
Zn-PNO	DMF/water (1:1 v/v)	2.8 (0.05 mmol)	98.3
Zn-PNO	DMF/water (1:1 v/v)	4.2 (0.075 mmol)	112.6
Zn-PNO	Water	3.4 (0.06 mmol)	106.7
Zn-PNO	Water	4.2 (0.075 mmol)	114.0
Zn-INO	Water	3.7 (0.065 mmol)	97.0
Zn-INO	Water	4.2 (0.075 mmol)	102.4
Cd-PNO	Water	3.7 (0.06 mmol)	100.5
Cd-PNO	Water	4.6 (0.075 mmol)	110.2
Cd-INO	Water	4.3 (0.07 mmol)	101.6
Cd-INO	Water	4.6 (0.075 mmol)	104.0

2. Scanning electron microscopy

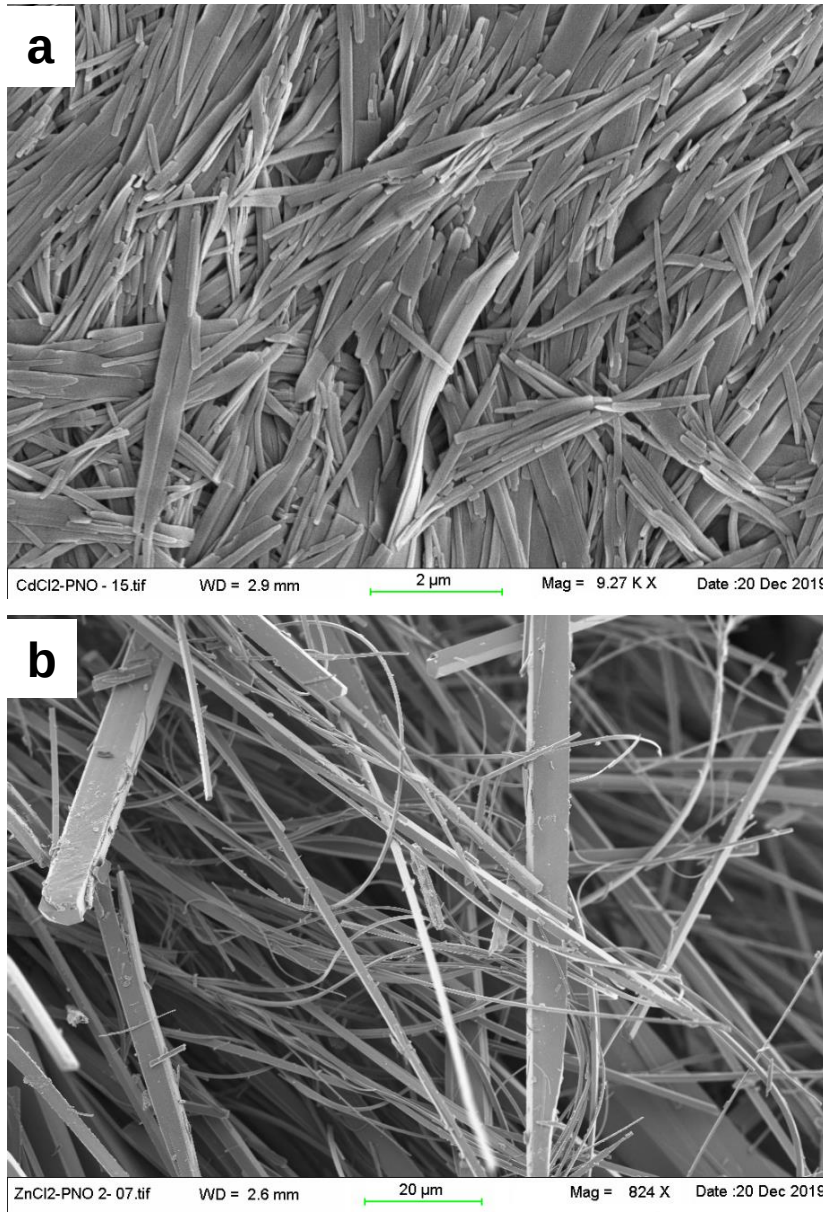

Figure S1: SEM images of xerogels of a Cd-**PNO** obtained from water at 3.7 wt% and b) Zn-**PNO** obtained from DMF/water (1:1, v/v) at 2.8 wt%.

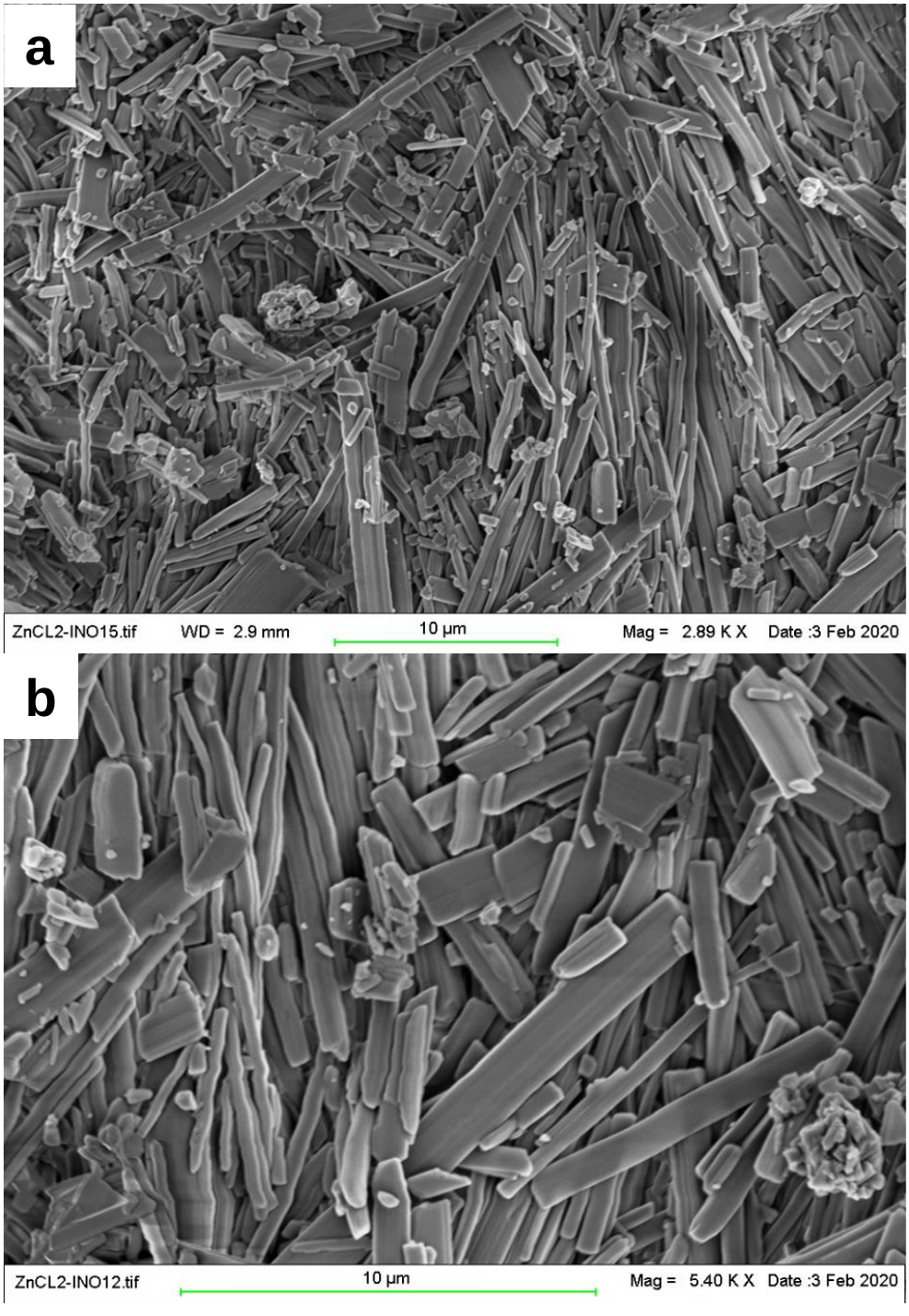

Figure S2: SEM images of xerogels of Zn-**INO** obtained from water at 3.7 wt%: a) overview and b) magnified image.

3. Crystal data

Table S8: Hydrogen-bonding table

$ZnCl_2$(**PNO**)$_2$						
Nr	Donor—H···Acceptor	D—H/**Å**	H···A/**Å**	D···A/**Å**	∠D—H···A/°	Symmetry operation
1	N(11)—H(11)···O(18)	0.86	1.97	2.783(3)	156	-1/4+x,3/4-y,-3/4+z
2	C(5) —H(5) ···O(10)	0.93	2.46	3.093(3)	125	3/2-x,1-y,-1/2+z
3	C(7) —H(7) ···O(18)	0.93	2.55	3.300(3)	138	-1/4+x,3/4-y,-3/4+z
4	C(16)—H(16)···Cl(2)	0.93	2.83	3.721(2)	162	1/4+x,3/4-y,7/4+z
5	C(17)—H(17)···O(18)	0.93	2.31	3.065(3)	138	-1/4+x,3/4-y,-3/4+z
$ZnCl_2$(**INO**)$_2$						
Nr	Donor—H···Acceptor	D—H/**Å**	H···A/**Å**	D···A/**Å**	∠D—H···A/°	Symmetry operation
1	N(9) —H(9) ···O(18)	0.86	2.05	2.8146(19)	148	2-x,1-y,1-z
2	C(7) —H(7) ···O(18)	0.93	2.54	3.248(2)	133	2-x,1-y,1-z
3	C(16)—H(16)···O(11)	0.93	2.30	3.142(2)	151	1+x,y,z

4. IR spectra of the complexes

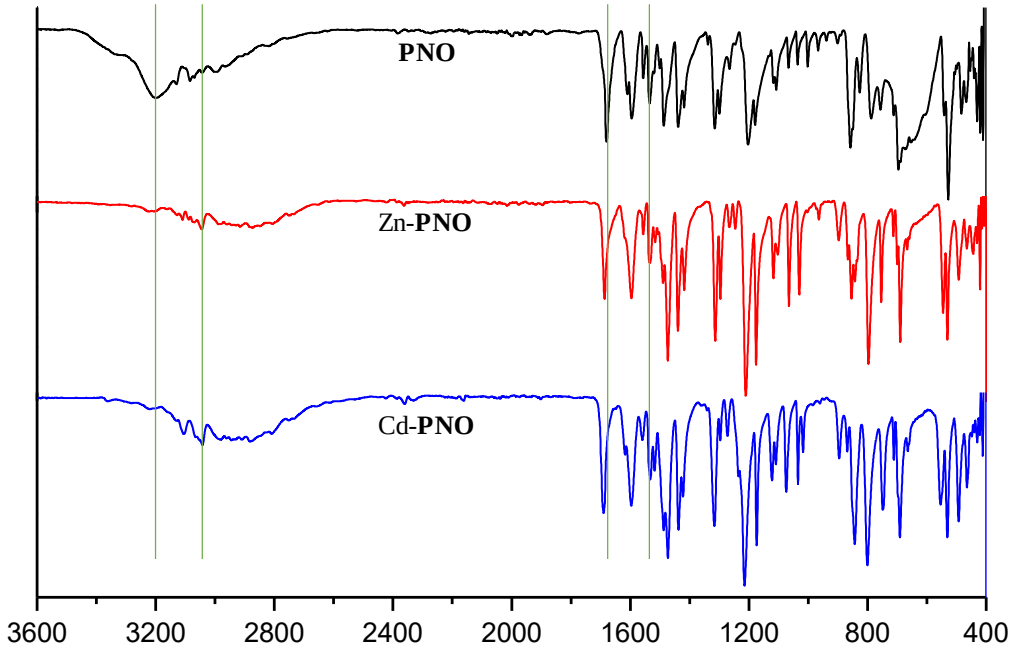

Figure S3: comparison of FT-IR spectra of **PNO**, **Zn-PNO** and **Cd-PNO**

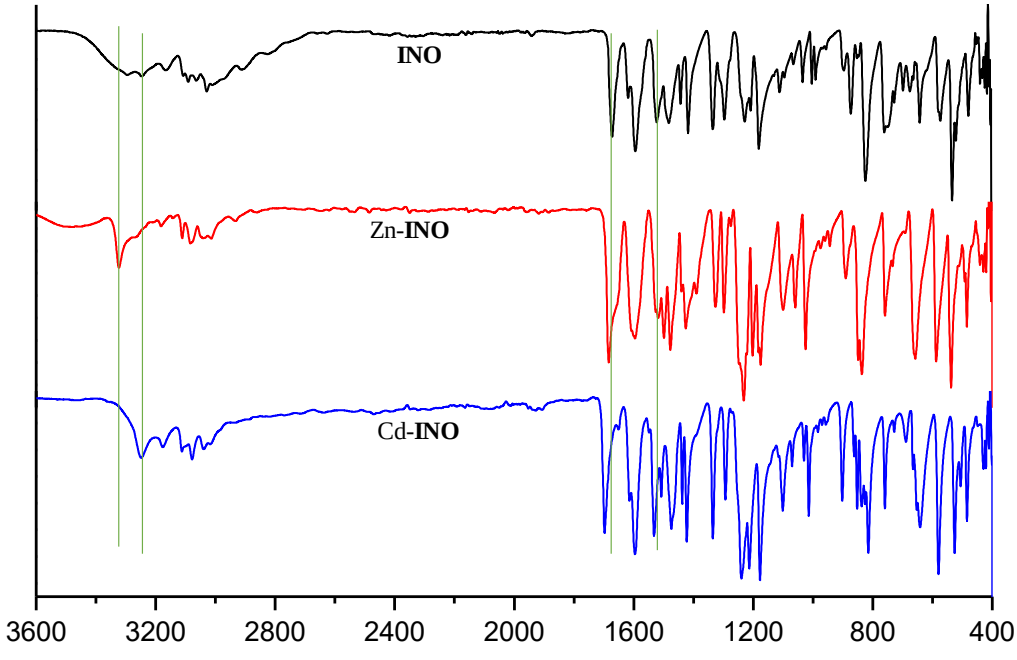

Figure S4: comparison of FT-IR spectra of **INO**, **Zn-INO** and **Cd-INO**

Table S9: IR-peaks for **PNO** and **INO** ligands and metal complexes.

Compound	Amide-A and amide-B (cm^{-1})	Amide-I (cm^{-1})	Amide-II (cm^{-1})
PNO	3193	1679	1556
Zn-PNO	3044	1686	1533
Cd-PNO	3042	1689	1532
INO	3247, 3029	1672	1522
Zn-INO	3323, 3083	1683	1518
Cd-INO	3248, 3078	1697	1532

5. X-ray powder diffraction

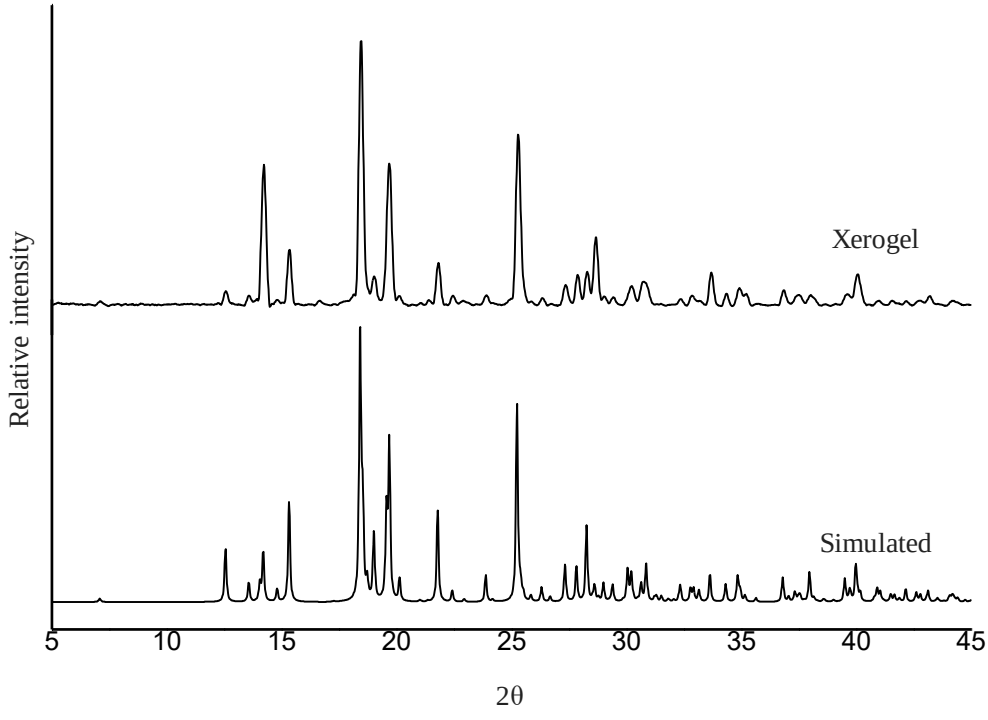

Figure S5: XRPD comparison of **Zn-INO**: simulated pattern obtained from single-crystal data (bottom) and xerogel (top) obtained from water at 3.7 wt%.

6. Anion sensing

Table S10: Effect of various anions on the metallogels

Metallogel	**Anions**				
	F^-	**Cl^-**	**Br^-**	**I^-**	**CN^-**
Zn-PNO	Gel was broken on adding 2 equivalent of F^-	Gel was stable up to 5 equivalent of Cl^-	Gel was stable up to 5 equivalent of Br^-	Gel was broken on adding 2 equivalent of I^-	Gel was broken on adding 2 equivalent of CN^-
Zn-INO	Gel was broken on adding 2 equivalent of F^-	Gel was stable up to 5 equivalent of Cl^-	Gel was stable up to 5 equivalent of Br^-	Gel was broken on adding 2 equivalent of I^-	Gel was broken on adding 2 equivalent of CN^-
Cd-PNO	Gel was stable up to 5 equivalent of F^-	Gel was stable up to 5 equivalent of Cl^-	Gel was stable up to 5 equivalent of Br^-	Gel was broken on adding 5 equivalent of I^-	Gel was broken on adding 2 equivalent of CN^-
Cd -INO	Gel was stable up to 5 equivalent of F^-	Gel was stable up to 5 equivalent of Cl^-	Gel was stable up to 5 equivalent of Br^-	Gel was broken on adding 5 equivalent of I^-	Gel was broken on adding 2 equivalent of CN^-

The equivalent amount was calculated with respect to the counter anion of the metal salt.

Zn-PNO and **Zn-INO** gels were prepared at 4.0 wt%, **Cd-PNO** and **Cd-INO** gels were prepared at 4.3 wt%. In both cases 0.07 mmol metal salt and 0.14 mmol ligand were dissolved in 1.0 mL water.

4 Analyzing the Self-Assembly Process of Multi-Component Gels Based on Enantiomers

Supramolecular gels constructed from multi-component systems have emerged as smart materials in recent time due to their application in tuning gel state properties.[23-24, 26, 149, 298-299] Multi-component gels are formed by mixing two or more components are in a well-defined stoichiometry resulting in either constructive (enhanced gel strength) or destructive (reduced gel strength) mixed gel. Mixing two or more components leads self-recognition at molecular level, and the individual components can be assembled separately (self-sorting), or randomly (random co-assembly), or combine in a well-ordered fashion (specific co-assembly) to construct a different network (*Scheme 1.7*).[149, 298] The process of self-sorting or co-assembly of the gelator is often dictated by the structural similarity between individual gels. However, predicting the self-assembly of multi-component gel is challenging due to the dynamic nature of LMWGs. Efforts have been made to understand the self-assembly process gelators from molecular to macroscopic level. Molecular level assembly are analyzed by various spectroscopic techniques such as UV-visible, infra-red (IR), nuclear magnetic resonance (NMR) and circular dichroism (CD).[158, 169-173] On the other hand, microscopic techniques such as scanning electron microscopy (SEM), transmission electron microscopy (TEM), cryogenic transmission electron microscopy (cryo-TEM), small angle scattering (SAXS) atomic force microscopy (AFM) and confocal laser scanning microscopy (CLSM) are widely used to visualize the morphology of self-assembled fibers in mesoscopic scale.[174-178] The effect of the self-assembly in the mixed gels are analyzed by evaluating physical properties such as differential scanning calorimetry (DSC), rheology, powder X-ray diffraction (PXRD), fiber X-ray diffraction etc.[159-160, 179-184]

A simple way to construct multi-component gel is by mixing enantiomers. Supramolecular gels based on chiral gelators have emerged as a special class of soft materials due to the potential application in asymmetric catalysis, chiral nanomaterials and chiral recognition. The molecular chirality is often translated at mesoscopic scale, which is evident from the helical morphology observed in SEM or AFM. Mixing two enantiomers lead to self-recognition at the molecular level, which can result to self-sorting or co-assembly of the enantiomers. The mixing can be either constructive or destructive, i.e., the mixed gel may display stronger or weaker gelling ability compared to pure enantiomers.

In this doctoral study, bis(urea) or bis(amide) have been used as gelator since they are excellent class of LMWGs, and capable of forming both hydro- and organogels. Bis(urea) gelators form α-tape type one-dimensional hydrogen bonded network through urea N—H and C=O moieties.[110] Similarly, bis(amide) forms β-tape network through amide N—H and C=O groups. Chirality is introduced by using methyl ester protected α-amino acids as amine components in the synthesis of bis(urea) or bis(amide). Amino acids are used due to the availability in both enantiomeric and racemate forms, feasible transformation to urea or amides and cost efficiency. The carboxylic acid group is protected by converting to corresponding methyl esters to prevent hydrogen bonding between carboxylic acid and urea/amide groups, resulting in self-aggregation of urea/amide moiety and forming the desired one-dimensional network.

4.1 Article V

The first system we studied is a bis-urea tagged with methyl phenylalaninate moiety. Bis-urea compounds has been extensively used as a supramolecular synthon for the self-assembly of LMWGs[110, 300] due to the ability of forming one-dimensional hydrogen bonded structures. Mixing the two enantiomeric bis(urea) will lead to reassembly of the compounds at molecular level, which will influence the overall gel network. Analysis of self-assembly in multi-component bis(urea) gelator and correlation to gel strength is reported in *Article-V*.

4.2 Article VI

The next multi-component system studied was a bis(amide) tagged with methyl valinate. 1,4-benzene diamides (BDA) are excellent supramolecular synthons due to the C_2 symmetric structure and BDA derivatives of amino acids have been reported to show impressive gelation properties. The 1,4-disubstiturted benzene derivatives are crystalline, which opens the possibility to probe the self-assembly by crystallographic evidence. Furthermore, the BDA derivatives can be synthesized in all stereoisomeric forms (*R*-*R*, *S*-*S* and *R*-*S*). The self-assembly of the individual gelators and the mix enantiomeric gel was studied, and we reported the first crystallographic evidence of specific co-assembly in multi-component gel based on enantiomers in *Article-VI*.

Article-V

This project is published in a peer reviewed journal and included as it was published. Slight differences might appear from the original article due to the formatting issue.

Publication details:

″Enhanced Mechanical and Thermal Strength in Mixed-Enantiomers-Based Supramolecular Gel″

Daníel Arnar Tómasson, Dipankar Ghosh, Zala Kržišnik, Luiz Henrique Fasolin, António A. Vicente, Adam D. Martin, Pall Thordarson and Krishna K. Damodaran*

Langmuir, **2018**, *34* (43), 12957–12967.

D.A.T. and **D.G.** contributed equally.

Author contributions:

K.K.D. planned and designed the research; D.A.T. synthesized and characterized the gelators, performed gelation experiments, SEM, AFM and optical rotation. **D.G.** synthesized the gelators, performed rheology, CD and solid-state NMR. L.H.F. and A.V. helped with rheometer instrument and A.D.M. and P.T. helped with AFM, CD and solid-state NMR instrument at collaboration. K.K.D. wrote the initial manuscript draft and all authors reviewed the main manuscript.

LANGMUIR Article
Cite This: Langmuir 2018, 34, 12957−12967 pubs.acs.org/Langmuir

Enhanced Mechanical and Thermal Strength in Mixed-Enantiomers-Based Supramolecular Gel

Daníel Arnar Tómasson,[†,∥] Dipankar Ghosh,[†,∥] Zala Kržišnik,[†] Luiz Henrique Fasolin,[‡] António A. Vicente,[‡] Adam D. Martin,[§] Pall Thordarson,[§] and Krishna K. Damodaran*[,†]

[†]Department of Chemistry, Science Institute, University of Iceland, Dunhagi 3, 107 Reykjavík, Iceland
[‡]Centre of Biological Engineering, University of Minho, Campus de Gualtar, 4710-057 Braga, Portugal
[§]School of Chemistry, The Australian Centre for Nanomedicine and the ARC Centre of Excellence in Convergent Bio-Nano Science and Technology, University of New South Wales, Sydney 2052, Australia

Supporting Information

ABSTRACT: Mixing supramolecular gels based on enantiomers leads to re-arrangement of gel fibers at the molecular level, which results in more favorable packing and tunable properties. Bis(urea) compounds tagged with a phenylalanine methyl ester in racemic and enantiopure forms were synthesized. Both enantiopure and racemate compounds formed gels in a wide range of solvents and the racemate (**1-rac**) formed a stronger gel network compared with the enantiomers. The gel (**1R+1S**) obtained by mixing equimolar amount of enantiomers (**1R** and **1S**) showed enhanced mechanical and thermal stability compared to enantiomers and racemate gels. The preservation of chirality in these compounds was analyzed by circular dichroism and optical rotation measurements. Analysis of the scanning electron microscopy (SEM) and atomic force microscopy (AFM) images revealed that the network in the mixed gel is a combination of enantiomers and racemate fibers, which was further supported by solid-state NMR. The analysis of the packing in xerogels by solid-state NMR spectra and the existence of twisted-tape morphology in SEM and AFM images confirmed the presence of both self-sorted and co-assembled fibers in mixed gel. The enhanced thermal and mechanical strength may be attributed to the enhanced intermolecular forces between the racemate and the enantiomer and the combination of both self-sorted and co-assembled enantiomers in the mixed gel.

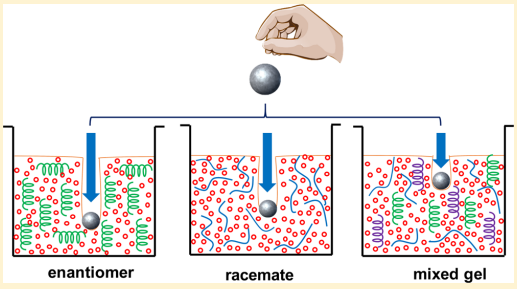

INTRODUCTION

Supramolecular gels based on low-molecular-weight gelators (LMWGs)[1−9] have witnessed a tremendous growth over the last decade due to their emerging potential applications[10−16] such as dynamic gels, biological applications using gels as cell growth scaffolds and also as a medium to control crystal growth, drug delivery, etc. Although the majority of these gelators are based on individual molecules, gels based on multicomponent systems have emerged as smart materials due to their application in tuning gel state properties.[17−30] Multicomponent gels are formed when two or more components are mixed together in a well-defined stoichiometry and also by introducing an external entity such as nanoparticles,[31] graphene,[32,33] carbon nanotubes,[34] clay nanosheets,[35] liquid crystal,[36] surfactants,[37,38] and polymers[39−41] to an individual system to trigger gelation process. Multicomponent gels based on mixing individual gels are less explored, which will lead to the co-assembly or self-sorting of individual gels either constructively or destructively, resulting in mixtures of gel and crystals[42] or "multi-gelator" gels.[20,43−45] The self-sorting processes of multicomponent gels can be analyzed by various analytical methods (NMR, X-ray diffraction, etc.)[8,45,46] and also by direct and real-time imaging of self-sorted supramolecular fibers.[47] However, predicting the formation of co-assembled or self-sorted multicomponent gels is challenging due to differences in their mutual interactions and the gelation conditions. The co-assembly and self-sorting is often dictated by the structural similarity between individual gels.[18] An excellent strategy is to use enantiomers, for example, chiral gels to design multicomponent systems with structurally similar components.

Chiral LMWGs have proved to be an excellent class of soft materials[14,43,48−50] due to their potential applications in the field of asymmetric catalysis, chiral nanomaterials, and chiral recognition. Gel fibers often show chirality at a mesoscopic scale, which is evident from their morphology (helical cylinders or multiple helices),[48] and Gunnlaugsson and Pfeffer's group showed that chirality of the gelator dictates the self-assembly

Received: August 10, 2018
Revised: September 27, 2018
Published: October 1, 2018

processes of gels resulting in the formation of helical materials.[51] Chirality plays an important role in controlling and mediating the self-assembly of LMWGs, which clearly explains the occurrence of stereogenic centers[14,43,48,49,52] in most LMWGs. LMWGs based on enantiomerically pure chiral molecules display strong gelling ability compared to their racemates.[43,46,53,54] Interestingly, when pure enantiomers are less efficient gelators or nongelators, a reverse phenomenon is observed.[55−62] A racemate LMWG can be considered as a multicomponent gel, where two structurally similar compounds are present in stoichiometric ratio. Mixing of enantiomers leads to self-recognition at the molecular level and pure enantiomers would interact with enantiomers, which may lead to more favorable packing and better gels.[18,63−65]

Multicomponent self-assembled gels obtained by mixing enantiomers have shown different properties compared to the individual gels.[63,65−69] For example, Schneider's group reported that mixing an equimolar ratio of enantiomers enhanced the mechanical strength of amino acid-based gels.[67,70] This is due to the structural similarity of enantiomers, which will either self-sort or co-assemble depending on the environment. Self-sorting occurs when enantiomers independently assemble and retain their chirality, whereas in the case of co-assembly, it may result in random or specific co-assembly similar to its racemate (Scheme 1). In a mixed enantiomer

Scheme 1. Self-Assembly Modes in Mixed Gels

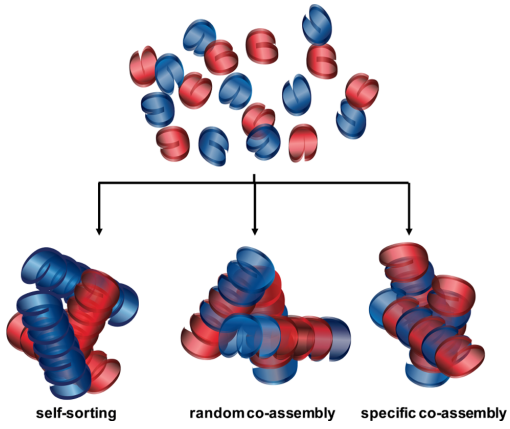

system, the interaction of enantiomers with the same conformation results in separate aggregates via self-sorting, which may lead to conglomerate formation.[18] Based on their studies on amphipathic peptides, Nilsson and co-workers proposed that enantiomers form co-assembled rippled β-sheet fibrils rather than self-sorting.[63] In this work, we have designed multicomponent gels based on amino acid compounds to analyze the difference between the self-assembly of pure and mixed enantiomers. Enantiomeric multicomponent gels based on amino acid derivatives are ideal candidates due to the fact that they are available in enantiomeric and racemic forms, easily accessible, relatively cheap, and easy to modify the substituent groups.[64]

EXPERIMENTAL SECTION

Materials and Methods. All the starting materials and reagents were commercially available (Sigma Aldrich) and used as supplied. Deionized water was used for gelation test and solvent chloroform was distilled over P_2O_5, and methanol over Mg turnings in the presence of small amount of iodine.

Synthesis. *Methyl-rac-phenylalaninate.* Five grams (30.0 mmol) of *rac*-phenylalanine was dissolved in 70 mL of methanol and 2 mL of conc. H_2SO_4 was added. The solution was refluxed overnight and then cooled to room temperature. Methanol was evaporated and the white oil obtained was stirred with 2% $NaHCO_3$ solution. The solution was extracted with DCM (3 × 75 mL), the combined organic layers were dried over Na_2SO_4 and evaporated to yield the ester as white powder. Yield: 4.99 g, 92%. ^{1}H NMR (400 MHz, $CDCl_3$): δ [ppm] = 7.32−7.18 (m, 5H), 3.74 (dd, J = 8.0, 5.2, 1H), 3.72 (s, 3H), 3.09 (dd, J = 13.5, 5.1, 1H), 2.86 (dd, J = 13.5, 7.9, 1H), 1.47 (s, 2H).

*General Synthesis of R−R Bis(urea) (**1R**) and S−S Bis(urea) (**1S**) Compounds.* The phenylalanine methyl ester hydrochloride (1.3 g, 6.0 mmol, either **R** or **S**) was dissolved in 60 mL chloroform and 3 mL of trimethylamine was added. A solution of 1,6-disocyanatohexane (482 μL, 3.0 mmol) in chloroform (40 mL) was added dropwise under N_2 atmosphere over a period of 1 h. The solution was then refluxed at 60 °C overnight, cooled to room temperature and the solvent was evaporated to yield a white oil. The oil was dried in air and suspended in 50 mL distilled water and stirred. The suspension was filtered, washed with ethyl acetate, and dried to yield the desired product as a white powder.

1R: Yield: 1.50 g, 95.0%. ^{1}H NMR (400 MHz, DMSO-d_6) δ 7.31−7.13 (m, 10H), 6.11 (d, J = 8.2 Hz, 2H), 6.05 (t, J = 5.7 Hz, 2H), 4.39 (td, J = 8.0, 5.6 Hz, 2H), 3.59 (s, 6H), 2.99−2.82 (m, 8H), 1.35−1.16 (m, 8H). ^{13}C NMR (100 MHz, DMSO-d_6) δ 173.19, 157.49, 137.19, 129.21, 128.34, 126.62, 54.09, 51.74, 39.15, 37.71, 29.94, 26.13. HRMS (APCI) Calcd for $C_{28}H_{38}N_4O_6$ 526.28; found 549.26 [M + Na]$^+$.

1S: Yield: 1.46 g, 92.3%. ^{1}H NMR (400 MHz, DMSO-d_6) δ 7.38−7.07 (m, 10H), 6.12 (d, J = 8.2 Hz, 2H), 6.06 (t, J = 5.9 Hz, 2H), 4.40 (td, J = 8.0, 5.6 Hz, 2H), 3.59 (s, 6H), 2.93 (m, J = 17.1, 8.9, 7.9 Hz, 8H), 1.42−1.09 (m, 8H). ^{13}C NMR (100 MHz, DMSO-d_6) δ 173.20, 157.52, 137.20, 129.22, 128.35, 126.64, 54.11, 51.76, 39.17, 37.73, 29.96, 26.14. HRMS (APCI) Calcd for $C_{28}H_{38}N_4O_6$ 526.28; found 549.26 [M + Na]$^+$.

*Synthesis of Racemic Bis(urea) (**1-rac**).* The *rac*-phenylalanine methyl ester (1.11 g, 6.2 mmol) was dissolved in 60 mL chloroform and 2 mL of trimethylamine was added. A solution of 1,6-disocyanatohexane (500 μL, 3.1 mmol) in chloroform (40 mL) was added dropwise under N_2 atmosphere over a period of 1 h. The resulting mixture was refluxed at 60 °C overnight, cooled to room temperature, and a similar reaction workup for **1R** was followed to yield the desired product as a white powder. Yield: 1.57 g, 96.3%. ^{1}H NMR (400 MHz, DMSO-d_6) δ 7.33−7.12 (m, 10H), 6.11 (d, J = 8.2 Hz, 2H), 6.05 (t, J = 5.7 Hz, 2H), 4.39 (td, J = 8.1, 5.6 Hz, 2H), 3.59 (s, 6H), 3.00−2.82 (m, 8H), 1.34−1.24 (m, 4H), 1.24−1.15 (m, 4H). ^{13}C NMR (100 MHz, DMSO-d_6) δ 173.22, 157.55, 137.21, 129.24, 128.37, 126.66, 54.13, 51.78, 39.18, 37.74, 29.97, 26.15. HRMS (APCI) Calcd for $C_{28}H_{38}N_4O_6$ 526.28; found 549.26 [M + Na]$^+$.

Gelation Details. *Gelation Test.* Ten milligrams of gelator was taken in a test tube and 1 mL of appropriate solvent was added. The mixed solution was heated until the compound was completely dissolved. The test tube was then sonicated and left undisturbed for gelation, and the gel formation was confirmed by inversion test.

Minimum Gel Concentration (MGC). Ten milligrams of the gelator **1R**, **1S**, or **1-rac** was placed in a vial and 1 mL of solvent was added. The vial was heated until a clear solution was obtained. The solution was then sonicated and left to cool to room temperature for gelation. Additional solvent was added in portions and the gelation process was repeated until a small amount of solvent was left on top of the gel. The excess solvent was then decanted and MGC was calculated by weight. Similar experiments were performed for the **1R**

DOI: 10.1021/acs.langmuir.8b02729
Langmuir 2018, 34, 12957−12967

Scheme 2. Synthesis of 1R, 1S, and 1-rac Bis(urea) Compounds

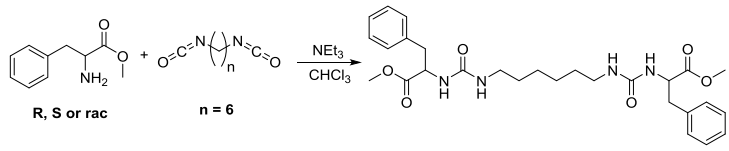

+1S mixed gel, which was prepared by mixing equal amounts of **1R** and **1S**.

T_{gel} Experiment. Ten milligrams of the gelator (**1R**, **1S**, or **1-rac**) was taken in a standard 7 mL vial and 1 mL of appropriate solvent was added. The solution was heated and sonicated to dissolve the compound and allowed to stand undisturbed. After 24 h, a small spherical glass ball (92 mg) was placed on the top of the gel. The vial was placed over an oil bath equipped with a magnetic stirrer and a thermometer. The oil bath was gradually heated and the observation was noted. The temperature at which the glass ball touched the bottom of the vial was recorded as T_{gel}. Similar experiments were performed for the **1R+1S** mixed gels by mixing 5 mg of each **1R** and **1S**.

Rheology. The rheological study was performed by using a TA Instruments Advanced Rheometer 2000 and toluene was selected as the gelling solvent. The gels of **1R**, **1S**, and **1-rac** were prepared by heating 50 mg of the corresponding gelator in 1 mL toluene and the resulting solutions were kept at room temperature without disturbing for 1 h. The **1R+1S** gel was prepared by mixing equal amounts of **1R** and **1S** (25 mg in 0.5 mL toluene), heating, and leaving at room temperature without disturbing for 1 h. A stainless steel cone-plate geometry (20 mm, 2° angle, truncation 64 μm) was used. Viscoelastic properties were evaluated by oscillatory measurements using a frequency sweep between 0.1 and 10 Hz within the linear viscoelasticity domain (0.05% deformation). Complex moduli (G^*) and tan δ were evaluated. Mechanical properties were determined by uniaxial compression measurements using a TA HD Plus Texture Analyzer (Stable Micro Systems, UK) with a stainless steel 0.5 mm probe. The probe penetrated 80% of the initial height using a crosshead speed of 1 mm/s.

Scanning Electron Microscopy (SEM). Twenty milligrams of the gelator (**1R**, **1S**, or **1-rac**) was dissolved in 1 mL of toluene/ethyl acetate by heating and sonicating. The solution was allowed to stand undisturbed to form the gel. After 24 h, it was filtered through a filter paper and the residue was dried in air. The **1R+1S** xerogel was prepared by same procedure using the gel obtained by mixing equal amounts of **1R** and **1S**. The xerogels were gold coated and placed on a Leo Supra 25 microscope for scanning electron microscopy and the morphologies of the dried gels were examined by SEM. The EtOH/water xerogels were lightly dusted onto double-sided carbon tape and then coated with a 30 nm layer of platinum using a Leica EM ACE600, where the thickness was monitored using a film thickness monitor. The SEM imaging for EtOH/water gels were undertaken on a NanoSEM 230 fitted with a through lens detector at an operating voltage of 5 kV, with a working distance between 4.9 and 5.7 mm.

Atomic Force Microscopy (AFM). Gels of **1R**, **1S** (0.7 wt %), **1-rac** (0.15 wt %), and **1R+1S** (0.3 wt %) were dispersed in appropriate solvent (toluene or EtOH/water), heated to dissolve, and cooled to form gels within 5 min. The solutions were diluted 5× (100 + 400 μL solvent) and 10× (100 + 900 μL solvent). One drop of the organogel in its solution phase was cast onto a mica substrate, followed by spreading of the drop over the mica using a glass slide, with the excess liquid wicked away using capillary action. The samples were left to dry overnight before imaging, which was undertaken on a Bruker Mulitmode 8 Atomic Force Microscope in Scanasyst Air (PeakForce Tapping) mode, which is based upon tapping mode AFM, but the imaging parameters are constantly optimized through the force curves that are collected, preventing damage to soft samples. Bruker Scanasyst-Air probes were used, with a spring constant of 0.4−0.8 nm and a tip radius of 2 nm.

Circular Dichroism (CD). The data were collected using a ChirascanPlus CD spectrometer (Applied Photophysics, UK) scanning between wavelengths of 180 and 500 nm with a bandwidth of 1 nm, 0.6 s per point, and step of 1 nm. The gels of **1R**, **1S**, **1-rac**, and (**R+1S** were prepared at their minimum gel concentration in EtOH/water (1:1 v/v). After 24 h, the gel was dispersed in EtOH/water (1:1 v/v) to obtain various concentrations (0.005, 0.025, and 0.05 wt %) for CD experiments. The CD experiments in the solution state were performed by dissolving 2.5 mg of the gelator (either **1R**, **1S**, **1-rac**, or **1R+1S**) in 10 mL of absolute ethanol.

Optical Rotation Measurements (OD). The OD experiments for both enantiomers, the racemic mixture, and the mixed gel (at 50/50 wt/wt) were carried out at 589 nm, on an Autopol V from Rudolph research analytical, in both a gelling solvent (toluene) and a nongelling solvent (2-butanol). Due to the opaque nature of the gel, the concentration was kept under the minimum gel concentration.

NMR Experiments. The solution state ^{1}H and ^{13}C NMR spectra were recorded on Bruker Advance 400 spectrometer (^{1}H NMR: 400 MHz, ^{13}C NMR: 100 MHz). The solid-state NMR spectra were recorded on Bruker Avance III 700 MHz spectrometer on xerogels of **1R**, **1S**, **1-rac**, and **1R+1S** in toluene at 1 wt %.

RESULTS AND DISCUSSION

We have selected the bis(urea) moiety as a hydrogen-bonding backbone, which has been extensively used as a supramolecular synthon for the self-assembly of gelators in LMWGs with tunable properties.[71−76] Compounds based on bis(urea) ligands form a α-urea tape structure, which will result in a one-dimensional tape-like network (fibrils), and these fibrils aggregate to form an interconnected, entangled 3-D framework capable of immobilizing solvent molecules, thereby inducing gelation in small molecules.[7,77−81] Enantiopure *R*−*R* (**1R**) and *S*−*S* (**1S**) bis(urea) compounds based on amino acid derivatives were synthesized by reacting 1,6-diisocyanatohexane and the corresponding methyl ester protected amino acid hydrochloride in chloroform.[81−83] The racemate bis(urea) compound (**1-rac**), which is a statistical mixture of *R*−*S*, *R*−*R*, and *S*−*S* (see the Supporting Information), was synthesized by reacting racemate phenylalanine methyl ester with 1,6-diisocyanatohexane in chloroform (Scheme 2). The gelation properties of these compounds were tested in a series of solvents.

Gelation Experiments. The initial screening was performed in a series of solvents with 1 wt % of the compound. In a typical experiment, the compounds were heated and sonicated in a particular solvent to get a clear solution, cooled to room temperature, and the gel formation was confirmed by inversion test (Figure 1). All the three bis(urea) compounds (**1R**, **1S**, and **1-rac**) formed gels in 1,2-dichloroethane, benzene, toluene, *o*-xylene, *m*-xylene, *p*-xylene, chlorobenzene, ethyl acetate, 2-butanone, and nitrobenzene. It is quite interesting that all the three forms (both enantiomeric and racemate) show gelation for a wide range of solvents. Generally, selective gelation is observed with either the enantiomers or racemate,[46,53,54,56,84] but gel formation of both enantiomers and racemate is rare.[56,57,85,86] The selective

DOI: 10.1021/acs.langmuir.8b02729
Langmuir 2018, 34, 12957−12967

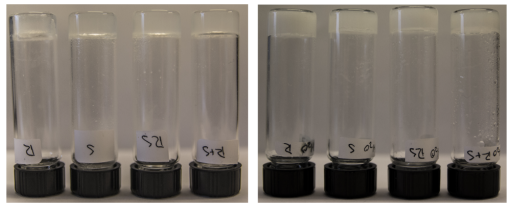

Figure 1. Gel images (left) in toluene and (right) EtOH/water (50% v/v).

gelation of **1-rac** at 1 wt % was observed in cyclohexanone and mesitylene (Table S1, see the Supporting Information). The occurrence of partial gels prompted us to check the gelation of the compounds at higher concentrations, and the gels were obtained at higher wt % for **1R** and **1S** in mesitylene (2 wt %). The gels were formed at 2 w% for the racemate **1-rac** in isopropanol, 2-pentanol, and *n*-pentanol and in ethanol at 3 wt %. We have also checked the gelation properties in aqueous solution by using 50% (v/v) of water and a co-solvent (either methanol, ethanol, DMA, DMF, and DMSO) to dissolve the compounds. The hydrogels were obtained at 1 wt % for most of the cases except for **1-rac** in DMF/water and DMSO/water, where gelation occurred at 2 wt %.

The minimum gel concentration of the gelators were evaluated in solvents such as ethyl acetate, 2-butanone, toluene, chlorobenzene, xylenes (*ortho*-, *meta*-, and *para*-), and nitrobenzene (Table S2, see the Supporting Information). Interestingly, **1-rac** compounds formed gels at lower concentration compared to **1R** and **1S**. The **1-rac** gels formed in toluene, chlorobenzene, and xylenes (*ortho*-, *meta*-, and *para*-) can be classified as supergelators. Specifically, less than half the concentration was required to form the gels for **1-rac** gels compared to enantiomerically pure gels, indicating that the presence of both isomers increases the gelling ability. This may be attributed to the $\pi-\pi$ interaction between the solvents and the gelator molecules in the 3-D network within which the solvent molecules are entrapped. Furthermore, the α-sheet-like structure of the urea network could be preserved due to the absence of the strong hydrogen-bonding moieties. These results clearly indicate that both **1R** and **1S** self-assemble to form a strong network in the racemate form **1-rac**. This leads to an interesting question, what happens when two enantiomers are mixed? Will **1R** and **1S** undergo self-sorting or co-assembly to form conglomerate or racemate? This prompted us to evaluate the gelation property of mixed enantiomers by mixing equal amounts of **1R** and **1S** in a series of solvents at 1 wt % resulting in mixed gels. The mixed gel turned out to be an excellent multicomponent gel, and the gels were formed in 23 solvents. Analyzing the gelation results revealed that **1R+1S** formed gel at 1 wt % in solvents such as acetonitrile, tetrahydrofuran, acetone, 2-butanol, *n*-butanol, and 1,4-dioxane and 2 wt % in *n*-propanol, whereas **1R**, **1S**, and **1-rac** did not form gel in these solvents (Table S1, see the Supporting Information). The experiments performed on mixed gels prepared by mixing equimolar solutions of **1R** and **1S** resulted in similar gelation properties.

Gel Strength. The thermal stability of the gel network was evaluated using gel-to-solution transition temperature test (T_{gel}). To compare the gel strength, we selected solvents such as toluene, ethyl acetate, xylenes (*ortho*-, *meta*-, and *para*-), 2-butanone, chlorobenzene, and EtOH/water (50% v/v) and the gel concentration was fixed at 1 wt %. The analysis of the results revealed that T_{gel} of **1R** in toluene, m-xylene, and *p*-xylene is higher compared to **1S** and **1-rac** gels (Table 1). In other cases, the **1-rac** gel displayed the highest T_{gel} value, indicating a thermally stronger network, whereas **1S** showed similar or lower values than **1R**. Interestingly, there is a distinct difference in **1R+1S** mixture T_{gel}, which is higher than that of pure enantiomers and racemate in all cases (Table 1). A difference of 10−20 °C was observed for toluene, ethyl acetate, and 2-butanone. This clearly indicates that the 3-D network in the enantiomers and the mixed gels is different. This was confirmed by variable temperature rheology experiments in toluene (Figure S1, see the Supporting Information). We have also compared the T_{gel} of the hydrogels obtained from EtOH/water (1:1, v/v), and **1R+1S** gels showed greater thermal stability compared to the enantiomers and the racemate gels. The enhanced thermal stability of the mixed gel (**1R+1S**) may be attributed to the self-assembly of these components into a new or mixed network as compared to the enantiomer and racemate fibrils. The T_{gel} experiments performed on 1 wt % of mixed gels by varying the concentration of both **1R** and **1S** revealed that the gel formation of **1R+1S** depends on **1R** and **1S** concentrations, respectively (Figure 2).

Table 1. Gel−Sol Transition Temperature (°C) of the Enantiomers, Racemate, and Mixed Gels at 1 wt %

solvent	1R	1S	1-rac	1R+1S
toluene	91.0	86.5	85.0	106.5
ethyl acetate	55.0	54.5	61.0	73.5
p-xylene	94.0	91.0	98.0	102.0
m-xylene	99.0	95.0	97.0	102.0
o-xylene	92.0	91.0	90.0	99.0
2-butanone	38.0	37.5	40.0	55.5
chlorobenzene	73.0	70.5	75.5	90.5
EtOH/water	51.5	44.5	52.5	55.5

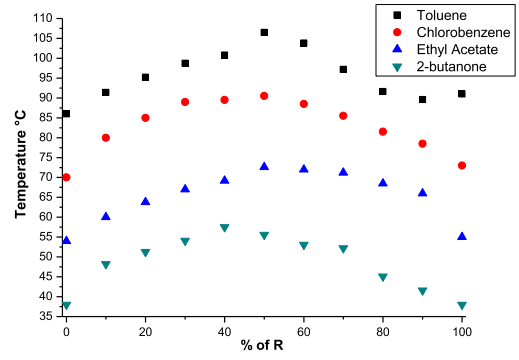

Figure 2. T_{gel} of **1R+1S** gels by varying the concentration of both **1S** and **1R** in toluene, ethyl acetate chlorobenzene, and 2-butanone.

Rheology. Rheology was used to evaluate the structural characteristics of supramolecular gels, which enables us to elucidate the information regarding factors controlling the gelation, gel strength, and the solid-like properties of pure gels. For example, Adams and co-workers reported that the combination of self-sorted LMWGs and photoresponsive

DOI: 10.1021/acs.langmuir.8b02729
Langmuir 2018, 34, 12957−12967

gelators offers the possibility of spatially controlling the rheological properties of LMWG.[45] We performed frequency sweep experiments to compare the relative gel behavior of **1R**, **1S**, **1-rac**, and **1R+1S** in toluene at 5 wt %. Elastic (G') and viscous (G'') moduli were evaluated, as well as the complex modulus ($G^* = \sqrt{G'^2 + G''^2}$) and tan δ (G''/G').

It is worth mentioning that a strain sweep was also carried out to determine the linear viscoelastic region. This ensured that the systems did not undergo an irreversible deformation during the experiments and the original structure of the organogels can be evaluated. All the organogels showed a gel-like behavior with no frequency dependence (Figure 3). The

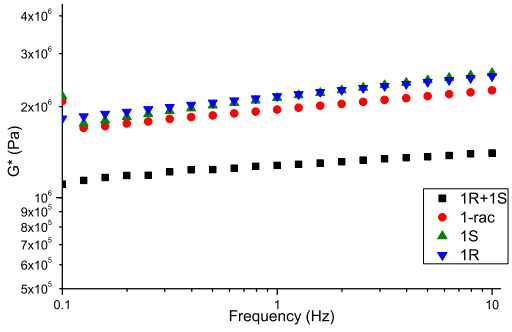

Figure 3. Complex modulus G^* for gels produced with **1R**, **1S**, **1-rac**, and **1R+1S** in toluene at 5 wt %.

1R, **1S**, and **1-rac** gels exhibited very similar G^* behavior. However, the **1R+1S** gel had a slightly lower complex modulus (G^*) value, indicating the presence of a weak fibrous network in comparison to other gels. It should be noted that the G' values of **1R+1S** were not so different from those of other gels, but the viscous contribution (G'') was higher for **1R**, **1S**, and **1-rac** systems, leading to higher values of G^*. Indeed, tan δ results presented lower values for the **1R+1S** system, whereas the other gels remained very close to each other (Figure S2, see the Supporting Information). The lower tan δ value indicates a prevailing elastic modulus (G'), i.e., more solid characteristic, which will enable the network to withstand higher applied forces without irreversible deformation. The mechanical strength of all the gels was compared by evaluating the force required to penetrate a certain distance through a gel, plotting force vs distance (Figure 4). Unlike rheological analysis, mechanical properties measure high and irreversible deformation, complementing the rheological results, which are performed at small deformations. These results clearly indicate that **1R**, **1S**, and **1-rac** showed similar behavior with maximum forces with same magnitude. On the other hand, a higher maximum force was observed for the mixed gels (**1R+1S**). Moreover, a larger area under the curve also means a stronger structure, which was observed for **1R+1S**, indicating that this gel was stronger in comparison to the other systems. Mechanical results corroborated rheological tests, showing that **1R+1S** presented more solid character with higher resistance to applied forces.

Gel Morphology. The morphologies of all the gels were analyzed by scanning electron microscopy (SEM). All the gels were prepared at 2 wt % in toluene and ethyl acetate, then filtered, and dried under a fume hood for 2−3 days. A small

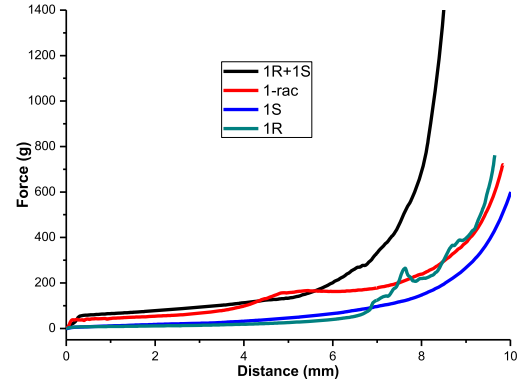

Figure 4. Comparison of mechanical strength for gels **1R**, **1S**, **1-rac**, and **1R+1S** in toluene at 5 wt %.

portion of the dried gel was placed on a pin mount with graphite planchets on top and coated with gold for 3 min. The SEM images revealed that all xerogels display typical fibrous and helical network (Figures 5 and 6). The SEM images of the xerogels from ethyl acetate showed that **1R** and **1S** form a helical fibrous network (Figure S3). The individual fibrils form

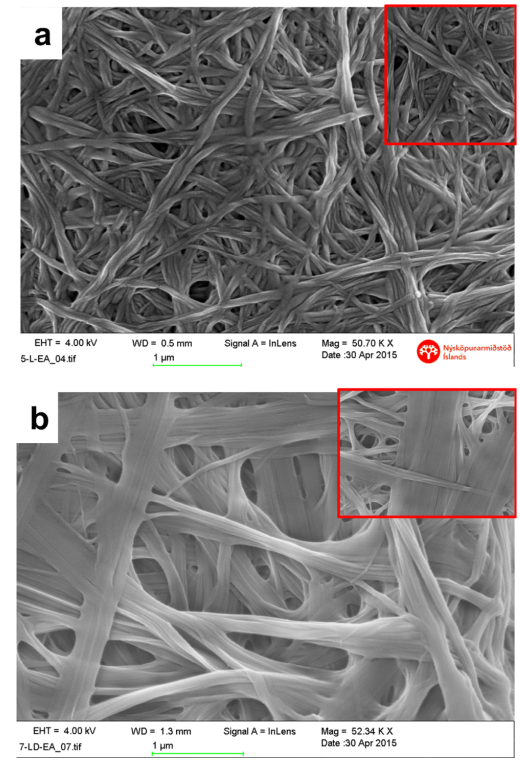

Figure 5. SEM images of (a) **1S** and (b) **1-rac** xerogels in ethyl acetate, inset shows the magnified images.

DOI: 10.1021/acs.langmuir.8b02729
Langmuir 2018, 34, 12957−12967

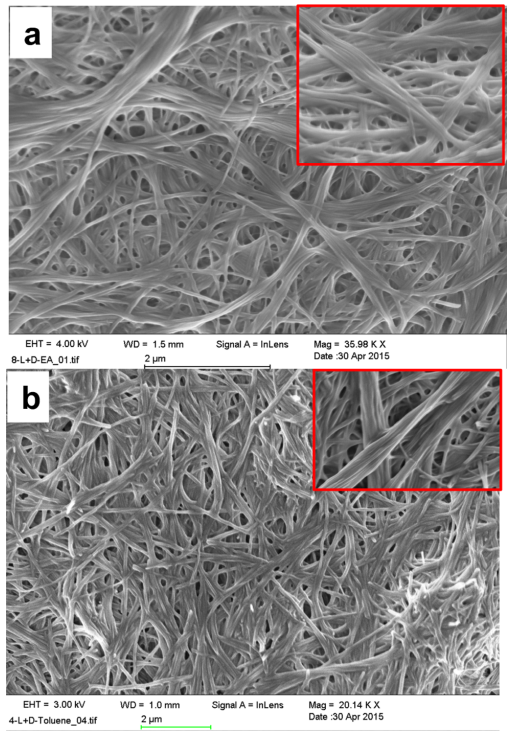

Figure 6. SEM images of **1R+1S** xerogels in (a) ethyl acetate and (b) toluene, inset shows the twisted-tape morphology.

helical fibrous aggregates with varying dimensions, and the thickness of each helical fiber varied from 25 to 40 nm. The larger bundles of 100−150 nm are formed by wrapping individual fibers around each other in a helical manner, resulting in physically entangled networks; this type of twisting is often observed in chiral compounds.[84,87,88] The helicity of single fibers for **1R** and **1S** clearly indicates that molecular chirality had been successfully transferred to the hierarchical aggregates (Figure 5a). The morphology of racemate xerogel **1-rac** showed tape-like fibers, which is different from that of its enantiomers (Figure 5b). The thickness of each fiber varied from 50 to 200 nm, with few fibrils wrapped around each other. Interestingly, a twisted tape-like architecture was observed in **1R+1S** with bundles of varying dimension from 50 to 200 nm, indicating the presence of both enantiomers and racemate (Figure 6a). The SEM of xerogels obtained from toluene showed similar morphologies, both **1R** and **1S** form helical fibrous network with a thickness of 30−70 nm (Figure S4, see the Supporting Information). These small fibers merge with each other to form a thicker helix of diameter 150−200 nm.

Xerogels of **1-rac** from toluene shows similar tape-like morphology (Figure S5, see the Supporting Information). The **1R+1S** xerogel displayed twisted-tape morphology similar to ethyl acetate gels and the diameter of the fibers was found to be 100−250 nm. The SEM analysis of the xerogels obtained from EtOH/water (50% v/v) also support the presence of mixed network in **1R+1S** gels (Figure S6, see the Supporting Information). The presence of two types of networks in the SEM images corroborate well with the rheology results. In mixed networks, elastic character of the gel network was increased due to higher entanglement, which is evident from the rheology results of **1R+1S** compared to other gels.

Atomic Force Microscopy (AFM). The morphology of the gel fibers was further analyzed by AFM studies. The gels were made by dissolving **1R** (0.7 wt %), **1S** (0.7 wt %), and **1-rac** (0.15 wt %) in toluene. The **1R+1S** gel was prepared by dissolving individual **1R** and **1S** in toluene (0.3 wt %) and then heating. All these gels were further dispersed in toluene (10×), dropped on a plate, dried at room temperature, and analyzed by AFM. Analysis of the AFM images of **1R** and **1S** revealed that both enantiomers have a twisted single helix with a uniform right- and left-handed morphology, respectively (Figure 7). However, a tape-like morphology was observed for **1-rac**, which clearly indicated that the helicity was canceled due to the co-assembly of both **R** and **S** fibrils (Figure 8).

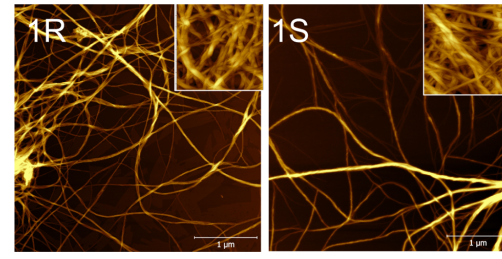

Figure 7. AFM images of **1R** and **1S** showing the left- and right-handed helical fibers; inset shows the magnified images.

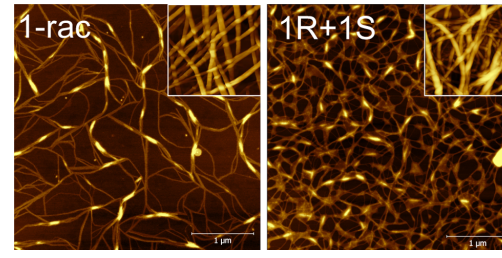

Figure 8. AFM images showing tape-like architecture of **1-rac** and a mixture of tape and helical morphology of **1R+1S**; inset shows the magnified images.

Interestingly, the mixed gel **1R+1S** showed both twisted and tape-like morphology. This may be attributed to the self-sorting and co-assembly of **1R** and **1S** fibrils when they are mixed and heated together. Similar morphologies were observed for EtOH/water (50% v/v) gels and the AFM images of **1R** and **1S** showed helical fibers, a tape-like morphology for **1-rac**, and both twisted and tape-like morphology for **1R+1S** (Figures S9 and S10, see the Supporting Information).

Circular Dichroism (CD). The sensitivity of CD to chiral perturbations will provide information about the molecular chirality and the difference between CD signals of self-assembled and isolated state will enable us to elucidate the structural information of the assembled hierarchical struc-

DOI: 10.1021/acs.langmuir.8b02729
Langmuir 2018, 34, 12957−12967

ture.[89] Although we screened a series of solvents, which are capable of forming gels with **1R**, **1S**, and **1-rac**, these solvents were discarded due to background absorption. We have selected EtOH/water mixture for our studies, which showed an absorption cutoff at around 190−200 nm. The CD experiments were performed at various concentrations in dispersed gel state and weak signals were observed below 0.005 wt % for all gelators. On the other hand, increasing the concentration above 0.05 wt % resulted in saturation of CD signals. Thus, we selected 0.025 wt % as the optimum concentration for the enantiomers, racemate, and mixed gels (Figure 9a). The CD

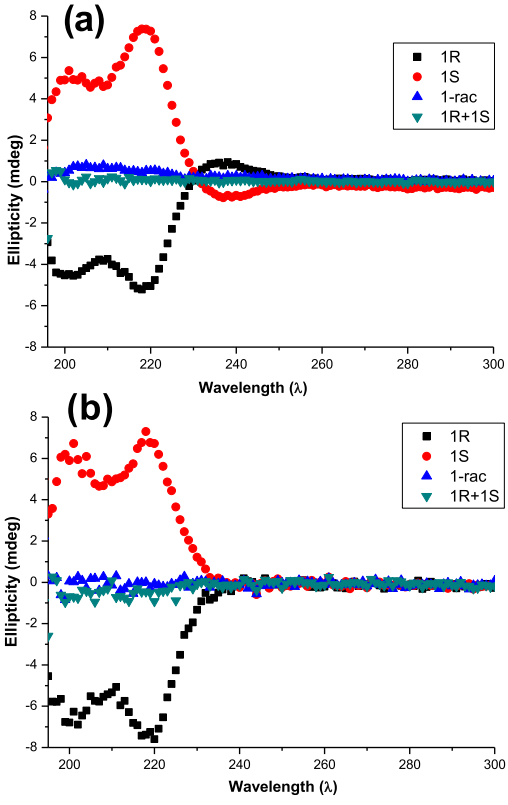

Figure 9. CD spectra of **1R**, **1S**, **1-rac**, and **1R+1S** in dispersed gel state (a) and in solution state (b).

signal maxima observed at 200 and 220 nm for **1S** may be attributed to the existence of $\pi-\pi$ stacking interactions from the aromatic units.[90,91] The CD spectrum of **1R** showed negative signals, which is similar to the mirror image of the CD signal of **1S**. The gels of **1-rac** and **1R+1S** (50% v/v) displayed a linear CD signal, indicating the presence of both enantiomers in the gel state. To get an insight into the self-assembly process, the CD of these compounds in the solution state was also analyzed (Figure 9b) and compared to the gel state CD, which indicated the formation of self-assembled networks in the gel state. The small peak at 240 nm observed in the gel state CD is likely due to the stacking of the aromatic phenylalanine groups within the gel. We have also performed the CD experiments of **1R+1S** by varying the concentration of **1R** and **1S**. The CD spectrum of **1R+1S** (75% **1R** v/v) mixture displayed negative maxima, indicating the presence of excess **1R** (Figure S11, see the Supporting Information). Similarly, the experiments with **1R+1S**(25% **1R** v/v) displayed positive maxima.

We have also performed optical rotation measurements for **1R**, **1S**, **1-rac**, and **1R+1S** at 589 nm in a solution (2-butanol) and a gelling solvent (toluene) at concentrations below the minimum gel concentrations (Table S4, see the Supporting Information). The observations were similar to that of the CD experiments.

Nuclear Magnetic Resonance (NMR) Spectroscopy. The self-assembly of **1R**, **1S**, **1-rac**, and **1R+1S** was studied by NMR spectroscopy. The ^{1}H and ^{13}C NMR of **1R**, **1S**, **1-rac**, and **1R+1S** in the solution state was recorded in DMSO-d_6 and similar NMR spectra suggest that enantiomers, racemate, and mixed enantiomers have identical environment in the solution state (Figures S12 and S13, see the Supporting Information). To analyze their self-assembly in the gel state, solid-state NMR was performed on the xerogels of **1R**, **1S**, **1-rac**, and **1R+1S** by filtering 1 wt % gels, followed by drying, and compared with the solution-state NMR (Figure 10).

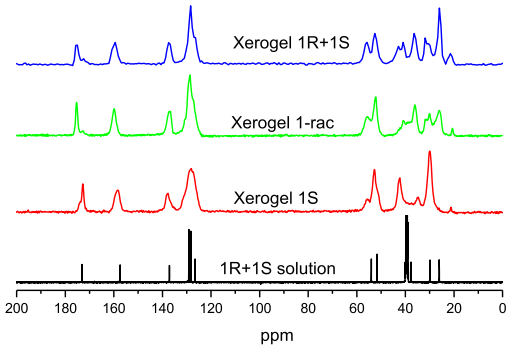

Figure 10. Comparison of the solid-state and solution-state ^{13}C NMR of **1R**, **1S**, **1-rac**, and **1R+1S**.

Analysis of the ^{13}C NMR of the four samples revealed that the solid-state packing of the xerogels is not identical (Figure S14, see the Supporting Information), which may be attributed to the difference in the molecular self-assembly. Generally, the morphology and molecular arrangement of original gels are translated to the xerogels, but in some cases, the removal of solvent may result in artefacts due to dissolution and recrystallization, changes in morphology, or polymorphic phase transition.[9] The NMR spectra of enantiopure **1R** and **1S** were identical due to the similar three-dimensional packing in these structures because of their mirror image. This observation corroborates nicely with the SEM and AFM images, where a helical fibrous network was observed for **1R** and **1S**. However, the peak at δ = 42.5 ppm was missing in racemic **1-rac**, but more peaks were observed at δ = 26.0, 31.8, 36.3, and 40.9 ppm (Figure 11). Thus, the self-assembly in the racemate is different from its enantiomers and evident from the tape-like fibers in the SEM and AFM images. The packing mode of **1R+1S** was analyzed by comparing the NMR spectra of **1R**, **1S**, and **1-rac** with that of **1R+1S** (Figure 11). It is clear

DOI: 10.1021/acs.langmuir.8b02729
Langmuir 2018, 34, 12957−12967

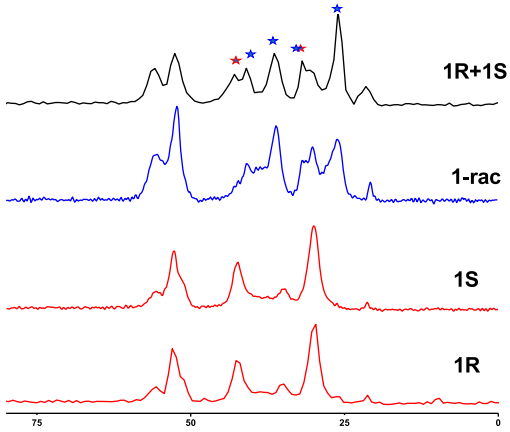

Figure 11. Comparison of the solid-state ^{13}C NMR of **1R**, **1S**, **1-rac**, and **1R+1S** for the aliphatic region showing the mixed network in solid state for **1R+1S** (*indicates the corresponding peaks in enantiomers and racemate).

from the spectra that **1R+1S** network is a mixture of fibers from both enantiomers and the racemate, which indicates the presence of both self-sorted and co-assembled fibers in **1R+1S**.

CONCLUSIONS

We have successfully synthesized the enantiopure (**1R**) and racemic (**1-rac**) forms of bis(urea)-based phenylalanine methyl ester. The known enantiomeric form (**1S**) was also synthesized and all the isomers were found to be excellent gelators capable of gelling a wide range of solvents. Multicomponent gels based on enantiomers were prepared by mixing equal amounts of pure enantiomers as well as varying individual enantiomer concentrations. The gels were characterized using standard gelation techniques and the morphology was analyzed by SEM, AFM, and solid state NMR. The mixed gel displayed a higher thermal and mechanical strength compared to the enantiomer and racemate gels. The CD experiments performed in the solution sate and gel state revealed the preservation of chirality in gel fibers. The enantiopure gels displayed helical fibers and the racemate showed a tape-like architecture, indicating co-assembly of individual enantiomers. The mixed gel of the enantiopure gels displayed twisted tapes, indicating the presence of both enantiomers and racemate gels. This was also confirmed by solid-state NMR studies, where the NMR spectrum of the xerogel of mixed gel displayed both forms. This clearly indicates that in mixed gels system, the fibrils rearrange to form self-sorted and co-assembled fibers. The enhanced mechanical and thermal stability of the mixed gel compared to the enantiomer and racemate gel may be attributed to the presence of both self-sorted and co-assembled fibers. The tuning of mechanical and thermal strength as a function of self-assembly will enable supramolecular chemists to design multicomponent systems with enhanced mechanical and thermal stability.

ASSOCIATED CONTENT

Supporting Information

The Supporting Information is available free of charge on the ACS Publications website at DOI: 10.1021/acs.langmuir.8b02729.

Further gelation test, MGC experiments, T_{gel} experiments, SEM, and AFM images, CD and OD experiments, rheology, and NMR spectra (PDF)

AUTHOR INFORMATION

Corresponding Author

*E-mail: krishna@hi.is. Tel: +354 525 4846. Fax: +354 552 8911.

ORCID

António A. Vicente: 0000-0003-3593-8878
Pall Thordarson: 0000-0002-1200-8814
Krishna K. Damodaran: 0000-0002-9741-2997

Author Contributions

‖D.A.T. and D.G. contributed equally to this work.

Notes

The authors declare no competing financial interest.

ACKNOWLEDGMENTS

We thank University of Iceland Research Fund for financial support. D.G. thanks University of Iceland for the Doctoral Research grant and Z.K. thanks University of Ljubljana for the Erasmus exchange program. We thankfully acknowledge Dr. A. Rawal, The Mark Wainwright Analytical Centre, UNSW for solid state NMR studies and Dr. Sigridur Jónsdóttir, University of Iceland for solution NMR and Mass spectroscopy. P.T. thanks the Australian Research Council for an ARC Centre of Excellence grant (CE140100036) and A.D.M. thanks the National Health and Medical Research Council for a Dementia Development Research Fellowship (APP1106751). L.F. and A.V. thank the FCT (UID/BIO/04469/2013), COMPETE 2020 (POCI-01-0145-FEDER-006684), and Norte2020—Programa Operacional Regional do Norte (BioTecNorte operation, NORTE-01-0145-FEDER-000004) for rheological studies. The rheological study was supported by a STSM Grant from COST Action CM1402 Crystallize.

REFERENCES

(1) Estroff, L. A.; Hamilton, A. D. Water Gelation by Small Organic Molecules. *Chem. Rev.* **2004**, *104*, 1201−1218.
(2) de Loos, M.; Feringa, B. L.; van Esch, J. H. Design and Application of Self-Assembled Low Molecular Weight Hydrogels. *Eur. J. Org. Chem.* **2005**, *2005*, 3615−3631.
(3) George, M.; Weiss, R. G. Molecular Organogels. Soft Matter Comprised of Low-Molecular-Mass Organic Gelators and Organic Liquids. *Acc. Chem. Res.* **2006**, *39*, 489−497.
(4) Dastidar, P. Supramolecular gelling agents: can they be designed? *Chem. Soc. Rev.* **2008**, *37*, 2699−2715.
(5) Hirst, A. R.; Escuder, B.; Miravet, J. F.; Smith, D. K. High-Tech Applications of Self-Assembling Supramolecular Nanostructured Gel-Phase Materials: From Regenerative Medicine to Electronic Devices. *Angew. Chem., Int. Ed.* **2008**, *47*, 8002−8018.
(6) Banerjee, S.; Das, R. K.; Maitra, U. Supramolecular gels 'in action'. *J. Mater. Chem.* **2009**, *19*, 6649−6687.
(7) Piepenbrock, M.-O. M.; Lloyd, G. O.; Clarke, N.; Steed, J. W. Metal- and Anion-Binding Supramolecular Gels. *Chem. Rev.* **2010**, *110*, 1960−2004.
(8) Yu, G.; Yan, X.; Han, C.; Huang, F. Characterization of supramolecular gels. *Chem. Soc. Rev.* **2013**, *42*, 6697−6722.

DOI: 10.1021/acs.langmuir.8b02729
Langmuir 2018, 34, 12957−12967

(9) Kumar, D. K.; Steed, J. W. Supramolecular gel phase crystallization: orthogonal self-assembly under non-equilibrium conditions. *Chem. Soc. Rev.* **2014**, *43*, 2080−2088.
(10) Foster, J. A.; Damodaran, K. K.; Maurin, A.; Day, G. M.; Thompson, H. P. G.; Cameron, G. J.; Bernal, J. C.; Steed, J. W. Pharmaceutical polymorph control in a drug-mimetic supramolecular gel. *Chem. Sci.* **2017**, *8*, 78−84.
(11) Terech, P.; Weiss, R. G. Low Molecular Mass Gelators of Organic Liquids and the Properties of Their Gels. *Chem. Rev.* **1997**, *97*, 3133−3160.
(12) Skilling, K. J.; Citossi, F.; Bradshaw, T. D.; Ashford, M.; Kellam, B.; Marlow, M. Insights into low molecular mass organic gelators: a focus on drug delivery and tissue engineering applications. *Soft Matter* **2014**, *10*, 237−256.
(13) Du, X.; Zhou, J.; Shi, J.; Xu, B. Supramolecular Hydrogelators and Hydrogels: From Soft Matter to Molecular Biomaterials. *Chem. Rev.* **2015**, *115*, 13165−13307.
(14) Babu, S. S.; Praveen, V. K.; Ajayaghosh, A. Functional π-Gelators and Their Applications. *Chem. Rev.* **2014**, *114*, 1973−2129.
(15) Worthington, P.; Pochan, D. J.; Langhans, S. A. Peptide Hydrogels − Versatile Matrices for 3D Cell Culture in Cancer Medicine. *Front Oncol.* **2015**, *5*, 92.
(16) Truong, W. T.; Su, Y.; Meijer, J. T.; Thordarson, P.; Braet, F. Self-Assembled Gels for Biomedical Applications. *Chem. Asian J.* **2011**, *6*, 30−42.
(17) Buerkle, L. E.; Rowan, S. J. Supramolecular gels formed from multi-component low molecular weight species. *Chem. Soc. Rev.* **2012**, *41*, 6089−6102.
(18) Raeburn, J.; Adams, D. J. Multicomponent low molecular weight gelators. *Chem. Commun.* **2015**, *51*, 5170−5180.
(19) Edwards, W.; Smith, D. K. Enantioselective Component Selection in Multicomponent Supramolecular Gels. *J. Am. Chem. Soc.* **2014**, *136*, 1116−1124.
(20) Smith, M. M.; Smith, D. K. Self-sorting multi-gelator gels-mixing and ageing effects in thermally addressable supramolecular soft nanomaterials. *Soft Matter* **2011**, *7*, 4856−4860.
(21) Fichman, G.; Guterman, T.; Adler-Abramovich, L.; Gazit, E. Synergetic functional properties of two-component single amino acid-based hydrogels. *CrystEngComm* **2015**, *17*, 8105−8112.
(22) Singh, N.; Maity, C.; Zhang, K.; Angulo-Pachón, C. A.; van Esch, J. H.; Eelkema, R.; Escuder, B. Synthesis of a Double-Network Supramolecular Hydrogel by Having One Network Catalyse the Formation of the Second. *Chem. Eur. J.* **2017**, *23*, 2018−2021.
(23) Singh, N.; Zhang, K.; Angulo-Pachon, C. A.; Mendes, E.; van Esch, J. H.; Escuder, B. Tandem reactions in self-sorted catalytic molecular hydrogels. *Chem. Sci.* **2016**, *7*, 5568−5572.
(24) Sandeep, A.; Praveen, V. K.; Kartha, K. K.; Karunakaran, V.; Ajayaghosh, A. Supercoiled fibres of self-sorted donor-acceptor stacks: a turn-off/turn-on platform for sensing volatile aromatic compounds. *Chem. Sci.* **2016**, *7*, 4460−4467.
(25) Safont-Sempere, M. M.; Fernández, G.; Würthner, F. Self-Sorting Phenomena in Complex Supramolecular Systems. *Chem. Rev.* **2011**, *111*, 5784−5814.
(26) Draper, E. R.; Wallace, M.; Schweins, R.; Poole, R. J.; Adams, D. J. Nonlinear Effects in Multicomponent Supramolecular Hydrogels. *Langmuir* **2017**, *33*, 2387−2395.
(27) Ramalhete, S. M.; Nartowski, K. P.; Sarathchandra, N.; Foster, J. S.; Round, A. N.; Angulo, J.; Lloyd, G. O.; Khimyak, Y. Z. Supramolecular Amino Acid Based Hydrogels: Probing the Contribution of Additive Molecules using NMR Spectroscopy. *Chem. Eur. J.* **2017**, *23*, 8014−8024.
(28) Draper, E. R.; Adams, D. J. How should multicomponent supramolecular gels be characterised? *Chem. Soc. Rev.* **2018**, *47*, 3395−3405.
(29) Cross, E. R.; Sproules, S.; Schweins, R.; Draper, E. R.; Adams, D. J. Controlled Tuning of the Properties in Optoelectronic Self-Sorted Gels. *J. Am. Chem. Soc.* **2018**, *140*, 8667−8670.
(30) Shigemitsu, H.; Fujisaku, T.; Tanaka, W.; Kubota, R.; Minami, S.; Urayama, K.; Hamachi, I. An adaptive supramolecular hydrogel comprising self-sorting double nanofibre networks. *Nat. Nanotechnol.* **2018**, *13*, 165−172.
(31) Nanda, J.; Adhikari, B.; Basak, S.; Banerjee, A. Formation of Hybrid Hydrogels Consisting of Tripeptide and Different Silver Nanoparticle-Capped Ligands: Modulation of the Mechanical Strength of Gel Phase Materials. *J. Phys. Chem. B* **2012**, *116*, 12235−12244.
(32) Adhikari, B.; Nanda, J.; Banerjee, A. Pyrene-Containing Peptide-Based Fluorescent Organogels: Inclusion of Graphene into the Organogel. *Chem. Eur. J.* **2011**, *17*, 11488−11496.
(33) Samanta, S. K.; Subrahmanyam, K. S.; Bhattacharya, S.; Rao, C. N. R. Composites of Graphene and Other Nanocarbons with Organogelators Assembled through Supramolecular Interactions. *Chem. Eur. J.* **2012**, *18*, 2890−2901.
(34) Samanta, S. K.; Pal, A.; Bhattacharya, S.; Rao, C. N. R. Carbon nanotube reinforced supramolecular gels with electrically conducting, viscoelastic and near-infrared sensitive properties. *J. Mater. Chem.* **2010**, *20*, 6881−6890.
(35) Wang, Q.; Mynar, J. L.; Yoshida, M.; Lee, E.; Lee, M.; Okuro, K.; Kinbara, K.; Aida, T. High-water-content mouldable hydrogels by mixing clay and a dendritic molecular binder. *Nature* **2010**, *463*, 339−343.
(36) Kato, T.; Hirai, Y.; Nakaso, S.; Moriyama, M. Liquid-crystalline physical gels. *Chem. Soc. Rev.* **2007**, *36*, 1857−1867.
(37) Heeres, A.; van der Pol, C.; Stuart, M.; Friggeri, A.; Feringa, B. L.; van Esch, J. Orthogonal Self-Assembly of Low Molecular Weight Hydrogelators and Surfactants. *J. Am. Chem. Soc.* **2003**, *125*, 14252−14253.
(38) Brizard, A.; Stuart, M.; van Bommel, K.; Friggeri, A.; de Jong, M.; van Esch, J. Preparation of Nanostructures by Orthogonal Self-Assembly of Hydrogelators and Surfactants. *Angew. Chem., Int. Ed.* **2008**, *47*, 2063−2066.
(39) Cornwell, D. J.; Okesola, B. O.; Smith, D. K. Hybrid polymer and low molecular weight gels - dynamic two-component soft materials with both responsive and robust nanoscale networks. *Soft Matter* **2013**, *9*, 8730−8736.
(40) Cornwell, D. J.; Okesola, B. O.; Smith, D. K. Multidomain Hybrid Hydrogels: Spatially Resolved Photopatterned Synthetic Nanomaterials Combining Polymer and Low-Molecular-Weight Gelators. *Angew. Chem., Int. Ed.* **2014**, *53*, 12461−12465.
(41) Wang, J.; Wang, Z.; Gao, J.; Wang, L.; Yang, Z.; Kong, D.; Yang, Z. Incorporation of supramolecular hydrogels into agarose hydrogels-a potential drug delivery carrier. *J. Mater. Chem.* **2009**, *19*, 7892−7896.
(42) Kölbel, M.; Menger, F. M. Molecular Recognition among Structurally Similar Components of a Self-Assembling Soft Material. *Langmuir* **2001**, *17*, 4490−4492.
(43) Moffat, J. R.; Smith, D. K. Controlled self-sorting in the assembly of 'multi-gelator' gels. *Chem. Commun.* **2009**, 316−318.
(44) Draper, E. R.; Adams, D. J. Self-sorting shows its true colours. *Nat. Chem.* **2016**, *8*, 737−738.
(45) Draper, E. R.; Eden, E. G. B.; McDonald, T. O.; Adams, D. J. Spatially resolved multicomponent gels. *Nat. Chem.* **2015**, *7*, 848−852.
(46) Morris, K. L.; Chen, L.; Raeburn, J.; Sellick, O. R.; Cotanda, P.; Paul, A.; Griffiths, P. C.; King, S. M.; O'Reilly, R. K.; Serpell, L. C.; Adams, D. J. Chemically programmed self-sorting of gelator networks. *Nat. Commun.* **2013**, *4*, No. 1480.
(47) Onogi, S.; Shigemitsu, H.; Yoshii, T.; Tanida, T.; Ikeda, M.; Kubota, R.; Hamachi, I. In situ real-time imaging of self-sorted supramolecular nanofibres. *Nat. Chem.* **2016**, *8*, 743−752.
(48) Brizard, A.; Oda, R.; Huc, I. Chirality effects in self-assembled fibrillar networks. *Top. Curr. Chem.* **2005**, *256*, 167−218.
(49) Zhang, L.; Jin, Q.; Liu, M. Enantioselective Recognition by Chiral Supramolecular Gels. *Chem. Asian J.* **2016**, *11*, 2642−2649.
(50) Leiras, S.; Freire, F.; Quinoa, E.; Riguera, R. Reversible assembly of enantiomeric helical polymers: from fibers to gels. *Chem. Sci.* **2015**, *6*, 246−253.

DOI: 10.1021/acs.langmuir.8b02729
Langmuir 2018, 34, 12957−12967

(51) Engstrom, J. R.; Savyasachi, A. J.; Parhizkar, M.; Sutti, A.; Hawes, C. S.; White, J. M.; Gunnlaugsson, T.; Pfeffer, F. M. Norbornene chaotropic salts as low molecular mass ionic organogelators (LMIOGs). *Chem. Sci.* **2018**, *9*, 5233−5241.
(52) Liu, M.; Zhang, L.; Wang, T. Supramolecular Chirality in Self-Assembled Systems. *Chem. Rev.* **2015**, *115*, 7304−7397.
(53) Jung, J. H.; Ono, Y.; Hanabusa, K.; Shinkai, S. Creation of Both Right-Handed and Left-Handed Silica Structures by Sol−Gel Transcription of Organogel Fibers Comprised of Chiral Diaminocyclohexane Derivatives. *J. Am. Chem. Soc.* **2000**, *122*, 5008−5009.
(54) Hasell, T.; Chong, S. Y.; Jelfs, K. E.; Adams, D. J.; Cooper, A. I. Porous Organic Cage Nanocrystals by Solution Mixing. *J. Am. Chem. Soc.* **2012**, *134*, 588−598.
(55) Liu, Z.; Sun, J.; Zhou, Y.; Zhang, Y.; Wu, Y.; Nalluri, S. K. M.; Wang, Y.; Samanta, A.; Mirkin, C. A.; Schatz, G. C.; Stoddart, J. F. Supramolecular Gelation of Rigid Triangular Macrocycles through Rings of Multiple C−H···O Interactions Acting Cooperatively. *J. Org. Chem.* **2016**, *81*, 2581−2588.
(56) Čaplar, V.; Frkanec, L.; Vujičić, N. Š.; Žinić, M. Positionally Isomeric Organic Gelators: Structure−Gelation Study, Racemic versus Enantiomeric Gelators, and Solvation Effects. *Chem. Eur. J.* **2010**, *16*, 3066−3082.
(57) Frkanec, L.; Zinic, M. Chiral bis(amino acid)- and bis(amino alcohol)-oxalamide gelators. Gelation properties, self-assembly motifs and chirality effects. *Chem. Commun.* **2010**, *46*, 522−537.
(58) He, Y.; Bian, Z.; Kang, C.; Gao, L. Self-discriminating and hierarchical assembly of racemic binaphthyl-bisbipyridines and silver ions: from metallocycles to gel nanofibers. *Chem. Commun.* **2011**, *47*, 1589−1591.
(59) Shen, Z.; Wang, T.; Liu, M. Tuning the Gelation Ability of Racemic Mixture by Melamine: Enhanced Mechanical Rigidity and Tunable Nanoscale Chirality. *Langmuir* **2014**, *30*, 10772−10778.
(60) Lin, J.; Guo, Z.; Plas, J.; Amabilino, D. B.; De Feyter, S.; Schenning, A. P. H. J. Homochiral and heterochiral assembly preferences at different length scales - conglomerates and racemates in the same assemblies. *Chem. Commun.* **2013**, *49*, 9320−9322.
(61) Borges, A. R.; Hyacinth, M.; Lum, M.; Dingle, C. M.; Hamilton, P. L.; Chruszcz, M.; Pu, L.; Sabat, M.; Caran, K. L. Self-Assembled Thermoreversible Gels of Nonpolar Liquids by Racemic Propargylic Alcohols with Fluorinated and Nonfluorinated Aromatic Rings. *Langmuir* **2008**, *24*, 7421−7431.
(62) Amemiya, R.; Mizutani, M.; Yamaguchi, M. Two-Component Gel Formation by Pseudoenantiomeric Ethynylhelicene Oligomers. *Angew. Chem., Int. Ed.* **2010**, *49*, 1995−1999.
(63) Swanekamp, R. J.; DiMaio, J. T. M.; Bowerman, C. J.; Nilsson, B. L. Coassembly of Enantiomeric Amphipathic Peptides into Amyloid-Inspired Rippled β-Sheet Fibrils. *J. Am. Chem. Soc.* **2012**, *134*, 5556−5559.
(64) Suzuki, M.; Hanabusa, K. l-Lysine-based low-molecular-weight gelators. *Chem. Soc. Rev.* **2009**, *38*, 967−975.
(65) Edwards, W.; Smith, D. Chiral Assembly Preferences and Directing Effects in Supramolecular Two-Component Organogels. *Gels* **2018**, *4*, 31.
(66) Das, R. K.; Kandanelli, R.; Linnanto, J.; Bose, K.; Maitra, U. Supramolecular Chirality in Organogels: A Detailed Spectroscopic, Morphological, and Rheological Investigation of Gels (and Xerogels) Derived from Alkyl Pyrenyl Urethanes. *Langmuir* **2010**, *26*, 16141−16149.
(67) Nagy, K. J.; Giano, M. C.; Jin, A.; Pochan, D. J.; Schneider, J. P. Enhanced Mechanical Rigidity of Hydrogels Formed from Enantiomeric Peptide Assemblies. *J. Am. Chem. Soc.* **2011**, *133*, 14975−14977.
(68) Adhikari, B.; Nanda, J.; Banerjee, A. Multicomponent hydrogels from enantiomeric amino acid derivatives: helical nanofibers, handedness and self-sorting. *Soft Matter* **2011**, *7*, 8913−8922.
(69) Cicchi, S.; Ghini, G.; Lascialfari, L.; Brandi, A.; Betti, F.; Berti, D.; Baglioni, P.; Di Bari, L.; Pescitelli, G.; Mannini, M.; Caneschi, A. Self-sorting chiral organogels from a long chain carbamate of 1-benzyl-pyrrolidine-3,4-diol. *Soft Matter* **2010**, *6*, 1655−1661.
(70) Nagy-Smith, K.; Beltramo, P. J.; Moore, E.; Tycko, R.; Furst, E. M.; Schneider, J. P. Molecular, Local, and Network-Level Basis for the Enhanced Stiffness of Hydrogel Networks Formed from Coassembled Racemic Peptides: Predictions from Pauling and Corey. *ACS Cent Sci.* **2017**, *3*, 586−597.
(71) George, M.; Weiss, R. G. Low Molecular-Mass Organic Gelators. In *Molecular Gels: Materials with Self-Assembled Fibrillar Networks*. In Weiss, R. G., Terech, P., Eds.; Springer: Dordrecht, Netherlands, 2006; pp 449−551.
(72) Schön, E.-M.; Marqués-López, E.; Herrera, R. P.; Alemán, C.; Díaz, D. D. Exploiting Molecular Self-Assembly: From Urea-Based Organocatalysts to Multifunctional Supramolecular Gels. *Chem. Eur. J.* **2014**, *20*, 10720−10731.
(73) Steed, J. W. Anion-tuned supramolecular gels: a natural evolution from urea supramolecular chemistry. *Chem. Soc. Rev.* **2010**, *39*, 3686−3699.
(74) Isare, B.; Pensec, S.; Raynal, M.; Bouteiller, L. Bisurea-based supramolecular polymers: From structure to properties. *C. R. Chim.* **2016**, *19*, 148−156.
(75) George, M.; Tan, G.; John, V. T.; Weiss, R. G. Urea and Thiourea Derivatives as Low Molecular-Mass Organogelators. *Chem. Eur. J.* **2005**, *11*, 3243−3254.
(76) Kumar, D. K.; Jose, D. A.; Das, A.; Dastidar, P. First snapshot of a nonpolymeric hydrogelator interacting with its gelling solvents. *Chem. Commun.* **2005**, 4059−4061.
(77) Kotova, O.; Daly, R.; dos Santos, C. M. G.; Boese, M.; Kruger, P. E.; Boland, J. J.; Gunnlaugsson, T. Europium-Directed Self-Assembly of a Luminescent Supramolecular Gel from a Tripodal Terpyridine-Based Ligand. *Angew. Chem., Int. Ed.* **2012**, *51*, 7208−7212.
(78) Piepenbrock, M.-O. M.; Lloyd, G. O.; Clarke, N.; Steed, J. W. Gelation is crucially dependent on functional group orientation and may be tuned by anion binding. *Chem. Commun.* **2008**, 2644−2646.
(79) Schoonbeek, F. S.; van Esch, J. H.; Hulst, R.; Kellogg, R. M.; Feringa, B. L. Geminal bis-ureas as gelators for organic solvents: Gelation properties and structural studies in solution and in the gel state. *Chem. Eur. J.* **2000**, *6*, 2633−2643.
(80) Padrela, L.; Rodrigues, M. A.; Velaga, S. P.; Matos, H. A.; Azevedo, E. G. d. Formation of indomethacin-saccharin cocrystals using supercritical fluid technology. *Eur. J. Pharm. Sci.* **2009**, *38*, 9−17.
(81) Foster, J. A.; Edkins, R. M.; Cameron, G. J.; Colgin, N.; Fucke, K.; Ridgeway, S.; Crawford, A. G.; Marder, T. B.; Beeby, A.; Cobb, S. L.; Steed, J. W. Blending Gelators to Tune Gel Structure and Probe Anion-Induced Disassembly. *Chem. Eur. J.* **2014**, *20*, 279−291.
(82) Lloyd, G. O.; Piepenbrock, M.-O. M.; Foster, J. A.; Clarke, N.; Steed, J. W. Anion tuning of chiral bis(urea) low molecular weight gels. *Soft Matter* **2012**, *8*, 204−216.
(83) Foster, J. A.; Johnson, D. W.; Pipenbrock, M.-O. M.; Steed, J. W. Using gel morphology to control pore shape. *New J. Chem.* **2014**, *38*, 927−932.
(84) Smith, D. K. Lost in translation? Chirality effects in the self-assembly of nanostructured gel-phase materials. *Chem. Soc. Rev.* **2009**, *38*, 684−694.
(85) Makarević, J.; Jokić, M.; Raza, Z.; Štefanić, Z.; Kojić-Prodić, B.; Žinić, M. Chiral Bis(amino alcohol)oxalamide Gelators—Gelation Properties and Supramolecular Organization: Racemate versus Pure Enantiomer Gelation. *Chem. Eur. J.* **2003**, *9*, 5567−5580.
(86) Watanabe, Y.; Miyasou, T.; Hayashi, M. Diastereomixture and Racemate of myo-Inositol Derivatives, Stronger Organogelators than the Corresponding Homochiral Isomers. *Org. Lett.* **2004**, *6*, 1547−1550.
(87) Friggeri, A.; van der Pol, C.; van Bommel, K. J. C.; Heeres, A.; Stuart, M. C. A.; Feringa, B. L.; van Esch, J. Cyclohexane-Based Low Molecular Weight Hydrogelators: A Chirality Investigation. *Chem. Eur. J.* **2005**, *11*, 5353−5361.
(88) Wu, X.; Ji, S.; Li, Y.; Li, B.; Zhu, X.; Hanabusa, K.; Yang, Y. Helical Transfer through Nonlocal Interactions. *J. Am. Chem. Soc.* **2009**, *131*, 5986−5993.

DOI: 10.1021/acs.langmuir.8b02729
Langmuir 2018, 34, 12957−12967

(89) Gottarelli, G.; Lena, S.; Masiero, S.; Pieraccini, S.; Spada, G. P. The use of circular dichroism spectroscopy for studying the chiral molecular self-assembly: An overview. *Chirality* **2008**, *20*, 471−485.
(90) Krysmann, M. J.; Castelletto, V.; McKendrick, J. E.; Clifton, L. A.; Hamley, I. W.; Harris, P. J. F.; King, S. M. Self-Assembly of Peptide Nanotubes in an Organic Solvent. *Langmuir* **2008**, *24*, 8158−8162.
(91) Gupta, M.; Bagaria, A.; Mishra, A.; Mathur, P.; Basu, A.; Ramakumar, S.; Chauhan, V. S. Self-Assembly of a Dipeptide-Containing Conformationally Restricted Dehydrophenylalanine Residue to Form Ordered Nanotubes. *Adv. Mater.* **2007**, *19*, 858−861.

DOI: 10.1021/acs.langmuir.8b02729
Langmuir 2018, 34, 12957−12967

Supporting Information

Enhanced mechanical and thermal strength in mixed enantiomers based supramolecular gel

Daníel Arnar Tómasson,[†] Dipankar Ghosh,[†] Zala Kržišnik,[†] Luiz Henrique Fasolin,[‡] António A. Vicente,[‡] Adam D. Martin,[§] Pall Thordarson,[§] and Krishna K. Damodaran*,[†]

[†] Department of Chemistry, Science Institute, University of Iceland, Dunhagi 3, 107 Reykjavík, Iceland. Tel: +354 525 4846, Fax: +354 552 8911.

[‡] Centre of Biological Engineering, University of Minho, Campus de Gualtar, 4710-057, Braga, Portugal

[§] School of Chemistry, The Australian Centre for Nanomedicine and the ARC Centre of Excellence in Convergent Bio-Nano Science and Technology, University of New South Wales, Sydney-2052, Australia

Table of Contents

1. Synthesis: **1-rac** was synthesized by reacting racemate phenylalanine methyl ester with 1,6-diisocyanatohexane in chloroform. While **1-rac** is a mixture of diastereomers; *R-S* (meso) and the enantiomeric pair *R-R* and *S-S*, these could not be distinguished by HPLC. This suggests that on the molecular level, the two stereocenters are too far away from each other to have any significant influence on the chemical properties of this compound. This, however, does not mean that these stereocenters could not influence the way in which these molecules self-assemble and form gels.

2. Gel Studies

2.1 Gelation test: Gelation tests for both enantiomers, racemate and the mixture of **1R+1S** (1:1 wt/wt) were performed at 1 wt%, using a typical heating and sonication technique.

Table S1: Gelation properties of **1R**, **1S**, **1-rac** and **1R+1S**

Solvent	**1R**	**1S**	**1-rac**	**1R+S**
Ethanol	S	C	G**	G*
2-Pentanol	S	S	G*	G
n-Pentanol	P	C	G*	G
Cyclohexanone	S	S	G	G
Isopropanol	S	S	G*	G*
Acetone	C	C	C	G
THF	P	P	P	G
Acetonitrile	P	P	P	G
n-Propanol	S	S	S	G*
2-Butanol	S	S	C	G
n-Butanol	S	S	C	G
1,4-Dioxane	C	C	C	G
Toluene	G	G	G	G
Ethyl acetate	G	G	G	G
Nitrobenzene	G	G	G	G
Chlorobenzene	G	G	G	G
Benzene	G	G	G	G
2-Butanone	G	G	G	G
p-Xylene	G	G	G	G
m-Xylene	G	G	G	G
o-Xylene	G	G	G	G
Mesitylene	G*	G*	G	G
1,2-Dichloroethane	G	G	G	G

G* = 2 wt%, G** = 3 wt%, S = soluble, P = precipitate, C = colloidal solution and G = gel.

2.2. Minimum Gel Concentration (MGC) experiments

MGC was determined by weighing 10 mg of gelator and 1 mL of the solvent was added, heated to get a clear solution and cooled to room temperature. Once the gel was formed, a small amount of solvent was added in portions and the gelation process was repeated until a layer of solvent was observed on top of the gel. The excess solvent was decanted and MGC was calculated based on weight of gelators with the gelled solvent.

Table S2: MGC of **1R**, **1S**, **1-rac** and **1R+1S** in wt%

Solvent	**1R**	**1S**	**1-rac**	**1R+S**
Ethyl acetate	0.952	0.962	0.505	0.361
2-butanone	1.00	1.00	1.00	0.476
Toluene	0.599	0.741	0.147	0.128
Chlorobenzene	0.412	0.368	0.257	0.201
p-xylene	0.862	0.513	0.141	0.138
m-xylene	0.656	0.503	0.138	0.111
o-xylene	0.26	0.303	0.128	0.118
Nitrobenzene	1.00	1.00	0.752	0.625
Ethanol/water (1:1 v/v)	0.79	0.975	0.77	0.51

2.3. T_{gel} experiment

10 mg of the gelator (**1R**, **1S**, **1-rac** or **1R+1S**) was taken in a standard 7 mL vial and 1 mL solvent was added to it. The solution was heated and sonicated to dissolve the compound and left without disturbing. After 24 hours, a small spherical glass ball (92 mg) was placed on the top of the gel. The vial was placed over an oil bath equipped with a magnetic stirrer and a thermometer. The oil bath was gradually heated and the observation was noted (Table 1). The temperature at which the glass ball touched the bottom of the vial was recorded as T_{gel}. The T_{gel} experiments were also performed on 1 wt% of mixed gels by varying the concentration of both **1S** and **1R** in various solvents (Table S3).

Table S3: T_{gel} (°C) of **1R+1S** gels by varying the concentration of both **1S** and **1R** in various solvents

R:S ratio	Ethyl Acetate	Toluene	2-butanone	Chlorobenzene
0:1	54.0	86.0	38.0	70.0
1:9	60.0	91.5	48.0	86.0
1:4	64.0	95.0	51.0	88.0
3:7	67.0	99.0	54.0	89.0
2:3	69.0	101.0	57.5	89.5
1:1	72.5	106.5	55.5	90.5
3:2	72.0	104.0	53.0	88.5
7:3	71.0	97.0	52.0	85.5
4:1	68.5	92.0	45.0	81.5
9:1	66.0	90.0	41.5	78.5
1:0	55.0	91.0	38.0	73.0

3. Rheology

Temperature Sweep: Oscillatory temperature sweep was performed at constant 0.05% strain and 1 Hz frequency, from 25 °C to 95 °C with an increment of 5 °C per minute.

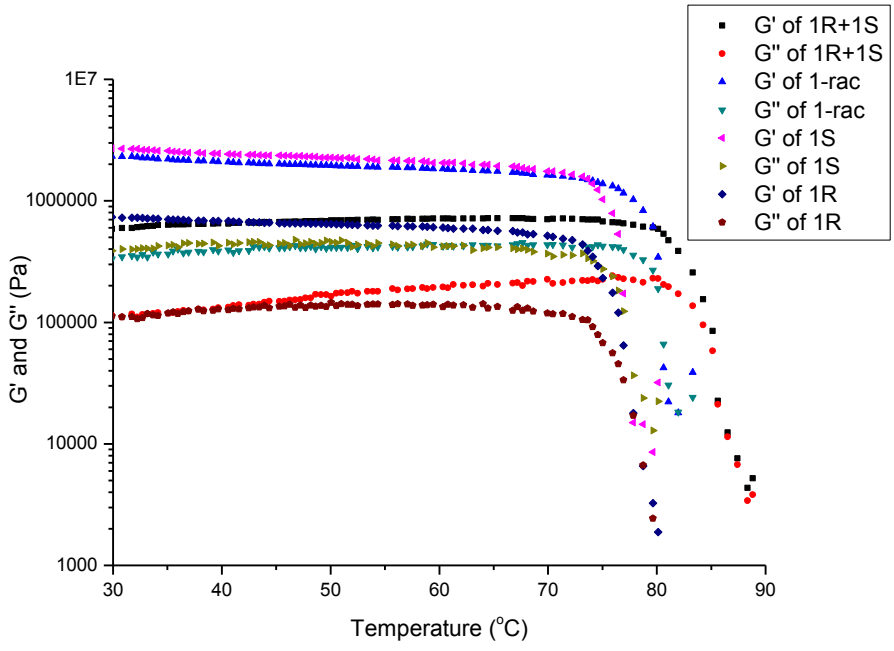

Figure S1: Temperature Sweep for all gels at 5 wt%.

Frequency sweep: Frequency sweep was performed from 0.1 Hz to 10 Hz at 0.05% stress at 25ºC. Various rheological parameters like elastic modulus (G'), viscous modulus (G") and tan(δ) were measured. Both G' and G'' were independent of frequency, which is characteristic for gel. Also G' (corresponds to solid property) was found to be higher than G'' (corresponds to liquid property), since gel is solid at room temperature. Tan(δ), which is a ratio of G'' and G', found to be less than 1, supporting gel behavior of the system (Figure S2).

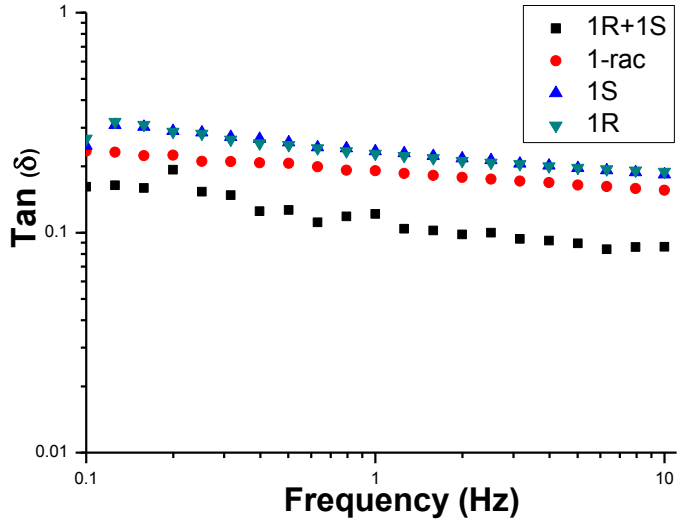

Figure S2: Gel behavior [Tan(δ)] of all gels at 5 wt%.

4. Scanning Electron Microscopy (SEM): 20 mg of the gelators (**1R**, **1S**, **1-rac** and **1R+1S**) were dissolved in 1 mL of toluene and ethyl acetate by heating and sonicating. It was allowed to stand without disturbing to form the gel. After 24 hours, it was filtered through Whatman filter paper. The residue was dried in fume hood. The xerogels were gold coated and placed on a Leo Supra 25 microscope for scanning electron microscopy. Morphologies of the dried xerogels were examined by SEM.

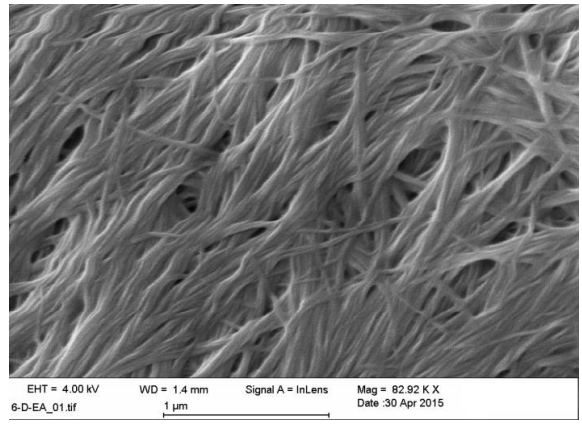

Figure S3: SEM image of **1R** xerogel from ethyl acetate showing similar morphology with **1S**

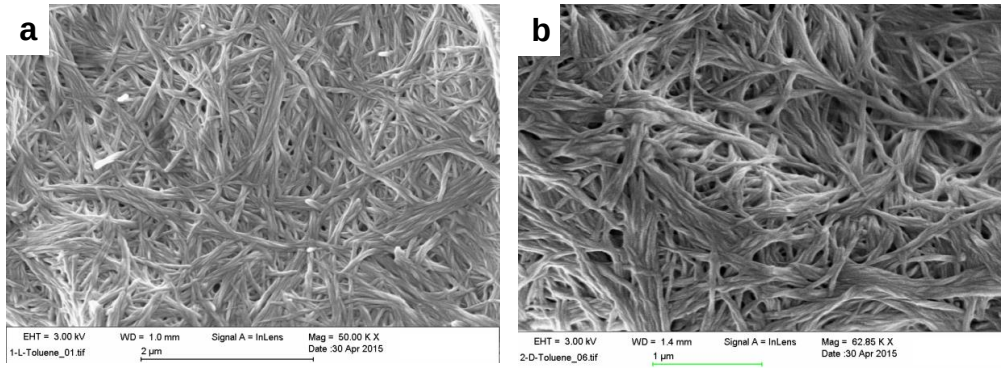

Figure S4: SEM image of xerogel obtained from toluene gel of (a) **1S** and (b) **1R**

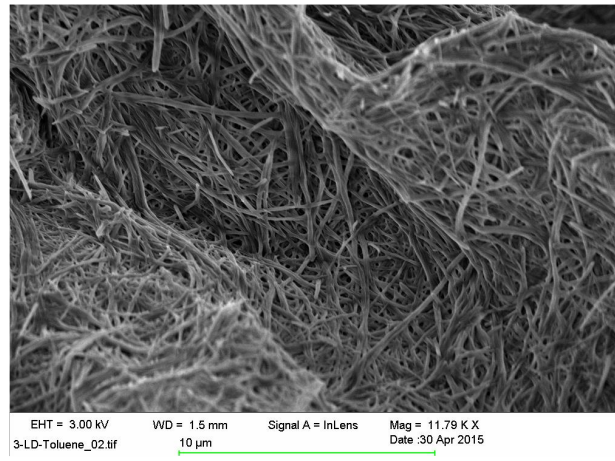

Figure S5: SEM image of xerogel obtained from toluene gel of **1-rac**

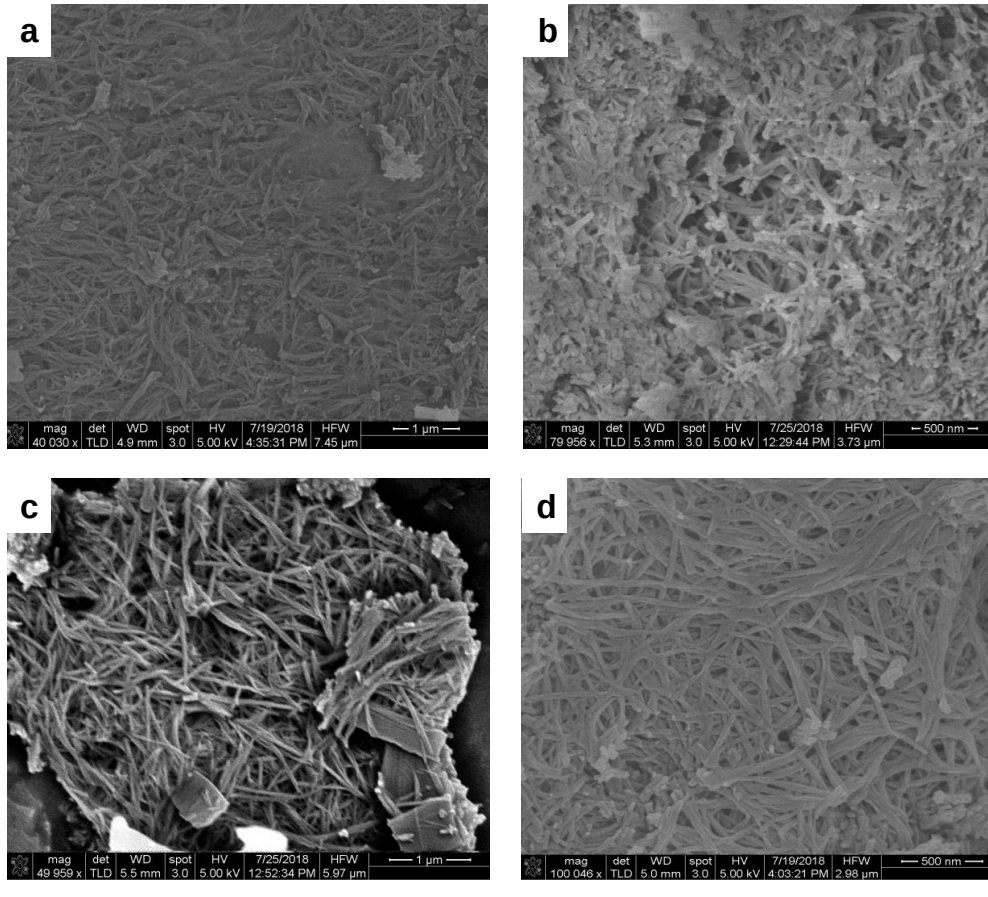

Figure S6: SEM image of xerogel obtained from EtOH/water (50%, v/v) of (a) **1R**, (b) **1S**, (c) **1-rac** and (d) **1R+1S**

5. Atomic Force Microscopy (AFM):

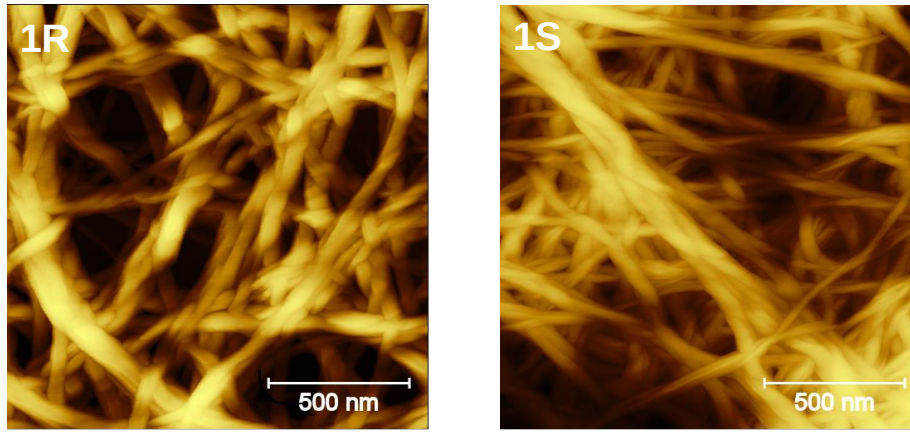

Figure S7: AFM image of **1R** and **1S** in toluene showing the helical fibers

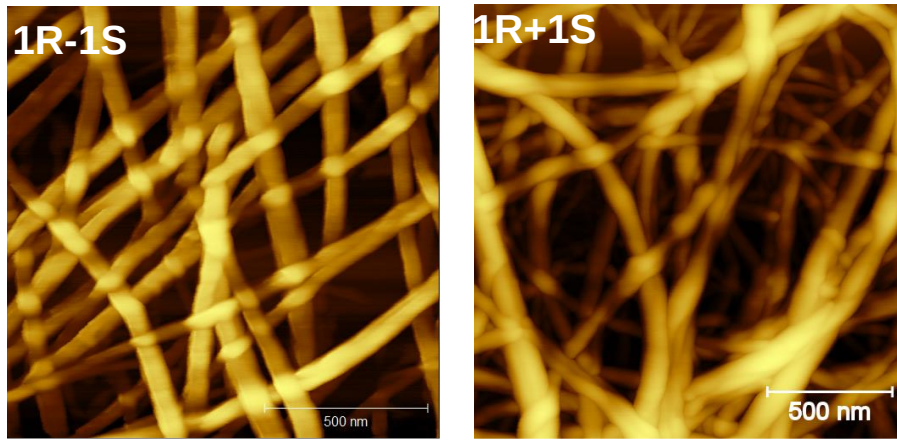

Figure S8: AFM image of **1-rac** and **1R+1S** in toluene showing tape like architecture and a mixture of tape and helical morphology respectively.

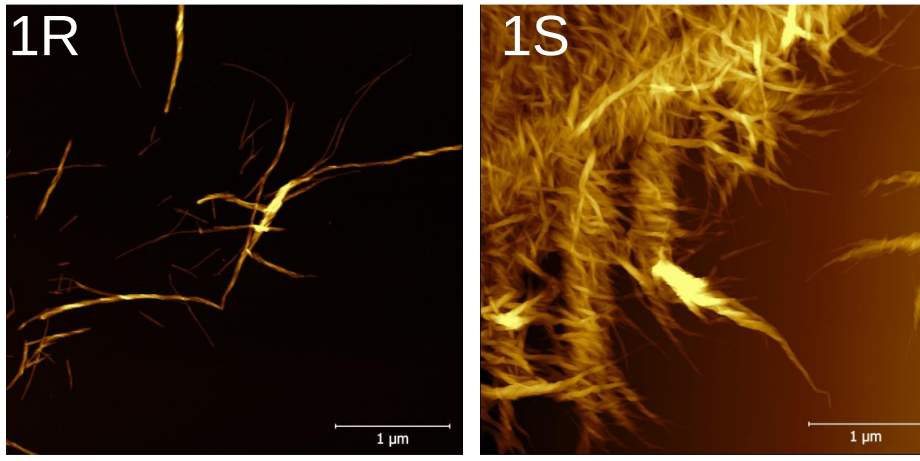

Figure S9: AFM image of **1R** and **1S** in EtOH/water (50%, v/v) showing the helical fibers

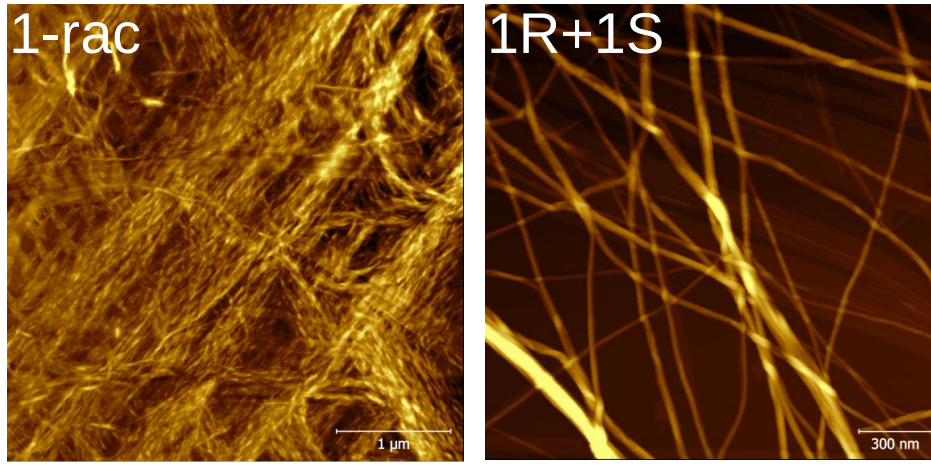

Figure S10: AFM image of **1-rac** and **1R+1S** in EtOH/water (50%, v/v) tape like architecture and a mixture of tape and helical morphology respectively.

6. Circular dichroism (CD) Experiments

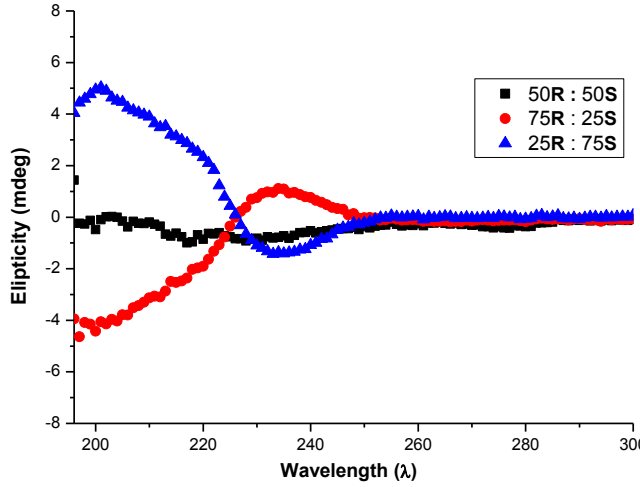

Figure S11: CD spectra of **1R+1S** (75% **1R** v/v), (50% **1R** v/v) and (25% **1R** v/v) mixture showing negative neutral and positive maxima.

7. Optical Rotation Experiments

Table S4: Optical Rotation of **1R**, **1S**, **1-rac** and **1R+1S** in solution (2-butanol) and gelling solvent (toluene) at concentrations below minimum gel concentrations

Solvent	Compound	Wt %	Optical rotation	Specific Rotation [α]D 25°C (°·mL·g^{-1}·dm^{-1})
2-Butanol	**1R**	1.0	-0.341	-33.762
	1S	1.0	0.375	36.667
	1-rac	1.0	-0.006 - 0.006	-0.6 to 0.6
	1R+1S	1.0	0.04	3.960
Toluene	**1R**	0.067	-0.021	-31.532
	1S	0.070	0.019	27.143
	1-rac	0.063	-0.001	-1.587
	1R+1S	0.055	-0.007	-14.000

8. NMR Experiments

8.1 ^{1}H NMR of all compounds in solution state

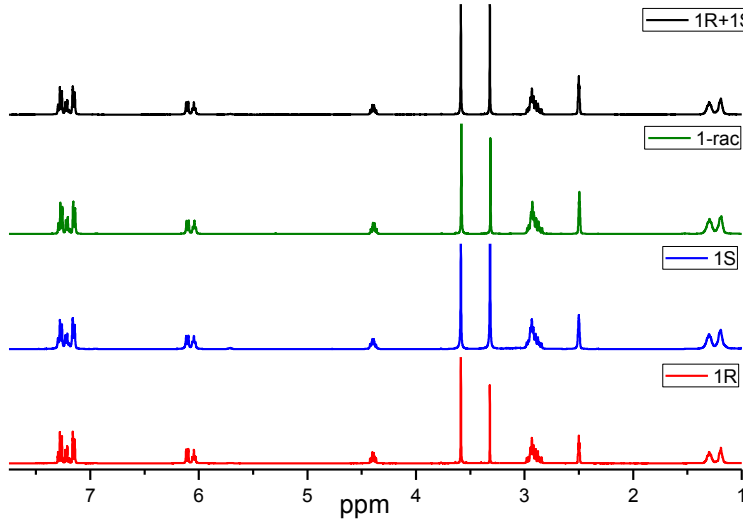

Figure S12: ^{1}H NMR of all compounds in solution state (DMSO-d_6)

8.2. ^{13}C NMR of all compounds in solution state

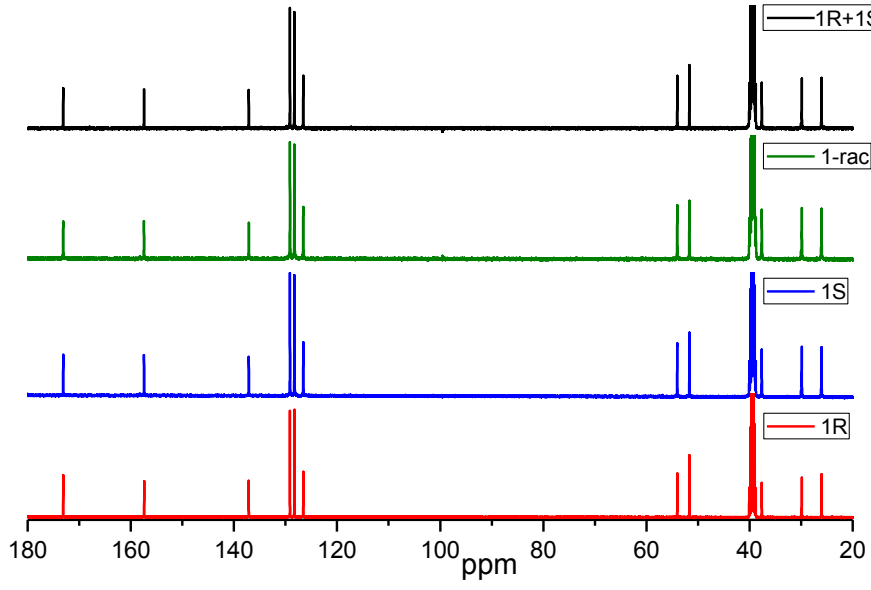

Figure S13: **^{13}C** NMR of all compounds in solution state (DMSO-d_6)

8.3. Solid state ^{13}C NMR of the xerogels from toluene

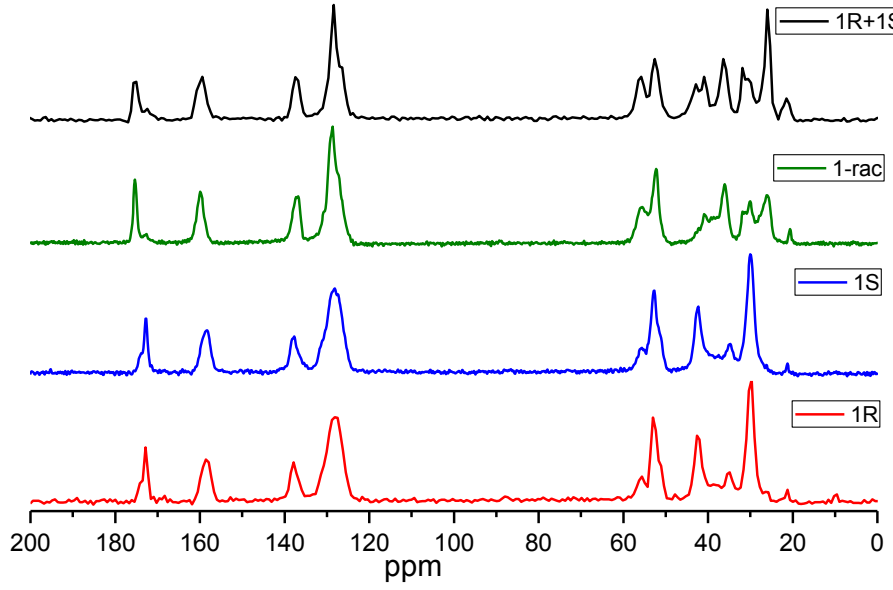

Figure S14: Solid state NMR of toluene xerogel of all compounds.

Article-VI

This project is published in a peer reviewed journal and included as it was published. Slight differences might appear from the original article due to the formatting issue.

Publication details:

Unravelling self-assembly modes in multi-component supramolecular gels using single crystal X-ray diffraction.

Dipankar Ghosh, Abbas D. Farahani, Adam D. Martin, Pall Thordarson* and Krishna K. Damodaran*

Chem. Mater., **2020**, *32* (8), 3517–3527.

Author contributions:

D.G. and K.K.D planned and designed the research; **D.G.** synthesized the gelators, performed characterizations, solved single crystal structures and evaluated gelation properties, SEM and CD experiments. A.D.F. performed rheology and A.D.M. performed AFM. **D.G.** and K.K.D. wrote the initial manuscript draft and **D.G.**, A.D.M., P.T. and K.K.D. reviewed the main manuscript.

CHEMISTRY OF MATERIALS

pubs.acs.org/cm

Article

Unraveling the Self-Assembly Modes in Multicomponent Supramolecular Gels Using Single-Crystal X-ray Diffraction

Dipankar Ghosh, Abbas D. Farahani, Adam D. Martin, Pall Thordarson,* and Krishna K. Damodaran*

Cite This: *Chem. Mater.* 2020, 32, 3517−3527

Read Online

ACCESS | Metrics & More | Article Recommendations | Supporting Information

ABSTRACT: The control and prediction of the self-assembly process in multicomponent supramolecular gels are challenging because the structure and properties rely mostly on the geometry and spatial arrangement of the building blocks. The understanding of noncovalent interactions between the individual gelators at the molecular level will enable us to tune the gelation properties of multicomponent gels. We have studied the self-assembly process of multicomponent gel based on enantiomers and herin we report the first crystallographic evidence of specific co-assembly in mixed enantiomeric gel, which is supported by scanning electron microscopy and atomic force microscopy images. The mode of interactions between the individual gelators from the molecular to macroscopic level, which are responsible for co-assembled fibers, was identified by single-crystal X-ray diffraction. We have proved that specific co-assembly leads to enhanced mechanical and thermal stability in the mixed gel compared to the *meso* and individual enantiomeric gels.

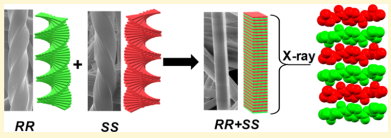

INTRODUCTION

Self-assembly is a ubiquitous process in life science, and nature has been successful in self-assembling simple building blocks to complex functional architectures with unique functions and properties.[1] The concept of supramolecular chemistry[2,3] has enabled chemists to mimic nature's self-assembly principles, resulting in functional materials with tailored properties,[4−6] but it is often challenging to control the structure and mechanism of such self-assembled structures and their formation in real time. Stimuli-responsive supramolecular systems[7−10] offer better control of the self-assembly/reassembly process, which can be either switched on/off by an external stimulus such as anions, heat, light, sound, and so forth. Supramolecular low molecular weight gelators (LMWGs)[11−19] based on multicomponent systems have emerged as an important class of stimuli-responsive soft materials because of their potential applications in tuning gel-state properties.[20−25] Multicomponent gels obtained by mixing individual gels offer a good platform to analyze the supramolecular assembly of individual gels. For example, the individual gelator molecules interact either constructively or destructively to form well-ordered fibers containing individual gelators (self-sorting), both gelators (specific co-assembly, Scheme 1), or a mixture of both (random co-assembly).[24,25] Multicomponent self-assembled gels obtained by mixing enantiomers[25−37] display interesting properties because of the interaction between pure enantiomers, which facilitate the formation of mixed enantiomeric gels with intriguing properties that are not achieved by individual enantiomeric gels. These interactions will lead to more favorable packing in mixed enantiomeric gels,[25−37] presumably because of the interaction of the individual enantiomers either constructively or destructively. Recently, we have shown that mixing enantiomeric bis(urea) compounds tagged with phenylalanine methyl ester led to a multicomponent gel with enhanced thermal and mechanical strength.[30]

Scheme 1. Self-Sorting and Specific Co-assembly of Enantiomers in Mixed Gels

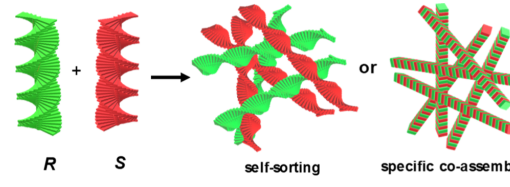

One of the main challenges in mixed gel systems is the prediction of the self-assembly process because it is hard to control the interactions between the individual gelators from the molecular to macroscopic level during the formation of fibrous networks.[25,38,39] The self-assembly process at the molecular level in multicomponent gels has been analyzed by various spectroscopic[40−46] and microscopic techniques.[47−51] Efforts have been made to unravel the self-assembly process of multicomponent enantiomeric gels by analyzing the physical properties using spectroscopic methods such as UV−vis, NMR, and IR and other methods such as differential scanning

Received: February 5, 2020
Revised: March 28, 2020
Published: April 1, 2020

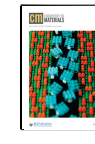

https://dx.doi.org/10.1021/acs.chemmater.0c00475
Chem. Mater. 2020, 32, 3517−3527

calorimetry and rheology.[52−59] We have studied the self-assembly process in mixed enantiomeric gels using scanning electron microscopy (SEM), atomic force microscopy (AFM), and solid-state NMR and showed that the resulting network is a mixture of self-sorted and co-assembled networks.[30] Recent developments in high-resolution X-ray diffraction have enabled researchers to differentiate self-sorted and co-assembled networks and identify the key parameters in the formation of multicomponent gel networks.[24,48,59−63] Adams and co-workers used fiber X-ray diffraction to show self-sorting in naphthalene-functionalized dipeptide hydrogelators.[59] Nisbet *et al.* showed that the small-angle X-ray scattering data of co-assembled system were different from the individual components.[60] Adams *et al.* proved that the individual components in multicomponent dipeptide gels are self-sorted by isolating the single crystals of one of the dipeptides in the gel network.[24]

Single-crystal X-ray diffraction (SCXRD) has been used to identify the key interactions in the solid-state structure of LMWGs,[64−71] which may provide some insight into the packing modes of these molecules in gel fibers. This approach was used by Pfeffer and co-workers to explain the gelation behavior of the enantiomers compared to the nongelator racemate.[72] However, the analysis of the self-assembly process in multicomponent gels based on enantiomers using SCXRD is not reported till date because of the lack of crystal structures of all possible stereoisomeric forms and the mixed enantiomers. The combination of single-crystal X-ray structure of the gelator and powder diffraction pattern of either the native gel or the xerogel will enable us to correlate the intermolecular interactions observed in the single-crystal structure with the molecular aggregation in the gel state. However, the removal of solvent to prepare a xerogel can result in artefacts because of dissolution, recrystallization, and changes in morphology or polymorphic phase transition, but this approach still remains as one of the practical methods to get insight into the self-assembly process in LMWGs.[12,19,71,73,74] Interestingly, this approach has not been explored for enantiomeric multicomponent gels because of the high scattering factor of the gel systems and also the nonavailability of the structural information for comparison. In this work, we have used X-ray diffraction to correlate the solid-state structures of multicomponent gel based on bis-amides of terephthalic acid and amino acid derivatives with the dried gel state. To the best of our knowledge, this is the first example correlating the self-assembly process of the gelator with its crystal structure in multicomponent gels based on enantiomers.

EXPERIMENTAL SECTION

Materials and Methods. All the starting materials and reagents were commercially available (Sigma-Aldrich and TCI Europe) and used as supplied. Enantiomeric (*S* or *R*)-methyl valinate was purchased as hydrochloride salt and the racemate in the acid form. Deionized water and freshly distilled ethanol were used for gelation and circular dichroism (CD) experiments. Dichloromethane (DCM) was distilled over CaH_2 prior to use in synthesis. Methyl *rac*-valinate was synthesized following the similar reported procedure.[75] ***SS*-TAV** is reported,[76] and ***RR*-TAV** and **TAV** were synthesized in similar fashion. The mono *tert*-butyl ester of terephthalic acid (**1**) was synthesized according to the literature.[77] ^{1}H and ^{13}C NMR spectra were recorded on a Bruker AVANCE 400 spectrometer. Attenuated total reflectance−Fourier transform infrared (ATR−FTIR) and CD were measured in a Nicolet iZ10 and a JASCO J-1100 CD spectrometer, respectively. SEM and AFM were performed on a Leo Supra 25 microscope and Bruker MultiMode 8, respectively. SCXRD and powder X-ray diffraction (PXRD) were carried out using Bruker D8 venture and Bruker D8 Focus instrument. High-performance liquid chromatography (HPLC) was performed on a Shimadzu Prominence LC-20A HPLC system to confirm purity of the compounds.

Synthesis. *Methyl rac-Valinate.* *rac*-Valine (3.0 g, 25.6 mmol) was dissolved in 50 mL of methanol, and 4 mL (6.5 g, 55.0 mmol) of thionyl chloride was added dropwise. The solution was refluxed at 65 °C for 8 h and then cooled to room temperature. Methanol was evaporated, and the white oil obtained was stirred with 2% $NaHCO_3$ solution. The solution was extracted with DCM (3 × 50 mL), and the combined organic layers were dried over Na_2SO_4 and evaporated to yield the ester as colorless oil. Yield: 2.6 g, 77%. ^{1}H NMR (400 MHz, $CDCl_3$): δ [ppm] 3.71 (3H, s), 3.29 (1H, d, J = 5.2), 2.01 (1H, m), 1.42 (2H, br s), 0.96 (3H, d, J = 6.8), 0.90 (3H, d, J = 6.8). ^{13}C NMR (100 MHz, $CDCl_3$): δ [ppm] 176.10, 60.08, 51.82, 32.32, 19.40, 17.32.

***SS*-TAV and *RR*-TAV.** Terephthaloyl dichloride (1.0 g, 4.9 mmol) and corresponding (*S* or *R*)-methyl valinate hydrochloride (1.7 g, 10.0 mmol) were taken in a two-neck RB flask under a dry N_2 atmosphere at 0 °C, and 40 mL of freshly distilled DCM was added to it. A solution of 3 mL (2.1 g, 21.5 mmol) of triethylamine in 30 mL dry DCM was added dropwise to the above solution, and the mixture was stirred overnight at room temperature. The clear solution was washed with 3.0% $NaHCO_3$ and 0.05 N HCl, followed by brine. The organic layer was dried over Na_2SO_4 and evaporated to yield the desired amide as the white solid.

SS-TAV. Yield 1.9 g, 98.5%. ^{1}H NMR (400 MHz, $CDCl_3$): δ [ppm] 7.87 (4H, s), 6.67 (2H, d, J = 8.4), 4.78 (2H, dd, J = 8.8, 5.0), 3.79 (6H, s), 2.29 (2H, m), 1.02 (6H, d, J = 6.8), 1.00 (6H, d, J = 7.2). ^{13}C NMR (100 MHz, $CDCl_3$): δ [ppm] 172.50, 166.30, 137.00, 127.40, 57.56, 52.33, 31.63, 18.99, 18.00. HRMS (APCI): calcd for $C_{20}H_{28}N_2O_6Na$ $[M + Na]^+$, 415.1840; found, 415.1831.

RR-TAV. Yield 1.88 g, 97.5%. ^{1}H NMR (400 MHz, $CDCl_3$): δ [ppm] 7.87 (4H, s), 6.69 (2H, d, J = 8.4), 4.78 (2H, dd, J = 8.8, 5.0), 3.78 (6H, s), 2.29 (2H, m), 1.02 (6H, d, J = 6.8), 1.00 (6H, d, J = 7.2). ^{13}C NMR (100 MHz, $CDCl_3$): δ [ppm] 172.47, 166.30, 136.98, 127.39, 57.55, 52.32, 31.62, 18.99, 18.00. HRMS (APCI): calcd for $C_{20}H_{28}N_2O_6Na$ $[M + Na]^+$, 415.1840; found, 415.1828.

TAV. The ternary mixture consisting of racemate and *meso* form (**TAV**) was synthesized in the similar procedure, except *rac*-methyl valinate (1.3 g, 10.0 mmol) was used in the amine form, and 1.5 mL (1.1 g, 11.0 mmol) of triethylamine was added during the reaction. Yield: 1.89 g, 98.0%. ^{1}H NMR (400 MHz, $CDCl_3$): δ [ppm] 7.86 (4H, s), 6.75 (2H, d, J = 8.4), 4.77 (2H, dd, J = 8.8, 5.0), 3.77 (6H, s), 2.28 (2H, m), 1.01 (6H, d, J = 7.2), 0.99 (6H, d, J = 6.8). ^{13}C NMR (100 MHz, $CDCl_3$): δ [ppm] 172.51, 166.51, 137.02, 127.56, 57.70, 52.45, 31.71, 19.12, 18.15. HRMS (APCI): cald for $C_{20}H_{28}N_2O_6Na$ $[M + Na]^+$ 415.1840; found, 415.1829.

tert-Butyl (S)-4-((1-Methoxy-3-methyl-1-oxobutan-2-yl)-carbamoyl)benzoate (2). 4-(*tert*-Butoxycarbonyl)benzoic acid (**1**)[77] (2.2 g, 10 mmol), 3 mL (4.9 g, 41.3 mmol) of thionyl chloride, and 5 mL of dry DCM were stirred in a RB flask under nitrogen at 45.0 °C overnight. The clear solution obtained was evaporated under reduced pressure to remove the volatile impurities leaving *tert*-butyl-4-(chlorocarbonyl)benzoate as the white solid, and 50 mL of dry DCM was added. Methyl *S*-valinate hydrochloride (1.7 g, 10.0 mmol) was added to this mixture and was cooled to at 0 °C under a N_2 atmosphere, followed by the dropwise addition of a solution of 3.5 mL (2.5 g, 25.1 mmol) of triethylamine in 50 mL of dry DCM. The mixture was stirred overnight at room temperature and then washed with 3.0% $NaHCO_3$, 0.05 N HCl, and brine. The organic layer was dried over Na_2SO_4 and evaporated to yield the mono-amide mono-*tert*-butyl ester (**2**) as a pale yellow solid. Yield 2.7 g, 80.6%. ^{1}H NMR (400 MHz, $CDCl_3$): δ [ppm] 8.04 (2H, d, J = 8.8), 7.83 (2H, d, J = 8.4), 6.68 (1H, d, J = 8.4), 4.78 (1H, dd, J = 8.6, 5.0), 3.78 (3H, s), 2.28 (1H, m), 1.60 (9H, s), 1.01 (3H, d, J = 6.8), 0.99 (3H, d, J = 7.2). ^{13}C NMR (100 MHz, $CDCl_3$): δ [ppm] 172.50, 166.52, 164.82, 137.48, 134.85, 129.66, 126.90, 81.67, 57.54, 52.33, 31.65, 28.13,

https://dx.doi.org/10.1021/acs.chemmater.0c00475
Chem. Mater. 2020, 32, 3517−3527

18.99, 18.01. HRMS (APCI): calcd for $C_{18}H_{25}NO_5Na$ $[M + Na]^+$, 358.1625; found, 358.1615.

*(S)-4-((1-Methoxy-3-methyl-1-oxobutan-2-yl)carbamoyl)-benzoic Acid (**3**).* To a solution of **2** (2.7 g, 8.0 mmol) in 16 mL DCM, 8 mL (11.9 g, 10.4 mmol) of trifluoracetic acid (TFA) was added. The reaction mixture was stirred overnight at room temperature, volatile impurities were evaporated, and the residue was passed through a column (silica gel, DCM/MeOH 4:1). The product was obtained as a white solid. Yield 2.1 g, 93.8%. ^{1}H NMR (400 MHz, $CDCl_3$): δ [ppm] ^{1}H NMR (400 MHz, $CDCl_3$): δ [ppm] 10.12 (1H, br s), 8.07 (2H, d, J = 8.4), 7.84 (2H, d, J = 8.8), 6.99 (1H, d, J = 8.8), 4.78 (1H, dd, J = 8.8, 5.2), 3.78 (3H, s), 2.30 (1H, m), 1.02 (3H, d, J = 6.8), 1.00 (3H, d, J = 6.4). ^{13}C NMR (100 MHz, $CDCl_3$): δ [ppm] 173.02, 169.74, 166.93, 138.41, 132.16, 130.31, 127.20, 57.70, 52.46, 31.41, 18.98, 17.99. HRMS (APCI) calcd for $C_{14}H_{17}NO_5Na$ $[M + Na]^+$, 302.0999; found, 302.1000.

***RS*-TAV (4).** To a suspension of mono carboxylic acid **3** (2.1 g, 7.5 mmol) in 5 mL of dry DCM, 2.2 mL (3.6 g, 30.3 mmol) of thionyl chloride was added under a N_2 atmosphere, and the reaction mixture was stirred at 45.0 °C overnight. A clear solution was observed, and the solvents were removed to yield the acid chloride methyl (4-(chlorocarbonyl)benzoyl)-*S*-valinate as a white solid powder. Dry DCM (50 mL) was charged to the acid chloride, and methyl *R*-valinate hydrochloride (1.3 g, 7.5 mmol) was subsequently added to a mixture under a N_2 atmosphere. A solution of 2.6 mL (1.9 g, 18.7 mmol) of triethylamine in 50 mL of dry DCM was added dropwise to the mixture at 0 °C and stirred overnight at room temperature. The solution was washed with 3.0% $NaHCO_3$, 0.05 N HCl, and brine. The organic layer was dried over Na_2SO_4 and evaporated to yield ***RS*-TAV** as a pale brown solid. Yield 2.7 g, 93.3%. The purity of the *meso* compound was confirmed by chiral HPLC (see Supporting Information, Figure S22). ^{1}H NMR (400 MHz, $CDCl_3$): δ [ppm] 7.87 (4H, s), 6.68 (2H, d, J = 8.8), 4.78 (2H, dd, J = 8.4, 4.8), 3.79 (6H, s), 2.29 (2H, m), 1.02 (6H, d, J = 7.2), 1.00 (6H, d, J = 7.2). ^{13}C NMR (100 MHz, $CDCl_3$): δ [ppm] 172.46, 166.29, 136.99, 127.38, 57.55, 52.43, 31.63, 18.91, 17.99. HRMS (APCI): calcd for $C_{20}H_{28}N_2O_6Na$ $[M + Na]^+$, 415.1840; found, 415.1834.

Gelation Details. *Gelation Test.* The required amount of the gelator was taken in a standard 7.0 mL vail, and 1.0 mL of appropriate solvent was added. The (***RR*+*SS*)-TAV** gel was prepared by mixing the equimolar ratio of individual ***RR*-TAV** and ***SS*-TAV** compounds, followed by the addition of the solvent/solvent mixture. The vial was closed, and the mixture was heated until a clear solution was observed. The solution was left undisturbed for gelation, and gel formation was confirmed by the inversion test.

Minimum Gel Concentration. Various amounts of the gelator were weighed, and gelation experiment was carried out as described above. The minimum amount of the gelator required to form gel after 24 h was noted as minimum gel concentration (MGC).

T_{gel} Experiment. The gelator (40.0 mg) was taken in a standard 7.0 mL vial, and 1.0 mL of appropriate solvent was added. The mixture was heated to form a clear solution and kept undisturbed. After 24 h, a small spherical glass ball (54.0 mg) was carefully placed on the top of the gel. The vial was immersed in an oil bath equipped with a magnetic stirrer and a thermosensor. Temperature of the oil bath was gradually increased by ∼10 °C per minute. The temperature at which the glass ball touched the bottom of the vial was recorded as T_{gel}.

Rheology. Rheological measurements for *m*-xylene gels were carried out using the MCR 102 Anton Paar modular compact rheometer using a 25.0 mm stainless steel parallel plate geometry configuration. The gels ***RR*-TAV**, ***SS*-TAV**, and ***RS*-TAV** were prepared by dissolving 80.0 mg of corresponding gelator in 2.0 mL of *m*-xylene. The (***RR*+*SS*)-*TAV*** gel was prepared by dissolving a mixture of 40.0 mg of ***RR*-TAV** and 40.0 mg of ***SS*-TAV** in 2.0 mL of *m*-xylene. Experiments were performed by scoping a ∼2.0 mL portion of gel on the plate. Viscoelastic properties were evaluated by oscillatory measurements at a constant temperature of 25.0 °C. Amplitude sweeps were performed with a constant frequency (f) of 1.0 Hz and log ramp strain (γ) = 0.01−100%, and frequency sweeps were carried out between 0.1 and 10.0 Hz within the linear viscoelasticity domain (0.1% strain). Rheology measurements for EtOH/water gels were made on an Anton Paar MCR 302 rheometer using a 25 mm stainless steel parallel plate geometry configuration and analyzed using the RheoCompass 1.24 software. Typical rheology measurements involved casting the sol [550 μL, 4.0 wt % in EtOH:H_2O (1:1, v/v)] onto one of the stainless-steel plates, lowering the other plate to the measurement position (1 mm), and for most of the cases, the gels were formed in 3 h. Then, gels were allowed to form, followed by applying constant frequency (f) = 1 Hz and strain (γ) = 0.2% until a plateau in the storage modulus was observed. To avoid evaporation and maintain a temperature of 25.0 °C for frequency and amplitude sweeps, we used a Peltier temperature control hood. Frequency sweeps were undertaken three times with a log ramp frequency (f) = 0.01−10 Hz in constant strain (γ) = 0.2%. Amplitude sweeps were also performed with constant frequency (f) = 1 Hz and log ramp strain (γ) = 0.1−100%.

Scanning Electron Microscopy. All gels were prepared at 4.0 wt % and filtered after 24 h. The residue was dried in air, and a small portion of the xerogel was placed on a pin mount with the carbon tab on top and was coated with gold for 3 min. Morphologies of the dried gels were examined on a Leo Supra 25 microscope with an in-lens detector at an operating voltage of 3 kV, with a working distance between 3 and 4 mm.

Atomic Force Microscopy. Solutions were prepared at 0.25 wt % in a 1:1 EtOH/water (v/v) mixture and cast onto a freshly cleaved mica substrate, followed by spreading of the drop over the mica using a glass slide, with the excess liquid wicked away using capillary action. These samples were left to dry in air overnight. Imaging was undertaken on a Bruker Multimode 8 atomic force microscope in Scanasyst mode in air, whereby the imaging parameters are constantly optimized through the force curves that are collected, preventing damage of soft samples. Bruker Scanasyst-Air probes were used, with a spring constant of 0.4−0.8 N/m and a tip radius of 2 nm.

Circular Dichroism. The data were collected using a JASCO J-1100 CD spectrometer between wavelengths of 190 and 350 nm at 20 nm per minute rate, bandwidth of 1 nm, and continuous scanning mode. All gels were prepared at 5.0 wt % in EtOH/water (1:1 v/v). After 24 h, the gels were dispersed in EtOH/water (1:1 v/v) to obtain various concentrations (0.025, 0.03, and 0.05 wt %), and 0.03 wt % was found to be the optimum concentration. CD experiments in the solution state were performed by dissolving 10.0 mg of the gelator in 3.0 mL of absolute EtOH and diluting ten times in the same solvent.

Crystallography. *Single-crystal X-ray Diffraction.* The compound (approximately 30.0 mg) was dissolved in 2.0 mL of suitable solvent and left in an open vial for crystallization. X-ray quality single crystals were isolated from mother liquor and quickly immersed in cryogenic oil and then mounted. The diffractions were collected using Cu Kα radiation (λ = 1.542 Å) on a Bruker D8 Venture (Photon100 CMOS detector) diffractometer equipped with a Cryostream (Oxford Cryosystems) open-flow nitrogen cryostats at a temperature of 120(2) K for the *meso* compound, and all other compounds were collected at 150(2) K. The unit cell determination, data collection, data reduction, structure solution/refinement, and empirical absorption correction were carried out using Apex-III (Bruker AXS: Madison, WI, 2015). All structure was solved by the direct method and refined by the full-matrix least squares on F^2 for all data using OLEX2[78] and SHELXTL[79] software. All nondisordered nonhydrogen atoms were refined anisotropically except for both the enantiomers. In these cases, the aromatic carbon atoms and the methoxy carbon atom of ester moieties were disordered, and the free variables were refined by FVAR instruction. All the hydrogen atoms were placed in the calculated positions and refined using a riding model. Crystallographic data for the structures have been deposited to the Cambridge Crystallographic Data Centre as supplementary publication (CCDC no: 1975764−1975767).

Powder X-ray Diffraction. The as-synthesized bulk compounds were ground to make a fine powder, and PXRD was performed on a Bruker D8 Focus instrument between a 2θ value of 4.0−60.0. PXRD was also performed on the xerogels obtained the similar way for SEM analysis.

https://dx.doi.org/10.1021/acs.chemmater.0c00475
Chem. Mater. 2020, 32, 3517−3527

Scheme 2. Synthesis of *RR*-TAV, *SS*-TAV, and TAV

Scheme 3. Synthesis of *RS*-TAV; (i) KOH and ^{t}BuOH, (ii) $SOCl_2$, *S*-Methyl Valinate Hydrochloride, Et_3N, and DCM, (iii) TFA and DCM, and (iv) $SOCl_2$, *R*-Methyl Valinate Hydrochloride, Et_3N, and DCM

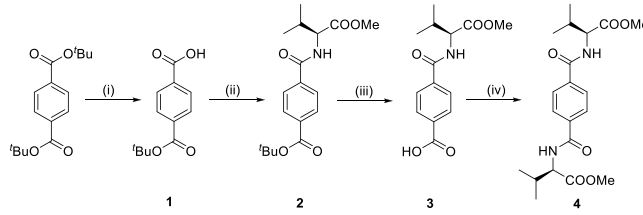

RESULTS AND DISCUSSION

The chiral and achiral bis-amide compounds such as enantiomeric and *meso* forms were synthesized and characterized using standard analytical techniques including SCXRD. Chiral LMWGs have emerged as a special class of soft materials because of their potential applications in chiral nanomaterials, chiral recognition, and asymmetric catalysis.[28,47,80−82] The molecular chirality of a particular enantiomer is often translated into gel fibres.[36,83] We have selected terephthalic amide of an amino acid ester (methyl valinate), owing to their ability to form C_2-symmetric chiral LMWGs.[84−90]

The terephthalic amide of amino acid ester is an ideal candidate for multicomponent gels based on enantiomers because of their availability in both enantiomeric and racemic forms, inexpensive starting materials, crystalline nature, and ease of modification.[91,92] The hydrogen-bonding interactions between the amide groups and $\pi-\pi$ interaction of the phenylene ring play an important role in the self-assembly process.[87−90] The diamides will display β-tape type self-assembly to form a well-defined fibrous network, resulting in the formation of various organo/hydrogels similar to the self-assembly process in peptides. The self-assembly mode of the amide group is preserved by introducing the ester derivatives, which will interfere the hydrogen bonding between amide and carboxylate functionalities.[93]

Thus, we have synthesized enantiopure *R*−*R*−, *S*−*S*−, and *R*−*S*-**TAV** based upon the valine methyl ester and terephthalic acid. Enantiopure ***RR*-TAV** and ***SS*-TAV** compounds were synthesized by reacting terephthaloyl dichloride and the corresponding *R*- or *S*-methyl valinate hydrochloride in DCM (Scheme 2) in the presence of triethylamine (Et_3N). The *meso* form ***RS*-TAV** with *R*−*S* configuration was synthesized by reacting mono ester-protected terephthalic acid chloride and *S*-methyl valinate hydrochloride to form a mono ester terephthalic amide with *S*-configuration, which was hydrolyzed, converted to acid chloride, and reacted with *R*-methyl valinate hydrochloride to form ***RS*-TAV** (Scheme 3). We have also synthesized **TAV** for comparison from terephthaloyl dichloride and racemate methyl valinate, which is expected to be a 1:1:2 mixture of *R*−*R*, *S*−*S*, and *R*−*S* isomers. The compounds were characterized by NMR, IR, mass spectroscopy, and SCXRD. The chirality of the compounds was confirmed by CD experiments, and the gelation properties were analyzed in a series of solvents using standard gelation techniques.

The gelation test was carried out by heating the gelator and the particular solvent in a sealed vial until a clear solution was obtained. The solution was sonicated prior to cooling in some cases to induce gelation, left undisturbed, and the gel formation was confirmed by a vial inversion test (Figure 1).

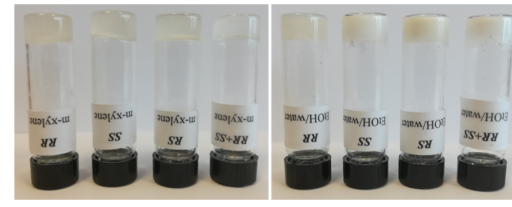

Figure 1. Gels obtained from **TAV** gelators (left) in *m*-xylene and (right) in EtOH/water (1:1 v/v).

Gelation was mostly observed in aromatic solvents for all compounds (see Supporting Information, Table S1) such as benzene, toluene, *o*-xylene, *m*-xylene, *p*-xylene, and mesitylene, which may be attributed to the $\pi-\pi$ interactions between the phenylene rings of the gelator and the aromatic solvents. In chlorobenzene, the *meso* compound (***RS*-TAV**) did not form a gel, but the enantiopure ***RR*-TAV** and ***SS*-TAV** formed a gel at 5.5 wt % (wt % refers to w/v % in all cases). Interestingly, gelation was not observed in various aliphatic solvents (<6.0 wt %) such as DCM, chloroform, 1,2-dichloroethane, acetone, butanone, THF, 1,4-dioxane, acetonitrile, methanol, ethanol, isopropanol, and butanol. The higher solubility of the gelator in these solvents may be attributed to the presence of strong hydrogen-bonding motifs or polar moieties, which hinders β-tape formation. The compounds were unable to form hydrogels because of their insolubility in water. This prompted us to check the gelation properties of these compounds in mixed solvent systems (1:1, v/v) by dissolving the compound in polar solvents (either methanol, ethanol, isopropanol or *tert*-butanol), followed by the addition of water. The resulting aqueous solutions were heated, cooled, and left undisturbed,

https://dx.doi.org/10.1021/acs.chemmater.0c00475
Chem. Mater. 2020, 32, 3517−3527

and gels were formed in all cases (see Supporting Information, Table S2).

The MGC of the gelators was evaluated in benzene, toluene, *o*-xylene, *m*-xylene, *p*-xylene, and mesitylene (Table 1). The

Table 1. Minimum Gel Concentration (MGC in wt %)

solvent	*RR*-TAV	*SS*-TAV	*RS*-TAV	(*RR*+*SS*)-TAV
benzene	2.3	2.3		2.0
toluene	3.0	3.0		2.0
o-xylene	2.5	2.5	3.5	2.0
m-xylene	2.5	2.5	3.0	1.5
p-xylene	2.5	2.5	3.5	2.0
mesitylene	1.5	1.5	2.0	1.2
chlorobenzene	5.5	5.5		4.0
EtOH/water (1:1)	4.0	4.0	4.0	3.5

MGC for *meso* form (***RS*-TAV**) was found to be higher compared to enantiopure ***RR*-TAV** and ***SS*-TAV**. The slow transformation of the ***RS*-TAV** gel network into crystalline materials indicates that the crystalline nature is predominant in the *meso* form. We also checked the MGC of **TAV**, which is a statistical mixture of ***RR*-TAV**, ***SS*-TAV**, and ***RS*-TAV** for comparison and found that the MGC was lower compared to the *meso* and enantiomeric forms. The strong gelation ability of **TAV** may be attributed to the presence of enantiomers (***RR*-TAV** and ***SS*-TAV**) and the *meso* form (***RS*-TAV**) in the ternary mixture (**TAV**). Recently, we have shown that the mixed gel of enantiopure *R*,*R*- and *S*,*S*-hexyl bis(urea) tagged with methyl phenylalaninate displayed enhanced thermal and mechanical stability compared to enantiopure gels as well as racemic mixture.[30]

This prompted us to analyze the gelation property of the multicomponent gel (***RR*+*SS*)-TAV** obtained by mixing equimolar ratio of enantiopure gels ***RR*-TAV** and ***SS*-TAV**. The gelation property of the mixture (***RR*+*SS*)-TAV** was analyzed in various solvents, and the mixture formed gels in various aromatic solvents such as benzene, toluene, *o*-xylene, *m*-xylene, *p*-xylene, mesitylene, and chlorobenzene (see Supporting Information, Table S1). The MGC of (***RR*+*SS*)-TAV** (Table 1) was lower compared to the corresponding enantiomers and *meso* gels but matched with the MGC of **TAV** mixture, indicating that the presence of enantiomeric mixtures increases the gelation ability in multicomponent gels (see Supporting Information, Table S3).

The thermal stabilities of the gel network were evaluated by gel to solution phase transition temperature test (T_{gel}) using the "dropping ball" method. The gels were prepared at 4.0 wt % in benzene, toluene, *o*-xylene, *m*-xylene, *p*-xylene, mesitylene, and ethanol/water mixture (1:1, v/v). The analysis of T_{gel} revealed that ***RR*-TAV** and ***SS*-TAV** had similar thermal stability (Table 1), which was not surprising because fibers should have identical strength with different optical rotations. The *meso* compound ***RS*-TAV** displayed significantly low T_{gel} indicating thermally weaker network compared to enantiomers. Interestingly, the mixture (***RR*+*SS*)-TAV** showed consistently high T_{gel} values in various solvents compared to both enantiopure (***RR*-TAV** and ***SS*-TAV**) and *meso* compound (***RS*-TAV**) (Table 2). This clearly indicates that mixing two enantiomers leads to a different self-assembly mode, resulting in enhanced thermal stability. We also determined T_{gel} for **TAV** for comparison (see Supporting Information, Table S5), which was found to be similar to the (***RR*+*SS*)-TAV** gel. This

Table 2. Sol−Gel Transition Temperature (T_{gel})

	T_{gel} (°C)			
Solvent	*RR*-TAV	*SS*-TAV	*RS*-TAV	(*RR*+*SS*)-TAV
p-xylene	87.2	87.6	60.0	106.2
m-xylene	90.4	90.2	76.0	102.0
o-xylene	85.2	85.0	63.0	96.3
Mesitylene	100.2	103.1	88.0	116.2
EtOH/water (1:1)	59.1	60.0	52.0	62.5

corroborates well with the fact that the existence of both enantiomers is a key factor and plays an important role in the thermal stability of gel network. The T_{gel} experiments of the hydrogels performed for enantiomers, *meso*, ternary mixture and the mixed enantiomeric gels did not show drastic differences, which may be attributed to the predominant crystalline nature of these compounds over the gel state in hydrophilic systems. The T_{gel} experiments of the mixed gels at 4.0 wt % performed by varying the concentration of both ***RR*-TAV** and ***SS*-TAV** in *m*-xylene and mesitylene revealed that the thermal stability of the mixed gel depends on the concentration of the enantiomers (see Supporting Information, Table S6).

The comprehensive structural characteristics such as semi solid-like properties and relative strength of the **TAV** gels were evaluated by rheology. Rheological measurements were performed at 4.0 wt % in *m*-xylene to evaluate mechanical properties of ***RR*-TAV**, ***SS*-TAV**, ***RS*-TAV**, and (***RR*+*SS*)-TAV**. Initially, a strain sweep was performed to determine the linear viscoelastic region (LVR), where the elastic modulus (G') was independent of the applied strain. The LVR ensured that the gels undergo reversible deformation during the experiments, which will enable us to evaluate the exact structural properties of the gels. The strain sweep measurement revealed that all the four gels displayed constant G' up to 0.1% of strain (see Supporting Information, Figure S1). The crossover points at which the gel networks collapsed to the liquid phase were found at around 0.5−3.0% of strain. Oscillatory frequency sweep experiment was performed between 0.1 and 10.0 Hz at 0.1% of strain. All organogels showed constant elastic (G') and viscous (G'') moduli under varying frequency, corroborating gel-like behavior (Figure 2).

The enantiopure and *meso* gels ***RR*-TAV**, ***SS*-TAV**, and ***RS*-TAV** displayed similar G' values in frequency sweep measurements. Interestingly, (***RR*+*SS*)-TAV** gel showed distinctly higher G' and G'' values compared to the enantiopure and *meso* gels, which indicates that the mixed gel displayed a relatively rigid network compared to other gels. Rheological measurements were also performed in EtOH/water (1:1, v/v) at 4.0 wt % for all gelators using a heat−cool method (see Supporting Information, Figures S2 and S3). The maximum storage modulus values (G') from frequency sweep measurements in EtOH/water indicate that the ***RR*-TAV** and ***SS*-TAV** gels were stiffer (>100 kPa) than the other gels (<30 kPa). The mechanical strength of the gels in EtOH/water compared to *m*-xylene gels was different presumably because of the favorable interactions of the enantiomers with hydrogen-bonding solvents.

The recent advances in microscopic techniques such as SEM, transmission electron microscopy (TEM), cryogenic TEM, AFM, and confocal laser scanning microscopy enabled researchers to visualize the morphology of self-assembled fibers in multicomponent gels.[47−51] SEM is one of the best techniques to visualize the morphology of the fibrous network

https://dx.doi.org/10.1021/acs.chemmater.0c00475
Chem. Mater. 2020, 32, 3517−3527

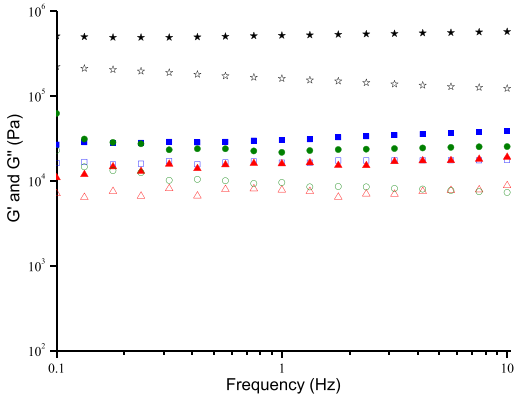

Figure 2. Frequency sweep of **TAV** gels (4.0 wt %) in *m*-xylene at 25.0 °C measured at a constant strain of 0.1%. Color codes: *G*′ ***RR*-TAV** (blue box solid), *G*″ ***RR*-TAV** (blue box), *G*′ ***SS*-TAV** (red triangle up solid), *G*″ ***SS*-TAV** (red triangle up open), *G*′ ***RS*-TAV** (circle solid), *G*″ ***RS*-TAV** (circle open), *G*′ (***RR*+*SS***)**-TAV** (star solid), and *G*″ (***RR*+*SS***)**-TAV** (star open).

in LMWGs, which could be used to differentiate self-sorted or co-assembled fibers in multicomponent systems. For example, fibers with similar morphologies as individual components were mostly observed in self-sorted systems but it is possible to visualize fibers with different morphologies in co-assembled systems. The organogels were prepared at 4.0 wt % in various solvents, and the hydrogel was obtained from EtOH/water (1:1, v/v) at 5.0 wt %. The gels were filtered after 24 h and dried overnight. The xerogels were placed on a carbon tab and gold coated for 3 min. The morphologies of the gels analyzed by SEM revealed typical fibrous morphologies in most of the cases (Figures 3 and see Supporting Information S4−S7).

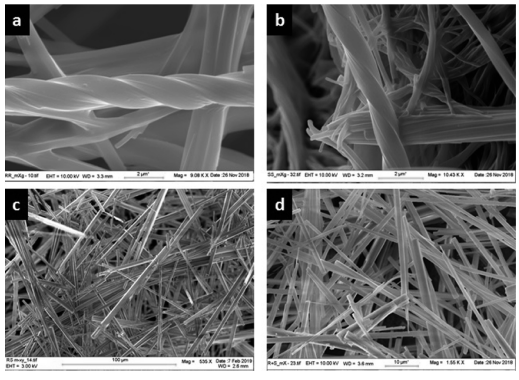

Figure 3. SEM images of (a) ***RR*-**, (b) ***SS*-**, (c) ***RS*-**, and (d) (***RR*+*SS***)-**TAV** xerogels in *m*-xylene at 4.0 wt %.

The enantiopure ***RR*-TAV** and ***SS*-TAV** displayed right-handed and left-handed twisted fibers, respectively, indicating that the molecular chirality has been translated into the hierarchical aggregates. The diameter of the thin fibers ranged from 250 to 400 nm, and the thick fibers were between 600 nm and 1.0 μm. The optically inactive *meso* compound ***RS*-TAV** showed a needle-like morphology with diameter ranging from 2.0 to 8.0 μm. The morphology of mixed (***RR*+*SS***)**-TAV** xerogel was different from individual enantiomers, displaying crystalline needle-like fibers in all solvents. This indicates the co-assembly of ***RR*-** and ***SS*-** compounds in the mixed gel, resulting in the cancellation of opposite helixes. The width of the needles ranged from 1.1 to 2.4 μm, and these needles did not show helicity across all lengths.

The SEM images of the dried hydrogels of all the compounds (5.0 wt %) in 1:1 (v/v) ethanol/water displayed needle and block-shaped morphologies (see Supporting Information, Figure S6), which may be attributed to the strong hydrogen-bonding interaction between the amide and the polar solvents. The enantiomers displayed the twisted needle-like morphology, and a mixture of needle and block shaped fibers was observed in the *meso* form. The hydrogel of (***RR*+*SS***)**-TAV** displayed the block-shaped morphology, indicating that the enantiomers interacted each other to form a co-assembled network, which was confirmed by the absence of self-sorted twisted fibers. The SEM image of the **TAV** in *m*-xylene and mesitylene indicated a mixture of tape and twisted tape-like fibers, which confirms the presence of enantiomers, *meso*, and the mixed gels in the ternary mixture (**TAV**) (see Supporting Information, Figure S7).

To confirm that the fibrous network morphology and handedness observed for all the xerogels from *m*-xylene were also present in 1:1 (v/v) EtOH/water gels, AFM was undertaken on these samples (Figure 4). As observed in the SEM images, right- and left-handed twisted fibers were observed for ***RR*-** and ***SS*-TAV** xerogels, respectively. Interestingly, EtOH/water xerogels of ***RS*-TAV** showed a tightly packed network of smaller fibers that almost appeared braided together, whereas the (***RR*+*SS***)**-TAV** xerogel showed long, branched fibers with no evidence of handedness. This is

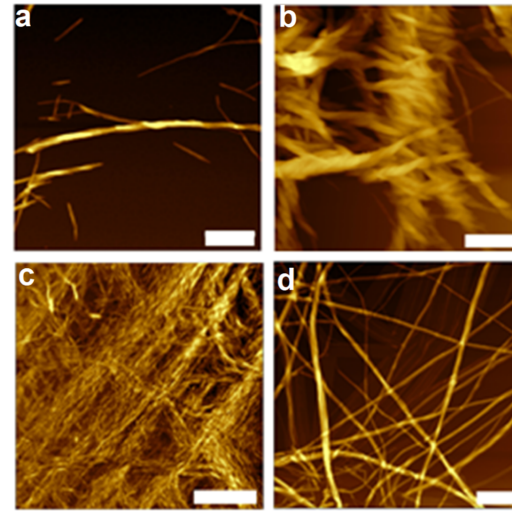

Figure 4. AFM images of (a) ***RR*-**, (b) ***SS*-**, (c) ***RS*-**, and (d) (***RR*+*SS***)**-TAV** gels in EtOH/water (1:1, v/v). Scale bar represents 300 nm in all images except (c), where the scale bar is 1 μm. Samples were spread coated onto freshly cleaved mica at 0.25 wt % apart from (***RR*+*SS***)**-TAV**, which was prepared at 0.5 wt %.

https://dx.doi.org/10.1021/acs.chemmater.0c00475
Chem. Mater. 2020, 32, 3517−3527

in excellent agreement with the handedness observed in SEM images and suggests a conservation of specific co-assembly mechanism across different solvent systems. Fiber diameters were largely similar across **TAV** xerogels of different handednesses, with diameters of 9.7 ± 2.9, 10.8 ± 1.6, and 8.4 ± 2.0 nm observed for (***RR***+***SS***)-, ***RS***-, and ***RR***-**TAV** xerogels, respectively. ***SS***-**TAV** xerogels yielded a slightly larger fiber diameter of 19.0 ± 6.0 nm, which likely represented a braided arrangement of two individual fibrils, as observed in Figure 4b. The discrepancy between fiber diameters measured through SEM and AFM can be ascribed to a combination of different gelation solvents, coupled with the different concentrations that the measurements were performed. At the higher concentrations (4.0 wt %) used for SEM imaging, it is expected that more aggregation will occur, leading to larger fiber diameters.

CD experiments help to elucidate the structural information of the assembled hierarchical aggregates. CD provides information about the chirality-driven self-assembly process, which can be obtained by comparing the CD signals of the solution and gel state. The solution-state CD experiments were performed in EtOH at 0.03 wt % to confirm the chirality of these compounds (see Supporting Information, Figure S8). The CD experiments of the gels in aromatic solvents were not possible because of the background absorption of the solvents in the CD spectrum. Thus, we have selected hydrogels in 1:1 (v/v) ethanol/water mixture for the CD experiments, which shows absorption cut off at around 190−200 nm. The hydrogels (5.0 wt %) obtained from 1:1 ethanol/water (v/v) mixture were dispersed in a dilute solution of the same solvent mixture to ensure homogenous dispersion of the fibers in the medium. The CD experiments performed at various concentrations revealed that 0.03 wt % was the optimum gelator concentration for these experiments.

The CD spectrum of ***RR***-**TAV** showed positive and negative maxima at 225 and 250 nm, respectively, and the spectrum was found to be mirror image of ***SS***-**TAV** (Figure 5). The peaks at 250 nm may be attributed to the β-sheet-like architecture observed in short peptide self-assembled gels, arising from amide hydrogen-bonding and $\pi-\pi$ stacking interactions.[94−96]

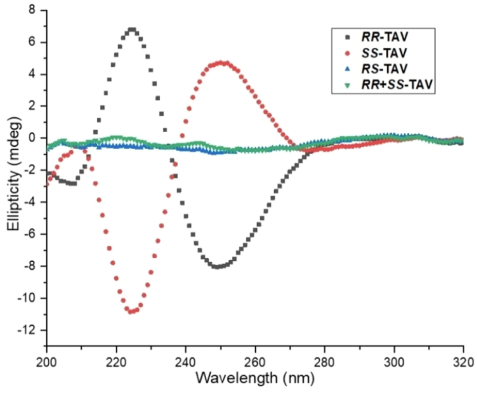

Figure 5. CD spectra of ***RR***-, ***SS***-, ***RS***-, and (***RR***+***SS***)-**TAV** in the dispersed gel state measured at 25.0 °C. Gels formed at 5.0 wt % in EtOH/water (1:1 v/v) were diluted with the same solvent system to 0.03 wt %.

The *meso* compound ***RS***-**TAV** displayed a linear CD signal, and the absence of strong absorption peaks at 225 and 250 nm confirmed the cancelation of the optical rotation because of the presence of opposite stereogenic centers. The CD spectrum of the mixed gel of equimolar mixture of ***RR***-**TAV** and ***SS***-**TAV** was similar to the *meso* compound (Figure 5). We have performed the CD at higher water concentration (EtOH/water, 1:4, v/v) for all gels, and similar spectra were observed in all cases (see Supporting Information, Figure S9). The experiments were also carried out with different ***RR***-**TAV** and ***SS***-**TAV** ratios in mixed gel. The mixture (***RR***-**TAV** and ***SS***-**TAV**, 75:25) displayed positive maxima, and the mixture (***RR***-**TAV** and ***SS***-**TAV**, 25:75) displayed negative maxima in both solution (see Supporting Information, Figure S10a) and dispersed gel state (see Supporting Information, Figure S10b) because of the presence of one of the enantiomers in excess.

ATR−FTIR spectroscopy has been used to extract information about the extent of hydrogen bonding in supramolecular gels,[43,46,97−99] and the difference between N−H stretching peaks in the solid state and gel state will enable elucidation of structural information for the self-assembled hierarchical **TAV** aggregates. The IR spectra recorded in the gel states indicated a slight broadening of the amide band, and the N−H stretching peaks were shifted toward lower wavenumber for ***RS***-**TAV** and (***RR***+***SS***)-**TAV**. The maximum shift (26.0 cm^{-1}) was observed for (***RR***+***SS***)-**TAV**, suggesting that the mixed gel network displayed stronger and extended hydrogen bonding compared to other gels (see Supporting Information, Figures S12−S15 and Table S7).

The crystallization experiments were performed in a wide range of solvent or solvent mixtures, and single crystals were obtained via slow evaporation over 2−3 days, depending upon the solvent used. Analysis of the crystal morphologies revealed that block-shaped crystals were obtained for ***RR***-**TAV**, ***SS***-**TAV**, and (***RR***+***SS***)-**TAV** by the vapor phase diffusion of diethyl ether into a toluene solution of the compound, and plate-shaped crystals were obtained for ***RS***-**TAV**. However, block-shaped crystals were obtained for ***SS***-**TAV**, ***RS***-**TAV**, and (***RR***+***SS***)-**TAV** in 1:1 (v/v) aqueous mixture (EtOH/water and 1,4-dioxane/water), whereas ***RR***-**TAV** formed needle-shaped crystals. The crystals of ***RR***-**TAV** and ***SS***-**TAV** isolated from different solvents displayed an identical structure, which was confirmed by SCXRD and PXRD. The crystallographic details and hydrogen-bonding parameters of the compounds are summarized in Tables S8 and S9 (see Supporting Information), respectively.

The enantiomers ***SS***-**TAV** and ***RR***-**TAV** crystallized in the chiral $P2_1$ space group (see Supporting Information, Figures S16 and S17) with three molecules in the asymmetric unit oriented orthogonally to each other. The methyl ester and the aromatic moieties of one of the molecules were disordered in both cases, and the structure and hydrogen-bonding patterns of these two enantiomers were similar. The nitrogen atom and the oxygen atom of the amide moieties of the gelator displayed N−H···O hydrogen-bonding interactions with four molecules to form a hydrogen bonded zig-zag sheet-like architecture. In the crystal structure, two zig-zag sheets were oriented perpendicular to each other, which might explain the helical twist in gel fibers of ***SS***-**TAV** and ***RR***-**TAV**. The *meso* compound ***RS***-**TAV** crystallized in the centrosymmetric $P2_1/c$ space group with an inversion center at the centroid of the phenylene ring (see Supporting Information, Figure S18),

https://dx.doi.org/10.1021/acs.chemmater.0c00475
Chem. Mater. 2020, 32, 3517−3527

making the molecule optically inactive. The amide moieties displayed similar N−H···O hydrogen-bonding interactions as the enantiomers, but a 2-D hydrogen-bonded sheet-like architecture was observed in ***RS*-TAV**.

The equimolar mixture of the two enantiomers (***RR*+*SS*)-TAV** crystallized in the centrosymmetric $P2_1/c$ space group with one enantiomer in the asymmetric unit (Figure 6a), which

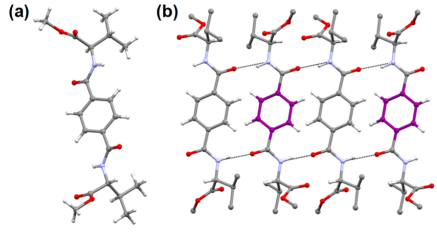

Figure 6. Single-crystal structure of (***RR*+*SS*)-TAV**: (a) asymmetric unit (b) H-bonded 1-D chain showing specific co-assembly; the phenyl carbon atoms of ***RR*-TAV** and ***SS*-TAV** are shown in gray and purple color, respectively, and the hydrogen atoms of the ester and isopropyl groups are omitted for clarity.

was related to the other enantiomer *via* an inversion center. Interestingly, the amide moieties displayed complementary amide hydrogen bonding and the adjacent enantiomer interacted *via* N−H···O interactions. These interactions resulted in a 1-D hydrogen-bonded tape with a sequence of −(*R*−*R*)−(*S*−*S*)−(*R*−*R*)−(*S*−*S*)−, confirming the specific co-assembly of two enantiomers (Figure 6b). The 1-D tape interacted with adjacent tapes *via* various nonbonding interactions, which was oriented perpendicular to each other. The extended 1-D chain-like architecture with co-assembled enantiomers explains the enhanced thermal and mechanical stability of the mixed gels.

The correlation of single-crystal structure and the gel network was analyzed by comparing the crystal structure with the PXRD data of the dried gel. The gels obtained from EtOH/water (1:1, v/v, 4.0 wt %) were filtered after 24 h and dried under a fume hood. The PXRD pattern of the xerogels was compared to the simulated pattern obtained from the crystal structure. The PXRD pattern of the xerogel obtained from the mixed (***RR*+*SS*)-TAV** gel matched perfectly with the simulated pattern (Figure 7), indicating that the crystal structure truly represents the hierarchical assembly of the xerogel network. This confirms that the translation of specific co-assembly of ***RR*-TAV** and ***SS*-TAV** enantiomers from the molecular level to mesoscopic xerogel network was achieved. The PXRD pattern of the xerogels of enantiomers (***RR*-TAV** and ***SS*-TAV**) was also found to be similar to the simulated pattern, but the peak intensities were lower (see Supporting Information, Figures S19 and S20) presumably because of the low order and less crystallinity of the xerogels compared to the crystalline state.

The PXRD pattern of ***RS*-TAV** xerogel matched with the simulated and bulk crystal pattern except a sharp peak at 8.5° (2θ), which may be attributed to the presence of hydrogen-bonded solvent molecules in the xerogel (see Supporting Information, Figure S21). The PXRD pattern of the xerogels and the bulk crystals with the corresponding crystal structures clearly indicates the phase purity of these compounds and proved that the solid-state structure truly represents the

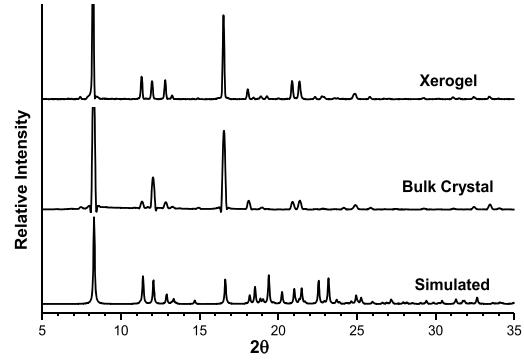

Figure 7. Comparison of PXRD pattern of (***RR*+*SS*)-TAV**: simulated, bulk crystals obtained from EtOH/water and xerogel at 4.0 wt % obtained from EtOH/water (1:1, v/v).

hierarchical assembly of the xerogel network. Thus, we have used the combination of single-crystal X-ray and powder X-ray diffraction to analyze the self-assembly modes in enantiomeric multicomponent gels. Importantly, the results do show unambiguously that (***RR*+*SS*)-TAV** co-assembles in both the solid and the gel states, explaining that this mixture has very different stability (T_{gel}) and mechanical properties from the individual enantiomers. The correlation of nonbonding interactions in the solid-state structure to the xerogel will add up to the ongoing efforts to identify the key interactions that control the self-assembly process.

CONCLUSIONS

The self-assembly modes in chiral bis-amide supramolecular gels in all three possible stereoisomeric forms (*R*−*R*, *S*−*S*, and *R*−*S*) and mixed enantiomers were studied using X-ray diffraction. The multicomponent gel (***RR*+*SS*)-TAV** based on enantiomers was prepared by mixing an equimolar ***RR*-TAV** and ***SS*-TAV**, and the mixed gel displayed enhanced mechanical and thermal stabilities compared to the enantiomers and the *meso* form. The preservation of chirality of the gel was analyzed by the CD experiment. The SCXRD revealed a chiral 2-D sheet architecture for both enantiomers, but the planar sheet architecture was observed for the *meso* form. The mixed gelator (***RR*+*SS*)-TAV** displayed specific co-assembly of the two enantiomers, resulting in a 1-D hydrogen-bonded network, which was further supported by SEM and AFM images. The increased thermal and mechanical strength of the mixed gel may be attributed to the enhanced intermolecular forces between the enantiomers, leading to specific co-assembly in the mixed gel. The understanding of noncovalent interactions between the individual gelators at the molecular level leading to the specific co-assembly process will enable supramolecular chemists to design multicomponent systems with tunable properties.

ASSOCIATED CONTENT

Supporting Information

The Supporting Information is available free of charge at https://pubs.acs.org/doi/10.1021/acs.chemmater.0c00475.

Further gelation studies, rheology, SEM images, CD experiments, IR spectra, hydrogen-bonding parameters,

https://dx.doi.org/10.1021/acs.chemmater.0c00475
Chem. Mater. 2020, 32, 3517−3527

comparison of powder X-ray pattern, and HPLC of ***RR***-, ***SS***-, and ***RS***-**TAV** (PDF)

X-ray crystallography data of ***SS***-**TAV** (CIF)

X-ray crystallography data of ***RS***-**TAV** (CIF)

X-ray crystallography data of (***RR***+***SS***)-**TAV** (CIF)

X-ray crystallography data of ***RR***-**TAV** (CIF)

AUTHOR INFORMATION

Corresponding Author

Krishna K. Damodaran − *Department of Chemistry, Science Institute, University of Iceland, 107, Iceland*; orcid.org/0000-0002-9741-2997; Phone: +354 525 4846; Email: krishna@hi.is; Fax: +354 552 8911

Authors

Dipankar Ghosh − *Department of Chemistry, Science Institute, University of Iceland, 107, Iceland*

Abbas D. Farahani − *School of Chemistry, The Australian Centre for Nanomedicine and the ARC Centre of Excellence in Convergent Bio-Nano Science and Technology, University of New South Wales, Sydney 2052, Australia*

Adam D. Martin − *Dementia Research Centre, Department of Biomedical Science, Faculty of Medicine and Health Sciences, Macquarie University, Sydney, New South Wales 2109, Australia*; orcid.org/0000-0002-5445-0299

Pall Thordarson − *School of Chemistry, The Australian Centre for Nanomedicine and the ARC Centre of Excellence in Convergent Bio-Nano Science and Technology, University of New South Wales, Sydney 2052, Australia*; orcid.org/0000-0002-1200-8814

Complete contact information is available at: https://pubs.acs.org/10.1021/acs.chemmater.0c00475

Notes

The authors declare no competing financial interest.

ACKNOWLEDGMENTS

We thank the University of Iceland Research Fund and Science Institute for funding. D.G. thanks the University of Iceland for the Doctoral Research and Teaching Assistantship grant. We thankfully acknowledge Poulami Chakraborty, School of Chemical Sciences, Indian Association for the Cultivation of Science (IACS), Kolkata, India for rheology measurements in *m*-xylene, Dr. Sigurdur Sveinn Jónsson, ÍSOR-Iceland for PXRD analysis, Kristinn Ragnar Óskarsson, University of Iceland for CD experiments and Dr. Sigridur Jónsdóttir, University of Iceland for NMR and Mass spectroscopy. We thank Rannís Iceland for infrastructure grants for a single-crystal X-ray diffractometer (150998-0031) and CD spectrometer (171448-0031). P.T. thanks the Australian Research Council for an ARC Centre of Excellence grant (CE140100036) and ARC Discovery Project grant (DP190101892). A.D.M. thanks the National Health and Medical Research Council for a Dementia Development Research Fellowship (APP1106751).

REFERENCES

(1) Ball, P. *The Self-Made Tapestry: Pattern Formation in Nature*; Oxford University Press, Inc.: Oxford, U.K., 2001; p 296.

(2) Lehn, J. M. *Supramolecular Chemistry: Concepts and Perspectives*; Wiley-VCH: Weinheim, Germany, 1995; p 262.

(3) *Comprehensive Supramolecular Chemistry*; Lehn, J. M., Atwood, J. L., Davies, J. E. D., MacNicol, D. D., Vögtle, F., Eds.; Pergamon: Oxford, U.K., 1996; Vol. *11*.

(4) Lehn, J.-M. Perspectives in Chemistry—Steps towards Complex Matter. *Angew. Chem., Int. Ed.* **2013**, *52*, 2836−2850.

(5) Lehn, J.-M. Constitutional Dynamic Chemistry: Bridge from Supramolecular Chemistry to Adaptive Chemistry. In *Constitutional Dynamic Chemistry*; Barboiu, M., Ed.; Springer: Berlin: Heidelberg, 2012; Vol. *322*, pp 1−32.

(6) Lehn, J.-M. Perspectives in Chemistry—Aspects of Adaptive Chemistry and Materials. *Angew. Chem., Int. Ed.* **2015**, *54*, 3276−3289.

(7) McConnell, A. J.; Wood, C. S.; Neelakandan, P. P.; Nitschke, J. R. Stimuli-Responsive Metal−Ligand Assemblies. *Chem. Rev.* **2015**, *115*, 7729−7793.

(8) Theato, P.; Sumerlin, B. S.; O'Reilly, R. K.; Epps, T. H., III Stimuli responsive materials. *Chem. Soc. Rev.* **2013**, *42*, 7055−7056.

(9) Shigemitsu, H.; Hamachi, I. Supramolecular Assemblies Responsive to Biomolecules toward Biological Applications. *Chem.—Asian J.* **2015**, *10*, 2026−2038.

(10) Segarra-Maset, M. D.; Nebot, V. J.; Miravet, J. F.; Escuder, B. Control of molecular gelation by chemical stimuli. *Chem. Soc. Rev.* **2013**, *42*, 7086−7098.

(11) Banerjee, S.; Das, R. K.; Maitra, U. Supramolecular gels 'in action'. *J. Mater. Chem.* **2009**, *19*, 6649−6687.

(12) Dastidar, P. Supramolecular gelling agents: can they be designed? *Chem. Soc. Rev.* **2008**, *37*, 2699−2715.

(13) de Loos, M.; Feringa, B. L.; van Esch, J. H. Design and Application of Self-Assembled Low Molecular Weight Hydrogels. *Eur. J. Org. Chem.* **2005**, 3615−3631.

(14) Estroff, L. A.; Hamilton, A. D. Water Gelation by Small Organic Molecules. *Chem. Rev.* **2004**, *104*, 1201−1218.

(15) George, M.; Weiss, R. G. Molecular Organogels Soft Matter Comprised of Low-Molecular-Mass Organic Gelators and Organic Liquids. *Acc. Chem. Res.* **2006**, *39*, 489−497.

(16) Hirst, A. R.; Escuder, B.; Miravet, J. F.; Smith, D. K. High-Tech Applications of Self-Assembling Supramolecular Nanostructured Gel-Phase Materials: From Regenerative Medicine to Electronic Devices. *Angew. Chem., Int. Ed.* **2008**, *47*, 8002−8018.

(17) Kumar, D. K.; Steed, J. W. Supramolecular gel phase crystallization: orthogonal self-assembly under non-equilibrium conditions. *Chem. Soc. Rev.* **2014**, *43*, 2080−2088.

(18) Steed, J. W. Anion-tuned supramolecular gels: a natural evolution from urea supramolecular chemistry. *Chem. Soc. Rev.* **2010**, *39*, 3686−3699.

(19) Yu, G.; Yan, X.; Han, C.; Huang, F. Characterization of supramolecular gels. *Chem. Soc. Rev.* **2013**, *42*, 6697−6722.

(20) Buerkle, L. E.; Rowan, S. J. Supramolecular gels formed from multi-component low molecular weight species. *Chem. Soc. Rev.* **2012**, *41*, 6089−6102.

(21) Edwards, W.; Smith, D. K. Enantioselective Component Selection in Multicomponent Supramolecular Gels. *J. Am. Chem. Soc.* **2014**, *136*, 1116−1124.

(22) Cross, E. R.; Sproules, S.; Schweins, R.; Draper, E. R.; Adams, D. J. Controlled Tuning of the Properties in Optoelectronic Self-Sorted Gels. *J. Am. Chem. Soc.* **2018**, *140*, 8667−8670.

(23) Draper, E. R.; Eden, E. G. B.; McDonald, T. O.; Adams, D. J. Spatially resolved multicomponent gels. *Nat. Chem.* **2015**, *7*, 848.

(24) Colquhoun, C.; Draper, E. R.; Eden, E. G. B.; Cattoz, B. N.; Morris, K. L.; Chen, L.; McDonald, T. O.; Terry, A. E.; Griffiths, P. C.; Serpell, L. C.; Adams, D. J. The effect of self-sorting and co-assembly on the mechanical properties of low molecular weight hydrogels. *Nanoscale* **2014**, *6*, 13719−13725.

(25) Raeburn, J.; Adams, D. J. Multicomponent low molecular weight gelators. *Chem. Commun.* **2015**, *51*, 5170−5180.

(26) Swanekamp, R. J.; DiMaio, J. T. M.; Bowerman, C. J.; Nilsson, B. L. Coassembly of Enantiomeric Amphipathic Peptides into Amyloid-Inspired Rippled β-Sheet Fibrils. *J. Am. Chem. Soc.* **2012**, *134*, 5556−5559.

(27) Edwards, W.; Smith, D. Chiral Assembly Preferences and Directing Effects in Supramolecular Two-Component Organogels. *Gels* **2018**, *4*, 31.
(28) Brizard, A.; Oda, R.; Huc, I. Chirality Effects in Self-assembled Fibrillar Networks. In *Low Molecular Mass Gelator*; Springer: Berlin: Heidelberg, 2005; pp 167−218.
(29) Smith, D. K. Lost in translation? Chirality effects in the self-assembly of nanostructured gel-phase materials. *Chem. Soc. Rev.* **2009**, *38*, 684−694.
(30) Tómasson, D. A.; Ghosh, D.; Kržišnik, Z.; Fasolin, L. H.; Vicente, A. A.; Martin, A. D.; Thordarson, P.; Damodaran, K. K. Enhanced Mechanical and Thermal Strength in Mixed-Enantiomers-Based Supramolecular Gel. *Langmuir* **2018**, *34*, 12957−12967.
(31) Das, R. K.; Kandanelli, R.; Linnanto, J.; Bose, K.; Maitra, U. Supramolecular Chirality in Organogels: A Detailed Spectroscopic, Morphological, and Rheological Investigation of Gels (and Xerogels) Derived from Alkyl Pyrenyl Urethanes. *Langmuir* **2010**, *26*, 16141−16149.
(32) Nagy, K. J.; Giano, M. C.; Jin, A.; Pochan, D. J.; Schneider, J. P. Enhanced Mechanical Rigidity of Hydrogels Formed from Enantiomeric Peptide Assemblies. *J. Am. Chem. Soc.* **2011**, *133*, 14975−14977.
(33) Adhikari, B.; Nanda, J.; Banerjee, A. Multicomponent hydrogels from enantiomeric amino acid derivatives: helical nanofibers, handedness and self-sorting. *Soft Matter* **2011**, *7*, 8913−8922.
(34) Cicchi, S.; Ghini, G.; Lascialfari, L.; Brandi, A.; Betti, F.; Berti, D.; Baglioni, P.; Di Bari, L.; Pescitelli, G.; Mannini, M.; Caneschi, A. Self-sorting chiral organogels from a long chain carbamate of 1-benzyl-pyrrolidine-3,4-diol. *Soft Matter* **2010**, *6*, 1655−1661.
(35) Nagy-Smith, K.; Beltramo, P. J.; Moore, E.; Tycko, R.; Furst, E. M.; Schneider, J. P. Molecular, Local, and Network-Level Basis for the Enhanced Stiffness of Hydrogel Networks Formed from Coassembled Racemic Peptides: Predictions from Pauling and Corey. *ACS Cent. Sci.* **2017**, *3*, 586−597.
(36) Duan, P.; Cao, H.; Zhang, L.; Liu, M. Gelation induced supramolecular chirality: chirality transfer, amplification and application. *Soft Matter* **2014**, *10*, 5428−5448.
(37) Liu, Z.; Sun, J.; Zhou, Y.; Zhang, Y.; Wu, Y.; Nalluri, S. K. M.; Wang, Y.; Samanta, A.; Mirkin, C. A.; Schatz, G. C.; Stoddart, J. F. Supramolecular Gelation of Rigid Triangular Macrocycles through Rings of Multiple C−H···O Interactions Acting Cooperatively. *J. Org. Chem.* **2016**, *81*, 2581−2588.
(38) Draper, E. R.; Adams, D. J. How should multicomponent supramolecular gels be characterised? *Chem. Soc. Rev.* **2018**, *47*, 3395−3405.
(39) Draper, E. R.; Wallace, M.; Schweins, R.; Poole, R. J.; Adams, D. J. Nonlinear Effects in Multicomponent Supramolecular Hydrogels. *Langmuir* **2017**, *33*, 2387−2395.
(40) Chen, L.; Revel, S.; Morris, K.; Adams, D. J. Energy transfer in self-assembled dipeptide hydrogels. *Chem. Commun.* **2010**, *46*, 4267−4269.
(41) Felip-León, C.; Díaz-Oltra, S.; Galindo, F.; Miravet, J. F. Chameleonic, Light Harvesting Photonic Gels Based on Orthogonal Molecular Fibrillization. *Chem. Mater.* **2016**, *28*, 7964−7972.
(42) Draper, E. R.; Lee, J. R.; Wallace, M.; Jäckel, F.; Cowan, A. J.; Adams, D. J. Self-sorted photoconductive xerogels. *Chem. Sci.* **2016**, *7*, 6499−6505.
(43) Abul-Haija, Y. M.; Roy, S.; Frederix, P. W. J. M.; Javid, N.; Jayawarna, V.; Ulijn, R. V. Biocatalytically Triggered Co-Assembly of Two-Component Core/Shell Nanofibers. *Small* **2014**, *10*, 973−979.
(44) Sarkar, A.; Dhiman, S.; Chalishazar, A.; George, S. J. Visualization of Stereoselective Supramolecular Polymers by Chirality-Controlled Energy Transfer. *Angew. Chem., Int. Ed.* **2017**, *56*, 13767−13771.
(45) Sugiyasu, K.; Kawano, S.-i.; Fujita, N.; Shinkai, S. Self-Sorting Organogels with p−n Heterojunction Points. *Chem. Mater.* **2008**, *20*, 2863−2865.
(46) Xing, P.; Chu, X.; Li, S.; Xin, F.; Ma, M.; Hao, A. Switchable and orthogonal self-assemblies of anisotropic fibers. *New J. Chem.* **2013**, *37*, 3949−3955.
(47) Moffat, J. R.; Smith, D. K. Controlled self-sorting in the assembly of 'multi-gelator' gels. *Chem. Commun.* **2009**, 316−318.
(48) Onogi, S.; Shigemitsu, H.; Yoshii, T.; Tanida, T.; Ikeda, M.; Kubota, R.; Hamachi, I. In situ real-time imaging of self-sorted supramolecular nanofibres. *Nat. Chem.* **2016**, *8*, 743.
(49) Singh, N.; Zhang, K.; Angulo-Pachón, C. A.; Mendes, E.; van Esch, J. H.; Escuder, B. Tandem reactions in self-sorted catalytic molecular hydrogels. *Chem. Sci.* **2016**, *7*, 5568−5572.
(50) Singh, N.; Maity, C.; Zhang, K.; Angulo-Pachón, C. A.; van Esch, J. H.; Eelkema, R.; Escuder, B. Synthesis of a Double-Network Supramolecular Hydrogel by Having One Network Catalyse the Formation of the Second. *Chem.—Eur. J.* **2017**, *23*, 2018−2021.
(51) An, B.; Wang, X.; Cui, M.; Gui, X.; Mao, X.; Liu, Y.; Li, K.; Chu, C.; Pu, J.; Ren, S.; Wang, Y.; Zhong, G.; Lu, T. K.; Liu, C.; Zhong, C. Diverse Supramolecular Nanofiber Networks Assembled by Functional Low-Complexity Domains. *ACS Nano* **2017**, *11*, 6985−6995.
(52) Xing, P.; Tham, H. P.; Li, P.; Chen, H.; Xiang, H.; Zhao, Y. Environment-Adaptive Coassembly/Self-Sorting and Stimulus-Responsiveness Transfer Based on Cholesterol Building Blocks. *Adv. Sci.* **2018**, *5*, 1700552.
(53) Halperin-Sternfeld, M.; Ghosh, M.; Sevostianov, R.; Grigoriants, I.; Adler-Abramovich, L. Molecular co-assembly as a strategy for synergistic improvement of the mechanical properties of hydrogels. *Chem. Commun.* **2017**, *53*, 9586−9589.
(54) Fichman, G.; Guterman, T.; Adler-Abramovich, L.; Gazit, E. Synergetic functional properties of two-component single amino acid-based hydrogels. *CrystEngComm* **2015**, *17*, 8105−8112.
(55) Smith, M. M.; Smith, D. K. Self-sorting multi-gelator gels—mixing and ageing effects in thermally addressable supramolecular soft nanomaterials. *Soft Matter* **2011**, *7*, 4856−4860.
(56) Li, D.; Shi, Y.; Wang, L. Mechanical Reinforcement of Molecular Hydrogel by Co-assembly of Short Peptide-based Gelators with Different Aromatic Capping Groups. *Chin. J. Chem.* **2014**, *32*, 123−127.
(57) Foster, J. A.; Edkins, R. M.; Cameron, G. J.; Colgin, N.; Fucke, K.; Ridgeway, S.; Crawford, A. G.; Marder, T. B.; Beeby, A.; Cobb, S. L.; Steed, J. W. Blending Gelators to Tune Gel Structure and Probe Anion-Induced Disassembly. *Chem.—Eur. J.* **2014**, *20*, 279−291.
(58) Das, A.; Ghosh, S. A generalized supramolecular strategy for self-sorted assembly between donor and acceptor gelators. *Chem. Commun.* **2011**, *47*, 8922−8924.
(59) Morris, K. L.; Chen, L.; Raeburn, J.; Sellick, O. R.; Cotanda, P.; Paul, A.; Griffiths, P. C.; King, S. M.; O'Reilly, R. K.; Serpell, L. C.; Adams, D. J. Chemically programmed self-sorting of gelator networks. *Nat. Commun.* **2013**, *4*, 1480.
(60) Horgan, C. C.; Rodriguez, A. L.; Li, R.; Bruggeman, K. F.; Stupka, N.; Raynes, J. K.; Day, L.; White, J. W.; Williams, R. J.; Nisbet, D. R. Characterisation of minimalist co-assembled fluorenylmethyloxycarbonyl self-assembling peptide systems for presentation of multiple bioactive peptides. *Acta Biomater.* **2016**, *38*, 11−22.
(61) Džolić, Z.; Wolsperger, K.; Žinić, M. Synergic effect in gelation by two-component mixture of chiral gelators. *New J. Chem.* **2006**, *30*, 1411−1419.
(62) Shigemitsu, H.; Fujisaku, T.; Tanaka, W.; Kubota, R.; Minami, S.; Urayama, K.; Hamachi, I. An adaptive supramolecular hydrogel comprising self-sorting double nanofibre networks. *Nat. Nanotechnol.* **2018**, *13*, 165−172.
(63) McAulay, K.; Dietrich, B.; Su, H.; Scott, M. T.; Rogers, S.; Al-Hilaly, Y. K.; Cui, H.; Serpell, L. C.; Seddon, A. M.; Draper, E. R.; Adams, D. J. Using chirality to influence supramolecular gelation. *Chem. Sci.* **2019**, *10*, 7801−7806.
(64) Kumar, D. K.; Jose, D. A.; Das, A.; Dastidar, P. First snapshot of a nonpolymeric hydrogelator interacting with its gelling solvents. *Chem. Commun.* **2005**, 4059−4061.

https://dx.doi.org/10.1021/acs.chemmater.0c00475
Chem. Mater. 2020, 32, 3517−3527

(65) Abraham, S.; Lan, Y.; Lam, R. S. H.; Grahame, D. A. S.; Kim, J. J. H.; Weiss, R. G.; Rogers, M. A. Influence of Positional Isomers on the Macroscale and Nanoscale Architectures of Aggregates of Racemic Hydroxyoctadecanoic Acids in Their Molecular Gel, Dispersion, and Solid States. *Langmuir* **2012**, *28*, 4955−4964.
(66) Xu, Y.; Kang, C.; Chen, Y.; Bian, Z.; Qiu, X.; Gao, L.; Meng, Q. In Situ Gel-to-Crystal Transition and Synthesis of Metal Nanoparticles Obtained by Fluorination of a Cyclic β-Aminoalcohol Gelator. *Chem.—Eur. J.* **2012**, *18*, 16955−16961.
(67) Wang, Y.; Tang, L.; Yu, J. Investigation of Spontaneous Transition from Low-Molecular-Weight Hydrogel into Macroscopic Crystals. *Cryst. Growth Des.* **2008**, *8*, 884−889.
(68) Braga, D.; d'Agostino, S.; D'Amen, E.; Grepioni, F. Polymorphs from supramolecular gels: four crystal forms of the same silver(i) supergelator crystallized directly from its gels. *Chem. Commun.* **2011**, *47*, 5154−5156.
(69) Byrne, P.; Lloyd, G. O.; Applegarth, L.; Anderson, K. M.; Clarke, N.; Steed, J. W. Metal-induced gelation in dipyridyl ureas. *New J. Chem.* **2010**, *34*, 2261−2274.
(70) Dastidar, P.; Roy, R.; Parveen, R.; Sarkar, K. Supramolecular Synthon Approach in Designing Molecular Gels for Advanced Therapeutics. *Adv. Ther.* **2019**, *2*, 1800061.
(71) Kumar, D. K.; Jose, D. A.; Dastidar, P.; Das, A. Nonpolymeric Hydrogelator Derived from N-(4-Pyridyl)isonicotinamide. *Langmuir* **2004**, *20*, 10413−10418.
(72) Engstrom, J. R.; Savyasachi, A. J.; Parhizkar, M.; Sutti, A.; Hawes, C. S.; White, J. M.; Gunnlaugsson, T.; Pfeffer, F. M. Norbornene chaotropic salts as low molecular mass ionic organogelators (LMIOGs). *Chem. Sci.* **2018**, *9*, 5233−5241.
(73) Ghosh, D.; Lebedytė, I.; Yufit, D. S.; Damodaran, K. K.; Steed, J. W. Selective gelation of N-(4-pyridyl)nicotinamide by copper(ii) salts. *CrystEngComm* **2015**, *17*, 8130−8138.
(74) Sahoo, P.; Kumar, D. K.; Raghavan, S. R.; Dastidar, P. Supramolecular Synthons in Designing Low Molecular Mass Gelling Agents: L-Amino Acid Methyl Ester Cinnamate Salts and their Anti-Solvent-Induced Instant Gelation. *Chem.−Asian J.* **2011**, *6*, 1038−1047.
(75) Anantharaj, S.; Jayakannan, M. Polymers from Amino acids: Development of Dual Ester-Urethane Melt Condensation Approach and Mechanistic Aspects. *Biomacromolecules* **2012**, *13*, 2446−2455.
(76) Karmakar, A.; Oliver, C. L.; Platero-Prats, A. E.; Laurila, E.; Örstrla, L. Crystal structures and hydrogen bond analysis of five amino acid conjugates of terephthalic and benzene-1,2,3-tricarboxylic acids. *CrystEngComm* **2014**, *16*, 8243−8251.
(77) Li, K.; Liang, S.; Lu, Y.; Wang, Q. Synthesis of Telechelic Fluoropolymers with Well-Defined Functional End Groups for Cross-Linked Networks and Nanocomposites. *Macromolecules* **2007**, *40*, 4121−4123.
(78) Dolomanov, O. V.; Bourhis, L. J.; Gildea, R. J.; Howard, J. A. K.; Puschmann, H. OLEX2: a complete structure solution, refinement and analysis program. *J. Appl. Crystallogr.* **2009**, *42*, 339−341.
(79) Sheldrick, G. M. Crystal structure refinement with SHELXL. *Acta Crystallogr., Sect. C: Struct. Chem.* **2015**, *71*, 3−8.
(80) Babu, S. S.; Praveen, V. K.; Ajayaghosh, A. Functional π-Gelators and Their Applications. *Chem. Rev.* **2014**, *114*, 1973−2129.
(81) Leiras, S.; Freire, F.; Quiñoá, E.; Riguera, R. Reversible assembly of enantiomeric helical polymers: from fibers to gels. *Chem. Sci.* **2015**, *6*, 246−253.
(82) Zhang, L.; Jin, Q.; Liu, M. Enantioselective Recognition by Chiral Supramolecular Gels. *Chem.−Asian J.* **2016**, *11*, 2642−2649.
(83) Hanabusa, K.; Yamada, M.; Kimura, M.; Shirai, H. Prominent Gelation and Chiral Aggregation of Alkylamides Derived from trans-1,2-Diaminocyclohexane. *Angew. Chem., Int. Ed.* **1996**, *35*, 1949−1951.
(84) Li, P.; Yin, Z.; Dou, X.-Q.; Zhou, G.; Feng, C.-L. Convenient Three-Dimensional Cell Culture in Supermolecular Hydrogels. *ACS Appl. Mater. Interfaces* **2014**, *6*, 7948−7952.
(85) Liu, G.-F.; Ji, W.; Feng, C.-L. Installing Logic Gates to Multiresponsive Supramolecular Hydrogel Co-assembled from Phenylalanine Amphiphile and Bis(pyridinyl) Derivative. *Langmuir* **2015**, *31*, 7122−7128.
(86) Wang, F.; Qin, M.; Peng, T.; Tang, X.; Yinme Dang-i, A.; Feng, C. Modulating Supramolecular Chirality in Alanine Derived Assemblies by Multiple External Stimuli. *Langmuir* **2018**, *34*, 7869−7876.
(87) Dou, X.; Li, P.; Zhang, D.; Feng, C.-L. C2-symmetric benzene-based hydrogels with unique layered structures for controllable organic dye adsorption. *Soft Matter* **2012**, *8*, 3231−3238.
(88) Yu, S.-L.; Dou, X.-Q.; Qu, D.-H.; Feng, C.-L. C2-symmetric benzene-based organogels: A rationally designed LMOG and its application in marine oil spill. *J. Mol. Liq.* **2014**, *190*, 94−98.
(89) Cai, W.; Feng, C.; Ma, X.; Chen, M.; Liu, J. C2-Symmetric Benzene-based Low Molecular Weight Hydrogel Modified Electrode for Highly Sensitive Detection of Copper Ions. *Electrochim. Acta* **2015**, *169*, 424−432.
(90) Yu, Y.; Wang, Y.; Feng, C. Hybrid hydrogels assembled from phenylalanine derivatives and agarose with enhanced mechanical strength. *Chem. Res. Chin. Univ.* **2016**, *32*, 872−876.
(91) Suzuki, M.; Hanabusa, K. l-Lysine-based low-molecular-weight gelators. *Chem. Soc. Rev.* **2009**, *38*, 967−975.
(92) Allix, F.; Curcio, P.; Pham, Q. N.; Pickaert, G.; Jamart-Grégoire, B. Evidence of Intercolumnar π−π Stacking Interactions in Amino-Acid-Based Low-Molecular-Weight Organogels. *Langmuir* **2010**, *26*, 16818−16827.
(93) Dirany, M.; Ayzac, V.; Isare, B.; Raynal, M.; Bouteiller, L. Structural Control of Bisurea-Based Supramolecular Polymers: Influence of an Ester Moiety. *Langmuir* **2015**, *31*, 11443−11451.
(94) Gupta, M.; Bagaria, A.; Mishra, A.; Mathur, P.; Basu, A.; Ramakumar, S.; Chauhan, V. S. Self-Assembly of a Dipeptide-Containing Conformationally Restricted Dehydrophenylalanine Residue to Form Ordered Nanotubes. *Adv. Mater.* **2007**, *19*, 858−861.
(95) Qin, S.-Y.; Pei, Y.; Liu, X.-J.; Zhuo, R.-X.; Zhang, X.-Z. Hierarchical self-assembly of a β-amyloid peptide derivative. *J. Mater. Chem. B* **2013**, *1*, 668−675.
(96) Shin, S.; Lim, S.; Kim, Y.; Kim, T.; Choi, T.-L.; Lee, M. Supramolecular Switching between Flat Sheets and Helical Tubules Triggered by Coordination Interaction. *J. Am. Chem. Soc.* **2013**, *135*, 2156−2159.
(97) Fornaro, T.; Burini, D.; Biczysko, M.; Barone, V. Hydrogen-Bonding Effects on Infrared Spectra from Anharmonic Computations: Uracil−Water Complexes and Uracil Dimers. *J. Phys. Chem. A* **2015**, *119*, 4224−4236.
(98) Nebot, V. J.; Armengol, J.; Smets, J.; Prieto, S. F.; Escuder, B.; Miravet, J. F. Molecular Hydrogels from Bolaform Amino Acid Derivatives: A Structure−Properties Study Based on the Thermodynamics of Gel Solubilization. *Chem.—Eur. J.* **2012**, *18*, 4063−4072.
(99) Tang, Y.-T.; Dou, X.-Q.; Ji, Z.-A.; Li, P.; Zhu, S.-M.; Gu, J.-J.; Feng, C.-L.; Zhang, D. C2-symmetric cyclohexane-based hydrogels: A rational designed LMWG and its application in dye scavenging. *J. Mol. Liq.* **2013**, *177*, 167−171.

Supporting Information

Unraveling the self-assembly modes in multi-component supramolecular gels using single crystal X-ray diffraction

Dipankar Ghosh, Abbas D. Farahani, Adam D. Martin, Pall Thordarson* and Krishna K. Damodaran*

1. Gelation Studies

Table S1: Gelation Experiments in Organic Solvents

	Gelation test at 3.0 wt %				
Solvent	***RR*-TAV**	**SS-TAV**	***RS*-TAV**	**(*RR+SS*)-TAV)**	**TAV**
tBu-Me ether	I	I	I	I	I
Chloroform	S	S	S	S	S
Acetone	S	S	S	S	S
Tetrahydrofuran	S	S	S	S	S
Methanol	S	S	S	S	S
1,2-dichloroethane	S	S	S	S	S
Ethyl acetate	S	S	S	S	S
Ethanol	S	S	S	S	S
Isopropanol	S	S	S	S	S
Tert-butanol	S	S	S	S	S
Acetonitrile	S	S	S	S	S
2-butanone	S	S	S	S	S
Benzene	G	G	PG‡	G	G
Toluene	G	G	PG‡	G	G
o-xylene	G	G	G*	G	G
m-xylene	G	G	G	G	G
p-xylene	G	G	G*	G	G
Mesitylene	G	G	G	G	G
Chlorobenzene	G§	G§	S	G**	G**
Nitrobenzene	S	S	S	S	S

** = 4.0 wt %, ** = 5.0 wt %, § = 5.5 wt %, ‡ = crystals in 2 days, I = insoluble, S = solution, G = gel, PG = partial gel, C = crystal.*

Table S2: Gelation Experiments in Aqueous Solvents (1:1, v/v)

Solvent	Gelation test at 4.0 wt %				
	***RR*-TAV**	**SS-TAV**	***RS*-TAV**	**(*RR+SS*)-TAV**	**TAV**
Water	I	I	I	I	I
EtOH/water	G	G	G	G	G
MeOH/water	G	G	G	G	G
iPrOH/water	G*	G*	G*	G*	G*
tBuOH/water	G*	G*	G*	G*	G*
MeCN/water	C	C	C	C	C
THF/water	C	C	C	C	C
1,4-dioxane/water	C	C	C	C	C

**= 5.0 wt %, I = insoluble, C = crystal, G = gel.*

Table S3: Determination of Minimum Gel Concentration (MGC in wt %)

Solvent	TAV
Benzene	1.8
Toluene	1.8
o-xylene	2.0
m-xylene	1.2
p-xylene	2.0
Mesitylene	1.2
Chlorobenzene	4.0
EtOH/water (1:1)	3.0

Table S4: Determination of Sol-gel Transition Temperature (T_{gel})

Compound	wt %	T_{gel}/°C			
		***RR*-TAV**	***SS*-TAV**	***RS*-TAV**	**(*RR+SS*)-TAV**
Benzene	4.0	48.7	49.5	-	106.2
Toluene	4.0	72.6	72.0	-	87.8
Chlorobenzene	5.0	-	-	-	67.5

Table S5: Determination of Sol-gel Transition Temperature (T_{gel}) of the Statistical Mixture (**TAV**)

Solvent	wt %	T_{gel}/°C
o-xylene	4.0	103.5
m-xylene	4.0	97.7
p-xylene	4.0	89.5
Mesitylene	4.0	104.0
Benzene	4.0	59.2
Toluene	4.0	79.8
Chlorobenzene	5.0	60.3
EtOH/water (1:1)	4.0	62.2

Table S6: Determination of T_{gel} at Different ***RR*-TAV** and ***SS*-TAV** Ratio at 4.0 wt %

***RR*/*SS*-TAV** composition (%)	T_{gel}/°C	
	m-xylene	mesitylene
0.0 ***RR***, 100.0 ***SS***	90.4	100.2
20.0 ***RR***, 80.0 ***SS***	91.5	102.0
40.0 ***RR***, 60.0 ***SS***	98.7	111.6
50.0 ***RR***, 50.0 ***SS***	102.0	116.2
60.0 ***RR***, 40.0 ***SS***	100.5	112.0
80.0 ***RR***, 20.0 ***SS***	92.2	103.7
100.0 ***RR***, 0.0 ***SS***	90.2	103.1

2. Rheology:

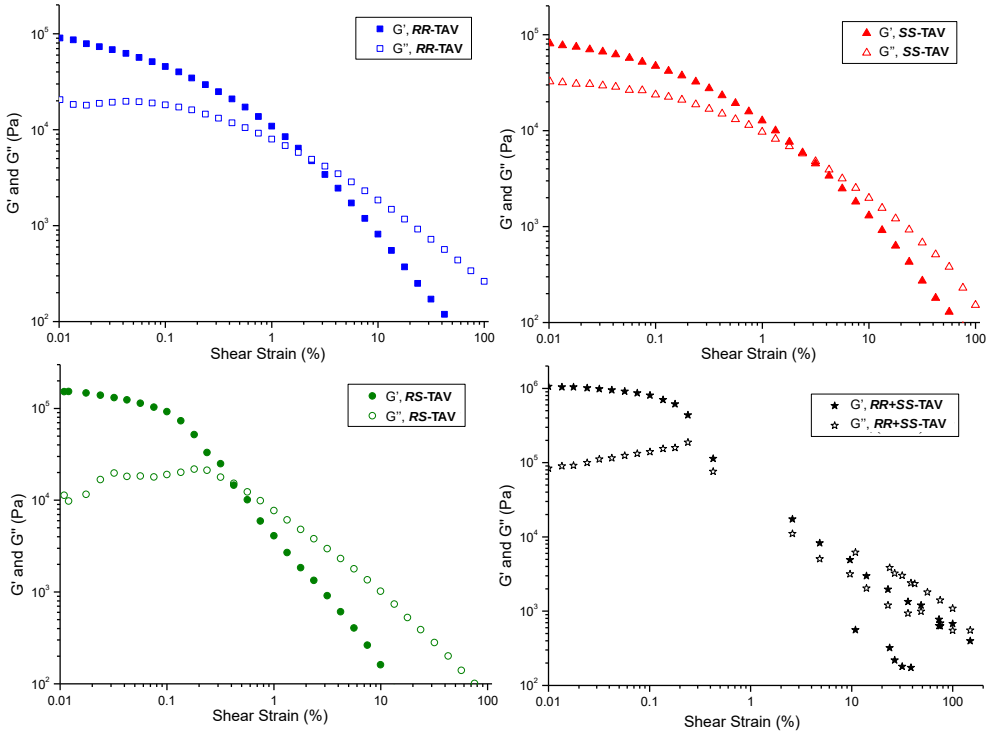

Figure S1: Strain sweep experiment with ***RR-***, ***SS-***, ***RS-*** and (***RR+SS***)**-TAV** gels (4.0 wt %) in *m*-xylene. Measurements were performed at 25.0 °C, at a constant frequency of 1.0 Hz.

Rheological measurements were performed to evaluate mechanical properties of the gels at 4.0 wt % in EtOH/water (1:1, v/v) for all gelators using a heat-cool method. The frequency sweep was performed on the gels (Figure S2) and the analysis of the frequency sweep data revealed that the gels behaved mainly in a frequency-independent way. The maximum storage modulus values (G') from frequency sweep measurements indicate that the ***RR*-TAV** and ***SS*-TAV** gels were stiffer (>100 kPa) than the other gels (<30 kPa). Strain sweeps were performed to study the amenability of the hydrogels in relation to external strain forces. In strain sweep measurements, the linear viscoelastic region (LVR) is defined as the region where the elastic modulus is independent of the applied strain. In this case, the LVR for gels were quite narrow, and the storage modulus starts to decrease almost immediately after the strain was increased above 0.1%. The crossover point of these gels was between 1.0% to 10.0% strain, which means the gel networks collapsed to liquid phase (Figure S3).

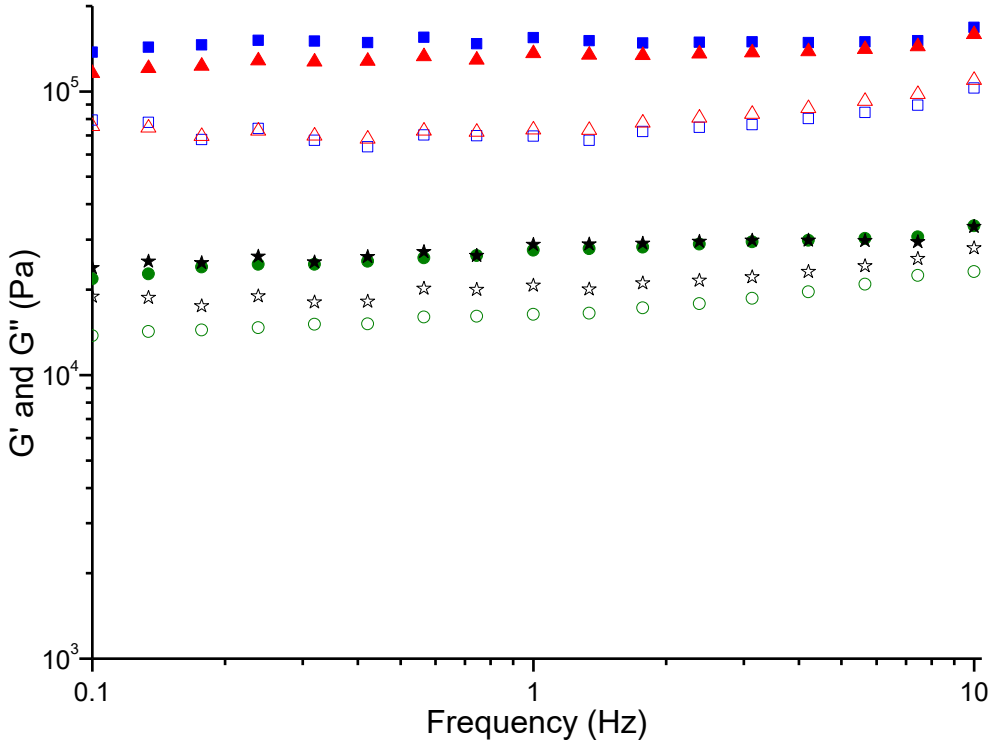

Figure S2: Frequency sweep experiment with ***RR*-**, ***SS*-**, ***RS*-** and (***RR+SS*)-TAV** gels (4.0 wt %) in EtOH/water (1:1 v/v). Measurements were performed at 25.0 °C, at a constant strain of 0.2%. Color codes: G' ***RR*-TAV** (■), G'' ***RR*-TAV** (□), G' ***RR*-TAV** (▲), G'' ***RR*-TAV** (△), G' ***RR*-TAV** (●), G'' ***RR*-TAV** (○), G' (***RR+SS*)-TAV** (★) and G'' (***RR+SS*)-TAV** (☆).

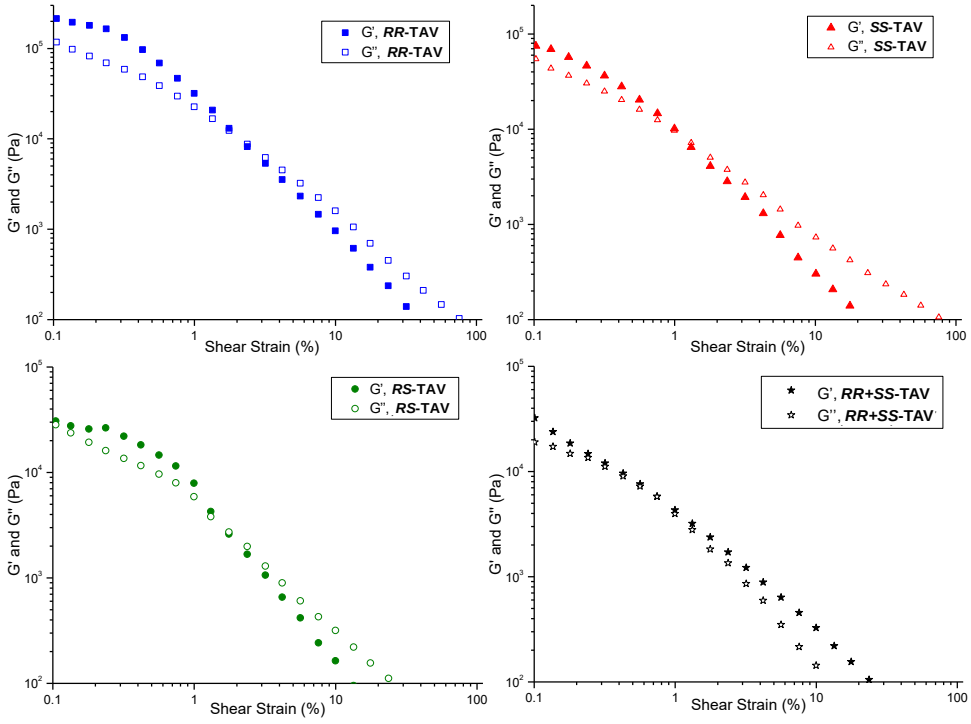

Figure S3: Strain sweep experiment with ***RR-***, ***SS-***, ***RS-*** and (***RR+SS***)**-TAV** gels (4.0 wt %) in EtOH/water (1:1 v/v). Measurements were performed at 25.0 °C, at a constant frequency of 1.0 Hz.

3. Scanning Electron Microscopy (SEM)

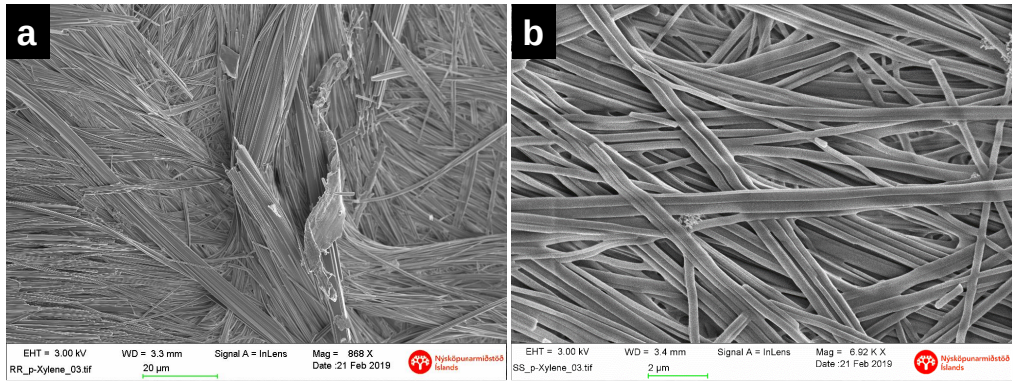

Figure S4: SEM images of (a) ***RR*-** and (b) ***SS*-TAV** xerogels obtained from *p*-xylene at 4.0 wt %.

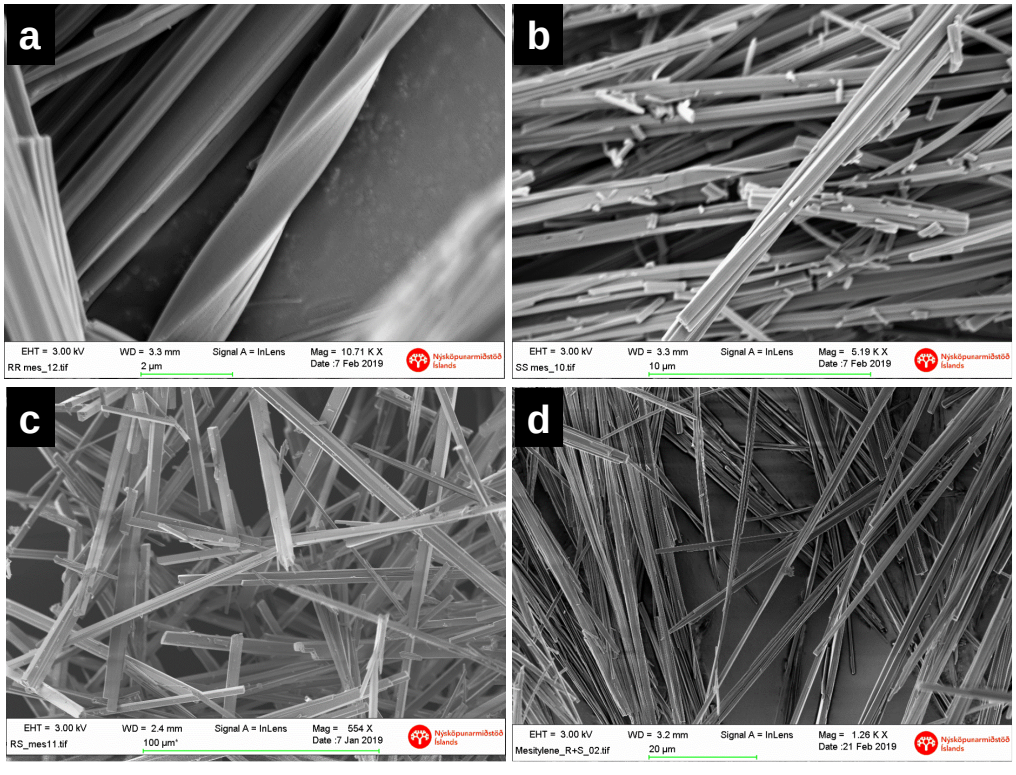

Figure S5: SEM images of (a) ***RR*-**, (b) ***SS*-**, (c) ***RS*-** and (d) (***RR*+*SS*)-TAV** xerogels obtained from mesitylene at 4.0 wt %.

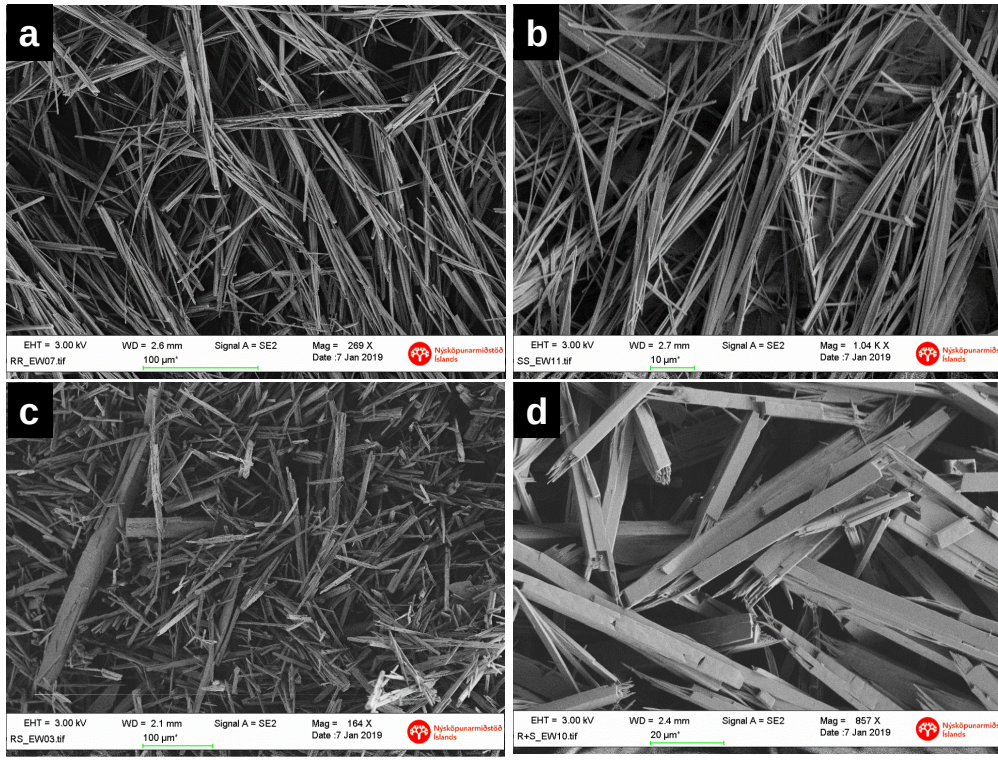

Figure S6: SEM images of (a) ***RR***-, (b) ***SS***-, (c) ***RS***- and (d) (***RR+SS***)-**TAV** xerogels obtained from EtOH/water (1:1, v/v) at 5.0 wt %.

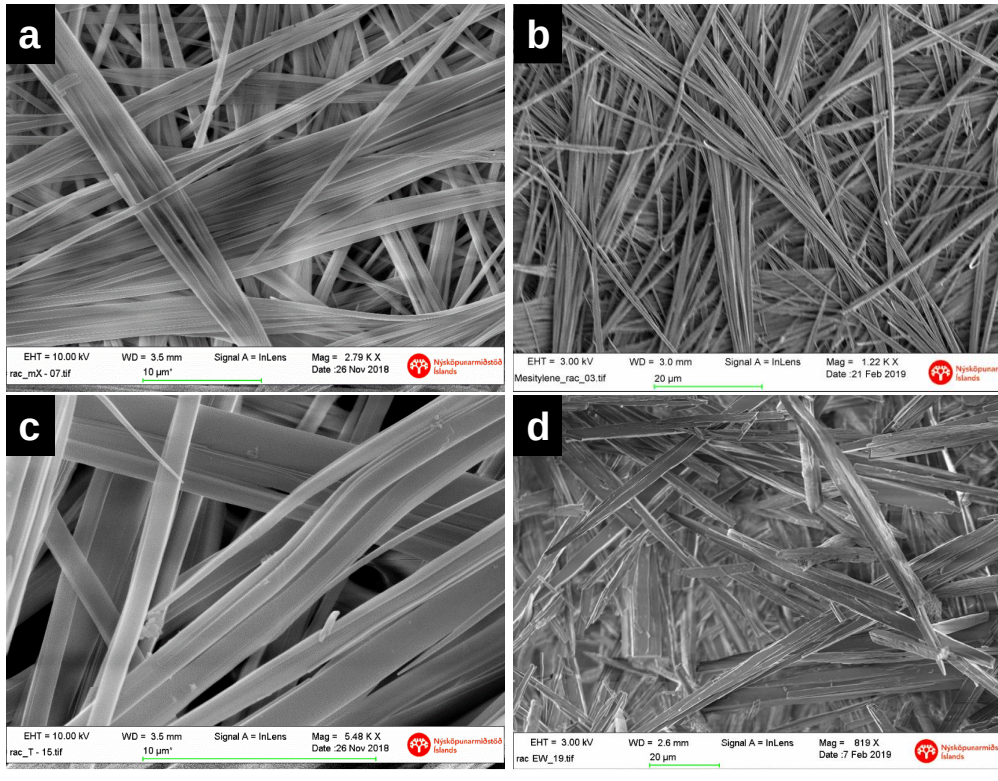

Figure S7: SEM images of **TAV** xerogels obtained at 4.0 wt % from (a) *m*-xylene, (b) mesitylene, (c) toluene and (d) 5.0 wt % from EtOH/water (1:1, v/v).

4. Circular dichroism (CD)

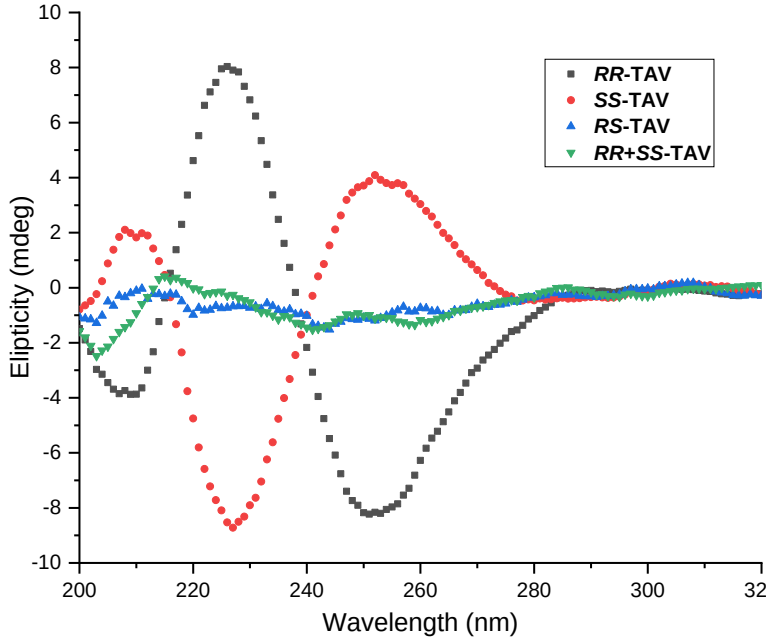

Figure S8: CD spectra of ***RR***-, ***SS***-, ***RS***- and (***RR+SS***)**-TAV** in solution state at 0.03 wt % in absolute EtOH.

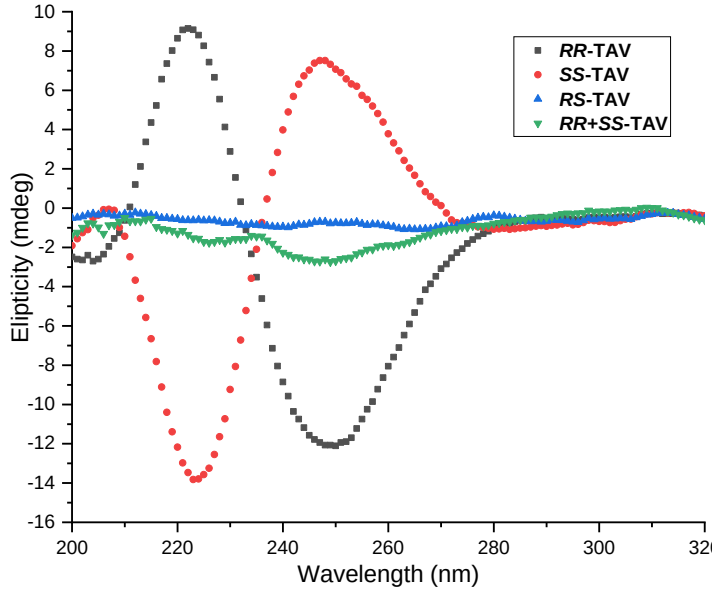

Figure S9: CD spectra of ***RR***-, ***SS***-, ***RS***- and (***RR+SS***)**-TAV** in dispersed gel state at 0.03 wt % in EtOH/water (1:4 v/v).

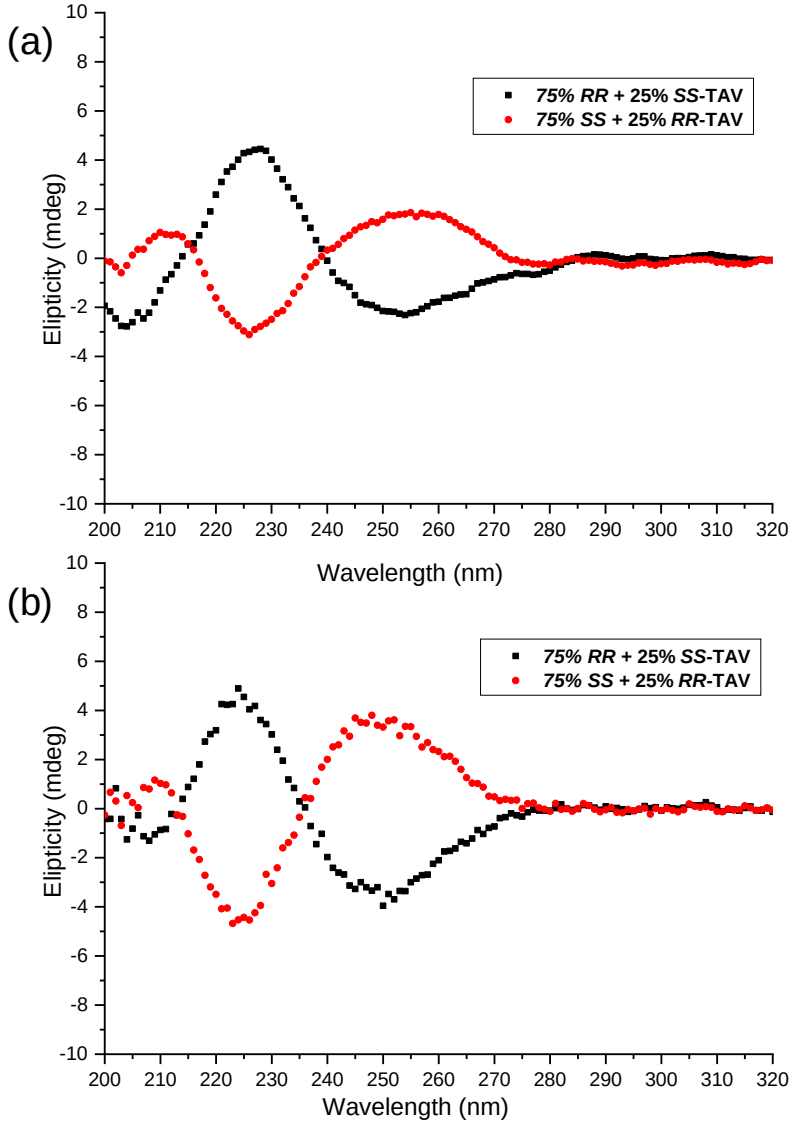

Figure S10: CD spectra of (75% ***RR*** + 25% ***SS***)-**TAV** and (25% ***RR*** + 75% ***SS***)-**TAV** mixture in (a) solution state at 0.03 wt % in absolute EtOH and (b) in dispersed gel state at 0.03 wt % in EtOH/water (1:1 v/v) showing positive and negative maxima.

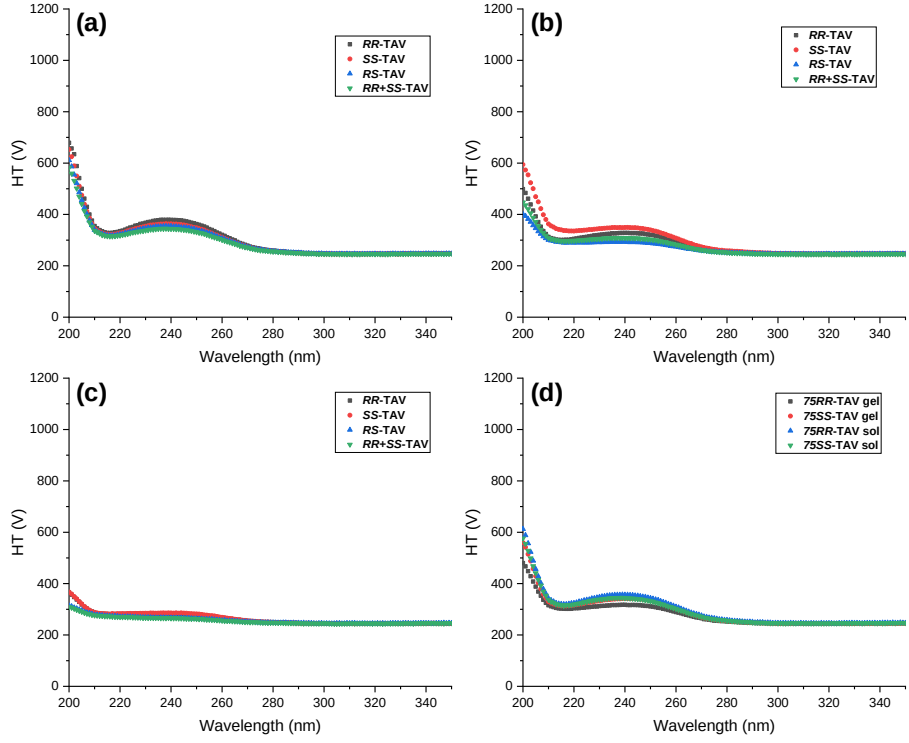

Figure S11: HT data for the CD spectra of all **TAV** samples in: (a) dispersed gel state at 0.03 wt % in EtOH/water (1:1 v/v), (b) solution state at 0.03 wt % in absolute EtOH, (c) dispersed gel state at 0.03 wt % in EtOH/water (1:4 v/v) and (d) dispersed gel and solution state of (75% ***RR*** + 25% ***SS***)-**TAV** and (25% ***RR*** + 75% ***SS***)-**TAV** at 0.03 wt % in EtOH/water (1:1 v/v) and absolute EtOH respectively.

5. IR Spectroscopy

The hydrogen bonding interactions lead to significant changes in IR spectra of supramolecular gels. For example, the N—H stretching peaks will provide information about the extent of hydrogen bonding between the amide groups. The difference between N—H stretching peaks in solid-state and gel state will enable us to elucidate the structural information of the self-assembled hierarchical aggregate. The ATR-FTIR spectra of the compounds were recorded and N—H stretching vibration signals were observed between 3295 to 3303 cm^{-1} in all cases. The C═O stretching peaks of ester and amide appeared at 1740-1750 and 1630-1640 cm^{-1} respectively, whereas aromatic and aliphatic C—H peaks were spotted around 2875-2970 cm^{-1}. The self-assembly of the gelator was analyzed by comparing the gel state IR with the solid-state. The ATR-FTIR spectra in the gel state was recorded by placing small amount of the gel (4.0 wt % in mesitylene) and was subtracted from background solvent contribution. Analysis of the peaks indicated that a slight broadening of the amide band and the peaks were shifted towards lower

wavenumber in all cases, which confirmed the extended hydrogen bonding in the gel state. The maximum shift (from 3303 to 3277 cm^{-1}) was observed for (***RR*+*SS*)-TAV** suggesting that the gel possesses most effective H-bonding among all systems (Figure S15).

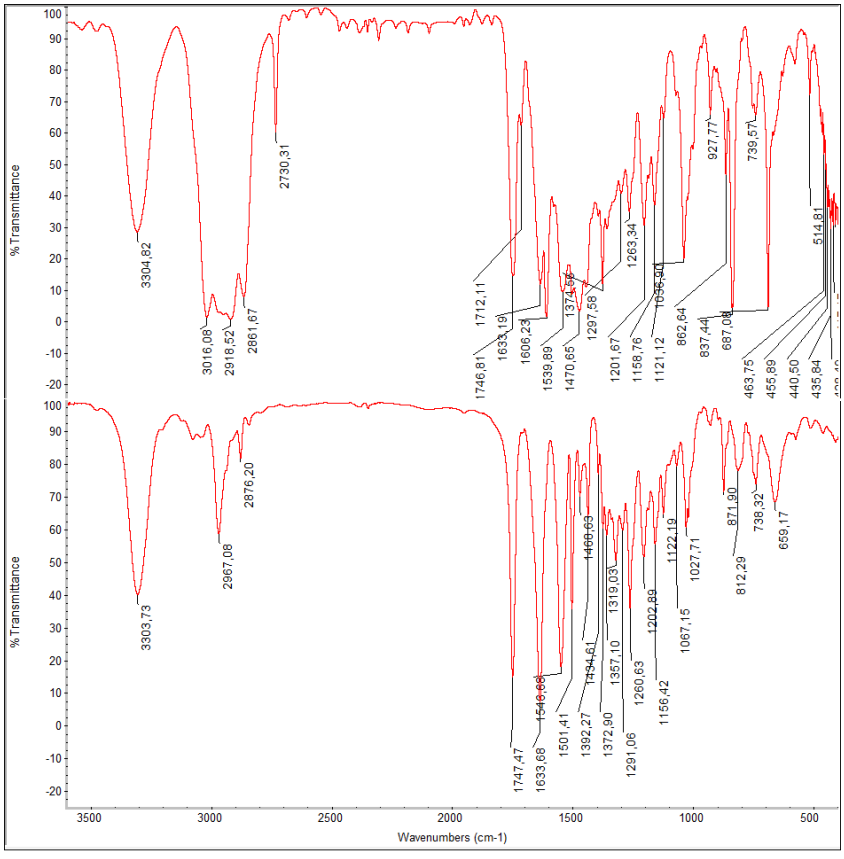

Figure S12: IR spectra of ***RR*-TAV**: bulk solid (bottom) and gel state in mesitylene at 4.0 wt %.

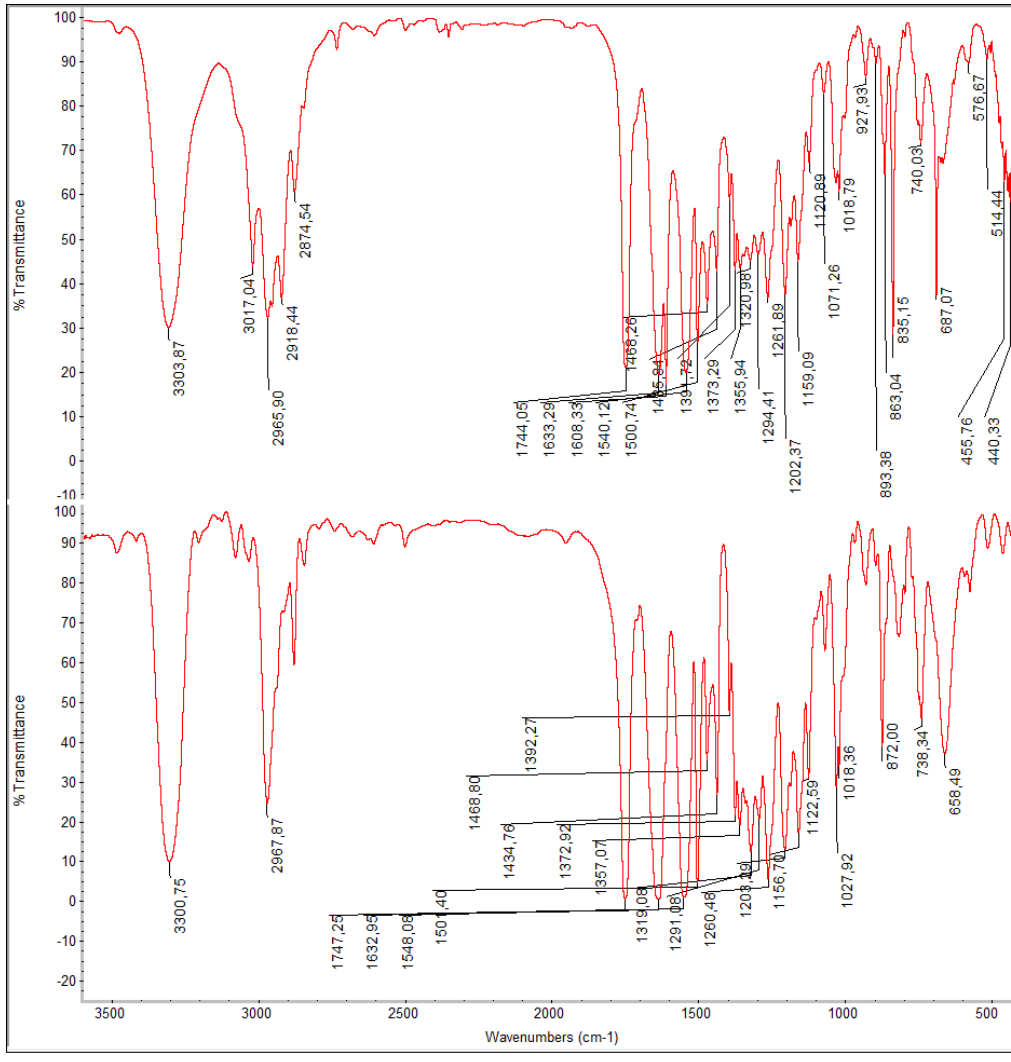

Figure S13: IR spectra of ***SS*-TAV**: bulk solid (bottom) and gel state in mesitylene at 4.0 wt %.

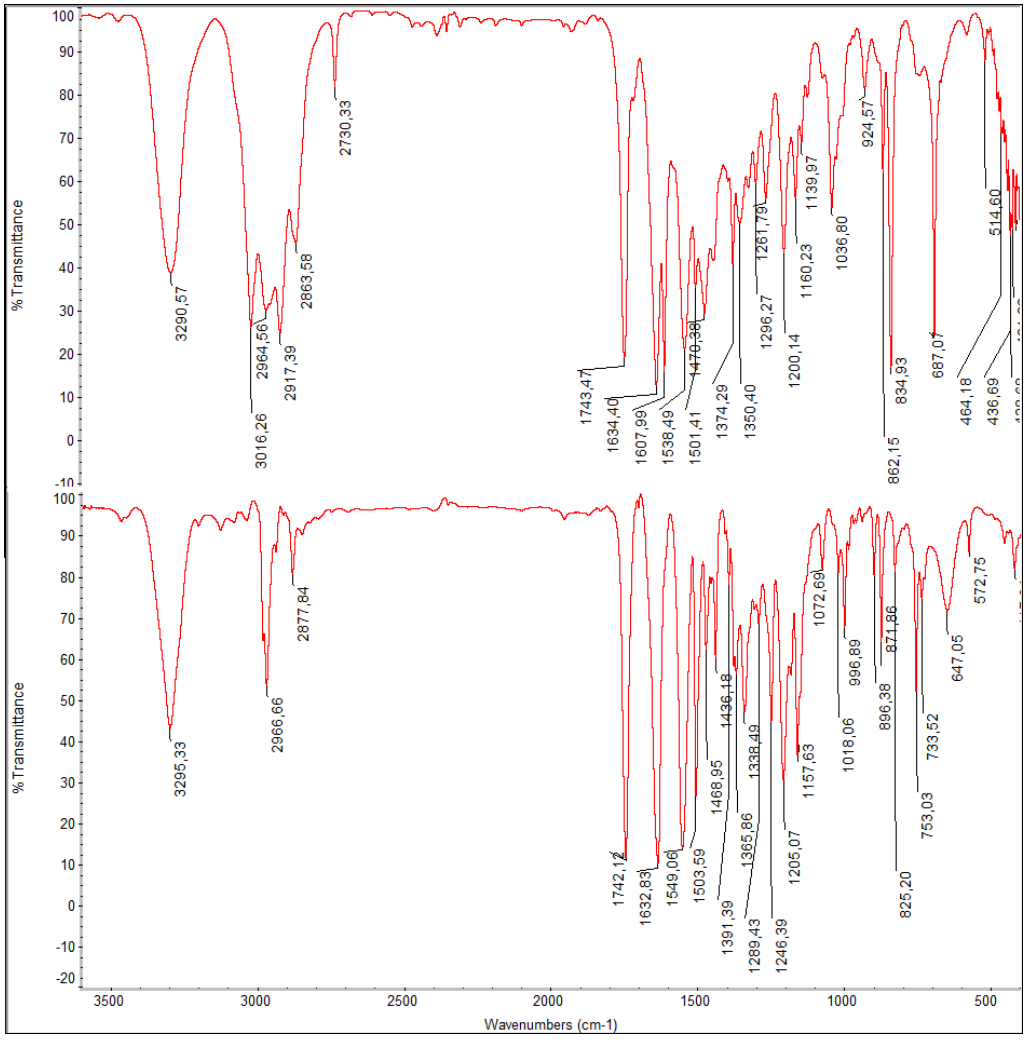

Figure S14: IR spectra of ***RS*-TAV**: bulk solid (bottom) and gel state in mesitylene at 4.0 wt %.

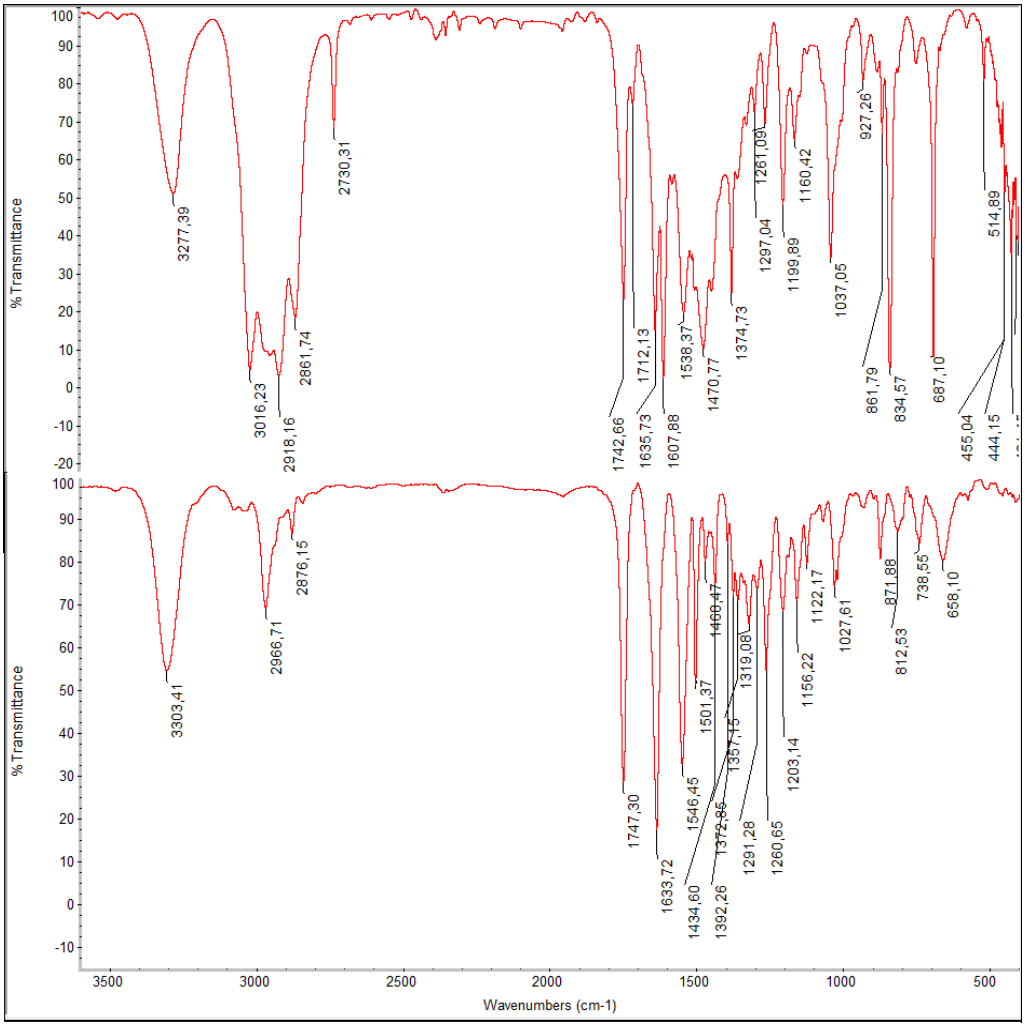

Figure S15: IR spectra of (***RR+SS***)**-TAV**: bulk solid (bottom) and gel state in mesitylene at 4.0 wt %.

Table S7: Comparison of IR spectra of **TAV** gelators (cm^{-1})

Bond	***RR***, solid	***RR***, gel	***SS***, solid	***SS***, gel	***RS***, solid	***RS***, gel	(***RR+SS***), solid	(***RR+SS***), gel
Amide-A (N—H stretching)	3303	3304	3300	3303	3295	3290	3303	3277
Amide-I (C=O stretching)	1633	1633, 1606	1632	1633, 1608	1632	1634, 1607	1633	1635, 1607
Amide-II (N-H bending)	1548	1539	1548	1540	1549	1538	1546	1538

6. X-ray crystallography

Table S8: Crystal data

Crystal data	***RR*-TAV**	***SS*-TAV**	***RS*-TAV**	(***RR+SS***)**-TAV**
Empirical formula	$C_{20}H_{28}N_2O_6$	$C_{20}H_{28}N_2O_6$	$C_{20}H_{28}N_2O_6$	$C_{20}H_{28}N_2O_6$
Color	colorless	colorless	colorless	colorless
Formula weight	392.44	392.44	392.44	392.44
Crystal size (mm)	0.41 x 0.16 x 0.10	0.55 x 0.18 x 0.12	0.31 x 0.18 x 0.05	0.50 x 0.24 x 0.15
Crystal system	monoclinic	monoclinic	monoclinic	monoclinic
Space group	$P2_1$	$P2_1$	$P2_1/c$	$P2_1/c$
a (Å)	9.9333(5)	9.9327(5)	16.0197(10)	9.8888(4)
b (Å)	9.8326(5)	9.8290(5)	6.7614(4)	15.5000(6)
c (Å)	33.0974(16)	33.1100(18)	9.9344(6)	15.1398(6)
β (°)	96.739(2)	96.721(2)	104.480(2)	104.6370(10)
Volume ($Å^3$)	3210.3(3)	3210.3(3)	1041.87(11)	2245.26(15)
Z	6	6	2	4
$D_{calc.}$ (g/cm^3)	1.218	1.218	1.251	1.161
F(000)	1260	1260	420	840
μ CuKα (mm^{-1})	0.745	0.745	0.765	0.710
Temperature (K)	150(2)	150(2)	120(2)	150(2)
Reflections collected/ unique/observed [I>2σ(I)]	59636/12072/11727	66905/12386/12045	12532/2044/1874	36510/4397/4020
Data/restraints/parameters	12072/1/823	12386/1/798	2044/0/134	4397/0/259
Goodness of fit on F^2	1.022	1.037	1.084	1.040
Final R indices [I>2σ(I)]	R_1 = 0.0367 wR_2 = 0.0947	R_1 = 0.0366 wR_2 = 0.0915	R_1 = 0.0428 wR_2 = 0.1156	R_1 = 0.0495 wR_2 = 0.1421
R indices (all data)	R_1 = 0.0378 wR_2 = 0.0957	R_1 = 0.0376 wR_2 = 0.0924	R_1 = 0.0469 wR_2 = 0.1190	R_1 = 0.0529 wR_2 = 0.1457

Table S9: Hydrogen bonding parameters

Donor—H···Acceptor	D—H/Å	H···A/Å	D···A/Å	∠D—H···A/°	Symmetry operation
***RR*-TAV**					
N(9)—H(9)···O(39)	0.88	2.04	2.895(2)	162	1+x,y,z
N(20)—H(20)···O(47)	0.88	2.05	2.921(2)	172	x,-1+y,z
N(37)—H(37)···O(11)	0.88	2.07	2.938(2)	171	-1+x,1+y,z
N(48)—H(48)···O(19)	0.88	2.00	2.858(3)	165	x,y,z
N(65)—H(65)···O(75)	0.88	2.05	2.911(3)	165	-x,-1/2+y,1-z
N(76)—H(76)···O(67)	0.88	1.97	2.836(3)	167	1-x,1/2+y,1-z
C(5)—H(5)···O(32)	1.00	2.41	3.371(3)	160	1+x,-1+y,z
C(14)—H(14)···O(47)	0.95	2.40	3.039(3)	124	x,-1+y,z
C(17)—H(17)···O(39)	0.95	2.43	3.331(3)	159	1+x,y,z
C(41)—H(41)···O(4)	0.95	2.57	3.266(3)	130	-1+x,1+y,z
C(44)—H(44)···O(19)	0.95	2.44	3.320(3)	153	x,y,z
C(49)—H(49)···O(25)	1.00	2.52	3.499(3)	166	x,1+y,z
C(69)—H(69)···O(75)	0.95	2.59	3.313(4)	133	-x,-1/2+y,1-z
C(72)—H(72)···O(67)	0.95	2.39	3.127(5)	134	1-x,1/2+y,1-z
***SS*-TAV**					
N(9)—H(9)···O(39)	0.88	2.04	2.895(2)	163	-1+x,y,z
N(20)—H(20)···O(47)	0.88	2.05	2.923(2)	172	x,1+y,z
N(37)—H(37)···O(11)	0.88	2.06	2.938(2)	172	1+x,-1+y,z
N(48)—H(48)···O(19)	0.88	2.00	2.856(2)	165	x,y,z
N(65)—H(65)···O(75)	0.88	2.05	2.911(3)	165	2-x,1/2+y,1-z
N(76)—H(76)···O(67)	0.88	1.97	2.833(3)	167	1-x,-1/2+y,1-z
C(5)—H(5)···O(32)	1.00	2.41	3.369(3)	160	-1+x,1+y,z
C(14)—H(14)···O(47)	0.95	2.41	3.040(3)	124	x,1+y,z
C(17)—H(17)···O(39)	0.95	2.43	3.332(3)	159	-1+x,y,z
C(41)—H(41)···O(4)	0.95	2.57	3.260(3)	130	1+x,-1+y,z
C(44)—H(44)···O(19)	0.95	2.45	3.320(3)	153	x,y,z
C(49)—H(49)···O(25)	1.00	2.52	3.499(3)	166	x,-1+y,z
C(70)—H(70)···O(67)	0.95	2.40	3.122(5)	133	1-x,-1/2+y,1-z
C(73)—H(73)···O(75)	0.95	2.60	3.318(4)	133	2-x,1/2+y,1-z

***RS*-TAV**					
N(8)—H(8)···O(10)	0.867(19)	2.106(19)	2.9586(15)	167.8(18)	x,1/2-y,-1/2+z
C(12)—H(12)···O(10)	0.95	2.47	3.3060(17)	147	x,1/2-y,-1/2+z
(*RR+SS*)-TAV					
N(9)—H(9)···O(19)	0.88	2.03	2.8729(15)	161	2-x,1-y,1-z
N(20)—H(20)···O(11)	0.88	2.03	2.8571(15)	155	1-x,1-y,1-z

Crystal Structures

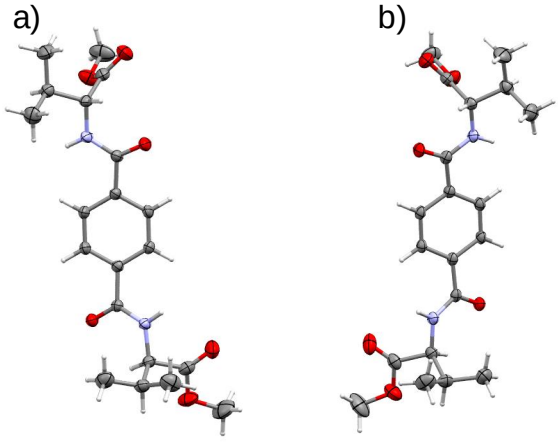

Figure S16: Asymmetric unit of (a) ***RR*-TAV** and (b) ***SS*-TAV** showing the mirror image of enantiomers

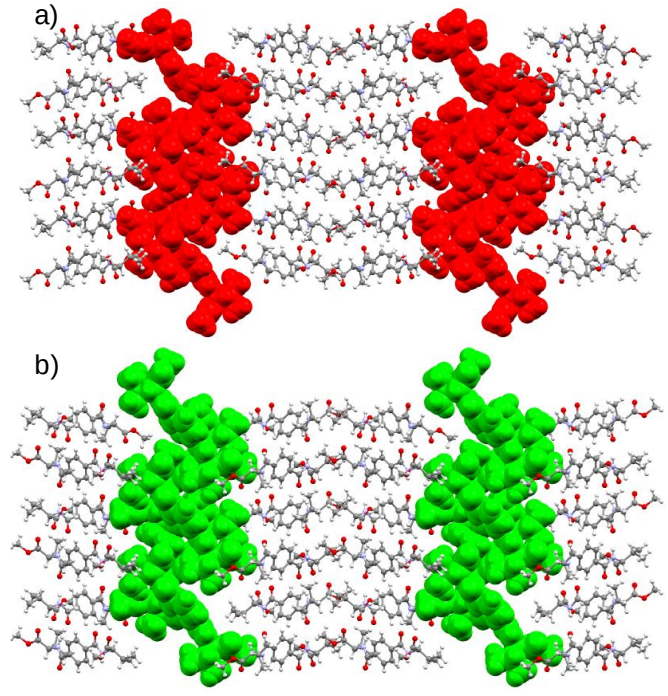

Figure S17: Crystal packing of (a) ***SS*-TAV** and (b) ***RR*-TAV** showing helicity, disordered carbons and hydrogen atoms are omitted for clarity.

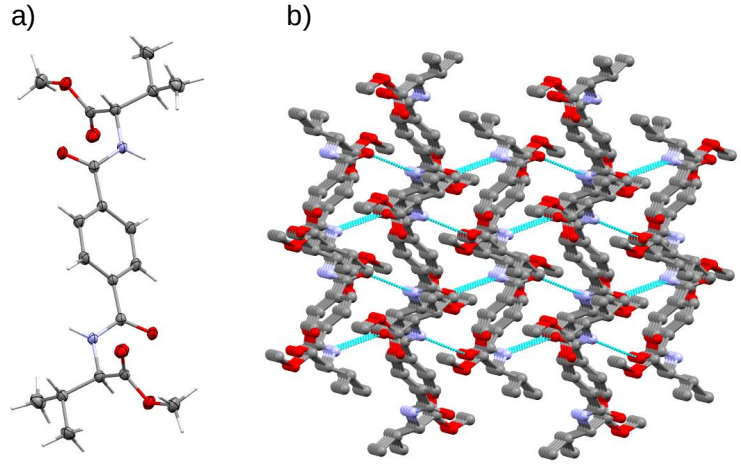

Figure S18: Crystal structure of ***RS*-TAV** (a) asymmetric unit, (b) formation of 2-D hydrogen bonded sheet architecture on the crystallographic *b-c* plane (hydrogen atoms are omitted for clarity).

7. Powder X-ray diffraction (PXRD):

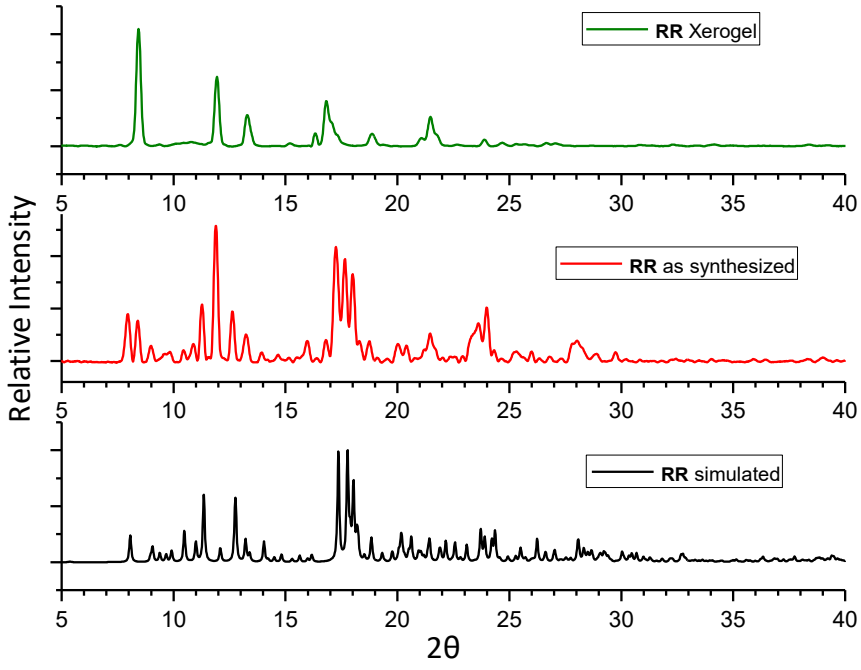

Figure S19: Comparison of PXRD pattern of ***RR*-TAV**: simulated, bulk crystals obtained from EtOH/water (1:1, v/v) and xerogel obtained from EtOH/water (1:1, v/v) at 4.0 wt %.

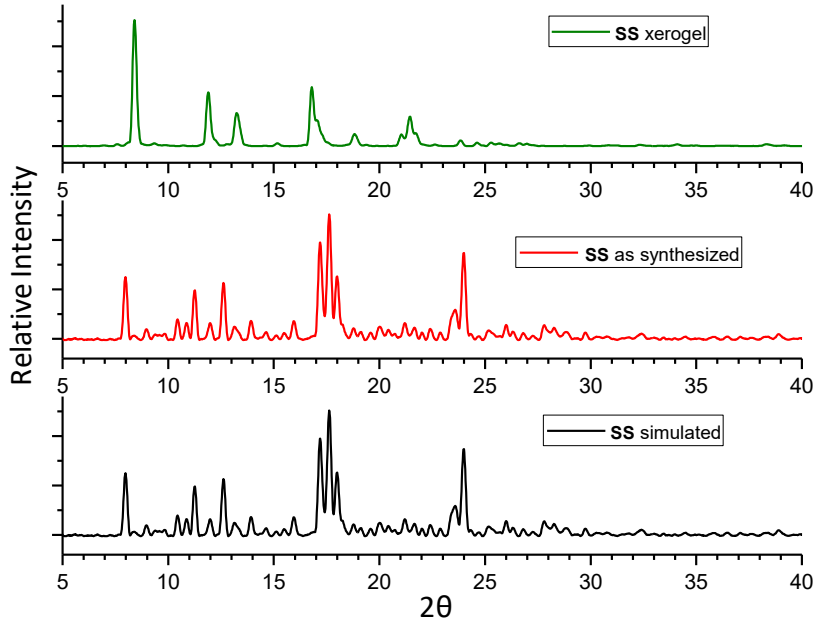

Figure S20: Comparison of PXRD pattern of ***SS*-TAV**: simulated, bulk crystals obtained from EtOH/water (1:1, v/v) and xerogel obtained from EtOH/water (1:1, v/v) at 4.0 wt %.

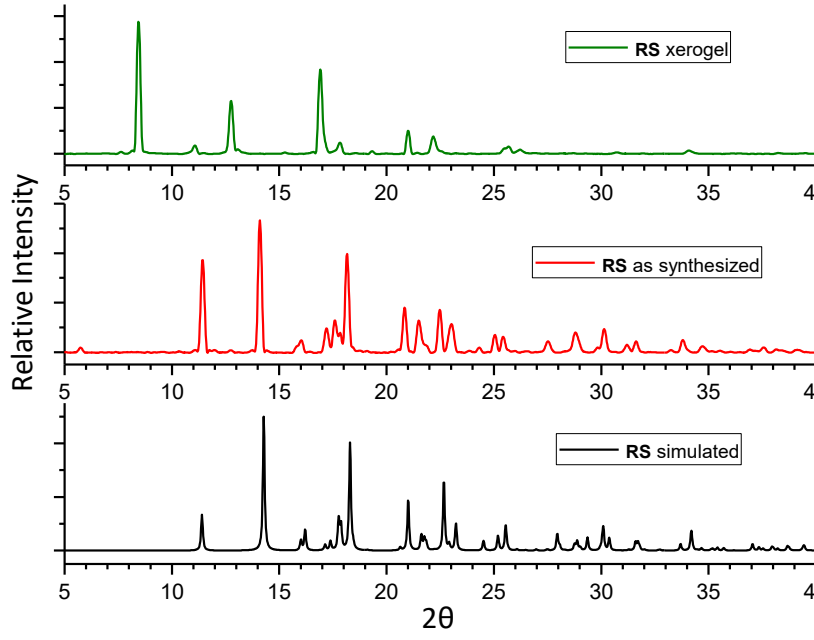

Figure S21: Comparison of PXRD pattern of ***RS*-TAV**: simulated, bulk crystals obtained from EtOH/water (1:1, v/v) and xerogel obtained from EtOH/water (1:1, v/v) at 4.0 wt %.

8. Purity of *RR-, SS- and RS-TAV*

High-Performance Liquid Chromatography (HPLC) was performed on a Shimadzu Prominence LC-20A HPLC system to confirm purity. An Astec CHIROBIOTIC™ T (5 µm 10 cm x 4.60 mm) analytical chiral column was used at a flow rate of 0.8 mL/min. The mobile phase consisted of eluents: A (Ethanol) and B (Heptane). The HPLC trace was obtained using an isocratic solvent system (10 % A and 90 % B) over 30 minutes.

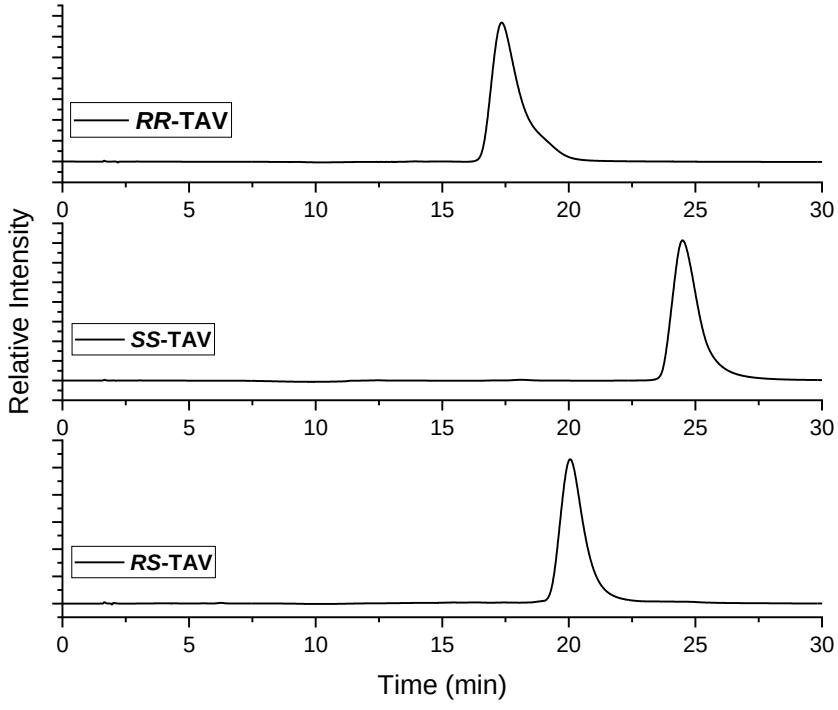

Figure S22: **Chiral** HPLC of ***RR-***, ***SS-*** and ***RS*-TAV** showing the purity of the compounds.

5 Application of Supramolecular Gels in Gel Phase Crystallization

Gel phase crystallization is a classic technique to influence the properties of the crystallite such as crystal size, crystal habit and polymorphism.[20] The control of polymorphism and crystal habit outcome of pharmaceuticals have been screening by crystallization in low molecular weight gels, and efforts were made to develop the technique by using gelators that mimic the crystallizing substance.[22, 212] Most of the pharmaceutical crystallizations were performed in organogels, [207-208] whereas hydrogels are more suitable to crystallize inorganic complexes.[204, 211] In this chapter, we aim to study the crystal habit modification of inorganic complexes and the influence of chirality of the gel medium in chiral MOMs.

4.1 Article V

In this project we studied the crystallization of an inorganic complex copper(II) isonicotinate-N-oxide, which is crystallized in at least three forms. The complex was chosen due to the availability at different forms having distinct coordination sphere and thermodynamic stability depending upon the crystallizing media. The gel phase crystallization was performed with various type of gelators such as PG, LMWG and gelator mimicking the ligand. The outcome of the work is reported in *Article-VII*.

4.2 Article VI

The gel phase crystallization was also studied for MOMs. A chiral MOM was synthesized from achiral starting materials via direct synthesis and solvent-mediated crystal-to-crystal transformation. The influence of the chirality of the gel fibers in crystallizing the MOM is discussed in *Article-VIII*.

.

Article-VII

This project is published in a peer reviewed journal and included as it was published. Slight differences might appear from the original article due to the formatting issue.

Publication details:

″Crystal habit modification of Cu(II) isonicotinate–N-oxide complexes using gel phase crystallisation”

Dipankar Ghosh, Katja Ferfolja, Žygimantas Drabavičius, Jonathan W. Steed* and Krishna K. Damodaran*

New J. Chem., **2018**, *42*, 19963-19970.

Author contributions:

K.K.D. planned and designed the research; **D.G.** synthesized the new polymer, solved single crystal structure, evaluated gelation properties, analyzed crystal habit modification and found selective crystallization. K.F. analyzed SCSC transformation and Ž.D. synthesized N-oxide gelator. K.K.D. wrote the initial manuscript draft and **D.G.**, K.K.D. and J.W.S. reviewed the main manuscript.

NJC

PAPER

Cite this: *New J. Chem.*, 2018, **42**, 19963

Crystal habit modification of Cu(II) isonicotinate–*N*-oxide complexes using gel phase crystallisation†

Dipankar Ghosh,[a] Katja Ferfolja,[a] Žygimantas Drabavičius,[a] Jonathan W. Steed*[b] and Krishna K. Damodaran*[a]

Received 4th October 2018,
Accepted 1st November 2018

DOI: 10.1039/c8nj05036h

rsc.li/njc

We report the crystallisation of three forms of the copper(II) isonicotinate–*N*-oxide complex and their phase interconversion *via* solvent-mediated crystal-to-crystal transformation. The different forms of the copper complex have been isolated and characterised by single crystal X-ray diffraction. Gel phase crystallisation performed in hydrogels, low molecular weight gels and gels of a tailored gelator showed crystal habit modification. Crystallisation in aqueous ethanol resulted in the concomitant formation of blue (form-I) and green (form-II/IV) crystals while the use of a low molecular weight gel resulted in the selective crystallization of the blue form-I under identical conditions. Comparison of the gel phase and the solution state crystallisation in various solvent compositions reveals that the blue form-I is the thermodynamically stable form under ambient conditions.

Introduction

Supramolecular gels based on low molecular weight gelators (LMWGs)[1–9] have witnessed tremendous growth over the last decade due to their emerging potential applications[5–8] such as dynamic behaviour, use as cell growth media, drug delivery and as media to control crystal growth. Gel phase crystallisation in hydrogels is a classical technique for inorganic compounds and biomolecules such as proteins.[11–15] The gel environment can influence the properties[16–22] such as crystal habit, crystal size and polymorphism. Polymorphism depends on a number of factors including the nucleation rate, which can give rise to the simultaneous crystallisation of two or more polymorphs with similar nucleation rates, known as concomitant polymorphism.[23] For decades, researchers have been using various techniques such as evaporative crystallization, solution cooling, melt crystallization and sublimation[24,25] to search for polymorphic modifications. While these methods are highly effective, they can sometimes fail to efficiently isolate slow-nucleating forms. LMWGs can provide various advantages as crystal growth media because of their versatility, stimuli-responsive properties and often facile synthesis. Gel phase crystallisation results in the shutdown of convection currents leading to diffusion limited growth, and the gel fibres can provide an active surface for heterogeneous nucleation. There have been a few recent reports of crystallisation within gels based on LMWGs[21,26–30] and small-molecule supramolecular hydrogels have been used to crystallise pharmaceuticals such a modafinil[26] and carbamazepine.[21] An inert gel matrix based on LMWGs (without drug-specific functionality) has been shown to influence the pharmaceutical crystallisation solid form and habit outcomes.[29] Efforts have also been made to develop supramolecular gel phase crystallisation using a gelator that mimics the anticancer drug cisplatin. This resulted in the crystal habit modification of cisplatin and the isolation of a novel solvate form.[28] LMWGs that are structurally similar to the crystallisation substrate have been shown to give rise to the selective crystallisation of the metastable R polymorph of the highly polymorphic drug precursor ROY.[31] The gel phase crystallisation of isoniazid gives rise to significant differences in the crystal habit and crystal size compared to solution control experiments.[22] In 2004, Hamilton's group demonstrated the use of a hydrogel medium to crystallize calcite,[32] while Gunnlaugsson's group reported that supramolecular gels can be used to produce single crystal nanowires based on NaCl, KCl, and KI in a gel medium.[33] In the present work, we report the use of LMWGs as crystallisation media for coordination compounds, which display several crystalline forms varying in the copper coordination environment. Specifically, we have selected the complexes of copper(II) with isonicotinic acid–*N*-oxide, which exhibits three

[a] *Department of Chemistry, Science Institute, University of Iceland, Dunhagi 3, 107 Reykjavik, Iceland. E-mail: krishna@hi.is; Fax: +354 552 8911; Tel: +354 525 4846*

[b] *Department of Chemistry, Durham University, South Road, Durham DH1 3LE, UK. E-mail: jon.steed@durham.ac.uk*

† Electronic supplementary information (ESI) available: Crystallisation of Cu(II) complexes, details of gelation experiments and gel phase crystallisation, and comparison of PXRD of form-IV. CCDC 1846767. For ESI and crystallographic data in CIF or other electronic format see DOI: 10.1039/c8nj05036h

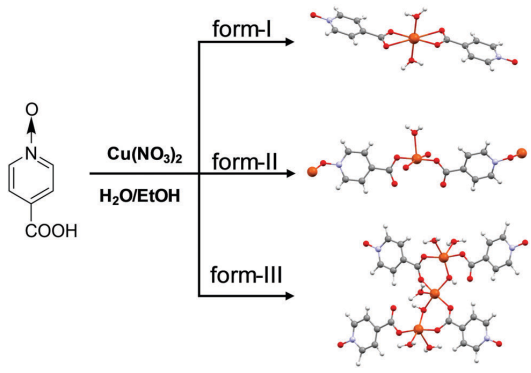

Scheme 1 Molecular structures of three copper(II) isonicotinate–*N*-oxide complexes deposited in the Cambridge Structural Database.[10]

forms[34–36] deposited within the Cambridge Structural Database[10] and these complexes can be easily isolated (Scheme 1). These three forms of the copper(II) isonicotinate–*N*-oxide complex are a discrete square planar diaqua species bound through monodentate carboxylate oxygen atoms $[Cu(C_6H_4NO_3)_2(H_2O)_2]$ (blue, form-I, CSD refcode BUXDED), a square pyramidal aqua complex involving bridging ligands bound by both carboxylate and *N*-oxide oxygen atoms $[Cu(\mu\text{-}C_6H_4NO_3)_2(H_2O)]_n$ (green, form-II, CSD refcode BEJCID) and a trinuclear hydroxyl-bridged species $[Cu(H_2O)(\mu\text{-}OH)_2\{Cu(C_6H_4NO_3)_2(H_2O)_2\}_2]\cdot 2H_2O$ (green, form-III, CSD refcode BULWIO), formed under basic conditions. A fourth form of formula $[\{Cu(C_6H_4NO_3)_2\}\{Cu(C_6H_4NO_3)NO_3\}_2]_n$ (green, form-IV) is reported herein.‡ The gelators are based on the amide N–H···O supramolecular synthon, an important class of stimuli-responsive supramolecular gels[7,37–53] with tuneable properties. Supramolecular gels based on trimesic amide derivatives[33,54–65] have been selected as gel media due to their typically very low minimum gel concentration (MGC). The candidate gel mimicking the pyridine *N*-oxide functional group of the isonicotinic acid–*N*-oxide ligand is reported.

Experimental

Materials and methods

All starting materials were purchased from Sigma Aldrich and were used as supplied. The tris-amide of trimesic acid with L-valine methyl ester (**Val-TMA**)[62] and aminopyridine[54] were synthesised following the reported procedures. The tailored *N*-oxide compound was synthesised by oxidizing the pyridyl group of tris-pyridyl trimesic amide.[54] Deionized water was used for all the experiments and absolute ethanol was obtained by distillation over Mg turnings and iodine.[66] ^{1}H-NMR and ^{13}C-NMR spectra were recorded on a Bruker Advance 400 spectrometer. Single crystal X-ray diffraction (SCXRD) was performed on a Bruker D8 venture, and powder X-ray diffraction (PXRD) was carried out using a Bruker D8 Focus instrument. The morphology of the xerogel was analysed by Scanning Electron Microscopy (SEM) using a Leo Supra 25 Microscope.

Synthesis

3,3′,3″-((Benzene-1,3,5-tricarbonyl)tris(azanediyl))tris-(pyridine 1-oxide) (L-3Nox). To a solution of N^1,N^3,N^5-tri(pyridin-3-yl)benzene-1,3,5-tricarboxamide (0.88 g, 2.0 mmol) in hot methanol (50 mL), *m*-chloroperbenzoic acid (1.86 g, 10.8 mmol) was added in portions over a period of 15 minutes. The reaction mixture was refluxed at 70 °C overnight. The mixture was cooled to room temperature. The solid obtained was filtered, washed with water followed by methanol, dried and the product was obtained as a white powder (0.76 g, 1.6 mmol). Yield: 78.0%. ^{1}H NMR (400 MHz, DMSO-d_6) δ: 10.95 (3H, s), 8.86 (3H, s), 8.74 (3H, s), 8.05 (3H, d, J = 6.4), 7.71 (3H, d, J = 8.4), 7.46 (3H, dd, J = 8.6, 6.2). ^{13}C NMR (100 MHz, DMSO-d_6) δ: 164.78, 138.10, 134.69, 134.40, 131.01, 130.51, 126.23, 116.84. HRMS (m/z) calcd for $C_{24}H_{18}N_6O_6Na$: 509.118; found: 509.118 [M − Na$^+$]. Anal. data for $C_{24}H_{18}N_6O_6$: calc. C, 59.26; H, 3.73; N, 17.28. Found: C, 59.10; H, 3.82; N, 17.00.

$[Cu(C_6H_4NO_3)_2(H_2O)_2]$ (form-I). 27.8 mg (0.2 mmol) of isonicotinic acid–*N*-oxide was dissolved in water (8.5 mL)/ethanol (1.5 mL) mixture and was layered over 5 mL aqueous solution of $Cu(NO_3)_2\cdot 3H_2O$ (24.1 mg, 0.1 mmol). Slow evaporation of the mixture resulted in blue crystals of form-I in 3–4 days.[34]

$[Cu(\mu\text{-}C_6H_4NO_3)_2(H_2O)]_n$ (form-II). 27.8 mg (0.2 mmol) of isonicotinic acid–*N*-oxide was dissolved in ethanol (10 mL) and layered over ethanolic solution (5 mL) of $Cu(NO_3)_2\cdot 3H_2O$ (24.1 mg, 0.1 mmol) and the vial was sealed. Plate shaped green crystals of form-II were obtained in 3–4 days.[36]

$[\{Cu(C_6H_4NO_3)_2\}\{Cu(C_6H_4NO_3)NO_3\}_2]_n$ (form-IV). 27.8 mg (0.2 mmol) of isonicotinic acid–*N*-oxide and 24.1 mg (0.1 mmol) of $Cu(NO_3)_2\cdot 3H_2O$ were added to 2 mL of ethanol and the mixture was heated at 85 °C in a sealed vial. Block shaped green crystals of form-IV were obtained overnight at 85 °C. Anal. data for $C_{24}H_{16}Cu_3N_6O_{18}$: calc. C, 33.25; H, 1.86; N, 9.69. Found: C, 33.16; H, 1.94; N, 9.70.

Single crystal X-ray diffraction

X-ray quality single crystals of form-IV were isolated from mother liquor, immediately immersed in cryogenic oil and then mounted. The diffractions were collected using MoKα radiation (λ = 0.71073 Å) on a Bruker D8 Venture (Photon100 CMOS detector) diffractometer equipped with a Cryostream (Oxford Cryosystems) open-flow nitrogen cryostats at a temperature of 150.0(2) K. The unit cell determination, data collection, data reduction, structure solution/refinement and empirical absorption correction (SADABS) were carried out using Apex-III (Bruker AXS: Madison, WI, 2015). The structure was solved by a direct method and refined by the full-matrix least squares on F^2 for all data using SHELXTL[67] and Olex2[68] software. All non-disordered non-hydrogen

‡ Crystal data for the Cu(II)–isonicotinic acid–*N*-oxide complex (form-IV): $C_{24}H_{16}Cu_3N_6O_{18}$, FW = 867.05, monoclinic, $P2_1/n$, a = 8.892(2), b = 15.096(4), c = 11.178(3) Å, β = 103.646(9)°, V = 3443(3) Å^3, Z = 4, D_c = 1.975 cm^3, $F(000)$ = 866, and T = 150 K. Final residuals (for 242 parameters) were R_1 = 0.0218 for 3288 reflections with $I > 2\sigma(I)$, and R_1 = 0.0218, wR_2 = 0.0581, and GOF = 0.989 for all 3052 reflections. CCDC 1846767 contains the supplementary crystallographic data for this paper.

atoms were refined anisotropically except for the disordered oxygen atom of the nitrate group, where the free variables were refined by the FVAR instruction. All the hydrogen atoms were placed in the calculated positions and refined using a riding model.

Gelation properties of tailored *N*-oxide compounds

The gelating ability of **L-3Nox** was screened in various solvent systems (see the ESI†). The gelator was soluble only in highly polar solvents such as DMF, DMA and DMSO and gels were formed only in DMSO/water mixtures. In a typical experiment, the compound was dissolved in a required amount of DMSO by heating and sonicating followed by the addition of water. The mixture was then sonicated to form a suspension, and left undisturbed to form a gel. The gel formation was confirmed by the inversion test.

Minimum gelation concentration. Various amounts (1.0 to 5.0 mg) of **L-3Nox** gelator were taken in standard vials (7 mL) and 0.5 mL of DMSO was added. The solution was heated and sonicated to dissolve the compound followed by the addition of 0.5 mL water, and the resulting mixture was left undisturbed to form the gel. After 24 hours, the gel formation was checked by an inversion test. The lowest concentration at which the gel was formed was recorded as the minimum gel concentration (MGC).

Gel–sol transition temperature. The required amount of **L-3Nox** gelator was taken in a standard 7 mL vial and the gel was prepared in DMSO/water (1 : 1 v/v) as per the above procedure. After 24 hours, a small spherical glass ball weighing 92.0 mg was placed on the gel surface, and the gel was heated gradually in an oil bath. The temperature at which the ball touched the bottom of the vial was recorded as the gel–sol transition temperature (T_{gel}).

Crystallisation experiments

Crystal-to-crystal transformation: transformation of a blue complex (form-I) to a green polymer (form-II). Form-I (3.0 mg) was added to absolute ethanol (10 mL) in a standard vial. The vial was sealed to prevent the evaporation of ethanol and left without disturbance. Green crystals of form-II were obtained over the course of one week and were characterized by SCXRD.

Transformation of a green polymer (form-II) to a blue complex (form-I). Water (1 mL) was added to form-II (3.0 mg). Excess water was avoided since form-II is sparingly soluble in water. The transparent green crystals almost instantly turned into an opaque blue material and the mixture was left undisturbed. X-ray quality blue crystals of form-I were obtained in 2–3 days and were characterized by SCXRD.

Transformation of a green polymer (form-IV) to a blue complex (form-I). Water (1 mL) was added to form-IV (3.0 mg) in a standard vial. X-ray quality blue crystals were obtained in 2–3 days and characterized by SCXRD.

Scanning electron microscopy. The gelator (**L-3Nox**) was dissolved in 0.7 mL of DMSO, the mixture was heated and sonicated, and 0.3 mL of water was added to form the gel. The gel was filtered through a filter paper after 24 hours and the residue was air-dried in a fume hood. The xerogels were gold coated and SEM was performed using a Leo Supra 25 Microscope.

Gel phase crystallisation

Crystallisation of $Cu(NO_3)_2{\cdot}3H_2O$ and isonicotinic acid–*N*-oxide was performed in the presence of hydrogelators (agarose and gelatin) and low molecular weight gelators (LMWGs). In a typical experiment, isonicotinic acid–*N*-oxide (2 equivalent) and the gelator were dissolved together in water (for agarose and gelatin) and then $Cu(NO_3)_2{\cdot}3H_2O$ (1 equivalent) was added. The solution was sonicated and left undisturbed to form the gel and crystallise. For **Val-TMA** and **L-3Nox**, isonicotinic acid–*N*-oxide and the gelator were dissolved in a polar organic solvent (DMF or DMSO) and $Cu(NO_3)_2{\cdot}3H_2O$ and water were added to this mixture in the quantities given below.

Crystallisation in agarose. Isonicotinic acid–*N*-oxide (13.9 mg, 0.1 mmol) and agarose (6.0 mg) were dissolved in water (1 mL) by heating, and $Cu(NO_3)_2{\cdot}3H_2O$ (12.1 mg, 0.05 mmol) was added to the resulting solution. X-ray quality crystals of form-I were obtained in 2 days.

Gel phase crystallisation in Val-TMA. Isonicotinic acid–*N*-oxide (27.8 mg, 0.2 mmol) and **Val-TMA** (40.0 mg, 4.0 wt%) were dissolved in DMF (0.5 mL) by heating and sonicating. Water (0.5 mL) and $Cu(NO_3)_2{\cdot}3H_2O$ (24.1 mg, 0.1 mmol) were added to this solution, and the mixture was left undisturbed to form a blue gel. X-ray quality crystals of form-I were obtained in 2–3 days.

Gel phase crystallisation in L-3Nox. Isonicotinic acid–*N*-oxide (27.8 mg, 0.2 mmol) and **L-3Nox** (8.0 mg) were dissolved in DMSO (0.5 mL) by heating and sonicating. Water (0.5 mL) and $Cu(NO_3)_2{\cdot}3H_2O$ (24.1 mg, 0.1 mmol) were added to this solution and leaving the mixture undisturbed yielded a blueish green gel. X-ray quality single crystals of form-I were obtained in 2 days.

Results and discussion

Solution phase crystallization

Layering an ethanolic solution of $Cu(NO_3)_2{\cdot}3H_2O$ over an aqueous ethanolic solution (5% of water, v/v) of isonicotinic acid–*N*-oxide at a 1 : 2 metal–ligand ratio results in the formation of a mixture of blue and green crystals over a period of three days (Fig. S1, ESI†). These crystals were isolated, and the structure was determined by single crystal X-ray diffraction. This technique shows that the samples match with the reported structures, namely form-I (blue crystals) and form-II (green crystals).[34,36] Formation of the hydroxyl-bridged species form-III is not expected under these conditions due to the absence of a base.[35] Basic conditions were not investigated because of the effect of changing pH on the gelation process in LMWGs.[69]

We have optimized the crystallisation conditions for these two forms and confirmed that crystallisation depends on the ethanol/water ratio. Form-I can be obtained in aqueous ethanol containing $>10\%$ of water (v/v), whereas the green form-II is formed at lower water content ($<3.5\%$ of water, v/v). Both forms are obtained simultaneously from aqueous ethanol containing 7% water (v/v). The monoaqua form-II transforms into the diaqua form-I over three days, presumably due to the absorption

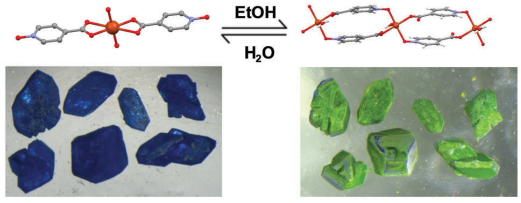

Fig. 1 Solvent mediated crystal-to-crystal transformation of form I and form-II.

of moisture from the mother liquor. The effect of temperature was studied by comparing the room temperature and low temperature (−15 °C) crystallisation for both forms. The yields of the single crystals in both cases were low compared to room temperature crystallisation. We have also performed low temperature crystallisation for form-I and form-II and interestingly, form-II does not disappear from the mixture even after three weeks. The conversion of green to blue crystals prompted us to explore the solvent-mediated solid-state transformation of form-I and form-II. Crystals of form-I were isolated, immersed in absolute ethanol and the crystals underwent conversion to green form-II over five days (Fig. 1). Similarly, treating form-II with water resulted in form-I overnight. The transformation of form-I to form-II was found to be reversible, which was confirmed by single crystal X-ray diffraction.

Heating copper(II) nitrate and isonicotinic acid–*N*-oxide at 85 °C in ethanol in a sealed vial resulted in block-shaped green crystals, a morphology that contrasts to the plate shaped form-II. Single crystal X-ray analysis of the block-shaped green crystals revealed a new coordination polymer (form-IV)‡ of the formula $[\{Cu(C_6H_4NO_3)_2\}\{Cu(C_6H_4NO_3)NO_3\}_2]_n$, which displays two different Cu(II) centres with distorted octahedral and square pyramidal geometries (Fig. 2a). The oxygen atoms of the carboxylate moiety of the isonicotinate–*N*-oxide ligands are coordinated to the two Cu(II) centres in a bidentate fashion forming an eight-membered metallo-macrocycle.

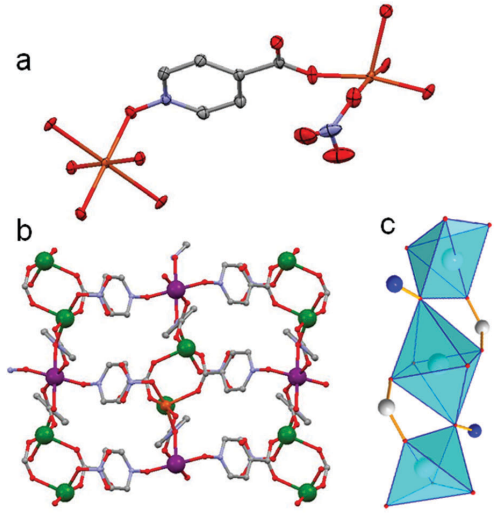

Fig. 2 (a) Molecular structure of form-IV $[\{Cu(C_6H_4NO_3)_2\}\{Cu(C_6H_4NO_3)NO_3\}_2]_n$, (b) representation of crystal structure showing octahedral (purple) and square pyramidal (green) metal centres and (c) interconnected octahedral and square pyramidal geometry.

The Cu(II) centres in the metallo-macrocycle display square pyramidal geometry with oxygen atoms of the *N*-oxide moiety, the nitrate anion and two carboxylate moieties in the equatorial site, and the axial position is coordinated to the oxygen atom of the carboxylate moiety. The oxygen atoms of the *N*-oxide moieties of isonicotinate–*N*-oxide in the metallo-macrocycle are coordinated to the Jahn–Teller distorted octahedral Cu(II) centre. In the octahedral Cu(II) centre, four isonicotinate–*N*-oxide ligands are coordinated to the equatorial position of the metal centre (two oxygen atoms of the *N*-oxide moiety and two carboxylate oxygen atoms), and the axial positions are coordinated to the oxygen atoms of the *N*-oxide moiety. The oxygen atom of the *N*-oxide moiety displays a bridging coordination mode and binds to the equatorial position of the distorted octahedral and square pyramidal copper(II) centres resulting in a complex 3-D network (Fig. 2b). Form-IV was found to convert to form-I when immersed in water (confirmed by single crystal X-ray diffraction).

Gel phase crystallization

The existence of at least four distinct copper(II) isonicotinate–*N*-oxide complexes prompted us to explore the selective crystallisation of this system in gel media. The copper(II) isonicotinate–*N*-oxide compounds were initially crystallised in gels of commercially available hydrogelators, namely agarose and gelatin. A blue gel was obtained by dissolving $Cu(NO_3)_2{\cdot}3H_2O$, isonicotinic acid–*N*-oxide and agarose in hot water, which subsequently produced X-ray quality crystals of blue form-I upon cooling. Crystallisation experiments performed at various concentrations of agarose, $Cu(NO_3)_2{\cdot}3H_2O$ and isonicotinic acid–*N*-oxide gave similar results; however, experiments with low concentration of metal salt and ligand did not yield any solid product. Crystals of isonicotinic acid–*N*-oxide (CSD refcode XUCPAO) were obtained at a higher concentration of metal salt and ligand. Experiments performed with 1 : 1 ethanol/water (v/v) gave similar results. Use of gelatin hydrogels as the crystallization medium resulted in blue gels, but crystals were not formed even after several weeks. Neither gelatin nor agarose formed gels in absolute ethanol. We then turned our attention to LMWGs based on **Val-TMA**[62] (Scheme 2 and ESI†).

Gel phase crystallisation was performed by mixing copper(II) nitrate trihydrate and isonicotinic acid–*N*-oxide at a 1 : 2 metal–ligand ratio with the gelator (4.0 wt%) in ethanol/water and DMF/water (1 : 1, v/v respectively). This resulted in blue crystals of form-I after two days (confirmed by single crystal X-ray diffraction). The formation of form-I in this 'generic' supramolecular gel medium prompted us to investigate the crystallisation of copper(II) isonicotinate–*N*-oxide complexes in the tailored LMWG gel, which is structurally similar to the crystallisation substrate. Recently we have shown that the tailored LMWG gel can enable selective crystallisation[31] of particular

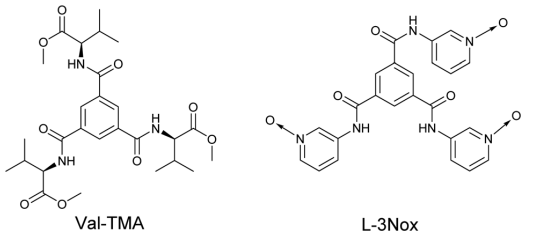

Scheme 2 Chemical structure of a non-tailored gelator (**Val-TMA**) and a tailored *N*-oxide gelator (**L-3Nox**).

polymorphs of the olanzapine precursor, ROY.[70] We have also reported the formation of crystalline materials in a supramolecular gel matrix of copper(II) metallogels with pyridyl amides.[71]

The gelator design involves trimesic pyridyl amide based compounds,[7,37] which show two types of hydrogen bonding motifs, one through a N–H···O synthon involving the amide moiety and the other through a N–H···N synthon involving the amide and the pyridyl ring nitrogen atom. Thus, a tailored gel was designed for the copper(II) isonicotinate–*N*-oxide system by modifying the pyridyl groups of trimesic amides to give *N*-oxides. In this context, we prepared a tailored tris-*N*-oxide compound (**L-3Nox**, Scheme 2) by oxidising *N*,*N*′,*N*″-tris(3-pyridyl)-trimesic amide[54] with *m*-chloroperbenzoic acid (ESI†). The gelation properties of **L-3Nox** were tested in aqueous solutions of highly polar DMSO, due to its poor solubility in other solvents. **L-3Nox** formed gels in various mixtures of DMSO and water (ESI†) and the gel formation was confirmed by an inversion test (Fig. 3). We selected a 7 : 3 DMSO/water mixture (v/v) for **L-3Nox** since the gel was transparent at this composition. The thermal stability of the tailored gel was evaluated by analysing the temperature at which the gel was converted into a liquid phase (T_{gel}). T_{gel} was found to be 107 °C at 0.5 wt% and the minimum gel concentration (MGC) was 0.15 wt% in the DMSO/water (7 : 3, v/v) mixture. T_{gel} and MGC were 105 °C at 0.5 wt% and 0.3 wt% in the 1 : 1 DMSO/water (v/v) mixture. Thus, replacing the pyridyl group with pyridyl *N*-oxide has a significant effect on the MGC of **L-3Nox** (0.15 wt%) compared to *N*,*N*′,*N*″-tris(3-pyridyl)-trimesic amide (0.03 wt%) in the DMSO/water (7 : 3, v/v) mixture.[54]

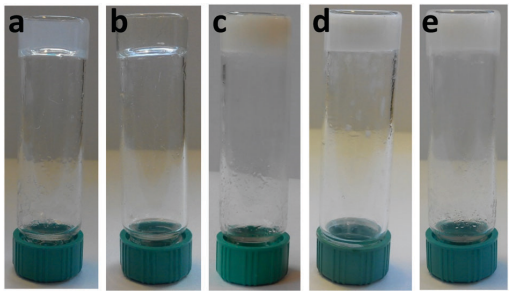

Fig. 3 Gels obtained from (a) agarose in water, (b) gelatin in water, (c) **Val-TMA** in DMF/water (1 : 1 v/v), (d) **Val-TMA** in ethanol and (e) **L-3Nox** in DMSO/water (1 : 1 v/v).

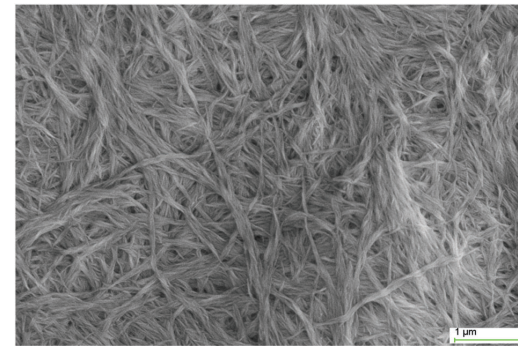

Fig. 4 SEM image of **L-3Nox** xerogel at 0.5 wt% obtained from DMSO/water (7 : 3, v/v).

Scanning electron microscopy (SEM) was performed on the xerogel of **L-3Nox** to elucidate the morphology of the xerogels (Fig. 4), which clearly indicates the fibrous nature of the gel network, and twisted fibres were observed in **L-3Nox**. The thickness of the individual fibres was found to be 20–40 nm and these fibres combine to form bundles with thickness ranging from 100 to 150 nm.

Gel phase crystallisation was performed by mixing copper(II) nitrate trihydrate and isonicotinic acid–*N*-oxide at a 1 : 2 metal–ligand ratio with **L-3Nox** gelator in DMSO/water. The mixture was heated to give a clear green solution and left without disturbing for 2 hours to form the gel (ESI†). The crystallisation experiments were performed at a higher concentration of **L-3Nox** gelator (greater than the MGC) to ensure gel formation. The crystallisation experiments were also performed with varying amounts of copper(II) nitrate trihydrate and isonicotinic acid–*N*-oxide. A greenish-blue gel was formed in an hour in all cases for **L-3Nox** gelator at 0.8 wt% in 1 : 1 (v/v) DMSO/water. The optimized concentration for crystallisation was found to be 0.06 mmol of copper(II) nitrate trihydrate and 0.12 mmol isonicotinic acid–*N*-oxide. Crystals were not formed for experiments with a lower metal–ligand concentration, whereas a concentration of 0.06 mmol or more copper(II) nitrate trihydrate produced blue crystals (form-I) in a week (Fig. 5c).

We have compared the morphologies of form-I crystals obtained from the gel phase crystallisation in different gelators. The solution phase crystallisation in an ethanol/water mixture without a gelator resulted in block shaped crystals. Similar crystals

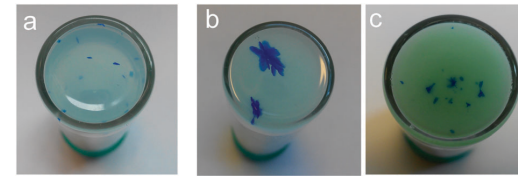

Fig. 5 Gel phase crystallisation of Cu(II) complexes from (a) agarose gel in water (1.5 wt%), (b) **Val-TMA** gel at 4.0 wt% in DMF/water (1 : 1, v/v) and (c) **L-3Nox** gel at 0.8 wt% in DMSO/water (1 : 1, v/v).

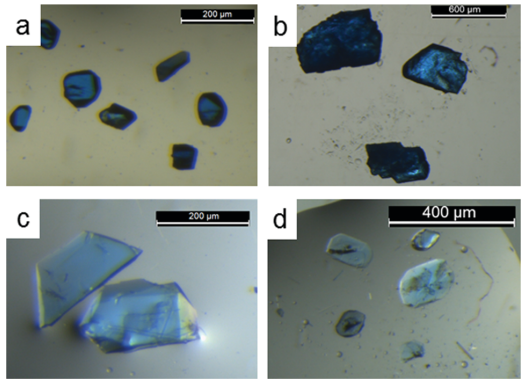

Fig. 6 Images of isolated crystals from (a) solution phase, (b) agarose gel, (c) **Val-TMA** gel and (d) **L-3Nox** gel.

of form-I were obtained in water with very low yield due to the crystallisation of the isonicotinic acid–*N*-oxide ligand. The gel phase crystallisation of the complex in an agarose gel yielded block-shaped crystals (Fig. 6). However, plate shaped crystals were obtained from **Val-TMA** and **L-3Nox** tailored gels indicating that the presence of similar functional groups in the gelator plays a role in crystal morphology. Crystallisation of copper(II) isonicotinate–*N*-oxide complexes was also performed in ethanolic supramolecular gel media. Since the tailored gelator and agarose do not form gels in absolute ethanol or a mixture of ethanol and other solvents, the gel phase crystallisation in ethanol was performed only with **Val-TMA** gelator. Adding copper(II) nitrate to a hot solution of isonicotinic acid–*N*-oxide and **Val-TMA** in absolute ethanol led to a green solution, which subsequently formed a green gel. However, crystals of Cu(II) isonicotinate–*N*-oxide complex were not formed and isonicotinic acid–*N*-oxide crystallised due to its poor solubility in ethanol at ambient temperature. The solubility of isonicotinic acid–*N*-oxide was increased by adding a trace amount of water. Thus, a mixture of isonicotinic acid–*N*-oxide (27.8 mg, 0.2 mmol) and **Val-TMA** (4.0 wt%) was heated in the ethanol/water (5% water, v/v) mixture, and copper(II) nitrate (24.1 mg, 0.1 mmol) was added to yield a green solution and the vial was sealed. The solution turned into a greenish blue gel in 15 minutes, and the blue colour intensified overnight resulting in blue crystals of form-I in the gel medium (Fig. 7a and b). Blue crystals of form-I were formed in almost every case, with one out of 25 trails forming green crystals of form-II, which might be due to accidental heteroseeding. Experiments were performed under identical conditions (the same solvent composition and the same concentration of copper(II) nitrate and isonicotinic acid–*N*-oxide) without **Val-TMA** by adding copper(II) nitrate to a hot solution of isonicotinic acid–*N*-oxide in ethanol/water (5% water, v/v), which resulted in a green solution. The vial was sealed, and a mixture of blue and green crystals was formed overnight (Fig. 7c and d). X-ray single crystal diffraction of these crystals revealed that the blue crystal belongs to form-I and the green crystals were either form-II or form-IV. Thus, concomitant crystallisation of different forms was observed from the solution. Most of the green crystals eventually turned blue over a week.

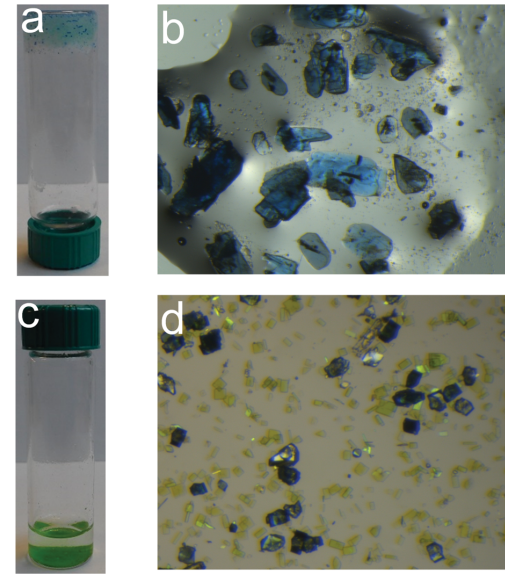

Fig. 7 Crystallisation experiments of the copper(II) isonicotinate–*N*-oxide complex in aqueous ethanol (5% water, v/v) (a) with **Val-TMA** gelator (4.0 wt%) and (b) the isolated crystals. Solution phase crystallisation (c) without gelator and (d) top view of crystals.

Conclusions

In summary, we report the crystallisation of three forms of copper(II) isonicotinate–*N*-oxide (form-I, form-II and form-IV) and their solvent-mediated interconversion. The crystal-to-crystal transformation of a concomitant mixture of blue and green crystals was also studied as a function of solvent concentration. We have designed a gelator that is structurally similar to the crystallisation substrate. Gel phase crystallisation of the complex was performed in hydrogels, the gels of low molecular weight gelators and tailored LMWG. The morphologies of the crystals obtained from solution and from agarose gel proved to be similar to each other while gel phase crystallisation performed in LMWGs and the tailored gelator resulted in plate shaped crystals indicating an influence of the gelator on the crystallization process. Crystallisation of copper(II) isonicotinate–*N*-oxide complexes in aqueous ethanol (5% water, v/v) resulted in a mixture of blue and green crystals, whereas gel phase crystallisation in **Val-TMA** gel under identical conditions resulted in only blue crystals indicating the influence of LMWGs in selective crystallisation of the thermodynamically stable form-I.

Conflicts of interest

There are no conflicts to declare.

Acknowledgements

We thank the University of Iceland Research Fund and the Science Institute for funding and Dr Sigurður Sveinn Jónsson,

ÍSOR-Iceland for powder X-ray diffraction analysis. DG thanks the University of Iceland for the Doctoral Research grant. KF and ZD thank the University of Ljubljana and Vilnius University respectively for the Erasmus exchange program. We thankfully acknowledge Dr Dmitry S. Yufit, the Department of Chemistry, Durham University, UK, for analysing the structures of form-I and form-II and Dr Sigríður Jónsdóttir, University of Iceland, for NMR and mass spectroscopy.

Notes and references

1 L. A. Estroff and A. D. Hamilton, *Chem. Rev.*, 2004, **104**, 1201–1218.
2 M. de Loos, B. L. Feringa and J. H. van Esch, *Eur. J. Org. Chem.*, 2005, 3615–3631.
3 M. George and R. G. Weiss, *Acc. Chem. Res.*, 2006, **39**, 489–497.
4 P. Dastidar, *Chem. Soc. Rev.*, 2008, **37**, 2699–2715.
5 A. R. Hirst, B. Escuder, J. F. Miravet and D. K. Smith, *Angew. Chem., Int. Ed.*, 2008, **47**, 8002–8018.
6 S. Banerjee, R. K. Das and U. Maitra, *J. Mater. Chem.*, 2009, **19**, 6649–6687.
7 M.-O. M. Piepenbrock, G. O. Lloyd, N. Clarke and J. W. Steed, *Chem. Rev.*, 2010, **110**, 1960–2004.
8 D. K. Kumar and J. W. Steed, *Chem. Soc. Rev.*, 2014, **43**, 2080–2088.
9 G. Yu, X. Yan, C. Han and F. Huang, *Chem. Soc. Rev.*, 2013, **42**, 6697–6722.
10 C. R. Groom, I. J. Bruno, M. P. Lightfoot and S. C. Ward, *Acta Crystallogr., Sect. B: Struct. Sci., Cryst. Eng. Mater.*, 2016, **72**, 171–179.
11 H. N. Holmes, *J. Phys. Chem.*, 1916, **21**, 709–733.
12 J. Eckstein, *Cryst. Res. Technol.*, 1996, **31**, 874.
13 M. C. Robert, O. Vidal, J. M. Garcia-Ruiz and F. Otalora, in *Crystallization of Nucleic Acids and Proteins*, ed. M. Ducruix and R. Giegé, Oxford University Press, 2nd edn, 1999, pp. 149–175.
14 M. Conejero-Muriel, J. A. Gavira, E. Pineda-Molina, A. Belsom, M. Bradley, M. Moral, J. d. D. G.-L. Durán, A. Luque González, J. J. Díaz-Mochón, R. Contreras-Montoya, Á. Martínez-Peragón, J. M. Cuerva and L. Álvarez de Cienfuegos, *Chem. Commun.*, 2015, **51**, 3862–3865.
15 T. K. Adalder, D. P. Kumar and P. Dastidar, *Cryst. Growth Des.*, 2014, **14**, 11–14.
16 Z. Yang, H. Gu, Y. Zhang, L. Wang and B. Xu, *Chem. Commun.*, 2004, 208–209.
17 *Polymorphism: In the Pharmaceutical Industry*, Wiley-VCH Verlag GmbH & Co. KGaA, 2006.
18 J. Bernstein, *Polymorphism in Molecular Crystals*, Oxford University Press, 2002.
19 C. Sudha, P. Parimaladevi and K. Srinivasan, *Mater. Sci. Eng., C*, 2015, **47**, 150–155.
20 J. Buendia, E. Matesanz, D. K. Smith and L. Sanchez, *CrystEngComm*, 2015, **17**, 8146–8152.
21 Y. Diao, K. E. Whaley, M. E. Helgeson, M. A. Woldeyes, P. S. Doyle, A. S. Myerson, T. A. Hatton and B. L. Trout, *J. Am. Chem. Soc.*, 2012, **134**, 673–684.
22 S. R. Kennedy, C. D. Jones, D. S. Yufit, C. E. Nicholson, S. J. Cooper and J. W. Steed, *CrystEngComm*, 2018, **20**, 1390–1398.
23 J. Bernstein, R. J. Davey and J.-O. Henck, *Angew. Chem., Int. Ed.*, 1999, **38**, 3440–3461.
24 M. R. Caira, in *Design of Organic Solids*, ed. E. Weber, Y. Aoyama, M. R. Caira, G. R. Desiraju, J. P. Glusker, A. D. Hamilton, R. E. Meléndez and A. Nangia, Springer, Berlin Heidelberg, 1998, pp. 163–208.
25 G. Dhanaraj, K. Byrappa, V. Prasad and M. Dudley, in *Springer Handbook of Crystal Growth*, ed. G. Dhanaraj, K. Byrappa, V. Prasad and M. Dudley, Springer, Berlin Heidelberg, 2010, pp. 3–16.
26 M. Pauchet, T. Morelli, S. Coste, J.-J. Malandain and G. Coquerel, *Cryst. Growth Des.*, 2006, **6**, 1881–1889.
27 F. Aparicio, E. Matesanz and L. Sanchez, *Chem. Commun.*, 2012, **48**, 5757–5759.
28 A. Dawn, K. S. Andrew, D. S. Yufit, Y. Hong, J. P. Reddy, C. D. Jones, J. A. Aguilar and J. W. Steed, *Cryst. Growth Des.*, 2015, **15**, 4591–4599.
29 J. A. Foster, M.-O. M. Piepenbrock, G. O. Lloyd, N. Clarke, J. A. K. Howard and J. W. Steed, *Nat. Chem.*, 2010, **2**, 1037–1043.
30 H. Wang, W. Zhu, J. Li, T. Tian, Y. Lan, N. Gao, C. Wang, M. Zhang, C. F. J. Faul and G. Li, *Chem. Sci.*, 2015, **6**, 1910–1916.
31 J. A. Foster, K. K. Damodaran, A. Maurin, G. M. Day, H. P. G. Thompson, G. J. Cameron, J. C. Bernal and J. W. Steed, *Chem. Sci.*, 2017, **8**, 78–84.
32 L. A. Estroff, L. Addadi, S. Weiner and A. D. Hamilton, *Org. Biomol. Chem.*, 2004, **2**, 137–141.
33 R. Daly, O. Kotova, M. Boese, T. Gunnlaugsson and J. J. Boland, *ACS Nano*, 2013, **7**, 4838–4845.
34 H. Knuuttila and P. Knuuttila, *Acta Chem. Scand., Ser. A*, 1983, **37**, 227–233.
35 H. Knuuttila, *Inorg. Chim. Acta*, 1983, **72**, 11–16.
36 X.-L. Li, J.-T. Chen, D.-Z. Niu, J.-T. Sheng and D.-P. Zhang, *Jiegou Huaxue*, 2003, **22**, 415–418.
37 D. K. Kumar, D. A. Jose, P. Dastidar and A. Das, *Langmuir*, 2004, **20**, 10413–10418.
38 A. Pal, Y. K. Ghosh and S. Bhattacharya, *Tetrahedron*, 2007, **63**, 7334–7348.
39 K. Kawamoto, S. C. Grindy, J. Liu, N. Holten-Andersen and J. A. Johnson, *ACS Macro Lett.*, 2015, **4**, 458–461.
40 Q. Jin, L. Zhang and M. Liu, *Chem. – Eur. J.*, 2013, **19**, 9234–9241.
41 S. Karak, S. Kumar, S. Bera, D. D. Diaz, S. Banerjee, K. Vanka and R. Banerjee, *Chem. Commun.*, 2017, **53**, 3705–3708.
42 K. K. Kartha, V. K. Praveen, S. S. Babu, S. Cherumukkil and A. Ajayaghosh, *Chem. – Asian J.*, 2015, **10**, 2250–2256.
43 Q. Liu, Y. Wang, W. Li and L. Wu, *Langmuir*, 2007, **23**, 8217–8223.
44 K. Ghosh, S. Panja and S. Bhattacharya, *RSC Adv.*, 2015, **5**, 72772–72779.
45 O. Kotova, R. Daly, C. M. G. dos-Santos, M. Boese, P. E. Kruger, J. J. Boland and T. Gunnlaugsson, *Angew. Chem., Int. Ed.*, 2012, **51**, 7208–7212.
46 F. Fages, F. Voegtle and M. Zinic, *Top. Curr. Chem.*, 2005, **256**, 77–131.
47 O. Kotova, R. Daly, C. M. G. dos Santos, P. E. Kruger, J. J. Boland and T. Gunnlaugsson, *Inorg. Chem.*, 2015, **54**, 7735–7741.

48 S. Mukhopadhyay, Ira, G. Krishnamoorthy and U. Maitra, *J. Phys. Chem. B*, 2003, **107**, 2189–2192.
49 K.-P. Tseng, M.-T. Kao, T. W. T. Tsai, C.-H. Hsu, J. C. C. Chan, J.-J. Shyue, S.-S. Sun and K.-T. Wong, *Chem. Commun.*, 2012, **48**, 3515–3517.
50 S. Bhattacharya and S. K. Samanta, *Langmuir*, 2009, **25**, 8378–8381.
51 M. Shirakawa, N. Fujita and S. Shinkai, *J. Am. Chem. Soc.*, 2003, **125**, 9902–9903.
52 U. K. Das, S. Banerjee and P. Dastidar, *Chem. – Asian J.*, 2014, **9**, 2475–2482.
53 H. H. Lee, S. H. Jung, S. Park, K.-M. Park and J. H. Jung, *New J. Chem.*, 2013, **37**, 2330–2335.
54 D. K. Kumar, D. A. Jose, P. Dastidar and A. Das, *Chem. Mater.*, 2004, **16**, 2332–2335.
55 S. Banerjee, N. N. Adarsh and P. Dastidar, *Soft Matter*, 2012, **8**, 7623–7629.
56 N. Shi, G. Yin, H. Li, M. Han and Z. Xu, *New J. Chem.*, 2008, **32**, 2011–2015.
57 T. R. Canrinus, F. J. R. Cerpentier, B. L. Feringa and W. R. Browne, *Chem. Commun.*, 2017, **53**, 1719–1722.
58 R. C. T. Howe, A. P. Smalley, A. P. M. Guttenplan, M. W. R. Doggett, M. D. Eddleston, J. C. Tan and G. O. Lloyd, *Chem. Commun.*, 2013, **49**, 4268–4270.
59 S. Y. Ryu, S. Kim, J. Seo, Y.-W. Kim, O.-H. Kwon, D.-J. Jang and S. Y. Park, *Chem. Commun.*, 2004, 70–71.
60 A. Desmarchelier, M. Raynal, P. Brocorens, N. Vanthuyne and L. Bouteiller, *Chem. Commun.*, 2015, **51**, 7397–7400.
61 F. Camerel and C. F. J. Faul, *Chem. Commun.*, 2003, 1958–1959.
62 Y. Ishioka, N. Minakuchi, M. Mizuhata and T. Maruyama, *Soft Matter*, 2014, **10**, 965–971.
63 J.-L. Zhong, X.-J. Jia, H.-J. Liu, X.-Z. Luo, S.-G. Hong, N. Zhang and J.-B. Huang, *Soft Matter*, 2016, **12**, 191–199.
64 J. J. van Gorp, J. A. J. M. Vekemans and E. W. Meijer, *J. Am. Chem. Soc.*, 2002, **124**, 14759–14769.
65 D. Spitzer, V. Marichez, G. J. M. Formon, P. Besenius and T. M. Hermans, *Angew. Chem., Int. Ed.*, 2018, **57**, 11349–11353.
66 W. L. F. Armarego and C. Chai, *Purification of Laboratory Chemicals*, Butterworth-Heinemann, 5th edn, 2003.
67 G. Sheldrick, *Acta Crystallogr., Sect. C: Cryst. Struct. Commun.*, 2015, **71**, 3–8.
68 O. V. Dolomanov, L. J. Bourhis, R. J. Gildea, J. A. K. Howard and H. Puschmann, *J. Appl. Crystallogr.*, 2009, **42**, 339–341.
69 X. Du, J. Zhou, J. Shi and B. Xu, *Chem. Rev.*, 2015, **115**, 13165–13307.
70 L. Yu, *Acc. Chem. Res.*, 2010, **43**, 1257–1266.
71 D. Ghosh, I. Lebedyte, D. S. Yufit, K. K. Damodaran and J. W. Steed, *CrystEngComm*, 2015, **17**, 8130–8138.

Supplementary Information

Crystal habit modification of Cu(II) isonicotinate-*N*-oxide complexes using gel phase crystallisation

Dipankar Ghosh,[a] Katja Ferfolja,[a] Žygimantas Drabavičius,[a] Jonathan W. Steed[b] and Krishna K. Damodaran[a]**

[a] Department of Chemistry, Science Institute, University of Iceland, Dunhagi 3, 107 Reykjavík, Iceland; Phone: +354 525 4846; Fax: +354 552 8911; E-mail: krishna@hi.is

[b] Department of Chemistry, Durham University, South Road, Durham DH1 3LE, UK; E-mail: jon.steed@durham.ac.uk.

Table of Contents

1. Concomitant crystallisation of blue and green crystals

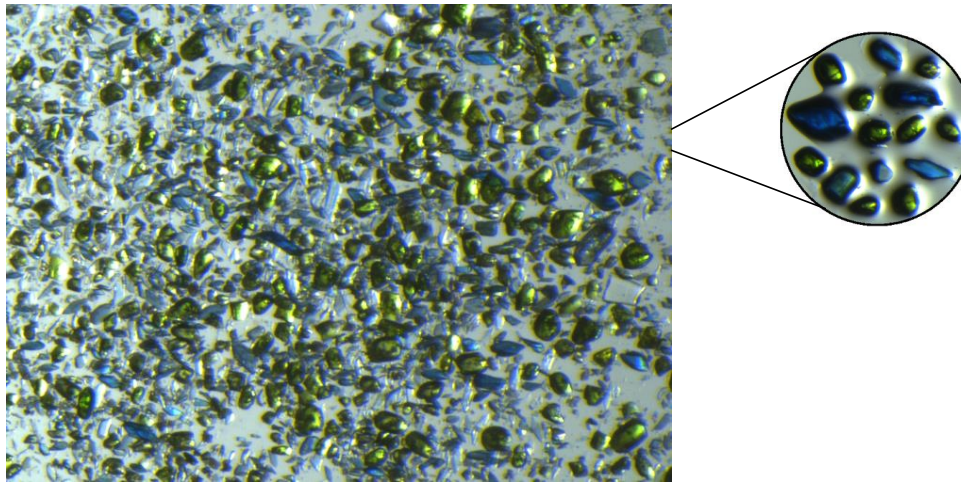

Figure S1: Concomitant crystals of copper(II) isonicotinate-*N*-oxide- form I (blue) and form II (green)

2.Crystallisation conditions for form-I and form-II

2.1. Crystals in different solvents: The crystals were isolated from the solution and dried in air. These crystals were transferred into small vials, approximately 0.5 mL of different solvent (water, methanol, ethanol, acetonitrile and THF) was added to each vail and sealed. We didn't add solvents to one of the vails to check the stability of these crystals in air.

2.1.1. Blue crystals: The crystals in ethanol changed colour to green in two hours. The crystals in methanol turned green in a couple of days and the crystals in water eventually dissolved. There was no change in colour for the crystals in THF, acetonitrile and the crystals were stable in air.

2.1.2. Green crystals: The crystals immersed in water dissolved completely after few hours. The crystals in methanol changed to darker green whereas crystals were partially soluble in ethanol. We did not observe any change with crystals in THF and acetonitrile.

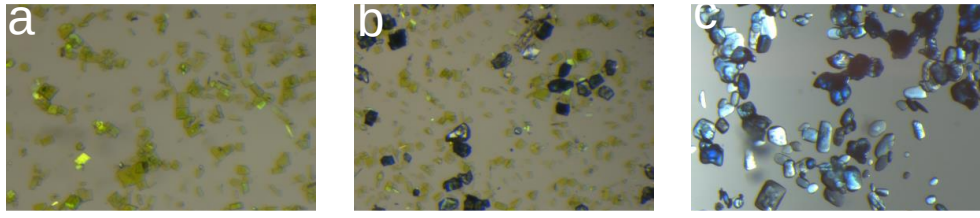

Figure S2: Crystallisation of (a) form-II (green) in (<3.5% water), (b) concomitant crystals (5-10% water) and (c) form-I (blue) (>10% water) in ethanol-water.

3. IR spectra of form-I, form-II and form-IV

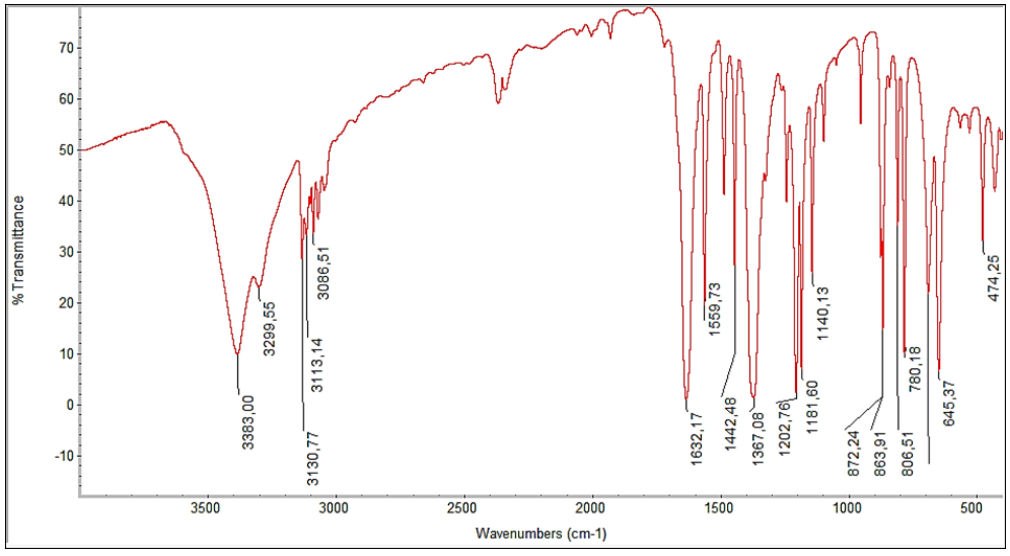

Figure S3: IR spectrum of form-I

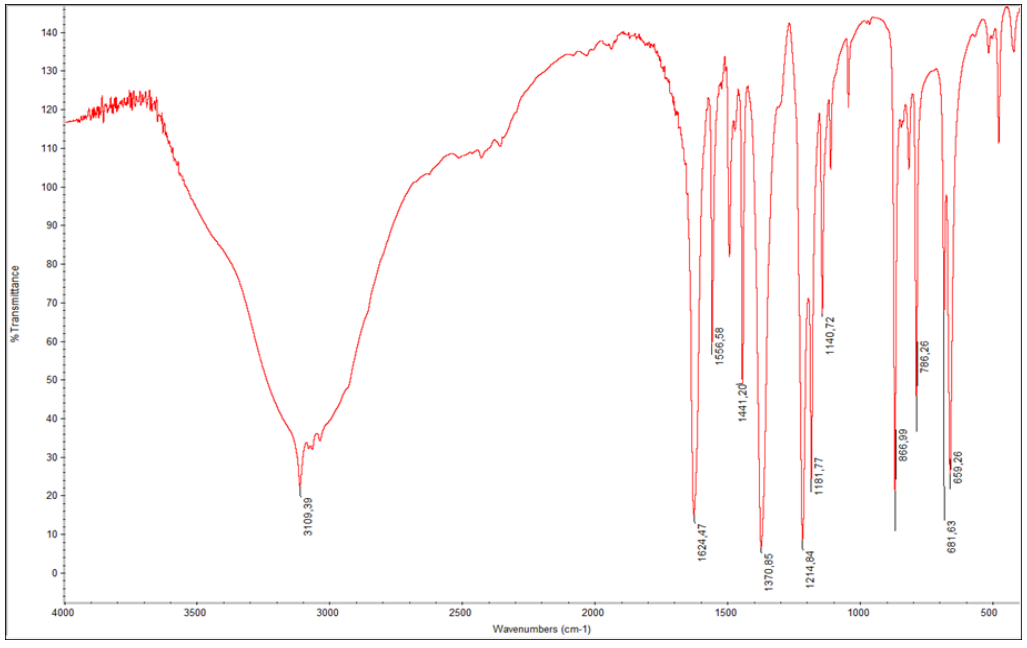

Figure S4: IR spectrum of form-II

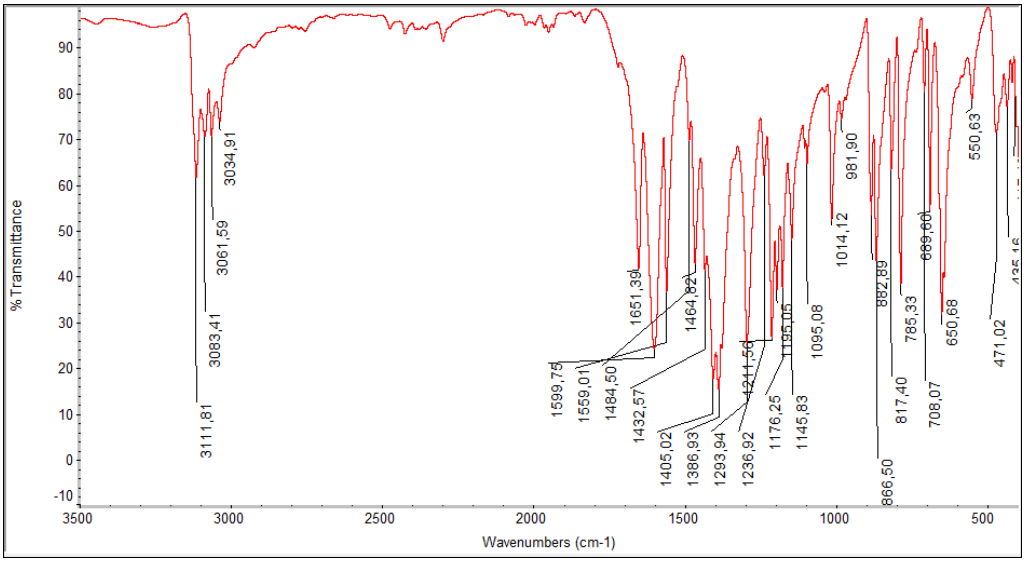

Figure S5: IR spectrum of form-IV

4. Single Crystal X-ray Diffraction: X-ray quality single crystals were obtained by heating ethanolic solution of copper(II) nitrate (24.1 mg, 0.1 mmol) and isonicotinic acid-*N*-oxide (27.8 mg, 0.2 mmol) at 85 °C in a sealed vial. The crystals were isolated from mother liquor, immediately immersed in cryogenic oil and then mounted. The X-ray single crystal data was collected using MoKα radiation (λ =0.71073Å) on a Bruker D8Venture (Photon100 CMOS detector) diffractometer equipped with a Cryostream (Oxford Cryosystems) open-flow nitrogen cryostats at the temperature 150.0(2) K.

5. Powder X-ray Diffraction: An ethanolic solution of copper(II) nitrate (24.1 mg, 0.1 mmol) and isonicotinic acid-*N*-oxide (27.8 mg, 0.2 mmol) was heated at 85 °C in a sealed vial. Resulting green crystals obtained overnight were filtered, dried in air and XRPD was recorded. XRPD pattern of the bulk solid was then compared with simulated pattern generated from single crystal data.

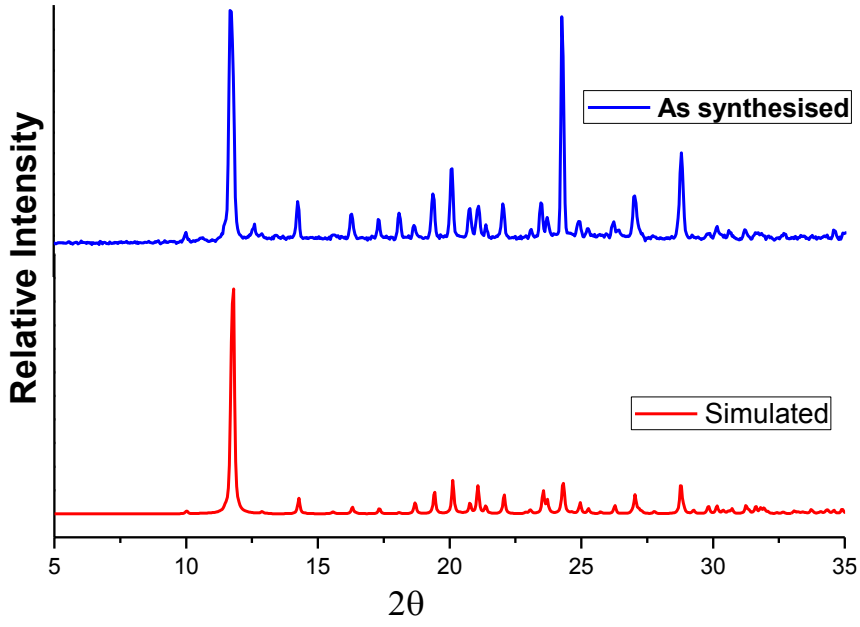

Figure S6: XRPD comparison of simulated and bulk solid of form-IV

6. Synthesis of gelators

6.1 General Scheme for all gelators.

Methyl L-valinate trimesic amide[1] and 3-pyridyl trimesic amide[2] were synthesised following literature procedure. Analytical and spectroscopic data of the synthesised compounds matched with reported compounds.

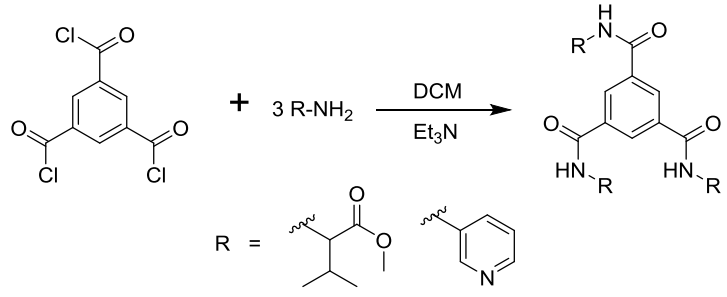

Scheme S1: General synthesis of trimesic amides

6.2 Synthesis of tailored L-3Nox compound.

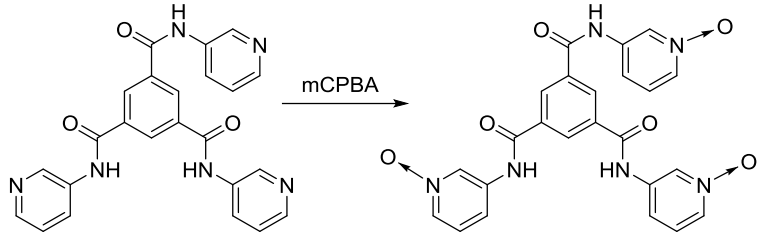

Scheme S2: Synthesis of *3,3',3''-((benzene-1,3,5-tricarbonyl)tris(azanediyl))tris-(pyridine 1-oxide) (**L-3Nox**)*

7. Gelation properties of tailored N-oxide compound {*3,3',3''-((benzene-1,3,5-tricarbonyl)tris-(azanediyl))tris(pyridine 1-oxide*)} (L-3Nox)

(a) Gelation test in various solvents

Gelation test for **L-3Nox** was performed in various solvent system. The gelator was soluble only in high polar solvents such as DMF, DMA, DMSO etc. In a typical experiment, **L-3Nox** was dissolved in required amount of solvent by heating and sonicating, cooled to room temperature and water was added. It was sonicated till a suspension was formed and left undisturbed.

Table S1: Gelation test of **L-3Nox** in various solvents

Amount	Solvents (mL)	Initial Observation	Final Observation
5.0 mg	DMF (0.5)/ water (0.5)	Solution	No gel
5.0 mg	DMA (0.5)/ water (0.5)	Solution	No gel
5.0 mg	DMSO (0.5)/ water (0.5)	Solution	Gel in ~1 hour
5.0 mg	DEF (0.5)/ water (0.5)	Solution	No gel
5.0 mg	DEA (0.5)/ water (0.5)	Solution	No gel

(b) Varying solvent composition

Gelation test of **L-3Nox** was performed at different DMSO/water composition. We did a solvent screening from 50% to 10% water (v/v) composition.

Table S2: Gelation of **L-3Nox** in various DMSO/water composition

Amount	DMSO	Water	Initial Observation	Final Observation
5.0 mg	500 µL	500 µL	Solution	Gel
5.0 mg	600 µL	400 µL	Solution	Gel
5.0 mg	700 µL	300 µL	Solution	Gel
5.0 mg	800 µL	200 µL	Solution	Gel
5.0 mg	900 µL	100 µL	Solution	No gel

(c) Finding minimum gelator concentration (MGC)

MGC test of **L-3Nox** gel was performed at 7:3 and 1:1 DMSO/water (v/v) composition, the gel formed at 7:3 DMSO-water ratio was most transparent. MGC was found to be 0.15 wt% at 7:3 DMSO/water and 0.3 wt% at 1:1 DMSO/water.

Table S3: Determination of MGC of **L-3Nox**

Amount	Solvents (mL)	Initial Observation	Final Observation
5.0 mg	DMSO (0.7)/ water (0.3)	Solution	Gel
4.0 mg	DMSO (0.7)/ water (0.3)	Solution	Gel
3.0 mg	DMSO (0.7)/ water (0.3)	Solution	Gel
2.0 mg	DMSO (0.7)/ water (0.3)	Solution	Gel
1.5 mg	DMSO (0.7)/ water (0.3)	Solution	Gel
1.0 mg	DMSO (0.7)/ water (0.3)	Solution	No gel
5.0 mg	DMSO (0.5)/ water (0.5)	Solution	Gel
4.0 mg	DMSO (0.5)/ water (0.5)	Solution	Gel
3.0 mg	DMSO (0.5)/ water (0.5)	Solution	Gel
2.5 mg	DMSO (0.5)/ water (0.5)	Solution	No gel

(d) Finding T_{gel}

Gel-sol transition temperature (T_{gel}) of **L-3Nox** was performed at 0.5 wt% (5 mg in 1 mL solvent) in 7:3 and 1:1 DMSO/water (v/v) composition, after 24 hours.

Table S4: Determination of T_{gel} of **L-3Nox**

Exp. no	Gelator	Solvents (mL)	Mass of glass ball	Time	T_{gel}
1	0.5 wt%	DMSO (0.5)/ water (0.5)	92.0 mg	24 hour	105 °C
2	0.5 wt%	DMSO (0.7)/ water (0.3)	92.0 mg	24 hour	106 °C

8. Gel Phase Crystallisation

8.1 In hydrogels

Crystallisation of $Cu(NO_3)_2.3H_2O$ and isonicotinic acid-*N*-oxide was performed in presence of hydrogelators like agarose, gelatin and some low molecular weight gelators (LMWGs). In a typical experiment, isonicotinic acid-*N*-oxide (2 equivalent) and the gelator were dissolved together in water (for agarose and gelatin), then $Cu(NO_3)_2.3H_2O$ (1 equivalent) was added to it and left undisturbed.

Table S5: Crystallisation of $Cu(NO_3)_2.3H_2O$ and isonicotinic acid-*N*-oxide in presence of hydrogelators

Exp no	$Cu(NO_3)_2.3H_2O$ (amount in mg)	Isonicotinic acid-*N*-oxide (amount in mg)	Gelator (amount in mg)	Solvent (in mL)	Initial Observation	Final Observation
1	25.0	28.8	agarose (12.0)	water (2.0)	Gel	No crystals
2	28.8	35.0	agarose (12.0)	water (2.0)	Gel	Blue crystals (I)
3	37.0	45.0	agarose (12.0)	water (2.0)	Gel	Blue crystals (I)
4	45.2	55.0	agarose (12.0)	water (2.0)	Gel	Precipitate
5	25.0	28.8	agarose (12.0)	EtOH (1.0)/water (1.0)	Gel	No crystals
6	28.8	35.0	agarose (12.0)	EtOH (1.0)/water (1.0)	Gel	Blue crystals (I)
7	37.0	45.0	agarose (12.0)	EtOH (1.0)/water (1.0)	Gel	Blue crystals (I)
8	45.2	55.0	agarose (12.0)	EtOH (1.0)/water (1.0)	Gel	Precipitate
9	25.0	28.8	agarose (12.0)	EtOH (2.0)	Suspension	No crystals
10	25.0	28.8	agarose (12.0)	EtOH (2.0)	Suspension	No crystals
11	25.0	28.8	Gelatin (50.0)	water (2.0)	Solution	No crystals
12	25.0	28.8	Gelatin (70.0)	water (2.0)	Gel	No crystals
13	37.0	45.0	Gelatin (70.0)	water (2.0)	Gel	Precipitate
14	25.0	28.8	Gelatin (50.0)	EtOH (1.0)/water (1.0)	Solution	No crystals
15	25.0	28.8	Gelatin (70.0)	EtOH (1.0)/water (1.0)	Solution	No crystals
16	45.2	55.0	Gelatin (70.0)	EtOH (1.0)/water (1.0)	Solution	Precipitate
17	25.0	28.8	Gelatin (50.0)	EtOH (2.0)	Suspension	No crystals
18	25.0	28.8	Gelatin (70.0)	EtOH (2.0)	Suspension	No crystals

8.2 In Low molecular weight gelators

We tried gel phase crystallisation in LMWGs based on trimesic amide of *L*-valine methyl ester.[1] In a typical experiment, isonicotinic acid-*N*-oxide and the gelator **Val-TMA** was dissolved in organic solvent, then an aqueous $Cu(NO_3)_2.3H_2O$ solution was added to it. It was sonicated and left undisturbed to form the gel. Blue crystals of form-I were obtained from these gels (characterized by SCXRD).

Table S6: Crystallization of $Cu(NO_3)_2.3H_2O$ and isonicotinic acid-*N*-oxide in presence of LMWGs

Exp. no	$Cu(NO_3)_2.3H_2O$ (mg)	Isonicotinic acid-*N*-oxide (mg)	Gelator (mg)	Solvents (mL)	Observation
1	24.1	27.8	**Val-TMA** (40.0)	DMF (0.5)/ water (0.5)	Blue crystals
2	24.1	27.8	**Val-TMA** (40.0)	DMSO (0.5)/ water (0.5)	No crystals
3	24.1	27.8	**Val-TMA** (40.0)	EtOH (0.5)/ water (0.5)	Blue crystals
4	24.1	27.8	**Val-TMA** (40.0)	EtOH (0.9)/ water (0.1)	Blue crystals

8.3 In tailored gel

Crystallisation of $Cu(NO_3)_2.3H_2O$ and isonicotinic acid-*N*-oxide was further investigated in presence of *N*-oxide gelator. In a typical experiment, isonicotinic acid-*N*-oxide (2 equivalent) and the *N*-oxide gelator were dissolved together in high polar organic solvent, and water was added. Then $Cu(NO_3)_2.3H_2O$ (1 equivalent) was added to this solution and the mixture was sonicated and left undisturbed.

Since the crystallisation depends on concentration of $Cu(NO_3)_2.3H_2O$ and isonicotinic acid-*N*-oxide, first we varied metal and ligand concentration in **L-3Nox** gel in 1:1 (v/v) DMSO-water.

Table S7: Crystallization of $Cu(NO_3)_2.3H_2O$ and isonicotinic acid-*N*-oxide in **L-3Nox** gel

L-3Nox (mg)	$Cu(NO_3)_2.3H_2O$	isonicotinic acid-*N*-oxide	Solvents (mL)	Observation after 24 h	Final observation
8.0 mg	6.0 mg	6.9 mg	DMSO (0.5)/water (0.5)	Gel	No crystal
8.0 mg	8.0 mg	9.2 mg	DMSO (0.5)/water (0.5)	Gel	No crystal
8.0 mg	10.0 mg	11.5 mg	DMSO (0.5)/water (0.5)	Gel	No crystal
8.0 mg	12.0 mg	13.8 mg	DMSO (0.5)/water (0.5)	Gel	No crystal
8.0 mg	14.0 mg	16.1 mg	DMSO (0.5)/water (0.5)	Gel	Blue crystals
8.0 mg	16.0 mg	18.4 mg	DMSO (0.5)/water (0.5)	Gel	Blue crystals
8.0 mg	18.0 mg	20.7 mg	DMSO (0.5)/water (0.5)	Gel	Blue crystals
8.0 mg	20.0 mg	23.0 mg	DMSO (0.5)/water (0.5)	Gel	Blue crystals
8.0 mg	24.0 mg	28.0 mg	DMSO (0.5)/water (0.5)	Gel	Blue crystals

We performed the crystallization of $Cu(NO_3)_2.3H_2O$ and isonicotinic acid-*N*-oxide with tailored **L-3Nox** gelator in various DMSO/water composition. Isonicotinic acid-*N*-oxide (27.8 mg, 0.2 mmol) and required amount (above MGC) of N-oxide gelator were dissolved together in DMSO, and water was added. To this mixture $Cu(NO_3)_2.3H_2O$ (24.1 mg, 0.1 mmol) was added and sonicated, left undisturbed for gel formation.

Table S8: Crystallisation of $Cu(NO_3)_2.3H_2O$ and isonicotinic acid-*N*-oxide in **L-3Nox** gel at various DMSO/water composition

N-oxide gelator	Amount	DMSO (mL)	Water (mL)	Observation after 24 h	Final observation
L-3Nox	8.0 mg	1.0	-	Clear solution	no crystal
L-3Nox	8.0 mg	0.9	0.1	Colloidal	no crystal
L-3Nox	8.0 mg	0.8	0.2	Gel	no crystal
L-3Nox	8.0 mg	0.7	0.3	Gel	blue crystal*
L-3Nox	8.0 mg	0.6	0.4	Gel	blue crystal*
L-3Nox	8.0 mg	0.5	0.5	Gel	blue crystal*

*(form-I), unit cell matched.

9. References

1. Y. Ishioka, N. Minakuchi, M. Mizuhata and T. Maruyama, *Soft Matter*, 2014, **10**, 965-971.

2. D. K. Kumar, D. A. Jose, P. Dastidar and A. Das, *Chem. Mater.*, 2004, **16**, 2332-2335.

Article-VIII

This project is in final stage and included as it is at the current version. The contribution from the collaborators is not completed since the study is still under progress.

Project details:

″Anion Induced Crystal to Crystal Transformation and Gel Phase Crystallization of Metal-Organic Materials (MOMs)″

Dipankar Ghosh, Vakare Merkyte, Marcin Górecki, Gennaro Pescitelli and Krishna K. Damodaran*

Author contributions:

D.G. and K.K.D. planned and designed the research; **D.G.** synthesized the ligand, analyzed the SCSC transformation, gel phase crystallization, solved single crystal structures and analyzed the selective crystallization in chiral gelator. K.F. synthesized the MOM and M.G. and G.P. performed the solid-state CD experiments. **D.G.** and K.K.D. wrote the initial manuscript draft and reviewing the main manuscript.

RESEARCH ARTICLE

Anion Induced Crystal to Crystal Transformation and Gel Phase Crystallization of Metal-Organic Materials (MOMs)

Dipankar Ghosh,[a] Vakare Merkyte,[a] Marcin Górecki,[b] Gennaro Pescitelli[b] and Krishna K. Damodaran*[a]

[a] Department of Chemistry, Science Institute, University of Iceland, Dunhagi 3, 107 Reykjavík, Iceland. E-mail: krishna@hi.is; Fax: +354 552 8911; Tel: +354 525 4846

[b] Department of Chemistry and Industrial Chemistry, University of Pisa, Moruzzi 13, 56124 Pisa, Italy

Supporting information for this article is given via a link at the end of the document.

Abstract: Anion induced crystal to crystal transformation of an achiral complex to chiral 3-dimensional metal–organic material (MOM) is reported. The transformation of the complex to a specific enantiomer was studied in solution and gel medium. The transformation performed in gel phase using a chiral gelator resulted in enantioselective solid-state structural transformation.

Introduction

Stimuli-responsive supramolecular systems constitute a fascinating class of materials,[1] offers better control of the self-assembly/reassembly process, which can be either switched on/off by an external stimulus such as anion, heat, light, sound etc. Metal–organic materials (MOMs)[1a, 2] are stimuli-responsive crystalline materials (1-D, 2-D, or 3-D) constructed from metal ions or clusters as nodes and organic ligands as linkers, including metal–organic frameworks (MOFs)[3] and coordination polymers.[2] MOMs are generally obtained by solvothermal or hydrothermal techniques and alternate routes to reduce the harshness of reaction condition and time are also reported.[4] The molecular-level description of the formation of MOMs has been studied via theoretical[5] and experimental methods[6] but the understanding of the self-assembly in MOMs is still challenging. Single-crystal to single-crystal (SCSC) transformation[7] can be considered as one of the best methods to unravel the solid-state self-assembly process of MOMs. The solid state transformation via SCSC will enable us to monitor the structural change during self-assembly and often lead to products, which are not accessible via routine synthetic routes.[8] However, synthesis of MOMs via SCSC transformation is challenging due to the restricted free movements of the molecules, since the molecules are closely bound to each other with strong ionic, covalent, coordination or metallic bonds in the crystal lattice.[8e, 9] The SCSC transformations of MOMs can be triggered by oxidation/reduction,[10] heat,[11] light,[12] mechanochemical forces,[13] sorption/desorption/exchange of the solvent or guest molecule,[8a, 14] cations,[15] post-synthetic modification (PSM)[16] and ion exchange.[17]

The SCSC transformations triggered by anion exchange has also been explored to control chemical and physical properties of MOMs through conscious interconversion of chemical compositions.[18] The significance of anion in MOMs enabled researchers to generate 3-D metal-organic materials[19] via anion-exchange process and convert 2-D network into helices[20] The SCSC transformation of MOMs triggered by anions are rare,[20-21] which will lead to interesting structural change or self-assembly. Hong and co-workers reported the transformation of copper nanocage complex into 1-D polymeric network via anion induced SCSC transformation.[21b] To the best of our knowledge, anion induced SCSC transformation of zero dimensional (0-D) complexes to 3-D MOMs are not reported. In this work, we report anion mediated solid-state structural transformation of copper(II) complexes of *N*-(4-pyridyl)nicotinamide (**Cu-4PNA**) in both solution and gel state to chiral 3-D MOMs (Scheme 1).

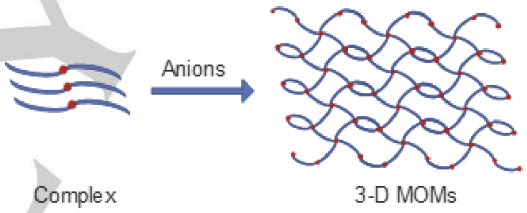

Scheme 1. Anion induced SCSC transformation of 0-D complex to 3-D MOMs.

Results and Discussion

The copper(II) complex $Cu(OAc)_2$(**4PNA**)$_2$ (**Cu-4PNA**) was synthesized by layering an ethanolic solution of *N*-(4-pyridyl)nicotinamide (**4PNA**) over an aqueous $Cu(OAc)_2.H_2O$ solution at 1:2 metal:ligand ratio.[22] The stimuli-responsive properties of **Cu-4PNA** complex in presence of halides (fluoride, chloride and bromide) were studied. The effect of iodide ion was not studied due to the possibility of iodide getting oxidized in presence of copper(II) ions. In a typical reaction, a solution of sodium or potassium salt of the appropriate anion (0.1 M) was added to **Cu-4PNA** crystals. The mixture was left undisturbed for a period of one week to ensure the completion of the solid-state transformation, if any. After a week, the mixture was filtered, washed thoroughly with deionized water and dried. The resulting solid was analyzed by single crystal X-ray (SCXRD) and powder X-ray diffraction (XRPD), which confirmed a solvent mediated single-crystal to single-crystal (SCSC) transformation was observed in presence of chloride and bromide salts.

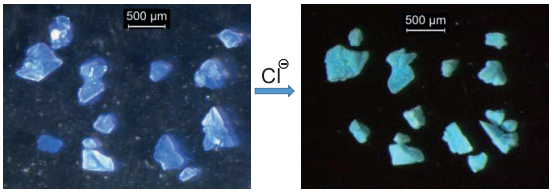

Figure 1. SCSC transformation of **Cu-4PNA** to **MOM-1**.

The solvent mediated SCSC transformation of **Cu-4PNA** with chloride salts was achieved by treating transparent purple crystals of **Cu-4PNA** with aqueous sodium chloride solution, which resulted in an opaque sky-blue solid in 2-3 h (Figure 1). X-ray quality single crystals were isolated from the sky-blue solid after a period of one week, and the structural analysis of these crystals revealed the conversion of the achiral complex to a 3-D chiral polymeric network $\{Cu(\mathbf{4PNA})_2Cl_2\}_n$ (**MOM-1**). **MOM-1** crystallized in the trigonal crystal system ($P3_221$) and the copper(II) metal center displayed a distorted octahedral geometry with chloride ions in the axial positions, and the nitrogen atoms of aminopyridine and nicotinoyl moieties of **4PNA** molecules occupying the equatorial positions. The comparison of the bond length revealed that the nitrogen atom of the aminopyridine moieties displayed stronger coordination compared to the nitrogen atoms of the nicotinoyl moiety. The non-coordinated nitrogen atoms of the nicotinoyl moiety of the parent **Cu-4PNA** complex was found to be coordinated in **MOM-1** resulting in the solid-state conversion of the complex to a 3-D polymeric network. The nicotinoyl moiety of **4PNA** was twisted from the aminopyridine plane by 53.7°, which induced chirality in **MOM-1** resulting in helical twist (Figure 2b). The formation of chiral MOMs by SCSC transformation route is interesting because the starting materials were achiral. The extended coordination of the nitrogen atoms of both nicotinoyl and aminopyridine moieties resulted in a 3-D chiral network with $6^4.8^2$ topology. These networks interacted each other via N–H···Cl interactions, where one of the chloride anions displayed bifurcated hydrogen bonding with the amide moieties.

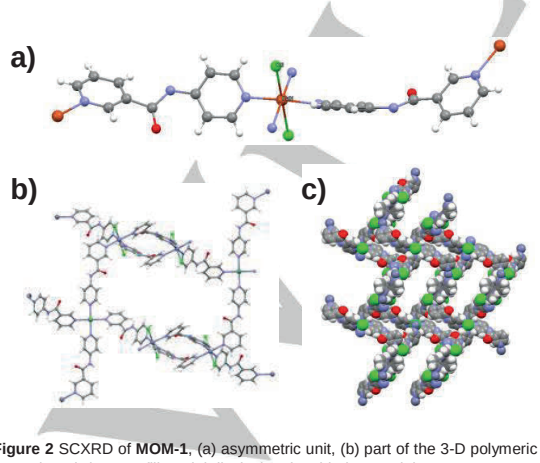

Figure 2 SCXRD of **MOM-1**, (a) asymmetric unit, (b) part of the 3-D polymeric network and c) space fill model displaying the chiral network in **MOM-1**.

The experiments were performed with bromide salts by adding aqueous sodium bromide solution to **Cu-4PNA** crystals, which resulted in a green solid and the analysis of the crystal structure revealed the formation of $\{Cu(4PNA)_2Br_2\}_n$ (**MOM-2**). **MOM-2** crystallized in trigonal crystal system ($P3_221$) and the structure was found to be isostructural with **MOM-1** (Figure S1, see Supporting information†). The experiments repeated with various chloride and bromide salts of alkali or alkaline earth metal such as potassium, ammonium, magnesium and calcium salts resulted in identical MOMs, which was confirmed by unit cell measurement in SCXRD and XRPD. The experiments were also performed in various solvents such as methanol, ethanol or dimethylformamide (DMF), which resulted in same MOMs. These results clearly indicate the role of chloride and bromide anions in inducing the solid-state transformation. We have also analyzed the effect of fluoride anions by treating **Cu-4PNA** with fluoride salts resulting in a light blue powder within an hour. The XRPD analysis of the blue material revealed the formation of an amorphous material, presumably due to the decomposition of the complex (Figure S2, see Supporting information†).

The solid-state structures of the **Cu-4PNA** complex and the 3-D chiral polymers (**MOM-1** & **MOM-2**) were compared to analyze the possible mechanism of the solid-state conversion. The copper(II) center in **Cu-4PNA** complex displayed a distorted octahedral geometry with two **4PNA** ligands in the axial position and the equatorial positions were coordinated by two acetate ligands in a chelate fashion. The nitrogen atoms of the nicotinoyl group was not coordinated to the metal center due to the chelate acetate anions and these nitrogen atoms did not show any non-bonding interaction. The addition of chloride/bromide salts resulted in the replacement of the acetate anion in **Cu-4PNA** complex, which resulted removal of the bidentate acetate with monodentate chloride/bromide anions. This process converted the copper(II) center to coordinatively unsaturated metal center with two free sites, which enabled the coordination of the nitrogen atom of the nicotinoyl group of the adjacent molecule to copper(II) metal center resulting in the polymerization of the complex (0-D) to 3-D MOMs.

The role of chloride/bromide anions in inducing structural transformation prompted us to extend our studies to analyze the effect of other anions on **Cu-4PNA** complex. We have selected various anions such as nitrate, nitrite, perchlorate, sulfate and azide anions. The structural transformation was not observed for labile anions such as nitrate, nitrite, perchlorate and sulfate, which was confirmed by SCXRD and XRPD experiments (Figure S3, see Supporting information†) by analyzing the crystals immersed in the corresponding anion solution for one week. This may be attributed to the weak coordinating ability of these anions to displace the acetate anions in **Cu-4PNA** compared chloride/bromide anions. The treatment of aqueous or ethanolic sodium azide solution on **Cu-4PNA** complex resulted in immediate color change (purple to green), indicating a possible anion replacement. The XRPD pattern showed solid-state structural transformation of the complex (Figure S4, see Supporting information†) but due to the unavailability of X-ray quality crystal the structural information was not elucidated. The reversible nature of the structural transformation was analyzed by treating **MOM-1**/**MOM-2** with aqueous sodium or ammonium acetate solution, which showed that the transformation was irreversible.

The phase purity of the compounds was analyzed by XRPD experiments, which will enable us to evaluate the phase purity of the materials and provide information about the extent of the solid-state transformation. The XRPD analysis performed on the bulk samples obtained from SCSC transformation was compared with the simulated pattern of the crystal structure obtained from SCXRD experiments. The pattern of **MOM-1** obtained for the SCSC transferred bulk solid showed excellent match with the simulated data (Figure 3), indicating the complete conversion in solid-state transformation. The experiments performed with the bulk samples obtained from SCSC of **MOM-2** salts also showed similar results (Figure S5, see Supporting information†).

The importance of SCSC transformation was analyzed by comparing the SCSC structures with the structures of **MOM-1** and **MOM-2** obtained by direct synthesis, for example, by reacting $CuCl_2$ or $CuBr_2$ with **4PNA**. This was achieved by mixing aqueous solution of metal salt and the ligand resulting in immediate precipitate, presumably due to the insolubility of MOMs in water. The direct synthesis of MOMs was repeated in mixed solvent systems by layering a dilute solution of **4PNA** in hydrophilic solvent (methanol, ethanol, acetonitrile or THF) over a dilute aqueous solution of $CuCl_2$ or $CuBr_2$ resulting in precipitate along with some crystals after three days. The crystal yield was increased by changing the solvents to aqueous solution of highly polar solvents such as DMF and DMSO and crystal of corresponding MOMs were also obtained at higher concentration. Single crystal X-ray analysis of MOMs crystal obtained from various solvents revealed the formation of two enantiomers.

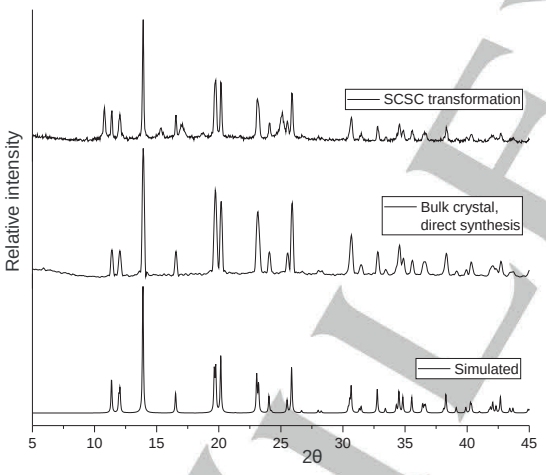

Figure 3. XRPD of **MOM-1**: simulated, bulk crystals obtained from direct synthesis and bulk SCSC transferred solid after one week.

This prompted us to systematically analyze the structures of compounds using SCXRD and XRPD experiments. The structural analysis of the crystal of $CuCl_2$ and **4PNA** mixture obtained from DMF/water and DMSO/water revealed the formation of different enantiomers, $P3_121$ and $P3_221$. Similarly, the direct reaction of $CuBr_2$ and **4PNA** resulted in space groups $P3_121$ and $P3_221$. The XRPD analysis was performed on the bulk samples obtained from direct synthesis were compared with bulk crystal of SCSC transformation and the simulated pattern obtained from the crystal structure. The XRPD patterns of the bulk crystals and the simulated pattern acquired from the single-crystal data of **MOM-1** were found to be virtually super-imposable (Figure 3), indicating similar structures in both the forms.

The formation of different enantiomers prompted us to check the enantioselectivity of the two synthetic routes using circular dichroism (CD) experiments, because XRPD pattern of enantiomers might be similar. Solid-state CD analysis was performed due to the insolubility of MOMs, which will enable us to differentiate the enantiomers obtained by two synthetic routes. For example, a sharp peak in the CD spectrum will confirm the presence of a particular enantiomer in excess, whereas a linear CD signal will indicate the formation of a conglomerate. The CD experiments in dispersed medium was avoided to prevent the possibility of structural rearrangement or polymorphic phase transition during the dissolution process. The solid-state CD performed on the bulk crystals from direct synthesis and SCSC transformation displayed broad peaks (Figure S6–S7, see Supporting information†). The CD spectra of **MOM-1** and **MOM-2** obtained via SCSC transformation of displayed characteristic peaks, indicating the presence of one enantiomer in excess. However, the CD spectra of the crystals from direct synthesis did not show such peaks, indicating the presence of both enantiomers. The presence of different enantiomers resulted in the inconsistency of the CD signals.

The presence of mixed enantiomers prompted us to study crystal growth of the MOMs in supramolecular gels. Supramolecular gels based on low-molecular weight gelators (LMWGs) [23] are excellent class of soft-materials due to their potential applications in tuning gel state properties.[24] Supramolecular gels have been used as an efficient media to control crystal growth and the gel synthon can induce selective crystallization by influencing the nucleation point.[23g, 25] We have shown that LMWGs can be used as medium for the crystallization of inorganic complexes and reported the selective crystallization of one particular form (form-I) of copper(II) isonicotinate–*N*-oxide complex.[25k] We have selected chiral gelators as crystalizing medium because gel fibers often show chirality at a mesoscopic scale, which is evident from the morphology of the gel fibers (helical cylinders or multiple helices).[26] The difference in the handedness of the crystals obtained from gel phase and solution phase will enable us to elucidate the role of the chirality in gel phase crystallization. Petrova *et al*. have utilized agarose in enantioselective crystallization of sodium chlorate, where either D-form or L-form of sodium chlorate was crystallized in excess in agarose hydrogel by varying the crystallization conditions.[27]

The gel phase crystallization of MOMs in agarose gel was performed in DMF/water (1:1, v/v) turned out to be unsuccessful due to the non-diffracting nature of the crystals. The crystallization was repeated in chiral LMWGs based on amino acids due to the easy synthetic procedure and availability in both enantiomeric and racemate forms. The initial crystallizations were performed in terephthalic amides of methyl phenylalaninate (**PAla-TA**)[28] and methyl valinate (**Val-TA**),[29] which are C_2-symmetric LMWGs (Scheme 2). The crystallization experiments in the LMWGs were performed by adding an aqueous solution of the metal salt to the DMF solution of gelator and the ligand (**4PNA**). The mixture was heated to obtain a clear solution, cooled to room temperature and left undisturbed. The crystalline materials obtained in **PAla-TA** gels

were weakly diffracting and gelation was not observed for **Val-TA**. The crystallization experiments performed in EtOH/water (1:1 v/v) for **Val-TA** resulted in immediate precipitate.

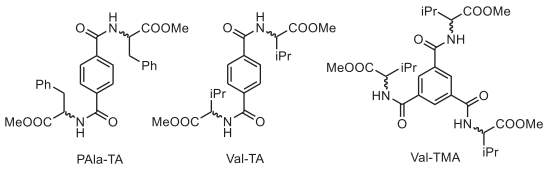

Scheme 2. Molecular structures of the chiral LMWGs used in gel phase crystallization of **MOM-1** and **MOM-2**.

Thus, we have selected a C_3-symmetric chiral gelator based on trimesic amide of methyl valinate (**Val-TMA**),[30] which forms gel in in DMF/water (1:1 v/v). The crystallization experiment was performed by adding an aqueous copper(II) solution to the DMF solution of the ligand and gelator, heated and cooled to room temperature to obtain the gel. X-ray quality microcrystals were obtained in 2-3 days. The experiments performed to optimize the crystallization conditions indicated 0.03 mmol of the ligand and 0.015 mmol of the metal salt was best concentration in 4.0 wt% gel and DMF/water (1:1, v/v) is the best solvent. Interestingly, SCXRD analysis on 15 crystals obtained from enantiopure ***RRR*-Val-TMA** gel (10 trials) revealed that $P3_121$ is formed in most cases but in one case a crystal with $P3_221$ space group was obtained, which might be a result of accidental heteroseeding. The crystallization experiments performed with enantiopure ***SSS*-Val-TMA** gel also resulted in $P3_221$ crystals, which is enantiomer of the crystals obtained from ***RRR*-Val-TMA** gel. The crystallization experiments performed in solution phase and crystallization in presence of the enantiopure **Val-TMA** gelator below minimum gel concentration (0.5 wt%) resulted in a mixture of both enantiomers of MOMs. These results clearly indicated that enantioselective crystallization was achieved by gel phase crystallization in direct synthesis of the MOMs. The ***SSS*-Val-TMA** gelator favors the crystallization of $P3_221$ and the enantiomer $P3_121$ was formed in ***RRR*-Val-TMA** gel. This indicates that the chirality of the supramolecular gel synthon can be potentially used as active media for enantioselective crystallization.

We are also performing the crystallization of the MOMs in solution state at higher concentration (4.0 wt%) of non-gelling substance, such as enantiopure phenylalanine methyl ester hydrochloride and dimethyl tartrate, which will reveal the role of chiral additives in crystallization. The CD experiments of the bulk crystals from gel phase collaboration with will be done in collaboration with Dr. Gennaro Pescitelli, University of Pisa, Italy, which is ongoing.

Conclusion

In summary, we have studied the anion induced stimuli-responsive property of **Cu-4PNA** complex, and the achiral complex displayed an irreversible structural transformation to a crystalline chiral 3-D polymeric material in presence of chloride and bromide ions. The compounds were characterized by SCXRD and the enantioselectivity was analyzed by solid-state CD experiments. The experiments repeated with various salts of chloride and bromide ions confirmed the structural transformation was anion induced. The SCSC transformation was compared with crystals obtained from direct synthesis, which indicated that direct synthesis yielded a mixture of enantiomers. The gel phase crystallization of the MOMs performed in enantiopure **Val-TMA** gels resulted in isolation of enantiopure crystals.

Acknowledgements

We thank University of Iceland Research Fund and Science Institute for funding. D.G. thanks the University of Iceland for the Doctoral Research and Teaching Assistantship grant. We thankfully acknowledge Dr. Sigurður Sveinn Jónsson, ÍSOR-Iceland for powder X-ray diffraction analysis, and Dr. Sigríður Jónsdóttir, University of Iceland for NMR and Mass spectroscopy. We thank Rannís Iceland for infrastructure grants for a single-crystal X-ray diffractometer (150998-0031).

Keywords: Single-crystal to single-crystal transformation • 0-D to 3-D • chiral MOM • gel phase crystallization • enantiospecific crystallization.

Reference

[1] a) A. J. McConnell, C. S. Wood, P. P. Neelakandan, J. R. Nitschke, *Chem. Rev.* **2015**, *115*, 7729-7793; b) P. Theato, B. S. Sumerlin, R. K. O'Reilly, I. I. I. T. H. Epps, *Chem. Soc. Rev.* **2013**, *42*, 7055-7056; c) S. Hajime, H. Itaru, *Chem. Asian J.* **2015**, *10*, 2026-2038; d) M. D. Segarra-Maset, V. J. Nebot, J. F. Miravet, B. Escuder, *Chem. Soc. Rev.* **2013**, *42*, 7086-7098.

[2] W.-X. Zhang, P.-Q. Liao, R.-B. Lin, Y.-S. Wei, M.-H. Zeng, X.-M. Chen, *Coord. Chem. Rev.* **2015**, *293-294*, 263-278.

[3] a) H.-C. Zhou, J. R. Long, O. M. Yaghi, *Chem. Rev.* **2012**, *112*, 673-674; b) H.-C. J. Zhou, S. Kitagawa, *Chem. Soc. Rev.* **2014**, *43*, 5415-5418; c) J. R. Long, O. M. Yaghi, *Chem. Soc. Rev.* **2009**, *38*, 1213-1214.

[4] a) Y.-R. Lee, J. Kim, W.-S. Ahn, *Korean J. Chem. Eng.* **2013**, *30*, 1667-1680; b) R. Seetharaj, P. V. Vandana, P. Arya, S. Mathew, *Arab. J. Chem.* **2019**, *12*, 295-315.

[5] a) D. Biswal, P. G. Kusalik, *ACS Nano* **2017**, *11*, 258-268; b) M. Yoneya, T. Yamaguchi, S. Sato, M. Fujita, *J. Am. Chem. Soc.* **2012**, *134*, 14401-14407; c) M. Yoneya, S. Tsuzuki, T. Yamaguchi, S. Sato, M. Fujita, *ACS Nano* **2014**, *8*, 1290-1296; d) M. Yoneya, S. Tsuzuki, M. Aoyagi, *PCCP* **2015**, *17*, 8649-8652.

[6] a) G. Férey, M. Haouas, T. Loiseau, F. Taulelle, *Chem. Mater.* **2014**, *26*, 299-309; b) S. Surblé, F. Millange, C. Serre, G. Férey, R. I. Walton, *Chem. Commun.* **2006**, 1518-1520; c) M. G. Goesten, E. Stavitski, J. Juan-Alcañiz, A. Martiñez-Joaristi, A. V. Petukhov, F. Kapteijn, J. Gascon, *Catal. Today* **2013**, *205*, 120-127; d) N. Stock, S. Biswas, *Chem. Rev.* **2012**, *112*, 933-969; e) M. R. E., *ChemPhysChem* **2009**, *10*, 327-329; f) M. Li, M. Dincă, *Chem. Mater.* **2015**, *27*, 3203-3206.

[7] a) H. Aggarwal, P. M. Bhatt, C. X. Bezuidenhout, L. J. Barbour, *J. Am. Chem. Soc.* **2014**, *136*, 3776-3779; b) J.-P. Zhang, P.-Q. Liao, H.-L. Zhou, R.-B. Lin, X.-M. Chen, *Chem. Soc. Rev.* **2014**, *43*, 5789-5814; c) G. K. Kole, J. J. Vittal, *Chem. Soc. Rev.* **2013**, *42*, 1755-1775; d) Y. Tian, P. K. Allan, C. L. Renouf, X. He, L. J. McCormick, R. E. Morris, *Dalton Transactions* **2014**, *43*, 1519-1523; e) Y. Miao, Y. Qiu, J. Cai, Z. Wang, X. Yu, W. Dong, *Sci. Rep.* **2016**, *6*, 37587.

[8] a) T.-Y. Ho, S.-M. Huang, J.-Y. Wu, K.-C. Hsu, K.-L. Lu, *Cryst. Growth Des.* **2015**, *15*, 4266-4271; b) Y.-C. He, J. Yang, Y.-Y. Liu, J.-F. Ma, *Inorg. Chem.* **2014**, *53*, 7527-7533; c) J.-Y. Wu, Y.-C. Liu, T.-C. Chao, *Inorg. Chem.* **2014**, *53*, 5581-5588; d) Q. Yao, J. Sun, K. Li, J. Su, M. V. Peskov,

X. Zou, *Dalton Transactions* **2012**, *41*, 3953-3955; e) A. Chaudhary, A. Mohammad, S. M. Mobin, *Cryst. Growth Des.* **2017**, *17*, 2893-2910.

[9] a) J. J. Vittal, *Coord. Chem. Rev.* **2007**, *251*, 1781-1795; b) Z. Ping, G. Wen, Z. Li-Zhi, L. Xin, T. Jin-Lei, Y. Shi-Ping, *Eur. J. Inorg. Chem.* **2008**, *2008*, 2971-2974.

[10] a) H.-H. Lee, I.-H. Park, S. Kim, E. Lee, H. Ju, J. H. Jung, M. Ikeda, Y. Habata, S. S. Lee, *Chem. Sci.* **2017**, *8*, 2592-2596; b) H. J. Choi, M. P. Suh, *J. Am. Chem. Soc.* **2004**, *126*, 15844-15851.

[11] a) H. Chunhua, E. Ulli, *Angew. Chem. Int. Ed.* **2005**, *44*, 2281-2283; b) G. Mahmoudi, A. Morsali, *Cryst. Growth Des.* **2008**, *8*, 391-394; c) S. K. Ghosh, J.-P. Zhang, S. Kitagawa, *Angew. Chem. Int. Ed.* **2007**, *46*, 7965-7968.

[12] a) H. Konaka, L. P. Wu, M. Munakata, T. Kuroda-Sowa, M. Maekawa, Y. Suenaga, *Inorg. Chem.* **2003**, *42*, 1928-1934; b) I. G. Georgiev, L. R. MacGillivray, *Chem. Soc. Rev.* **2007**, *36*, 1239-1248.

[13] S. Jie, D. Fangna, Y. Wenbing, B. Wenhua, Z. Xiaoliang, S. Wenming, S. Daofeng, *Angew. Chem. Int. Ed.* **2011**, *50*, 7061-7064.

[14] a) Y.-Q. Lan, H.-L. Jiang, S.-L. Li, Q. Xu, *Inorg. Chem.* **2012**, *51*, 7484-7491; b) M. C. Das, P. K. Bharadwaj, *J. Am. Chem. Soc.* **2009**, *131*, 10942-10949.

[15] H. Wang, W. Meng, J. Wu, J. Ding, H. Hou, Y. Fan, *Coord. Chem. Rev.* **2016**, *307*, 130-146.

[16] a) Z. Zhang, L. Zhang, L. Wojtas, P. Nugent, M. Eddaoudi, M. J. Zaworotko, *J. Am. Chem. Soc.* **2012**, *134*, 924-927; b) T. Haneda, M. Kawano, T. Kawamichi, M. Fujita, *J. Am. Chem. Soc.* **2008**, *130*, 1578-1579; c) J. Li, P. Huang, X.-R. Wu, J. Tao, R.-B. Huang, L.-S. Zheng, *Chem. Sci.* **2013**, *4*, 3232-3238.

[17] a) Y. Noori, K. Akhbari, *RSC Advances* **2017**, *7*, 1782-1808; b) C.-P. Li, H. Zhou, Y.-H. Mu, W. Guo, Y. Yan, M. Du, *Cryst. Growth Des.* **2017**, *17*, 2024-2033.

[18] a) O. Moonhyun, M. C. A., *Angew. Chem. Int. Ed.* **2006**, *45*, 5492-5494; b) S.-i. Noro, R. Kitaura, M. Kondo, S. Kitagawa, T. Ishii, H. Matsuzaka, M. Yamashita, *J. Am. Chem. Soc.* **2002**, *124*, 2568-2583.

[19] a) M. Du, Y.-M. Guo, S.-T. Chen, X.-H. Bu, S. R. Batten, J. Ribas, S. Kitagawa, *Inorg. Chem.* **2004**, *43*, 1287-1293; b) G. S. K., Z. Jie-Peng, K. Susumu, *Angew. Chem. Int. Ed.* **2007**, *46*, 7965-7968.

[20] O.-S. Jung, Y. J. Kim, Y.-A. Lee, H. K. Chae, H. G. Jang, J. Hong, *Inorg. Chem.* **2001**, *40*, 2105-2110.

[21] a) H.-R. Fu, Z.-X. Xu, J. Zhang, *Chem. Mater.* **2015**, *27*, 205-210; b) N. Li, F. Jiang, L. Chen, X. Li, Q. Chen, M. Hong, *Chem. Commun.* **2011**, *47*, 2327-2329; c) A. Michaelides, S. Skoulika, *Cryst. Growth Des.* **2009**, *9*, 2039-2042; d) Z. Zhang, L. Xu, R. Cao, *New J. Chem.* **2018**, *42*, 5593-5601; e) C.-P. Li, J. Chen, W. Guo, M. Du, *J. Solid State Chem.* **2015**, *223*, 95-103; f) X. Li, H. Xu, F. Kong, R. Wang, *Angew. Chem. Int. Ed.* **2013**, *52*, 13769-13773.

[22] D. Ghosh, I. Lebedyte, D. S. Yufit, K. K. Damodaran, J. W. Steed, *CrystEngComm* **2015**, *17*, 8130-8138.

[23] a) S. Banerjee, R. K. Das, U. Maitra, *J. Mater. Chem.* **2009**, *19*, 6649-6687; b) P. Dastidar, *Chem. Soc. Rev.* **2008**, *37*, 2699-2715; c) M. de Loos, B. L. Feringa, J. H. van Esch, *Eur. J. Org. Chem.* **2005**, *2005*, 3615-3631; d) L. A. Estroff, A. D. Hamilton, *Chem. Rev.* **2004**, *104*, 1201-1218; e) M. George, R. G. Weiss, *Acc. Chem. Res.* **2006**, *39*, 489-497; f) A. R. Hirst, B. Escuder, J. F. Miravet, D. K. Smith, *Angew. Chem. Int. Ed.* **2008**, *47*, 8002-8018; g) D. K. Kumar, J. W. Steed, *Chem. Soc. Rev.* **2014**, *43*, 2080-2088; h) J. W. Steed, *Chem. Soc. Rev.* **2010**, *39*, 3686-3699; i) G. Yu, X. Yan, C. Han, F. Huang, *Chem. Soc. Rev.* **2013**, *42*, 6697-6722.

[24] a) L. E. Buerkle, S. J. Rowan, *Chem. Soc. Rev.* **2012**, *41*, 6089-6102; b) W. Edwards, D. K. Smith, *J. Am. Chem. Soc.* **2014**, *136*, 1116-1124; c) E. R. Cross, S. Sproules, R. Schweins, E. R. Draper, D. J. Adams, *J. Am. Chem. Soc.* **2018**, *140*, 8667-8670; d) E. R. Draper, E. G. B. Eden, T. O. McDonald, D. J. Adams, *Nat. Chem.* **2015**, *7*, 848; e) C. Colquhoun, E. R. Draper, E. G. B. Eden, B. N. Cattoz, K. L. Morris, L. Chen, T. O. McDonald, A. E. Terry, P. C. Griffiths, L. C. Serpell, D. J. Adams, *Nanoscale* **2014**, *6*, 13719-13725; f) J. Raeburn, D. J. Adams, *Chem. Commun.* **2015**, *51*, 5170-5180.

[25] a) A. Dawn, K. S. Andrew, D. S. Yufit, Y. Hong, J. P. Reddy, C. D. Jones, J. A. Aguilar, J. W. Steed, *Cryst. Growth Des.* **2015**, *15*, 4591-4599; b) J. A. Foster, K. K. Damodaran, A. Maurin, G. M. Day, H. P. G. Thompson, G. J. Cameron, J. C. Bernal, J. W. Steed, *Chem. Sci.* **2017**, *8*, 78-84; c) S. R. Kennedy, C. D. Jones, D. S. Yufit, C. E. Nicholson, S. J. Cooper, J. W. Steed, *CrystEngComm* **2018**, *20*, 1390-1398; d) J. A. Foster, M.-O. M. Piepenbrock, G. O. Lloyd, N. Clarke, J. A. K. Howard, J. W. Steed, *Nat. Chem.* **2010**, *2*, 1037; e) Y. Diao, K. E. Whaley, M. E. Helgeson, M. A. Woldeyes, P. S. Doyle, A. S. Myerson, T. A. Hatton, B. L. Trout, *J. Am. Chem. Soc.* **2012**, *134*, 673-684; f) L. A. Estroff, L. Addadi, S. Weiner, A. D. Hamilton, *Org. Biomol.* **2004**, *2*, 137-141; g) M. Pauchet, T. Morelli, S. Coste, J.-J. Malandain, G. Coquerel, *Cryst. Growth Des.* **2006**, *6*, 1881-1889; h) F. Aparicio, E. Matesanz, L. Sanchez, *Chem. Commun.* **2012**, *48*, 5757-5759; i) L. Kaufmann, S. R. Kennedy, C. D. Jones, J. W. Steed, *Chem. Commun.* **2016**, *52*, 10113-10116; j) R. Daly, O. Kotova, M. Boese, T. Gunnlaugsson, J. J. Boland, *ACS Nano* **2013**, *7*, 4838-4845; k) D. Ghosh, K. Ferfolja, Ž. Drabavičius, J. W. Steed, K. K. Damodaran, *New J. Chem.* **2018**, *42*, 19963-19970.

[26] A. Brizard, R. Oda, I. Huc, *Top. Curr. Chem.* **2005**, *256*, 167-218.

[27] R. I. Petrova, J. A. Swift, *J. Am. Chem. Soc.* **2004**, *126*, 1168-1173.

[28] a) P. Li, Z. Yin, X.-Q. Dou, G. Zhou, C.-L. Feng, *ACS Appl. Mater. Interfaces* **2014**, *6*, 7948-7952; b) X. Dou, P. Li, D. Zhang, C.-L. Feng, *Soft Matter* **2012**, *8*, 3231-3238.

[29] D. Ghosh, A. D. Farahani, A. D. Martin, P. Thordarson, K. K. Damodaran, *Chem. Mater.* **2020**.

[30] a) T. Kataoka, Y. Ishioka, M. Mizuhata, H. Minami, T. Maruyama, *ACS Appl. Mater. Interfaces* **2015**, *7*, 23346-23352; b) K. Knoll, M. Leyendecker, C. M. Thiele, *Eur. J. Org. Chem.* **2019**, *2019*, 720-727.

Supporting Information

Anion Induced Crystal to Crystal Transformation and Gel Phase Crystallization of Metal-Organic Materials (MOMs)

Dipankar Ghosh,[a] Vakare Merkyte,[a] Marcin Górecki,[b] Gennaro Pescitelli[b] and Krishna K. Damodaran[a]*

Table of Contents

1. Crystal structure of $Cu(4PNA)_2Br_2$

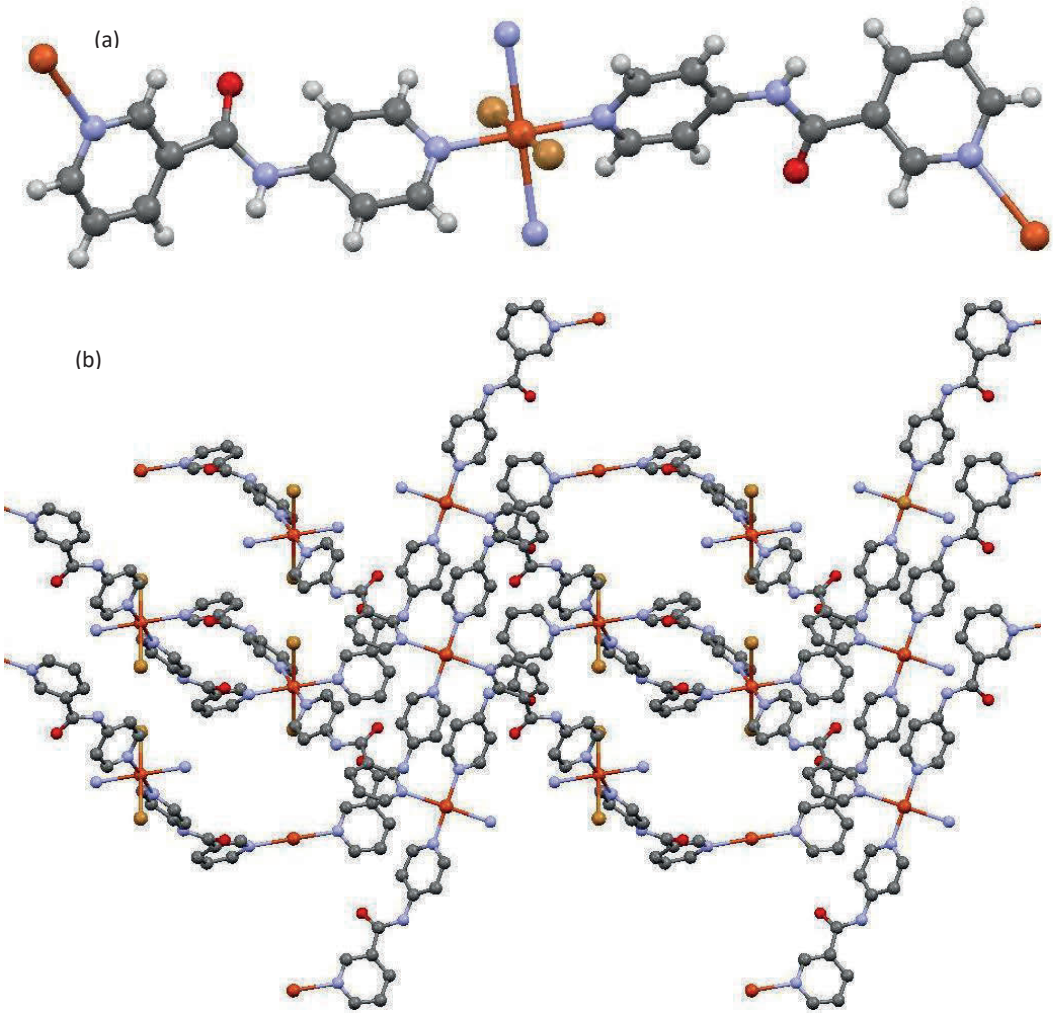

Figure S1: Single crystal structure of $Cu(4PNA)_2Br_2$: (a) asymmetric unit and (b) crystal packing viewed along b-axis, hydrogen atoms are omitted for clarity.

2. Crystal data of $Cu(4PNA)_2Cl_2$ and $Cu(4PNA)_2Br_2$

Table S1: crystal data of $Cu(4PNA)_2Cl_2$ and $Cu(4PNA)_2Br_2$

Crystal data	$Cu(4PNA)_2Cl_2$	$Cu(4PNA)_2Br_2$
Empirical formula	$C_{22}H_{18}Cl_2CuN_6O_2$	$C_{22}H_{18}Br_2CuN_6O_2$
Colour	Green	Green
Formula weight	532.86	621.78
Crystal size (mm)	0.243 x 0.131x 0.115	0.234 x 0.163 x 0.112
Crystal system	trigonal	trigonal
Space group	P 3_2 2 1	P 3_2 2 1
a (Å)	8.9790(8)	8.978(2)
b (Å)	8.9790(8)	8.978(2)
c (Å)	22.1895(18)	23.456(5)
α (°)	90	90
β (°)	90	90
γ (°)	120	120
Volume ($Å^3$)	1549.3(3)	1637.4(8)
Z	3	3
$D_{calc.}$(g/cm^3)	1.713	1.892
F(000)	813	921
μ MoKα (mm^{-1})	1.352	4.695
Temperature (K)	291(2)	291(2)
Reflections collected/ unique/observed [I>2σ(I)]	25985/2543/2463	29363/2709/2573
Data/restraints/parameters	2543/0/155	2709/0/155
Goodness of fit on F^2	0.634	0.642
Final R indices [I>2σ(I)]	R_1 = 0.0210 wR_2 = 0.0682	R_1 = 0.0220 wR_2 = 0.0699
R indices (all data)	R_1 = 0.0221 wR_2 = 0.0699	R_1 = 0.0251 wR_2 = 0.0740

3. XRPD

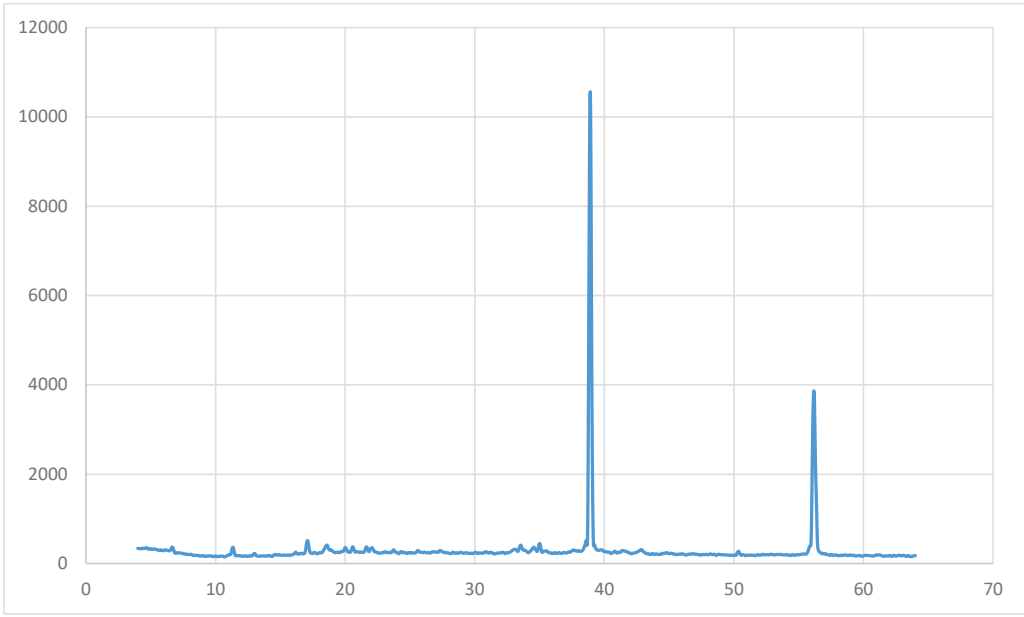

Figure S2: XRPD of $Cu(4PNA)_2(OAc)_2$ after treatment of NaF/KF.

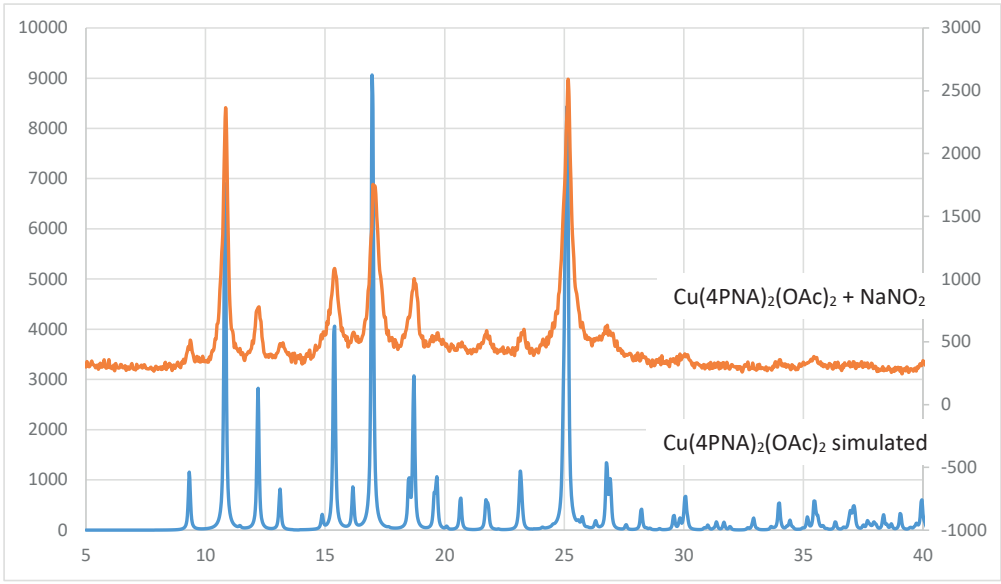

Figure S3: XRPD of $Cu(4PNA)_2(OAc)_2$ simulated and after treatment of $NaNO_2$.

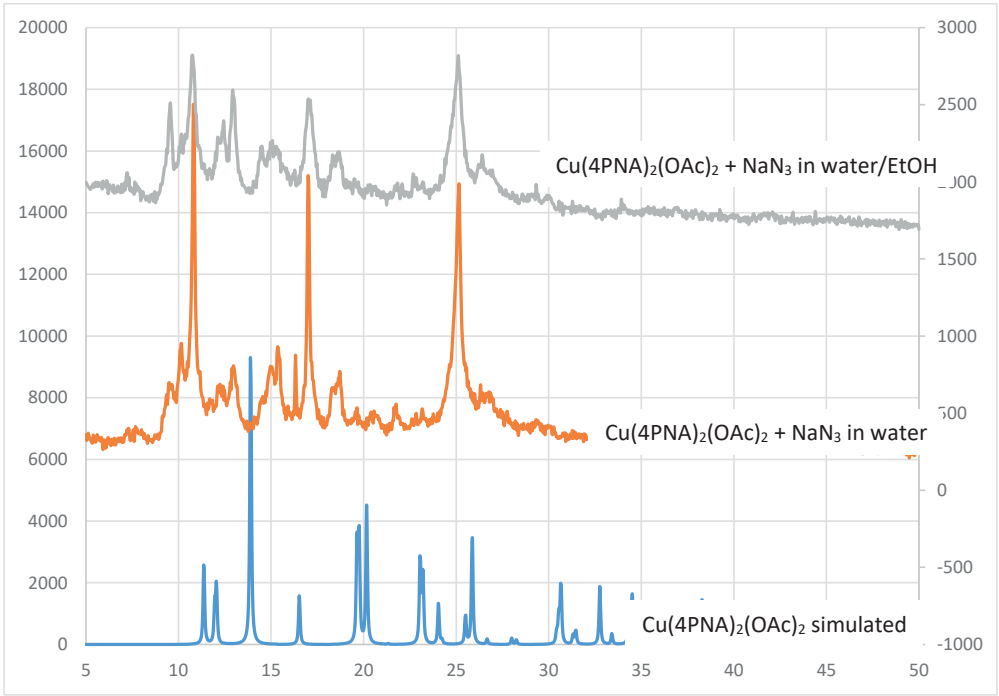

Figure S4: XRPD of $Cu(4PNA)_2(OAc)_2$ after treatment of NaN_3 in water and water/EtOH.

XRPD of **MOM-2** $\{Cu(4PNA)_2Br_2\}_n$

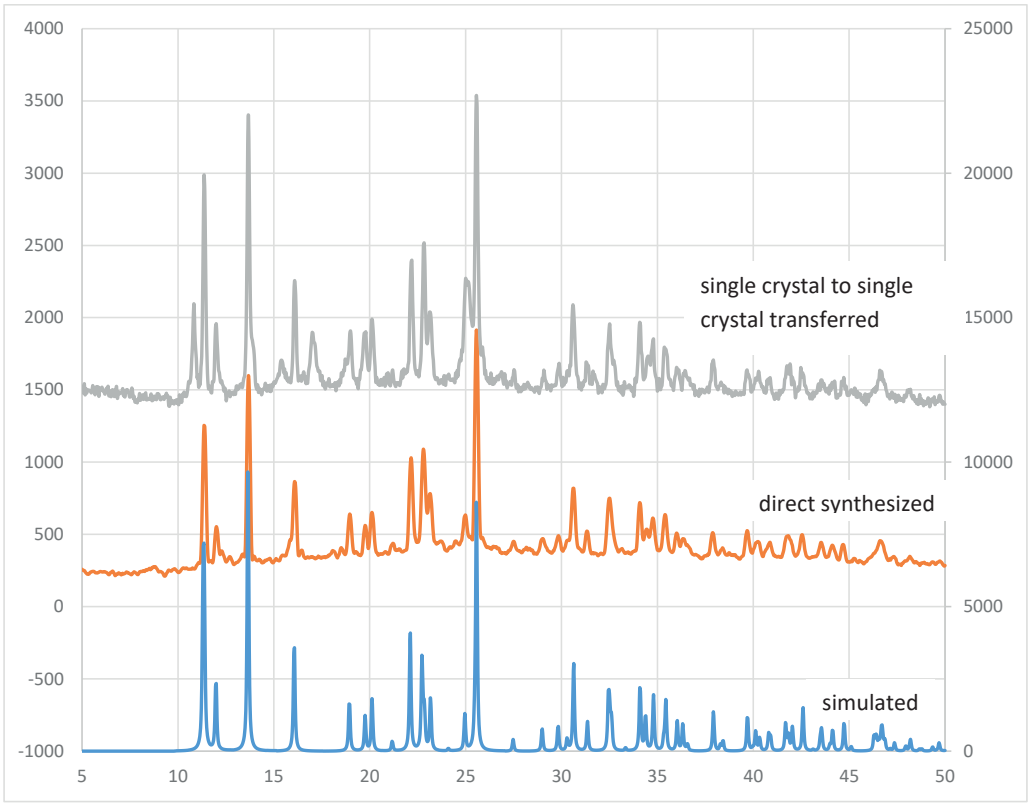

Figure S5: XRPD of $Cu(4PNA)_2Br_2$, simulated, direct synthesized and single crystal to single crystal transferred

4. Solid-state ECD

The solid-state ECD spectra were measured using the pellet technique. The investigated compounds were mixed with ca. 100 mg of dried KCl, then finely ground and pressed at 10 tons under vacuum for ca. 10 min to obtian a transparent disc. On each sample, several ECD spectra (at least 4) were measured upon rotation of the pellet around the incident axis direction at various rotation angles, to exclude linear dichroism artefacts. For each compound two pellets were prepared independently to test reproducibility. All ECD spectra were obtained using the following parameters: 200 nm/min scanning speed, 0.5 nm step size, 2 nm band-width, 0.5 sec response time, accumulation of 4 scans, continuous scanning mode, and standard sensitivity (100 mdeg). No smoothing or noise reduction was applied.

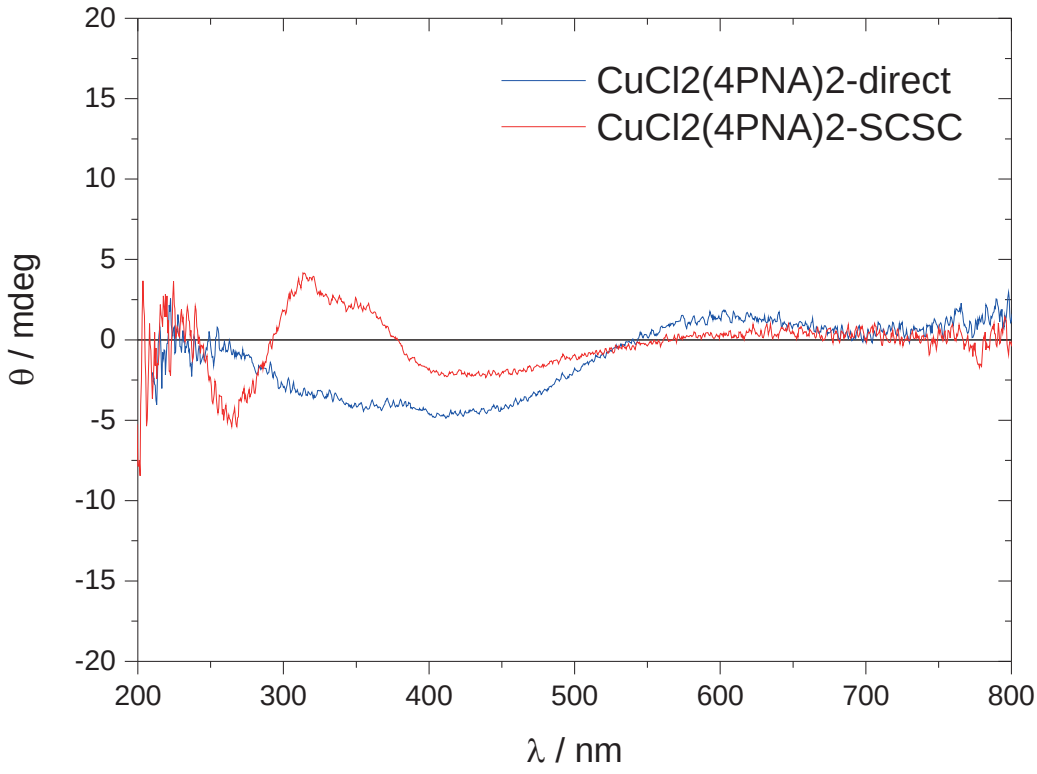

Figure S6: Solid state CD of **MOM-1**: crystal obtained from direct synthesis and SCSC transformation.

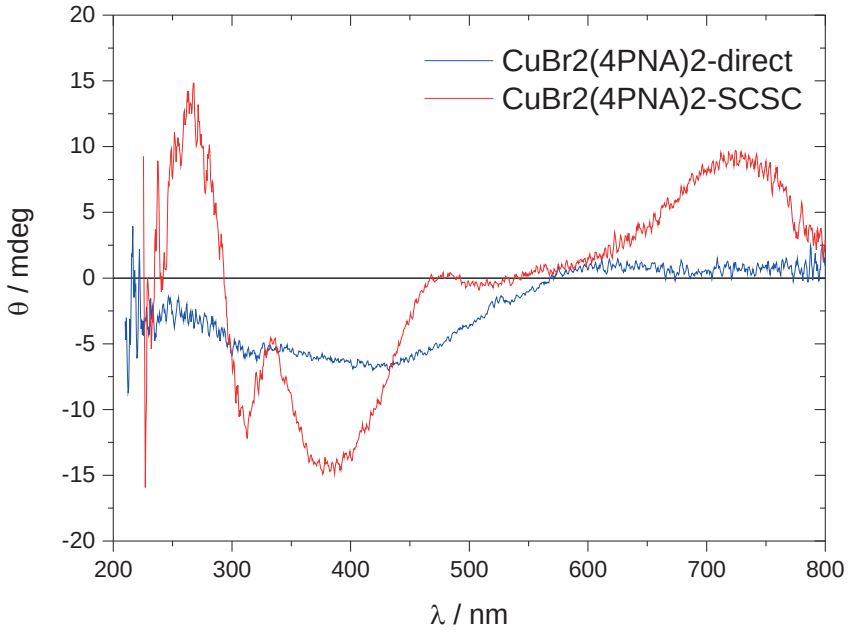

Figure S7: Solid state CD of **MOM-2**: crystal obtained from direct synthesis and SCSC transformation.

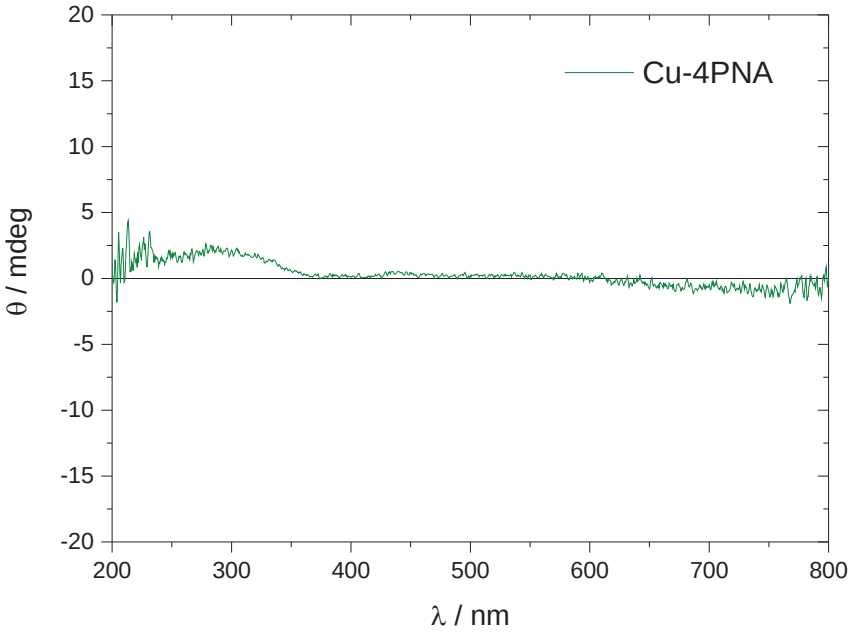

Figure S8: Solid state CD of the achiral complex $Cu(OAc)_2(4PNA)_2$ showing no signals.

6 Conclusions

This doctoral study demonstrates the scope of assembling diverse small molecules into complex functional architecture by non-covalent interactions. The hierarchical structure was classified mainly in two categories- metal-organic materials (MOMs) fabricated by metal-ligand coordination and supramolecular gels involving weak non-bonding interactions. Various multi-functional ligands were synthesized via multi-step organic reactions, and structurally characterized by standard analytical techniques, including SCXRD. Metalation of these ligands resulted in the formation of metalloligands, which was utilized to construct catalytically active MOMs. In most of the cases, incorporation of multi-functional ligands and metalloligands into MOMs was unsuccessful, however, a MOM **HI-101** consisting copper(II) paddle-wheel and urea moieties was obtained. **HI-101** displayed efficient catalytic activity in various reactions like CO_2 conversion, methanolysis and alcohol oxidation.

The self-assembly via non-bonding interactions were studied in low molecular weight gels (LMWGs) to elucidate the key structural information responsible for the gel network formation. The structural modification of existing gelators was explored, which proved to be an excellent strategy to analyze the self-assembly process of LMWGs. This was achieved by altering the functional groups of known gelators, for example, pyridyl amide and pyridyl urea were converted to pyridyl-*N*-oxide amide and pyridyl-*N*-oxide urea, respectively by oxidizing the pyridyl moiety with *m*-chloroperbnezoic acid. The C—H···N non-bonding interaction of the parent gelator was disrupted in the modified gelator, and the relative gel strength of the parent and modified gelators were compared to elucidate the importance of these interactions. The combination of single crystal structure and powder X-ray data of the dried gel proved to be a reliable tool to explore the role of different non-bonding interactions in gel formation. Furthermore, the gelation was induced in non-gelators via metal coordination to obtain metallogels. The strong coordination bond between the metal center and organic linker resulted in entangled 3D network of the metallogels, which was further stabilized by various non-covalent interactions. The comparison of the single crystal structure of the gelling complex and the corresponding non-gelator ligand provided insight to the fundamental interactions responsible for gel

formation. The study of the stimuli-responsive properties of the LMWGs tuning of the gel state properties was studied in presence of various anions, which showed that LMWGs can be utilized in useful applications such as anion sensing.

The self-assembly process was further investigated in multi-component systems. Mixing two or more gelators results in self-recognition at the molecular level, leading to the formation of fibers containing individual (self-sorting) or both components (co-assembly). Multi-component gels were obtained by mixing two enantiomers of bis(urea) and bis(amide) gelators. The multi-component gels displayed enhanced mechanical and thermal stabilities in both cases. Self-assembly modes of these systems were analyzed by various analytical techniques such as SEM, AFM, CD, FT-IR, solid-state NMR and X-ray diffraction. We reported the first crystallographic evidence of specific co-assembly in mixed enantiomeric gel and used solid state interaction to corroborate the enhanced gel strength in mixed multi-component gel.

Finally, the supramolecular gels were utilized as media to control crystal growth. The crystals grown in gel often display improved physical characteristics due to restricted Brownian motions and sedimentation in the gel medium. Furthermore, gel matrix can also act as an active medium by influencing the nucleation point of the crystal. We have demonstrated that the copper(II) isonicotinate-*N*-oxide complex can be selectively crystallized in the thermodynamically stable form in a gel matrix. Currently, we are studying the enantioselective crystallization of MOMs using chiral LMWGs. We believe that these studies will add significant efforts in understanding the formation of complex supra-molecular superstructures and help chemists to design new functional materials with unique properties.

References

1. Ball, P., *The Self-Made Tapestry: Pattern Formation in Nature*. Oxford University Press, Inc.: 2001; p 312.
2. Jean-Marie, L., Perspectives in Chemistry—Steps towards Complex Matter. *Angew. Chem. Int. Ed.* **2013,** *52* (10), 2836-2850.
3. Lehn, J.-M., Constitutional Dynamic Chemistry: Bridge from Supramolecular Chemistry to Adaptive Chemistry. In *Constitutional Dynamic Chemistry*, Barboiu, M., Ed. Springer Berlin Heidelberg: Berlin, Heidelberg, 2012; pp 1-32.
4. Jean-Marie, L., Perspectives in Chemistry—Aspects of Adaptive Chemistry and Materials. *Angew. Chem. Int. Ed.* **2015,** *54* (11), 3276-3289.
5. Zhang, M.; Gu, Z.-Y.; Bosch, M.; Perry, Z.; Zhou, H.-C., Biomimicry in metal–organic materials. *Coord. Chem. Rev.* **2015,** *293-294*, 327-356.
6. Lehn, J. M., *Supramolecular Chemistry: Concepts and Perspectives*. VCH: 1995; p 262 pp.
7. Atwood, J. L.; Lehn, J. M., *Comprehensive Supramolecular Chemistry*. Pergamon: 1996.
8. Lehn, J.-M., Supramolecular Chemistry—Scope and Perspectives Molecules, Supermolecules, and Molecular Devices (Nobel Lecture). *Angew. Chem. Int. Ed.* **1988,** *27* (1), 89-112.
9. Reinhoudt, D. N., Supramolecular Chemistry and Heterocycles. In *Reference Module in Chemistry, Molecular Sciences and Chemical Engineering*, Elsevier: 2013.
10. Savyasachi, A. J.; Kotova, O.; Shanmugaraju, S.; Bradberry, S. J.; Ó'Máille, G. M.; Gunnlaugsson, T., Supramolecular Chemistry: A Toolkit for Soft Functional Materials and Organic Particles. *Chem* **2017,** *3* (5), 764-811.
11. Zhou, H.-C.; Long, J. R.; Yaghi, O. M., Introduction to Metal–Organic Frameworks. *Chem. Rev.* **2012,** *112* (2), 673-674.
12. Chakrabarty, R.; Mukherjee, P. S.; Stang, P. J., Supramolecular Coordination: Self-Assembly of Finite Two- and Three-Dimensional Ensembles. *Chem. Rev.* **2011,** *111* (11), 6810-6918.
13. Isaeva, V. I.; Kustov, L., The application of metal-organic frameworks in catalysis (Review). *Pet. Chem.* **2010,** *50*, 167-180.
14. Wang, Q.; Astruc, D., State of the Art and Prospects in Metal–Organic Framework (MOF)-Based and MOF-Derived Nanocatalysis. *Chem. Rev.* **2019**.
15. Wang, L.; Han, Y.; Feng, X.; Zhou, J.; Qi, P.; Wang, B., Metal-Organic Frameworks for Energy Storage: Batteries and Supercapacitors. *Coord. Chem. Rev.* **2015,** *307*.
16. Draper, E. R.; Adams, D. J., Low-Molecular-Weight Gels: The State of the Art. *Chem* **2017,** *3* (3), 390-410.
17. Steed, J. W., Supramolecular gel chemistry: developments over the last decade. *Chem. Commun.* **2011,** *47* (5), 1379-1383.
18. Yamanaka, M., Urea derivatives as low-molecular-weight gelators. *J. Incl. Phenom. Macro.* **2013,** *77* (1), 33-48.
19. Lloyd, G. O.; Steed, J. W., Anion-tuning of supramolecular gel properties. *Nat. Chem.* **2009,** *1*, 437.
20. Kumar, D. K.; Steed, J. W., Supramolecular gel phase crystallization: orthogonal self-assembly under non-equilibrium conditions. *Chem. Soc. Rev.* **2014,** *43* (7), 2080-2088.

21. Yamamichi, S.; Jinno, Y.; Haraya, N.; Oyoshi, T.; Tomitori, H.; Kashiwagi, K.; Yamanaka, M., Separation of proteins using supramolecular gel electrophoresis. *Chem. Commun.* **2011,** *47* (37), 10344-10346.
22. Foster, J. A.; Damodaran, K. K.; Maurin, A.; Day, G. M.; Thompson, H. P. G.; Cameron, G. J.; Bernal, J. C.; Steed, J. W., Pharmaceutical polymorph control in a drug-mimetic supramolecular gel. *Chem. Sci.* **2017,** *8* (1), 78-84.
23. Buerkle, L. E.; Rowan, S. J., Supramolecular gels formed from multi-component low molecular weight species. *Chem. Soc. Rev.* **2012,** *41* (18), 6089-6102.
24. Edwards, W.; Smith, D. K., Enantioselective Component Selection in Multicomponent Supramolecular Gels. *J. Am. Chem. Soc.* **2014,** *136* (3), 1116-1124.
25. Draper, E. R.; Adams, D. J., How should multicomponent supramolecular gels be characterised? *Chem. Soc. Rev.* **2018,** *47* (10), 3395-3405.
26. Draper, E. R.; Eden, E. G. B.; McDonald, T. O.; Adams, D. J., Spatially resolved multicomponent gels. *Nat. Chem.* **2015,** *7*, 848.
27. Robin, A. Y.; Fromm, K. M., Coordination polymer networks with O- and N-donors: What they are, why and how they are made. *Coord. Chem. Rev.* **2006,** *250* (15), 2127-2157.
28. Spokoyny, A. M.; Kim, D.; Sumrein, A.; Mirkin, C. A., Infinite coordination polymer nano- and microparticle structures. *Chem. Soc. Rev.* **2009,** *38* (5), 1218-1227.
29. Eddaoudi, M.; Moler, D. B.; Li, H.; Chen, B.; Reineke, T. M.; O'Keeffe, M.; Yaghi, O. M., Modular Chemistry: Secondary Building Units as a Basis for the Design of Highly Porous and Robust Metal−Organic Carboxylate Frameworks. *Acc. Chem. Res.* **2001,** *34* (4), 319-330.
30. Kumar, G.; Gupta, R., Molecularly designed architectures - the metalloligand way. *Chem. Soc. Rev.* **2013,** *42* (24), 9403-9453.
31. Pan, L.; Sander, M. B.; Huang, X.; Li, J.; Smith, M.; Bittner, E.; Bockrath, B.; Johnson, J. K., Microporous Metal Organic Materials: Promising Candidates as Sorbents for Hydrogen Storage. *J. Am. Chem. Soc.* **2004,** *126* (5), 1308-1309.
32. Loukopoulos, E.; Kostakis, G. E., Review: Recent advances of one-dimensional coordination polymers as catalysts. *J. Coord. Chem.* **2018,** *71* (3), 371-410.
33. Zhao, D.; Timmons, D. J.; Yuan, D.; Zhou, H.-C., Tuning the Topology and Functionality of Metal−Organic Frameworks by Ligand Design. *Acc. Chem. Res.* **2011,** *44* (2), 123-133.
34. Lu, W.; Wei, Z.; Gu, Z.-Y.; Liu, T.-F.; Park, J.; Park, J.; Tian, J.; Zhang, M.; Zhang, Q.; Gentle Iii, T.; Bosch, M.; Zhou, H.-C., Tuning the structure and function of metal–organic frameworks via linker design. *Chem. Soc. Rev.* **2014,** *43* (16), 5561-5593.
35. Yuan, S.; Lu, W.; Chen, Y.-P.; Zhang, Q.; Liu, T.-F.; Feng, D.; Wang, X.; Qin, J.; Zhou, H.-C., Sequential Linker Installation: Precise Placement of Functional Groups in Multivariate Metal–Organic Frameworks. *J. Am. Chem. Soc.* **2015,** *137* (9), 3177-3180.
36. Garberoglio, G.; Skoulidas, A. I.; Johnson, J. K., Adsorption of Gases in Metal Organic Materials: Comparison of Simulations and Experiments. *J. Phys. Chem. B* **2005,** *109* (27), 13094-13103.
37. Ren, J.; Langmi, H. W.; North, B. C.; Mathe, M., Review on processing of metal–organic framework (MOF) materials towards system integration for hydrogen storage. *Int. J. Energy Res.* **2015,** *39* (5), 607-620.
38. Drobek, M.; Kim, J.-H.; Bechelany, M.; Vallicari, C.; Julbe, A.; Kim, S. S., MOF-Based Membrane Encapsulated ZnO Nanowires for Enhanced Gas Sensor Selectivity. *ACS Appl. Mater. Interfaces* **2016,** *8* (13), 8323-8328.

39. Horcajada, P.; Serre, C.; Vallet-Regí, M.; Sebban, M.; Taulelle, F.; Férey, G., Metal–Organic Frameworks as Efficient Materials for Drug Delivery. *Angew. Chem. Int. Ed.* **2006,** *45* (36), 5974-5978.
40. Lee, J.; Farha, O. K.; Roberts, J.; Scheidt, K. A.; Nguyen, S. T.; Hupp, J. T., Metal–organic framework materials as catalysts. *Chem. Soc. Rev.* **2009,** *38* (5), 1450-1459.
41. Farha, O. K.; Hupp, J. T., Rational Design, Synthesis, Purification, and Activation of Metal−Organic Framework Materials. *Acc. Chem. Res.* **2010,** *43* (8), 1166-1175.
42. Suzuki, M.; Hanabusa, K., l-Lysine-based low-molecular-weight gelators. *Chem. Soc. Rev.* **2009,** *38* (4), 967-975.
43. Gangu, K. K.; Maddila, S.; Mukkamala, S. B.; Jonnalagadda, S. B., A review on contemporary Metal–Organic Framework materials. *Inorg. Chim. Acta* **2016,** *446*, 61-74.
44. Furukawa, H.; Kim, J.; Ockwig, N. W.; O'Keeffe, M.; Yaghi, O. M., Control of Vertex Geometry, Structure Dimensionality, Functionality, and Pore Metrics in the Reticular Synthesis of Crystalline Metal−Organic Frameworks and Polyhedra. *J. Am. Chem. Soc.* **2008,** *130* (35), 11650-11661.
45. Song, F.; Wang, C.; Falkowski, J. M.; Ma, L.; Lin, W., Isoreticular Chiral Metal−Organic Frameworks for Asymmetric Alkene Epoxidation: Tuning Catalytic Activity by Controlling Framework Catenation and Varying Open Channel Sizes. *J. Am. Chem. Soc.* **2010,** *132* (43), 15390-15398.
46. Manna, K.; Ji, P.; Lin, Z.; Greene, F. X.; Urban, A.; Thacker, N. C.; Lin, W., Chemoselective single-site Earth-abundant metal catalysts at metal–organic framework nodes. *Nat. Commun.* **2016,** *7* (1), 12610.
47. Reinares-Fisac, D.; Aguirre-Díaz, L. M.; Iglesias, M.; Snejko, N.; Gutiérrez-Puebla, E.; Monge, M. Á.; Gándara, F., A Mesoporous Indium Metal–Organic Framework: Remarkable Advances in Catalytic Activity for Strecker Reaction of Ketones. *J. Am. Chem. Soc.* **2016,** *138* (29), 9089-9092.
48. Falkowski, J. M.; Liu, S.; Lin, W., Metal-Organic Frameworks as Single-Site Solid Catalysts for Asymmetric Reactions. *Isr. J. Chem.* **2012,** *52* (7), 591-603.
49. Liu, J.; Chen, L.; Cui, H.; Zhang, J.; Zhang, L.; Su, C.-Y., Applications of metal-organic frameworks in heterogeneous supramolecular catalysis. *Chem. Soc. Rev.* **2014,** *43* (16), 6011-6061.
50. Ma, L.; Abney, C.; Lin, W., Enantioselective catalysis with homochiral metal–organic frameworks. *Chem. Soc. Rev.* **2009,** *38* (5), 1248-1256.
51. Hasegawa, S.; Horike, S.; Matsuda, R.; Furukawa, S.; Mochizuki, K.; Kinoshita, Y.; Kitagawa, S., Three-Dimensional Porous Coordination Polymer Functionalized with Amide Groups Based on Tridentate Ligand: Selective Sorption and Catalysis. *J. Am. Chem. Soc.* **2007,** *129* (9), 2607-2614.
52. Kumar, G.; Gupta, R., Molecularly designed architectures – the metalloligand way. *Chem. Soc. Rev.* **2013,** *42* (24), 9403-9453.
53. Xie, M.-H.; Yang, X.-L.; He, Y.; Zhang, J.; Chen, B.; Wu, C.-D., Highly Efficient C□H Oxidative Activation by a Porous MnIII–Porphyrin Metal–Organic Framework under Mild Conditions. *Chem. Eur. J.* **2013,** *19* (42), 14316-14321.
54. Senthilkumar, S.; Goswami, R.; Smith, V. J.; Bajaj, H. C.; Neogi, S., Pore Wall-Functionalized Luminescent Cd(II) Framework for Selective CO2 Adsorption, Highly Specific 2,4,6-Trinitrophenol Detection, and Colorimetric Sensing of Cu2+ Ions. *ACS Sustain. Chem. Eng.* **2018,** *6* (8), 10295-10306.
55. Song, F.; Zhang, T.; Wang, C.; Lin, W., Chiral porous metal-organic frameworks with dual active sites for sequential asymmetric catalysis. *P. Roy. Soc. A-Math. Phy.* **2012,** *468* (2143), 2035-2052.

56. Cmarik, G. E.; Kim, M.; Cohen, S. M.; Walton, K. S., Tuning the Adsorption Properties of UiO-66 via Ligand Functionalization. *Langmuir* **2012,** *28* (44), 15606-15613.
57. Jasuja, H.; Huang, Y.-g.; Walton, K. S., Adjusting the Stability of Metal–Organic Frameworks under Humid Conditions by Ligand Functionalization. *Langmuir* **2012,** *28* (49), 16874-16880.
58. Béziau, A.; Baudron, S. A.; Pogozhev, D.; Fluck, A.; Hosseini, M. W., Stepwise construction of grid-type Cu(ii)–Cd(ii) heterometallic MOFs based on an imidazole-appended dipyrrin ligand. *Chem. Commun.* **2012,** *48* (83), 10313-10315.
59. Li, F.; Lindoy, L. F., Metalloligand Strategies for Assembling Heteronuclear Nanocages – Recent Developments. *Aust. J. Chem.* **2019,** *72* (10), 731-741.
60. Kalinke, L. H. G.; Cangussu, D.; Lloret, F.; Bruno, R.; Armentano, D.; Pardo, E.; Ferrando-Soria, J., A Metalloligand Approach for the Self-Assembly of a Magnetic Two-Dimensional Grid-of-Grids. *Cryst. Growth Des.* **2019,** *19* (7), 3905-3912.
61. Huang, S.-L.; Liu, N.; Ling, Y.; Luo, H.-K., IrIII-based Octahedral Metalloligands Derived Primitive Cubic Frameworks for Enhanced CO2/N2 Separation. *Chem. Asian J.* **2017,** *12* (24), 3110-3113.
62. Canali, L.; C. Sherrington, D., Utilisation of homogeneous and supported chiral metal(salen) complexes in asymmetric catalysis. *Chem. Soc. Rev.* **1999,** *28* (2), 85-93.
63. Burrows, A. D.; Cassar, K.; Mahon, M. F.; Warren, J. E., The stepwise formation of mixed-metal coordination networks using complexes of 3-cyanoacetylacetonate. *Dalton Trans.* **2007,** (24), 2499-2509.
64. Burrows, A. D.; Frost, C. G.; Mahon, M. F.; Raithby, P. R.; Renouf, C. L.; Richardson, C.; Stevenson, A. J., Dipyridyl β-diketonate complexes: versatile polydentate metalloligands for metal–organic frameworks and hydrogen-bonded networks. *Chem. Commun.* **2010,** *46* (28), 5067-5069.
65. Burrows, A. D.; Mahon, M. F.; Renouf, C. L.; Richardson, C.; Warren, A. J.; Warren, J. E., Dipyridyl β-diketonate complexes and their use as metalloligands in the formation of mixed-metal coordination networks. *Dalton Trans.* **2012,** *41* (14), 4153-4163.
66. Escudero-Adán, E. C.; Benet-Buchholz, J.; Kleij, A. W., Creation of a Nonsymmetric Dimethanolpyridine Ligand: A Rare Zn(salphen) Template Effect. *Inorg. Chem.* **2008,** *47* (2), 410-412.
67. Ren, Y.; Cheng, X.; Yang, S.; Qi, C.; Jiang, H.; Mao, Q., A chiral mixed metal–organic framework based on a Ni(saldpen) metalloligand: synthesis, characterization and catalytic performances. *Dalton Trans.* **2013,** *42* (27), 9930-9937.
68. Eyele-Mezui, S.; Delahaye, E.; Rogez, G.; Rabu, P., Functional Hybrid Materials Based on Layered Simple Hydroxide Hosts and Dicarboxylate Schiff Base Metal Complex Guests. *Eur. J. Inorg. Chem.* **2012,** *2012* (32), 5225-5238.
69. Huang, Y.; Liu, T.; Lin, J.; Lü, J.; Lin, Z.; Cao, R., Homochiral Nickel Coordination Polymers Based on Salen(Ni) Metalloligands: Synthesis, Structure, and Catalytic Alkene Epoxidation. *Inorg. Chem.* **2011,** *50* (6), 2191-2198.
70. Burnett, B. J.; Barron, P. M.; Choe, W., Recent advances in porphyrinic metal–organic frameworks: materials design, synthetic strategies, and emerging applications. *CrystEngComm* **2012,** *14* (11), 3839-3846.
71. Zhan, H.; Lamare, S.; Ng, A.; Kenny, T.; Guernon, H.; Chan, W.-K.; Djurišić, A. B.; Harvey, P. D.; Wong, W.-Y., Synthesis and Photovoltaic Properties of New Metalloporphyrin-Containing Polyplatinyne Polymers. *Macromolecules* **2011,** *44* (13), 5155-5167.

72. Deenadayalan, M. S.; Sharma, N.; Verma, P. K.; Nagaraja, C. M., Visible-Light-Assisted Photocatalytic Reduction of Nitroaromatics by Recyclable Ni(II)-Porphyrin Metal–Organic Framework (MOF) at RT. *Inorg. Chem.* **2016,** *55* (11), 5320-5327.
73. Choi, E.-Y.; Wray, C. A.; Hu, C.; Choe, W., Highly tunable metal–organic frameworks with open metal centers. *CrystEngComm* **2009,** *11* (4), 553-555.
74. Guo, Z.; Yan, D.; Wang, H.; Tesfagaber, D.; Li, X.; Chen, Y.; Huang, W.; Chen, B., A Three-Dimensional Microporous Metal–Metalloporphyrin Framework. *Inorg. Chem.* **2015,** *54* (1), 200-204.
75. Azhdari Tehrani, A.; Esrafili, L.; Abedi, S.; Morsali, A.; Carlucci, L.; Proserpio, D. M.; Wang, J.; Junk, P. C.; Liu, T., Urea Metal–Organic Frameworks for Nitro-Substituted Compounds Sensing. *Inorg. Chem.* **2017,** *56* (3), 1446-1454.
76. Forgan, R. S.; Marshall, R. J.; Struckmann, M.; Bleine, A. B.; Long, D.-L.; Bernini, M. C.; Fairen-Jimenez, D., Structure-directing factors when introducing hydrogen bond functionality to metal–organic frameworks. *CrystEngComm* **2015,** *17* (2), 299-306.
77. Kitson, P. J.; Marshall, R. J.; Long, D.; Forgan, R. S.; Cronin, L., 3D Printed High-Throughput Hydrothermal Reactionware for Discovery, Optimization, and Scale-Up. *Angew. Chem. Int. Ed.* **2014,** *53* (47), 12723-12728.
78. Rao, P. C.; Mandal, S., Friedel–Crafts Alkylation of Indoles with Nitroalkenes through Hydrogen-Bond-Donating Metal–Organic Framework. *ChemCatChem* **2017,** *9* (7), 1172-1176.
79. Eddaoudi, M.; Kim, J.; Rosi, N.; Vodak, D.; Wachter, J.; O'Keeffe, M.; Yaghi, O. M., Systematic Design of Pore Size and Functionality in Isoreticular MOFs and Their Application in Methane Storage. *Science* **2002,** *295* (5554), 469-472.
80. Karmakar, A.; Pombeiro, A. J. L., Recent advances in amide functionalized metal organic frameworks for heterogeneous catalytic applications. *Coord. Chem. Rev.* **2019,** *395*, 86-129.
81. Esrafili, L.; Gharib, M.; Morsali, A., Selective detection and removal of mercury ions by dual-functionalized metal–organic frameworks: design-for-purpose. *New J. Chem.* **2019,** *43* (46), 18079-18091.
82. Bucci, A.; Mondal, S. S.; Martin-Diaconescu, V.; Shafir, A.; Lloret-Fillol, J., Cobalt Amide Imidate Imidazolate Frameworks as Highly Active Oxygen Evolution Model Materials. *ACS Appl. Mater. Interfaces* **2019,** *2* (12), 8930-8938.
83. Zhang, M.; Chen, C.; Shi, Z.; Huang, K.; Fu, W.; Zhou, W., Inserting Amide into NOTT-101 to Sharply Enhance Volumetric and Gravimetric Methane Storage Working Capacity. *Inorg. Chem.* **2019,** *58* (20), 13782-13787.
84. Zhu, C.; Tang, H.; Yang, K.; Wu, X.; Luo, Y.; Wang, J.; Li, Y., A urea-containing metal-organic framework as a multifunctional heterogeneous hydrogen bond-donating catalyst. *Catal. Commun.* **2020,** *135*, 105837.
85. Janiak, C., Engineering coordination polymers towards applications. *Dalton Trans.* **2003,** (14), 2781-2804.
86. Kitagawa, S.; Kitaura, R.; Noro, S.-i., Functional Porous Coordination Polymers. *Angew. Chem. Int. Ed.* **2004,** *43* (18), 2334-2375.
87. Kitagawa, S.; Uemura, K., Dynamic porous properties of coordination polymers inspired by hydrogen bonds. *Chem. Soc. Rev.* **2005,** *34* (2), 109-119.
88. Li, N.; Feng, R.; Zhu, J.; Chang, Z.; Bu, X.-H., Conformation versatility of ligands in coordination polymers: From structural diversity to properties and applications. *Coord. Chem. Rev.* **2018,** *375*, 558-586.

89. Yan, Y.; Yang, S.; Blake, A. J.; Schröder, M., Studies on Metal–Organic Frameworks of Cu(II) with Isophthalate Linkers for Hydrogen Storage. *Acc. Chem. Res.* **2014,** *47* (2), 296-307.
90. Janiak, C.; Vieth, J. K., MOFs, MILs and more: concepts, properties and applications for porous coordination networks (PCNs). *New J. Chem.* **2010,** *34* (11), 2366-2388.
91. Duan, J.; Jin, W.; Kitagawa, S., Water-resistant porous coordination polymers for gas separation. *Coord. Chem. Rev.* **2017,** *332*, 48-74.
92. Xie, Z.; Ma, L.; deKrafft, K. E.; Jin, A.; Lin, W., Porous Phosphorescent Coordination Polymers for Oxygen Sensing. *J. Am. Chem. Soc.* **2010,** *132* (3), 922-923.
93. Zhang, X.; Wang, W.; Hu, Z.; Wang, G.; Uvdal, K., Coordination polymers for energy transfer: Preparations, properties, sensing applications, and perspectives. *Coord. Chem. Rev.* **2015,** *284*, 206-235.
94. Wu, Z.; Xie, J.; Xu, Z. J.; Zhang, S.; Zhang, Q., Recent progress in metal–organic polymers as promising electrodes for lithium/sodium rechargeable batteries. *J. Mater. Chem. A* **2019,** *7* (9), 4259-4290.
95. Corma, A.; García, H.; Llabrés i Xamena, F. X., Engineering Metal Organic Frameworks for Heterogeneous Catalysis. *Chem. Rev.* **2010,** *110* (8), 4606-4655.
96. Horcajada, P.; Surblé, S.; Serre, C.; Hong, D.-Y.; Seo, Y.-K.; Chang, J.-S.; Grenèche, J.-M.; Margiolaki, I.; Férey, G., Synthesis and catalytic properties of MIL-100(Fe), an iron(iii) carboxylate with large pores. *Chem. Commun.* **2007,** (27), 2820-2822.
97. Dybtsev, D. N.; Nuzhdin, A. L.; Chun, H.; Bryliakov, K. P.; Talsi, E. P.; Fedin, V. P.; Kim, K., A Homochiral Metal–Organic Material with Permanent Porosity, Enantioselective Sorption Properties, and Catalytic Activity. *Angew. Chem. Int. Ed.* **2006,** *45* (6), 916-920.
98. Chen, E. Y. X., Coordination Polymerization of Polar Vinyl Monomers by Single-Site Metal Catalysts. *Chem. Rev.* **2009,** *109* (11), 5157-5214.
99. Falkowski, J. M.; Wang, C.; Liu, S.; Lin, W., Actuation of Asymmetric Cyclopropanation Catalysts: Reversible Single-Crystal to Single-Crystal Reduction of Metal–Organic Frameworks. *Angew. Chem. Int. Ed.* **2011,** *50* (37), 8674-8678.
100. Lin, Z.; Zhang, Z.-M.; Chen, Y.-S.; Lin, W., Highly Efficient Cooperative Catalysis by CoIII(Porphyrin) Pairs in Interpenetrating Metal–Organic Frameworks. *Angew. Chem. Int. Ed.* **2016,** *55* (44), 13739-13743.
101. Zhuang, J.-L.; Ceglarek, D.; Pethuraj, S.; Terfort, A., Rapid Room-Temperature Synthesis of Metal–Organic Framework HKUST-1 Crystals in Bulk and as Oriented and Patterned Thin Films. *Adv. Funct. Mater.* **2011,** *21* (8), 1442-1447.
102. Majano, G.; Ingold, O.; Yulikov, M.; Jeschke, G.; Pérez-Ramírez, J., Room-temperature synthesis of Fe–BTC from layered iron hydroxides: the influence of precursor organisation. *CrystEngComm* **2013,** *15* (46), 9885-9892.
103. Parkin, I. P., Supramolecular chemistry. J.W. Steed and J.L. Atwood. John Wiley & Sons Ltd, Chichester, 2000. 745 pages. ISBN 0-471-98791-3. *Appl. Organomet. Chem.* **2001,** *15* (3), 236-236.
104. Banerjee, S.; Das, R. K.; Maitra, U., Supramolecular gels 'in action'. *J. Mater. Chem.* **2009,** *19* (37), 6649-6687.
105. Dastidar, P., Supramolecular gelling agents: can they be designed? *Chem. Soc. Rev.* **2008,** *37* (12), 2699-2715.
106. de Loos, M.; Feringa, B. L.; van Esch, J. H., Design and Application of Self-Assembled Low Molecular Weight Hydrogels. *Eur. J. Org. Chem.* **2005,** *2005* (17), 3615-3631.

107. Estroff, L. A.; Hamilton, A. D., Water Gelation by Small Organic Molecules. *Chem. Rev.* **2004,** *104* (3), 1201-1218.
108. George, M.; Weiss, R. G., Molecular Organogels. Soft Matter Comprised of Low-Molecular-Mass Organic Gelators and Organic Liquids†. *Acc. Chem. Res.* **2006,** *39* (8), 489-497.
109. Hirst, A. R.; Escuder, B.; Miravet, J. F.; Smith, D. K., High-Tech Applications of Self-Assembling Supramolecular Nanostructured Gel-Phase Materials: From Regenerative Medicine to Electronic Devices. *Angew. Chem. Int. Ed.* **2008,** *47* (42), 8002-8018.
110. Piepenbrock, M.-O. M.; Clarke, N.; Steed, J. W., Shear induced gelation in a copper(ii) metallogel: new aspects of ion-tunable rheology and gel-reformation by external chemical stimuli. *Soft Matter* **2010,** *6* (15), 3541-3547.
111. Yu, G.; Yan, X.; Han, C.; Huang, F., Characterization of supramolecular gels. *Chem. Soc. Rev.* **2013,** *42* (16), 6697-6722.
112. Flory, P. J., Molecular Size Distribution in Three Dimensional Polymers. I. Gelation1. *J. Am. Chem. Soc.* **1941,** *63* (11), 3083-3090.
113. Noro, A.; Hayashi, M.; Matsushita, Y., Design and properties of supramolecular polymer gels. *Soft Matter* **2012,** *8* (24), 6416-6429.
114. Carretti, E.; Bonini, M.; Dei, L.; Berrie, B. H.; Angelova, L. V.; Baglioni, P.; Weiss, R. G., New Frontiers in Materials Science for Art Conservation: Responsive Gels and Beyond. *Acc. Chem. Res.* **2010,** *43* (6), 751-760.
115. Suzuki, M.; Hanabusa, K., Polymer organogelators that make supramolecular organogels through physical cross-linking and self-assembly. *Chem. Soc. Rev.* **2010,** *39* (2), 455-463.
116. Wichterle, O.; LÍM, D., Hydrophilic Gels for Biological Use. *Nature* **1960,** *185* (4706), 117-118.
117. Jensen, O. M.; Hansen, P. F., Water-entrained cement-based materials: II. Experimental observations. *Cement Concrete Res.* **2002,** *32* (6), 973-978.
118. Kulicke, W.-M.; Kull, A. H.; Kull, W.; Thielking, H.; Engelhardt, J.; Pannek, J.-B., Characterization of aqueous carboxymethylcellulose solutions in terms of their molecular structure and its influence on rheological behaviour. *Polymer* **1996,** *37* (13), 2723-2731.
119. McConnell, A. J.; Wood, C. S.; Neelakandan, P. P.; Nitschke, J. R., Stimuli-Responsive Metal–Ligand Assemblies. *Chem. Rev.* **2015,** *115* (15), 7729-7793.
120. Theato, P.; Sumerlin, B. S.; O'Reilly, R. K.; Epps, I. I. I. T. H., Stimuli responsive materials. *Chem. Soc. Rev.* **2013,** *42* (17), 7055-7056.
121. Hajime, S.; Itaru, H., Supramolecular Assemblies Responsive to Biomolecules toward Biological Applications. *Chem. Asian J.* **2015,** *10* (10), 2026-2038.
122. Segarra-Maset, M. D.; Nebot, V. J.; Miravet, J. F.; Escuder, B., Control of molecular gelation by chemical stimuli. *Chem. Soc. Rev.* **2013,** *42* (17), 7086-7098.
123. Zhang, J.; Hu, Y.; Li, Y., Supramolecular Gels. In *Gel Chemistry: Interactions, Structures and Properties*, Springer Singapore: Singapore, 2018; pp 9-59.
124. Flory, P. J., Introductory lecture. *Faraday Discussions of the Chemical Society* **1974,** *57* (0), 7-18.
125. Terech, P.; Weiss, R. G., Low Molecular Mass Gelators of Organic Liquids and the Properties of Their Gels. *Chem. Rev.* **1997,** *97* (8), 3133-3160.
126. Banerjee, S.; Das, R. K.; Maitra, U., Supramolecular gels 'in action'. *Journal of Materials Chemistry* **2009,** *19* (37), 6649-6687.
127. Du, X.; Zhou, J.; Shi, J.; Xu, B., Supramolecular Hydrogelators and Hydrogels: From Soft Matter to Molecular Biomaterials. *Chem. Rev.* **2015,** *115* (24), 13165-13307.

128. Babu, S. S.; Praveen, V. K.; Ajayaghosh, A., Functional π-Gelators and Their Applications. *Chem. Rev.* **2014,** *114* (4), 1973-2129.
129. Worthington, P.; Pochan, D. J.; Langhans, S. A., Peptide Hydrogels – Versatile Matrices for 3D Cell Culture in Cancer Medicine. *Front. Oncol.* **2015,** *5* (92).
130. Truong, W. T.; Su, Y.; Meijer, J. T.; Thordarson, P.; Braet, F., Self-Assembled Gels for Biomedical Applications. *Chem. Asian J.* **2011,** *6* (1), 30-42.
131. Tomasini, C.; Castellucci, N., Peptides and peptidomimetics that behave as low molecular weight gelators. *Chem. Soc. Rev.* **2013,** *42* (1), 156-172.
132. Piepenbrock, M.-O. M.; Lloyd, G. O.; Clarke, N.; Steed, J. W., Metal- and Anion-Binding Supramolecular Gels. *Chem. Rev.* **2010,** *110* (4), 1960-2004.
133. Tam, A. Y.-Y.; Yam, V. W.-W., Recent advances in metallogels. *Chem. Soc. Rev.* **2013,** *42* (4), 1540-1567.
134. Gavara, R.; Llorca, J.; Lima, J. C.; Rodríguez, L., A luminescent hydrogel based on a new Au(i) complex. *Chem. Commun.* **2013,** *49* (1), 72-74.
135. Terech, P.; Gebel, G.; Ramasseul, R., Molecular Rods in a Zinc(II) Porphyrin/Cyclohexane Physical Gel: Neutron and X-ray Scattering Characterizations. *Langmuir* **1996,** *12* (18), 4321-4323.
136. Zhang, Y.; Zhang, B.; Kuang, Y.; Gao, Y.; Shi, J.; Zhang, X. X.; Xu, B., A Redox Responsive, Fluorescent Supramolecular Metallohydrogel Consists of Nanofibers with Single-Molecule Width. *J. Am. Chem. Soc.* **2013,** *135* (13), 5008-5011.
137. Adarsh, N. N.; Sahoo, P.; Dastidar, P., Is a Crystal Engineering Approach Useful in Designing Metallogels? A Case Study. *Cryst. Growth Des.* **2010,** *10* (11), 4976-4986.
138. de Hatten, X.; Bell, N.; Yufa, N.; Christmann, G.; Nitschke, J. R., A Dynamic Covalent, Luminescent Metallopolymer that Undergoes Sol-to-Gel Transition on Temperature Rise. *J. Am. Chem. Soc.* **2011,** *133* (9), 3158-3164.
139. Hamilton, T. D.; Bučar, D.-K.; Baltrusaitis, J.; Flanagan, D. R.; Li, Y.; Ghorai, S.; Tivanski, A. V.; MacGillivray, L. R., Thixotropic Hydrogel Derived from a Product of an Organic Solid-State Synthesis: Properties and Densities of Metal−Organic Nanoparticles. *J. Am. Chem. Soc.* **2011,** *133* (10), 3365-3371.
140. Hanabusa, K.; Maesaka, Y.; Suzuki, M.; Kimura, M.; Shirai, H., Low Molecular Weight Gelator Containing β-Diketonato Ligands: Stabilization of Gels by Metal Coordination. *Chem. Lett.* **2000,** *29* (10), 1168-1169.
141. Kumar, D. K.; Jose, D. A.; Dastidar, P.; Das, A., Nonpolymeric Hydrogelator Derived from N-(4-Pyridyl)isonicotinamide. *Langmuir* **2004,** *20* (24), 10413-10418.
142. Lloyd, G. O.; Piepenbrock, M.-O. M.; Foster, J. A.; Clarke, N.; Steed, J. W., Anion tuning of chiral bis(urea) low molecular weight gels. *Soft Matter* **2012,** *8* (1), 204-216.
143. Zhao, C.; Bai, B.; Wang, H.; Qu, S.; Xiao, G.; Tian, T.; Li, M., Self-assemblies, helical ribbons and gelation tuned by solvent–gelator interaction in a bi-1,3,4-oxadiazole gelator. *J. Mol. Struct.* **2013,** *1037*, 130-135.
144. Nebot, V. J.; Armengol, J.; Smets, J.; Prieto, S. F.; Escuder, B.; Miravet, J. F., Molecular Hydrogels from Bolaform Amino Acid Derivatives: A Structure–Properties Study Based on the Thermodynamics of Gel Solubilization. *Chem. Eur. J.* **2012,** *18* (13), 4063-4072.
145. Yang, Z.; Gu, H.; Zhang, Y.; Wang, L.; Xu, B., Small molecule hydrogels based on a class of antiinflammatory agents. *Chem. Commun.* **2004,** (2), 208-209.
146. Houton, K. A.; Morris, K. L.; Chen, L.; Schmidtmann, M.; Jones, J. T. A.; Serpell, L. C.; Lloyd, G. O.; Adams, D. J., On Crystal versus Fiber Formation in Dipeptide Hydrogelator Systems. *Langmuir* **2012,** *28* (25), 9797-9806.

147. Mears, L. L. E.; Draper, E. R.; Castilla, A. M.; Su, H.; Zhuola; Dietrich, B.; Nolan, M. C.; Smith, G. N.; Doutch, J.; Rogers, S.; Akhtar, R.; Cui, H.; Adams, D. J., Drying Affects the Fiber Network in Low Molecular Weight Hydrogels. *Biomacromolecules* **2017,** *18* (11), 3531-3540.
148. Adams, D. J., Does Drying Affect Gel Networks? *Gels* **2018,** *4* (2), 32.
149. Raeburn, J.; Adams, D. J., Multicomponent low molecular weight gelators. *Chem. Commun.* **2015,** *51* (25), 5170-5180.
150. Miao, W.; Qin, L.; Yang, D.; Jin, X.; Liu, M., Multiple-Stimulus-Responsive Supramolecular Gels of Two Components and Dual Chiroptical Switches. *Chem. Eur. J.* **2015,** *21* (3), 1064-1072.
151. Hirst, A. R.; Smith, D. K., Two-Component Gel-Phase Materials—Highly Tunable Self-Assembling Systems. *Chem. Eur. J.* **2005,** *11* (19), 5496-5508.
152. Hirst, A. R.; Smith, D. K.; Feiters, M. C.; Geurts, H. P. M., Two-Component Dendritic Gel: Effect of Spacer Chain Length on the Supramolecular Chiral Assembly. *Langmuir* **2004,** *20* (17), 7070-7077.
153. Basit, H.; Pal, A.; Sen, S.; Bhattacharya, S., Two-Component Hydrogels Comprising Fatty Acids and Amines: Structure, Properties, and Application as a Template for the Synthesis of Metal Nanoparticles. *Chem. Eur. J.* **2008,** *14* (21), 6534-6545.
154. Adarsh, N. N.; Kumar, D. K.; Dastidar, P., Composites of N,N′-bis-(pyridyl) urea-dicarboxylic acid as new hydrogelators—a crystal engineering approach. *Tetrahedron* **2007,** *63* (31), 7386-7396.
155. Fuhrhop, J. H.; Schnieder, P.; Rosenberg, J.; Boekema, E., The chiral bilayer effect stabilizes micellar fibers. *J. Am. Chem. Soc.* **1987,** *109* (11), 3387-3390.
156. Fuhrhop, J. H.; Svenson, S.; Boettcher, C.; Roessler, E.; Vieth, H. M., Long-lived micellar N-alkylaldonamide fiber gels. Solid-state NMR and electron microscopic studies. *J. Am. Chem. Soc.* **1990,** *112* (11), 4307-4312.
157. Das, R. K.; Kandanelli, R.; Linnanto, J.; Bose, K.; Maitra, U., Supramolecular Chirality in Organogels: A Detailed Spectroscopic, Morphological, and Rheological Investigation of Gels (and Xerogels) Derived from Alkyl Pyrenyl Urethanes. *Langmuir* **2010,** *26* (20), 16141-16149.
158. Sugiyasu, K.; Kawano, S.-i.; Fujita, N.; Shinkai, S., Self-Sorting Organogels with p−n Heterojunction Points. *Chem. Mater.* **2008,** *20* (9), 2863-2865.
159. Džolić, Z.; Wolsperger, K.; Žinić, M., Synergic effect in gelation by two-component mixture of chiral gelators. *New J. Chem.* **2006,** *30* (10), 1411-1419.
160. Li, D.; Shi, Y.; Wang, L., Mechanical Reinforcement of Molecular Hydrogel by Co-assembly of Short Peptide-based Gelators with Different Aromatic Capping Groups. *Chin. J. Chem.* **2014,** *32* (2), 123-127.
161. Koga, T.; Matsuoka, M.; Higashi, N., Structural Control of Self-Assembled Nanofibers by Artificial β-Sheet Peptides Composed of d- or l-Isomer. *J. Am. Chem. Soc.* **2005,** *127* (50), 17596-17597.
162. Edwards, W.; Smith, D. K., Chiral Assembly Preferences and Directing Effects in Supramolecular Two-Component Organogels. *Gels* **2018,** *4* (2), 31.
163. Smith, D. K., Lost in translation? Chirality effects in the self-assembly of nanostructured gel-phase materials. *Chem. Soc. Rev.* **2009,** *38* (3), 684-694.
164. Zhang, L.; Jin, Q.; Liu, M., Enantioselective Recognition by Chiral Supramolecular Gels. *Chem. Asian J.* **2016,** *11* (19), 2642-2649.
165. Leiras, S.; Freire, F.; Quiñoá, E.; Riguera, R., Reversible assembly of enantiomeric helical polymers: from fibers to gels. *Chem. Sci.* **2015,** *6* (1), 246-253.

166. de Loos, M.; van Esch, J.; Kellogg, R. M.; Feringa, B. L., Chiral Recognition in Bis-Urea-Based Aggregates and Organogels through Cooperative Interactions. *Angew. Chem. Int. Ed.* **2001,** *40* (3), 613-616.
167. Das, A.; Ghosh, S., A generalized supramolecular strategy for self-sorted assembly between donor and acceptor gelators. *Chem. Commun.* **2011,** *47* (31), 8922-8924.
168. Draper, E. R.; Wallace, M.; Schweins, R.; Poole, R. J.; Adams, D. J., Nonlinear Effects in Multicomponent Supramolecular Hydrogels. *Langmuir* **2017,** *33* (9), 2387-2395.
169. Chen, L.; Revel, S.; Morris, K.; Adams, D. J., Energy transfer in self-assembled dipeptide hydrogels. *Chem. Commun.* **2010,** *46* (24), 4267-4269.
170. Felip-León, C.; Díaz-Oltra, S.; Galindo, F.; Miravet, J. F., Chameleonic, Light Harvesting Photonic Gels Based on Orthogonal Molecular Fibrillization. *Chem. Mater.* **2016,** *28* (21), 7964-7972.
171. Draper, E. R.; Lee, J. R.; Wallace, M.; Jäckel, F.; Cowan, A. J.; Adams, D. J., Self-sorted photoconductive xerogels. *Chem. Sci.* **2016,** *7* (10), 6499-6505.
172. Abul-Haija, Y. M.; Roy, S.; Frederix, P. W. J. M.; Javid, N.; Jayawarna, V.; Ulijn, R. V., Biocatalytically Triggered Co-Assembly of Two-Component Core/Shell Nanofibers. *Small* **2014,** *10* (5), 973-979.
173. Sarkar, A.; Dhiman, S.; Chalishazar, A.; George, S. J., Visualization of Stereoselective Supramolecular Polymers by Chirality-Controlled Energy Transfer. *Angew. Chem. Int. Ed.* **2017,** *56* (44), 13767-13771.
174. Moffat, J. R.; Smith, D. K., Controlled self-sorting in the assembly of 'multi-gelator' gels. *Chem. Commun.* **2009,** (3), 316-318.
175. Onogi, S.; Shigemitsu, H.; Yoshii, T.; Tanida, T.; Ikeda, M.; Kubota, R.; Hamachi, I., In situ real-time imaging of self-sorted supramolecular nanofibres. *Nat. Chem.* **2016,** *8*, 743.
176. Singh, N.; Zhang, K.; Angulo-Pachón, C. A.; Mendes, E.; van Esch, J. H.; Escuder, B., Tandem reactions in self-sorted catalytic molecular hydrogels. *Chem. Sci.* **2016,** *7* (8), 5568-5572.
177. Singh, N.; Maity, C.; Zhang, K.; Angulo-Pachón, C. A.; van Esch, J. H.; Eelkema, R.; Escuder, B., Synthesis of a Double-Network Supramolecular Hydrogel by Having One Network Catalyse the Formation of the Second. *Chem. Eur. J.* **2017,** *23* (9), 2018-2021.
178. An, B.; Wang, X.; Cui, M.; Gui, X.; Mao, X.; Liu, Y.; Li, K.; Chu, C.; Pu, J.; Ren, S.; Wang, Y.; Zhong, G.; Lu, T. K.; Liu, C.; Zhong, C., Diverse Supramolecular Nanofiber Networks Assembled by Functional Low-Complexity Domains. *ACS Nano* **2017,** *11* (7), 6985-6995.
179. Foster, J. A.; Edkins, R. M.; Cameron, G. J.; Colgin, N.; Fucke, K.; Ridgeway, S.; Crawford, A. G.; Marder, T. B.; Beeby, A.; Cobb, S. L.; Steed, J. W., Blending Gelators to Tune Gel Structure and Probe Anion-Induced Disassembly. *Chem. Eur. J.* **2014,** *20* (1), 279-291.
180. Xing, P.; Tham, H. P.; Li, P.; Chen, H.; Xiang, H.; Zhao, Y., Environment-Adaptive Coassembly/Self-Sorting and Stimulus-Responsiveness Transfer Based on Cholesterol Building Blocks. *Adv. Sci.* **2018,** *5* (1), 1700552.
181. Morris, K. L.; Chen, L.; Raeburn, J.; Sellick, O. R.; Cotanda, P.; Paul, A.; Griffiths, P. C.; King, S. M.; O'Reilly, R. K.; Serpell, L. C.; Adams, D. J., Chemically programmed self-sorting of gelator networks. *Nat. Commun.* **2013,** *4*, 1480.
182. Halperin-Sternfeld, M.; Ghosh, M.; Sevostianov, R.; Grigoriants, I.; Adler-Abramovich, L., Molecular co-assembly as a strategy for synergistic improvement of the mechanical properties of hydrogels. *Chem. Commun.* **2017,** *53* (69), 9586-9589.

183. Fichman, G.; Guterman, T.; Adler-Abramovich, L.; Gazit, E., Synergetic functional properties of two-component single amino acid-based hydrogels. *CrystEngComm* **2015,** *17* (42), 8105-8112.
184. Smith, M. M.; Smith, D. K., Self-sorting multi-gelator gels—mixing and ageing effects in thermally addressable supramolecular soft nanomaterials. *Soft Matter* **2011,** *7* (10), 4856-4860.
185. Dou, X.-Q.; Li, P.; Zhang, D.; Feng, C.-L., RGD anchored C2-benzene based PEG-like hydrogels as scaffolds for two and three dimensional cell cultures. *J. Mater. Chem. B* **2013,** *1* (29), 3562-3568.
186. Vieira, V. M. P.; Lima, A. C.; de Jong, M.; Smith, D. K., Commercially Relevant Orthogonal Multi-Component Supramolecular Hydrogels for Programmed Cell Growth. *Chem. Eur. J.* **2018,** *24* (56), 15112-15118.
187. Li, P.; Dou, X.-Q.; Feng, C.-L.; Zhang, D., Mechanical reinforcement of C2-phenyl-derived hydrogels for controlled cell adhesion. *Soft Matter* **2013,** *9* (14), 3750-3757.
188. Banerjee, S.; Das, R. K.; Maitra, U., Supramolecular gels 'in action'. *J. Mater. Chem.* **2009,** *19* (37), 6649-6687.
189. van Bommel, K. J. C.; Stuart, M. C. A.; Feringa, B. L.; van Esch, J., Two-stage enzyme mediated drug release from LMWG hydrogels. *Org. Biomol. Chem.* **2005,** *3* (16), 2917-2920.
190. Bhuniya, S.; Seo, Y. J.; Kim, B. H., (S)-(+)-Ibuprofen-based hydrogelators: an approach toward anti-inflammatory drug delivery. *Tetrahedron Lett.* **2006,** *47* (40), 7153-7156.
191. Bolla, P. K.; Rodriguez, V. A.; Kalhapure, R. S.; Kolli, C. S.; Andrews, S.; Renukuntla, J., A review on pH and temperature responsive gels and other less explored drug delivery systems. *J. Drug. Deliv. Sci. Tec.* **2018,** *46*, 416-435.
192. Díaz Díaz, D.; Kühbeck, D.; Koopmans, R. J., Stimuli-responsive gels as reaction vessels and reusable catalysts. *Chem. Soc. Rev.* **2011,** *40* (1), 427-448.
193. Schiaffino, L.; Ercolani, G., Unraveling the Mechanism of the Soai Asymmetric Autocatalytic Reaction by First-Principles Calculations: Induction and Amplification of Chirality by Self-Assembly of Hexamolecular Complexes. *Angew. Chem. Int. Ed.* **2008,** *47* (36), 6832-6835.
194. Lan, Y.; Corradini, M. G.; Weiss, R. G.; Raghavan, S. R.; Rogers, M. A., To gel or not to gel: correlating molecular gelation with solvent parameters. *Chem. Soc. Rev.* **2015,** *44* (17), 6035-6058.
195. Adams, D. J.; Morris, K.; Chen, L.; Serpell, L. C.; Bacsa, J.; Day, G. M., The delicate balance between gelation and crystallisation: structural and computational investigations. *Soft Matter* **2010,** *6* (17), 4144-4156.
196. Lan, Y.; Corradini, M. G.; Liu, X.; May, T. E.; Borondics, F.; Weiss, R. G.; Rogers, M. A., Comparing and Correlating Solubility Parameters Governing the Self-Assembly of Molecular Gels Using 1,3:2,4-Dibenzylidene Sorbitol as the Gelator. *Langmuir* **2014,** *30* (47), 14128-14142.
197. Wang, Y.; Tang, L.; Yu, J., Investigation of Spontaneous Transition from Low-Molecular-Weight Hydrogel into Macroscopic Crystals. *Cryst. Growth Des.* **2008,** *8* (3), 884-889.
198. Xu, Y.; Kang, C.; Chen, Y.; Bian, Z.; Qiu, X.; Gao, L.; Meng, Q., In Situ Gel-to-Crystal Transition and Synthesis of Metal Nanoparticles Obtained by Fluorination of a Cyclic β-Aminoalcohol Gelator. *Chem. Eur. J.* **2012,** *18* (52), 16955-16961.
199. Cui, J.; Shen, Z.; Wan, X., Study on the Gel to Crystal Transition of a Novel Sugar-Appended Gelator. *Langmuir* **2010,** *26* (1), 97-103.

200. Moffat, J. R.; Smith, D. K., Metastable two-component gel—exploring the gel–crystal interface. *Chem. Commun.* **2008,** (19), 2248-2250.
201. Nonappa; Lahtinen, M.; Behera, B.; Kolehmainen, E.; Maitra, U., Unraveling the packing pattern leading to gelation using SS NMR and X-ray diffraction: direct observation of the evolution of self-assembled fibers. *Soft Matter* **2010,** *6* (8), 1748-1757.
202. Holmes, H. N., The Formation of Crystals in Gels. *J. Phys. Chem.* **1917,** *21* (9), 709-733.
203. Patel, A. R.; Venkateswara Rao, A., Crystal growth in gel media. *Bull. Mater. Sci.* **1982,** *4* (5), 527-548.
204. Estroff, L. A.; Addadi, L.; Weiner, S.; Hamilton, A. D., An organic hydrogel as a matrix for the growth of calcite crystals. *Org. Biomol. Chem.* **2004,** *2* (1), 137-141.
205. Daly, R.; Kotova, O.; Boese, M.; Gunnlaugsson, T.; Boland, J. J., Chemical Nano-Gardens: Growth of Salt Nanowires from Supramolecular Self-Assembly Gels. *ACS Nano* **2013,** *7* (6), 4838-4845.
206. Pauchet, M.; Morelli, T.; Coste, S.; Malandain, J.-J.; Coquerel, G., Crystallization of (±)-Modafinil in Gel: Access to Form I, Form III, and Twins. *Cryst. Growth Des.* **2006,** *6* (8), 1881-1889.
207. Foster, J. A.; Piepenbrock, M.-O. M.; Lloyd, G. O.; Clarke, N.; Howard, J. A. K.; Steed, J. W., Anion-switchable supramolecular gels for controlling pharmaceutical crystal growth. *Nat. Chem.* **2010,** *2* (12), 1037-1043.
208. Aparicio, F.; Matesanz, E.; Sánchez, L., Cooperative self-assembly of linear organogelators. Amplification of chirality and crystal growth of pharmaceutical ingredients. *Chem. Commun.* **2012,** *48* (46), 5757-5759.
209. Dawn, A.; Mirzamani, M.; Jones, C. D.; Yufit, D. S.; Qian, S.; Steed, J. W.; Kumari, H., Investigating the effect of supramolecular gel phase crystallization on gel nucleation. *Soft Matter* **2018,** *14* (46), 9489-9497.
210. Cudney, R.; Patel, S.; McPherson, A., Crystallization of macromolecules in silica gels. *Acta Crystallogr. D* **1994,** *50* (4), 479-483.
211. Petrova, R. I.; Swift, J. A., Selective Growth and Distribution of Crystalline Enantiomers in Hydrogels. *J. Am. Chem. Soc.* **2004,** *126* (4), 1168-1173.
212. Dawn, A.; Andrew, K. S.; Yufit, D. S.; Hong, Y.; Reddy, J. P.; Jones, C. D.; Aguilar, J. A.; Steed, J. W., Supramolecular Gel Control of Cisplatin Crystallization: Identification of a New Solvate Form Using a Cisplatin-Mimetic Gelator. *Cryst. Growth Des.* **2015,** *15* (9), 4591-4599.
213. Kaufmann, L.; Kennedy, S. R.; Jones, C. D.; Steed, J. W., Cavity-containing supramolecular gels as a crystallization tool for hydrophobic pharmaceuticals. *Chem. Commun.* **2016,** *52* (66), 10113-10116.
214. Diao, Y.; Whaley, K. E.; Helgeson, M. E.; Woldeyes, M. A.; Doyle, P. S.; Myerson, A. S.; Hatton, T. A.; Trout, B. L., Gel-Induced Selective Crystallization of Polymorphs. *J. Am. Chem. Soc.* **2012,** *134* (1), 673-684.
215. Norskov, J. K.; Bligaard, T.; Rossmeisl, J.; Christensen, C. H., Towards the computational design of solid catalysts. *Nat. Chem.* **2009,** *1* (1), 37-46.
216. Qiao, J.; Liu, Y.; Hong, F.; Zhang, J., A review of catalysts for the electroreduction of carbon dioxide to produce low-carbon fuels. *Chem. Soc. Rev.* **2014,** *43* (2), 631-675.
217. Yang, Z.-Z.; He, L.-N.; Gao, J.; Liu, A.-H.; Yu, B., Carbon dioxide utilization with C-N bond formation: carbon dioxide capture and subsequent conversion. *Energy Environ. Sci.* **2012,** *5* (5), 6602-6639.
218. Ruddy, D. A.; Schaidle, J. A.; Ferrell Iii, J. R.; Wang, J.; Moens, L.; Hensley, J. E., Recent advances in heterogeneous catalysts for bio-oil upgrading via "ex situ catalytic fast

pyrolysis": catalyst development through the study of model compounds. *Green Chem.* **2014,** *16* (2), 454-490.
219. MacLellan, P., Heterogeneous organocatalysis: Catalytic cloth. *Nat. Chem.* **2013,** *5* (11), 896-897.
220. George, S. M., Introduction: Heterogeneous Catalysis. *Chem. Rev.* **1995,** *95* (3), 475-476.
221. Eddaoudi, M.; Sava, D. F.; Eubank, J. F.; Adil, K.; Guillerm, V., Zeolite-like metal-organic frameworks (ZMOFs): design, synthesis, and properties. *Chem. Soc. Rev.* **2015,** *44* (1), 228-249.
222. Guillerm, V.; Kim, D.; Eubank, J. F.; Luebke, R.; Liu, X.; Adil, K.; Lah, M. S.; Eddaoudi, M., A supermolecular building approach for the design and construction of metal-organic frameworks. *Chem. Soc. Rev.* **2014,** *43* (16), 6141-6172.
223. Lee, Y.-R.; Kim, J.; Ahn, W.-S., Synthesis of metal-organic frameworks: A mini review. *Korean J. Chem. Eng.* **2013,** *30* (9), 1667-1680.
224. Chughtai, A. H.; Ahmad, N.; Younus, H. A.; Laypkov, A.; Verpoort, F., Metal-organic frameworks: versatile heterogeneous catalysts for efficient catalytic organic transformations. *Chem. Soc. Rev.* **2015,** *44* (19), 6804-6849.
225. Sathre, R.; Masanet, E., Prospective life-cycle modeling of a carbon capture and storage system using metal-organic frameworks for CO2 capture. *RSC Adv.* **2013,** *3* (15), 4964-4975.
226. Purewal, J.; Liu, D.; Sudik, A.; Veenstra, M.; Yang, J.; Maurer, S.; Müller, U.; Siegel, D. J., Improved Hydrogen Storage and Thermal Conductivity in High-Density MOF-5 Composites. *J. Phys. Chem. C* **2012,** *116* (38), 20199-20212.
227. Zhao, Z.; Li, Z.; Lin, Y. S., Adsorption and Diffusion of Carbon Dioxide on Metal−Organic Framework (MOF-5). *Ind. Eng. Chem. Res.* **2009,** *48* (22), 10015-10020.
228. Rosi, N. L.; Eckert, J.; Eddaoudi, M.; Vodak, D. T.; Kim, J.; O'Keeffe, M.; Yaghi, O. M., Hydrogen Storage in Microporous Metal-Organic Frameworks. *Science* **2003,** *300* (5622), 1127-1129.
229. Zhang, Z.; Yao, Z.-Z.; Xiang, S.; Chen, B., Perspective of microporous metal-organic frameworks for CO2 capture and separation. *Energy Environ. Sci.* **2014,** *7* (9), 2868-2899.
230. Jiang, H.-L.; Xu, Q., Porous metal-organic frameworks as platforms for functional applications. *Chem. Commun.* **2011,** *47* (12), 3351-3370.
231. Saha, D.; Deng, S., Structural Stability of Metal Organic Framework MOF-177. *J. Phys. Chem. Lett.* **2010,** *1* (1), 73-78.
232. Tan, Y.-X.; He, Y.-P.; Zhang, J., Tuning MOF Stability and Porosity via Adding Rigid Pillars. *Inorg. Chem.* **2012,** *51* (18), 9649-9654.
233. Furukawa, S.; Reboul, J.; Diring, S.; Sumida, K.; Kitagawa, S., Structuring of metal-organic frameworks at the mesoscopic/macroscopic scale. *Chem. Soc. Rev.* **2014,** *43* (16), 5700-5734.
234. Chen, S.; Xue, M.; Li, Y.; Pan, Y.; Zhu, L.; Qiu, S., Rational design and synthesis of NixCo3-xO4 nanoparticles derived from multivariate MOF-74 for supercapacitors. *J. Mater. Chem. A* **2015,** *3* (40), 20145-20152.
235. Zhu, Q.-L.; Xu, Q., Metal-organic framework composites. *Chem. Soc. Rev.* **2014,** *43* (16), 5468-5512.
236. Kotova, O.; Daly, R.; dos Santos, C. M. G.; Kruger, P. E.; Boland, J. J.; Gunnlaugsson, T., Cross-Linking the Fibers of Supramolecular Gels Formed from a Tripodal Terpyridine Derived Ligand with d-Block Metal Ions. *Inorg. Chem.* **2015,** *54* (16), 7735-7741.

237. Shultz, A. M.; Sarjeant, A. A.; Farha, O. K.; Hupp, J. T.; Nguyen, S. T., Post-Synthesis Modification of a Metal–Organic Framework To Form Metallosalen-Containing MOF Materials. *J. Am. Chem. Soc.* **2011,** *133* (34), 13252-13255.
238. Zeng, M.-H.; Yin, Z.; Tan, Y.-X.; Zhang, W.-X.; He, Y.-P.; Kurmoo, M., Nanoporous Cobalt(II) MOF Exhibiting Four Magnetic Ground States and Changes in Gas Sorption upon Post-Synthetic Modification. *J. Am. Chem. Soc.* **2014,** *136* (12), 4680-4688.
239. Zhang, C.; Koros, W. J., Tailoring the Transport Properties of Zeolitic Imidazolate Frameworks by Post-Synthetic Thermal Modification. *ACS Appl. Mater. Interfaces* **2015,** *7* (42), 23407-23411.
240. Shekhah, O.; Liu, J.; Fischer, R. A.; Woll, C., MOF thin films: existing and future applications. *Chem. Soc. Rev.* **2011,** *40* (2), 1081-1106.
241. Halper, S. R.; Do, L.; Stork, J. R.; Cohen, S. M., Topological Control in Heterometallic Metal−Organic Frameworks by Anion Templating and Metalloligand Design. *J. Am. Chem. Soc.* **2006,** *128* (47), 15255-15268.
242. Kobayashi, A.; Suzuki, Y.; Ohba, T.; Ogawa, T.; Matsumoto, T.; Noro, S.-i.; Chang, H.-C.; Kato, M., Systematic Syntheses and Metalloligand Doping of Flexible Porous Coordination Polymers Composed of a Co(III)–Metalloligand. *Inorg. Chem.* **2015,** *54* (6), 2522-2535.
243. Beyzavi, M. H.; Stephenson, C. J.; Liu, Y.; Karagiaridi, O.; Hupp, J. T.; Farha, O. K., Metal–Organic Framework-Based Catalysts: Chemical Fixation of CO2 with Epoxides Leading to Cyclic Organic Carbonates. *Front. Energy Res.* **2015,** *2* (63).
244. Möller, F.; Merz, K.; Herrmann, C.; Apfel, U. P., Bimetallic nickel complexes for selective CO2 carbon capture and sequestration. *Dalton Trans.* **2016,** *45* (3), 904-907.
245. Lindahl, P. A., The Ni-Containing Carbon Monoxide Dehydrogenase Family: Light at the End of the Tunnel? *Biochemistry* **2002,** *41* (7), 2097-2105.
246. Dixon, N. E.; Gazzola, C.; Blakeley, R. L.; Zerner, B., Jack bean urease (EC 3.5.1.5). Metalloenzyme. Simple biological role for nickel. *J. Am. Chem. Soc.* **1975,** *97* (14), 4131-4133.
247. Park, I.-S.; Hausinger, R. P., Metal Ion Interactions with Urease and UreD-Urease Apoproteins. *Biochemistry* **1996,** *35* (16), 5345-5352.
248. Huang, D.; Makhlynets, O. V.; Tan, L. L.; Lee, S. C.; Rybak-Akimova, E. V.; Holm, R. H., Kinetics and mechanistic analysis of an extremely rapid carbon dioxide fixation reaction. *Proc. Natl. Acad. Sci. U.S.A.* **2011,** *108* (4), 1222-1227.
249. Huang, D.; Makhlynets, O. V.; Tan, L. L.; Lee, S. C.; Rybak-Akimova, E. V.; Holm, R. H., Fast Carbon Dioxide Fixation by 2,6-Pyridinedicarboxamidato-nickel(II)-hydroxide Complexes: Influence of Changes in Reactive Site Environment on Reaction Rates. *Inorg. Chem.* **2011,** *50* (20), 10070-10081.
250. Möller, F.; Castañeda-Losada, L.; Junqueira, J. R. C.; Miller, R. G.; Reback, M. L.; Mallick, B.; van Gastel, M.; Apfel, U. P., Modulation of the CO2 fixation in dinickel azacryptands. *Dalton Trans.* **2017,** *46* (17), 5680-5688.
251. Gamage, N.-D. H.; Mei, Y.; Garcia, J.; Allen, M. J., Oxidatively Stable, Aqueous Europium(II) Complexes through Steric and Electronic Manipulation of Cryptand Coordination Chemistry. *Angew. Chem. Int. Ed.* **2010,** *49* (47), 8923-8925.
252. Wei, P.; Xia, B.; Zhang, Y.; Yu, Y.; Yan, X., A responsive supramolecular polymer formed by orthogonal metal-coordination and cryptand-based host–guest interaction. *Chem. Commun.* **2014,** *50* (30), 3973-3975.
253. Mateus, P.; Lima, L. M. P.; Delgado, R., Di- and trinuclear copper(II) complexes of polyaza macrocycles and cryptands as anion receptors. *Polyhedron* **2013,** *52*, 25-42.

254. Inokuchi, Y.; Boyarkin, O. V.; Kusaka, R.; Haino, T.; Ebata, T.; Rizzo, T. R., UV and IR Spectroscopic Studies of Cold Alkali Metal Ion–Crown Ether Complexes in the Gas Phase. *J. Am. Chem. Soc.* **2011,** *133* (31), 12256-12263.
255. Inokuchi, Y.; Boyarkin, O. V.; Kusaka, R.; Haino, T.; Ebata, T.; Rizzo, T. R., Ion Selectivity of Crown Ethers Investigated by UV and IR Spectroscopy in a Cold Ion Trap. *J. Phys. Chem. A* **2012,** *116* (16), 4057-4068.
256. Choi, C. M.; Kim, H. J.; Lee, J. H.; Shin, W. J.; Yoon, T. O.; Kim, N. J.; Heo, J., Ultraviolet Photodepletion Spectroscopy of Dibenzo-18-Crown-6-Ether Complexes with Alkali Metal Cations. *J. Phys. Chem. A* **2009,** *113* (29), 8343-8350.
257. Chen, T.-H.; Schneemann, A.; Fischer, R. A.; Cohen, S. M., Metal–organic frameworks constructed from crown ether-based 1,4-benzenedicarboxylic acid derivatives. *Dalton Trans.* **2016,** *45* (7), 3063-3069.
258. Beer, P. D.; Kocian, O.; Mortimer, R. J.; Ridgway, C., Syntheses, coordination, spectroscopy and electropolymerisation studies of new alkynyl and vinyl linked benzo- and aza-crown ether-bipyridyl ruthenium(II) complexes. Spectrochemical recognition of group IA/IIA metal cations. *J. Chem. Soc., Chem. Commun.* **1991,** (20), 1460-1463.
259. Pond, S. J. K.; Tsutsumi, O.; Rumi, M.; Kwon, O.; Zojer, E.; Brédas, J.-L.; Marder, S. R.; Perry, J. W., Metal-Ion Sensing Fluorophores with Large Two-Photon Absorption Cross Sections: Aza-Crown Ether Substituted Donor−Acceptor−Donor Distyrylbenzenes. *J. Am. Chem. Soc.* **2004,** *126* (30), 9291-9306.
260. Gustowski, D. A.; Gatto, V. J.; Mallen, J.; Echegoyen, L.; Gokel, G. W., Direct correlation of cation binding strengths to Hammett parameters in substituted N-benzylaza-15-crown-5 lariat ether and N,N'-dibenzyl-4,13-diaza-18-crown-6 BiBLE derivatives. *J. Org. Chem.* **1987,** *52* (23), 5172-5176.
261. Ngo, H. T.; Liu, X.; Jolliffe, K. A., Anion recognition and sensing with Zn(ii)–dipicolylamine complexes. *Chem. Soc. Rev.* **2012,** *41* (14), 4928-4965.
262. Hernández-Gil, J.; Ferrer, S.; Salvador, E.; Calvo, J.; Garcia-España, E.; Mareque-Rivas, J. C., A dinucleating ligand which promotes DNA cleavage with one and without a transition metal ion. *Chem. Commun.* **2013,** *49* (35), 3655-3657.
263. Belousoff, M. J.; Tjioe, L.; Graham, B.; Spiccia, L., Synthesis, X-Ray Crystal Structures, and Phosphate Ester Cleavage Properties of bis(2-Pyridylmethyl)amine Copper(II) Complexes with Guanidinium Pendant Groups. *Inorg. Chem.* **2008,** *47* (19), 8641-8651.
264. Pan, Y.; Yan, Y.; Li, Y.; Gao, X.-W.; Chao, D., A fast-responsive fluorescent probe based on a terpyridine-Zn2+ complex for sensing hypochlorous acid in aqueous solution and its application in real water samples and bioimaging. *New J. Chem.* **2019,** *43* (38), 15120-15125.
265. O'Neil, E. J.; Smith, B. D., Anion recognition using dimetallic coordination complexes. *Coord. Chem. Rev.* **2006,** *250* (23), 3068-3080.
266. Tse, E. C. M.; Schilter, D.; Gray, D. L.; Rauchfuss, T. B.; Gewirth, A. A., Multicopper Models for the Laccase Active Site: Effect of Nuclearity on Electrocatalytic Oxygen Reduction. *Inorg. Chem.* **2014,** *53* (16), 8505-8516.
267. Carreira-Barral, I.; Riopedre-Fernández, M.; de Blas, A.; Mosquera, J.; Vázquez, M. E.; Platas-Iglesias, C.; Esteban-Gómez, D., Ditopic binuclear copper(II) complexes for DNA cleavage. *J. Inorg. Biochem.* **2020,** *205*, 110995.
268. Shinde, V. N.; Bhuvanesh, N.; Kumar, A.; Joshi, H., Design and Syntheses of Palladium Complexes of NNN/CNN Pincer Ligands: Catalyst for Cross Dehydrogenative Coupling Reaction of Heteroarenes. *Organometallics* **2020,** *39* (2), 324-333.

269. Hansen, J.; Davies, H. M. L., High Symmetry Dirhodium(II) Paddlewheel Complexes as Chiral Catalysts. *Coord. Chem. Rev.* **2008,** *252* (5-7), 545-555.
270. Kumar, D. K.; Filatov, A. S.; Napier, M.; Sun, J.; Dikarev, E. V.; Petrukhina, M. A., Dirhodium Paddlewheel with Functionalized Carboxylate Bridges: New Building Block for Self-Assembly and Immobilization on Solid Support. *Inorg. Chem.* **2012,** *51* (8), 4855-4861.
271. Zhu, B.; Liu, G.; Chen, L.; Qiu, L.; Chen, L.; Zhang, J.; Zhang, L.; Barboiu, M.; Si, R.; Su, C.-Y., Metal–organic aerogels based on dinuclear rhodium paddle-wheel units: design, synthesis and catalysis. *Inorg. Chem. Frontiers* **2016,** *3* (5), 702-710.
272. Collins, L. R.; Auris, S.; Goddard, R.; Fürstner, A., Chiral Heterobimetallic Bismuth–Rhodium Paddlewheel Catalysts: A Conceptually New Approach to Asymmetric Cyclopropanation. *Angew. Chem. Int. Ed.* **2019,** *58* (11), 3557-3561.
273. Agterberg, F. P. W.; Provó Kluit, H. A. J.; Driessen, W. L.; Oevering, H.; Buijs, W.; Lakin, M. T.; Spek, A. L.; Reedijk, J., Dinuclear Paddle-Wheel Copper(II) Carboxylates in the Catalytic Oxidation of Carboxylic Acids. Unusual Polymeric Chains Found in the Single-Crystal X-ray Structures of [Tetrakis(μ-1-phenylcyclopropane-1-carboxylato-O,O‘)bis(ethanol-O)dicopper(II)] and catena-Poly[[bis(μ-diphenylacetato-O:O‘)dicopper](μ3-diphenylacetato-1-O:2-O‘:1‘-O‘)(μ3-diphenylacetato-1-O:2-O‘:2‘-O‘)]. *Inorg. Chem.* **1997,** *36* (20), 4321-4328.
274. Collins, L. R.; van Gastel, M.; Neese, F.; Fürstner, A., Enhanced Electrophilicity of Heterobimetallic Bi–Rh Paddlewheel Carbene Complexes: A Combined Experimental, Spectroscopic, and Computational Study. *J. Am. Chem. Soc.* **2018,** *140* (40), 13042-13055.
275. Chui, S. S.-Y.; Lo, S. M.-F.; Charmant, J. P. H.; Orpen, A. G.; Williams, I. D., A Chemically Functionalizable Nanoporous Material $[Cu_3(TMA)_2(H_2O)_3]$n. *Science* **1999,** *283* (5405), 1148-1150.
276. Doitomi, K.; Xu, K.; Hirao, H., The mechanism of an asymmetric ring-opening reaction of epoxide with amine catalyzed by a metal–organic framework: insights from combined quantum mechanics and molecular mechanics calculations. *Dalton Trans.* **2017,** *46* (11), 3470-3481.
277. Motoyama, Y.; Morii, K.; Ishizuka, S.; Inomoto, S.; Zhang, Z.; Yoon, S.-H., Specific Inhibition of the Hydrogenolysis of Benzylic C−O Bonds Using Palladium Nanoparticles Supported on Nitrogen-Doped Carbon Nanofibers. *ChemCatChem* **2018,** *10* (3), 505-509.
278. Liu, M.; Liang, L.; Li, X.; Gao, X.; Sun, J., Novel urea derivative-based ionic liquids with dual-functions: CO2 capture and conversion under metal- and solvent-free conditions. *Green Chem.* **2016,** *18* (9), 2851-2863.
279. Drewe, W. C.; Nanjunda, R.; Gunaratnam, M.; Beltran, M.; Parkinson, G. N.; Reszka, A. P.; Wilson, W. D.; Neidle, S., Rational Design of Substituted Diarylureas: A Scaffold for Binding to G-Quadruplex Motifs. *J. Med. Chem.* **2008,** *51* (24), 7751-7767.
280. Tehrani, A. A.; Abedi, S.; Morsali, A.; Wang, J.; Junk, P. C., Urea-containing metal-organic frameworks as heterogeneous organocatalysts. *J. Mater. Chem. A* **2015,** *3* (40), 20408-20415.
281. Sakakura, T.; Kohno, K., The synthesis of organic carbonates from carbon dioxide. *Chem. Commun.* **2009,** (11), 1312-1330.
282. Shaikh, A.-A. G.; Sivaram, S., Organic Carbonates. *Chem. Rev.* **1996,** *96* (3), 951-976.
283. Song, J.; Zhang, Z.; Hu, S.; Wu, T.; Jiang, T.; Han, B., MOF-5/n-Bu4NBr: an efficient catalyst system for the synthesis of cyclic carbonates from epoxides and CO2 under mild conditions. *Green Chem.* **2009,** *11* (7), 1031-1036.

284. Maina, J. W.; Pozo-Gonzalo, C.; Kong, L.; Schutz, J.; Hill, M.; Dumee, L. F., Metal organic framework based catalysts for CO2 conversion. *Mater. Horiz.* **2017,** *4* (3), 345-361.
285. Zalomaeva, O. V.; Chibiryaev, A. M.; Kovalenko, K. A.; Kholdeeva, O. A.; Balzhinimaev, B. S.; Fedin, V. P., Cyclic carbonates synthesis from epoxides and CO2 over metal–organic framework Cr-MIL-101. *J. Catal.* **2013,** *298*, 179-185.
286. Verma, A.; De, D.; Tomar, K.; Bharadwaj, P. K., An Amine Functionalized Metal–Organic Framework as an Effective Catalyst for Conversion of CO2 and Biginelli Reactions. *Inorg. Chem.* **2017,** *56* (16), 9765-9771.
287. Zhao, D.; Liu, X.-H.; Guo, J.-H.; Xu, H.-J.; Zhao, Y.; Lu, Y.; Sun, W.-Y., Porous Metal–Organic Frameworks with Chelating Multiamine Sites for Selective Adsorption and Chemical Conversion of Carbon Dioxide. *Inorg. Chem.* **2018,** *57* (5), 2695-2704.
288. Fernando, C. G.; Giovanni, S.; W., K. A.; Carles, B., A DFT Study on the Mechanism of the Cycloaddition Reaction of CO2 to Epoxides Catalyzed by Zn(Salphen) Complexes. *Chem. Eur. J.* **2013,** *19* (20), 6289-6298.
289. Hongming, H.; A., P. J.; Guangshan, Z.; Shengqian, M., Metal-Organic Frameworks for CO2 Chemical Transformations. *Small* **2016,** *12* (46), 6309-6324.
290. Garibay, S. J.; Wang, Z.; Cohen, S. M., Evaluation of Heterogeneous Metal−Organic Framework Organocatalysts Prepared by Postsynthetic Modification. *Inorg. Chem.* **2010,** *49* (17), 8086-8091.
291. Taher, A.; Kim, D. W.; Lee, I.-M., Highly efficient metal organic framework (MOF)-based copper catalysts for the base-free aerobic oxidation of various alcohols. *RSC Adv.* **2017,** *7* (29), 17806-17812.
292. Graffner-Nordberg, M.; Marelius, J.; Ohlsson, S.; Persson, Å.; Swedberg, G.; Andersson, P.; Andersson, S. E.; Åqvist, J.; Hallberg, A., Computational Predictions of Binding Affinities to Dihydrofolate Reductase: Synthesis and Biological Evaluation of Methotrexate Analogues. *J. Med. Chem.* **2000,** *43* (21), 3852-3861.
293. Khan, G. S.; Dickson, B. D.; Barker, D., Synthesis of benzoic acids and polybenzamides containing tertiary alkylamino functionality. *Tetrahedron* **2012,** *68* (6), 1790-1801.
294. Barrett, A. G. M.; Hamprecht, D.; James, R. A.; Ohkubo, M.; Procopiou, P. A.; Toledo, M. A.; White, A. J. P.; Williams, D. J., Synthesis and Characterization of Coronanes: Multicyclopropane-Fused Macrocyclic Arrays. *J. Org. Chem.* **2001,** *66* (7), 2187-2196.
295. Kumar, D. K.; Jose, D. A.; Das, A.; Dastidar, P., First snapshot of a nonpolymeric hydrogelator interacting with its gelling solvents. *Chem. Commun.* **2005,** (32), 4059-4061.
296. Pandurangan, K.; Kitchen, J. A.; Blasco, S.; Paradisi, F.; Gunnlaugsson, T., Supramolecular pyridyl urea gels as soft matter with antibacterial properties against MRSA and/or E. coli. *Chem. Commun.* **2014,** *50* (74), 10819-10822.
297. Liu, Q.; Wang, Y.; Li, W.; Wu, L., Structural Characterization and Chemical Response of a Ag-Coordinated Supramolecular Gel. *Langmuir* **2007,** *23* (15), 8217-8223.
298. Colquhoun, C.; Draper, E. R.; Eden, E. G. B.; Cattoz, B. N.; Morris, K. L.; Chen, L.; McDonald, T. O.; Terry, A. E.; Griffiths, P. C.; Serpell, L. C.; Adams, D. J., The effect of self-sorting and co-assembly on the mechanical properties of low molecular weight hydrogels. *Nanoscale* **2014,** *6* (22), 13719-13725.
299. Cross, E. R.; Sproules, S.; Schweins, R.; Draper, E. R.; Adams, D. J., Controlled Tuning of the Properties in Optoelectronic Self-Sorted Gels. *J. Am. Chem. Soc.* **2018,** *140* (28), 8667-8670.

300. Schön, E.-M.; Marqués-López, E.; Herrera, R. P.; Alemán, C.; Díaz, D. D., Exploiting Molecular Self-Assembly: From Urea-Based Organocatalysts to Multifunctional Supramolecular Gels. *Chem. Eur. J.* **2014,** *20* (34), 10720-10731.